

Air infiltration modelling based on low-pressure airtightness measurements

Alan Emmanuel Vega Pasos

BSc., MSc.

Supervisors:

Dr. Christopher Wood

Prof. Mark Gillott

Dr. Xiaofeng Zheng

Thesis submitted to the University of Nottingham for the degree of Building Technology Doctor of Philosophy

Buildings, Energy and Environment, Research Group

Architecture and Built Environment

Faculty of Engineering

University of Nottingham

June 2020

Abstract

The building sector has been responsible for around 30% of carbon emissions. These emissions come from the construction materials, but mainly by the building operation. The largest energy user of a building usually is the Heating, Ventilation and Air Conditioning system (HVAC). The ventilation efficiency depends on a correct design; however there is an unintended part of the ventilation called air infiltration. One-third of the heating load of a building is related to infiltration. The fewer leakage paths the building envelope has, the less infiltration it will allow. These leakage paths define the airtightness of a building. Air infiltration mainly (but not only) depends on the airtightness.

Air infiltration measurements are taken through invasive and disruptive tracer gas methods. Infiltration energy losses are calculated via air infiltration predictions obtained using infiltration models. Examples of infiltration models are LBL, AIM-2 AIDA, CONTAM, or DOMVENT3D. Airtightness is typically measured at a high-pressure differential. Infiltration occurs most of the time in a lower pressure difference. Infiltration is then predicted based on those high-pressure airtightness measurements. This project found that there are no models predicting infiltration using low-pressure airtightness measurements.

The steady pressurisation method is the most common airtightness measuring test. It measures the building airtightness typically between 10-60 Pa pressure difference (quoted at 50 Pa). This method has shortcomings such as the disruption of building integrity, the potential creation of new leakage paths, and the uncertainty created when extrapolating from high to low pressure. Pulse is a low-pressure airtightness testing method. It measures the building airtightness typically between 1-10 Pa pressure difference (quoted at 4 Pa). Pulse maintains the building integrity and its measurements avoid the uncertainties created by extrapolation.

Pulse is used in this thesis to obtain infiltration predictions based on modified infiltration models. This project aims to review, calibrate, test and validate infiltration models based on airtightness measurements taken using the Pulse technique. The overall methodology is to do air infiltration and airtightness tests in

various dwellings across the East-Midlands in the UK. Dwelling parameters and environmental conditions are also recorded. Measurements and predictions are compared and statistically analysed.

The first model tested was a leakage-infiltration ratio: the "divide-by-20" rule of thumb. The rule of thumb overestimated the infiltration rate for all dwellings. A divide-by-38 rule fitted better the data obtained. When using low-pressure airtightness measurements, a divide-by-8 rule fitted the data. It was concluded that leakage-infiltration ratios are not accurate when predicting infiltration.

The LBL model was used to predict air infiltration from high (LBL50) and low (LBL4) pressure airtightness measurements. Both LBL models delivered similar results: comparable standard errors and relative percentage difference. DOMVENT3D model was used to predict air infiltration using both airtightness methods' measurements (DOMVENT3D-50 when using the steady pressurisation method measurements and, DOMVENT3D-4 when using Pulse). DOMVENT3D-4 model turned to predict with and RPD accuracy of 3% $\pm$ 14%. Both models are comparable and can be used regardless of the airtightness inputs. A sensitivity analysis of all the models showed that the variables used interact similarly.

Comparing all models, DOMVENT3D-4 was the most accurate model (mean RPD 3%), whereas the LBL-50 was the one with the lowest standard error (3%). The least accurate is the divide-by-20 rule of thumb (95%). The best overall predictions were given by the DOMVENT3D-4 model: 3% $\pm$ 14%. The conclusion is that measurements from the Pulse method can be used to predict infiltration. Regardless of the infiltration model, when using the Pulse method, there is not added error or uncertainty compared with the standard steady pressurisation method. Recommendations regarding the creation or revision of legislation and the extension of Pulse's development are given.

Acknowledgements

This PhD project would not have been achieved without support of a number of academics and organisations which I would like to mention.

First of all, the Mexican council of science and technology (CONACYT) for fully funding this PhD project. Support to science must always be recognised, and I thank the council for giving me the opportunity to start a career in science.

Dr. Christopher Wood, Professor Mark Gillott and Dr. Xiaofeng Zheng from the University of Nottingham, for providing guidance, patience, and knowledge to the project. For giving me the opportunity to involve my project to the Pulse and low-pressure airtightness measuring, and for teaching me how to be a researcher. Building physics would not be as fun without your input. In addition, I would like to thank Dr. Benjamin Jones from the University of Nottingham, for helping me with statistics and mathematical modelling, I would not have found my curiosity for uncertainties without his input. Finally I acknowledge Dr. Edward Cooper for first taking me into the project.

Thank you to Dr. Lucelia Rodrigues, Professor Mark Gillott, Dr. Christopher Wood from the University of Nottingham and Dr. Joana Soares Goncalves from the University of Sao Paulo, for allowing me to carry out airtightness tests in Sao Paulo, Brasil.

Saint Gobain Recherche for the provision of the tracer gas testing materials and equipment used to perform all the test from the fourth chapter of the thesis. In addition, the collaboration to papers published from Saint Gobain's collaborators is also acknowledged.

Most of the data collected in this project was possible thanks to Build Test Solutions (BTS). Properties tested, airtightness data and tracer gas equipment were provided by them, I would specially like to thank Luke Smith and Adam Moring for all the effort and resources that they put on my project.

Finally the University of Nottingham Graduate School travel grant for proving the funds to attend the Sustainable Energy Technologies international conference in 2019.

Dedicatory

I would like to dedicate this thesis to all the people whose friendship, love and support made it possible.

Chris and Ken, more than my supervisors you became part of my family, thanks for all the work and non-work related talks, the laughs, the help, the support, the advice, everything, I am happy that our professional and personal paths crossed. Thanks to you I think that doing a PhD was the best professional decision I could have made.

All the people in Mark Group house, I have seen people come an go in the last four years but most of you left something in me, thanks for the fuddles, the coffee, the snacks, and those "research breaks" at tea time. All of you are acknowledged here but specially Ana, Eldar, Lia, Sean and Vasilis. And thank you Zeny for being the most important person for a PhD student in the department, I do not have the words to thank you for all the help.

To the team in Rutland Hall, you made me spent two of the most amazing years in my life. Ana, Anjani, Carlos, Haya, Hauwa, Layla and Zain. I will miss those de-stressing dinners that took me away from work. And, most important thanks to Professor Jan Bradley who taught me how to be a leader and, for being a role model, you were the most influential person in my PhD, outside of my PhD.

Thanks to the always supportive Mexican community in the University of Nottingham. I met many of the greatest minds in the world here, I am happy to call them friends now. Your joy will always cheer me up, you are so many that I cannot mention all without forgetting someone.

The completion of this work is also dedicated to the person who first introduced me to science and research: Dr. Roger Gonzalez Herrera from UADY, here I fulfil the promise I made in 2010, thank you!

To all my family and friends who are always cheering for me no matter where I am.

And finally, but most importantly, to my wife Monica, thanks for giving me that smile to continue my work everyday, your patience, for being there unconditionally

on the happiest and the most stressful times, and for joining me in this 4-year adventure. Not a single word of this thesis would have been written without your presence. You are the reason why I am able to accomplish my goals. I love you.

Thank you all.

Alan Vega Pasos

Contents

1 Introduction **1**

1.1 Introduction 1

1.1.1 Introduction to airtightness and air infiltration modelling research 4

1.2 Aim 6

1.3 Objectives 7

1.4 Structure of project and Thesis overview 8

1.4.1 Methodology 10

2 Literature Review **11**

2.1 Introduction 11

2.2 Airtightness measuring techniques 11

2.2.1 Building airtightness context 11

2.2.2 Steady pressurisation method: blower door 14

2.2.3 The Pulse method 18

2.2.4 Other airtightness measuring methods 24

2.2.5 Modern research on airtightness measuring 26

2.3 Air infiltration measurement 26

2.3.1 Tracer gas methods 27

2.4 Prediction of air infiltration 36

2.4.1 Air infiltration models 37

2.4.2 Historical research on air infiltration 51

2.4.3 Discussion on air infiltration and lessons learnt 53

2.5 Chapter conclusions 55

3 Introduction to the Pulse method and preliminary tests **57**

3.1 Introduction 57

3.2 Description of an airtightness test using the Pulse Method 58

3.3 Experimental studies on dwellings 61

3.4 Experimental studies on small enclosures . . . 66
3.5 Instrumentation uncertainties in Pulse . . . 69
3.5.1 Process of calculation of instrumentation uncertainty for the Pulse method . . . 69
3.6 Chapter conclusions . . . 73

4 Case study on the investigation of the impact of airtightness and environmental conditions on air infiltration 76
4.1 Introduction . . . 77
4.2 Chapter methodology . . . 78
4.2.1 Test house and setup . . . 78
4.2.2 Equipment . . . 80
4.2.3 Testing arrangement . . . 84
4.3 Results . . . 86
4.3.1 Airtightness measurements . . . 86
4.3.2 Air infiltration rate measurements . . . 90
4.3.3 The correlation between air infiltration and airtightness . . . 97
4.3.4 Impact of environmental conditions on the infiltration measurements and the airtightness-infiltration correction . . . 99
4.3.5 Impact of wind on the pressure profiles . . . 103
4.4 Discussion . . . 109
4.5 Chapter conclusion . . . 111

5 Field investigation on the infiltration - leakage correlation 113
5.1 Introduction . . . 113
5.2 Methodology . . . 114
5.2.1 Description of the test houses . . . 114
5.2.2 Measurements: airtightness, environmental conditions and air infiltration . . . 117
5.2.3 Pulse airtightness temperature corrections . . . 128
5.3 Results . . . 133
5.3.1 Airtightness . . . 133
5.3.2 Air infiltration - Tracer gas decay method . . . 138
5.4 Discussion . . . 139
5.4.1 Correlating air infiltration and airtightness . . . 139
5.4.2 Statistical analysis and validation . . . 142
5.5 Chapter conclusions . . . 145

6 Leakage-infiltration ratios, testing the simplest way of predicting air infiltration 147
6.1 Introduction . . . 147
6.1.1 UK context . . . 148
6.2 Chapter methodology . . . 149
6.3 Results and discussion . . . 150
6.3.1 Air Permeability q_{50} (air leakage rate n_{50}) – infiltration n_1 ratios. . . . 150
6.3.2 Air Permeability q_4 (air change rate n_4) – infiltration n_1 ratios. 162
6.4 Chapter conclusion . . . 165

7 Prediction of infiltration from low-pressure leakage measurements using the LBL model 167
7.1 Introduction . . . 167
7.2 Chapter methodology . . . 168
7.3 Predicting infiltration rates with the LBL model . . . 172
7.3.1 From high- pressure airtightness measurements: Steady pressurisation method . . . 172
7.3.2 From low-pressure airtightness measurements: Pulse method 177
7.4 Monte Carlo analysis . . . 183
7.4.1 Defining distributions . . . 183
7.5 Sensitivity analysis . . . 192
7.5.1 Introduction to sensitivity analysis . . . 192
7.5.2 Scatter plots LBL50 and LBL4 assumptions 1 and 3 . . . 195
7.5.3 Regression and ranking of variables . . . 212
7.5.4 Scatter plots LBL50 and LBL4 assuming volume and envelope area as constants . . . 218
7.5.5 Regression and ranking of variables taking volume and envelope area as constants . . . 227
7.5.6 Sensitivity analysis: major findings . . . 232
7.6 Conclusions . . . 233

8 Modifying an infiltration model to predict based on low pressure airtightness measurements 236
8.1 Introduction . . . 236
8.2 Chapter method . . . 237
8.3 Predicting infiltration rates with DOMVENT3D . . . 239
8.4 Montecarlo simulations . . . 242

8.5 Sensitivity analysis . . . 243
8.5.1 Scatter plots DOMVENT3D-50 and DOMVENT3D-4 245
8.5.2 Regression and ranking of variables . . . 254
8.5.3 Regression and ranking of variables taking volume and envelope area as constants . . . 258
8.6 Conclusions . . . 262

9 Discussion, conclusion and recommendation for future research 264
9.1 Discussion . . . 264
9.1.1 Airtightness testing . . . 264
9.1.2 Air infiltration rate measurements: tracer gas . . . 266
9.1.3 The correlation between airtightness and air infiltration: predictions using models . . . 268
9.1.4 Implication of the impact of the findings on the practice. . . . 272
9.2 Conclusion . . . 273
9.3 Future research . . . 274

Appendix A Temperature correction code 291

Appendix B Tracer gas tests in the case study house 294

Appendix C Wind and pressure graphs from the case study house tests 316

Appendix D Statistical distributions of pressure tests in the case study house 321

Appendix E Tracer gas tests and environmental conditions measurements in Field Trials stage. 325
E.1 Tracer gas concentration decay tests and uncertainty calculation . . 325
E.2 Environmental conditions measurements in test dwellings . . . 336

Appendix F LBL50 and LBL4 MATLAB code 355

Appendix G DOMVENT3D-50 and DOMVENT3D-4 MATLAB code 364

List of Figures

2.1 Steady airtightness measuring method, door fan in pressurisation . 14
2.2 A typical steady-state airtightness test (Log-log plot) 15
2.3 Standard Minneapolis blower door unit (photo source: Wikimedia) 15
2.4 Gravity-powered piston device for generating a pressure pulse in the testing room [Cooper and Etheridge, 2007b] 19
2.5 Pulse connection of compressed air and piston unit [Cooper et al., 2014] 20
2.6 Nozzle-based pulse unit [Cooper and Etheridge, 2007b] 20
2.7 Schematic diagram of the Pulse nozzle unit with a composite tank [Zheng et al., 2019a] 20
2.8 Photo of the Pulse nozzle unit with composite tank [Cooper et al., 2016, Zheng et al., 2019a] 21
2.9 Photo of the Pulse modified nozzle unit with control box integrated 22
2.10 Latest version of the Pulse unit 22
2.11 Example of a concentration decay of tracer gas in one zone of a building 29
2.12 Example of calculation of infiltration rate from a decay test, the Y-axis represents the logarithmic of the concentration; and, the slope in the equation of the line represents the infiltration rate 30
2.13 Apparatus and Procedure of the tracer gas decay method [American Society for Testing and Materials, 2011] 31
2.14 Apparatus for the constant injection method, taken from [American Society for Testing and Materials, 2011] 32
2.15 Diagram of the apparatus of the constant concentration technique [American Society for Testing and Materials, 2011] 33
2.16 Gas analyser, gas controller (multiplexer) with pumps and filters, and a data acquisition computer for tracer gas constant concentration method. 33

2.17 a) Multi-zone assumption, air exchange between zones and indoor-outdoor; b) single-zone assumption, outdoor-indoor air exchange. . . . 38
2.18 From [Lowe, 2000]. Vertical cross-section through a dwelling, showing the direction and magnitude of infiltration and exfiltration across the envelope. AA' is the neutral plane. . . . 49

3.1 Single test Pulse graph . . . 59
3.2 Example of a Pulse step test and fitting of Power law . . . 60
3.3 Overlapping measurements of the PULSE technique (0-10 Pa) and the blower door (10-70 Pa) . . . 63
3.4 Test pods, left: Passivhaus pod (pod 2), right: a standard pod (pod 1) . . . 66
3.5 Pulse unit, with a 20-litre tank . . . 67
3.6 Unsealed condition of the Passivhaus pod when the blower door is in place. . . . 68
3.7 Histogram of frequencies of instrumentation uncertainties in BRE houses . . . 73

4.1 Location of the test house. . . . 79
4.2 South façade of the test house . . . 79
4.3 Floorplans of the test house and location of testing devices, left: ground floor; right: first floor. . . . 80
4.4 Schematic of the differential pressure transducers FCO-44 used in the tests. . . . 82
4.5 Differential pressure transducers FCO-44 used in the tests, with data logger. . . . 82
4.6 Tube in the south façade of the test dwelling. . . . 83
4.7 Tracer gas equipment, gas analyser, 6 channel multiplexer and, data acquisition computer. . . . 83
4.8 Location of indoor temperature sensors PT100. . . . 84
4.9 Blower door tests results. . . . 88
4.10 Air permeability at 4 Pa given by PULSE-60. . . . 89
4.11 Wind speed change during tests. . . . 90
4.12 Air infiltration rates measured from tracer gas methods. . . . 92
4.13 Box and whisker plot from a) Pulse test results and b) Infiltration rates obtained using the tracer gas decay method. . . . 98

4.14 Infiltration rates (h^{-1}) against temperature difference (K), example of a graph when wind speed is low, taken from the results in test 2, from the 19th to the 23rd of January 2018. 99
4.15 Infiltration rates (h^{-1}) against temperature difference (K), taken from the results in test 4, from the 30th of January to the 1st of February 2018. 100
4.16 Infiltration rates (h^{-1}) against temperature difference (K), example of a graph when wind speed is low, taken from the results in test 8, from the 13th to the 14rd of February 2018. 100
4.17 Infiltration rates (h^{-1}) against Wind speed (m/s), example of a graph witch high wind speeds, taken from the results in test 2, from the 19th to the 23rd of January 2018. 101
4.18 Infiltration rates (h^{-1}) against Wind speed (m/s), example of a graph witch high wind speeds, taken from the results in test 4, from the 30th of January to the 1st of February 2018. 101
4.19 Infiltration rates (h^{-1}) against Wind speed (m/s), example of a graph witch high wind speeds, taken from the results in test 8, from the 13th to the 14rd of February 2018. 102
4.20 Impact of wind and temperature [Liddament, 1996] 102
4.21 Transition from stack to wind dominant flow, taken from [Liddament, 1996] 103
4.22 Pressure difference against wind of the test house during 10 minutes when high wind gusts were occurring, on the 26th of February in the a) east, b) north, c) west and, d) south façades. 105
4.23 Pressure distributions in the windward (east and north) and leeward façades (west and south)of the test building for eleven minutes on the 24th of February 106
4.24 Pressure difference repetitions for the 23rd to the 28th of February 2018 in the test house 108

5.1 Dwellings tested. 116
5.2 Latest version of the Pulse unit. 118
5.3 Example of sealed conditions in dwelling 6 with vents and trickle vents sealed. 119
5.4 Blower door unit used in the field investigation study (photo by The Energy Conservatory). 120
5.5 Location of Wind sensor in house number 10. 123
5.6 Concentration decay of dwelling 12. 125

5.7 Natural logarithm of the decay of dwelling 12 versus time wit time of best fit via linear regression. 126
5.8 Measured wind speed during the tracer gas concentration decay test in dwelling 12 126
5.9 Measured indoor and outdoor temperatures (and calculated temperature difference) during the tracer gas concentration decay test in dwelling 12 127
5.10 Calculation of infiltration rate, uncertainty and confidence intervals for dwelling 12. 128
5.11 Fit of temperature fall from an experimental study on tank temperatures using data from multiple tests of three pulse steps. 131
5.12 Warming between pulses versus difference in end temperature of the previous pulse and the ambient using all data from multiple tests of three pulse steps. 132
5.13 Simplified process of the change in temperature of the air inside the tank (not to scale) during a three-step test. 132
5.14 Results from steady pressurisation tests (air leakage rate and flow exponent). 135
5.15 Results from Pulse tests (air leakage rate and flow exponent). . . . 137
5.16 Linear correlation between steady pressurisation tests (airtightness) and air infiltration rate. 140
5.17 Power correlation between steady pressurisation tests (airtightness) and air infiltration rate. 140
5.18 Linear correlation between Pulse tests (airtightness) and air infiltration rate. 141
5.19 Power correlation between Pulse tests (airtightness) and air infiltration rate. 141

6.1 N_{UK} of all testing dwellings with their uncertainties, boxes representing the best case scenario for $\delta E_a = 3\%$ and, lines representing the worst case scenario $\delta E_a = 10\%$. 156
6.2 Comparison of measured and predicted air infiltration in re-tested dwellings 165

7.1 Diagram of the evaluation of the LBL model during the present Chapter. 171
7.2 Relative percentage differences (RPD) in the LBL50 model. 175

7.3 Absolute value of the relative percentage differences (RPD) in the LBL50 model. 176
7.4 Relative percentage differences (RPD) in the LBL4 model. 180
7.5 Absolute value of the relative percentage differences (RPD) in the LBL4 model. 181
7.6 Air leakage rate @50 Pa(n_{50}) distribution from $1x10^5$ samples. . . . 184
7.7 Air leakage rate @4 Pa(n_4) distribution from $1x10^5$ samples. 185
7.8 Predicted air infiltration rates (using LBL50 model) against air leakage rate. 186
7.9 Wind speed distribution from $1x10^5$ samples. 188
7.10 Wind direction distribution from $1x10^5$ samples. 188
7.11 Temperature difference distribution from $1x10^5$ samples. 189
7.12 Dwelling volume distribution from $1x10^5$ samples. 190
7.13 Dwelling envelope area distribution from $1x10^5$ samples. 191
7.14 Cumulative distribution function (CDF) for predicted infiltration rates using the LBL models for assumptions 1 and 3. 194
7.15 Predicted air infiltration rates (using LBL50 model Assumption 1) against wind speed. 196
7.16 Predicted air infiltration rates (using LBL4 model Assumption 1) against wind speed. 196
7.17 Predicted air infiltration rates (using LBL50 model Assumption 3) against wind speed. 197
7.18 Predicted air infiltration rates (using LBL4 model Assumption 3) against wind speed. 197
7.19 Predicted air infiltration rates (using LBL50 model Assumption 1) against temperature difference. 198
7.20 Predicted air infiltration rates (using LBL4 model Assumption 1) against temperature difference. 199
7.21 Predicted air infiltration rates (using LBL50 model Assumption 3) against temperature difference. 199
7.22 Predicted air infiltration rates (using LBL4 model Assumption 3) against temperature difference. 200
7.23 Predicted air infiltration rates (using LBL50 model Assumption 1) against wind speed and temperature difference 201
7.24 Predicted air infiltration rates (using LBL4 model Assumption 1) against wind speed and temperature difference form low infiltration 201

7.25 Predicted air infiltration rates (using LBL50 model Assumption 1) against air leakage rate (n_{50}). 202
7.26 Predicted air infiltration rates (using LBL50 model Assumption 3) against air leakage rate (n_{50}. 203
7.27 Predicted air infiltration rates (using LBL4 model Assumption 1) against air leakage rate (n_4). 203
7.28 Predicted air infiltration rates (using LBL4 model Assumption 3) against air leakage rate (n_4). 204
7.29 Predicted air infiltration rates (using LBL50 model Assumption 1) against flow exponent. 205
7.30 Predicted air infiltration rates (using LBL4 model Assumption 1) against flow exponent. 205
7.31 Predicted air infiltration rates (using LBL50 model Assumption 3) against flow exponent. 206
7.32 Predicted air infiltration rates (using LBL4 model Assumption 3) against flow exponent. 206
7.33 Predicted air infiltration rates (using LBL50 model Assumption 1) against house volume. 207
7.34 Predicted air infiltration rates (using LBL50 model Assumption 1) against house envelope area. 207
7.35 Predicted air infiltration rates (using LBL50 model Assumption 1) against shielding condition. 208
7.36 Predicted air infiltration rates (using LBL50 model Assumption 3) against house volume. 208
7.37 Predicted air infiltration rates (using LBL50 model Assumption 3) against house envelope area. 209
7.38 Predicted air infiltration rates (using LBL4 model Assumption 1) against house volume. 210
7.39 Predicted air infiltration rates (using LBL4 model Assumption 1) against house envelope area. 210
7.40 Predicted air infiltration rates (using LBL4 model Assumption 1) against shielding condition. 211
7.41 Predicted air infiltration rates (using LBL4 model Assumption 3) against house volume. 211
7.42 Predicted air infiltration rates (using LBL4 model Assumption 3) against house envelope area. 212

7.43 Predicted and regression values of infiltration rate for LBL50 Assumption 1 sensitivity analysis, $R^2 = 0.996$. 213
7.44 Predicted and regression values of infiltration rate for LBL4 Assumption 1 sensitivity analysis, $R^2 = 0.997$. 214
7.45 Predicted and regression values of infiltration rate for LBL50 Assumption 3 sensitivity analysis, $R^2 = 0.923$. 216
7.46 Predicted and regression values of infiltration rate for LBL4 Assumption 3 sensitivity analysis, $R^2 = 0.998$. 216
7.47 Predicted air infiltration rates (using LBL50 model Assumption 1) against wind speed with Volume and Envelope Area as true constants. 219
7.48 Predicted air infiltration rates (using LBL4 model Assumption 1) against wind speed with Volume and Envelope Area as true constants. 219
7.49 Predicted air infiltration rates (using LBL50 model Assumption 3) against wind speed with Volume and Envelope Area as true constants. 220
7.50 Predicted air infiltration rates (using LBL4 model Assumption 3) against wind speed with Volume and Envelope Area as true constants. 220
7.51 Predicted air infiltration rates (using LBL50 model Assumption 1) against temperature difference with Volume and Envelope Area as true constants. 221
7.52 Predicted air infiltration rates (using LBL4 model Assumption 1) against temperature difference with Volume and Envelope Area as true constants. 221
7.53 Predicted air infiltration rates (using LBL50 model Assumption 3) against temperature difference with Volume and Envelope Area as true constants. 222
7.54 Predicted air infiltration rates (using LBL4 model Assumption 3) against temperature difference with Volume and Envelope Area as true constants. 222
7.55 Predicted air infiltration rates (using LBL50 model Assumption 1) against air leakage rate with Volume and Envelope Area as true constants. 223
7.56 Predicted air infiltration rates (using LBL50 model Assumption 3) against air leakage rate with Volume and Envelope Area as true constants. 223
7.57 Predicted air infiltration rates (using LBL4 model Assumption 1) against air leakage rate with Volume and Envelope Area as true constants. 224

7.58 Predicted air infiltration rates (using LBL4 model Assumption 3) against air leakage rate with Volume and Envelope Area as true constants. . . . 224
7.59 Predicted air infiltration rates (using LBL50 model Assumption 1) against flow exponent with Volume and Envelope Area as true constants. . . . 225
7.60 Predicted air infiltration rates (using LBL4 model Assumption 1) against flow exponent with Volume and Envelope Area as true constants. . . . 225
7.61 Predicted air infiltration rates (using LBL50 model Assumption 3) against flow exponent with Volume and Envelope Area as true constants. . . . 226
7.62 Predicted air infiltration rates (using LBL4 model Assumption 3) against flow exponent with Volume and Envelope Area as true constants. . . . 226
7.63 Predicted and regression values of infiltration rate for LBL50 Assumption 1 sensitivity analysis with Volume and Envelope Area as true constants, $R^2 = 0985$. . . . 228
7.64 Predicted and regression values of infiltration rate for LBL4 Assumption 1 sensitivity analysis with Volume and Envelope Area as true constants, $R^2 = 0984$. . . . 228
7.65 Predicted and regression values of infiltration rate for LBL50 Assumption 3 sensitivity analysis with Volume and Envelope Area as true constants, $R^2 = 0982$. . . . 230
7.66 Predicted and regression values of infiltration rate for LBL4 Assumption 3 sensitivity analysis with Volume and Envelope Area as true constants, $R^2 = 0989$. . . . 230

8.1 Diagram of the evaluation of the DOMVENT3D model during the present Chapter. . . . 238
8.2 Distribution of infiltration predictions (n_1, h^{-1}) in the DOMVENT3D-50 model. . . . 244
8.3 Cumulative Distribution Function (CDF) for the predictions of the DOMVENT3D models 244
8.4 Predicted air infiltration rates (using DOMVENT3D-50 model) against wind speed. . . . 245
8.5 Predicted air infiltration rates (using DOMVENT3D-4 model) against wind speed. . . . 245

8.6 Predicted air infiltration rates (using DOMVENT3D-50 model) against temperature difference. 246
8.7 Predicted air infiltration rates (using DOMVENT3D-4 model) against temperature difference. 247
8.8 Predicted air infiltration rates (using DOMVENT3D-50 model) against air leakage rate. 248
8.9 Predicted air infiltration rates (using DOMVENT3D- model) against air leakage rate. 248
8.10 Predicted air infiltration rates (using DOMVENT3D-50 model) against flow exponent. 249
8.11 Predicted air infiltration rates (using DOMVENT3D-4 model) against flow exponent. 249
8.12 Predicted air infiltration rates (using DOMVENT3D-50 model) against dwelling volume. 250
8.13 Predicted air infiltration rates (using DOMVENT3D-4 model) against dwelling volume. 250
8.14 Predicted air infiltration rates (using DOMVENT3D-50 model) against dwelling envelope area. 251
8.15 Predicted air infiltration rates (using DOMVENT3D-4 model) against dwelling envelope area. 251
8.16 Predicted air infiltration rates (using DOMVENT3D-50 model) against shielding type. 252
8.17 Predicted air infiltration rates (using DOMVENT3D-4 model) against shielding type. 252
8.18 Predicted air infiltration rates (using DOMVENT3D-50 model) against dwelling type. 253
8.19 Predicted air infiltration rates (using DOMVENT3D-4 model) against dwelling type. 253
8.20 Predicted and regression values of infiltration rate for DOMVENT3D-50 sensitivity analysis, $R^2 = 0.5646$. 255
8.21 Predicted and regression values of infiltration rate for DOMVENT3D-4 sensitivity analysis, $R^2 = 0.6580$. 255
8.22 Predicted and regression values of infiltration rate for DOMVENT3D-50 sensitivity analysis with Volume and Envelope Area as true constants, $R^2 = 0.5466$. 259

8.23 Predicted and regression values of infiltration rate for DOMVENT3D-4 sensitivity analysis with Volume and Envelope Area as true constants, $R^2 = 0.6413$. 259

B.1 Comparison between occurring temperature difference and measured infiltration rate in test 1 295
B.2 Comparison between occurring temperature difference and measured infiltration rate in test 2 295
B.3 Comparison between occurring temperature difference and measured infiltration rate in test 3 296
B.4 Comparison between occurring temperature difference and measured infiltration rate in test 4 296
B.5 Comparison between occurring temperature difference and measured infiltration rate in test 6 297
B.6 Comparison between occurring temperature difference and measured infiltration rate in test 7 297
B.7 Comparison between occurring temperature difference and measured infiltration rate in test 8.1 298
B.8 Comparison between occurring temperature difference and measured infiltration rate in test 8.2 298
B.9 Comparison between occurring temperature difference and measured infiltration rate in test 9.1 299
B.10 Comparison between occurring temperature difference and measured infiltration rate in test 9.2 299
B.11 Comparison between occurring temperature difference and measured infiltration rate in test 9.3 300
B.12 Comparison between occurring temperature difference and measured infiltration rate in test 10.1 300
B.13 Comparison between occurring temperature difference and measured infiltration rate in test 10.2 301
B.14 Comparison between occurring temperature difference and measured infiltration rate in test 10.3 301
B.15 Comparison between occurring temperature difference and measured infiltration rate in test 11 301
B.16 Comparison between occurring wind velocities and measured infiltration rate in test 1 302
B.17 Comparison between occurring wind velocities and measured infiltration rate in test 2 302

B.18 Comparison between occurring wind velocities and measured infiltration rate in test 3 . . . 303
B.19 Comparison between occurring wind velocities and measured infiltration rate in test 4 . . . 303
B.20 Comparison between occurring wind velocities and measured infiltration rate in test 6 . . . 304
B.21 Comparison between occurring wind velocities and measured infiltration rate in test 7 . . . 304
B.22 Comparison between occurring wind velocities and measured infiltration rate in test 8.1 . . . 305
B.23 Comparison between occurring wind velocities and measured infiltration rate in test 8.2 . . . 305
B.24 Comparison between occurring wind velocities and measured infiltration rate in test 9.1 . . . 306
B.25 Comparison between occurring wind velocities and measured infiltration rate in test 9.2 . . . 306
B.26 Comparison between occurring wind velocities and measured infiltration rate in test 9.3 . . . 307
B.27 Comparison between occurring wind velocities and measured infiltration rate in test 10.1 . . . 307
B.28 Comparison between occurring wind velocities and measured infiltration rate in test 10.2 . . . 308
B.29 Comparison between occurring wind velocities and measured infiltration rate in test 10.3 . . . 308
B.30 Comparison between occurring wind velocities and measured infiltration rate in test 11 . . . 308
B.31 Tracer gas concentration decay calculation for test 2 . . . 309
B.32 Tracer gas concentration decay calculation for test 3.1 . . . 309
B.33 Tracer gas concentration decay calculation for test 3.2 . . . 310
B.34 Tracer gas concentration decay calculation for test 4.1 . . . 310
B.35 Tracer gas concentration decay calculation for test 4.2 . . . 311
B.36 Tracer gas concentration decay calculation for test 5.1 . . . 311
B.37 Tracer gas concentration decay calculation for test 5.2 . . . 311
B.38 Tracer gas concentration decay calculation for test 5.3 . . . 312
B.39 Tracer gas concentration decay calculation for test 6 . . . 312
B.40 Tracer gas concentration decay calculation for test 7 . . . 312
B.41 Tracer gas concentration decay calculation for test 8 . . . 313

B.42 Tracer gas concentration decay calculation for test 9.1 313
B.43 Tracer gas concentration decay calculation for test 9.2 313
B.44 Tracer gas concentration decay calculation for test 9.3 314
B.45 Tracer gas concentration decay calculation for test 10.1 314
B.46 Tracer gas concentration decay calculation for test 10.2 314
B.47 Tracer gas concentration decay calculation for test 10.3 315
B.48 Tracer gas concentration decay calculation for test 11 315
B.49 Tracer gas concentration decay calculation for test 12 315

C.1 Wind speed against measured pressure in all the façades of the case study house 317
C.2 Wind speed against measured pressure in all the façades of the case study house in the 24th of February 2018 318
C.3 Wind speed against measured pressure in all the façades of the case study house in the 25th of February 2018 319
C.4 Wind speed against measured pressure in all the façades of the case study house in the 26th of February 2018 320

D.1 Distribution of measured pressures in different facades of the case study house in the 24th of February 2018 322
D.2 Distribution of measured pressures in different facades of the case study house in the 25th of February 2018 323
D.3 Distribution of measured pressures in different facades of the case study house in the 26th of February 2018 324

E.1 Tracer gas decay test graph for dwelling 1 with best fit for uncertainty and confidence at 99%. 326
E.2 Tracer gas decay test graph for dwelling 2 with best fit for uncertainty and confidence at 99%. 326
E.3 Tracer gas decay test graph for dwelling 3 with best fit for uncertainty and confidence at 99%. 327
E.4 Tracer gas decay test graph for dwelling 4 with best fit for uncertainty and confidence at 99%. 327
E.5 Tracer gas decay test graph for dwelling 5 with best fit for uncertainty and confidence at 99%. 328
E.6 Tracer gas decay test graph for dwelling 6 with best fit for uncertainty and confidence at 99%. 328
E.7 Tracer gas decay test graph for dwelling 7 with best fit for uncertainty and confidence at 99%. 329

E.8 Tracer gas decay test graph for dwelling 8 with best fit for uncertainty and confidence at 99%. 329
E.9 Tracer gas decay test graph for dwelling 9 with best fit for uncertainty and confidence at 99%. 330
E.10 Tracer gas decay test graph for dwelling 10 with best fit for uncertainty and confidence at 99%. 330
E.11 Tracer gas decay test graph for dwelling 11 with best fit for uncertainty and confidence at 99%. 331
E.12 Tracer gas decay test graph for dwelling 12 with best fit for uncertainty and confidence at 99%. 331
E.13 Tracer gas decay test graph for dwelling 13 with best fit for uncertainty and confidence at 99%. 332
E.14 Tracer gas decay test graph for dwelling 14 with best fit for uncertainty and confidence at 99%. 332
E.15 Tracer gas decay test graph for dwelling 15 with best fit for uncertainty and confidence at 99%. 333
E.16 Tracer gas decay test graph for dwelling 16 with best fit for uncertainty and confidence at 99%. 333
E.17 Tracer gas decay test graph for dwelling 17 with best fit for uncertainty and confidence at 99%. 334
E.18 Tracer gas decay test graph for dwelling 18 with best fit for uncertainty and confidence at 99%. 334
E.19 Tracer gas decay test graph for dwelling 19 with best fit for uncertainty and confidence at 99%. 335
E.20 Tracer gas decay test graph for dwelling 20 with best fit for uncertainty and confidence at 99%. 335
E.21 Temperature difference, indoor and outdoor temperatures in dwelling 2. 336
E.22 Temperature difference, indoor and outdoor temperatures in dwelling 3. 337
E.23 Temperature difference, indoor and outdoor temperatures in dwelling 4. 337
E.24 Temperature difference, indoor and outdoor temperatures in dwelling 5. 338
E.25 Temperature difference, indoor and outdoor temperatures in dwelling 6. 338

E.26 Temperature difference, indoor and outdoor temperatures in dwelling 7. 339
E.27 Temperature difference, indoor and outdoor temperatures in dwelling 8. 339
E.28 Temperature difference, indoor and outdoor temperatures in dwelling 9. 340
E.29 Temperature difference, indoor and outdoor temperatures in dwelling 10. 340
E.30 Temperature difference, indoor and outdoor temperatures in dwelling 11. 341
E.31 Temperature difference, indoor and outdoor temperatures in dwelling 12. 341
E.32 Temperature difference, indoor and outdoor temperatures in dwelling 13. 342
E.33 Temperature difference, indoor and outdoor temperatures in dwelling 14. 342
E.34 Temperature difference, indoor and outdoor temperatures in dwelling 15. 343
E.35 Temperature difference, indoor and outdoor temperatures in dwelling 16. 343
E.36 Temperature difference, indoor and outdoor temperatures in dwelling 17. 344
E.37 Temperature difference, indoor and outdoor temperatures in dwelling 18. 344
E.38 Temperature difference, indoor and outdoor temperatures in dwelling 19. 345
E.39 Measurements of wind speed in dwelling 2. 345
E.40 Measurements of wind speed in dwelling 3. 346
E.41 Measurements of wind speed in dwelling 4. 346
E.42 Measurements of wind speed in dwelling 5. 347
E.43 Measurements of wind speed in dwelling 6. 347
E.44 Measurements of wind speed in dwelling 7. 348
E.45 Measurements of wind speed in dwelling 8. 348
E.46 Measurements of wind speed in dwelling 9. 349
E.47 Measurements of wind speed in dwelling 10. 349
E.48 Measurements of wind speed in dwelling 11. 350
E.49 Measurements of wind speed in dwelling 12. 350

E.50 Measurements of wind speed in dwelling 13. 351
E.51 Measurements of wind speed in dwelling 14. 351
E.52 Measurements of wind speed in dwelling 15. 352
E.53 Measurements of wind speed in dwelling 16. 352
E.54 Measurements of wind speed in dwelling 17. 353
E.55 Measurements of wind speed in dwelling 18. 353
E.56 Measurements of wind speed in dwelling 19. 354
E.57 Measurements of wind speed in dwelling 20. 354

List of Tables

2.1 Examples of domestic airtightness requirements in different countries [RDH Building Engineering Ltd., 2013] 13
2.2 Comparisons of three tracer gas techniques [Sandberg and Blomqvist, 1985, Laussmann and Helm, 2011, Sherman, 1989, 1998] 28
2.3 Minimum durations between the initial and final samples for the concentration decay method [American Society for Testing and Materials, 2011] 28
2.4 Brief description of some infiltration predicting models 39
2.5 Estimates for shelter coefficients (S_{wo}) for no flue in the AIM-2 model (from Walker and Wilson [1990]) 45

3.1 Pulse measurements taken the 15th and 16th of February in the test house quoted @4 Pa of pressure difference 62
3.2 Reported airtightness values with their uncertainty quoted @4 Pa of pressure difference 62
3.3 Deviations from average (%) of measurements taken the 15th and 16th of February in the test house 62
3.4 Airtightness measurements quoted @4 Pa of pressure difference in new-built dwellings in Nottingham, UK. 64
3.5 Reported airtightness values quoted @4 Pa of pressure difference with their uncertainty in new-built dwellings in Nottingham, UK. . 65
3.6 Deviations from average (%) of airtightness measurements in new-built dwellings in Nottingham, UK. 65
3.7 Envelope area and volume of the test pods 67
3.8 Airtightness of the test pods, and relative percentage difference (RPD) between sealed and unsealed scenarios 68
3.9 Equipment uncertainty given by manufacturer 69
3.10 Number of tests in BRE properties 72
3.11 Number of tests in BRE properties 72

3.12 Calculation of Pulse uncertainty: Statistical information from BRE houses 73

4.1 Equipment utilised in the experimental study in the test house. . . 81
4.2 Distribution of tracer gas tests and heating conditions. 85
4.3 Permeability ($m^3h^{-1}m^{-2}$) measured by both methods and relative percentage difference (RPD) against the average. 87
4.4 Mean, minimum and maximum airtightness measurements during the testing period, ... 88
4.5 Air infiltration (h^{-1}) measurements using the constant concentration and concentration decay methods. 91
4.6 Reproducibility of infiltration rate measurements, using the a) constant concentration and b) decay method. 94
4.7 Uncertainty from tracer gas constant concentration tests 95
4.8 Uncertainty from tracer gas concentration decay tests 96
4.9 Summary and comparisons of air infiltration measurements using the tracer gas decay method and the Pulse method. 97
4.10 Statistical figures from measured pressure differences when wind gusts were captured by the anemometer 107
4.11 Most repeated ranges of pressures when wind gusts were captured. . 107
4.12 Heat loss calculation as per SAP from blower door tests. 109
4.13 Calculation of heat losses as per SAP from different tracer gas constant concentration tests. 110

5.1 Description of test houses. 115
5.2 Survey information of test houses. 117
5.3 Orientation of the main door of dwellings and blower door. 121
5.4 Environmental conditions measuring equipment. 122
5.5 Air infiltration concentration decay method equipment. 124
5.6 Examples of minimum durations between the initial and final samples for the concentration decay method. From ASTM E741-11 [American Society for Testing and Materials, 2011]. 124
5.7 Summary of the environmental conditions present during tracer gas concentration decay tests. 127
5.8 Measured ambient and tank temperatures at the beginning of the test. 130
5.9 Steady pressurisation method measurements results. 134
5.10 Pulse results. 136

5.11 Tracer gas concentration decay method results. 138
5.12 Errors from the leave-one-out cross-validation approach. 143
5.13 Results from re-test of properties 4 and 5. 143
5.14 Air infiltration rate (h^{-1}) predictions based on steady pressurisation and pulse airtightness measurements, and, error using the empirical models in the re-tested properties. 144

6.1 Air permeability (@50 Pa) - infiltration ratios. 151
6.2 q_{50}/n_1 statistical figures. 152
6.3 Air change rate(@50 Pa) - infiltration ratios. 153
6.4 n_{50}/n_1 statistical figures. 153
6.5 Sources or error in obtaining N_{UK}. 154
6.6 Air change rates(h^{-1}) calculated using SAP, values of N from values calculated, and their error compared to measured values. 159
6.7 Air change rates(h^{-1}) calculated using SAP and measured wind speeds, values of N from values calculated, and their error compared to measured values. 161
6.8 Airtightness measurements (@4Pa) and estimated infiltration ratios using air permeability and air change rate as metrics. 163
6.9 q_4/n_1 and n_4/n_1 statistical figures. 164

7.1 Average environmental conditions measured for every dwelling to be used as inputs for the LBL model. 169
7.2 Air infiltration rate predictions using the LBL50 model. The letter A stands for the assumption used. 173
7.3 Standard error and percentage difference between measurements for all the assumptions in the LBL50 model 174
7.4 Statistical figures for the overall relative percentage difference between measurements for all the assumptions in the LBL50 model when taking the absolute value of each RPD 176
7.5 Air infiltration rate predictions using the LBL4 model. 178
7.6 Standard error and percentage difference between measurements for all the assumptions in the LBL4 model 179
7.7 Standard error and percentage difference between measurements for all the assumptions in the LBL4 model 181
7.8 Mean and standard deviation from all the measurements (Chapter 5) of airtightness using the blower door and Pulse methods. 185

7.9 Mean and standard deviation from all the measurements of environmental conditions. 187
7.10 Mean and standard deviation from all the measurements of Volume and Envelope Area. 190
7.11 Probability of shielding and dwelling factor. 191
7.12 Sum of squares (SS) and coefficient of multiple determination (R^2) for sensitivity analysis of LBL50 and LBL4 infiltration models (assumption 1) for $1x10^5$ samples. 213
7.13 Model coefficients (b_n), Standardised Regression Coefficients (SRC) and, Correlation Coefficients (CC) for the model created in the Sensitivity analysis for LBL50 and LBL 4 assumption 1. 215
7.14 Sum of squares (SS) and coefficient of multiple determination (R^2) for sensitivity analysis of LBL50 and LBL4 infiltration models (assumption 3) for $1x10^5$ samples. 215
7.15 Model coefficients (b_n), Standardised Regression Coefficients (SRC) and, Correlation Coefficients (CC) for the model created in the Sensitivity analysis for LBL50 and LBL 4 assumption 3. 217
7.16 Sum of squares (SS) and coefficient of multiple determination (R^2) for sensitivity analysis of LBL50 and LBL4 infiltration models (assumption 1) for $1x10^5$ samples when the Volume and Envelope area are considered as constants. 227
7.17 Model coefficients (b_n), Standardised Regression Coefficients (SRC) and, Correlation Coefficients (CC) for the model created in the Sensitivity analysis for LBL50 and LBL4 models assumption 1 when Volume and Envelope are taken as constants. 229
7.18 Sum of squares (SS) and coefficient of multiple determination (R^2) for sensitivity analysis of LBL50 and LBL4 infiltration models (assumption 3) for $1x10^5$ samples when the Volume and Envelope area are considered as constants. 229
7.19 Model coefficients (b_n), Standardised Regression Coefficients (SRC) and, Correlation Coefficients (CC) for the model created in the Sensitivity analysis for LBL50 and LBL4 models assumption 3 when Volume and Envelope are taken as constants. 231

8.1 Air infiltration rate (h^{-1}) predictions from the DOMVENT3D model, from high and low pressure difference airtightness measurements. . . 240
8.2 Standard error and relative percentage difference between assumptions for the DOMVENT3D models 241

8.3 Sum of squares and (SS) and coefficient of multiple determination (R^2) for sensitivity analysis of DOMVENT3D-50 and DOMVENT3D-4 infiltration models for $1x10^5$ samples. 254
8.4 Model coefficients (b_n), Standardised Regression Coefficients (SRC) and, Correlation Coefficients (CC) for the models created in the Sensitivity Analysis for DOMVENT3D. 256
8.5 Sum of squares and (SS) and coefficient of multiple determination (R^2) for sensitivity analysis of DOMVENT3D-50 and DOMVENT3D-4 infiltration models for $1x10^6$ samples when the Volume and Envelope area are considered as constants. 258
8.6 Model coefficients (b_n), Standardised Regression Coefficients (SRC) and, Correlation Coefficients (CC) for the models created in the Sensitivity Analysis for DOMVENT3D with Volume and Envelope Area as true constants. 260

9.1 Comparisons of average and standard error reported values between three different infiltration models, using high and low-pressure air-tightness inputs 271

List of Symbols

a	Flow coefficient for fully developed laminar friction losses	
A	Leakage area	m^2
A_c	Leakage area of celing	m^2
A_f	Leakage area of floor level leaks	m^2
A_{flue}	Leakage area of the flue	m^2
A_o	Total leakage area	m^2
$B1$	Interaction coefficient	
B	Coefficient for entry, exit and turbulent flow losses	
b	Flow exponent	
b_{50}	Flow exponent referenced at 50 Pa	
b_4	Flow exponent referenced at 4 Pa	
C	Flow coeffcient	$m^3h^{-1}Pa^{-b}$
c	Shielding coefficient	
d	Thickness	m
E_a	Envelope Area	m^2
ELA	Effective leakage area	m^2
E	Relative leakage area	-
E_N	Predicted standard error for regression	
F	Flow function	$kgm^{-2}s{-}1$
f_w	Wind factor	
f_s	Stack factor	
G	Tracer gas emission rate	ppm/s
g	Acceleration of gravity	$ms{-}2$
H	Building eaves height	m
H_s	Stack height	m
h_0	Height of neutral plane	m
I	Heat transfer coefficient	WK^{-1}

K	Concentration	ppm
L	Length	m
$\dot{m}$	Mass flow rate	kgs^{-1}
N	Ratio constant	
n_{50}	Air change rate referenced at 50 Pa	h^{-1}
n_4	Air change rate referenced at 4 Pa	h^{-1}
n_1	Air infiltration rate	m^3s^{-1}, h^{-1}
P	Pressure	Pa
P_{met}	Wind speed exponent at metheorological station	
P_{site}	Wind speed exponent at building site	
Q	Flow rate	m^3s^{-1}
q_{50}	Air permeability referenced at 50 Pa	$m^3h{-}1m^{-2}$
q_4	Air permeability referenced at 4 Pa	$m^3h{-}1m^{-2}$
Q_s	Stack induced infiltration	m^3s^{-1}
Q_w	Wind induced infiltration	m^3s^{-1}
Q_{mv}	Contribution of mechanical ventilation to infiltration	m^3s^{-1}
q	Air flow rate	m^3s^{-1}
R	Gas constant	$JKg^{-1}K^{-1}$
R^2	Coefficient of determination	
S	Shelter coefficient	
SE	Standard Error	
T	Temperature	$K, ^\circ C$
T_i	Indoor temperature	$K, ^\circ C$
T_o	Outdoor temperature	$K, ^\circ C$
V	Volume	m^3
U_e	Building height (at site) wind speed	ms^{-1}
U_{met}	Weather station wind speed	ms^{-1}
W	Width	m
z	Distance	m
z_m	Height at which the meteorological station measures wind speed	m
α	Terrain coefficient	
Δh_0	Differential of mean heights of each façade neutral plane	m
ΔP	Pressure difference	Pa

ΔT	Temperature difference	K
μ	Dynamic viscosity	$Pa - s$
ρ	Density	kgm^{-3}
σ	Standard deviation	
τ	Terrain coefficient	

Chapter 1

Introduction

1.1 Introduction

The most crucial challenge for this generation is to reduce carbon emissions and to tackle climate change. As first stated in 1987 by the United Nations' World Commission on Environment and Development; and then acknowledged in the "Paris Agreement" [United Nations, 2015], climate change is a concern for all humankind. A global goal must not only be to tackle climate change, but also to sustain our resources while preserving a healthy environment and people [United Nations, 2015]. Governments, scientists, and communities are the stakeholders when delivering solutions to change the habits acquired during the industrial revolution. Two ways of cutting carbon emissions are first, to change the method of energy generation: using more efficient fuels, or using renewable sources to generate electricity and second, to reduce overall energy demand i.e. to be less energy-intensive. There is not a single industry that is not forced to do this. In Paris, in 2015 during the UN Framework on Climate Change conference of the parts (COP21), most of the governments in the world agreed on the magnitude of the problem and, committed to addressing it [United Nations, 2015].

The building sector is been responsible for around 30% of the carbon emissions [Clark, 2013]. The reduction of energy-intensity in buildings decreased from 2% in 2015 to 0.6% in 2018 [International Energy Agency, 2019a]. Carbon emissions come from the construction materials, but mainly from building operation. Also, the majority of the energy used in a building comes from non-renewable sources. The consumption rate is higher than the availability of de-carbonised energy. As a result, in 2018, the International Energy Agency (IEA) reported a record in CO_2 emissions [International Energy Agency, 2019a]; buildings use primary energy from the grid, and predominately are not able to generate their energy; therefore energy

efficiency of the building fabric plays an essential role in the building sector. It has become imperative to improve the energy efficiency of buildings in order to reduce the overall energy demand. Agreements and initiatives suggest that the path to take is to de-carbonise the building sector by the year 2050 [International Energy Agency, 2019a]. It is essential to mention that at the current time the building sector is not accomplishing the goals set for a low-carbon transition [International Energy Agency, 2019b]

A building needs to provide shelter for people, a healthy indoor environment, good air quality, and also comfort; all of these are related to the ventilation of a building [Allard, 1998]. A building can have natural ventilation strategies, where no mechanical system is involved; this solution does not require electricity to provide ventilation [Etheridge, 2012]. However, it is not always possible to implement it, and when it does, it might create different problems such as over-heating or more energy losses due to an increase in opening areas [Etheridge, 2012]. On the other hand, a mechanical ventilation system is a way to ensure correct airflow, however, with an energy cost.

In most situations, a building requires heating or an air conditioning system to provide comfort to the occupants and; these systems tend to be responsible for the greatest energy demands of the building. 59% of heating technologies depend on fossil fuels, and energy usage due to cooling continues to increase in buildings [International Energy Agency, 2019a].

These ventilation, heating and air conditioning systems depend on a good design to be efficient. In turn, the design is dependent on the building fabric. Correct design of the location of windows, doors, flues, and chimneys is important, as the designer can locate these to improve the efficiency of the ventilation systems. In other words, these are the purposely provided ventilation devices [Liddament, 1986]. Alternatively, there is a part of the ventilation which the designer cannot control. This uncontrolled or unintended ventilation of air coming into a building is known as infiltration (or exfiltration where air leaves the building) and amounts to the exchange of indoor and external air through the gaps and the cracks within the building fabric, driven by pressure differentials across the building envelope (i.e. external layer of the building). Air infiltration can be attributable to up to one-third of the heating load of a building [American Society of Heating, Refrigerating and Air Conditioning Engineers, 2017, Santamouris and Asimakopoulos, 1996].

Infiltration is dependent on how “well” or “sealed” a building is constructed [Etheridge, 2015]. A building envelope with the fewer “paths” for air to flow through will therefore have a lower infiltration potential. These “paths”, when

accounted for all, define the "airtightness" of a building. Air infiltration and airtightness are directly proportional, and the first mainly (but not only) depends on the latter. Air infiltration plays a critical role when meeting ventilation needs [Liddament, 1986].

There are two main differences between infiltration and airtightness. First, infiltration is airflow, changing in the short term and varying due to external factors acting upon a building. Second, this change is dependent on the wind, temperature difference and location of the building; these forces impose an indoor-outdoor pressure difference [Liddament, 1986]. I.e. Air infiltration is concerned with the movement of air in the buildings natural state in response to the vagaries of its environment. However, airtightness which is measured at artificially imposed and elevated pressure differentials is a function of the fabric construction of the building. If a building's airtightness level changes this must be due to the creation of new leakage paths. Airtightness can and does change with ageing of materials but more often that not is due to human involvement for this to happen. Infiltration is important not only in the energy efficiency of buildings but also for the building's indoor air quality and comfort [Liddament, 1986, Sherman and Dickinson, 1985]; hence why the International Energy Agency (IEA), created the Air Infiltration and Ventilation Centre (AIVC).

In summary, strategies to improve the energy efficiency of a building requires the reduction in air infiltration by means of sealing or preventing leakage paths [Sherman and Dickinson, 1985, Etheridge, 2015]. Measuring air infiltration is not common in the industry, whereas in many countries, airtightness testing is [International Organization for Standardization, 2015].

Currently, air infiltration is predicted from airtightness measurements or assumed. Moreover, this is only for those countries that already have legislation in place for air infiltration or airtightness. Nevertheless, most of the developing world has not implemented legislation on that matter. Chapter 2 presents more information in regards to legislation.

As mentioned, climate conditions affect the infiltration of a building [Sherman and Grimsrud, 1980]. Changes in pressure (induced by environmental conditions) drive infiltration [Moss, 2007, Liddament, 1986], creating an indoor-outdoor pressure differential. While airtightness is commonly measured at a 50 Pa pressure difference (which is artificially created) [International Organization for Standardization, 2015], infiltration occurs most of the time in a lower pressure difference [Cooper and Etheridge, 2007a].

Infiltration is then predicted based on those airtightness measurements at high-

pressure difference [Liddament, 1986, Jones et al., 2015]. Currently, there has been no established method for predicting infiltration from airtightness measurements taken at low-pressure differences, *circa* 4 Pa. That is because the standard steady state method of measuring airtightness shows several uncertainties when measuring at such low pressure [Remi Carrie and Leprince, 2016] and also; because there was no alternative to the standard testing method. However, more recently a novel technology that measures airtightness at low-pressure difference exists, and this potentially provides an opportunity to predict infiltration rates with greater accuracy and lower uncertainty.

A gap in knowledge has been found. Can predicting infiltration from low-pressure airtightness tests be more accurate than current methods? More accurate predictions can lead to more efficient ventilation systems, better air quality, closer control of thermal comfort for the user and importantly less energy consumption in heating or cooling buildings. For these reasons, this research project aims to answer the question: "What is the correlation between airtightness values measured at 4 Pa, the associated climate conditions and the air infiltration in buildings?". Considering that infiltration energy losses represent a proportion of the ventilation energy losses, answering these two questions presented would aid the decision-making process when not only designing but legislating for a more efficient built environment.

1.1.1 Introduction to airtightness and air infiltration modelling research

Air infiltration in a building is the non-intended part of the ventilation. Santamouris and Asimakopoulos [1996] defines it as the flow of air through leakage pathways in the building envelope; the ventilation that occurs in the adventitious openings or cracks in the building also defines air infiltration [Etheridge, 2015]; an "airtight" building is the one that minimises air infiltration [Santamouris and Asimakopoulos, 1996].

Airtightness is the air movement through leakage paths or cracks; however, it describes how well a building is "sealed". The airtightness determines the level of air infiltration occurring in the building. The difference between airtightness and air infiltration is that infiltration varies with different factors, weather conditions (wind and temperature difference), shielding conditions and building geometry. [Santamouris and Asimakopoulos, 1996, Sherman and Grimsrud, 1980]; airtightness is a building property that fundamentally determines air infiltration.

Weather-driven forces, namely wind or stack effect lead to a pressure differential across the building envelope, which in consequence, drives air to flow across the building envelope via cracks and gaps [Turner et al., 2012].

Buildings in the European Union account for around 40% of overall energy consumption [Lapillonne et al., 2015]. The heat losses caused by air infiltration accounts for up to one-third of the heating load of a building, this remarks the importance of determining the air infiltration and airtightness properties of a building [Etheridge, 2015, Liddament and Allen, 1983, Sherman, 1983, Sherman and Dickinson, 1985, Energy Saving Trust, 2006]. Infiltration is always present (a building with no adventitious openings does not exist), and it must be considered at the design stage [Etheridge, 2015] to assess the building energy load and sizing HVAC systems.

Measuring airtightness is the starting point to understand building infiltration. Airtightness is quantified in a variety of ways. "Air permeability" is defined as the rate of leakage per area across the envelope ($m^3h^{-1}m^2$); alternatively when measured as part of the ventilation and flow (m^3/s), it is not normalised by volume and envelope area and, is named air leakage rate or air change rate(h^{-1}). The steady pressurisation method, commonly known as "blower door", is the method to obtain all metrics presented. The blower door pressurizes (or depressurises) the building to a range of pressures (typically between 10 and 60 Pa) and quotes air leakage at 50 Pa of pressure difference. Various countries adopt airtightness metrics in their regulations and testing standards. Taking the United Kingdom as an example, building regulations require to measure the air permeability and quote it at 50 Pa.

If a building has high air permeability, it will lose much heat during the heating season (or gain heat if cooling is required). As a result, it will need more energy to condition the indoor environment [American Society of Testing and Materials, 1991]. Nonetheless, different countries have different regulations, and therefore, a "high" permeability is defined differently in different locations. The Air Tightness Testing and Measurements Association [2016] mentions that a permeability lower than $5m^3h^{-1}m^2$ will lead to a poor indoor air quality (IAQ), and in consequence to health problems. For these cases, the standard advises using mechanical ventilation; on the other hand, a permeability level higher than $10m^3h^{-1}m^2$ will result in higher energy usage due to air infiltration. Some authors have studied how infiltration enhances the growth of mould [Chen et al., 2016]. Thus air infiltration and airtightness are not only part of the energy efficiency of the building, but also a potential health and safety issue which also affects the occupant's thermal

comfort.

In the United Kingdom, the Standard Assessment Procedure (SAP) is the calculation process to determine the energy demand of a dwelling, which includes losses due to infiltration. The calculation for infiltration within SAP consists of dividing the permeability level of a dwelling by 20 and modifying the value with weather and shielding factors [Building Research Establishment, 2013]. The Air Conditioning Contractors of America (ACCA), developed their manual to calculate the energy load of a house. The ACCA Manual J standard in section 12 relates the envelope leakage level, location and building parameters to the infiltration energy losses to obtain an overall heating or cooling load. The envelope leakage level can be defined as tight, semi-tight, average, semi-loose; the definitions of these parameters can be obtained in [American Society of Heating, Refrigerating and Air Conditioning Engineers, 2017]. U.S. and U.A.E. regulation [Government of Abu Dhabi, 2014] recommend this manual. The Australian Government suggests to use the ASHRAE 140-2001, which mentions that the energy load should be calculated by building modelling software, with the assumption to maintain a constant infiltration rate of 0.5 h^{-1} [ASHRAE]. Furthermore, this standard also recognised the ACCA Manual J method as a different approach. The New Zealand Government [Standards New Zealand, 2009] proposes a similar figure.

The European standard suggests a minimum infiltration rate of 0.41 h^{-1} to enter into the energy loss calculation [ISO, 2017]. For heat losses, heat flow rate due to air entering an enclosed space divided by the difference between the internal air temperature and the supply air temperature gives the infiltration heat transfer coefficient (Equation 1.1).

$$I_{ve,k;t} = \rho_a \cdot c_a q_{V,k;t} \tag{1.1}$$

Where $I_{ve,k;t}$ is the heat transfer coefficient by ventilation airflow element k, in W/K, $\rho_a \cdot c_a$ is the heat capacity of air per volume in $J/(m^3K)$; and, $q_{V,k;t}$ is the airflow rate of airflow element, k, in m^3/s.

The Canadian government [Canadian commission on Building and Fire Codes, 2017] refers to both, the ASHRAE [American Society of Heating, Refrigerating and Air Conditioning Engineers, 2017] standard and the ISO standard [ISO, 2017]. The standard also uses a value of $0.25Ls^{-1}m^{-2}(0.9m^3h^{-1}m^{-2})$ saying that is a typical infiltration rate at 5 Pa. Countries like Chile only include a minimum airtightness level depending on the area of the country; nevertheless, they do not mention an air infiltration requirement [Ministerio de vivienda y urbanismo, 2018].

There has been extensive research aiming to find a correlation between airtight-

ness and air infiltration [Blomsterberg et al., 1979, Dols et al., 2000, Sherman, 1980, Liddament, 1989, 1996]. Such efforts led to the development of predicting tightness-infiltration ratios and models. However, all rely on the airtightness results given by the high-pressure methods despite the development of new technologies.

1.2 Aim

As mentioned in the introductory section, improving airtightness measurements, and in consequence, air infiltration prediction will lead to a reduction in the energy losses of a building. The prediction of air infiltration can improve the building's energy efficiency.

The aim of this research is to develop a correlation between low-pressure airtightness measurements and infiltration rates within buildings. In order to achieve this aim there will be a review, calibration, and validation testing of infiltration models based on airtightness measurements taken using the novel Pulse technique (low-pressure airtightness testing method). In other words, airtightness testing is used to validate mathematically calibrated infiltration models. These models are also validated in their original form and in the new calibrated form. This work will seek to provide such correlations with a statistical degree of confidence in order to demonstrate the reliability of these models.

Once the models are proved correct with a statistical degree of confidence, the research question will be answered, and the correlation will be found. Therefore, the models are the correlation. In addition, part of the aim is to find the most accurate model when using low-pressure airtightness measuring methods.

1.3 Objectives

The following objectives are defined in order to accomplish the main aim of the research project.

- Analyse the current state of the art in relation to air infiltration, air leakage, infiltration modelling and infiltration applications. Furthermore, investigate previous attempts on correlating airtightness and air infiltration to design the most suitable methodology to follow.
- Investigate the different air infiltration models (LBL, AIM-2, CONTAM, DOMVENT3D), and decide if it is feasible to re-calibrate and test them.

Also to define which models might work better when predicting with low-pressure airtightness measurements.

- Use the Pulse technique in different scenarios, buildings and conditions, to test and analyse its capacities, advantages and shortcomings. Furthermore, as a comparative benchmark, to use the standard pressurization technique (blower door) to measure airtightness referenced at 50 Pa.
- Compare the performance of the Pulse and blower door techniques in order to assess the accuracy, reproducibility and uncertainties of the Pulse technique. To assess if the Pulse method would be the appropriate method to fulfil the main aim of the project.
- Perform tracer gas decay and constant concentration tests in order to measure air infiltration. Furthermore, to analyse the procedure and results of the tests, to understand the uncertainties associated with the methods.
- Develop experiments to measure the pressure fields around a building, to understand how these are related to infiltration and its driving forces.
- Perform tracer gas tests in at least 20 dwellings to determine their infiltration rate and obtain enough data to input models.
- Determine a correlation between the results of air leakage rate (@4Pa) given by the Pulse method and the infiltration rate obtained from measurements using a tracer gas technique to validate different models. All these measurements carried out during different weather conditions and on different buildings.
- Calibrate different infiltration models according to the results obtained during the experimentation stage and the correlation found, to make it predict infiltration rates from low-pressure airtightness measurements.
- Compare the predicted results based on measurements of the steady pressurisation method and the Pulse technique, to determine the potential inclusion of Pulse in infiltration models.
- Test and compare different infiltration models in terms of accuracy based on which predicted values reflect better the real measurements, to determine which infiltration model more closely represents the data used.
- To assess the feasibility of using the Pulse method to predict infiltration rate and a potential integration into energy legislation.

1.4 Structure of project and Thesis overview

This thesis contains nine chapters, with each one providing a role in fulfilling the above objectives. Overall the thesis has is overarched by chapters under three areas. The first five chapters analyse the currently available literature and legislation, and additionally, they include how data was collected. Chapters six to eight include the integration of low-pressure airtightness measuring into different infiltration models, with each chapter using a different infiltration model. The last chapter includes the analysis on which model or models can be used when predicting air infiltration from low-pressure airtightness measurements. Specially the individual chapters contain the following:

Chapter two presents an overview of research made over the last few decades in the fields of airtightness measurement and infiltration prediction, how prior research relates to the topic and also includes how the research in this study adds to the body of knowledge in the area. As a literature review chapter, it discusses the research guidelines, investigation articles and building standards. After reading the chapter, the reader will be able to understand how this project fills a knowledge and technical gap in the airtightness and air infiltration correlation.

Chapter three details the initial experiments on airtightness measuring with the Pulse method. It also introduces Pulse's technical information, advantages and shortcomings of the technique and includes analyses on practicality and reproducibility. Details of the uncertainty analysis and a modification of the algorithm of the Pulse method are also discussed.

Chapter four introduces the first experiments on air infiltration in one dwelling. The tracer gas tests carried out in the test house are analysed. Chapter four also presents tests and experiments on pressure fields. The results from this chapter were presented in the AIVC conference 2018 in Antibes-Juan-les-pins, France in September 2018, and are included in the conference proceedings [Vega Pasos et al., 2018a,b].

Chapter five describes the experimentation carried out in 20 dwellings during 2018: airtightness and tracer gas tests were carried out in different places in the East Midlands in the United Kingdom. This Chapter presents the description of test properties, tests and expected outcomes of a period called "field trials". In addition, all measured and calculated data is provided.

Chapter six discusses the usage of airtightness - air infiltration ratios. Infiltration ratios are the simplest way of predicting air infiltration and are therefore commonly used (as rule of thumb). The Chapter introduces and challenges the

usage of the divide by 20 rule, based on the results from Chapter five. In addition new ratios are proposed when quoting airtightness at both, high and low pressure.

Chapter seven uses chapter five's measurements and compare them with predicted results of the calibrated version of the LBL infiltration model. A similar analysis is made for predicted results of the DOMVENT3D infiltration model; results are presented in chapter eight. In both cases, how predictions based on Pulse and blower door's measurements compare are discussed.

Chapter nine gives a summary of the results and concludes this thesis. There is a discussion on the feasibility of using Pulse in legislation and infiltration prediction. Finally, it presents a comparison of the results between models and provides direction in relation to further applications of the outcomes of this study and recommended research guidelines.

in essence the thread running through this thesis is one of starting from understanding how to measure airtightness and air infiltration; passing through a data collection stage, and ending on the usage of the collected data to assess the usage of airtightness measuring techniques into infiltration predicting models.

1.4.1 Methodology

Each experimental chapter includes their particular methodology. Nevertheless, the overall methodology of this thesis can be simplified in:

- Literature and standards review: Extensive revision of the literature aiming to understand the research carried out in the field. The literature is analysed focusing on research carried out for the existing technology to identify potential research guidelines for the Pulse method. Once that is identified, the analysis focuses on which new research paths for both air infiltration modelling and low-pressure airtightness measurement. Finally, in-depth analysis and comparison of different infiltration models aid to decide which ones can be selected to accomplish this project.

- Training and initial experimentation: Before starting the experimental stage of the project, extensive training on airtightness (Pulse and blower door tests) and air infiltration testing was undertaken. Furthermore, the work within this study covers how airtightness testing is helpful with different research objectives. For example, Chapter 3 describes how different experiments aided on the development of the Pulse method.

- Data collection and experimental stage: Following the initial experimentation, the main experimental stage commences. Several properties were tested

covering a range of climatic conditions. The data is analysed individually to obtain results such as the validity of tests, airtightness and air infiltration results and, the uncertainty associated with each measurement.

- Modelling: Data is introduced in previously calibrated models, air infiltration predictions are obtained and a brief analysis on measurement-prediction is given.

- Comparisons and conclusions: The data is analysed as a whole, different statistical methods (described in chapters 6, 7 and 8) are utilised. The results are then compared for both airtightness measuring techniques and the infiltration models results are also compared against each other.

Chapter 2

Literature Review

2.1 Introduction

This chapter reviews first, the steady pressurisation method and different airtightness measuring technologies; it presents the advantages and shortcomings of the methods, and describes some of the existing airtightness-infiltration predicting models.

The objective of this chapter is to present the prior research in this field and provide context to the research gap considered in this study.

2.2 Airtightness measuring techniques

2.2.1 Building airtightness context

Building airtightness, as mentioned, is the property of a building that impacts the most on air-infiltration. Measuring the airtightness is the first step towards the calculation (or prediction) of air infiltration heat losses; therefore, it is closely related to the energy efficiency of buildings. There are different ways to refer to airtightness; for example, air leakage rate is a different name for airtightness, or air permeability is the metric which results from normalising the air leakage rate using the envelope area. There are different units to describe airtightness: as a flow of air through the envelope (m^3/s), as part of the ventilation in air changes per hour (h^{-1}), leakage area (m^2) or in air permeability units ($m^3h^{-1}m^{-2}$). Nevertheless, all of them account for the "amount" of adventitious openings in the building envelope. Airtightness is a property of the building, and should not vary with sudden changes in climate conditions; however, it can change due to ageing of the building or modifications to the envelope (i.e. drilling holes). On the other hand,

air infiltration is the property that varies with outdoor climate conditions.

Airtightness and air infiltration have long been recognised as a concern and led to the creation of the Air Infiltration Centre (AIVC) in 1979. It is essential to take the airtightness into account in the building qualitative and quantitative evaluation, considering its contribution to building energy loss and, the fact that the energy consumption in the building sector represents a large portion of the overall energy use. The need for a reduction of energy usage in buildings ties up with the global target on reducing carbon emission made by EU directive, Kyoto Protocol and discussed in the climate change talks held in Paris in 2015.

Understanding the airtightness of a building is fundamental in quantifying the level of infiltration in a building (leading to heat losses). Theoretically, the measurement of building airtightness can be implemented by measuring the airflow rate across the building's thermal envelope, while under a particular indoor-outdoor pressure difference. Usually, this is done in a range of pressure differences, which can be established by methods like blowing air in or taking air out of a building using a device such as a fan blower or duct blower. The correlation between the pressure difference and the corresponding airflow rate across the building envelope determines the building air leakage characteristics (airtightness). The building airtightness is described differently in different countries; it is quoted at a specific building pressure difference. The quoted building pressure also varies with countries, typically at 4 Pa (France and Switzerland) or 50 Pa (Germany, Ireland Belgium, U.S.A. and U.K), but sometimes at 75 Pa (U.A.E.) or 10 Pa. RDH Building Engineering Ltd. [2013] summarises the airtightness standard requirements in different countries, a glimpse of these is included in Table 2.1; it is important to notice the different units required in each country.

Table 2.1: Examples of domestic airtightness requirements in different countries [RDH Building Engineering Ltd., 2013]

Country	**Requirement**
Denmark	1.5 $Ls^{-1}m^{-2}$ @50 Pa
France	0.8 - 1.2 $m^3h^{-1}m^{-2}$ @4 Pa
Germany	1.5 - 3.0 h^{-1} @50 Pa
Germany (Passivhaus)	0.6 h^{-1} @50 Pa
Japan	2.24 cm^2 (Leakage Area)
Norway	0.6 h^{-1} @50 Pa
Qatar	0.6 - 2.2 $m^3h^{-1}m^{-2}$ @4 Pa
Abu Dhabi, U.A.E.	2.0 $Ls^{-1}m^{-2}$ @75 Pa
United Kingdom compliance	10 $m^3h^{-1}m^{-2}$ @50 Pa
United Kingdom best practice	5 $m^3h^{-1}m^{-2}$ @50 Pa

One of the main challenges in measuring building air leakage rate is in the measurement of the building pressure. Under natural conditions, a building would experience pressure caused by wind (outdoor air movement) and buoyancy effects (indoor-outdoor temperature difference). This pressure is typically in the region of 0-10 Pa. In order to obtain a precise value for the actual building pressure, this naturally occurring pressure difference from across the building envelope would ideally need to be removed. In practice, it can be challenging to achieve due to the random nature of the wind. This issue becomes even more significant when the wind condition is adverse. One of the approaches to overcome this issue is to measure the building leakage rate at high pressures. High-pressure measurements negate or shadow the impact of wind/buoyancy effects; for this reason, the most widely used method to measure airtightness increases the pressure difference and quotes the results at 50 Pa. For the countries that need to quote the results at 4 Pa or to predict infiltration rates, a process of extrapolation (from high-pressure results to low pressure) has to be carried out.

For these reasons, several methods to measure airtightness are described and analysed in the following section in terms of maintaining building integrity, time for setting up and tear down, background pressure measurement, test duration, pressure range and results, leakage detection, and, the level of skill required.

2.2.2 Steady pressurisation method: blower door

The steady pressurisation method (blower door) is the most developed, known and widely used method to measure the airtightness of a building. It has been standardised, and several countries have adopted it as the method to measure the airtightness [International Organization for Standardization, 2015, The Air Tightness Testing and Measurements Association, 2016]. The method is commonly known as the "blower door" method.

The blower door measures the building airtightness in a range of pressures, typically between 10-60 Pa. It is implemented by creating a steady pressure difference across the building envelope and measuring the corresponding indoor-outdoor airflow exchange rate. In practice, this is achieved by mounting a fan blower in a doorway, as shown in Figure 2.1. Despite being a "pressurisation" method, the building can actually be pressurised or depressurised. The imposed pressure difference can be created by blowing air into the building (pressurisation) or taking air out creating a suction (depressurisation). Good practice when measuring the airtightness is to perform a pressurisation test, a depressurisation test, and, calculate an average of both. Although, for the United Kingdom, only a depressurisation test is required.

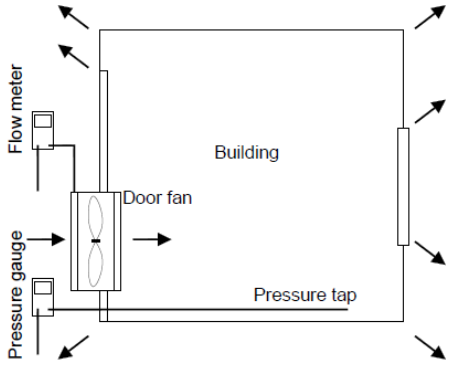


Figure 2.1: Steady airtightness measuring method, door fan in pressurisation

A pressure gauge measures the pressure difference across the building envelope, and a flow meter measures the resulting flow rate. The leakage-pressure correlation establishes the building leakage characteristic. Figure 2.2 shows a correlation curve of a typical steady-state airtightness test. The building airtightness from a blower door test is quoted at 50 Pa in the UK (but can be extrapolated to other pressure differences). Results can be in terms of q_{50} ($m^3h^{-1}m^{-2}$) or n_{50} (h^{-1}). High-pressure measurements shadow noise coming from outdoor wind and buoyancy. Hence the

method has good repeatability and reproducibility.

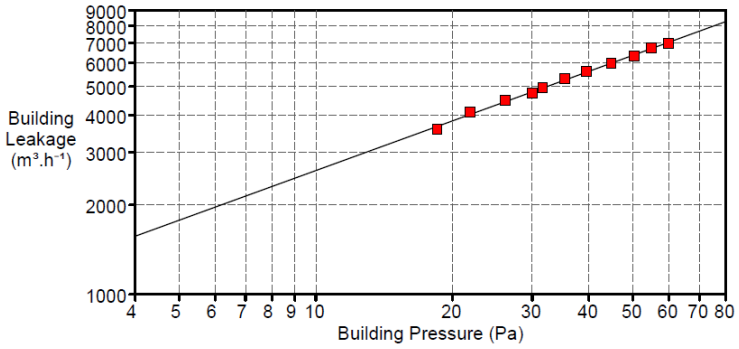


Figure 2.2: A typical steady-state airtightness test (Log-log plot)

The steady pressurisation method has gone through significant developments from early bulky, heavy versions, which were made of materials like plywood and formica to the latest lighter and more compact equipment. The latest commercially available blower door comes with three main pieces, a variable speed blower door fan, a fabric adjustable door frame which allows the unit to be fitted into doors of different sizes and, a pressure and flow gauge used to measure pressure difference across building envelope and the corresponding flow rate of air moving through the fan respectively (Figure 2.3).



Figure 2.3: Standard Minneapolis blower door unit (photo source: Wikimedia)

The blower door is the most commonly used technique for measuring building airtightness in the field and identifying the locations of leakage pathways.Orme et al. [1994] and Chan et al. [2003] did an early summary of the blower door test. Also, it has been adopted as a standard testing method by American Society

for Testing and Materials [2019], Standards Council of Canada [1996], and ISO [International Organization for Standardization, 2015] and used for demonstrating compliance.

A complete blower door test consists of the set-up of the blower door unit, test implementation and tear-down of the unit. The test implementation comprises the measurement of zero flow pressure, environmental conditions including the indoor and outdoor temperatures, wind speed and barometric pressure and, pressures of building and blower door fan (sometimes air leakage rate is measured directly instead of fan pressure, depending on the country) [Energy Conservatory, 2017].

Jones et al. [2013b], Cooper and Etheridge [2007a] calculated the errors and uncertainties when measuring airtightness using the steady pressurisation method. The authors confirmed that when the wind speeds are higher than 10 m/s, the error increases more than 12% at a reference pressure of 50 Pa. Low pressures are more representative of natural conditions; however, when measuring airtightness at low pressures uncertainty due to high wind speed is more significant.

Sherman and Palmiter [1995] mentions two kinds of error for the steady pressurization technique: errors associated with measurements, and, model specification errors; wind was defined as the most important cause of measurement errors. The accuracy of the blower door technique is limited by the uncertainties when measuring at the lowest pressures (where natural phenomena such as wind and buoyancy take place); hence the importance of covering high pressures when testing.

Remi Carrie and Leprince [2016] studied the effects of steady wind on the blower door test. The authors were not able to find an equation to include the stack effect (this might induce more uncertainties to the measurement). The study concluded that it is better to use a pressure reference of 50 Pa rather than 4 Pa since lower pressures will lead to more substantial errors (up to 60%). At natural pressure levels (around 4 Pa) wind and stack effects impact more on the accuracy of the pressurization tests. These results agree with what Sherman and Palmiter [1995] found years before. Uncertainty due to zero flow pressures have been studied as well by Prignon et al. [2019] and Delmotte [2017].

In order to achieve the desired pressure range across the building envelope, air needs to be blown (or taken out) into the building enclosure. For example, a house with a volume of 343 m^3 and a permeability of 5.68 $m^3h^{-1}m^{-2}$ at 50 Pa, would require a flow rate of net fluid of between 600-2000 m^3/h to achieve a pressure range of 10-60 Pa. For a house with a volume of 446 $m^3$and a permeability of 10 $m^3h^{-1}m^{-2}$ at 50 Pa, the maximum flow rate of net fluid for testing could go up to 5000 m^3/h. The usage of a large amount of net fluid flow and significant change

to indoor environment conditions makes the steady pressurisation tests unsuitable for buildings or spaces where strict environment conditions are required due to safety and performance reasons.

Some of the practical shortcomings of the steady pressurisation method are, first, that it installs a duct or blower fan in an external doorway. The leakage characteristics of that door could change; the replacement can be tighter or leakier depending on the installation quality and door condition. This happens especially when the frame has an irregular shape or when secure door and lock fittings are mounted in the door frame, hence this makes it difficult to maintain the same leakage characteristic. This situation is a particular problematic when testing very airtight or small buildings, where the door seal could potentially be a non-insignificant contributor to the overall building leakage. Second, the artificially high-pressure range where the measurement is taken can potentially create additional openings during testing [Cooper et al., 2016].

Regarding the practicality and set-up of the steady pressurisation method, there are two major steps [Energy Conservatory, 2017] as follows:

1. *Setup of door panel* - fitting the blower door frame and fabric into an external doorway of the test building, placing tubes through the fabric and installing the fan blower in the fabric.

2. *Connecting the gauge to the blower door* - mounting the gauge to the blower door frame or door panel, connecting two pressure tubes to the gauge, fan blower and outdoor environment, and also plugging the fan controlling cable to the fan blower.

The setup or teardown of a blower door kit usually takes 5-10 minutes depending on the experience of the test operative.

The background pressure is defined as the pressure experienced by buildings under natural conditions, namely pressure variation caused by wind and buoyancy effects. By measuring it during a standard test, the impact of background pressure could be taken out from the raw measurement and uncertainties could be minimized or eliminated. For a steady environmental condition, theoretically, a limited number of measurements before and after the test is sufficient to represent the pressure variation trend. When the environment condition is unsteady, the frequency of measuring background pressure needs to be increased in order to represent the trend with adequate accuracy [Delmotte, 2017].

The measurement of background pressure is called the zero flow pressure reading. It is typically done by taking ten pressure readings in 30 seconds before

and after the test with the fan blower off and covered [International Organization for Standardization, 2015]. These background pressure readings account for what occurs during the testing period. The background pressure measurement can be representative when the external wind condition is stable, but not when fluctuation is present in the external environment conditions.

The time taken to run a steady pressurisation test (either pressurisation or depressurisation) is usually between 10-20 minutes. The time varies depending on the operator's proficiency and weather conditions.

An advantage of the steady pressurisation method is that it can detect the location of leakages with the assistance of either a thermal image camera or a smoke pen [Lerma et al., 2018]. The detection can be done by fixing the blower door unit in an existing doorway or other openings, and to depressurise the building and walk around with a thermal camera or smoke pen to identify the leakages in the building envelope. The leakage detection is essential when the presence of certain leaks has a significant impact on the performance or safety of systems in the building. The leakage detection becomes less critical when the pressure differences are relatively low, and the leaks are either unavoidable or desirable, such as the shell of a house or an acoustic enclosure [Sherman and Modera, 1986].

The steady pressurisation method has been adopted internationally as the standard method for measuring building airtightness. In order to certify the validity and accuracy of the test, the operative needs to be trained and qualified to carry out tests correctly. In the United Kingdom, for instance, standard steady pressurisation tests are needed before calculating the building heat losses due to air infiltration, as stated by the UK's Standard Assessment Procedure [Building Research Establishment, 2013].

2.2.3 The Pulse method

The Pulse method is an alternative to the steady pressurisation method to measure the airtightness of a building. Pulse has been developed by the University of Nottingham. Low-pressure measurements quoted at 4 Pa are Pulse's main feature [Cooper and Etheridge, 2007b, Cooper and Zu, 2011, Cooper et al., 2014, 2016].

The Pulse method generates an instant pressure rise in the building enclosure. The pressure variation is monitored and used to determine the building airtightness. It requires a volume change at the order of 0.004% to generate a pulse pressure in the order of 4 Pa. This technique can be implemented by releasing a certain amount of compressed air into the building enclosure, to obtain low-pressure rise, typically between 1-10 Pa.

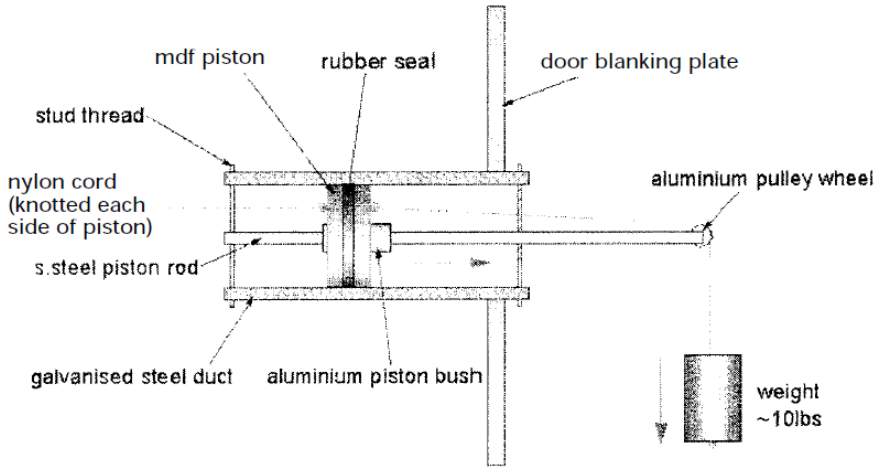


Figure 2.4: Gravity-powered piston device for generating a pressure pulse in the testing room [Cooper and Etheridge, 2007b]

The first Pulse unit used a gravity-driven piston (Figure 2.4); it was designed and tested by Carey and Etheridge [2001]. At a later stage in 2004 [Cooper and Etheridge, 2004], a more practical version was developed, in which a supply of compressed air released via an electronically-controlled solenoid valve drives the piston (Figure 2.5). The piston unit demonstrated good test repeatability [Cooper and Etheridge, 2007b].

In order to avoid air leaks from the narrow gap between the piston and cylinder wall, a nozzle unit was developed to substitute the piston. The nozzle method determines the mass flow rate of air directly by measuring the change in pressure of the air receiver whilst the pulse is firing (Figure 2.6) [Cooper and Zu, 2011]. The later version contained a separate control box and a composite tank. Figures 2.7 and 2.8 show the unit setup and schematic diagram of this version. This unit, having the control and measurement parts simplified into a single control box, is autonomous and able to display testing results instantly without relying on other procedure or software to analyse the test data.

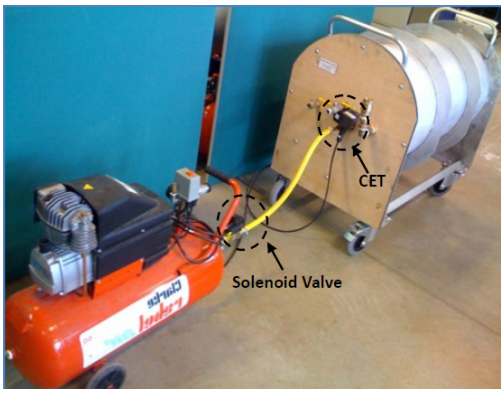


Figure 2.5: Pulse connection of compressed air and piston unit [Cooper et al., 2014]

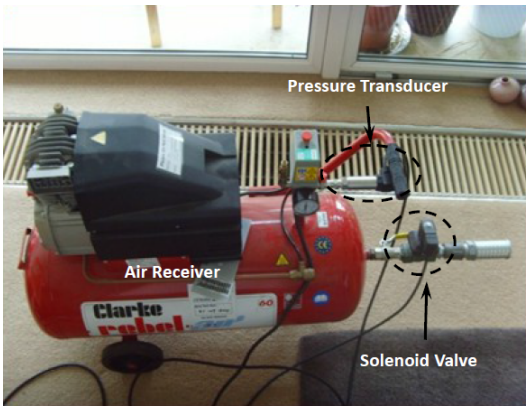


Figure 2.6: Nozzle-based pulse unit [Cooper and Etheridge, 2007b]

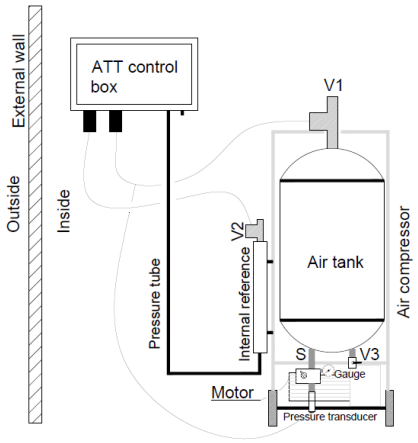


Figure 2.7: Schematic diagram of the Pulse nozzle unit with a composite tank [Zheng et al., 2019a]



Figure 2.8: Photo of the Pulse nozzle unit with composite tank [Cooper et al., 2016, Zheng et al., 2019a]

The later development contained an aluminium tank, a nozzle valve, a solenoid valve, a pressure gauge, which are enclosed in a box to provide robustness. A touch screen display within the control box includes the software to run the calculations (Figures 2.9 and 2.10).

The pulse unit in its current form does not require sophisticated setup, apart from some simple connections of cables, and also the input of a few parameters related to the building, tester and the pulse unit. The test is implemented by a series of button operations on a control box; the software analyses the data, and the results are displayed instantly on the electronic display. It needs to be noted that at the time of writing this study, the assessment of the test validity needs confirmation from a specialist, and extra time is required when a specific tank pressure level is in demand. Usually large and leaky buildings require larger tanks to obtain the desired pressure range whereas small and tight spaces (i.e. cleanrooms) could require small tanks. A 60 litre tank would be sufficient for buildings with an airtightness level between 0.5 - 2.5 h^{-1} @ 4 Pa; a smaller tank (20 litre) will be useful for very tight buildings (¡0.5 h^{-1} @4 Pa); for leaky buildings, two 60 litre tanks can be used.

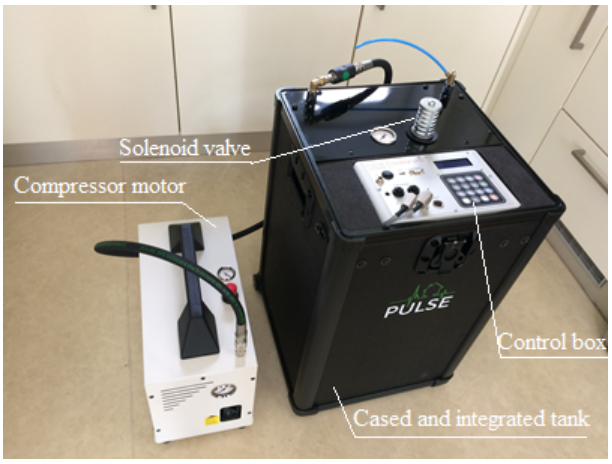


Figure 2.9: Photo of the Pulse modified nozzle unit with control box integrated



Figure 2.10: Latest version of the Pulse unit

A Pulse technique test is implemented within the building enclosure. Therefore, the building integrity is maintained; it is a standalone and portable device which needs to be plugged to the wall socket and possibly some quick connections to the control box depending on if the unit contains a control box. The time required for setup and teardown of the unit is about 1-2 minutes.

Pulse measures the background pressure at a sampling rate of 20 Hz for 2 seconds before and after the pulse. The whole test is conducted over a short duration. Therefore, the way that the background pressure is measured is deemed to be representative of background pressure trend caused by ambient conditions [Cooper and Etheridge, 2007b].

The test can be carried out as a single or as a step test, which is a combination of three single steps each one fired with lower pressure in the tank than the previous one. The objective of a step test is to cover a broader pressure range than in a single test. A Single test has a duration of 6 seconds and a step test of 14 seconds. Nevertheless, the time needed to re-charge the tank shadows the duration of the test itself, depending on the compressor used and, the size of the tank, a full charge of a 60-litre tank takes between 6-10 minutes, and one charge is equivalent to one step test.

2.2.3.1 Pulse algorithm

In order to measure the airtightness properties of a building, Pulse requires to calculate the mass flow rate of the released compressed air. Equation 2.1 describes the calculation procedure.

$$\dot{m}_p(t) = -\frac{V'}{\gamma R T_0}\Big[\frac{P(t)}{P_0}\Big]^{\frac{1-\gamma}{\gamma}}\dot{P}(t) \tag{2.1}$$

Where $\dot{m}_p$ is the mass flow rate of released compressed air (kgs), V' is the volume of the tank (m^3), γ is the ratio of specific heat, equals to 1.4, R is the gas constant, equal to $287.058\frac{J}{Kg\cdot K}$. $P(t)$ is the transit tank air pressure (Pa). P_0 (Pa) and T_0 (K) are the initial pressure and temperature of the tank air before every test launched.

The volumetric flow rate is calculated using Equation 2.2.

$$Q_p(t) = \frac{\dot{m}_p(t)}{\rho_i} \tag{2.2}$$

Where Q_p (m^3/s)is the volumetric flow rate from the compressed air release, ρ_i (kg/m^3)represents the density of indoor air which depends on the measured indoor air temperature.

Finally, Equation 2.3 is used to calculate the building's leakage rate.

$$q\{t\} = Q_p\{t\} - \frac{V}{\gamma P_i}\frac{dp_i}{dt} \tag{2.3}$$

Where q is the building air permeability, V is the volume of the building, and P_i is the building's pressure in the Pulse's quasi-steady period. The calculations are computed within the Pulse's control box and can be exported to a spreadsheet for greater analysis.

2.2.4 Other airtightness measuring methods

2.2.4.1 Decay method

The decay airtightness measuring method consists in increasing the pressure inside an enclosure by supplying air until it achieves the desired level [Moller et al., 2010]. When the air supply stops, the pressure decays due to air leakage through the envelope. The pressure decay over time is recorded and used together with the air leakage rate to describe airtightness characteristics of the test space.

The process of the measurements consists of three phases, pressure rise, pressure stabilising and pressure decay. The pressurisation can be achieved in two ways: one is releasing compressed air from a compressor. Unstable environmental factors or large air leakage rate make it difficult to obtain the correct pressure profile. [Nishioka et al., 2003].

This method has been used to measure the airtightness of a bio-containment laboratory of class CL4 [Granne, 2001], Furthermore, the method has been employed more scientifically by Mattsson [2007] in determining the airtightness of an enclosure.

The measurement of wind pressure has not been discussed in previous research for the decay method. The studies related to the decay method have been carried out in a laboratory where the environment condition is controlled and the background pressure is sufficiently stable for the test. The decay method has taken measurements at various pressure levels, 0-50 Pa [Moller et al., 2010], 6-100 Pa [Mattsson, 2007] and 70-400 Pa [Nishioka et al., 2003]. The leakage results are quoted at 50 Pa [Moller et al., 2010, Mattsson, 2007].

Conclusions from using this method showed that it can estimate the airtightness level during construction process but it is not suitable to replace the current steady pressurisation method due to insufficient accuracy [Moller et al., 2010].

2.2.4.2 AC Method (repeated sinusoidal volume change)

AC pressurisation method, shortly known as “AC method”, was inspired by physical principles of fluctuating pressures, a well-known phenomenon that occurs when the flow begins to reverse [Sharples and D., 1996, Siren, 1997].

The AC method is described in [Sherman and Modera, 1986, Card et al., 1978]. Based on a steady pressure, the technique creates a repeated sinusoidal volume change to the building by a reciprocating piston and measures the unsteadiness. The data is analysed by recording the time-averaged values of the imposed flow rate and the pressure difference.

The AC method, also know as "infrasonic method" can make real-time leakage measurements at low pressures without inducing large flows through the building envelope [Card et al., 1978]. Watanabe et al. [1999] describes the apparatus and analytical technique and the laboratory measurements that determined the specifications for the field device. The measurement of background pressure has not been discussed in previous studies on the AC method, nor the duration of the tests or the capability for detecting leaks. The investigations using the AC method have taken measurements in pressure ranges of 1-10 Pa [Card et al., 1978], 4-22 Pa [Watanabe et al., 1999] and quoted the results at 4 Pa and 25 Pa respectively.

It was concluded the accuracy of the AC method was rather low, compared with the conventional steady fan pressurisation with a factor of three [Watanabe et al., 1999]. At a later study, it was reported [Sherman and Modera, 1986] that the accuracy has been improved significantly and the discrepancy between those two techniques went down to 14%. Although the AC method was quicker to set up and implement, the results are more difficult to interpret. The measurement is limited to certain opening size as further increase in the opening size does not affect the test results. For this reason, the AC method has not been as widely used as the steady pressurisation method.

2.2.4.3 Acoustic method

Previous research studies of acoustic methods [Ringger and Hartmann, 1989, Keast and Pei, 1979, Sherman and Modera, 1988, Raman et al., 2014] primarily focused on building leak detection rather than the measurement of airtightness level. However, research of using an acoustic method to infer airtightness by measuring sound transmission through cracks and gaps has been carried out since the early 1980s. Airtightness can be inferred by establishing a correlation between air and noise transfer phenomena through adventitious openings [Iordache and Catalina, 2012]. A sound source radiates sound waves at a known frequency inside or outside a building element such as windows. Sound level is sampled on both sides using devices such as a sonometer. Early experimental attempts to find the correlation between the sound transmission loss (STL) and airtightness were made in the 1980s [Ringger and Hartmann, 1989, Sonoda and Peterson, 1986, Benedetto and Brosio, 1981]but with no concrete findings.

More recently, acoustic methods for evaluating the airtightness of building components has been briefly reported by Hassan [2013] but without giving many experimental details. Results were not compared with the steady pressurisation method or any other method. Iordache and Catalina [2012] used an in-situ setup

of the acoustic test and the steady pressurisation test for measuring STL and permeability through windows. By comparing the results of the blower door test and acoustic loss test, a correlation between airtightness and sound transmission loss of test windows has been obtained, showing an inverse proportional relation between STL and airtightness.

Varshney et al. [2013] compared this method with the steady pressurisation method. The author found it potentially useful for determining air infiltration in building components. The measurement of airtightness using the acoustic method is limited to the specimen and not suitable for on-site measurement due to the complexity. However, its use in leak detection has been discussed more extensively and potentially offers some promise for this purpose.

2.2.5 Modern research on airtightness measuring

Airtightness has been studied for over 40 years now. Nowadays, the goal is to obtain regulations that minimize the infiltration heat losses (or gains). That is why most of the studies relating airtightness are intending to validate standards or characterising buildings.

In Portugal, a study found that some houses do not comply with airtightness standards and have leakage rates larger than in other countries [Salehi et al., 2017], in the same country, Ramos et al. [2015] studied the airtightness characteristics of social housing. Extensive characterisation of Finnish house airtightness was done between 2002 and 2005 and was reported by Vinha et al. [2015]. Similar studies characterising the housing stock have been done in Spain [Fernandez-Aguera et al., 2016, 2019, Feijo-Muñoz et al., 2019]. Johnston and Miles-Shenton [2018] studied the airtightness characteristics of holiday homes and Tanyer et al. [2018] in container houses.

Studies in Ireland [Sinott and Dyer, 2012], North America [Urquhart et al., 2015, Logue et al., 2013] and China [Ji et al., 2017] showed that refurbishments and renovations improve the airtightness of a building considerably, even when these changes are not done with that objective (i.e. changing windows). Research has focused on building parts such as joints that are known to be common leakage paths [Kalamees et al., 2017].

In China for example [Ji et al., 2017] it was shown that most of the air leakage pathways come from the discharge flue or the exhaust airway, rather than windows or doors which is what would be expected considering that the buildings were multi-unit high rise buildings. Pan [2010] showed that in the UK, flats (apartments) are generally tighter than houses and, also mentions that the construction

method is a relevant factor for the airtightness of a building.

Notably, improving the quality and energy efficiency of buildings defines current airtightness research guidelines, mainly in countries where the regulation is young or is not yet applied.

2.3 Air infiltration measurement

A knowledge of a building's air infiltration rate is required to determine the energy losses associated with this movement of air through the building envelope. As discussed previously, airtightness testing provides a metric for the "leakiness" of a building but its result cannot be used directly for energy loss assessment. i.e. a correlation factor or model must be used to link airtightness to infiltration. However, in order to validate such correlations, the infiltration rate itself must be measured to provide the necessary data.

Tracer gas is the ideal substance to track the bulk movement of air in a building. Furthermore, it can also be used to detect building leaks. There are several tracer gas methods to measure the air infiltration rate, yet they all work behind the conservation of mass principle and the continuity equation. Monitoring the concentration and supply of the tracer gas for a period is necessary to calculate the air infiltration rate. Thus, the main advantage of the tracer gas methods is the possibility of measuring air movement regardless the location and number of leaks, cracks or gaps and the difficulty of measuring flow in each one of them. Despite the advantages of the tracer gas methods, they are not used routinely in building assessment because tracer gas methods are invasive, disruptive, expensive and time taking; hence the need for airtightness testing.

According to standard [International Organization for Standardization, 2017, Liddament, 1996], a tracer gas must be safe, non-reactive, measurable, unique and insensible. Examples of gases employed for infiltration measurements are F_6, N_2O, C_2H_6, CH_4, CFC, H_2, He and CO_2, being the latter the most common one due to its availability and low cost. Gases can be classified by their molecular weight as heavy, light and similar (relative to the weight of air).

2.3.1 Tracer gas methods

There are several methods to measure the air infiltration rate by tracer gas means; however, three have been standardised globally: concentration decay method, constant injection method and, constant concentration method [International Organization for Standardization, 2017, American Society for Testing and Materials,

2011]. The concentration decay method is the most widely used method due to its low cost (no high-spec equipment required). Nevertheless, it has its shortcomings, such as the limited duration of the test and, that it only delivers one average infiltration rate value for the duration of the test. The constant injection and the constant concentration methods are automated tests that can measure the infiltration rate in real time, yet they require expensive gas monitoring equipment. Table 2.2 shows a summary of the mentioned tracer gas methods.

Table 2.2: Comparisons of three tracer gas techniques [Sandberg and Blomqvist, 1985, Laussmann and Helm, 2011, Sherman, 1989, 1998]

Method	**Duration of the Test**	**Airtightness level @50Pa**	**Building Size**	**Accuracy (Deviation of the mean)**
Concentration Decay	Hours	$< 10\ h^{-1}$	$<500\ m^3$	11±6%
Constant Injection	Hours to seasons	$> 0.3h^{-1}$	-	No information
Constant Concentration	Hours to season	All	-	6±3%

The decay method is widely used due to its low cost and simplicity (compared to the other methods). A certain mass of gas is inserted to the enclosed space to a required concentration level. The gas is mixed with air; typically with the aid of fans, to ensure a uniform starting concentration. The concentration decay is measured over a period of time, at various points within the building. The recommended minimum time (stated in ASTM E741-11) is proportional to the airtightness of the building (Table 2.3) [American Society for Testing and Materials, 2011]. Finally, the infiltration rate is calculated using Equation 2.4.

Table 2.3: Minimum durations between the initial and final samples for the concentration decay method [American Society for Testing and Materials, 2011]

Air change rate (h^{-1})	Minimum duration of test (h)
0.25	4
0.5	2
1	1
2	0.5
4	0.25

$$K_t = K_0 e^{-\frac{q}{V}t} \tag{2.4}$$

Where K_0 is tracer gas concentration at the beginning of the test; K_t is the real-time tracer gas concentration, $\frac{q}{V}$ is the air change rate, which can be determined by plotting the logarithm of tracer gas concentration over time (regression method).

Commonly, more than one zone is defined in the building; each zone will be measured at least twice during the test. For the regression method, an average concentration rate is calculated for different times, then its logarithm is calculated. The concentration has to be uniform in all the measured zones. Figure 2.11 and Figure 2.12 are examples of the concentration decay and its logarithm respectively. The slope of the best-fit line of the average concentration logarithms represents the infiltration rate. Okuyama and Onishi [2012] presents a different calculation approach; however, it has not been included in the standards.

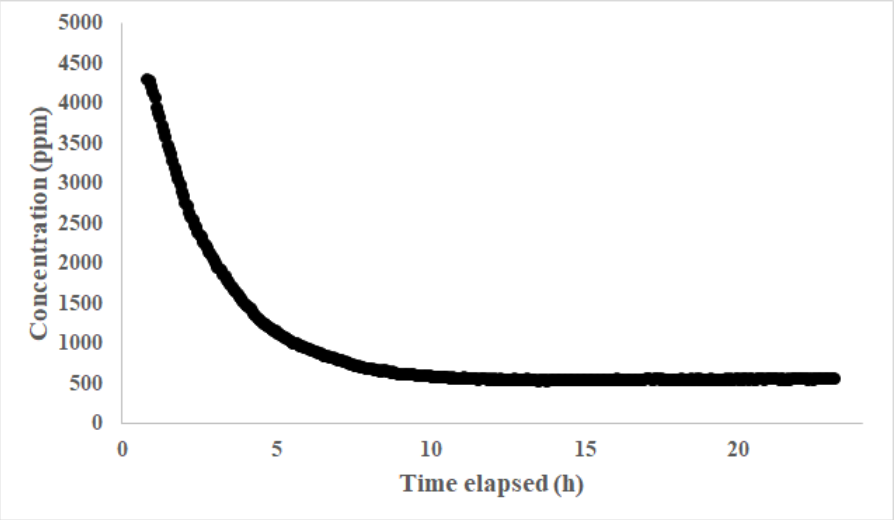


Figure 2.11: Example of a concentration decay of tracer gas in one zone of a building

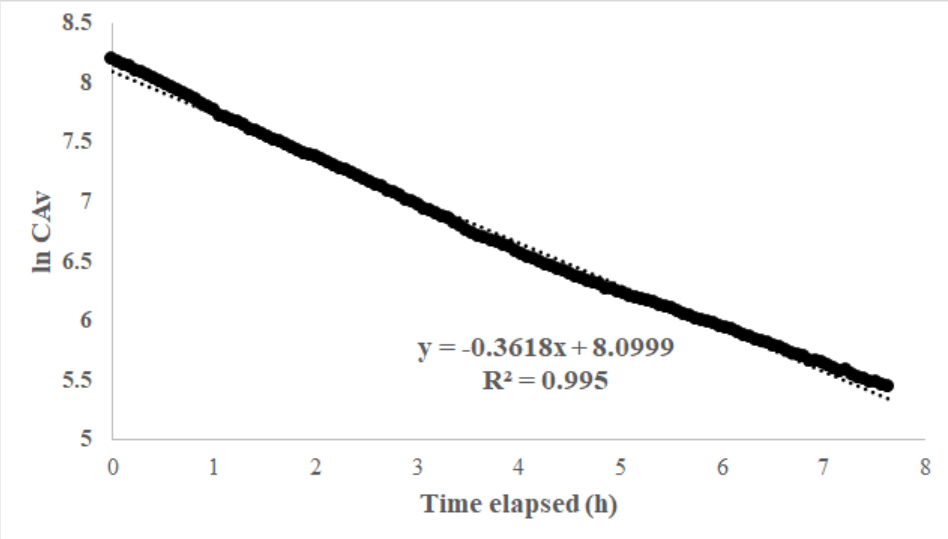


Figure 2.12: Example of calculation of infiltration rate from a decay test, the Y-axis represents the logarithmic of the concentration; and, the slope in the equation of the line represents the infiltration rate

The gas mixture and the concentration uniformity are related to the test accuracy; hence why fans are beneficial to achieve a correct mixture when a heavy or light gas is used [Sherman, 1989]. Carbon dioxide (CO_2) is the most common tracer gas, which is heavier than air and therefore fans must be used. The decay method has been reported to be appropriate for single-zone buildings with a volume of $500m^3$ or less; with medium or low air change rate (airtightness $< 6h^{-1}$ at 50 Pa).

There are several ways to measure the gas concentration in a decay test, such as samples using bags or syringes, or the usage of loggers capable of measuring different gases. One limitation to the decay method is the fact that the fans introduce a different pressure in the test building, i.e. a different environment from the normal occupied condition. The method is therefore not appropriate for measuring the infiltration rate of a single room in a multi-room building. For more information related to the decay method test and infiltration calculation it is advised to revise [American Society for Testing and Materials, 2011] and [International Organization for Standardization, 2017]. Figure 2.13 shows the apparatus of the tracer gas decay method.

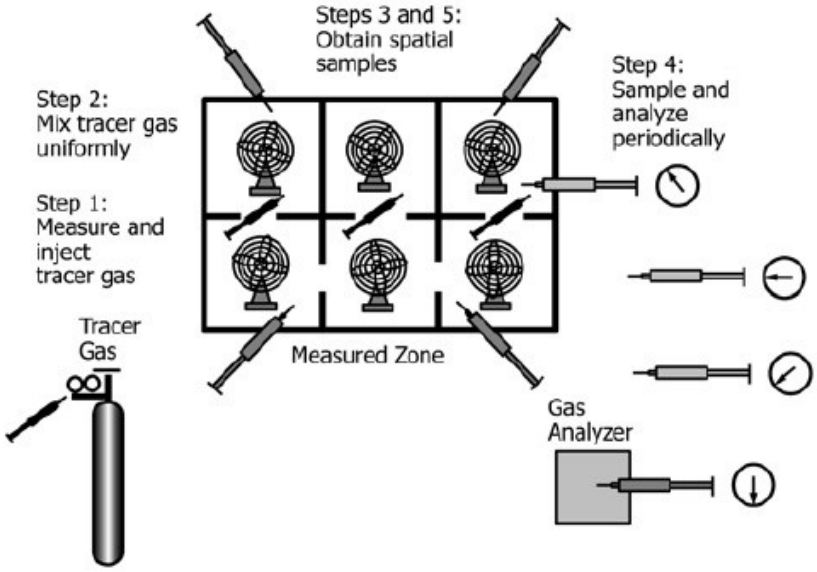


Figure 2.13: Apparatus and Procedure of the tracer gas decay method [American Society for Testing and Materials, 2011]

The constant injection (or sometimes called constant emissions) method consists of inserting a known quantity of tracer gas in the space permanently for the duration of the tests. The concentration variation is measured until uniformity is achieved; the infiltration rate is calculated using Equation 2.5, which is based on the equilibrium of the gas and the known injection rate.

$$K_t = \frac{G}{q} + (K_0 - \frac{G}{q})e^{-\frac{q}{V}t} \tag{2.5}$$

Where, G is the emission rate of tracer gas; q is air change rate, kg/s or m^3/s. The initial advantage is that the infiltration rate can be calculated for all the duration of the test; in steady conditions with a (relatively) constant infiltration rate, the method is accurate. Even so, the method is not suitable when the ventilation rate varies, i.e. conditions of high wind. Furthermore, it is complicated to reach equilibrium. A uniform concentration is difficult to achieve when the gas is supplied in different zones. Because of these disadvantages, the method has not been widely utilised; furthermore, it requires an automated supply of the tracer gas. Nevertheless, Sandberg and Sundberg [1987] described the constant injection method as an excellent option to measure the emission of metabolic carbon dioxide when the building is occupied. Figure 2.14 shows a simple diagram of the apparatus required for the tracer gas constant injection method.

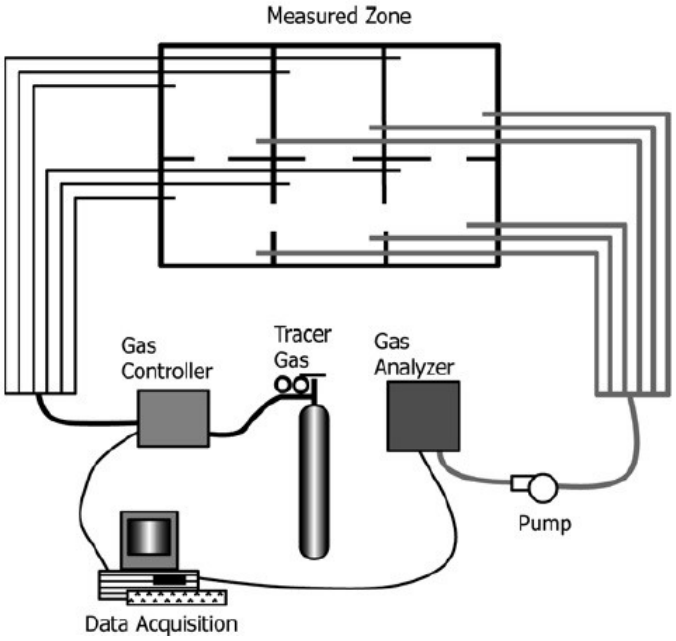


Figure 2.14: Apparatus for the constant injection method, taken from [American Society for Testing and Materials, 2011]

The constant concentration method consists of an automated continuous injection of tracer gas, utilising similar equipment as used with the constant injection method. The automated injection aims to maintain a pre-determined concentration in the whole building. The infiltration rate is calculated from the amount of air injected in each one of the injection/measuring zones and the time intervals of injections [American Society for Testing and Materials, 2011]. The procedure starts by defining zones where the tracer gas is to be injected and measured. The gas is continuously released in each zone in variable amounts to maintain a near to constant concentration. Depending on the equipment utilised, each zone is sampled every 2 to 15 minutes. Figure 2.15 represents the diagram of the apparatus. Finally, Figure 2.16 shows the LumaSense 1412 photoacoustic gas monitor and the LumaSense 1303 multipoint sampler and doser, which are some of the commercially available equipment to perform a constant concentration method.

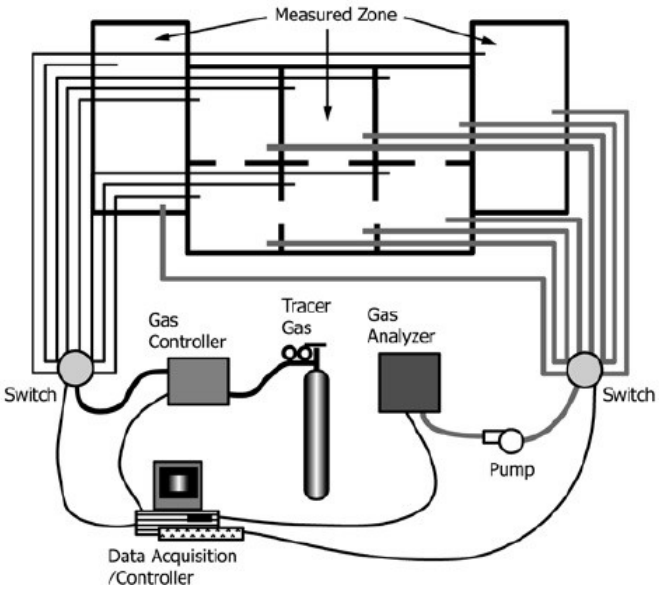


Figure 2.15: Diagram of the apparatus of the constant concentration technique [American Society for Testing and Materials, 2011]

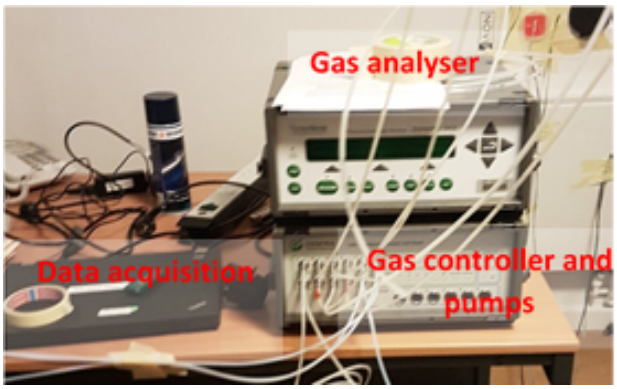


Figure 2.16: Gas analyser, gas controller (multiplexer) with pumps and filters, and a data acquisition computer for tracer gas constant concentration method.

The constant concentration method calculates the infiltration rate by relating the time that it takes to inject tracer gas with the released amount of tracer gas, as mathematically described by Equation 2.6.

$$q = \frac{G}{K} \tag{2.6}$$

When carrying out a constant concentration test, the volumes of the zones are not needed to determine the rate of outdoor air entering the enclosed spaces. The main advantage of the method is that it injects the amount of tracer gas depending

on how much "fresh" air entered; consequently, the method can adapt to changing infiltration conditions. It can also measure in leaky buildings where the tracer gas would escape rapidly. The method has not been used regularly because of the need for high-spec equipment which is usually bulky and expensive.

The constant concentration method can measure for short times; however, its strengths lie in its capability of measuring for prolonged periods, such as whole seasons (assuming a supply of gas is available). Monitoring over longer periods enables different infiltration rates to be captured against different external influences i.e. samples could be taken every 2 to 15 minutes, over days, weeks or months. The set-up of the equipment is time consuming and tubes for injection and measuring have to be allocated; therefore, it is risky to occupy the building while the test is running. Furthermore, the method cannot measure inter-room airflow. Hence, research is the primary use of this method. Equally, the method has been catalogued as the most accurate tracer gas method to measure infiltration rates [Sandberg and Blomqvist, 1985], yet the costliest [Laussmann and Helm, 2011, Sherman, 1998] due to the complicated control and monitoring of tracer gas emissions in real-time.

2.3.1.1 Accuracy and practicality of tracer gas methods

There is little information or discussion in previous investigations about the time of set-up/tear-down of tracer gas methods; in fact, it is not discussed in the standards. The first part of a tracer gas test is to divide the building in "zones" depending on the building volume and equipment available.

Depending on the equipment, a decay method test set-up would take from 10 to 30 minutes, including the emission and a first mixture of the gas. The tear-down process is quicker (5-15 minutes). On the other hand, for a constant concentration method, the set-up consists of putting the gas analyser and controller in place, installing the tracer gas canister, defining injection zones, and finally, setting the injection and measuring tubes. The whole process can take up to two or three hours. The second stage of the test is to program the controller in the required settings using the software provided by the equipment manufactured (15 minutes). The tear-down process can also be time-taking (1 hour). These periods, longer than the decay method, are shadowed by the long duration of the test (months or even seasons). Independently of the test, at least 5 minutes before measuring is recommended for a mixing process [Benedetto and Brosio, 1981, Condon et al., 1978].

During the tests, measurements may be "instantaneous" or "time-averaged",

depending on the test, the duration can span for several weeks [Benedetto and Brosio, 1981]. A decay method lasts no longer than one day, but the minimum time is 30 minutes; however, a different study [McWilliams, 2003] reported 10 minutes is possible when the building is leaky enough.

The accuracy of the results depends on building type and if it is single or multi-zone, being the latter the most accurate one [Sherman, 1998] due to the smaller volume of the divided test space. Investigations agree that the constant concentration method delivers the most accurate results, although the cost barrier is regularly a problem. Furthermore, this method is also the most complicated to set-up. The second best method is the constant injection, but the fact that this method is not suitable for variation in ventilation rate makes it limited to specific scenarios. Finally the decay method is "least accurate" of the three methods presented in Table 2.2; yet, this method is the most popular one because it is reliable, relatively cheap and quick to perform. The accuracy of the method is however still considered high enough to provide good results, and therefore all these reasons have made the method the most widely used in both, industry and academia[Laussmann and Helm, 2011, Sandberg and Blomqvist, 1985].

2.3.1.2 Historical research using tracer gas methods

The accuracy of the tracer gas methods (concentration decay and constant concentration) was studied by Sandberg and Blomqvist [1985], who concluded that:

- It can be difficult to achieve a uniform concentration of the gas without the aid of fans. Light or heavy gases (due to their densities) would cause stratification and the study recommends using fans despite the difference created compared to a "normal" scenario.
- Both studied methods are accurate enough to measure the air infiltration rate of a building. The standard deviation of the decay method ranges 4% and 20% in different cases [Sherman, 1989], and the constant concentration proved to be better with standard deviations of the measurements between 1% and 10% [Sandberg and Blomqvist, 1985, Sherman, 1989, 1998].

A different study was carried out by Sherman [1998]. The objective was to test and analyse different tracer gas methods to measure air infiltration rate:

- simple decay
- two-point decay

- integral decay
- charge up
- pulse
- constant injection
- long-term integral, and,
- constant concentration.

Uncertainty and bias error were analysed. The study found that when using a multi-gas technique, the accuracy improves with only 1% of error; though due to the complications, multi-gas methods are rarely used nowadays. The most accurate single-gas technique is the constant concentration with only 5% of error; however, if the building is divided into many zones (data points), the error could be further reduced [Sherman, 1989]. Most of the potential biases found in tracer gas techniques are related to the uniformity of the gas in the building and the correct definition of the zonal-model. Furthermore, methods taking more extended periods, e.g. constant concentration; are more accurate than methods with a short duration such as the decay method. Other studies have used the decay method to revise the ventilation rates in buildings [Gough et al., 2018] or validate measuring techniques [Liu et al., 2018].

2.3.1.3 Tracer gas methods used in this research project

From knowledge of the different tracer gas testing approaches, this study makes use of both the constant concentration and the concentration decay methods for different types of testing. In Chapter 4, the constant concentration method is used to compare the changing infiltration rate with the varying weather conditions. The equipment utilised was the one showed in Figure 2.16. Furthermore, in Chapter 5 the decay method was selected to measure the infiltration rate in a number of different dwellings. This was due to the need for quicker set-up and tear-down time and also because of multiple tests were performed, the overall cost of the test was a key factor.

2.4 Prediction of air infiltration

In order to find a non-invasive, quick and accurate way of calculating air infiltration rate, several models that predict air infiltration have been developed, which

also serve as tools to calculate heating/cooling loads and design ventilation systems. They have been used for more than 30 years; however, their complexity and applications have changed. The following sections refer to infiltration models available in the literature. An understanding of the process underlying these models is essential when adapting them to predict air infiltration from airtightness measurements taken at a low pressure difference.

2.4.1 Air infiltration models

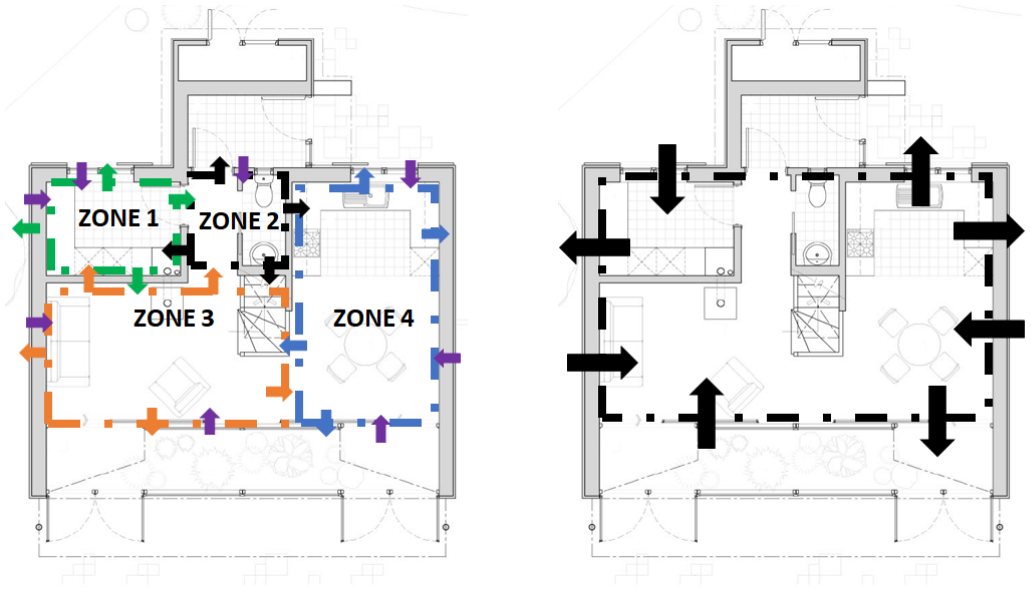
The non-disruptive and non-invasive approach to predict the air infiltration rate is via infiltration models. These models rely on a airtightness measurements. Infiltration models have been used since the 1970s in the United Kingdom. Regularly, air leakage rate (n_{50}, h^{-1}) is measured at high pressure difference, however, if the measurement is needed to calculate the impact of infiltration in the ventilation and heat losses, it has to be transformed into a useful air infiltration unit, $n_1, (h^{-1})$ [Jones et al., 2016]. The quickest and most common way to do this is through a leakage - infiltration ratio (N).

$$\frac{n_{50}}{n_1} = N \tag{2.7}$$

The term N takes typically the value of 20 in the UK (known as the rule-of-20); however, some authors have disputed the use of this ratio, the arguments are that it is rather crude and should not be used outside the United States where it was first used and created [Jones et al., 2016]. Using this ratio will lead to an uncertainty of ±28%. The rule-of-20 has been adopted in different countries including the UK, where the standard assessment procedure (SAP) [Building Research Establishment, 2013] for building energy assessment uses it as the basis to predict the unintended ventilation and the heat losses attached to it. Despite its simple approach more accurate models are available to predict infiltration rates.

Infiltration prediction is not only related to the measurement of building airtightness but also on geographical, environmental, and physical conditions of the building. Infiltration can be predicted using a model at a particular time or over a period, e.g. the winter when heating is mostly needed; and it can be used to predict infiltration associated energy losses.

The International Energy Agency assessed several models [Liddament and Allen, 1983], which include single (building treated as one cell) and multi-zone (many cells) models. A multi-zone assumption permits to model flows between the defined zones, and outdoor-indoor air exchange; whereas a single-zone model



a)Multi-zone b)Single zone

Figure 2.17: a) Multi-zone assumption, air exchange between zones and indoor-outdoor; b) single-zone assumption, outdoor-indoor air exchange.

would treat the building a single cell only allowing outdoor-indoor air exchange modelling (Figure 2.17). The models were tested in different parts of the world and consider different wind and temperature conditions. Most of the models did well under different conditions. The accuracy of the predictions is more dependent on the input values that the user specifies. The four most important parameters in the models are the flow equations used in the models; the wind pressures occurring in the building, stack pressures, the leakage distribution and air leakage rate. This draws to the conclusion that air infiltration and leakage are proportional.

A compilation of different models can be found in [Liddament and Allen, 1983] and [Orme and Leksmono, 2005]; from these two texts, the evolution of building infiltration modelling is clear. The models have changed from simplified ones to complex pieces of software.

This section of the thesis reviews, and states the virtues and shortcomings of some models used in the last 35 years including the LBL model, AIM-2, CONTAM, AIDA, DOMVENT 2D and DOMVENT 3D. A summary of the described models is given in Table 2.4.

2.4.1.1 Mathematical representation

The scientific community has been discussing over the last decades the validity, applicability and accuracy of the mathematical representation on building infiltra-

Table 2.4: Brief description of some infiltration predicting models

Model	**Complexity**	**Main use**	**Zonal definition**	**Validation**
LBL	Simplified	Infiltration prediction	Single	Yes
AIM-2	Simplified	Infiltration prediction	Single	Yes
AIDA	Complex	Infiltration prediction	Single	
CONTAM	Complex	Pollutant transport	Multi-zone	Yes
DOMVENT3D	Complex	Stock modelling	Single	No

tion: the power law and the quadratic equations [Walker and Wilson, 1998, Chiu and Etheridge, 2002, Walker et al., 1997]. Walker et al. [1997] compared the two most important equations. Both were assessed on their accuracy when extrapolating to lower pressures (natural conditions). Walker concluded that the power law (Equation 2.8) is applicable for describing the building leakage characteristics at low pressures.

The Power Law

$$Q = C\Delta P^b \tag{2.8}$$

C is the flow coefficient and, b is the flow exponent (between 0.5 and 1 from turbulent to laminar flow).

The quadratic form is described by Eq. 2.9.

$$\Delta P = a{\cdot}Q + B{\cdot}Q^2 \tag{2.9}$$

Therefore

$$Q = \frac{-a + \sqrt{a^2 + 4B\Delta P}}{2B} \tag{2.10}$$

Where:

$$a = \frac{12\mu z}{Ld^3} \tag{2.11}$$

$$B = \frac{\rho Y}{2d^2L^2} \tag{2.12}$$

Where a is the flow coefficient for fully developed laminar friction losses and B is the coefficient for entry, exit and turbulent flow losses. μ is the dynamic viscosity, L is the width of the crack, d is the gap thickness, z is the distance in the flow direction, ρ is the fluid density and Y depends on the crack geometry [Walker et al., 1997].

From the measurement of airtightness using a steady pressurisation test, it can be implied that "*a different flow coefficient, C, and flow exponent, b, apply at the low pressures that a building experiences due to natural conditions than at the elevated pressures of a steady pressurization test*" [Walker et al., 1997]. This was mentioned regarding the usage of different airtightness measurement techniques at different pressure differences (taking into account that the steady pressurisation method uses high-pressure measurements). In addition, it was found that the values C and b of the Power law (Equation 2.8)are true constants that describe the leakage characteristics of the building. Furthermore, the study mentions that the power law represents better the infiltration flows, and its validity was demonstrated for the natural conditions pressure range. The study by Walker et al. [1997] suggests that extrapolation from high pressure to low pressure will not introduce a bias while predicting air infiltration rate. On the other hand, different studies dispute this; they claim that the extrapolation (from 50 to 4 Pa), introduces uncertainties up to 40% when calculating the infiltration rate [Cooper and Etheridge, 2007a, American Society of Heating, Refrigerating and Air Conditioning Engineers, 2017, Cooper and Zu, 2011].

A different study disputing what Walker et al. [1997] found showed through the usage of CFD (Computational Fluid Dynamics) technologies that the quadratic equation (Equation 2.9) is more representative of the infiltration. Even when the power law can give a good fit to airtightness results at high pressure, it introduces a significant error when extrapolating to low pressure [Chiu and Etheridge, 2002]. Chiu and Etheridge mention that the results in [Walker et al., 1997] were misleading and the experimentation results (which were carried out using a flue) are not representative of typical adventitious openings and leakage paths. A large opening (such as a flue) takes the flow exponent (b) value closer to 0.5, making the power law more accurate. The errors can be more substantial for small adventitious openings using the power law, compared to the quadratic equations.

Finally, Baker and Sharples [1987] tested both mathematical formulations to find which one described better the airflow through cracks. Measuring and calculating the flow through three different known cracks was part of the experimentation; the quadratic equation turned out to be better or as good as the power law in

84% of the studied cases. Baker and Sharples [1987] concluded that the quadratic flow model can be used as a rule of thumb to estimate leakage through cracks.

2.4.1.2 Simplified models: The Lawrence Berkeley Laboratory and the Alberta Air Infiltration models

Sherman, in the early '80s, developed an infiltration model [Sherman, 1980], which now is known as the Lawrence Berkeley Laboratory infiltration model (LBL), which uses the power law (Eq. 2.8) as a governing equation. Where Q is the flow through the envelope (m^3/s), ΔP the pressure difference (Pa), b the flow exponent which varies from 0.5 to 1 from turbulent to laminar; and, C is the flow coefficient. C and b, are obtained from pressurization tests; most of the infiltration models depend on these two constants.

The LBL model treats the building as one single space, i.e. a single-zone model. It is also a "simplified" model due to the assumptions used (i.e. superposition, stack and wind infiltration are added in quadrature). Therefore, it requires low computational capabilities. When measuring airtightness, for the building to be considered as "single-zone", all the internal door must be open [Etheridge, 2012].

A different single-zone and simplified model was developed by Walker and Wilson [1990], this model is called the Alberta Air Infiltration Model or AIM-2. Similarly to the LBL model, AIM-2 uses the Power law as the governing equation. The main difference between the two models is that AIM-2 considers crawlspaces, basements, flues, and fireplaces as leakage paths. The accuracy and validity of both models have been proved by several studies. Furthermore, they have the advantage of being simplified models which means that they are easy to use and understand [Hayati et al., 2014, Grot and Persily, 1986, Wang et al., 2009, Sherman and Grimsrud, 1980, Walker and Wilson, 1998]

LBL and AIM-2 rely on superposition techniques that simplify the calculation of air infiltration. Moreover, both models were widely used during the '90s and '00s. Currently, they are still in use to predict infiltration rates in different types of buildings, due to their simplicity, reliability and proven accuracy [Wang et al., 2009, Hayati et al., 2014].

The LBL model included in its algorithm the location of the Neutral Pressure Level (NPL), which is the point where no outdoor-indoor pressure difference occurs. It also introduced the concept of Effective Leakage Area (ELA, $m^2 or ft^2$), defined as the total surface area of the opening in the envelope where air flows, showed mathematically in Equation 2.13.

$$ELA = \frac{Q_4}{[\frac{2}{\rho}\Delta P_4]^{0.5}} \tag{2.13}$$

Where ρ is the air density (kg/m^3) and the subscript "4" stands for a pressure difference of 4 Pa. Note that the air leakage measurement is taken at high-pressure difference. Therefore, extrapolation is necessary, and this process introduces uncertainty [Cooper and Etheridge, 2007a, Remi Carrie and Leprince, 2016].

The superposition in the LBL model assumes that the flow is proportional to the square root of the pressure; hence the stack and wind infiltration flows are added in quadrature to find the total infiltration rate.

$$Q = \sqrt{Q_w^2 + Q_s^2} \tag{2.14}$$

In Equation 2.14, Q_s is the stack induced infiltration, which is grouped in three categories: floor, walls, and ceiling areas; and, Q_w is the wind-induced infiltration considering the shielding factors [Sherman and Dickinson, 1985]. The superposition assumptions simplified the calculation and delivered accurate results. However, Lyberg [1997] challenged it, mentioning that it is not physically realistic; therefore, the utilisation of superposition is questionable. LBL uses the following mathematical procedure to predict air infiltration [Sherman and Grimsrud, 1980, Sherman and Dickinson, 1985, Sherman, 1980, 1987, 1991].

$$X = \frac{A_c - A_f}{A_o} \tag{2.15}$$

$$R = \frac{A_c + A_f}{A_o} \tag{2.16}$$

Where: A_c is the leakage area of the ceiling, A_f is the leakage area of floor level leaks, and A_o is the total leakage area. The stack induced infiltration (Q_s) is defined by

$$Q_s = Lf_s\sqrt{gH_S\Big|\frac{\Delta T}{T_i}\Big|} \tag{2.17}$$

H_s is the stack height of the building (m), g is the acceleration of the gravity (m/s^2), ΔT is the temperature difference (indoor-outdoor) (K), T_i is the indoor temperature (K) and, f_s is the stack factor.

$$f_s = \frac{1 + (\frac{R}{2})}{3}\Big(1 - \frac{X^2}{(2-R)^2}\Big)^{\frac{3}{2}} \tag{2.18}$$

from Equation 2.14 Q_w is the wind-induced infiltration, defined as:

$$Q_w = \Big(ELA\Big) U_e f_w \tag{2.19}$$

Where U_e is the site measured wind speed in m/s (building height [Sherman and Dickinson, 1985]) and f_w is the wind factor:

$$f_w = c\Big(1 - R\Big)^{\frac{1}{3}} \cdot \frac{\alpha_b \Big(\frac{H_b}{10}\Big)^{\tau_b}}{\alpha_t \Big(\frac{H_t}{10}\Big)^{\tau_t}} \tag{2.20}$$

Where c is the shielding coefficient and can be extracted from Table 1 of [Sherman and Grimsrud, 1980], furthermore, α and τ are terrain parameters that depend on the type of shielding conditions and can be obtained from Table 2 in [Sherman and Grimsrud, 1980]. H (m) stands for height, the subscript b stands for test building, and the subscript t refers to the weather station where the wind speed was measured [Sherman, 1980].

The author of the model modified it and developed a more robust version which accounts for stack infiltration [Sherman and Grimsrud, 1982]. This version introduces the stack height and the Neutral Pressure Level. The model now assumes that leakage can be different in the walls and, leakage under and above the NPL is evenly distributed. By making the building equivalent to a box (fixed floor and ceiling height), the model becomes more robust for most single-zone buildings [Sherman, 1991].

The AIM-2 model shares some characteristics with the LBL model; however, it includes the infiltration from flues, chimneys and crawlspaces, which the LBL model does not consider. Validation of the AIM-2 model was carried out by the authors and showed that the calculated infiltration rates differed $\pm 10\%$ of the measured values. The second biggest difference between AIM-2 and LBL is that the first uses a different superposition technique, a first-order NPL shift.

$$Q = \Big(Q_s^{\frac{1}{b}} + Q_w^{\frac{1}{b}} + B_1 (Q_s Q_w)^{\frac{1}{2b}}\Big)^b \tag{2.21}$$

Q represents the flow, s and w subscripts stand for stack effect and wind effect respectively; B_1 is the interaction (stack and wind) coefficient assumed as $-1/3$, b is the flow exponent obtained from a steady pressurisation test. The algorithm of AIM-2 is given by Walker and Wilson in [Walker and Wilson, 1990, 1993, 1998]; there are two possibilities of analysing infiltration rates in a building: when there is a flue and when there is not. Both simplified models (LBL and AIM-2) assume that the wind factor is steady and does not change with wind direction. The ratio parameters R, X and Y define the leakage distribution.

$$X = \frac{A_c - A_f}{A_o} \tag{2.22}$$

$$R = \frac{A_c + A_f}{A_o} \tag{2.23}$$

$$Y = \frac{A_{flue}}{A_0} \tag{2.24}$$

Where: A_{flue} is the leakage area of the flue, A_c is the leakage area of the ceiling, A_f is the leakage area of floor level leaks, A_w is the leakage area of walls (uniformly distributed leaks) and A_o is the total leakage area and

$$A_0 = A_c + A_f + A_w + A_{flue} \tag{2.25}$$

When a flue is not present, the following equations can be used to calculate the infiltration rate; more information is presented in the AIM-2 bibliography mentioned above. The following relation calculates the stack effect:

$$Q_s = C f_s P_s^b \tag{2.26}$$

Where C is the total leakage coefficient obtained from a pressurization test. P_s is the stack effect reference pressure (Pa).

$$P_s = \rho_o g H \Big(\frac{T_i - T_o}{T_i} \Big) \tag{2.27}$$

g is the gravitational acceleration (9.8 m/s^2), ρ_o is the outdoor air density (kg/m^3); T_i is the indoor temperature (K), T_o is the outdoor temperature (K), H is the building eaves height (m) and f_s is the stack flow factor and it is given by:

$$f_s = \Big(\frac{1 + bR}{b + 1} \Big) \left(\frac{1}{2} - \frac{1}{2} \Big(\frac{X^2}{2 - R} \Big)^{\frac{5}{4}} \right)^{b+1} \tag{2.28}$$

The effect of the wind in the infiltration rate is given by:

$$Q_w = C f_w P_w^b \tag{2.29}$$

Where P_w is the reference wind pressure (Pa)

$$P_w = \rho_0 \frac{(S_w U_e)^2}{2} \tag{2.30}$$

U_e is the unobstructed wind speed at eaves height at the building site (m/s); S_w is the local wind shelter coefficient given by:

Table 2.5: Estimates for shelter coefficients (S_{wo}) for no flue in the AIM-2 model (from Walker and Wilson [1990])

Shelter coefficient S_{wo}	**Description**
1.00	No obstructions or local shielding
0.90	Light local shielding with few obstruction within two house heights
0.70	Heavy shielding, many large obstructions within two house heights
0.50	Very heavy shielding, many large obstructions within one house height
0.30	Complete shielding, with large buildings immediately adjacent

$$S_w = S_{wo}(1 - Y) + S_{wflue}(1.5Y) \tag{2.31}$$

S_{wflue} can be 1 if it is an unsheltered flue or equals to S_{wo} if it has the same sheltering conditions as the rest of the building; if there is not a flue $S_w = S_{wo}$. S_{wo} is extracted from Table 2.5. The wind factor f_w is defined by:

$$f_w = 0.19(2 - b)\left(1 - \left(\frac{X + R}{2}\right)^{\frac{3}{2}}\right) \tag{2.32}$$

Finally,

$$U_e = \left(\frac{600}{z_m}\right)^{P_{met}} \left(\frac{H}{600}\right)^{P_{site}} U_{met} \tag{2.33}$$

Where z_m is the height at which the meteorological station measures wind speed, typically at 10 meters. H is the building eaves height (m), P_{met} is the wind speed exponent at the meteorological station, P_{site} is the wind exponent at the building site and U_{met} is the wind speed taken at the meteorological station. P_m and P_s exponents can be extracted from Table 1 of [Walker and Wilson, 1990].

In AIM-2, B_1 is the only constant determined by measured data; other empirical data such as wind coefficients and sheltering factors are obtained from different sources. AIM-2 was tested in single zone churches (large single-zone buildings) in a study by Hayati et al. [2014]. The author introduced a correction factor of 0.8 as AIM-2 seemed to be over predicting the infiltration value in these types of build-

ings. When the correction was used, the author obtained more realistic results, closer to the measured ones. It is important to remark that the study was limited to churches and it is unknown if the correction factor would remain valid for other types of large single zone buildings in the same or different climate conditions.

Simplified models such as LBL and AIM-2, are easy to use and produce reliable results in different situations [Wang et al., 2009, Hayati et al., 2014], that is why they have been used globally for a long time. When both models were compared, AIM-2 proved to be slightly more accurate.

2.4.1.3 AIDA and CONTAM

With the development of new information technology and computational power increase, access to computers became widely available. The effect on infiltration models was the development of computer-aided models. This section introduces a second generation of infiltration models: AIDA and CONTAM. AIDA was developed by Liddament [1989] and modified later by Palmiter [1990] for the Air Infiltration and Ventilation Centre (AIVC). AIDA stands for the Air Infiltration Development Algorithm. CONTAM is a multi-zonal model (the only multi-zonal model reviewed in this project) developed to calculate the pollution transport within a building. CONTAM indirectly calculates the infiltration rates [Dols et al., 2000].

AIDA is a single-zone infiltration model which considers mass flow and density. To calculate infiltration, the balance of volumetric airflow is needed, shown in Equation 2.34. A number of parameters are required as inputs to AIDA such as; the flow exponent b from steady pressurisation tests, wind pressure, air leakage rate extrapolated to 1 Pa, indoor and outdoor temperatures and densities, and, wind velocity at the building's location have to be input to AIDA. The model outputs the building's infiltration rate Q (m^3/s) and the air change rate (h^{-1}). The advantage of AIDA is that the algorithm can be adapted to suit different situations and scenarios; by only defining the openings of the building based on a reference height.

$$\sum_{i=1}^{j} Q_{vi} = 0 \tag{2.34}$$

Where Q_{vi} is the volumetric airflow rate passing through the i'th path, and j is the total number of paths providing air infiltration into the building.

AIDA found that if 11 vertical leakage paths equally spaced in every facade are assumed, the results are more accurate. When using a lower number of leakage paths, the error can be as high as 100% [Orme and Leksmono, 2005]. More modern

models, such as DOMVENT3D still use this assumption [Jones et al., 2013a,b]. The infiltration rate in AIDA is obtained by:

$$Q_{(vi)} = C_i(P_i - P_{int})^{(b_i)} \quad if \quad P_i > P_{int} \tag{2.35}$$

$$Q_{vi} = -C_i(P_{int} - P_i)^{b_i} \quad if \quad P_i < P_{int} \tag{2.36}$$

the subscript i represents the i'th path, C and b are the flow coefficient and exponent respectively taken from steady pressurisation test; P_i is the external pressure (Pa) of the i'th path and P_{int} is the internal pressure (Pa). AIDA requires to consider the contribution of the wind and stack effect separately.

$$P_s = -\rho_0 g 273\Big(h_2 - h_1\Big[\frac{1}{T_{ext}} - \frac{1}{T_{int}}\Big]\Big) \tag{2.37}$$

Where P_s is the stack pressure (Pa), h is the height (m) of the selected opening (1 or 2), ρ_0 is the air density at 273 K, g is the gravitational acceleration (m/s^2), T_{ext} is the external air temperature (K), and T_{int} is the internal air temperature (K).

$$P_w = \frac{\rho C_p U_e^2}{2} \tag{2.38}$$

P_w is the wind pressure (Pa), ρ is the air density (kg/m^3), C_p, is the pressure coefficient, and, U_e is the local wind speed at building height (m/s).

When ready, the model starts by iterating until it finds a solution for the flow balance in the order of 0.0001 m^3/s; the model then calculates the pressure at this point. Finally, the model stops and prints the infiltration solution. In [Palmiter, 1990] a modification was introduced, and the model started considering the mass flow rate, this addition, once again, is used in modern models.

Different from the already reviewed models, CONTAM [Dols et al., 2000] is a multi-zonal model, which means that the model considers every room in a building as a single space, therefore, there is airflow from one zone to the other [Etheridge, 2015]. CONTAM's original purpose was to predict pollutant transport in a building. However, it can also predict air infiltration rates. It is one of the most used models nowadays because it has a graphic interface. In order to obtain predictions, the building is modelled in CONTAM. Input data is defined (including the ventilation strategy).

The graphical interface outputs the results as vectors; each vector corresponds to a leakage path; due to the multi-zonal nature, there can be vectors between zones (or rooms) of the enclosed space. CONTAM is a powerful tool to be used

from the design stage of a building. CONTAM can simulate the occupancy of the building [Dols et al., 2000, Orme and Leksmono, 2005] and, in addition, provides an accurate infiltration prediction; both are particularly important when selecting the ventilation strategy and the correct HVAC system (considering Energy Efficiency and Indoor Air Quality). The downside of CONTAM is that it can be time-consuming, especially for complex buildings; hence, it is not the most suitable model when quick or in-situ results are required. Even so, the model can be very useful for series-constructed projects, large buildings and, with the development of Building Information Modelling (BIM), the model can gain relevance in new-construction projects.

Both industry and research use CONTAM; for instance, CONTAM was utilised in an investigation when 209 dwellings in the United States were modelled [Persily et al., 2006]. The results were used to analyse the ventilation rates, the infiltration rates, the indoor air quality and, the pollutant transport; these aided to develop a better characterisation of buildings in the region.

2.4.1.4 DOMVENT 2D and 3D

Simplified models, which were the most used ones in the late '90s, relied on superposition techniques. Lyberg [1997] showed that superposition techniques are not representative of real flows. If one of the flows (stack, wind, mechanical ventilation) is non-zero, the law of conservation of mass is not fulfilled and an error is generated. Therefore, for more physically realistic models, a new mathematical approach was needed. Lyberg formulated the following assumption to model building's ventilation:

$$Q_{net} = \int\int EF(|\Delta P|)\varepsilon(\Delta p)dS + Q_{mv} \tag{2.39}$$

where E is the relative leakage area (dimensionless), Q_{net} is the flow of mass across the building's envelope (kg/s), F is the flow function (kg/m^2s), ΔP is the pressure difference across the leakage path (Pa), which is an infinitesimal section dS, $\varepsilon(x) = 1$ if $x > 0$ or -1 if $x < 0$, Q_{mv} is the contribution to the flow of the mechanical ventilation system (kg/s) [Lowe, 2000, Lyberg, 1997].

In Lyberg's study, nine propositions needed to be fulfilled for Equation 2.39 to work. More information about the proposition is found in [Lyberg, 1997], which also defines other basics of airflow.

The pressure difference (Δp) includes the impact of both: buoyancy and wind pressure difference:

$$\Delta p_{stack} = \rho g(h - h_0)\frac{\Delta T}{T} \tag{2.40}$$

$$\Delta p_{wind} = -\frac{1}{2}\rho c_p U^2 \tag{2.41}$$

h_0 is the mean height of the neutral plane (no flow).

With Lyberg's new proposals, Lowe [2000] followed the research guideline in a different study. The author created a new two-dimensional model following Lyberg's assumptions. The model assumed fully airtight horizontal surfaces in the building; meaning that infiltration from this surfaces does not exist; in addition, it assumes that the pressure coefficients are uniform across the windward and leeward sides of the building. The governing equation, as in the previous models, is the power law (Equation 2.8).

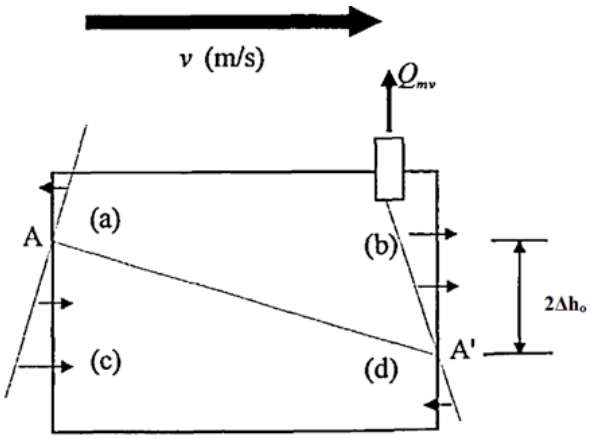


Figure 2.18: From [Lowe, 2000]. Vertical cross-section through a dwelling, showing the direction and magnitude of infiltration and exfiltration across the envelope. AA' is the neutral plane.

Lowe identified four zones depending on where infiltration and exfiltration occur, windward and leeward exfiltration (a and b), and windward and leeward infiltration (c and d), as shown in Figure 2.18. The model was named DOMVENT2D. Δh_0 is the differential of the mean heights of the neutral planes of each façade and is defined as:

$$\Delta h_0 = (c_1 - c_2)v^2\Big(\frac{T}{4g\Delta T}\Big) \tag{2.42}$$

Using Equations 2.39, 2.40 and 2.41, DOMVENT2D formulates a single integral for each of the four zones defined in Figure 2.18, once solved, the resulting equations are:

$$Q_{inf} = \frac{LEC(\rho g \frac{\Delta T}{T})}{(b+1)} \begin{cases} +(h_0 + \Delta h_0)^{b+1} \\ -(h_0 + \Delta h_0 - H)^{b+1}\Big|_{h_0+\Delta h_0>H} \\ +(h_0 - \Delta h_0)^{b+1}\Big|_{\Delta h_0<h_0} \\ -(h_0 - \Delta h_0 - H)^{b+1}\Big|_{h_0-\Delta h_0>H} \end{cases} \tag{2.43}$$

L and H (m) are the length and total height of the building respectively, C and b are the flow constant and exponent from pressurisation tests.

DOMVENT's original objective was to investigate the CO_2 emissions attributed to air infiltration heat losses and the ventilation system (or strategy). The main disadvantage of the model was its bi-dimensional nature. A whole-building case is challenging to analyse when only planes are studied. In the original paper [Lowe, 2000], DOMVENT2D was used to compare the efficiency of different mechanical ventilation systems.

Another use of DOMVENT2D was to analyse the effect of the party wall infiltration, carried out by Jones et al. [2013b]. The fact that in the United Kingdom most of the dwellings have at least one party wall motivated this study. Results showed that there is a big difference in infiltration rate when walls are considered fully permeable or impermeable. These findings led the author to create a modified version of the Lowe's model: DOMVENT3D [Jones et al., 2013a]. This new version (three-dimensional) addressed the problems created by the two-dimensional nature of DOMVENT2D.

In DOMVENT3D, the airflow from every façade of the building is considered, despite differences in geometries between façades. As in the previous version, the governing equation is Eq. 2.8, the model assumes that the power law is applied to an infinitesimal section of a vertical façade. The flow exponent (b) is assumed to be 0.5 for simplification purposes, regularly b would take a value between 0.6 and 0.7. The difference of air densities substitutes the flow function (F),because they direct the flow direction. From these modifications of the model, one can define the mass flow rates (Q_f).

$$Q_f = E\alpha W\varepsilon(\rho_o - \rho_i)\{|(\rho_o - \rho_i)|g\}^b \begin{cases} + \int_0^{minh_{0.H}} (h - h_0)^b dh \\ - \int_{maxh_{0.H}}^{H} (h - h_0)^b dh \end{cases} \tag{2.44}$$

Where E is the dimensionless relative leakage area, W (m) is the façade width, and, a is taken as $(2\rho)0.5$. The solution of the integrals created from Equation 2.44 leads to two different equations:

$$Q_1 = \frac{E\alpha W\varepsilon(\rho_o - \rho_i)}{b+1}\{|(\rho_o - \rho_i)|g\}^b \begin{cases} +h_0^{b+1}\Big|_{h_0>0} \\ -(h_0 - H)^{b+1}\Big|_{h_0>H} \end{cases} \tag{2.45}$$

$$Q_2 = \frac{E\alpha W\varepsilon(\rho_o - \rho_i)}{b+1}\{|(\rho_o - \rho_i)|g\}^b \begin{cases} +(H - h_0)^{b+1}\Big|_{h_0<H} \\ -(-h_0)^{b+1}\Big|_{h_0<0} \end{cases} \tag{2.46}$$

Three equations (for the three-dimensional model) are needed by DOMVENT3D to predict air infiltration: Equations 2.8, 2.45 and 2.46, however, only two of them will be used for each façade, depending on if it is vertical or horizontal and outdoor and indoor densities. The authors of DOMVENT3D found that the major shortcoming of the model is that it is only valid for houses and low-rise buildings. In high-rise buildings, temperature stratification plays a significant role in air infiltration and therefore it must be considered; however, in the current state of the model, stratification is neglected for simplification purposes. Consideration of temperature stratification in high-rise buildings would considerably increase the computational requirements for the model to run.

One of the advantages of DOMVENT3D is that it can be used to predict whole-stock infiltration rates. The model was used by Jones et al. [2015] to predict the infiltration rate of the English housing stock using a stochastic approach. The model was shown to be a powerful tool for policymakers when large quantities of data can be analysed in a -relatively- short time; furthermore, the model can be re-coded to account for any housing stock if the information is available.

DOMVENT3D, which is a theoretically robust model, has proven to be very useful to predict infiltration rates for more than one building. However, to date no published literature exists showing that the model has been field validated. Field validation could give the model more reliability if proven accurate.

2.4.2 Historical research on air infiltration

Research on air infiltration has taken different paths, such as the creation or validation of infiltration models [Sherman, 2008, Walker and Wilson, 1998], comparisons between infiltration models [Liddament and Allen, 1983, Orme and Leksmono, 2005], prediction of air infiltration in different buildings or stocks [Jones et al., 2013b, Persily et al., 2006] revision of infiltration of buildings [Hayati et al., 2014, Francisco and Palmiter, 1994, Emmerich and Persily, 1998], understanding the

physical phenomena driving air infiltration [Kraniotis et al., 2013, 2014b,a, Kraniotis, 2014], among others. This section presents some of the existing investigations and their results and gives comments and suggestions on different topics for further research.

A study to 170 Finnish houses with different kind of constructions, found that the massive ones (built with concrete, blocks, etc.) present a lower leakage rate than those built with timber or lighter materials. However, the flow exponent b from the power law (Eq. 2.8) was seen to have minor dependence on construction type [Jokisalo et al., 2009]. The most important result obtained by Jokisalo et al. [2009] was the fact that the dependence of infiltration on weather and climate conditions is significant. The more exposed the studied house was, the more significant the effect the wind had on the infiltration. The study also found that during the heating season, when the temperature difference between indoor and outdoor conditions increased, the infiltration rate also increased. These results go hand in hand with the shielding factors introduced by the infiltration models.

A novel (at that time) study by Sherman and Grimsrud [1982] prepared a squared mobile test unit to measure climate conditions (wind speed, wind direction, interior and exterior temperatures) pressure coefficients, and infiltration using tracer gas infiltration measurements. The test unit was named MITU. The unit was also employed to monitor the pressures inside and outside of the mobile unit [Sherman, 1983].

A representative set of 25 office buildings in the U.S. was studied by Emmerich and Persily [1998] to understand the effect of infiltration and airtightness on energy consumption. The study found that high-rise buildings, with 15 or more storeys, tend to be tighter than low-rise buildings. The authors also found that, on average, air infiltration causes 25% of the heating load and 4% of the cooling load in office buildings in the United States. The main factors that make the cooling load less affected by infiltration are first, that the difference between indoor and outdoor temperatures is smaller (than when heating is needed), and second, that the driving forces for infiltration tend to have smaller magnitude during the cooling season [Emmerich and Persily, 1998]. The heating and cooling loads due to infiltration are higher when the building is under depressurised conditions.

Air infiltration also affects historic buildings, as reported in a study that evaluates two single-zone infiltration models. The investigation carried out in three large single zone churches in Sweden found out that for the churches, buoyancy had a stronger impact on the infiltration than wind [Hayati et al., 2014], due to the height of the building. The author remarks on the importance of locating the

Neutral Pressure Level (NPL) to identify the locations where the leakages must occur, and, understand the behaviour of the building. However, the study stated that it is not easy to determine the exact location of the NPL for single-zone large buildings.

Multi-family buildings were tested using a multi-tracer gas constant injection system by Francisco and Palmiter [1994], one gas per unit. The research study found that the bottom floors have more infiltration from outdoor than from other floors, mainly because there was no stack ventilation coming from other floors. On the other hand, the flow between units (floors) was caused by the stack effect mainly [Francisco and Palmiter, 1994]. Studies show that the stack effect is the leading cause of the inter-zonal flows; and, units in the upper floors have a higher amount of air from other units due to the stack effect. In multi-family (multi-zone) buildings, Bohac et al. [2007] proved that every unit could have utterly different leakage and infiltration than other units in the same building. These findings proved that every unit must be analysed as a single space. These results go hand in hand with what Jones et al. [2013b] suggested years later, that a party wall can have a significant impact on the way to predict air infiltration rates.

Most of the research performed was based on the assumption that a "steady" wind was present. Moreover, it is known that for low rise buildings, the wind is the most influencing driving force for infiltration [Shaw, 1981]. Kraniotis [2014] has focused his research on investigating how the gustiness of the wind affects air infiltration. In a low-rise building with known leakage paths and using the tracer gas decay method, the author studied the effect of wind gusts on air infiltration. The results from Kraniotis et al. [2014a] showed that wind direction and wind gusts have great importance on the infiltration of buildings. The authors could not correlate the air change rate with the wind fluctuations; however, they concluded that high wind speed fluctuation frequency has the potential to cause higher air change rates in the enclosure. The authors in another study [Kraniotis et al., 2013] using an exposed building in Norway, analysed the capacity to estimate air infiltration rates with only the wind speed and direction with known air leakage rates. This study encountered that more air leakage rate is found when leakages are equally distributed in the windward and leeward façades. In addition, the authors recommended considering leakages distribution as important factors, especially when wind gusts are present.

2.4.3 Discussion on air infiltration and lessons learnt

During the last 35 years, many infiltration models have been developed; however, not all of them have been used globally. Even when the models evolved from simplified to sophisticated ones that can analyse large amounts of data, the principle behind most of them is the same, and they share similar advantages and disadvantages.

LBL and AIM-2 were developed more than 25 years ago, nevertheless, they are still being used due to the simplicity and relatively good accuracy, even when the usage of superposition techniques has been proved to be physically inaccurate. Both models have been validated on several occasions using tracer gas techniques, and the correlation between the experiments and their prediction has been obtained, which led to their extensive use.

AIDA and DOMVENT are based on different theoretical backgrounds, and they have only been used in the countries where they were created, probably due to lack of experimental validation. CONTAM and other multi-zone models are useful when used at the design stage due to its user-friendly graphical interface. However, a long time is required to model a building before predicting an infiltration rate, even when this calculation is not the main output from CONTAM.

Most infiltration models rely on the power law (Equation 2.8) even when the quadratic form (Equation 2.9) was proven to represent better air infiltration; and, that the extrapolation using C and b (from the power law) to a lower pressure creates uncertainty [Remi Carrie and Leprince, 2016, Cooper and Etheridge, 2007a]. Models that take their input parameters from airtightness measurements obtained using a different technology than the blower door do not exist. The fact that infiltration naturally occurs in the realm of 1-10 Pa, might lead to the conclusion that air leakage measurements taken in this pressure range will theoretically be more accurate. Methods such as the A/C method [Card et al., 1978] or the Pulse technique [Cooper and Etheridge, 2007b, Cooper et al., 2016, Cooper and Etheridge, 2004] measure air leakage at low pressures and could be the basis of new infiltration models. The correlation between airtightness measurements (low pressure) and air infiltration has to be found to create new models or at least to modify the existing ones.

The creation of models that predict infiltration from low-pressure airtightness measurements would reduce the uncertainty of calculating infiltration by avoiding extrapolation (from high to low pressure). This path, however has not been deeply explored. The present investigation aims to explore the possibility of establishing a correlation between the low-pressure measurement and infiltration rate based on

existing models.

Further research guidelines on air infiltration measuring and modelling also include the improvement of infiltration models, including more accurate ways of calculation, e.g. adapting models to run with the quadratic form. There is a need for more understanding of physical phenomena such as wind gustiness [Kraniotis, 2014] or density stratification for high rise buildings [Jones et al., 2013a].

Sherman [2008] analysed Infiltration Standards published by ASHRAE (136 and 62.2). The analysis concluded that a revision must be performed to include new parameters such as the efficiency of ventilation systems. Another study found that in flats or any other attached dwellings, it has to be assumed that the partition walls are (1) fully permeable or (2) impermeable [Jones et al., 2013b]. However, the difference between both is so significant that the infiltration rates can broadly differ from each other; therefore, the standards that assume that there is no permeability between party walls should be revised.

It is considered from reviewing the literature that the impact of infiltration on building cooling demand has not been fully explored but has the potential of reducing energy consumption in some parts of the world. Studies argue that the energy loads due to infiltration are lower for cooling conditions than for heating conditions, due to the smaller indoor-outdoor temperature difference. Nevertheless, this is not necessarily true for all parts of the world, extreme hot climates can have large temperature differentials, and therefore infiltration can contribute significantly to the cooling load in this case. Undertaking studies in extreme (hot) climates is necessary; and, a correlation of infiltration and energy usage of buildings must be conducted in order to fully understand the effect of air infiltration in different climate conditions.

2.5 Chapter conclusions

This chapter discussed the importance of the measurement or prediction of air infiltration in buildings; the energy usage due to infiltration can be as high as 40% in some cases. Research on the topic has been carried out for more than 30 years, and yet there is much to be done. Air infiltration now is more relevant than ever before, as the clash between global energy consumption and climate change is increasing.

Airtightness is the characteristic of a building that impacts the most on air infiltration, therefore measuring it is relevant for air infiltration prediction. The steady pressurisation method has been the standard one for measuring building

airtightness in many nations. However, it has its own shortcomings, which become ever more relevant as the requirement to reduce the energy use of buildings increases. The most significant disadvantage of the steady pressurisation method is that it is required to be performed at an elevated pressure difference considerably away from those pressure differences experienced by buildings in the ambient or natural state. As a result, an extrapolation of the results to low pressures must be done (to relate it to air infiltration), creating significant uncertainties. Furthermore, conditions such as high wind velocities or the measurement of zero-flow pressures will introduce error.

The alternatives to the steady pressurisation method were reviewed. Each has its advantages over the steady pressurisation method but also adds their own disadvantages, which have been compared in this study across a few key aspects. This chapter concluded that the steady pressurisation method has obvious advantages over other methods on leakage detection, maturity of development and degree of acceptance. However, it does have its negative points, which include the inability of fully maintaining building integrity, extensive involvement of manual operation, coarse interpretation of background pressure caused by wind and buoyancy effects, relatively long test cycle and the demand for high testing skills.

Other methods, such as AC method, decay method and Pulse method, offer the solutions to some of the issues shown in the steady pressurisation method, e.g. fully maintaining building integrity, shorter test cycle, realistic pressure range, and potentially de-skilled operation. However, shortcomings do exist in most of them, which include the inability of detecting the leakage and poor accuracy.

Tracer gas techniques are currently the most widely accepted means for measuring air infiltration, due to its direct measurement with reasonably good accuracy. However, due to its invasive and time-consuming nature, these techniques are typically used for scientific research or specialised applications. With a quick measure of building airtightness, an infiltration model could predict the building's infiltration rate; thus avoids performing the invasive tests.

Over the years, several infiltration models, simplified and computer-aided, have been developed including LBL, AIM-2, AIDA, DOMVENT, and the multi-zone model CONTAM, which rely on the measurement of building airtightness such as a pressurization test in a range of high pressures.

Many studies on characterizing buildings in order to standardize a quality construction have been carried out; it is essential to expand these investigations in order to obtain results globally. Finally, new potential research guidelines were presented: 1. New infiltration models based on different assumptions or measure-

ments; 2. The creation of new standards for different places (or climate conditions); 3. The finding of a correlation between air leakage taken at low pressures and air infiltration.

Finally, after the review of the literature, it was concluded that this project would focus on how to avoid extrapolation procedures when measuring airtightness and predicting air infiltration. It is considered that performing airtightness testing at pressures at or closer to the natural pressure differentials experienced by buildings could provide the basis for a more accurate conversion to infiltration rate. The novel Pulse method appears to be an obvious candidate for these low-pressure measurements and the literature shows that infiltration models, which already exist could provide the basis for the required correlations.

Chapter 3

Introduction to the Pulse method and preliminary tests

3.1 Introduction

This research project aims to assess the usage of the Pulse method to predict infiltration rates in buildings. Currently, infiltration models rely on the conventional steady pressurisation method (blower door) to measure airtightness. Even when the measurements include a low-pressure reading, the final low-pressure airtightness has to be the result of an extrapolation. Also as discussed earlier there are other shortcomings of using a increased pressure when measuring airtightness (Chapter 2). Pulse is a low-pressure airtightness testing method.

The Pulse method has been developed by the University of Nottingham [Cooper and Etheridge, 2004, 2007b, Cooper and Zu, 2011, Cooper et al., 2016, Zheng et al., 2018]. Pulse development efforts have led to a UK-wide airtightness testing campaign to provide empirical evidence in support of its potential inclusion in UK building regulations. Furthermore, the method has been put to the test by the University of Nottingham and different laboratories. The main advantage of Pulse is that it measures airtightness at low pressure difference and quotes it at 4 Pa, thus potentially mitigating the error created from a high-to-low pressure extrapolation.

The Pulse technique has gone through various developmental stages for optimisation on the system design, software, practicality, among others. During which, a large number of research studies have been carried out to validate each change made, making sure a sufficient accuracy is retained during the development. Zheng et al. [2019b] made a technically detailed summary of the method and studies carried out. However, to provide a systematic understanding of the method and an

overview of the key performance indexes of the Pulse technique, further studies using the field trial prototype have been carried out and introduced herein alongside some previous investigations. The chapter provides detail of the initial tests performed in this research study, which delivered initial findings that went on to inform later investigations within this work.

3.2 Description of an airtightness test using the Pulse Method

A Pulse test can be divided into three parts:

First, charging of the tank. Pulse can work with 14, 20, 40, 60 or 80 litres tanks, utilizing two tanks is also possible; an air compressor fills the tank until the pressure gauge reaches 10 bar. This stage can take up to ten minutes when using a 60 litres tank and the standard air compressor included with Pulse (See figure 2.10). While the tank is being charged, the building must be prepared, with internal doors open (to make the building a single zone building), external doors and windows closed and vents sealed in accordance with the ISO and ATTMA standards [International Organization for Standardization, 2015, The Air Tightness Testing and Measurements Association, 2016].

Second, the building parameters are input into the Pulse control unit (See figure 2.10). These parameters of envelope area and the building volume are measured typically during the charging stage. The tester initials and the tank size also are entered into the control unit. The tester must then set the type of test; there are two different types: single and step test. A single test consists in releasing one "pulse" (or one "step"), regularly this happens when the tank is fully charged. A step test consists in releasing up to three "pulses", the first one with a fully charged tank, the second and third "steps" with the remaining pressure in the tank. Step tests are useful to cover a broader range of pressure differences in the building. The duration of this part of the test is less than one minute.

The final part of the test procedure is the test launch. The nozzle valve (See figure 2.9) releases the compressed air up to three times; each "step" takes between 4 and 6 seconds, a three-step test has a duration of 14 seconds. The tank is depleted after the last step. If a new test is needed, the tank must be charged again repeating the first and third parts of the procedure. Once the test is finished, results appear in Pulse's screen; however, more information can be obtained from the raw data which can be exported to a USB memory storage.

Each step produces a graph representing the measured pressure difference,

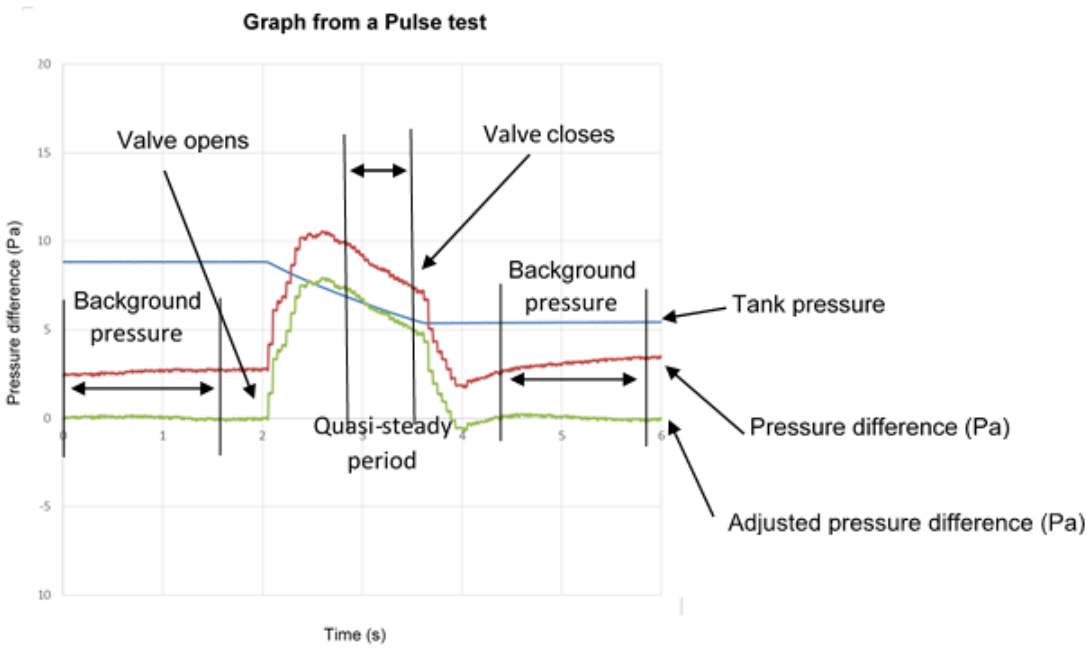


Figure 3.1: Single test Pulse graph

the adjusted pressure difference using the background pressure readings and the pressure drop in the air tank. Figure 3.1 shows an example of how a Pulse graph looks.

Pulse measures the background pressure for a period of two seconds. When the nozzle valve releases compressed air, the pressure in the enclosed space starts to rise and the pressure inside the tank falls. When the indoor pressure reaches to a maximum, it starts decreasing. Importantly air is still flowing from the air tank albeit at a reducing rate, whilst the building pressure is falling. The period when this decrease stabilizes in a linear decline is where the "quasi-steady" period occurs; this period lasts for - circa - half of a second. After this, the valve closes, and no more air enters the building. The building pressure fall quickly to background pressure and this background pressure is measured again over the final two seconds. The background pressure measurements are used to adjust the Pulse pressure, to account for any external factors which affect the natural building pressure over the time period of the test. In a step test, the process is repeated. Each "quasi-steady" period is used to define the airtightness properties of the building by fitting the data using the power law (Equation 2.8)). The power law has been widely used and accepted in academia and industry by scientists and practitioners [Walker and Wilson, 1998]. In order to keep it simple and easy to use, the Pulse technique adopted the power law equation to mathematically represent the leakage-

pressure relationship. However, the equation that fundamentally supports the Pulse principle is the quadratic equation.

The building parameters are used in the delivery of the results. Since different metrics can be used, Pulse gives results in the following metrics:

- Air leakage rate (ALR), or flow, referred in the literature as Q in flow units m^3/s.
- Air permeability, used in UK regulation, $m^3h^{-1}m^{-2}$.
- Air change rate (ACH) used to compare against ventilation, often referred to in the literature as n, in air changes per hour (h^{-1}).
- Effective leakage area (ELA), given in m^2, used to approximate the area of leakage paths in the building envelope.

Figure 3.2 gives an example of how the results fit the power law; the blue dots represent the measured values, each group represents one step, this example shows that the test covered pressure differences between 1 and 19 Pa approximately. Furthermore, the graph includes the best fitting power law.

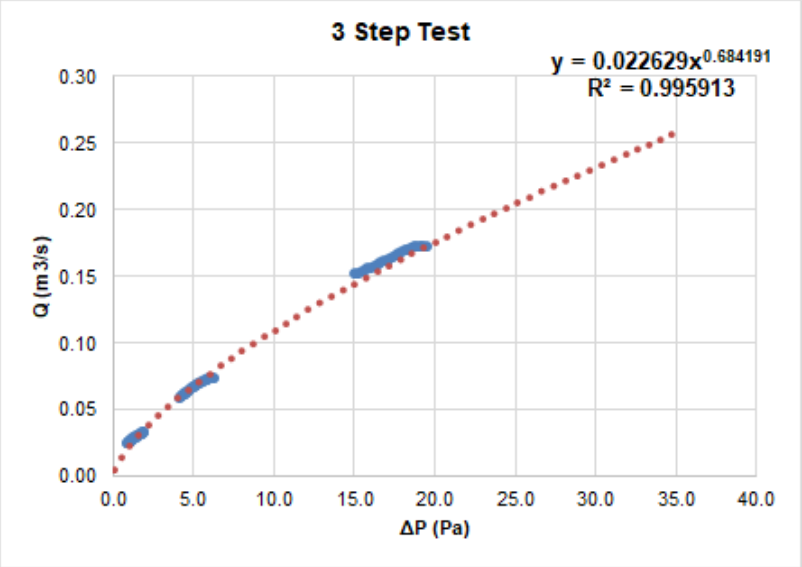


Figure 3.2: Example of a Pulse step test and fitting of Power law

For a test to be considered valid, first, the range of pressures tested must include 4 Pa. Furthermore, one or more steps can be discarded if the r^2 coefficient of the fitting of the power law is less than 0.98 and, the flow exponent (b) is lower than 0.5 or higher than 1. If one step is discarded, the overall result is drawn from the remaining steps.

3.3 Experimental studies on dwellings

The objective of this section is to present a typical example of how Pulse is used in airtightness testing. The dwellings presented in this section were tested using a composite tank version of the Pulse, which is not the same version used in later stages of this project. The Pulse version used had an external pressure reference tank and was not as robust as the version used in the following chapters; nevertheless, the calculation algorithm and result interpretation are the same across all the versions of Pulse used during the completion of this project.

During the days between the 13th of February and the 3rd of March 2017 several Pulse tests were carried out in a house located in the University of Nottingham with different purposes:

1. To determine the air leakage characteristics of the tested house.
2. To revise the accuracy of the Pulse unit during different weather conditions.
3. To test the differences between results using single tests and step tests.
4. To prove the reproducibility of the Pulse technique.

During the 15th and 16th of February 2017, ten repeated tests with the Pulse unit (with composite tank) were carried out. All the tests were step-tests and the tank used was an 80-litre tank (Table 3.1). Prior to the test, building volume and envelope area were measured and as a reference, a steady pressurisation test was also carried out. The testing conditions were according to standard [The Air Tightness Testing and Measurements Association, 2016], which meant, internal doors open, vents closed, external doors and windows closed, among other building preparations.

More single and step tests were carried out during the 24th of February 2017 using both, the 60 and the 80-litre composite tanks. The results were compared between each other and to the reference measurements (taken on the 15th and 16th of February 2017) aiming to test Pulse repeatability.

Table 3.1: Pulse measurements taken the 15th and 16th of February in the test house quoted @4 Pa of pressure difference

Metric @4Pa	**Test**										Average
	1	**2**	**3**	**4**	**5**	**6**	**7**	**8**	**9**	**10**	
Airflow (m^3/s)	0.1028	0.1076	0.1098	0.1066	0.1077	0.0898	0.1054	0.1017	0.1083	0.1055	**0.1045**
Permeability ($m^3h^{-1}m^{-2}$)	1.2768	1.3361	1.3627	1.3239	1.3370	1.1146	1.3080	1.2620	1.3450	1.3097	**1.2976**
ACH (h^{-1})	1.2251	1.3135	1.3396	1.3015	1.3143	1.0957	1.2859	1.2406	1.3222	1.2875	**1.2726**
ELA (m^2)	0.0135	0.0140	0.0142	0.0136	0.0137	0.0118	0.0138	0.0130	0.0138	0.0136	**0.0135**

Table 3.2: Reported airtightness values with their uncertainty quoted @4 Pa of pressure difference

Metric @4Pa	**Reported value**	**Standard error (%)**
Airflow (m^3/s)	0.1045 ± 0.0017	1.64
Permeability ($m^3h^{-1}m^{-2}$)	1.2976 ± 0.0214	1.65
ACH (h^{-1})	1.2726 ± 0.0215	1.69
ELA (m^2)	0.0135 ± 0.0006	1.50

Table 3.3: Deviations from average (%) of measurements taken the 15th and 16th of February in the test house

Metric	**Test**									
	1	**2**	**3**	**4**	**5**	**6**	**7**	**8**	**9**	**10**
Airflow (m^3/s)	1.65	-2.95	-5.05	-1.99	-3.04	14.08	-0.84	2.70	-3.62	-0.94
Permeability ($m^3h^{-1}m^{-2}$)	1.60	-2.97	-5.02	-2.03	-3.04	14.10	-0.80	2.74	-3.65	-0.93
ACH (h^{-1})	1.61	-2.97	-5.02	-2.03	-3.03	14.10	-0.81	2.74	-3.65	-0.93
ELA (m^2)	0.00	-3.70	-5.19	-0.74	-1.48	12.60	-2.22	3.73	-2.22	-0.74

Tables 3.1, 3.2 and 3.3 show the repeatability of the measurements taken on the 15th and 16th of February 2017; most of the tests range between ±5% of deviation from the average (relative percentage difference, RPD). If test 6 is not taken into account, these results become closer to each other and the repeatability of the tests is improved. It appears that test 6 represents an anomaly in these tests.

In order to prove the Pulse technique's accuracy, the measurements must be compared with the ones obtained using the steady pressurisation method (blower door). The leakage-pressure curves obtained in both tests are plotted in Figure 3.3 with a trend line added to the blower door test result. It shows how both methods were overlapped (Pulse in blue dots, steady pressurisation with orange dots and steady depressurisation with black dots), and how high-pressure measurements compare with low-pressure measurements. It is important to mention that for every Pulse step, many data points (pressure difference) are collected, whereas, for the blower door only between five to ten points are measured (seven for Figure 3.3 in pressurisation and eight for depressurisation).

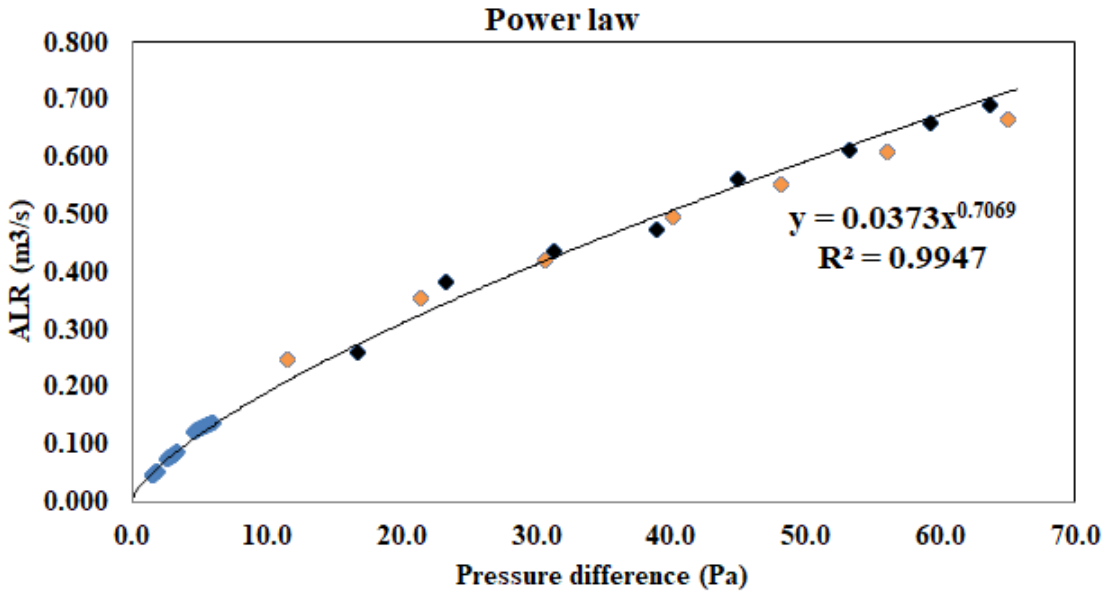


Figure 3.3: Overlapping measurements of the PULSE technique (0-10 Pa) and the blower door (10-70 Pa)

In a different study, on the last days of April 2017, airtightness tests were performed in two new-built dwellings in the Trent Basin development in Nottingham, UK. The Trent Basin project is a low-energy development located in Nottingham that comprises more than 40 dwellings. The tested houses were new build (2017-

2018) with the intention to have an improved airtightness compared to those built in the previous century.

The first property had 301 m^2 of envelope area and 309 m^3 of volume, whereas the second had 333 m^2 and 351 m^3 for both properties. The Pulse unit utilised was the 80-litre Pulse with composite tank. A summary of the results of the airtightness tests is shown in Table 3.4. It is clear that due to similar design and construction, both properties have similar airtightness characteristics.

Table 3.4: Airtightness measurements quoted @4 Pa of pressure difference in new-built dwellings in Nottingham, UK.

Test house	**Metric @4Pa**	**Test**			**Average**
		1	**2**	**3**	
1	Airflow (m^3/s)	0.1050	0.1079	0.1189	0.1106
	Permeability ($m^3h^{-1}m^{-2}$)	1.2556	1.2904	1.4224	1.3228
	ACH (h^{-1})	1.2231	1.2570	1.3856	1.2885
	ELA (m^2)	0.0159	0.0166	0.0192	0.0172
2	Airflow (m^3/s)	0.1106	0.1016		0.1061
	Permeability ($m^3h^{-1}m^{-2}$)	1.1954	1.0983		101469
	ACH (h^{-1})	1.1341	1.0420		1.0880
	ELA (m^2)	0.0173	0.0154		0.0163

To give a better insight of the results, Table 3.5 gives the reported value and the calculated standard error; due to the statistical nature of this, more measurements would reduce the uncertainty in the reported value which is the average plus (or minus) the standard error. Moreover, the difference from the average of the tests is presented in Table 3.6. As before, the results do not differ much, except from one test. This anomaly is probably due to a malfunction of the reference tank.

Table 3.5: Reported airtightness values quoted @4 Pa of pressure difference with their uncertainty in new-built dwellings in Nottingham, UK.

Test house	**Metric @4Pa**	**Reported value**	**Standard error (%)**
1	Airflow (m^3/s)	0.1106 ± 0.0035	3.14
	Permeability ($m^3h^{-1}m^{-2}$)	1.3228 ± 0.0415	3.14
	ACH (h^{-1})	1.2885 ± 0.0404	3.14
	ELA (m^2)	0.0172 ± 0.0014	4.71
2	m^3/s	0.1061 ± 0.0032	2.99
	Permeability ($m^3h^{-1}m^{-2}$)	1.1469 ± 0.0343	2.99
	ACH (h^{-1})	1.0880 ± 0.0326	2.99
	ELA (m^2)	0.0163 ± 0.0007	4.00

Table 3.6: Deviations from average (%) of airtightness measurements in new-built dwellings in Nottingham, UK.

Test house	**Metric**	**Test**		
		1	**2**	**3**
1	Airflow (m^3/s)	5.08	2.45	-7.53
	Permeability ($m^3h^{-1}m^{-2}$)	5.08	2.45	-7.53
	ACH (h^{-1})	5.08	2.45	-7.53
	ELA (m^2)	7.71	3.59	-11.30
2	Airflow (m^3/s)	-4.23	4.23	
	Permeability ($m^3h^{-1}m^{-2}$)	-4.23	4.23	
	ACH (h^{-1})	-4.23	4.23	
	ELA (m^2)	-5.66	5.66	

A simple conclusion is that for more accurate results, the tester must perform as many Pulse tests as possible; nevertheless, this will eliminate the advantage of Pulse's quick test. Several tests, similar to the ones presented in this section, were carried out in several properties; these tests were performed with the current version (at that time) of the Pulse. The major conclusions were as follows:

- The Pulse test is quick to perform and easy to understand. A successful training on airtightness testing was achieved.
- The reproducibility of the test seems to be the highest point of uncertainty. Tests that produce a statistically different result (compared to a different method) could happen at any time.

- A step test seems to be more accurate when two or more steps are valid. The higher the pressure range covered, the more accurate the results can be.
- The selection of tank is essential, for example a large tank for large or leaky houses. A tank which does not contain a high enough volume of air would result in the pressure range not covering 4 Pa. Conversely, for a very tight house, using a fully pressured large tank can result in the pressure elevation being to high leading to results far above 4 Pa.

3.4 Experimental studies on small enclosures

With the purpose of reducing heat losses, tighter buildings have been built in the recent times. The German standard Passivhaus requires a maximum airtightness level of $0.6h^{-1}$ at 50 Pa. Prior to this work it was unknown how Pulse would operate in such a tight environment, which can also be found in some laboratories or clean rooms.

The University of Nottingham built two small buildings, with a volume of less than 22 m^3. Each one has a different airtightness level: first, a standard construction one, and, second, a Passivhaus one. These small buildings are called "pods" and can be seen in Figure 3.4. It is clear from the pictures that doors are different; with the Passivhaus pod having a heavier more tightly sealed wooden construction, whereas the standard one has a regular UPVC house door. Furthermore, the characteristics of the pods are given in Table 3.7.



Figure 3.4: Test pods, left: Passivhaus pod (pod 2), right: a standard pod (pod 1)

Table 3.7: Envelope area and volume of the test pods

	1:Standard pod	**2:Passivhaus pod**
Volume (m^3)	21	22
Envelope area (m^2)	47	48
Approximate ACH @ 50 Pa (h^{-1})	6	1.65

As mentioned before, small and tight buildings airtightness is difficult to measure using a large-tank Pulse unit. Therefore, a twenty-litre tank was selected for this experiment (Figure 3.5). The Pulse airtightness test was carried out with the objectives of: testing Pulse in airtight environments, comparing the usage of a small tank (to a large tank), evaluating the pressure range that can be achieved by Pulse in tight environments, and testing the airtightness difference between the standard and the Passivhaus pod.



Figure 3.5: Pulse unit, with a 20-litre tank

As part of the test, steady pressurisation tests were also carried out. The advantages and disadvantages of each method were mentioned in chapter 2, and, as discussed, the blower door modifies the building envelope, which in the situation of the small pods could potentially contribute to a high proportion of the overall leakage. Figure 3.6 depicts that when the blower door is in place, there are gaps between the blower door frame and the POD door's frame.



Figure 3.6: Unsealed condition of the Passivhaus pod when the blower door is in place.

In order to provide comparable scenarios, each door was sealed; in consequence, the buildings were immediately tighter than before. The airtightness results are given in Table 3.8.

Table 3.8: Airtightness of the test pods, and relative percentage difference (RPD) between sealed and unsealed scenarios

	1:Standard pod			**2:Passivhaus pod**		
	Sealed	Unsealed	RPD	Sealed	Unsealed	RPD
Airflow (m^3/s)	0.006	0.007	14%	0.002	0.002	12%
n_4 (h^{-1})	0.986	1.146	14%	0.276	0.312	12%

The findings are:

- Pulse can perform well in very tight environments using a small tank i.e. Pulse pressure profiles were produced, which provided a quasi-steady period for analysis.
- By sealing the doors, the airtightness was affected; therefore, a blower door frame must also affect the airtightness level of a building.
- Pulse can cover up to 50 Pa of pressure difference; however, this is out of the scope of this project.

Table 3.9: Equipment uncertainty given by manufacturer

Variable	Uncertainty	Unit
$P(t)$	$0.035\% \pm 50$	Pa
P_0	$0.035\% \pm 50$	Pa
T_0	$0.5\% \pm 0.2$	K
V'	± 0.4	litres

- Airtightness differed by a factor of four from one pod to the other.

These tests were part of a more extensive study of comparing airtightness measurement techniques in airtight scenarios, which does not form part of this particular research study. All the results are included in Wood et al. [2018], including the ones mentioned in this section.

3.5 Instrumentation uncertainties in Pulse

Despite many tests carried out in different places, the manufacturers of the Pulse unit used had not reported a value of instrumentation uncertainty. The only information related to inaccuracy of measurement was the reproducibility of the tests and, not the uncertainty created by the equipment used within the Pulse. The following points relating to uncertainty are directly related to the algorithm in the Pulse method.

3.5.1 Process of calculation of instrumentation uncertainty for the Pulse method

An analysis of typical Pulse test results was carried out based on the Pulses' algorithm, the propagation of error theory and the calculation of uncertainty. The following uncertainty analysis is based upon the work of Hughes and Hase [2010] (Chapter 4). For the propagation of error, one needs to start with the first equation in the algorithm for the Pulse, which calculates the mass flow rate of released compressed air.

$$\dot{m}_p(t) = -\frac{V'}{\gamma R T_0}\left[\frac{P(t)}{P_0}\right]^{\frac{1-\gamma}{\gamma}} \dot{P}(t) \tag{3.1}$$

Equation 3.1 presents four variables which uncertainties have to be considered; Table 3.9 presents the accuracy of the equipment used to measure those variables.

The uncertainty for the mass flow rate is calculated using Equation 3.2

$$\begin{aligned}[\alpha_m p]^2 = [\dot{m}(P+\alpha_p, P_0, T_0, V') - \dot{m}_p(P, P_0, T_0, V')]^2 \\ +[\dot{m}(P, P_0+\alpha_{P0}, T_0, V') - \dot{m}_p(P, P_0, T_0, V')]^2 \\ +[\dot{m}(P+, P_0, T_0+\alpha_{T0}, V') - \dot{m}_p(P, P_0, T_0, V')]^2 \\ +[\dot{m}(P, P_0, T_0, V'+\alpha_{V'}) - \dot{m}_p(P, P_0, T_0, V')]^2\end{aligned} \tag{3.2}$$

The Greek letter α represents the accuracy (or uncertainty) of the measurement equipment or variable. $\dot{m}_p$ is the mass flow rate of released compressed air (kgs), V' is the volume of the tank (m^3), P is the transit tank air pressure (Pa). P_0 (Pa) and T_0 (K) are the initial pressure and temperature of the tank air before every test launched. After obtaining the uncertainty for the mass flow rate, the next equation to calculate its uncertainty is:

$$Q_p(t) = \frac{\dot{m}_p(t)}{\rho_i} \tag{3.3}$$

For Equation 3.3 the only variable which uncertainty must be considered is the mass flow rate (which was obtained in the previous step). The uncertainty in the volumetric flow rate (Q_p) is calculated using Equation 3.4.

$$\alpha_{Qp} = Q_p(\dot{m}_p + \alpha_{mp'}) - Q_p(\dot{m}_p) \tag{3.4}$$

Finally,

$$q\{t\} = Q_p\{t\} - \frac{V}{\gamma P_i}\frac{dp_i}{dt} \tag{3.5}$$

P_i is measured using an LDE sensor with reported accuracy of $0.075\%+0.06Pa$. Equation 3.5 is multivariable, the uncertainties in P_i and Q_p must be considered. Equation 3.6 is the last step to calculate the uncertainty in q.

$$[\alpha_q]^2 = [q(Q_p+\alpha_{Qp}, P_i) - q(Q_p, P_i)]^2 + [q(Q_p, P_i+\alpha_{Pi}) - q(Q_p, P_i)]^2 \tag{3.6}$$

Equations 3.5 and 3.6 assume that the volume of the building does not add a new uncertainty in the calculation.

The outcome of this process is that two different uncertainty values are obtained: one at the start of the quasi-steady period and one at the end of it. If the Pulse is launched three times in a step-test, six different uncertainties are estimated. From these six uncertainties, a spectrum can be obtained. It is important to remark that these calculations require real or simulated data to produce a value for the error in the measurement. If enough data is statistically analysed, a value for

Pulse's uncertainty could be obtained, a case to study exercise is carried out and explained in section 1.5.1.2.

3.5.1.1 Assumptions and considerations

The analysis made assumes that the following measurements do not add further uncertainties:

- Measurement of the building volume.
- Calculation of density of room air from temperature measurements.
- Usage of absolute pressure, atmospheric pressure is assumed as $101325Pa$, since it is not currently measured within Pulse, it is considered as a constant. Pulse assumes this atmospheric value in its algorithm.

A final assumption is that the tank air temperature (T_0) is the same as the room air temperature, and the uncertainty used is the one quoted earlier in this section. It is relevant to remark that this analysis is for the calculation of uncertainty created by the propagation of instrumentation error. In other words, the parameters adding to the uncertainty are those that are measured. The uncertainty from each equipment is known and provided by the manufacturer, or from calibration. This analysis does not include induced error due to human error, accuracy or repeatability of the tests, which are expected to be higher than the instrumentation uncertainty. The human error in the Pulse technique has been considered to be low; as explained, only input of the measurement of the building parameters and connections have human involvement and, as mentioned, it is assumed that those parameters do not add further uncertainty in this study. Additionally, it is difficult con quantify the uncertainty due to human error but it is considered to be lower than other types of error such as model or precision errors [Zheng et al., 2019b, Cooper and Etheridge, 2007b]. It is also believed that this human error uncertainty can be disregarded due to low human involvement, nevertheless this has not been scientifically proven yet.

3.5.1.2 Results obtained by case studies for uncertainty analysis

In order to illustrate the magnitude and variation of instrumentation uncertainty, analysis has been performed on results from five different properties. The tested properties are all located at the Building Research Establishment (BRE) facilities. The tests were carried out as part of an airtightness testing campaign by the developers of the Pulse method. The houses were designed to work energy efficiently;

currently, they function as showrooms for construction methods and materials. A brief description of the building characteristics is given in Table 3.10.

Table 3.10: Number of tests in BRE properties

Property	**Envelope area** m^2	**Volume** m^3	**Main feature**
Prince's house	287	290	Energy efficiency
Renewables house	236	243	Low carbon materials
Trillium home	279	292	Airtight
Userhuus	237	232	Factory produced
Zero bill's home	291	311	Super insulated

Each test was a three-step test; for the analysis, two points were considered in every step: the beginning and end of the quasi-steady period. Which equates to a total of 114 cases from which uncertainty can be obtained (Table 3.11).

Table 3.11: Number of tests in BRE properties

Property	**Number of tests**
Prince's house	4
Renewables house	3
Trillium home	4
Userhuus	4
Zero bill's house	4

3.5.1.3 Instrumentation uncertainty results

Figure 3.7 depicts a histogram of the uncertainties calculated for all the 114 cases. It is important to remark that all the cases from which the extreme results are obtained came from one single property (zero bill's house).

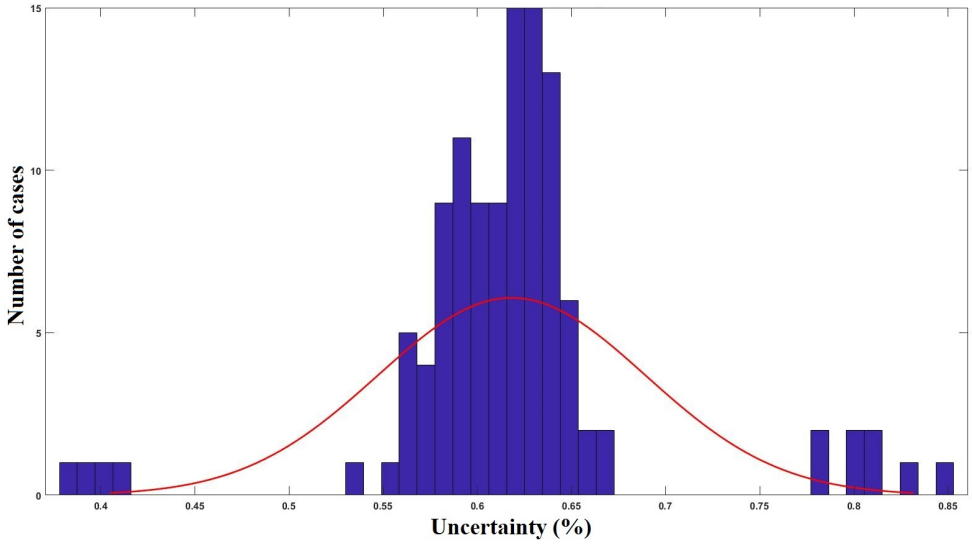


Figure 3.7: Histogram of frequencies of instrumentation uncertainties in BRE houses

In addition, the statistical data is included in (table 3.12).

Table 3.12: Calculation of Pulse uncertainty: Statistical information from BRE houses

Average	0.618%
Maximum	0.849%
Standard deviation	0.071%
Number of tests	114
Standard error	0.007%

From the results, it can be concluded that the Pulse's maximum instrumentation uncertainty can be quoted as ±0.6248%. Instrumentation uncertainty is small due to the high accuracy of the equipment utilised in the Pulse, furthermore, using absolute pressure as part of the calculation and assuming the atmospheric pressure as constant produce minimal uncertainties.

3.6 Chapter conclusions

From the tests carried out, the validity and analysis of tests were studied and, the advantages and disadvantages of different airtightness testing methods were experienced from first hand. After the first airtightness tests, it was ascertained

that the airtightness tests can vary depending on house type, construction type, leaks, and also on the tester preparation.

The blower door method is well positioned; nevertheless, there is new technology available. The Pulse method was used for a number of occasions and several advantages and shortcomings were found, addressing these would lead to a quicker development of the technology.

A Pulse test was defined in three parts: tank charging, input of building parameters, and test launch. In terms of practicality of the Pulse test, the most time taking part is to fill the tank using an air compressor. The tests can be carried out using the same building preparations as for the steady pressurisation test. Results, once knowing their meaning, are easy to analyse. The most significant advantage found was that building integrity is maintained. Furthermore, instrumentation uncertainty is maintained low. Despite the previous comments, Pulse has its shortcomings. If a step test is performed, when analysing results, the validity of each step has to be determined. The reproducibility was proved to be good, but, it brings the most considerable uncertainty to the test; this one shadows other uncertainties.

More robust units that are not affected by the outdoor wind can be constructed. Inclusion of an automated step by step validity analysis can be considered in the algorithm to improve the accuracy and reproducibility of the test.

During this project, many tests with the Pulse unit were carried out in different buildings. The uncertainties and repeatability of the method were put to the test. A step test proved to be the best way to conduct a Pulse test; however, the disadvantage is that sometimes is difficult to determine which steps are valid within the full test [Vega Pasos et al., 2018a]. Zheng et al. [2018] and Wood et al. [2018] reported the latest developments of Pulse where the technology was tested in different scenarios. Initial tests showed that in the same building the method had a deviation from the average lower than 5% in most tests, hence an acceptable repeatability was obtained. The instrumentation uncertainty turned to be $\pm 0.6248\%$, which is small compared to its repeatability error.

When tested in small and airtight enclosures, it was found that Pulse can perform well using a 20 litre (small) tank. It was seen that when using a blower door frame in a tight environment the airtightness is affected considerably. And airtightness differed by a factor of four from one small building (pod) to a similar one; therefore, construction matters. Results were compared to the blower door ones and agreed. It was also seen that Pulse measurements can reach 50 Pa of pressure difference in these environments.

Finally, it is relevant to take into account that when the tests presented in this chapter were carried out, a different Pulse model was available. With the newer version, many shortcomings have been addressed (such as the robustness of the equipment and method). Therefore, it can be concluded that there is potential for the method to be developed towards the inclusion in energy legislation.

The steady pressurisation method has to be used as a guideline or benchmark due to its acceptance and development. However, the Pulse method shows good potential to be compared with the blower door. Therefore, including Pulse's results into the existing building infiltration models is a task that could lead to a more accurate prediction of building heat losses. It is important also to compare field infiltration measurements (tracer gas), with predicted results using modified (using measurements at 4 Pa) infiltration models. It is also concluded that the Pulse method is a suitable technology to measure airtightness at low pressure difference and quote it at 4 Pa due to its accuracy (acceptable repeatability and reproducibility) and low uncertainty. For this reason, Pulse will be used to develop this research project to calculate infiltration rates from its airtightness measurements. The following chapters will discuss comparisons between the steady pressurisation method and Pulse. In addition, Pulse will be the basis for calibrating infiltration models, in order to predict air infiltration from its measurements.

Chapter 4

Case study on the investigation of the impact of airtightness and environmental conditions on air infiltration

Part of the work covered in this chapter was previously presented as a short and long presentation at the Air Infiltration and Ventilation Centre conference 2018, and at the Sustainable Energy Technologies international conference 2019 in:

A. Vega Pasos, X. Zheng, V. Sougkakis, M. Gillott, J. Meulemans, O. Samin, F. Alzetto, L. Smith, S. Jackson, and C. Wood. Experimental investigation of the impact of environmental conditions on the measurement of building infiltration, and its correlation with airtightness. In *39th AIVC Conference Proceedings*, Juan-les-Pins/Antibes, France, 2018a

A. Vega Pasos, X. Zheng, V. Sougkakis, M. Gillott, J. Meulemans, O. Samin, F. Alzetto, L. Smith, S. Jackson, and C. Wood. Experimental study on the measurement of building infiltration and air leakage rates (at 4 and 50 pa) by means of tracer gas, blower door and the novel pulse technique in a detached uk home. In *39th AIVC Conference Proceedings*, Juan-les-Pins/Antibes, France, 2018b

A. Vega Pasos, X. Zheng, M. Gillott, and C. Wood. Experimental study on the pressure differential at which building air leakage should be measured. In *SET (Sustainable Energy Technlogies) 2019 Conference Proceedings*, Kuala Lumpur, Malaysia, 2019a

4.1 Introduction

Air Infiltration Rate (AIR) is fundamentally determined by the building's airtightness [Sherman and Grimsrud, 1980] and is driven by wind and stack effects [Kraniotis et al., 2014b,a]. Other factors such as external terrain, leakage distribution and sheltering factor affect air infiltration. Different countries have different ways to account for the infiltration heat losses, but as a first step, airtightness has to be understood. For instance, in the United Kingdom, infiltration heat losses are calculated after estimating the air infiltration rate from an airtightness measurement [Building Research Establishment, 2013].

AIR is measured through tracer gas tests, [International Organization for Standardization, 2017, Liddament, 1996]. The method to measure AIR with the highest accuracy is the constant concentration method; however, the decay method has been widely used due to its advantages of being low cost and quick-to-perform [Sherman, 1998]. The steady pressurization method (commonly known as "blower door") is the most used method for measuring airtightness [Energy Conservatory, 2017]. Alternatively, a novel method called the Pulse technique measures airtightness at low pressures [Cooper et al., 2014, Cooper and Etheridge, 2007a, Cooper et al., 2016].

Few studies have experimentally looked into how environmental conditions affect the infiltration rate by monitoring pressure distribution across a building. Given the above, a different insight on how wind and buoyancy effects impact the infiltration can be gained by the monitoring of pressure difference across the building envelope.

The way that the UK government predicts the air infiltration rate is from Equation 4.1, where the air permeability at 50 Pa, measured by the blower door is divided by 20. The usage of this rule –the divide-by-20 rule of thumb– has been questioned by different authors due to its crudeness [Keig et al., 2016, Jones et al., 2016]. Furthermore, in the UK's standard, heat losses are calculated as a third of the infiltration rate multiplied by the dwelling's volume [Building Research Establishment, 2013].

$$\frac{q_{50}}{n_1} = N \tag{4.1}$$

Where:

q_{50} = air permeability at 50 pa ($m^3h^{-1}m^{-2}$);

n_1 = air infiltration rate (h^{-1}); and,

N = ratio constant.

This chapter has an aim of establishing a simple correlation between the Pulse test result and the actual air infiltration rate (AIR) of a building. This does not suggest that such a simple correlation like the divide-by-20 rule is the most appropriate method of providing AIR for the purpose of building energy loss calculations. However, the experimental work performed here does provide an initial basis for comparative work against the standard method and also for providing an insight to the environmental effects which impact upon AIR. Infiltration measurements are performed by tracer gas tests. Airtightness testing is also performed by the steady pressurisation method. The simple ratio approach is assessed on the energy performance assessment of the test building for both the steady state and the Pulse technique. The effect of the environmental conditions on the AIR is also assessed.

4.2 Chapter methodology

Testing was performed during January and February 2018, in a two storey house situated on the University Park, Nottingham. A number of different airtightness and air infiltration tests were carried out during this period. The environmental conditions and the pressure fields were monitored continuously. In summary, four different measurements were performed during this study:

1. Air infiltration rate using tracer gas methods.
2. Outdoor-indoor pressure difference on different sides of the building envelope.
3. The dwelling's airtightness, using blower door and the pulse technique.
4. Environmental conditions including wind, outdoor and indoor temperatures.

The air infiltration tests are the basis of the study; parameters such as wind and internal/external temperature were measured yo investigate the impact of changes in infiltration rate due to their variation. Moreover, the pressure difference measurements served to study how pressure fields are affected by the changes in environmental conditions. It is essential to mention that Pulse and blower door measure the outdoor-indoor pressure difference, hence why pressure fields can be used to correlate with changes in the weather conditions. These measured pressure fields can provide insights on a new way of measuring wind and temperature, as an effect of a pressure change, rather than measuring them directly.

4.2.1 Test house and setup

The test house is a two-storey house located on the University Park campus in the University of Nottingham, Nottingham, United Kingdom. It is located in a suburban terrain with six other houses on top of a hill and blocked by a barrier of trees at a distance of 30m away due south, 5m from the house on the east and west there are two other detached houses with a road on the North (Figure 4.1). The building has light local shielding as defined by [Walker and Wilson, 1990].

The conditioned space of the house has an envelope area of approximately 290 m^2 and a volume of 285 m^3. In this investigation both constant concentration and concentration decay tracer gas methods were used. For the tracer gas tests, six zones were defined within the house;, each zone had a tracer gas dosing tube, a CO_2 measuring tube and a CO_2 sensor. Fan heaters were employed to vary the house internal temperature. Zones 1, 2, 3 and 4 were on the first floor while zones 5 and 6 were on the ground floor. Figure 4.2 depicts the south façade of the test house and Figure 4.3 shows the floorplans of the house and the location of dosers and samplers for the tracer gas analysis.



Figure 4.1: Location of the test house.



Figure 4.2: South façade of the test house

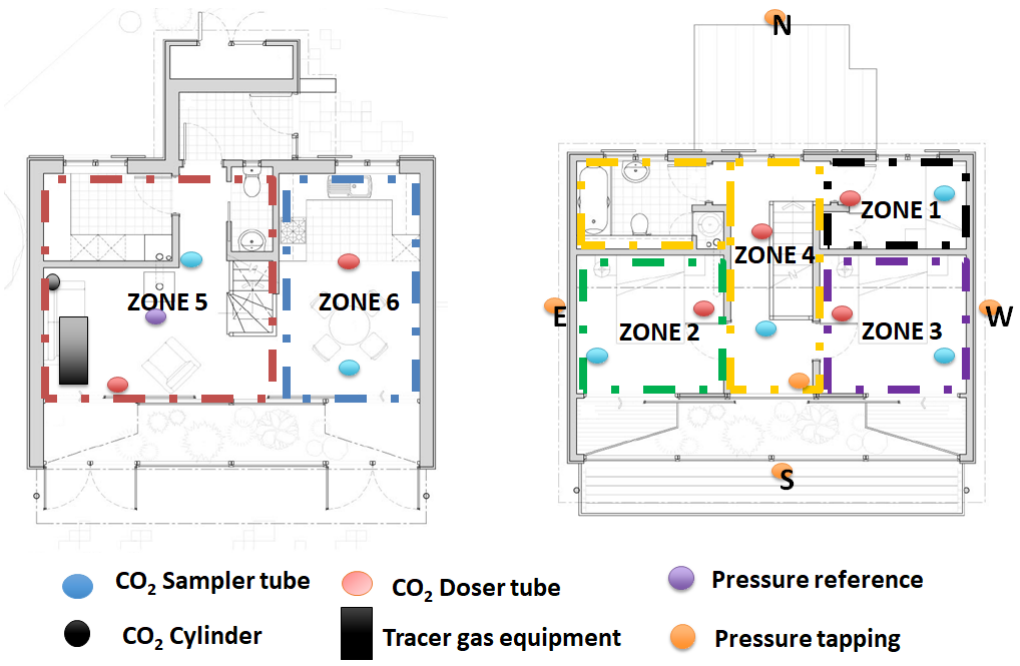


Figure 4.3: Floorplans of the test house and location of testing devices, left: ground floor; right: first floor.

4.2.2 Equipment

AIR is measured using tracer gas methods; this study employed both the concentration decay and constant concentration as per the ASTM E741-11 and ISO ISO 12569:2017 standards [International Organization for Standardization, 2017, American Society for Testing and Materials, 2011, Sherman, 1998]. The concentration decay method has the advantage of being less costly and quicker to perform; however, the constant concentration method is considered to be the most accurate tracer gas method [Sherman, 1989] and is able to deliver real-time AIR results, i.e. AIR variations with environmental influences such as wind gusts can be observed. However, constant concentration methods require highly specialised dosing and sampling equipment and the setup arrangement is more complex. The equipment used in this study is described in Table 4.1. The tracer gas used for testing was carbon dioxide (CO_2). Furthermore, the equipment used automatically revises the concentration of the carbon dioxide to always maintain uniformity of concentration between zones as required by the standards; this uniformity was maintained $\pm 5\%$ from the average concentration and checked through the analysis.

Table 4.1: Equipment utilised in the experimental study in the test house.

Airtightness	Pulse Mark 2.1 (PULSE-60)	
	TEC Blower door model 4. (BD-4)	
Tracer Gas	Gas	Carbon Dioxide
	Gas measuring	INNOVA 1412i gas analyser
		0 to 5000 ppm (±3%) TinyTag CO_2 logger
	Gas sampling/dosing	LumaSense 1303 multipoint gas sampler and doser
Other	Fan heaters	
	Wind Speed low inertia cup and wind vane WSD1 (2% accuracy)	
	±20 Pa Differential pressure transducers FCO-44 (¡1% accuracy)	
	Temperature sensors PT100 RTD	

For the purpose of measuring pressure differentials across the exterior of the building, four differential pressure transducers (FCO-44) with tappings were distributed on the exterior of test house; one on each façade. The transducers were located in the porch area of the building and the tappings consisted of lengths of polyethylene tubing, which ran along the perimeter of the house. Note that the porch are is a single storey construction, which does not form part of the tested envelope in this study. The tubing was secured by taping to prevent flexing of the tube which could cause erroneous pressure readings. The end of the tube tapping was positioned such that the opening of the tube was facing downwards and not in the direction of any incident wind against the façade. A fifth pressure transducer with tapping was located at the highest-indoor point in the house. All the differential pressure transducers were connected to the same reference located in the centre of the ground floor of the house. Finally, the FCO-44 transducers were connected to a data logger, which was recording every second during several days of testing. Figure 4.4 shows a schematic of the FCO-44 that were used in the experiment, Figure 4.5 shows a photo of the FCO-44, Figure 4.6 shows how the tubing was placed and secured in the south façade of the building and; Figure 4.7 shows the tracer gas equipment. The FCO-44 measured differential pressure between the outdoor and indoor environment, i.e. when wind hits one side of the building a change in pressure difference is expect on the building, mainly on the façade where the wind impacted originally. Furthermore, this measurement can be compared with theoretically calculated dynamic pressure forced by the wind; however, the dynamic pressure is a function based on the fluid velocity (wind speed in this case), and therefore will present similar results if only wind speed is compared against pressure.

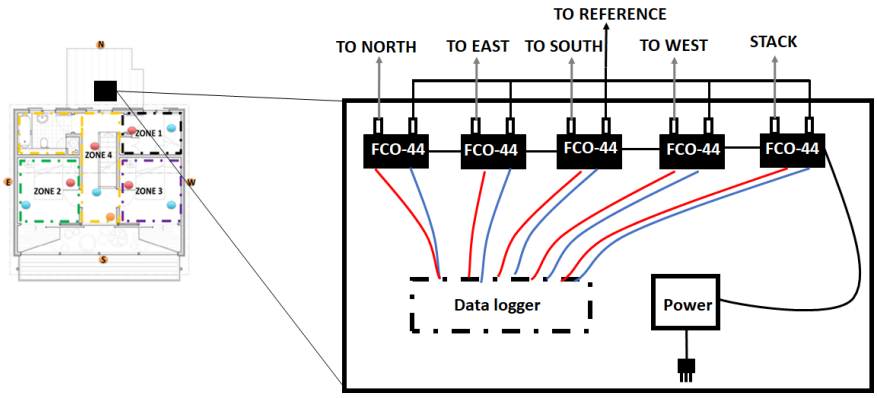


Figure 4.4: Schematic of the differential pressure transducers FCO-44 used in the tests.

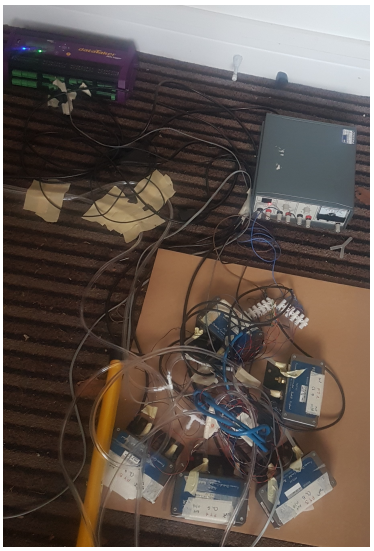


Figure 4.5: Differential pressure transducers FCO-44 used in the tests, with data logger.

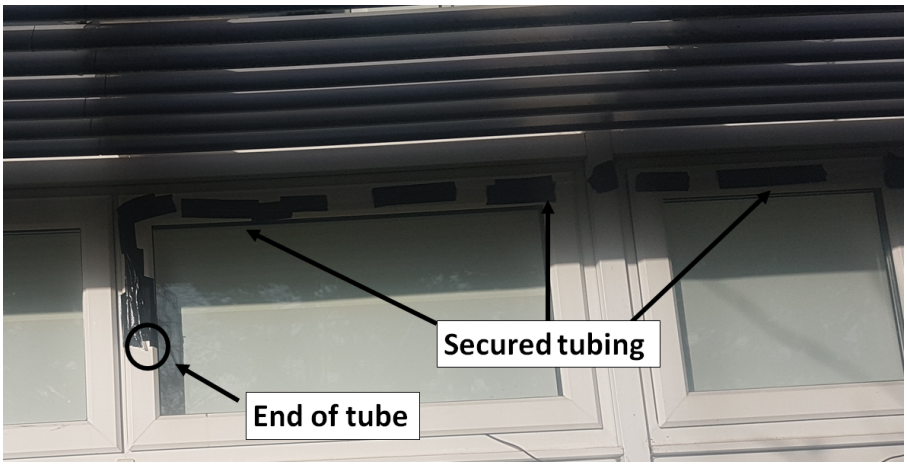


Figure 4.6: Tube in the south façade of the test dwelling.

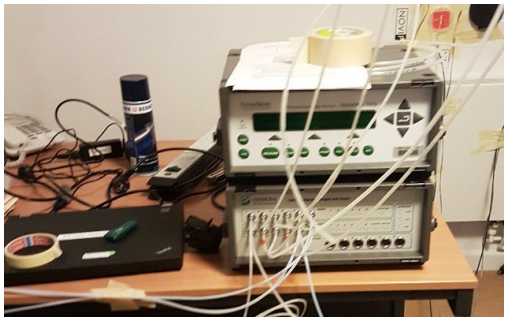


Figure 4.7: Tracer gas equipment, gas analyser, 6 channel multiplexer and, data acquisition computer.

Airtightness testing was carried out at various testing points using both the blower door and Pulse techniques. The blower door and Pulse unit models can be seen in Table 4.1 and the equipment photo can be seen in Figures 2.3 and 2.9 from Chapter 2.

An anemometer and an outdoor temperature sensor took readings every second; both were installed in the rooftop of a neighbouring house 10m away from the test house (Figure 4.1). Furthermore, ten different indoor temperature sensors were placed at locations throughout the house (Figure4.8). These sensors were connected to a data logger that was logging every minute. This study aimed to simulate different occupation scenarios; therefore, the indoor temperature was adjusted using fan heaters. Table 4.2 shows the heating schedule defined for the tests.

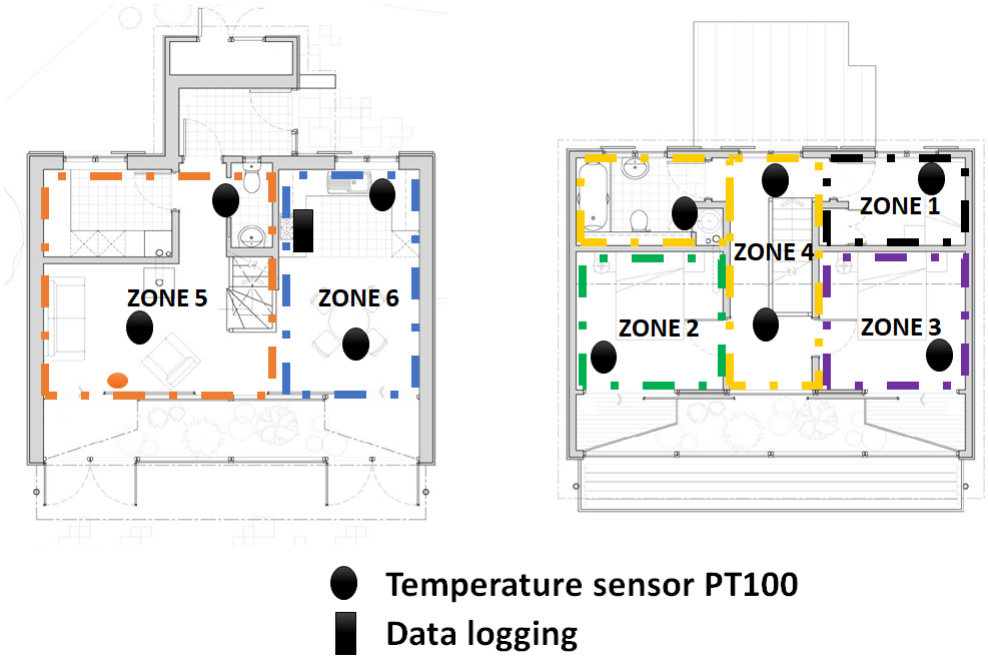


Figure 4.8: Location of indoor temperature sensors PT100.

4.2.3 Testing arrangement

The testing ran for a period of two months where within that time period a number of separate tests were performed. Internal temperature variation was one of the parameters investigated, to assess its impact upon AIR. Table 4.2 shows different tracer gas tests' performed across the testing period and how the heating conditions fluctuated in the tests. All the tests were performed in the wintertime of 2018. Therefore, an increase in indoor temperature would create a high temperature difference against the external temperature. At the end of each constant concentration test, the CO_2 was allowed to decay, providing the decay test results. Steady pressurisation and depressurisation blower door tests were performed before and after every tracer gas period. Blower door could not be performed on a daily basis as this would inevitably have had the consequence of removing the CO_2 from the building. However, as Pulse requires no large volumetric air floes, Pulse could be performed daily. At least three Pulse tests were conducted every weekday (Monday to Friday).

Table 4.2: Distribution of tracer gas tests and heating conditions.

Test	Dates	Tracer gas test	Heating conditions	Duration
1	18–23 Jan	Constant Concentration for 110 hours + decay method for 8 hours	Heating from 5 pm to 12 am	5 days
2	23-26 Jan	Constant concentration for 61 hours + decay method 5 hours (7am to 12 pm)	Heating from 5 pm to 12 am	3 days
3	26-29 Jan	Constant concentration from 3 pm to 7 am and decay method from 7 am to 3 pm	Heating from 5 pm to 12 am	3.5 days
4	29 Jan – 02 Feb	Constant concentration for 80 hours + decay method for 8 hours	Heating from 5 pm to 12 am	4 days
5	02-05 Feb	Constant concentration from 2 am to 6 pm and decay method from 6 pm to 2 am	Heating from 6 pm to 12.00 am	3 days
6	05-09 Feb	Constant concentration for 86 hours + decay method 7 hours	Constant temperature 23°C	4 days
7	09-12 Feb	Constant concentration from 4 pm to 6 am + decay method from 6 am to 4 pm	Constant temperature 23°C	3 days
8	12-16 Feb	Constant concentration for 85 hours + decay method 5 hours (7am to 12 pm)	No heating, allowing heat losses	4 days
9	16-19 Feb	Constant concentration from 3 pm to 7 am and decay method from 7 am to 3 pm	No heating, allowing heat losses	3 days
10	19-22 Feb	Constant concentration from 8 am to 12 am and decay method from 12 am to 8 am	Heating from 5 pm to 12 am	3 days
11	23-28 Feb	Constant concentration for 131 hours + decay method for 9 hours	Heating from 5 pm to 12 am	6 days
12	28 Feb – 01 Mar	Decay method for 24 hours	Heating from 5 pm to 12 am	1 days

4.3 Results

4.3.1 Airtightness measurements

Table 4.3 lists air permeability measurement values using both blower door and PULSE-60 with average weather conditions. In blower door's case, both pressurisation and depressurisation tests were carried out, an average figure is presented. All tests were carried out according to standard [International Organization for Standardization, 2015].

Table 4.3: Permeability ($m^3h^{-1}m^{-2}$) measured by both methods and relative percentage difference (RPD) against the average.

		18 Jan	19 Jan	22 Jan	23 Jan	25 Jan	26 Jan	29 Jan	30 Jan	31 Jan	1 Feb
	Pressurisation	7.48	-	-	7.21	-	7.45	7.35	-	-	-
	RPD	-2%	-	-	2%	-	-1%	0%	-	-	-
BD-4	Depressurisation	7.70	-	-	7.73	-	7.84	7.43	-	-	-
@50Pa	RPD	-1%	-	-	-1%	-	-3%	3%	-	-	-
	Average	7.59	-	-	7.47	-	7.65	7.39	-	-	-
	RPD	0%	-	-	0%	-	-1%	1%	-	-	-
PULSE-60 @4 Pa		1.54	1.45	1.59	1.56	1.49	1.58	1.58	1.60	1.43	1.60
RPD		5%	-1%	8%	6%	1%	7%	8%	9%	-3%	4%
Maximum wind speed (m/s)		7.50	11.90	7.50	7.50	7.50	4.50	10.45	5.97	11.90	10.45
Average wind speed (m/s)		2.72	3.32	2.32	2.71	2.86	1.00	3.33	2.31	4.48	4.48
Average outdoor temperature (°C)		6.44	4.29	8.27	11.92	8.05	7.59	8.34	7.22	6.13	3.84

		2 Feb	5 Feb	6 Feb	8 Feb	9 Feb	12 Feb	13 Feb	14 Feb	15 Feb	16 Feb
	Pressurisation	7.30	7.60	-	-	-	-	-	-	-	7.04
	RPD	1%	-4%	-	-	-	-	-	-	-	-2%
BD-4	Depressurisation	7.64	7.95	-	-	-	-	-	-	-	7.78
@50Pa	RPD	0%	-4%	-	-	-	-	-	-	-	-2%
	Average	7.47	7.78	-	-	-	-	-	-	-	7.41
	RPD	0%	-2%	-	-	-	-	-	-	-	0%
PULSE-60 @4 Pa		1.54	1.49	1.38	1.41	1.40	1.43	1.19	1.37	1.42	1.49
RPD		5%	1%	-6%	-4%	-4%	-3%	-19%	-7%	-3%	2%
Maximum wind speed (m/s)		7.50	11.90	7.50	7.5	2.99	10.45	8.95	8.95	13.40	7.50
Average wind speed (m/s)		2.84	4.17	1.83	2.40	0.45	2.92	3.38	3.38	4.49	2.14
Average outdoor temperature (°C)		5.25	6.63	6.92	3.96	1.63	7.18	4.71	4.22	7.46	8.63

		19 Feb	20 Feb	21 Feb	22 Feb	23 Feb	26 Feb	27 Feb	28 Feb	1 Mar
	Pressurisation	7.60	-	-	6.91	-	-	-	-	7.60
	RPD	-3%	-	-	4%	-	-	-	-	-3%
BD-4	Depressurisation	7.72	-	-	7.32	-	-	-	-	7.24
@50Pa	RPD	-1%	-	-	4%	-1%	-	-	-	5%
	Average	7.66	-	-	7.12	-	-	-	-	7.42
	RPD	-3%	-	-	3%	-	-	-	-	1%
PULSE-60 @4 Pa		1.51	1.54	1.45	1.33	1.49	1.53	1.42	1.53	1.38
RPD		3%	5%	-1%	-9%	1%	4%	-4%	4%	-6%
Maximum wind speed (m/s)		5.97	11.90	5.97	7.47	8.96	8.96	8.96	7.50	11.90
Average wind speed (m/s)		1.69	3.23	1.52	2.68	2.32	2.78	2.37	2.92	3.83
Average outdoor temperature (°C)		10.38	8.49	7.46	2.83	2.55	0.62	-0.31	-2.86	-3.27

On the other hand, Table 4.4 presents the mean, minimum and maximum airtightness measurements during the testing period.

Table 4.4: Mean, minimum and maximum airtightness measurements during the testing period,

		MEAN	MIN	MAX
BD-4 @50 Pa	Pressurisation	7.35	6.91	7.60
	Depressurisation	7.64	7.24	7.95
	Average	7.49	7.12	7.78
PULSE-60 @4 Pa		1.47	1.19	1.60

The permeability results given by the blower door and the Pulse methods are plotted in Figure 4.9 and Figure 4.10. The BD-4 test results performed on different days do not differ from each other significantly. The small variations might be the effect of a slight change in the weather conditions. Hence, good repeatability during the testing period has been demonstrated.

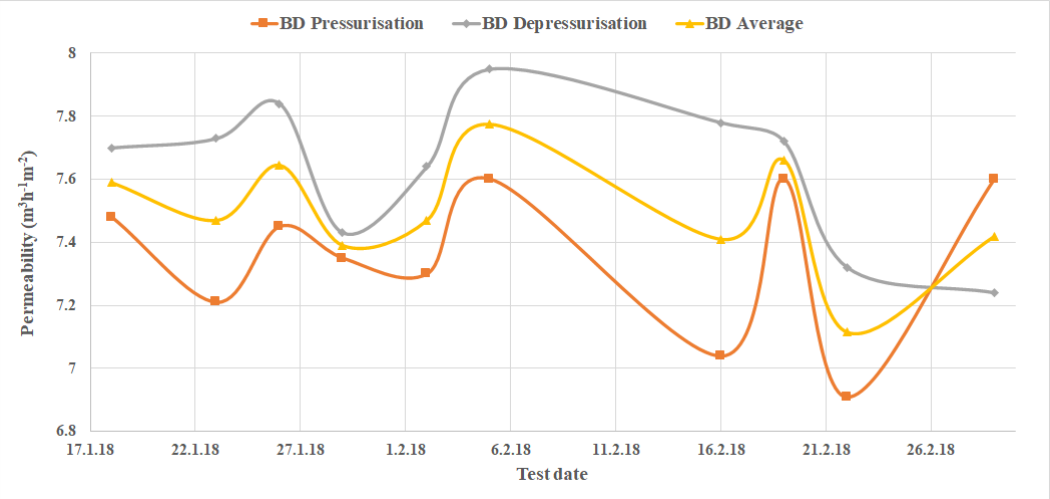


Figure 4.9: Blower door tests results.

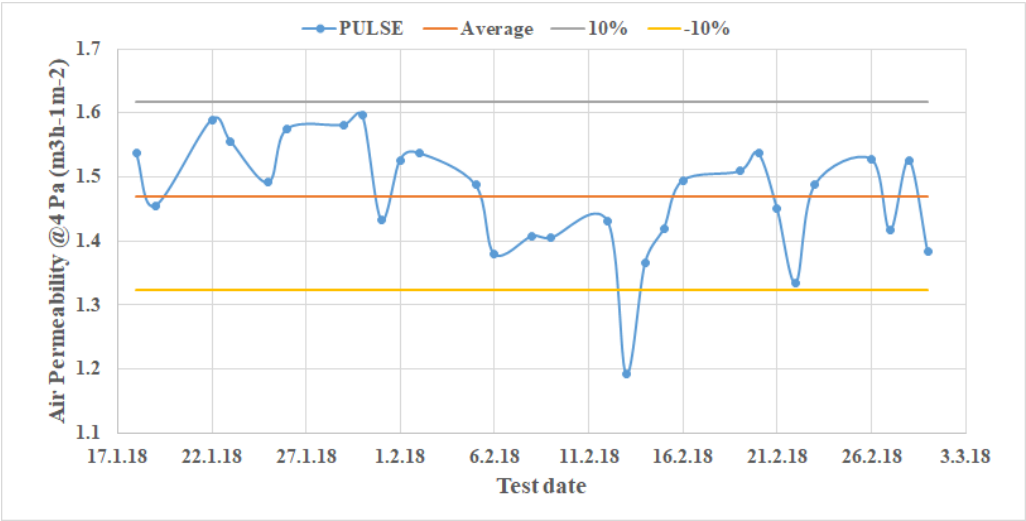


Figure 4.10: Air permeability at 4 Pa given by PULSE-60.

For the PULSE-60 results (Figure 4.10), repeatability of the tests mostly lies within ±9% of the average, which agrees with previous findings [Cooper et al., 2016]. This deviation from RPD for Pulse is higher than the figure for blower door of ±4%. However, Pulse results are based on tests that were carried out on more days and exposed to a wider range of weather conditions due to the test arrangement, which may account for greater variability from the mean.

Table 4.3 shows the average wind and outdoor temperature during Pulse tests, this can also be seen in Figure 4.11. Different conditions were captured, and it was seen that high wind speed has a relatively higher impact on the Pulse test at lower pressures. The test results presented in this chapter did not exclude the lower range test (step three from a three-step Pulse test). When the lower range measurements were taken out from the analysis, the agreement with the average value improved significantly. Agreeing with recent findings [Zheng et al., 2018]; these findings suggest that to reduce the wind impact on the Pulse test data analysis when high wind conditions are present the lower range measurements should be discarded. Wind can impact greatly in the much lower pressure pulse.

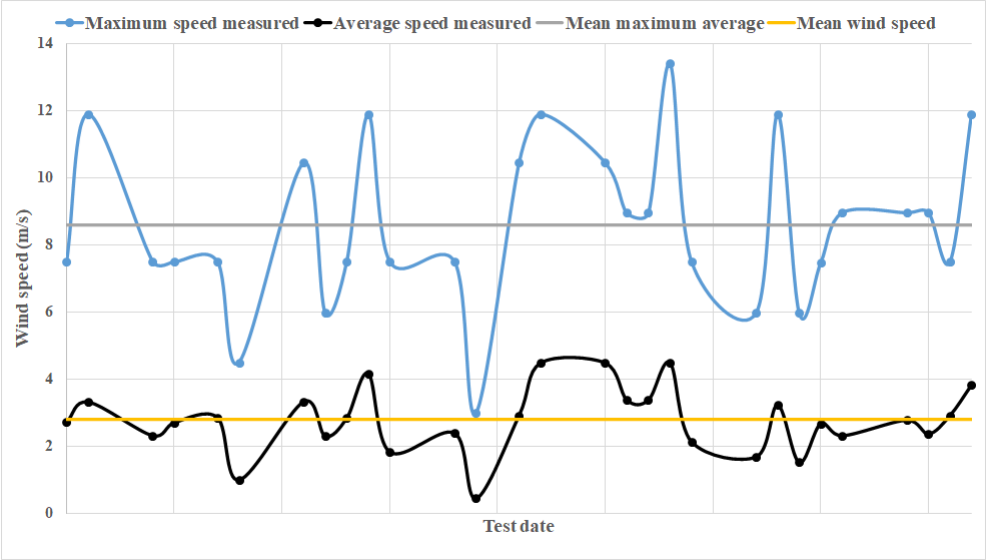


Figure 4.11: Wind speed change during tests.

4.3.2 Air infiltration rate measurements

AIR results taken by both tracer gas methods are shown in Table 4.5. The measurement and calculation procedures for the tracer gas methods were given in Chapter 2. Overall, 15 constant concentration and 19 decay tests were performed. The subtests are the test carried out during one scheduled test (see Table 4.2). In test 3, only one constant concentration test could be performed according to standards, therefore a second decay method tests was carried out (test 3.2). Moreover, due to shortage of gas,in test 4 a decay method test (test 4.1) was decided to be carried out before the constant concentration test, and a second after (test 4.2). the The target concentration in the constant concentration test was 2500 ppm, which was also the initial concentration for the decay method. Different from the rest of the decay tests, test 12 had an initial concentration of 4000 ppm in order to achieve a larger concentration drop.

Table 4.5: Air infiltration (h^{-1}) measurements using the constant concentration and concentration decay methods.

		Test	1	2	3		4		5			6	7
		Subtest			3.1	3.2	4.1	4.2	5.1	5.2	5.3		
Infiltration Rate (h^{-1})	**Constant Concentration**	**Range (Min - Max)**	0.05 - 0.30	0.19 - 0.27	0.12 - 0.26		0.13 - 0.32		NOT VALID			0.18 - 0.30	0.19 - 0.26
		Average	0.24	0.23	0.21		0.25		NOT VALID			0.26	0.25
	Decay		N/A	0.27	0.27	0.26	0.26	0.25	0.31	0.33	0.33	0.29	0.30
		Test	8		9			10			11	12	
		Subtest	8.1	8.2	9.1	9.2	9.3	10.1	10.2	10.3			
Infiltration Rate (h^{-1})	**Constant Concentration**	**Range (Min - Max)**	0.14 - 0.20	0.10 - 0.27	0.11 - 0.17	0.09 - 0.20	0.07 - 0.25	0.17 - 0.23	0.21 - 0.25	0.22 - 0.24	0.19 - 0.29	N/A	
		Average	0.17	0.18	0.15	0.14	0.14	0.20	0.22	0.22	0.24	N/A	
	Decay		0.25		0.26	0.19	0.14	0.28	0.29	0.32	0.31	0.36	

Infiltration Rate (h^{-1})		MEAN	MIN	MAX
	Constant Concentration	0.21	0.14	0.26
	Decay	0.27	0.14	0.36

It can be seen in Table 4.5, that there are differences between the results given by both tracer gas methods. The tracer gas constant concentration method shows large ranges and the averages in the constant concentration are higher than the results given by the decay method. The value quoted as infiltration rate in the decay method in tests 3.1, 7, 9.1, 10.1, 10.2, 10.3 and 11 is not included within the limits of the range of infiltration rates measured in the constant concentration method do. These differences are due to two main factors. First, the nature of the constant concentration method, which is to measure real-time infiltration rates; therefore, the quoted value is an average of three consecutive days of testing. Second, the initial concentration for the decay method (2500 ppm), was probably too low, and the decay curve was not optimal.

Figure 4.12 shows the change in infiltration rate from test to test using both tracer gas methods. The first results were taken during changing weather, mild during the day and cold during the night. Some days the highest temperature reached 15°, and the lowest -3°. The change in temperature from day to night was greater than 6K every day; these tests showed some discrepancies from method to method. After the 11th of February, days were consistently cold (both day and night); in most days the highest temperature was under 7°C, and the temperature

swing was lower than 4K. It is important to remark that for test 12, weather conditions were extremely cold with snow and high wind speed; therefore, an increase in the infiltration rate was expected. Despite the differences, the infiltration results follow the same trend.

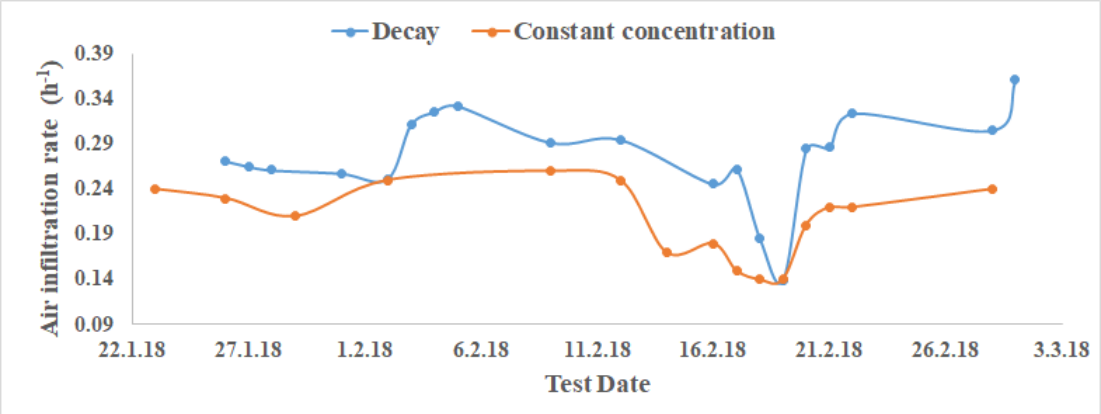


Figure 4.12: Air infiltration rates measured from tracer gas methods.

The advantage of the constant concentration method is that it measures in real-time. For this study, an infiltration rate was calculated every three and a half minutes. The results from the constant concentration method are higher first due to the factors mentioned at the beginning of this section (real-time measurements in constant concentration method and low initial concentration for decay method). Second, because the house was exposed to changing weather from different days, this means higher infiltration (due to higher ΔT, and wind). The result quoted in Figure 4.12 is an average of all the measurements in the constant concentration test.

The decay method was usually carried out during periods where the temperature and wind were mild. It is important to mention that in constant concentration tests performed between two decay tests, e.g. test 4, the range of air infiltration rate measurements in the constant concentration tests includes the infiltration rate value measured with the decay test.

This initial investigation provided a basis for understanding how Pulse compares with measured infiltration rate and also against the steady state blower door results. It also provided a knowledge of how best to proceed with testing for the greater investigation of multiple dwellings later in this research. The decay method is adopted due to its low cost and delivery of reliable results. On the other hand, the constant concentration method is known for using high-spec equipment but, also for delivering accurate results and measuring real-time infiltration rates.

Both methods were chosen for this study. The authors were looking for AIR trends (constant concentration) and what is the impact of environmental conditions in the infiltration rate. Also, specific infiltration rate values were needed to compare directly with airtightness measurements. The usage of the decay method for an extended study was assessed from the data obtained in this case study. The low 2500 ppm initial concentration for the decay method proved to deliver high uncertainty. However, when using over 4000 ppm as starting concentration gave results more similar to those ones obtained using the constant concentration method. Along with economic advantages, this led to extend this study to multiple dwellings using the concentration decay method to measure the air infiltration rate.

Table 4.6 contains the deviations from the average of the air infiltration rate results. It is expected that there would be variation in the results due to the environmental impacts upon the building. The table shows that variation from the mean us up to 33% for constant concentration and 50% for the decay method. This means that changing weather will be reflected in different air infiltration rates; thus, it is crucial to understand the weather, construction and shielding factors of the building and its surroundings, when assessing directly measured air infiltration rates or indeed airtightness measurements.

Table 4.6: Reproducibility of infiltration rate measurements, using the a) constant concentration and b) decay method.

a) Infiltration Rate (h^{-1}) Constant Concentration				b)Infiltration Rate (h^{-1}) Decay method			
Test	**Sub-test**	**CC Average (h^{-1})**	**Dev. from Average**	**Test**	**Sub-test**	**Decay (h^{-1})**	**Dev. from Average**
1		0.24	15%	1		N/A	
2		0.23	9%	2		0.27	2%
3	3.1	0.21	3%	3	3.1	0.27	4%
	3.2				3.2	0.26	6%
4	4.1	0.25	21%	4	4.1	0.26	7%
	4.2				4.2	0.25	9%
6		0.26	24%		5.1	0.31	12%
7		0.25	20%	5	5.2	0.33	18%
8	8.1	0.17	17%		5.3	0.33	20%
	8.2	0.18	12%	6		0.29	5%
9	9.1	0.15	29%	7		0.30	7%
	9.2	0.14	33%	8	8.1	0.25	11%
	9.3	0.14	31%		8.2		
10	10.1	0.20	3%	9	9.1	0.26	5%
	10.2	0.22	8%		9.2	0.19	33%
	10.3	0.22	9%		9.3	0.14	50%
11		0.24	16%	10	10.1	0.28	3%
					10.2	0.29	3%
					10.3	0.32	17%
				11		0.31	10%
				12		0.36	31%

4.3.2.1 Uncertainty in air infiltration measurements

All the uncertainties from the measured infiltration rates were calculated according to Annex A from the standard [International Organization for Standardization, 2017]. For the multipoint decay method, the predicted standard error, E_N, or uncertainty is calculated by Equation 4.2.

$$E_N = \frac{s}{\sqrt{\sum_{i=1}^{k}(t_i - \bar{t})^2}} \tag{4.2}$$

and

$$s^2 = \frac{\sum_{i=1}^{k}(Y_i - \hat{Y}_i)^2}{k-2} \tag{4.3}$$

where Y_i is the measured value of the logarithm of the concentration K in i, $\hat{Y}_i$ is the estimated value (regression) of the logarithm of the concentration K in i, t_i is the measurement time for each sample (h), $\bar{t}$ is the average value of the measurement times (h) and, k is the number of samples.

For the constant concentration method the variance is calculated by Equation 4.4.

$$s^2 = \frac{k\sum_{i=1}^{k} K_i^2 - (\sum_{i=1}^{k} K_i)^2}{k(k-1)} \tag{4.4}$$

The standard error is then calculated by:

$$SE = \frac{s}{\sqrt{k-1}} \tag{4.5}$$

Table 4.7 describes the calculated uncertainties for the tracer gas constant concentration tests.

Table 4.7: Uncertainty from tracer gas constant concentration tests

Test	**Sub-test**	**CC Average** (h^{-1})	**Uncer-tainty** (h^{-1})	**Uncer-tainty** (%)
1		0.24	0.006	2.5
2		0.23	0.020	8.7
3		0.21	0.022	10.5
4		0.25	0.009	3.6
5		N/A	N/A	N/A
6		0.26	0.010	3.8
7		0.25	0.030	12
8	8.1	0.17	0.011	6.5
	8.2	0.18	0.009	
9	9.1	0.15	0.013	8.7
	9.2	0.14	0.009	6.4
	9.3	0.14	0.009	6.4
10	10.1	0.20	0.017	8.5
	10.2	0.22	0.017	7.7
	10.3	0.22	0.016	7.2
11		0.24	0.014	5.8

Most of the uncertainties are under ±10%, except for two. It was seen that the uncertainty was inversely proportional to the test duration; the longer the test and the number of measurements, the lower the uncertainty.

For the tracer gas concentration decay method three different uncertainties were calculated, the data uncertainty, the regression uncertainty (according to Hughes and Hase [2010]), and, the uncertainty recommended by International Organization for Standardization [2017]. Table 4.8 reports the highest of the calculated uncertainties.

Table 4.8: Uncertainty from tracer gas concentration decay tests

Test	**Sub-test**	**DM** (h^{-1})	**Uncer-tainty** (h^{-1})	**Uncer-tainty** (%)
1		N/A	N/A	N/A
2		0.27	0.002	0.9
3	3.1	0.27	0.007	2.8
	3.2	0.26	0.005	2.0
4	4.1	0.26	0.003	1.1
	4.2	0.25	0.009	3.7
5	5.1	0.31	0.003	1.2
	5.2	0.33	0.004	1.1
	5.3	0.33	0.004	1.2
6		0.29	0.006	1.9
7		0.30	0.009	2.9
8		0.25	0.001	0.6
9	9.1	0.26	0.002	0.8
	9.2	0.19	0.001	0.6
	9.3	0.14	0.002	1.3
10	10.1	0.28	0.001	0.4
	10.2	0.29	0.004	1.2
	10.3	0.32	0.004	1.1
11		0.31	0.006	2.1
12		0.36	0.005	1.4

The most substantial uncertainty for most cases was the one calculated using the standards. The remaining calculated uncertainties were lower and were more related to the statistical procedure, rather than specifics of the method. The decay method showed a smaller uncertainty than the constant concentration method; nevertheless, the constant concentration tests also proved low uncertainty. Fur-

thermore, the starting concentration for every decay test, except test 12 was 2500 ppm. In a typical test, the CO_2 concentration decays to 800 ppm; the decay range is believed not to be as large as desired. An increase in the initial concentration might improve the accuracy of the test; that is why it is believed that test 12 is the most accurate decay test.

4.3.3 The correlation between air infiltration and airtightness

As a starting point for understanding the correlation between the Pulse test results and the air infiltration rate, a side-by-side comparison between the two is given in Table 4.9 and Figure 4.13. The decay method is the only one used in this comparison; because it is a more practical and simpler method than the other two tracer gas methods. Furthermore, according to the comparison made in the previous section, the decay method can provide comparable measurements with the constant concentration method.

Table 4.9: Summary and comparisons of air infiltration measurements using the tracer gas decay method and the Pulse method.

Test	1	2	3		4		5			6	7
Subtest			3.1	3.2	4.1	4.2	5.1	5.2	5.3		
Infiltration Rate (h^{-1})		0.1780	0.1455	0.1478	01775	0.1322	0.1835	0.1829	0.1850	0.1499	0.1492
Pulse (h^{-1})	1.5630	1.5820	1.6049		1.5642		1.5459			1.4422	1.4486

Test	8		9			10			11	12
Subtest	8.1	8.2	9.1	9.2	9.3	10.1	10.2	10.3		
Infiltration Rate (h^{-1})	0.1551		0.1653	0.1269	0.099	0.1935	0.1913	0.2042	0.1737	0.2426
Pulse (h^{-1})	1.4156		1.5298			1.4882			1.4681	N/A

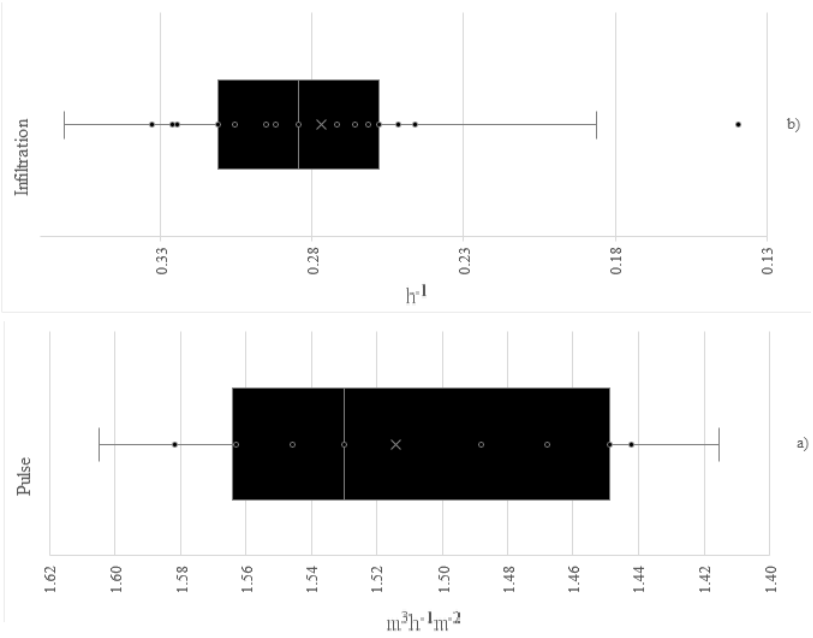


Figure 4.13: Box and whisker plot from a) Pulse test results and b) Infiltration rates obtained using the tracer gas decay method.

The box and whiskers plot showed that results vary more in the air infiltration rate. Usually, the infiltration rate (n_1, h^{-1}) is predicted through a leakage-infiltration ratio when the building airtightness is measured. For instance, the infiltration rate can be predicted by using the divide-by-20 rule [Building Research Establishment, 2013, Jones et al., 2016], i.e. the air change rate at 50 Pa (n_{50}, h^{-1}) divided by 20 [Sherman, 1987]. In the UK, the divide-by-20 rule is used to predict the infiltration rate; however, the air permeability at 50 Pa (q_{50}, $m^3h^{-1}m^{-2}$) is used instead of n_{50}. This change assumes that the building has a volume - envelope area ratio of 1. If a leakage – infiltration ratio is to be used (Equation 4.6, where n_4 represents the air change per hour at 4 Pa in h^{-1} measured by Pulse and n_1 is the infiltration rate in h^{-1}), N would range from 4 to 6.5, with an average value at 5.25. As stated before, in the UK context, q_4 would be used. In this case study, the volume-envelope area ratio is close to 1; therefore, the values of N using q_4 would be similar to the ones obtained using n_4.

$$\frac{n_4}{n_1} = N \tag{4.6}$$

If the same exercise were done using the value of n_{50} obtained in blower door tests instead of n_4, N would take values between 22.5 and 33.2. The results obtained here go hand in hand with what others have found or recommended [Johnston and Stafford, 2016, Keig et al., 2016]. The discrepancies between the

measurements and the predictions used in ratios lead to an overestimation of air infiltration, and in consequence, heat losses. The blower door introduces an uncertainty when using ratios of circa 20%, whereas the Pulse only around 5%.

4.3.4 Impact of environmental conditions on the infiltration measurements and the airtightness-infiltration correction

Figure 4.14 depicts the real-time infiltration rate and the temperature difference. It is clearly shown that the infiltration rate follows a similar trend as the temperature difference. It is also clear how the changes in indoor temperature (heating on) create a higher ΔT and therefore, higher infiltration rate. These results were also seen in different tests however, as seen in Figure 4.15, it was more evident when wind velocity was lower than 2.5 m/s. A different test where this pattern is clearly seen is shown in Figure 4.16.

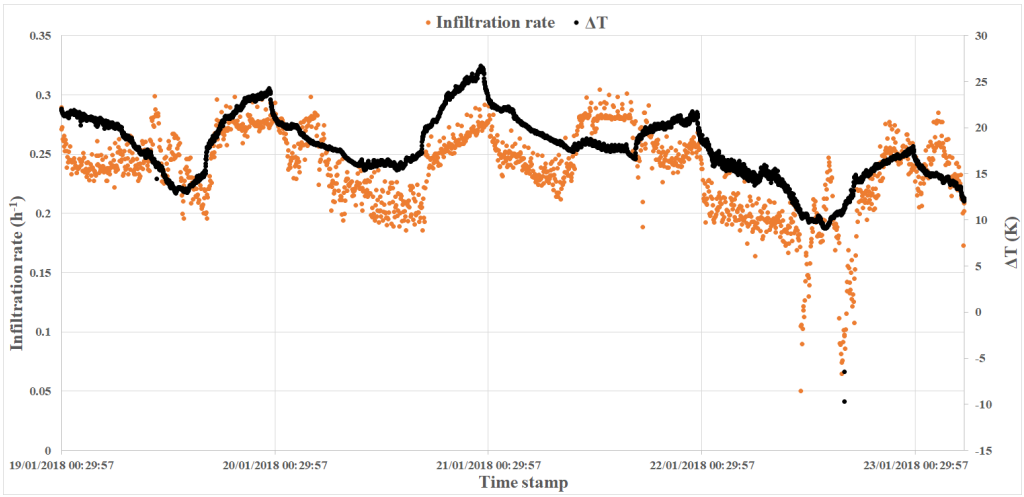


Figure 4.14: Infiltration rates (h^{-1}) against temperature difference (K), example of a graph when wind speed is low, taken from the results in test 2, from the 19th to the 23rd of January 2018.

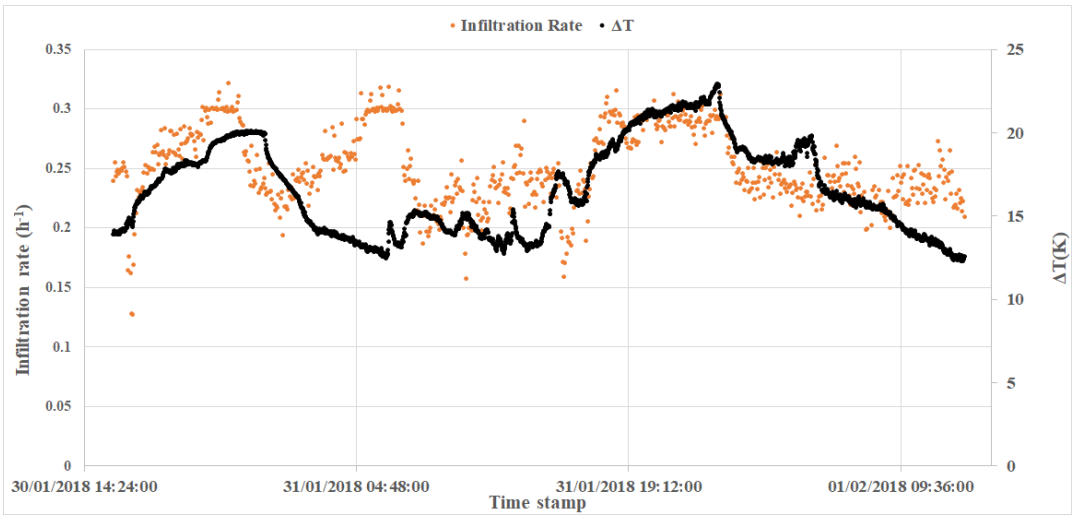


Figure 4.15: Infiltration rates (h^{-1}) against temperature difference (K), taken from the results in test 4, from the 30th of January to the 1st of February 2018.

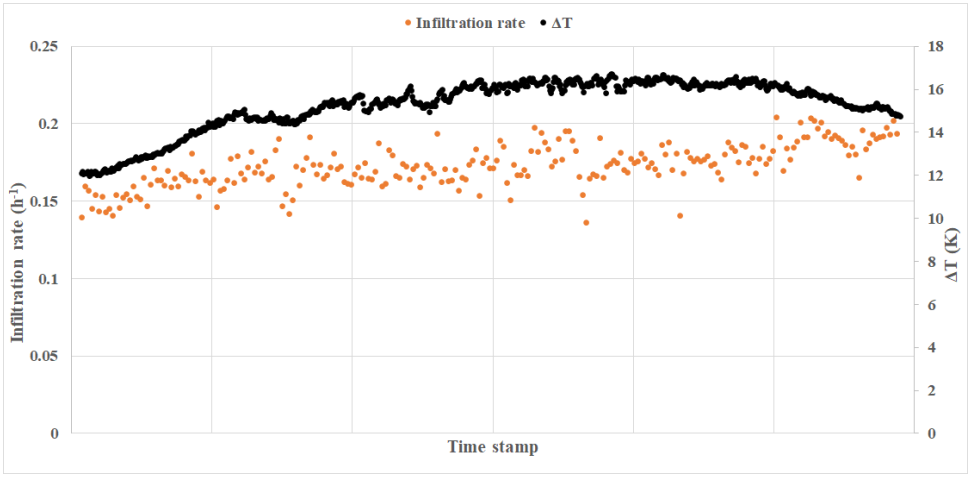


Figure 4.16: Infiltration rates (h^{-1}) against temperature difference (K), example of a graph when wind speed is low, taken from the results in test 8, from the 13th to the 14rd of February 2018.

Conversely, Figure 4.17 shows, for the same period as Figure 4.14, the infiltration rate against the wind speed. When wind increases, the infiltration rate gets a peak. Even when some authors suggest that wind is the main driving force [Kraniotis et al., 2014a]. This study showed that when temperature differences across the building envelope are high enough (achieved temperature difference was higher than 23K) and wind is below 2.5 m/s, the infiltration rate is dominated by the temperature difference (ΔT). Hence, it can be concluded that, the airtightness level of the house defines a minimum infiltration rate, both temperature difference

and wind speed affects the infiltration rate and shapes its trend. In addition Figures 4.18 and 4.19 show similar results.These findings are consistent with previous studies [Liddament, 1996], which are shown in Figures 4.20 and 4.21.

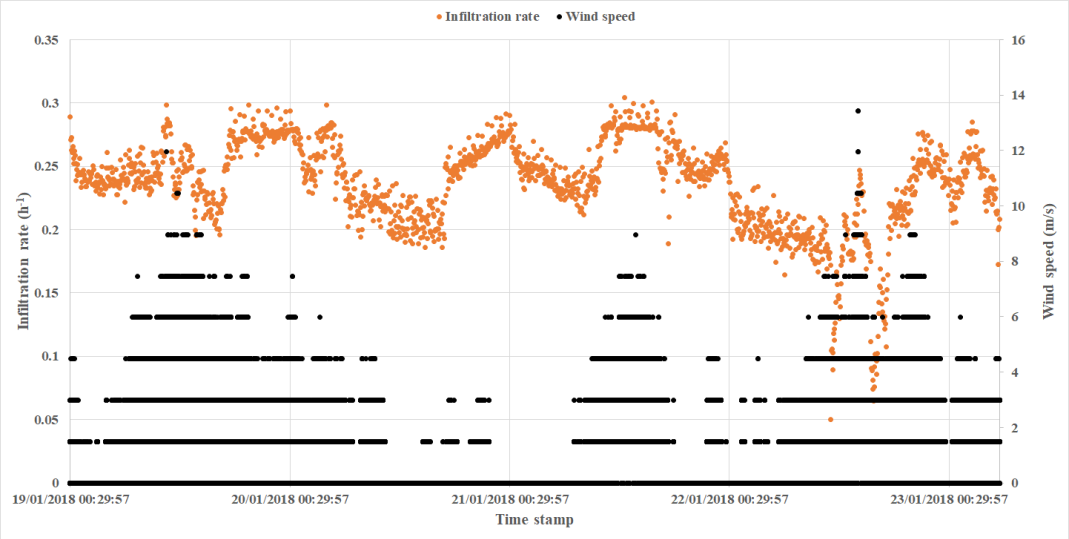


Figure 4.17: Infiltration rates (h^{-1}) against Wind speed (m/s), example of a graph witch high wind speeds, taken from the results in test 2, from the 19th to the 23rd of January 2018.

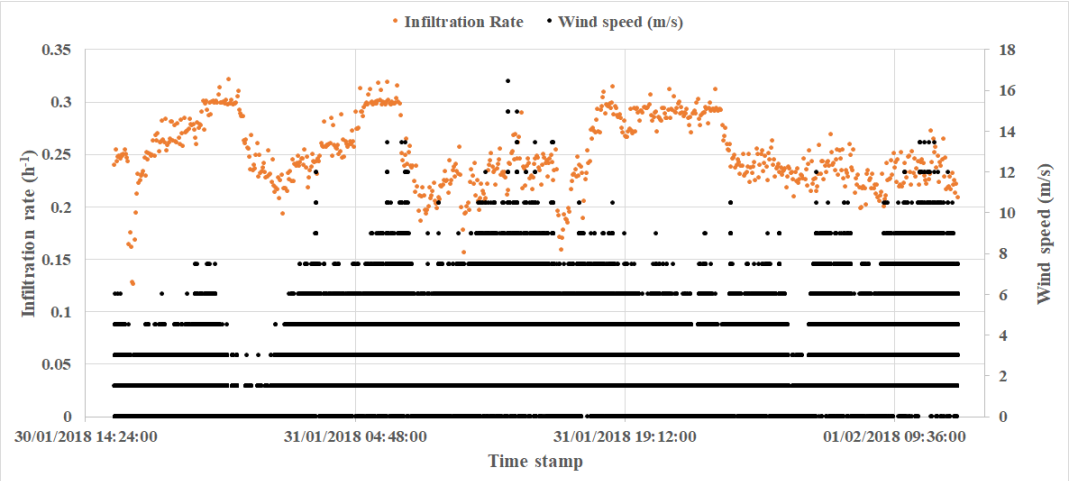


Figure 4.18: Infiltration rates (h^{-1}) against Wind speed (m/s), example of a graph witch high wind speeds, taken from the results in test 4, from the 30th of January to the 1st of February 2018.

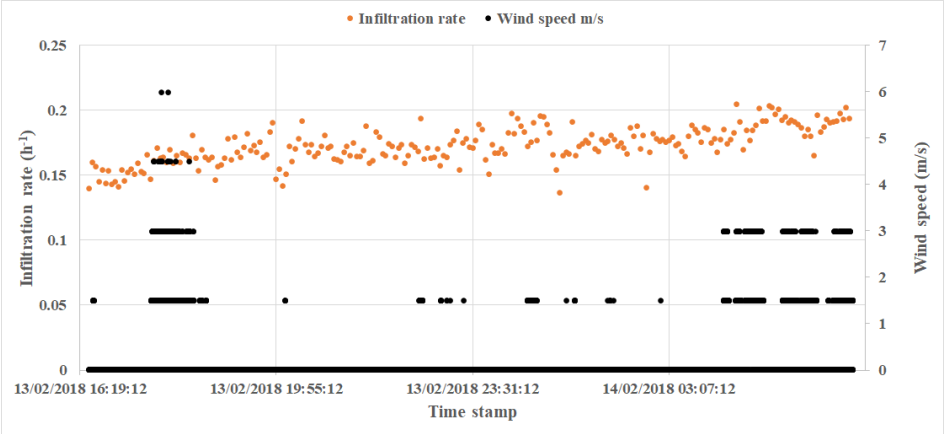


Figure 4.19: Infiltration rates (h^{-1}) against Wind speed (m/s), example of a graph witch high wind speeds, taken from the results in test 8, from the 13th to the 14rd of February 2018.

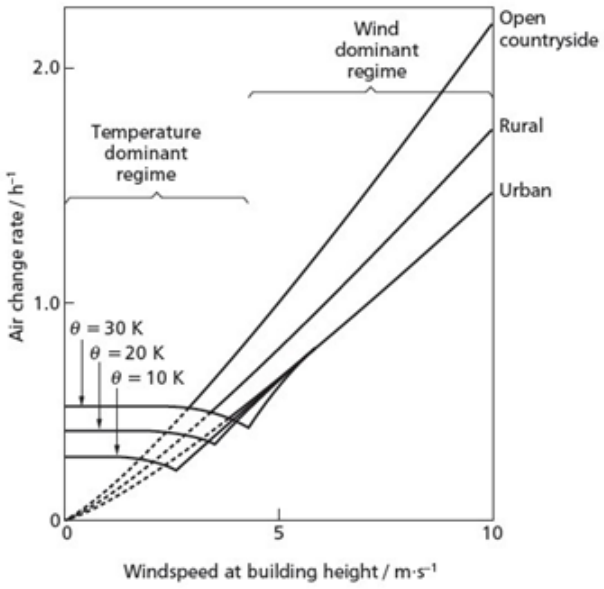


Figure 4.20: Impact of wind and temperature [Liddament, 1996]

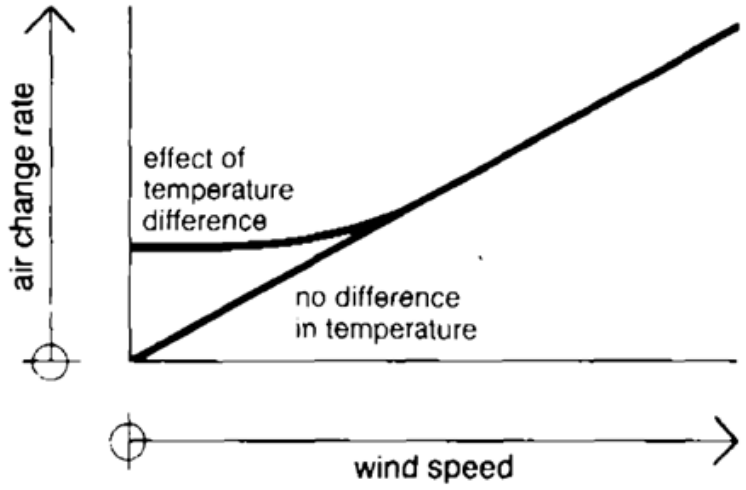


Figure 4.21: Transition from stack to wind dominant flow, taken from [Liddament, 1996]

Other similar analysis were made for different constant concentration tests, these are included in Appendix B, nevertheless the results are clearer in the previously referenced figures.

4.3.5 Impact of wind on the pressure profiles

The pressure fields around the building's envelope are key to understanding how air infiltration rate is affected by the changing outdoor wind. As mentioned before, the test house was tapped with pressure tubes in every façade, and the anemometer was located in a neighbouring house (refer to Figure 4.1). It is important to mention that all the outdoor pressure tapings were set at similar heights, therefore it was not possible to measure outdoor temperature stratification. From all the measurements of both, wind and pressure difference, the data containing high wind speeds was separated from the rest, as a result, short periods were considered to analyse how wind gusts are captured in terms of pressure difference. This is important because wind gusts make measuring the air leakage rate more difficult due to a sudden change of pressure difference [Kraniotis et al., 2014b]. Data from this time will aid to gain insight into the effect of the changing wind speed on the building pressure distribution and air infiltration.

During the studied time, the wind was mainly varying from 3 to 10 m/s. The pressure difference across the façades of the test house is illustrated in Figure 4.22 together with the wind speed. It can be noted that, when the wind speed peaks, the pressure difference does so too, but there is a short delay between the two. It

could have been caused by the fact that the weather station is located 10 meters away in the upstream from the east façade of the test house. Furthermore, the time delay observed in the east façade was also observed in the west façade, the main differences were that, in the west façade the pressure difference peaks were negative and, it occurred 2 seconds (approximately) after the east façade. The south and north façades showed a similar behaviour regarding the effect of strong winds.

Consistent results with Figure 4.22 were obtained for different periods: gusts were captured as extreme pressure differences depending on the side of the building exposed to the direction and magnitude of wind gusts. There is an almost immediate (in the range of 1 to 5 seconds) reaction from the pressure changes after the wind hits the building. Graphs for other two period with high wind gusts, where a similar analysis was made, can be found in Appendix C. A wider data set was studied to relate the mentioned pressure change to the infiltration rate: the main finding was that the sudden change in pressure difference is not immediately reflected in the change of infiltration rate; it might take minutes to build up and see the change. This empirical conclusion has to be validated with more similar studies.

These results showed that the pressure transducers can be correlated with the wind speed to determine a different way to account the wind acting on the building's envelope, however, this is not part of the scope of this study.

When considering the pressure analysis for the buoyancy effect, the main finding is that it had no immediate effect on the building pressure. Probable reasons are: only one pressure tap was allocated to evaluate the buoyancy effect; the difference in height between the reference point and the buoyancy taping was only six meters; the wind was much more dominant than the stack effect and its effect in pressure was shadowed. For future studies several buoyancy tapings in a controlled environment could provide better insights.

A period with high wind gusts was used to analyse the distributions of pressure differentials. Figure 4.23 shows how the differentials are distributed and two main conclusions can be drawn: the pressure distributions seem to follow a normal distribution and; the majority of the pressure difference occurs in the range of 0 to 5 Pa. It is important to remark that these figures only represent a gusty 11-minute time window on 24th of February 2018; nevertheless similar results were found in other analysis which are given in Appendix D.

The mean pressure differences in all four facades of the test house for all the measurements taken is 3.17 Pa with an uncertainty of ± 0.0022 Pa, however, the

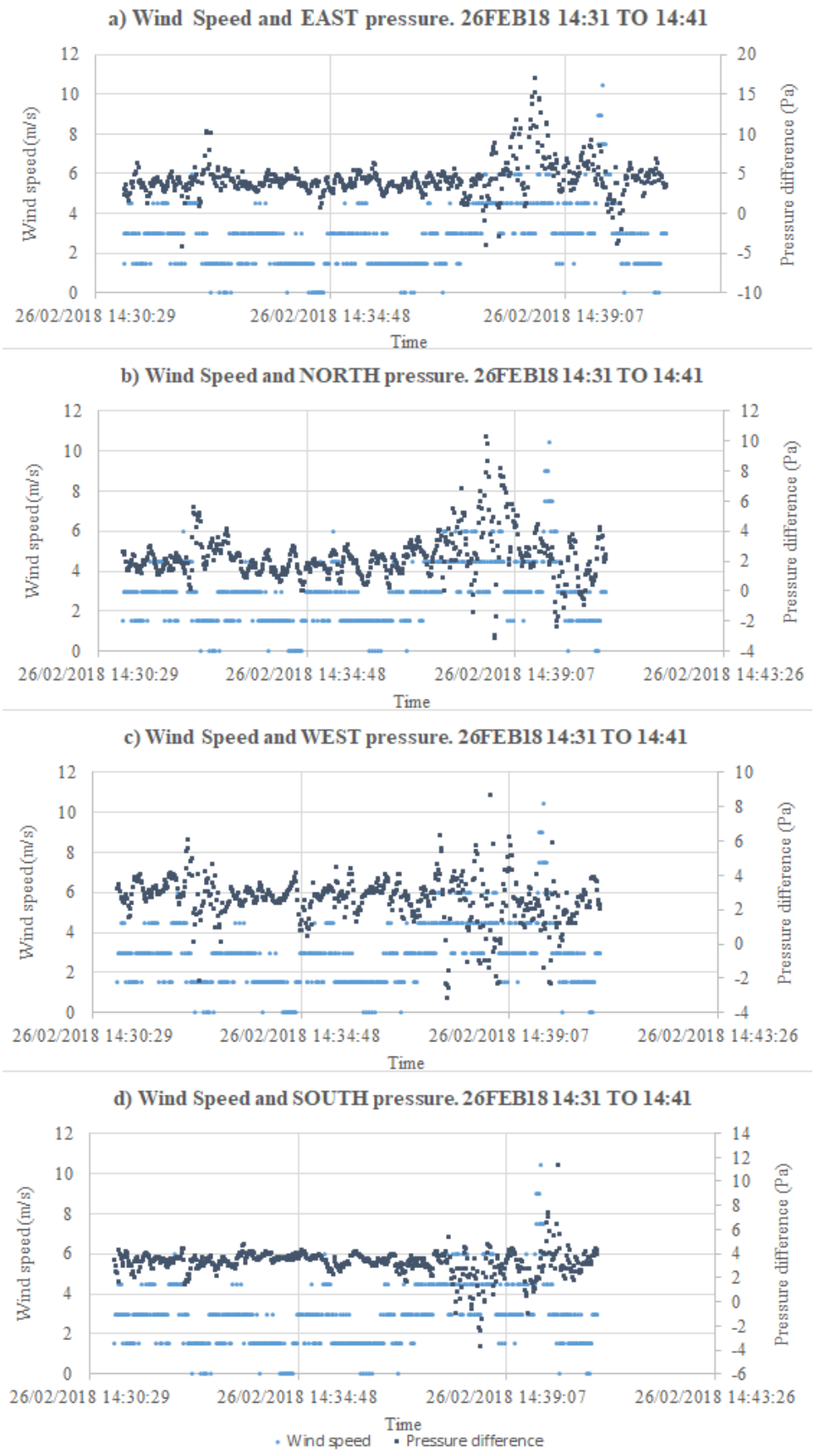


Figure 4.22: Pressure difference against wind of the test house during 10 minutes when high wind gusts were occurring, on the 26th of February in the a) east, b) north, c) west and, d) south façades.

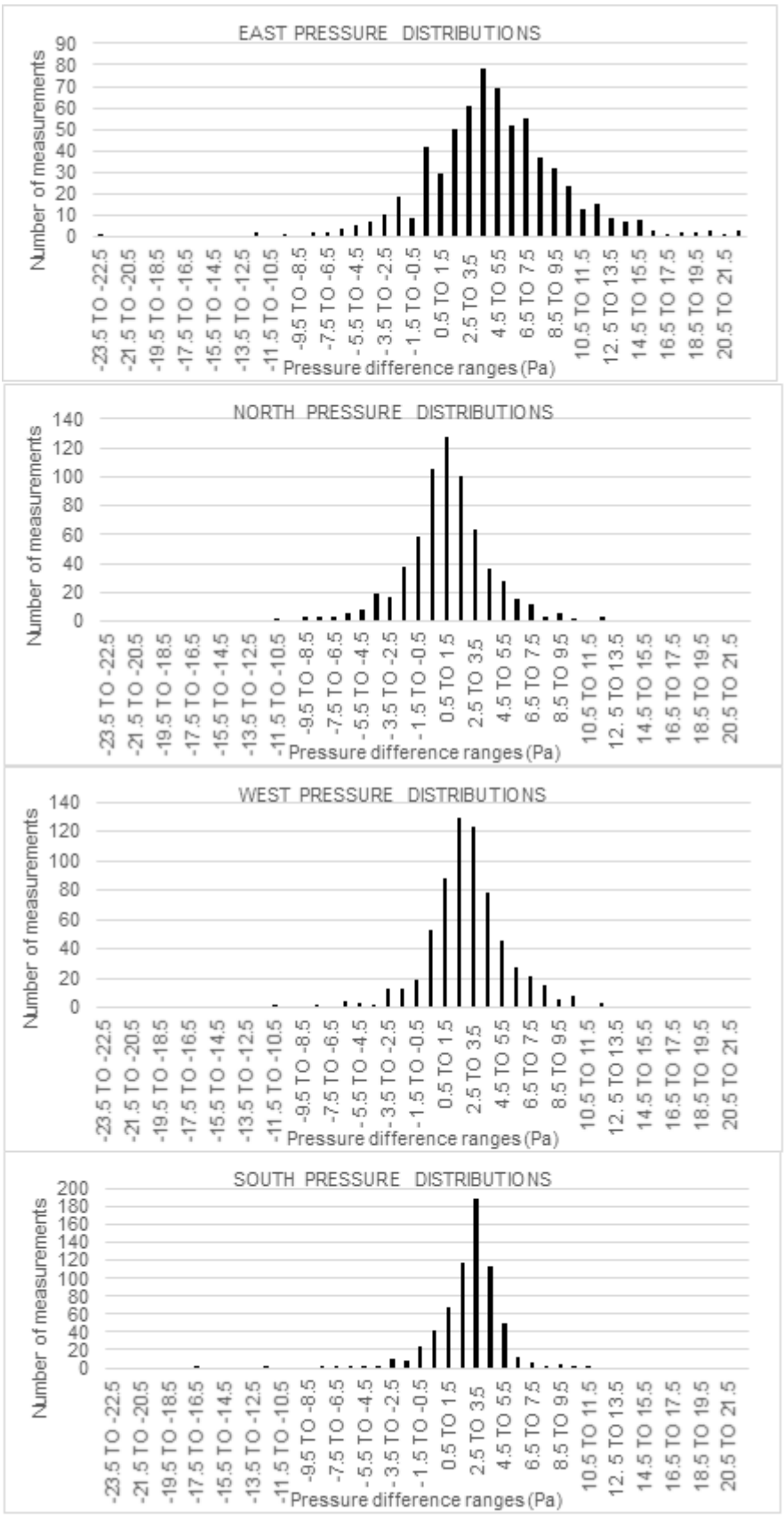


Figure 4.23: Pressure distributions in the windward (east and north) and leeward façades (west and south)of the test building for eleven minutes on the 24th of February

Table 4.10: Statistical figures from measured pressure differences when wind gusts were captured by the anemometer

Test	Feb 24th 15:15-15:26				Feb 25th 17:07-17:17				Feb 26th 14:31-14:41				Average
Façade	E	N	S	W	E	N	S	W	E	N	S	W	
Average pressure difference (Pa)	4.86	1.01	2.49	2.50	3.68	1.34	3.53	3.14	4.33	2.29	3.25	2.64	2.92
Standard error (Pa)	0.19	0.12	0.09	0.12	0.11	0.07	0.05	0.07	0.09	0.06	0.04	0.05	0.09

Table 4.11: Most repeated ranges of pressures when wind gusts were captured.

Test	Feb 24th 15:15-15:26				Feb 25th 17:07-17:17				Feb 26th 14:31-14:41			
Façade	E	N	S	W	E	N	S	W	E	N	S	W
Most repeated range (Pa)	3.5 - 4.5	0.5 - 1.5	1.5 - 2.5	2.5 - 3.5	2.5 - 3.5	0.5 - 1.5	3.5 - 4.5	2.5 - 3.5	3.5 - 4.5	1.5 - 2.5	3.5 - 4.5	2.5 - 3.5

most repeated value for the east façade is the range covering between 3.5 and 4.5 Pa, this was valid for the windward side of the house.

The statistical figures from different periods when wind gusts were captured are summarised in Table 4.10.

The mean pressure difference for these periods is 2.92 Pa, it is clearly seen that for the leeward façade (north) the pressure difference is less than those in where the wind is directly hitting the envelope of the building. The most repeated ranges vary from façade to façade, for the three periods of high gusts these are shown in Table 4.11.

High wind speeds are not always present and wind gusts occur in the fraction of a second. That is why an analysis of all the measurements from the 23rd to the 28th of February 2018 was made, this is shown in Figure 4.24. It can clearly be seen that for this period, where different weather conditions were captured, the majority of the pressure differences captured in the windward façade (east) are in the range of 3.0 to 4.5 Pa. Measurements on façades exposed to direct wind (windward) showed similar results, on leeward façades the pressure differentials were lower (1.5-2.5 Pa).

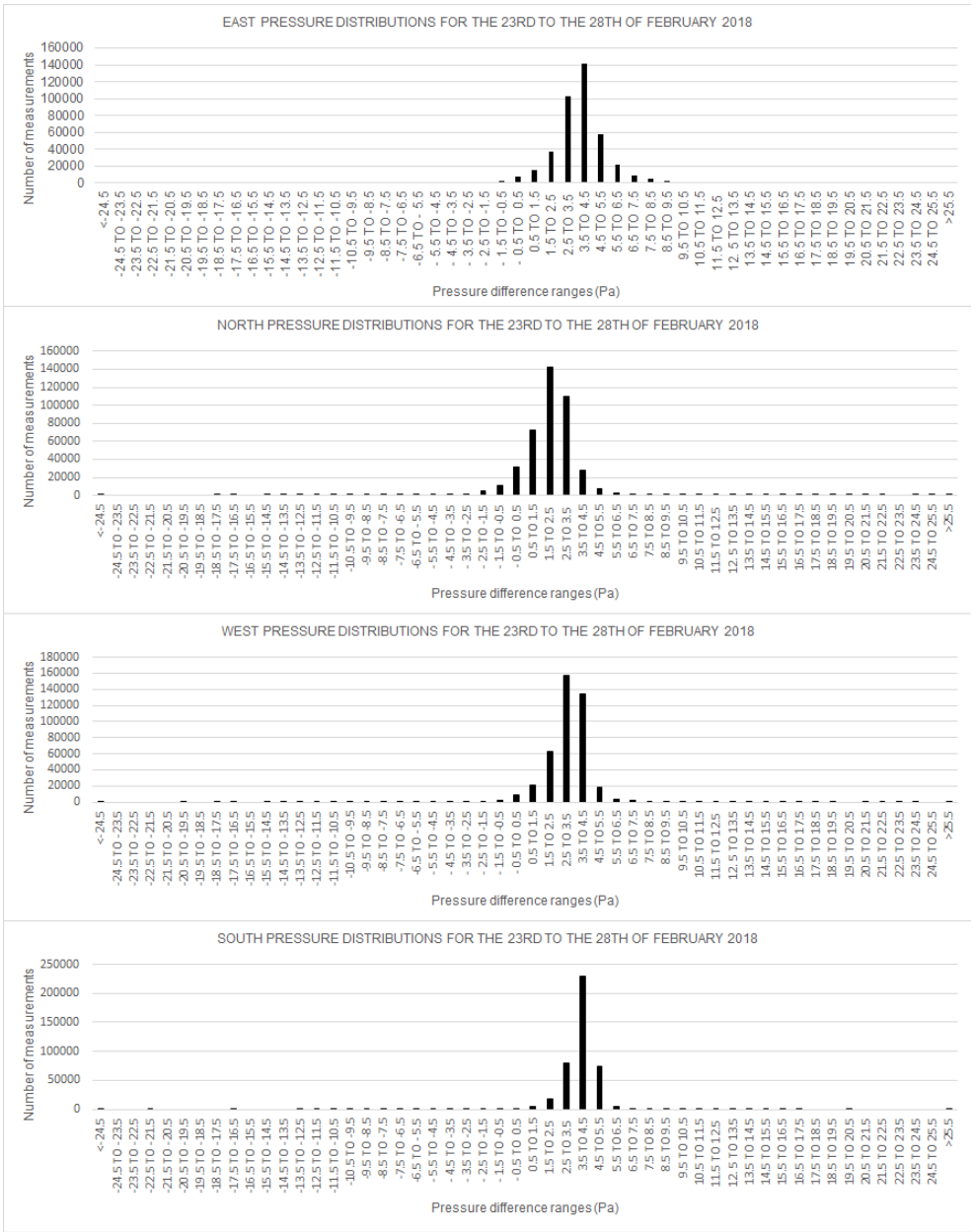


Figure 4.24: Pressure difference repetitions for the 23rd to the 28th of February 2018 in the test house

The results showed the building pressure difference incurred under natural conditions. The majority of results lied in a range from 1.5 to 4.5 Pa. This is consistent with what Cooper and Etheridge [2007a] found, and this suggests that measuring airtightness at lower pressures should be more representative and infiltration rates obtained from airtightness measured directly at low pressures should be more accurate. It is suggested that airtightness measured at 4 Pa should reduce the uncertainty created by the extrapolation from high to low pressure. The Pulse technique quotes and measures airtightness at 4 Pa. This justifies the usage of Pulse in the current research study.

4.4 Discussion

Regulation in the United Kingdom uses estimations of air infiltration rate. With those estimations, the dwellings heat losses are calculated. SAP takes into account the measured air permeability and the divide-by-20 rule to make the calculation. For this particular study, using the average value of the measurements taken with the blower door, the heat losses are calculated as SAP requires. This is shown in Table 4.12. The calculations already include the modifying factor given by SAP, there are two options: an average monthly heat loss and; the heat loss during the month when the blower door test was carried out.

Table 4.12: Heat loss calculation as per SAP from blower door tests.

Mean air permeability $m^3h^{-1}m^{-2}$ (q_{50})	$q_{50}/20$	Shelter factor	SF*$q_{50}/20$	SAP n_1 during month	SAP n_1 annual average	Volume m^3	Heat loss during month W/K	Heat loss annual average W/K
7.490	0.375	1	0.745	0.610	0.585	285	57.330	55.004

SAP calculation of the heat loss in the dwelling results in around 55 W/K. As a point of comparison, if the measurements of the tracer gas constant concentration method are taken as real infiltration values, the associated heat losses for every tests can be calculated. Table 4.13 shows the monthly heat losses for every measured infiltration rate. At the bottom, an average of the calculated heat losses is given.

The highest heat loss value obtained was 24 W/K, this figure is not even half of the estimated value using the regular SAP procedure. If the average result is

Table 4.13: Calculation of heat losses as per SAP from different tracer gas constant concentration tests.

Test		Constant Concentration n_1 h^{-1}	Volume m^3	Heat loss W/K
1		0.2368	285	22.270
2		0.2257	285	21.229
3	3.1	0.2135	285	20.081
	3.2		285	
4	4.1	0.2503	285	23.537
	4.2		285	
6		0.2568	285	24.151
7		0.2470	285	23.227
8	8.1	0.1723	285	16.204
	8.2	0.1822	285	17.133
9	9.1	0.1461	285	13.738
	9.2	0.1381	285	12.992
	9.3	0.1432	285	13.470
10	10.1	0.1995	285	20.048
	10.2	0.2238	285	21.048
	10.3	0.2242	285	21.086
11		0.2399	285	22.567
Average		0.2066		17.147

taken (17W/K), the heat losses are less than one third of the calculated ones.

These results suggest that UK regulation overestimates both, the air infiltration rate and the heat losses associated to it. The usage of the divide-by-20 rule makes a first overestimation, as was discussed in section 4.3.3; the modifying factors increase the infiltration rate, making the predicted value much greater than the actual one. The overestimation is more evident for tighter dwellings since an addition of 0.5 h^{-1} is carried out during the calculations, this figure is sometimes much higher than the original real infiltration rate for tight dwellings.

Further investigations can lead to a better way of predicting a building's heat losses. In addition, Love et al. [2017] shows how in the UK, steady pressurisation tests have been carried out in previous years, building airtightness has improved, nevertheless, it is uncertain if this has led to a higher energy efficiency in dwellings, or the airtightness tests are carried out "just to pass". A door is open for changes in the regulatory system to include new technologies and to update the existing ones in order to achieve the improvement in energy efficiency.

The results presented in this and the previous section show that new technologies can be included in regulation. Pulse has shown a good performance to be considered, however, regulation in most countries only permit steady pressurisation tests to comply with the standard. A study including a greater number of dwellings to test these results would be important to give the basis on how to update the existing regulation; and, to get a better understanding on how –real- air infiltration rate is affecting the energy efficiency of dwellings.

4.5 Chapter conclusion

A set of airtightness, tracer gas and pressure measurement tests were carried out in a property at the University of Nottingham during the winter of 2018, with the objective of understanding the correlation between airtightness and air infiltration, and, finding how the infiltration rate is affected by the environmental conditions, particularly wind and temperature.

Initial results showed the infiltration is fundamentally determined by the airtightness but it can also be affected by environmental conditions. The predominant factors that affect the infiltration rate are outdoor wind and indoor-outdoor temperature difference. It was also shown that there was a two-second delay in the impact of the wind on the pressures of windward and leeward sides. The pressure difference occurring around the tested building lies in a range of 1.5 – 4.5 Pa. This suggests that the measurement of airtightness at low pressures is more represen-

tative of the pressure under which the building infiltration occurs. Which gives a justification of using the Pulse method in this project.

The repeatability of the BD-4 and PULSE-60 unit is within ±6% and ±10%, respectively. However, it was noted that Pulse was subject to a wider range of environmental conditions whereas the blower door was not. Air infiltration was measured using the tracer gas constant concentration and decay methods. The tests showed a variation from the average due to the changing weather of up to 33% in the constant concentration and up to 50% in the decay method. The results also showed that the prediction of infiltration largely depends on the weather and shielding conditions.

The airtightness/air infiltration correlation showed that if ratios are to be used to calculate an average infiltration rate from Pulse's results, N in Equation 4.6 can take a value of 5.25. For the blower door's results, the corresponding ratio ranges from 22.5 to 33.2, deviating from the divide-by-20 rule of thumb. Hence, in this case study, the divide-by-20 rule would overestimate the infiltration rate and the heat losses calculated by SAP.

Further research must be developed if a statistical correlation is to be found; and, a better method to predict air infiltration from Pulse is to be developed. The next stage of the study is to extend the tests to a larger data set, which includes different archetypes, aiming to capture different weather conditions; results can be used to validate the results obtained in this study. Finally it is a goal of this project to find a way to predict air infiltration which can produce more accurate results than those ones obtained using the current UK legislation method.

Chapter 5

Field investigation on the infiltration - leakage correlation

5.1 Introduction

The previous chapter described airtightness and air infiltration testing, with the main findings providing the basis for further research. Initial findings such as the effect of environmental conditions on infiltration or; a possible correlation between the Pulse test results and air infiltration gave the background for further testing. Furthermore, air infiltration tests in the case study house provided optimum training to carry out different tests in different scenarios. A testing campaign which involved different constraints such as house availability, test time, weather conditions, transportation of tester and equipment, among others. Therefore, the knowledge and capabilities gained enabled the design of the testing campaign discussed within this chapter, assuring the optimization of resources and the collection of suitable data.

This chapter explains all the testing campaign carried out in 2018. The intention was to obtain a significant number of field investigations aiming to derive an infiltration - leakage correlation with sufficient supporting evidence. At the end of this testing campaign, twenty dwellings were tested.

The main objective of this chapter is to obtain test data for directly measured infiltration and airtightness values. Existing and modified infiltration models take the measurements from this campaign as inputs in the following chapters. This chapter explains the developed methodology to obtain the data and its uncertainty (air infiltration). Moreover, an analysis of an empirical airtightness - infiltration correlation is given.

5.2 Methodology

In this study 20 dwellings were tested and airtightness measured, using both steady pressurisation (blower door) and Pulse methods. Air infiltration, as mentioned previously, was measured through tracer gas tests [American Society for Testing and Materials, 2011]. The dwellings were all within a "reachable" radius from the University of Nottingham i.e. within the East Midlands of the UK. The execution of this project was coordinated with Build Test Solutions Ltd. (BTS) as part of the validation of the Pulse method.

At the end of the field trials phase, two of the dwellings were re-tested; with their results used to validate the results obtained in the initial field trials stage.

Each house tested was put forward by the owner voluntarily. The testing team involved two people: the author and, a member of BTS. The team arrived on the morning of the test day and an initial inspection of the dwelling was performed to collate specific parameters in relation to the house, i.e. measurements of building volume and envelope area, and also the finding of vents or other purposely-provided ventilation sources.

The following sections detail the test dwellings and the tests that were carried out. Also, a brief description of the analysis of the data will be provided.

5.2.1 Description of the test houses

From April to October 2018, twenty different houses were tested in the East Midlandss of the United Kingdom. It was intended to have as many "different" houses in terms of building type, building age, construction, etc. A brief description of the houses tested is given in Table 5.1. Table 5.1 includes the test number (which will be the same throughout this thesis), date when the tests were performed, volume and envelope area. It is interesting to notice that the volume - envelope area ratio for the houses is close to 1, this means that dwellings volume and envelope area are similar. The dwelling type, from mid-terrace to detached houses; shielding conditions, from no shielding to heavily shielded houses, as defined by Sherman and Dickinson [1985]; terrain conditions, from rural to urbanised areas; and; the shielded façades depending on the orientation of the dwelling were also listed.

Table 5.1: Description of test houses.

Number	Date	Volume (m^3)	Envelope Area (m^2)	Dwelling form	Shielding	Terrain	Shielded façades
1	25/04/2018	278	269	4	MS	3	-
2	22/05/2018	264	252	3	LS	3	E
3	06/06/2018	272	296	4	LS	3	-
4	03/08/2018	188	227	4	LS	3	-
5	16/08/2018	478	435	4	MS	3	-
6	22/08/2018	203	210	3	HS	3	E
7	10/09/2018	222	265	2	HS	2	N & S
8	07/06/2018	264	252	3	LS	3	E
9	12/07/2018	215	224	1	HS	2	E
10	30/08/2018	197	205	1	MS	3	N
11	24/09/2018	164	182	2	LS	3	E & W
12	27/09/2018	153	218	4	MS	3	-
13	01/10/2018	160	176	3	HS	2	N
14	04/10/2018	248	269	3	HS	2	N
15	05/10/2018	281	294	4	LS	3	-
16	08/10/2018	143	170	1	LS	3	N
17	09/10/2018	316	304	3	NO	6	S
18	10/10/2018	251	287	2	HS	2	E & W
19	18/10/2018	391	387	4	LS	3	-
20	31/10/2018	333	294	3	HS	3	E

Dwelling form

1= end of terrace

2= mid terrace

3= semi detached

4= detached

Shielding

HS= Heavy shielding. Obstructions found around the perimeter.

MS= Moderate shielding. Some obstructions within two dwelling heights.

LS= Light shielding. Few obstructions.

NO= No shielding. No obstructions or local shielding.

Terrain

1= city

2= urban

3= suburban town

4= rural residential

5= village centre

6= rural

Shielded façades

N= North

E= East

S= South

W= West

Figure 5.1 depicts twelve of the dwellings tested. All test houses were located in the Nottinghamshire and Leicestershire counties (United Kingdom).



Dwelling 2



Dwelling 3



Dwelling 6



Dwelling 10



Dwelling 11



Dwelling 12



Dwelling 13



Dwelling 14



Dwelling 15



Dwelling 16



Dwelling 17



Dwelling 19

Figure 5.1: Dwellings tested.

Further information about the construction of dwellings is included in Table 5.2.

Table 5.2: Survey information of test houses.

Number	Construction type	Type	Construction year	Ventilation
1	Cavity	Existing	1950 - 1966	PIV
2	Solid	Existing	1996 - 2002	Passive stack
3	Stone	Existing	Before 1900	Natural
4	Timber frame	Existing	2003 - 2006	MVHR
5	Solid	Retrofit	1976 - 1982	Natural
6	Solid	Existing	1983 - 1990	Natural
7	Solid	Existing	1900 - 1929	Natural
8	Solid	Existing	1996 - 2002	Passive stack
9	Cavity	Existing	1976 - 1982	Natural
10	Cavity	Existing	1991 - 1995	Natural
11	Cavity	Existing	1991 - 1995	Natural
12	Cavity	Existing	2003 - 2006	Natural
13	Solid	Existing	1900 - 1929	Natural
14	Solid	Existing	1991 - 1995	MVHR
15	Cavity	Existing	2012 onwards	Natural
16	Solid	Existing	1991 - 1995	Natural
17	System	New build	2012 onwards	MVHR
18	Solid	Existing	1930 - 1949	Natural
19	Cavity	Existing	1983 - 1990	Natural
20	Solid	Existing	1950 - 1966	Natural

It is important to remark that the system construction mentioned for dwelling 17 refers to modular construction manufactured on a factory and assembled on site.

5.2.2 Measurements: airtightness, environmental conditions and air infiltration

The tests were divided into four different stages:

1. House survey and equipment set-up: the volume and envelope area of the house were recorded; thermal zones are defined. The characteristics of the house are taken. Purposely provided vents identified. At the same time, the tracer gas and environmental conditions measuring equipment (described in the next sections) is prepared.

2. Airtightness testing with the Pulse method.

3. Airtightness testing with the steady pressurisation method.

4. Air infiltration testing using the tracer gas (carbon dioxide) concentration decay method.

5.2.2.1 Airtightness

As mentioned before, two different airtightness tests were carried out: Pulse and steady pressurisation (blower door) methods.

5.2.2.1.1 Pulse method

The Pulse method, described in Chapter 3, was the first airtightness testing method exercised.

Pulse tests consisted of sealing all provided vents such as grills, cooker hood vents, trickle vents, among others. Standards require these sealings for compliance [The Air Tightness Testing and Measurements Association, 2016, International Organization for Standardization, 2015]. Three three-step tests are performed. The unit used for the test was the latest mark3.0 prototype version of the Pulse from BTS Ltd, shown in Figure 5.2. All house preparations complied with the standards [The Air Tightness Testing and Measurements Association, 2016, International Organization for Standardization, 2015].



Figure 5.2: Latest version of the Pulse unit.

5.2.2.1.2 Steady pressurisation method

After all Pulse tests were performed, the house was left in the "sealed" conditions (sealing in vents, trickle vents, drains, cooker hoods and other purposely

provided ventilation devices, see figure 5.3 for an example. One pressurisation and one de-pressurisation test was performed. The average result of both pressurisation/depressurisation was also recorded. The equipment used was the "Mini-Fan Blower Door System", using a Minneapolis duct blaster fan and a DG-1000 pressure and flow gauge, manufactured by "The Energy Conservatory" (Figure 5.4). The measurements were carried out according to standard [International Organization for Standardization, 2015, The Air Tightness Testing and Measurements Association, 2016]; the results were computed using the TECtite software from "The Energy Conservatory". In all cases the blower door was placed in the main door of the dwellings, which only in one case faced the recorded average direction of the wind. Table 5.3 shows the orientation of the main door and if the blower door was facing the average direction of the wind.

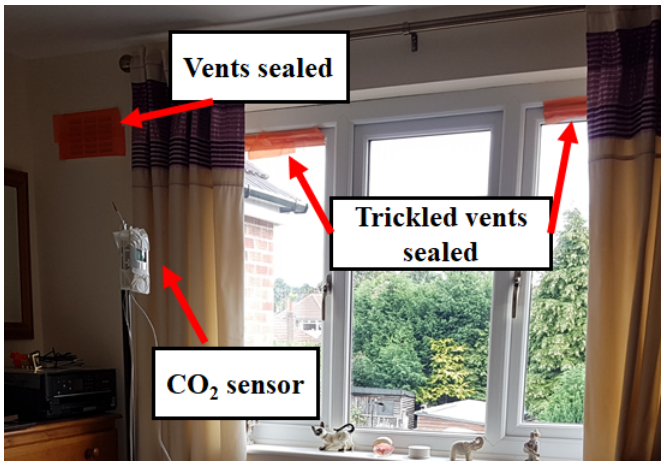


Figure 5.3: Example of sealed conditions in dwelling 6 with vents and trickle vents sealed.



Figure 5.4: Blower door unit used in the field investigation study (photo by The Energy Conservatory).

Table 5.3: Orientation of the main door of dwellings and blower door.

Dwelling	**Orientation of main door (°)**	**Blower door facing direction of wind**
1	30	NO
2	15	NO
3	285	NO
4	5	NO
5	45	NO
6	180	NO
7	345	NO
8	15	NO
9	180	YES
10	90	NO
11	0	NO
12	345	NO
13	270	NO
14	90	NO
15	90	NO
16	90	NO
17	285	NO
18	45	NO
19	75	NO
20	180	NO

5.2.2.2 Environmental conditions

Three different environmental parameters are necessary for the tests involved in this study: wind, indoor temperature, and outdoor temperature. These were measured once every second while the tests were being performed. Table 5.4 presents the equipment used for these measurements. .

Table 5.4: Environmental conditions measuring equipment.

Measurement	**Equipment**	**Number of pieces**
Indoor temperature	Temperature sensors PT100 RTD (±0.8°C at 0°C)	up to 6
Outdoor temperature	Temperature sensor PT100 RTD (±0.8°C at 0°C)	1
Wind	GILL instruments WindSonic Ultrasonic Wind Sensor option 1 (±2% @12m/s)	1
Data logging	Data logger data taker DT-85	1
Other	Tripods	6

All sensors were connected to the same data logging equipment (Datataker DT85) conveniently located inside the house.

Indoor temperature sensors were installed in every thermal zone of the house. The number of zones in a dwelling was dependent upon the size and layout of the house; however, for most of the tests, six different zones were defined. The temperature sensors were positioned at 1.5 meters of height using a tripod placed at least one meter away from walls in all directions. The outdoor temperature sensor was installed in the same tripod used for the wind sensor.

Wind measurement presented different complications from house to house. Locating the anemometer in a non-shielded area such as the roof was the most desirable option; however, this was not possible due to the lack of access to this area. The wind sensor was located based on the accessibility. In the majority of tests, the most accessible location was the backyard; nevertheless, it is acknowledged that an error is present due to wind turbulence created by fences, vegetation, neighbouring houses or the test house itself. While in most of the cases, the anemometer was placed on top of a two-meter tripod; sometimes it was possible to place it higher, on top of fences (see Figure 5.5).



Figure 5.5: Location of Wind sensor in house number 10.

After completion of all the tests, the measurements were downloaded to a CSV file. Environmental conditions measurements were put together with airtightness and air infiltration results.

5.2.2.3 Air Infiltration

The last parameter to measure in each dwelling, was the air infiltration rate. The selected method was the tracer gas concentration decay. The advantages of the method, presented in Chapters 2 and 4, were decisive when selecting a quick, reliable and inexpensive way to measure the infiltration rate.

Concentration decay method was carried out according to the American (ASTM E741-11) and European (ISO 12569:2017) standards [American Society for Testing and Materials, 2011, International Organization for Standardization, 2017]. The calculation selected was the regression method due to the number of data points collected.

The carbon dioxide sensors were installed one in each zone on the same tripods as the temperature sensors. Note that the equipment was not suitable for outdoor uses; therefore, for calculations purposes outdoor CO_2 concentration was assumed to be 400 ppm.

The CO_2 sensors were connected to the same data logger as the temperature and wind sensors, with a sampling rate of 1 Hz. Fans were used to obtain a homogeneous distribution of the gas in the air. A summary of the equipment is given in Table 5.5.

Table 5.5: Air infiltration concentration decay method equipment.

Measurement	**Equipment**	**Number of pieces**
Tracer gas	Carbon Dioxide (CO_2)	one 6 litre tank
Gas monitoring	Sontay 0-5000 ppm CO_2 sensor (GS-CO2-1001-T-HR) ± 5%	up to 6
Gas mixing	fans	up to 6
Data logging	Data logger data taker DT-85	1
Other	Tripods	6

The ASTM E741-11 standard [American Society for Testing and Materials, 2011] mentions a minimum duration of the decay method test (see Table 5.6). This duration was not possible to accomplish in every single test due to time constraints; however, for most of the properties, the standard was followed entirely. Carbon dioxide sensors monitored the decay of the tracer gas during the test period. Figure 5.6 shows a typical decay curve of the average concentration measured from the sensors.

Table 5.6: Examples of minimum durations between the initial and final samples for the concentration decay method. From ASTM E741-11 [American Society for Testing and Materials, 2011].

Air change rate (h^{-1})	Minimum duration of test (h)
0.25	4
0.5	2
1	1
2	0.5
4	0.25

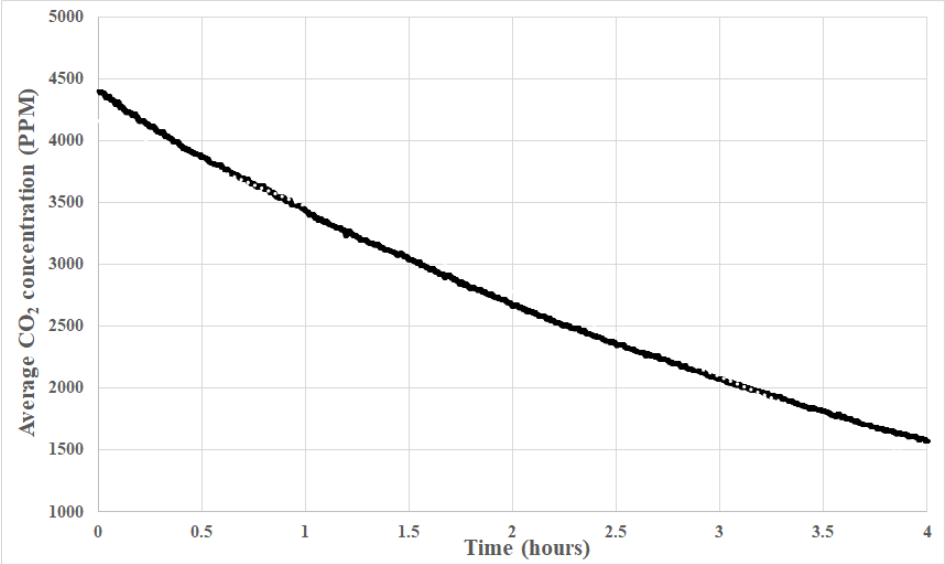


Figure 5.6: Concentration decay of dwelling 12.

The test starts by dispersing carbon dioxide in every thermal zone until the concentration approached 5000ppm. All personnel are removed from the property and with the vents sealed, doors and winds closed, the gas is then left to decay. The testing team returned to the house when either, the elapsed time is enough to obtain a decay according to standard (Table 5.6), or, the permitted time to use the house elapsed.

The data was downloaded to a laptop computer on the day of the test. The equipment packed and the house cleared. An average infiltration rate (from the test hours) was determined and analysed according to the standards.

The results obtained by the tracer gas decay method (namely air infiltration rate) were only representative of the conditions present during the tests. The air infiltration rate was given in the unit of air changes per hour (n_1, h^{-1}).

According to the standards, a least-squares regression between the natural logarithm of the concentration and the time must be computed. The best linear fit is produced and the slope of the equation represents the air infiltration rate of the building. Figure 5.7 shows the time against the natural logarithm of the concentration regression in dwelling 12; it also shows the equation of the best fit and the r^2 value. In both, Figures 5.6 and 5.7, dwelling 12 was used as an example to illustrate how a tracer gas test analysis is done.

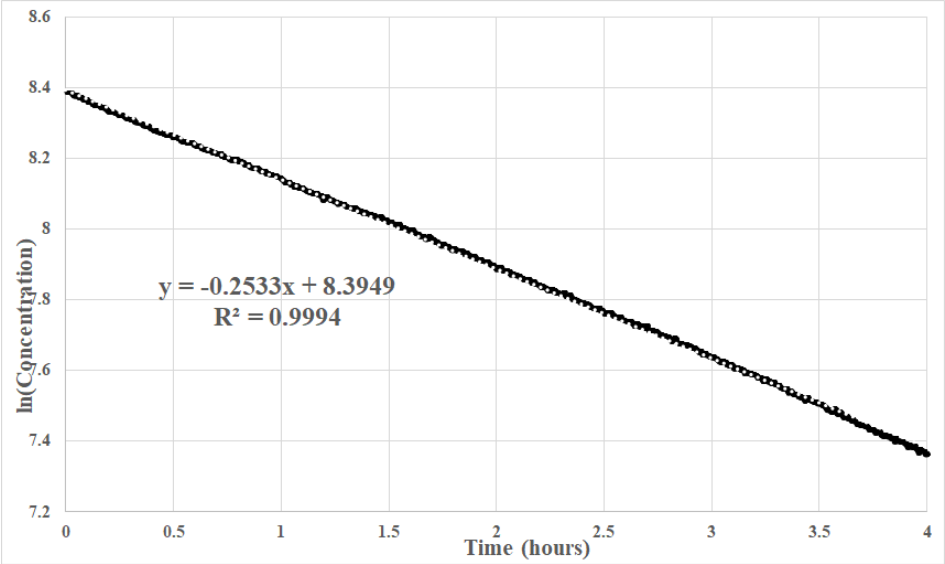


Figure 5.7: Natural logarithm of the decay of dwelling 12 versus time wit time of best fit via linear regression.

During the execution of tracer gas tests, the environmental conditions were measured. Figures 5.8 and 5.9 illustrate the measured wind and temperature in dwelling 12. It is pertinent to remark that the equipment was recording measurements at 1 Hz of frequency. These figures aided when calculating representative figures of the environmental conditions (Table 5.7). Similar figures as 5.8 and 5.9 for all dwellings are included in Appendix E.

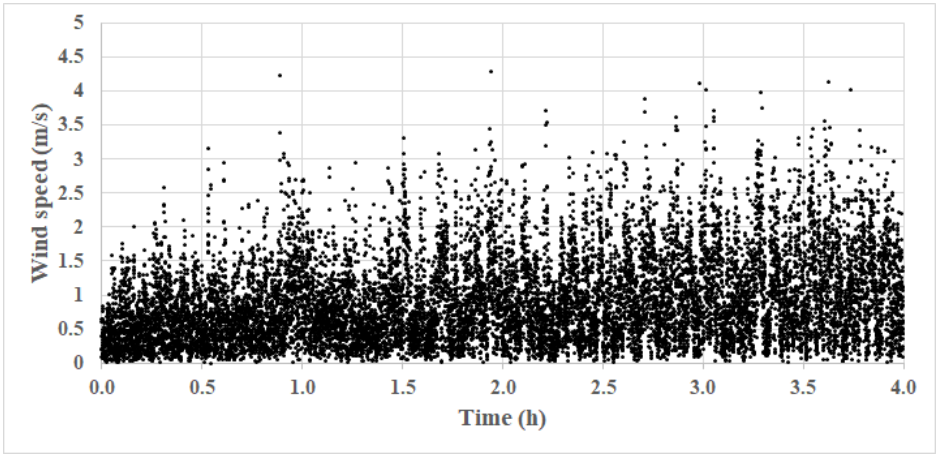


Figure 5.8: Measured wind speed during the tracer gas concentration decay test in dwelling 12

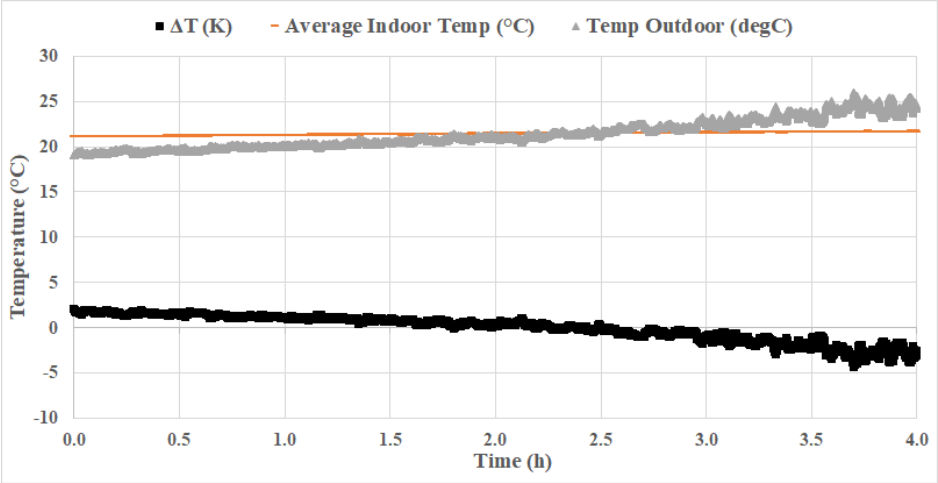


Figure 5.9: Measured indoor and outdoor temperatures (and calculated temperature difference) during the tracer gas concentration decay test in dwelling 12

Table 5.7: Summary of the environmental conditions present during tracer gas concentration decay tests.

dwelling	**Mean ΔT (K)**	**Mean wind speed (m/s)**	**Mean wind direction (°)**
1	4.73	2.74	224
2	2.05	1.17	185
3	1.13	0.57	192
4	3.69	1.08	250
5	3.40	0.71	216
6	0.19	0.93	87
7	2.87	0.86	170
8	1.71	1.70	195
9	1.66	0.51	177
10	1.65	0.51	193
11	3.72	0.76	205
12	0.01	0.91	249
13	6.13	0.67	121
14	1.31	0.85	197
15	1.96	0.93	227
16	4.83	0.75	199
17	11.08	0.36	178
18	0.70	1.03	163
19	3.91	0.59	229
20	3.55	1.70	83

5.2.2.3.1 Calculation of uncertainty

The uncertainty in air infiltration results was also estimated. Three different uncertainties were considered:

1. Uncertainty in the data [Hughes and Hase, 2010].
2. Uncertainty in the regression.
3. Uncertainty and confidence intervals calculation as per the ASTM standard [American Society for Testing and Materials, 2011].

Results report the highest of the three. A graph including the calculated uncertainty and the confidence intervals is plotted for every test. Figure 5.10 shows an example of these graphs. The graphs for all the test carried out are included in Appendix E.

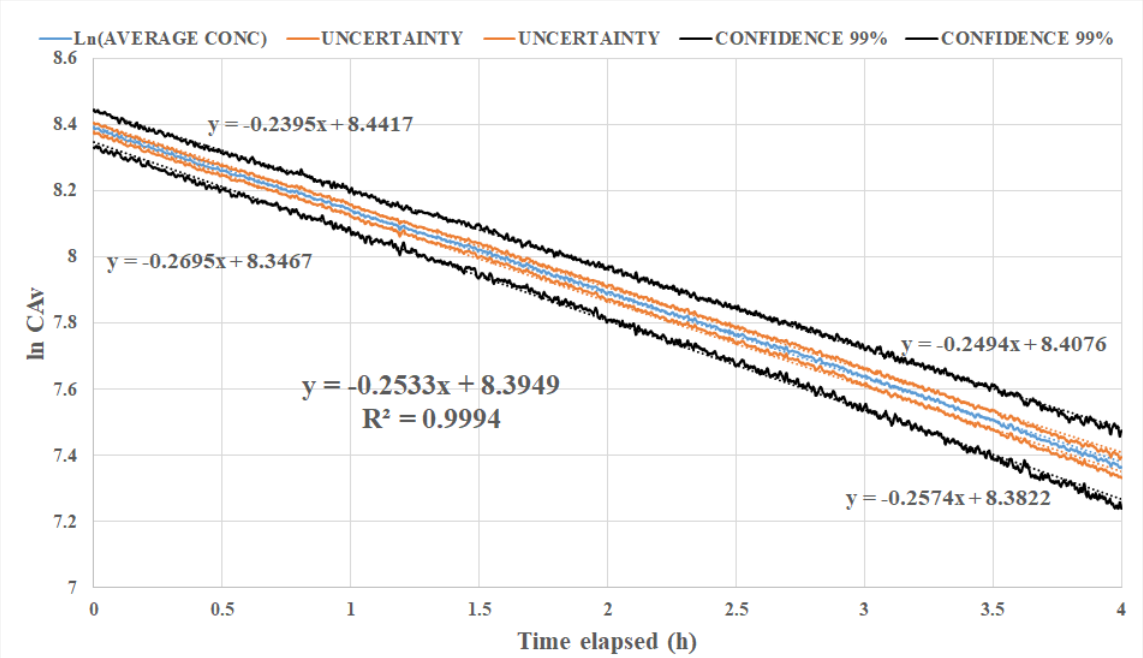


Figure 5.10: Calculation of infiltration rate, uncertainty and confidence intervals for dwelling 12.

5.2.3 Pulse airtightness temperature corrections

In order to determine the mass flow rate of air from the air tank, when a pulse of air is released the temperature of air in the tank must be measured to calculate the air density. The Pulse unit performs this as part of its measurement and calculation function. For simplification purposes, the initial Pulse units measured

room temperature and assumed this to be the initial tank temperature. This assumption provided good results based on a single-step test.

As mentioned in Chapter 3, a Pulse test, can include three "steps" or three "pulses". Each time air is released, the temperature falls rapidly and the original algorithm used in Pulse did not account for this change.

In order to test the impact of the inclusion of a change in temperature, data from five tests in different dwellings were taken and corrections were made to the density of air based upon changes in the tank temperature. For these five tests, three-step tests were modified $\pm 5^{\circ}$ for one or more steps; there were in total 27 combinations. Results showed that for that minimum (5°) change in temperature, there was a change of up to 3% in the calculated air leakage rate.

Due to these findings, it was necessary to determine a temperature correction process, which could be applied to the date from the field trial.

Bench tests were performed with a 60L aluminium tank, whereby air was released as per the timings/duration of typical Pulse tests. Temperature was measured inside the tank with a fine probe NTC thermistor at a length such that the temperature was being measured in the centre of the tanks volume.

Results from eighteen different tests showed that the starting temperature of the tank was on average $3^{\circ}C$ above the ambient temperature (Table 5.8). This can be explained due to the process of charging the tank via the air being compressed, through the reciprocating compressor.

Table 5.8: Measured ambient and tank temperatures at the beginning of the test.

Test	**Ambient temp. (°C)**	**Tank temp. (°C)**	**Difference (K)**
1	25.22	29.72	4.50
2	25.31	27.09	1.78
3	25.25	26.88	1.63
4	25.17	28.45	3.28
5	25.08	26.81	1.73
6	24.97	28.62	3.65
7	24.94	27.07	2.13
8	24.91	28.01	3.09
9	22.38	23.25	0.87
10	18.19	21.01	2.82
11	17.19	22.11	4.92
12	16.25	23.63	7.38
13	15.77	22.32	6.55
14	21.62	23.56	1.94
15	22.08	23.74	1.66
16	23.15	25.50	2.35
17	23.95	25.95	2.00
18	24.63	27.11	2.48
		Average	3.04
		Std. dev.	1.72
		Std. error	0.4

Therefore,

$$T_{0A} = T_{ab} + 3 \tag{5.1}$$

where T_{0A} is the tank temperature in $°C$ before the first step, or step "A", and T_{ab} is the measured ambient temperature in $°C$. As can be seen there is a general temperature elevation of a charged tank compared to the background ambient.

There is a temperature drop in the tank due to the fast air release; this effect is called the "temperature fall" in a pulse (Equation 5.2). Following the initial fall, warming is observed in the tank; therefore, the temperature rises (Equation 5.3).

$$T_{fallA} = 15.077 + ln(P_{fallA}) + 27.552 \tag{5.2}$$

$$T_{warmA} = 0.2807(\Delta_{tankA}) - 8.1002 \tag{5.3}$$

where T_{fall} is the temperature fall in $°C$, P_{fall} is the tank pressure fall in bar, T_{warm} is the effect of warming in the tank in $°C$, and Δ_{tank} is defined by Equation 5.4. Suffix A refers to pulse A, before starting pulse (or step) B.

$$\Delta_{tank} = T_{ab} - T_{0A} - T_{fallA} \tag{5.4}$$

All these equations are based on the results of the experimental bench study. The empirical relations were obtained from data taken in different conditions and scenarios. Figures 5.11 and 5.12 display the data.

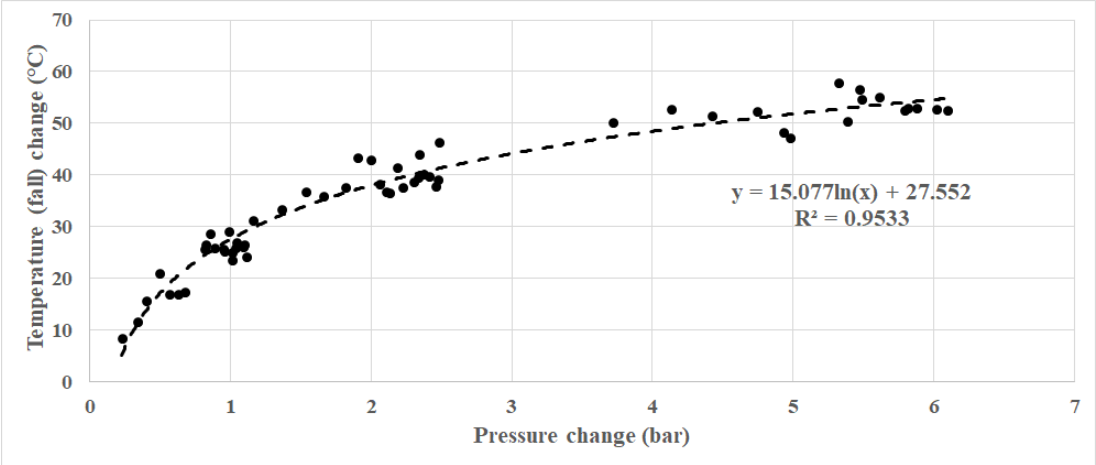


Figure 5.11: Fit of temperature fall from an experimental study on tank temperatures using data from multiple tests of three pulse steps.

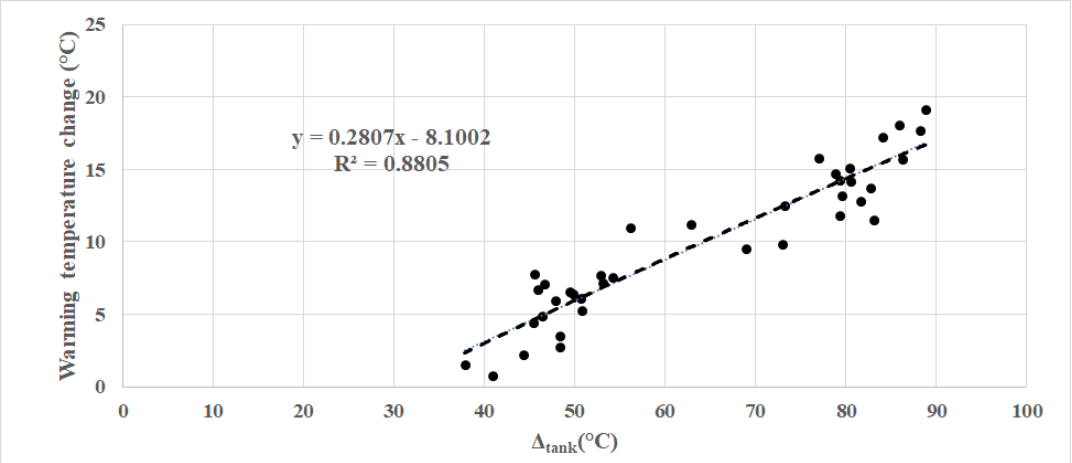


Figure 5.12: Warming between pulses versus difference in end temperature of the previous pulse and the ambient using all data from multiple tests of three pulse steps.

The equations fitting the data have relatively large r^2 values, meaning that the correlation is strong. After repeating the calculations, the final temperature change process would in a simplified form look like that shown in Figure 5.13.

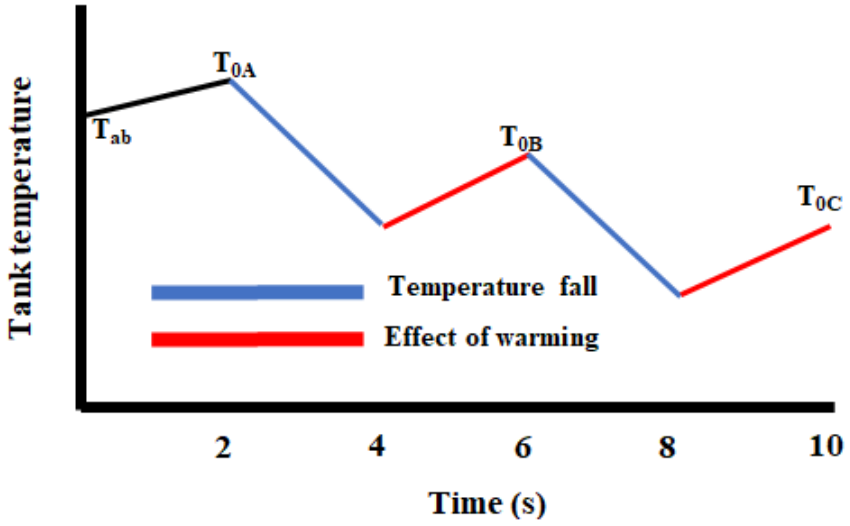


Figure 5.13: Simplified process of the change in temperature of the air inside the tank (not to scale) during a three-step test.

Therefore, the equation for a temperature correction at the beginning of step B or C is given by:

$$T_{0B} = T_{0A} - T_{fallA} + T_{warmA}$$
$$T_{0C} = T_{0B} - T_{fallB} + T_{warmB} \tag{5.5}$$

T_{fallB} and T_{warmB} follow the same equations as for step A, using the data obtained for step B.

After testing this newly developed temperature correction with several Pulse tests, it was seen that there was an average relative difference of 18% between the original and the corrected measurements. This procedure made a physical correction of an assumption used in the pulse technique.

Before the temperature correction, Pulse underpredicted the air permeability. It is believed that when the temperatures are corrected, the results are more accurate. These modifications were used to correct more than 600 pulse tests, three steps on each test, therefore there were more than 1800 points to modify. A MATLAB code was created to modify these tests. Appendix A includes the code used. All the Pulse results presented from this point in the field data collection stage of the project are corrected.

5.3 Results

5.3.1 Airtightness

5.3.1.1 Steady pressurisation method results

The results obtained using the steady pressurisation method are divided into three categories: pressurisation, depressurisation and an average of both methods. The averages are regarded as the "true" airtightness values. A complete list of the measurements is found in Table 5.9; the airtightness measurements reported at 50 Pa are given in air change or air leakage rate (h^{-1}) and air permeability ($m^3h^{-1}m^{-2}$) units. Additionally, the measured flow exponent (b_{50}) is presented.

Table 5.9: Steady pressurisation method measurements results.

Dwelling	Depressurisation			Pressurisation			Average		
	Air leakage rate @50 Pa, n_{50} h^{-1}	Air permeability @50 Pa, q_{50} $m^3h^{-1}m^{-2}$	flow exponent b_{50}	Air leakage rate @50 Pa, n_{50} h^{-1}	Air permeability @50 Pa, q_{50} $m^3h^{-1}m^{-2}$	flow exponent b_{50}	Air leakage rate @50 Pa, n_{50} h^{-1}	Air permeability @50 Pa, q_{50} $m^3h^{-1}m^{-2}$	flow exponent b_{50}
1	7.37	7.62	0.62	7.87	8.13	0.587	7.62	7.88	0.604
2	5.76	6.03	0.624	5.76	6.03	0628	5.76	6.03	0.626
3	8.96	8.23	0.609	8.23	7.56	0561	8.59	7.90	0.585
4	5.31	4.40	0682	5.31	4.40	0.636	5.31	4.40	0.659
5	3.50	3.84	0.639	3.53	3.88	0.553	3.51	3.86	0.596
6	7.43	7.18	0.688	8.30	8.02	0.518	7.86	7.60	0.603
7	8.23	6.89	0.681	9.00	7.54	0.708	8.61	7.22	0.695
8	5.77	6.04	0.626	5.77	6.04	0.559	5.77	6.04	0.626
9	6.85	6.57	0.639	7.35	7.05	0.559	7.10	6.81	0.633
10	10.41	10.00	0.617	10.49	10.08	0.612	10.45	10.04	0.634
11	9.38	8.45	0.718	10.08	9.08	0.515	9.73	8.77	0.612
12	8.14	5.71	0.664	8.52	5.98	0.592	8.33	5.85	0.628
13	14.82	13.47	0.620	15.13	13.75	0.567	14.97	13.61	0.594
14	4.98	4.59	0.736	5.16	4.76	0.690	5.07	4.68	0.713
15	5.46	5.22	0.650	5.69	5.44	0.619	5.58	5.33	0.635
16	13.21	11.11	0.625	13.33	11.21	0.541	13.27	11.16	0.583
17	3.98	4.14	0.674	4.27	4.44	0.535	4.13	4.29	0.605
18	11.25	9.84	0.712	11.43	10.00	0.662	11.34	9.92	0.687
19	12.09	12.21	0.680	14.49	14.64	0.504	13.29	13.43	0.592
20	12.08	13.68	0.751	12.41	14.05	0.760	12.24	13.87	0.756

The average air leakage (change) rate is 8.43 h^{-1} with a standard deviation of 3.22 h^{-1} at 50 Pa and at the same time the figures for air permeability are 7.93 $m^3h^{-1}m^{-2}$ and 3.08 $m^3h^{-1}m^{-2}$ respectively (at 50 Pa). The average flow exponent is 0.633 (standard deviation 0.46). A graphic description is given in Figure 5.14.

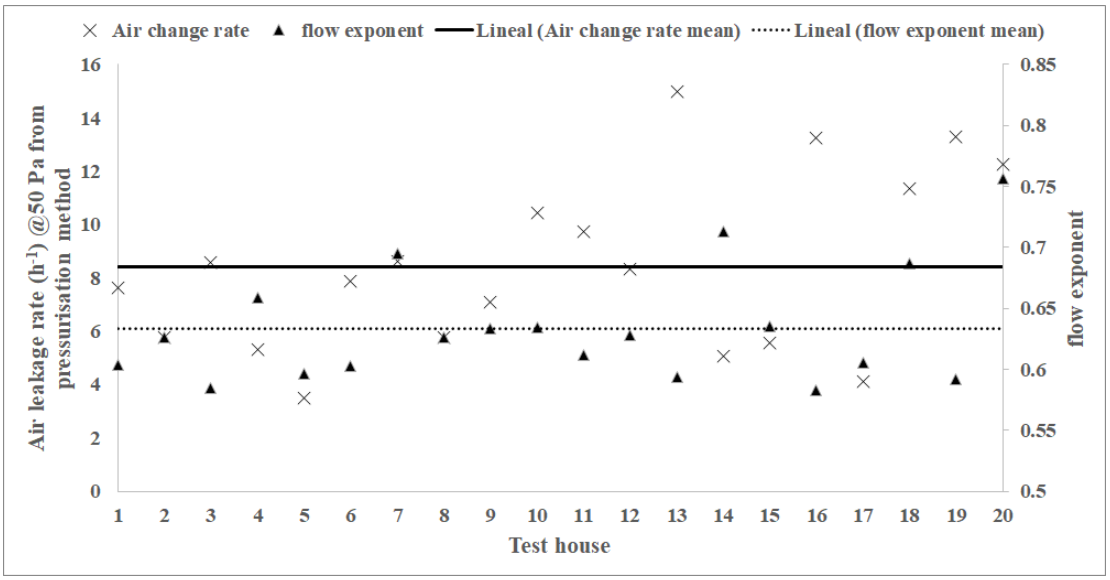


Figure 5.14: Results from steady pressurisation tests (air leakage rate and flow exponent).

Requirements under Part L of the UK building regulations for new build homes [HM government, 2013] asks for a maximum air permeability of 10 $m^3h^{-1}m^{-2}$. For this sample, five dwellings do not comply with this, i.e. 75% of dwellings are complying with the standard [Building Research Establishment, 2013, HM government, 2013]. On the other hand, four dwellings have an air permeability lower than 5 $m^3h^{-1}m^{-2}$; these can be considered as "tight" houses, two of those houses were built after 2003, one after 1991, and the last one (dwelling 5) was retrofitted to improve the airtightness. It can be pointed out that the building sector is progressively constructing "tighter" dwellings with time as regulation becomes stricter.

5.3.1.2 Pulse method results

Pulse tests' results are given in Table 5.10. Table 5.10 presents data reported at 4 Pa for the measured air leakage rate (h^{-1}), air permeability ($m^3h^{-1}m^{-2}$) and flow exponent. Additionally, the error due to reproducibility (Relative Percentage Difference) is given (from all the tests performed); for tests 17 and 19 only one (valid) test was performed due to time and house availability constraints.

Table 5.10: Pulse results.

Dwelling	**Pulse results**			
	Air leakage rate @4 Pa,n_{50} h^{-1}	Air permeability @4 Pa,q_{50} $m^3h^{-1}m^{-2}$	flow exponent b_4	Mean repeatability (%)
1	1.525	1.576	0.680	7.3
2	1.221	1.279	0.680	1.0
3	2.074	1.906	0.652	5.8
4	1.010	0.836	0.707	1.3
5	0.717	0.788	0.675	6.5
6	1.408	1.361	0.758	0.3
7	1.785	1.495	0.696	1.7
8	1.227	1.285	0.604	2.3
9	1.643	1.577	0.634	1.2
10	2.385	2.292	0.743	3.1
11	1.886	1.699	0.713	0.3
12	1.696	1.190	0.681	0.2
13	3.698	3.362	0.738	2.7
14	0.907	0.836	0.741	2.6
15	1.186	1.134	0.648	3.4
16	2.640	2.220	0.706	1.0
17	1.027	1.067	0.550	N/A
18	2.109	1.844	0.709	4.6
19	3.158	3.190	0.821	N/A
20	2.489	2.819	0.629	6.3

The mean measured air leakage rate and air permeability are 1.79 h^{-1} and 1.69 $m^3h^{-1}m^{-2}$ respectively (at 4 Pa), for the flow exponent the mean is 0.688; these results are shown in Figure 5.15.

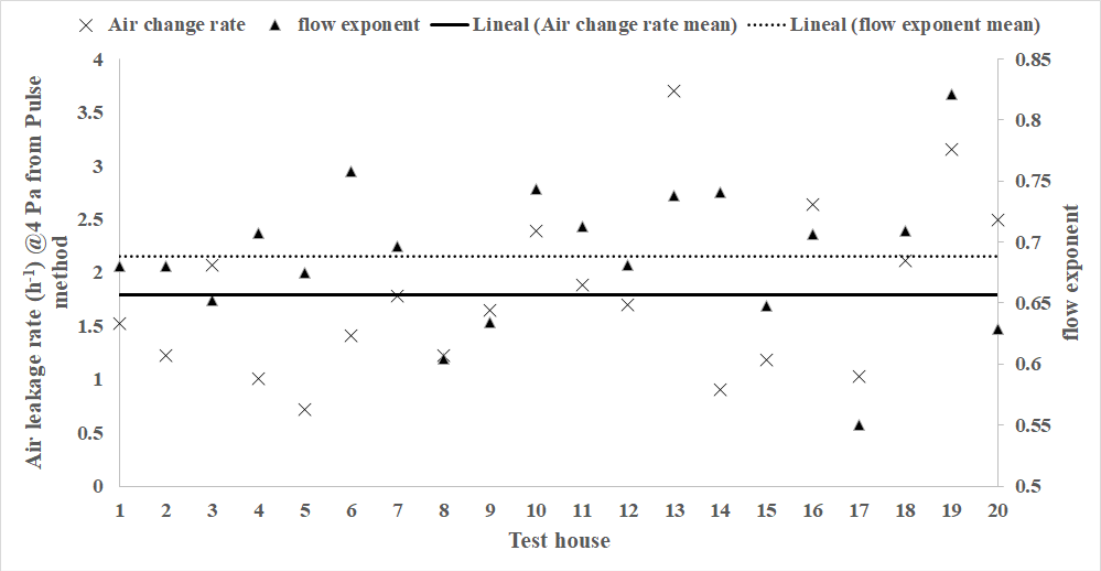


Figure 5.15: Results from Pulse tests (air leakage rate and flow exponent).

There has been interest from industry and regulatory agencies to know how the results from the steady pressurisation method and Pulse compare. Zheng et al. [2019b] and Zheng et al. [2019a] have addressed this question by carrying out a testing campaign with both methods. To understand this, it is essential to remember that both methods involve the usage of the power law ($Q = C\Delta P^b$, as defined in Equation 2.8)). The steady pressurisation method uses a pressure difference (ΔP) of 50 Pa and Pulse of 4 Pa. Moreover, an average flow exponent can be taken as 0.66. If a theoretical but simple ratio is to be developed using these values (Equation 5.6), N_{50-4} takes a value of 5.3. Zheng et al. reported a value very close to that figure from their studies where empirical values obtained by Pulse and steady state methods were used. Furthermore, the authors also mentioned that the value of N in most cases lies between 4 and 6.

$$N_{50-4} = \frac{50^{0.66}}{4^{0.66}} \tag{5.6}$$

For this study, the ratio found is 4.79 $\pm$ 0.105, which lies in the range given by Zheng et al. [2019a] and close to the theoretical 5.3. This ratio was found by dividing each of the airtightness measurements of the steady pressurisation method (average from pressurisation and depressuration) by the Pulse method. The ratio is the average of all test houses.

5.3.2 Air infiltration - Tracer gas decay method

Infiltration rates were estimated using measurements of the concentration decay method. Measurements from all dwellings are included in Table 5.11. The infiltration rate is given in air changes (h^{-1}), the duration of the test and the maximum uncertainty is also mentioned. Likewise, the average environmental conditions during the tests are given.

Table 5.11: Tracer gas concentration decay method results.

Dwelling number	**Air infiltration rate,**n_1 h^{-1}	r^2	**Test duration** (h)	**Uncertainty** $\pm h^{-1}$	**Average wind** (m/s)	**Average** $\Delta T(K)$
1	0.1484	1	7.32	0.0009	2.736	4.73
2	0.2093	0.997	9.00	0.0192	1.174	-1.83
3	0.2080	0.999	5.00	0.0069	0.569	1.13
4	0.1241	1	8.5	0.0019	1.08	3.69
5	0.0787	0.998	8.00	0.0036	0.710	3.39
6	0.3171	0.998	6.67	0.0071	0.930	0.19
7	0.3512	0.999	4.50	0.0305	0.860	2.87
8	0.1645	0.997	4.17	0.0020	1.700	0.94
9	0.1514	0.999	3.00	0.0027	0.510	1.66
10	0.2344	0.993	6.50	0.0004	0.500	1.64
11	0.2284	0.998	4.33	0.0026	0.760	3.73
12	0.2533	0.999	4.00	0.0041	0.910	0.01
13	0.4192	1	4.17	0.0259	0.67	6.13
14	0.0849	0.995	3.43	0.0014	0.850	1.30
15	0.1504	0.996	3.75	0.0033	0.930	1.95
16	0.5189	1	3.25	0.0111	0.750	4.83
17	0.0998	0.989	13.5	0.0059	0.350	11.00
18	0.3594	0.998	2.33	0.0303	1.030	-0.70
19	0.2928	0.999	3.25	0.0303	0.59	3.91
20	0.2753	0.991	2.5	0.0171	1.7	3.55

The majority of the test durations were higher than that required by the standard, except from tests 9, 14 and 15, which should have taken over 4 hours. Despite having co plied with the standards it is acknowledged that the duration of tests 5, 8, 18, 19 and 20 should have been longer due to the calculated infiltration result;

nevertheless the time that the properties were available was a constraint for this study. The average infiltration rate from the 20 houses is 0.2335 h^{-1}. The decay method tests showed to provide accurate results with -relatively- low uncertainty (within the limits showed by other authors [Sherman, 1989]); except for properties 16 and 19 (uncertainties above 10%). Furthermore, the r^2 values given in the decay tests are close to one; therefore, tests can be considered as valid.

5.4 Discussion

The main objective of this thesis is to find a correlation between airtightness measurements taken ata low-pressure differential (i.e. Pulse) and air infiltration. It is known that airtightness fundamentally determines the infiltration rate (despite the interaction of different parameters). Hence a potential direct correlation between airtightness and air infiltration can be studied.

With all the gathered data, an empirical model can be obtained and then analysed. With information from both, the steady pressurisation method, and the Pulse method, different models can be created and tested. The following sections discuss the development, test and validation of these models.

5.4.1 Correlating air infiltration and airtightness

Results from measurements are analysed to find an empirical infiltration - airtightness correlation. The data presented in this section only represents the sample of tested properties. The objective of this exercise is to understand the uncertainty created by only using airtightness to predict air infiltration.

By using airtightness as an independent variable and air infiltration as a dependent variable, the measured data was placed on a graph, and a curve was fitted to develop a simple model. It was observed that a linear and power model provided a best fit for the data.

Using the steady pressurisation method measurements, Figures 5.16 and 5.17 represent the linear and power models. These figures have airtightness in the x-axis and air infiltration in the y-axis, both in air changes per hour (h^{-1}). The linear model obtained is:

$$n_1 = 0.0299(n_{50}) - 0.0189 \tag{5.7}$$

where n_1 is the predicted infiltration rate and n_{50} is the measured air leakage rate from the steady pressurisation method, both in h^{-1}. Furthermore, the power

model obtained:

$$n_1 = 0.0197 n_{50}^{1.142}. \tag{5.8}$$

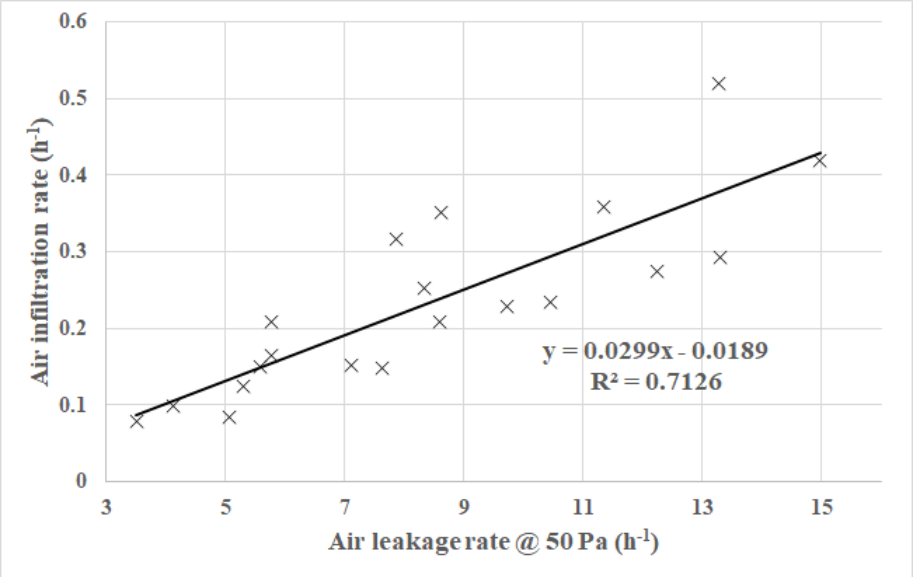


Figure 5.16: Linear correlation between steady pressurisation tests (airtightness) and air infiltration rate.

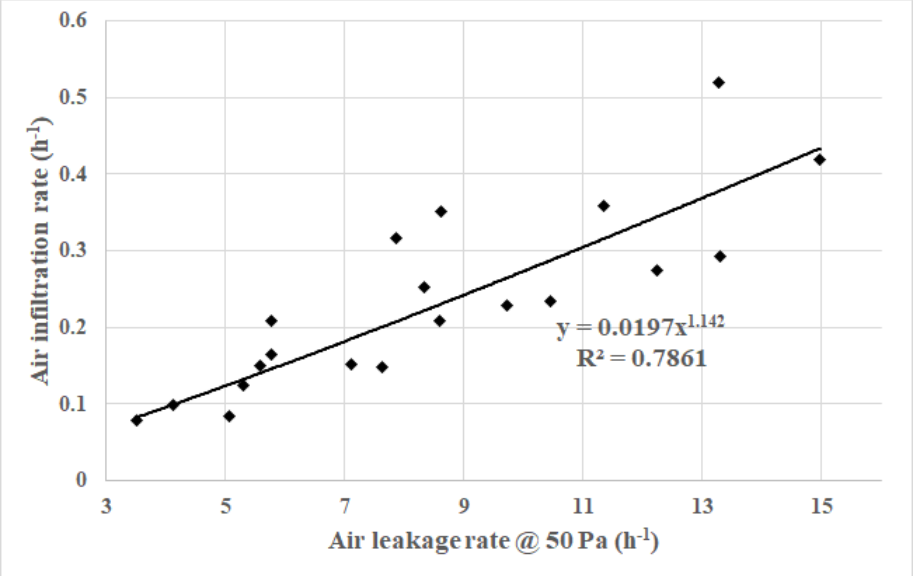


Figure 5.17: Power correlation between steady pressurisation tests (airtightness) and air infiltration rate.

the linear and power models have an r-squared value of 0.7126 and 0.7861 respectively. Theoretically, the models have an accuracy of over 70%. It is impor-

tant to remark that these models do not account for the weather, shielding or terrain conditions.

A similar exercise was carried out for the measurements taken by the Pulse method. Figures 5.18 and 5.19 include the linear and power models based on Pulse measurements.

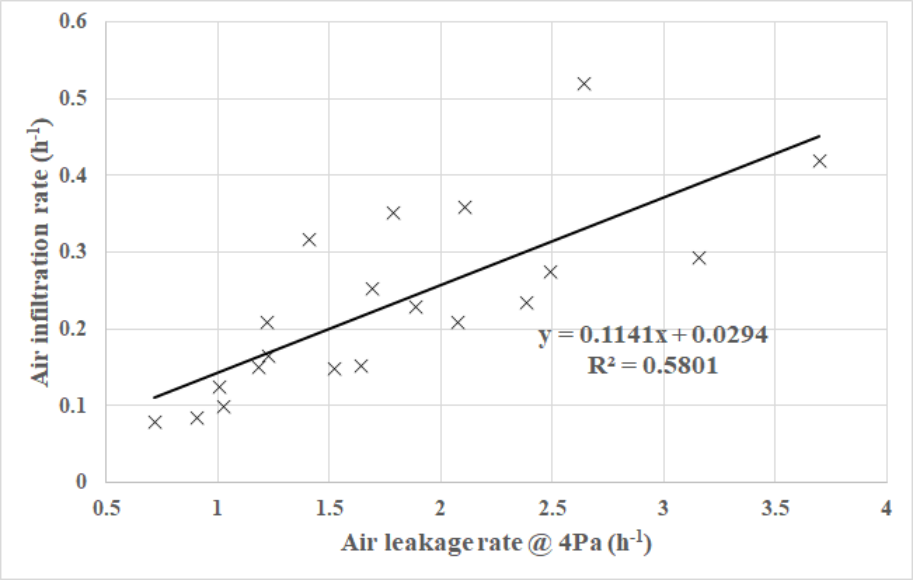


Figure 5.18: Linear correlation between Pulse tests (airtightness) and air infiltration rate.

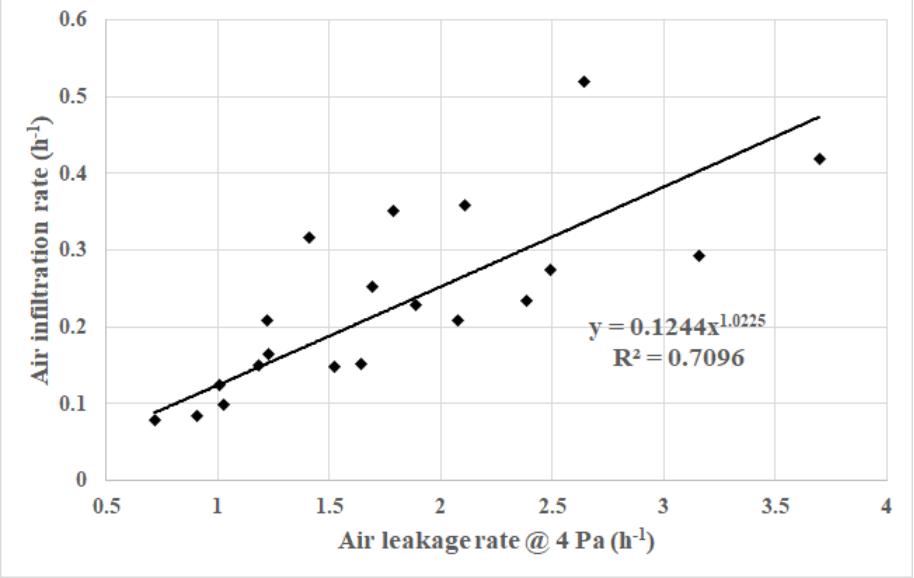


Figure 5.19: Power correlation between Pulse tests (airtightness) and air infiltration rate.

The linear model:

$$n_1 = 0.1141(n_4) + 0.0294 \tag{5.9}$$

where n_4 is the air leakage rate (h^{-1}) measured with the Pulse method. The power model:

$$n_1 = 0.1244 n_4^{1.0225}. \tag{5.10}$$

The r-squared values are 0.5801 and 0.7096 for the linear and power models respectively. The exponent in the power model is very close to one, meaning that the model is close to a linear model with an intersect of 0. Despite this approximation, the coefficient of determination is closer to one for the power model than for the linear model.

Comparing both techniques, the models created using the steady pressurisation method measurements are more accurate; however, these need a validation procedure.

5.4.2 Statistical analysis and validation

Due to the number of data points and the empirical nature of this analysis, a suitable cross-validation method for the models is the "leave-one-out" approach. Both the linear and the power models were cross-validated for the steady pressurisation and Pulse methods.

The leave-one-out approach uses all the data except for one data point and, re-testing the models to predict the outcome of the point that was left out. For example, in this case, twenty properties were used to create the models, in the leave-one-out approach, only nineteen are used to create 20 different models (each one leaving out one of the twenty properties). The next step is to use the new model to predict the dependent variable (air infiltration rate) using the independent variable (airtightness air leakage rate). In the end, the errors between measured and predicted values are accounted, and the average is reported. This approach is used to validate models with few data points.

In this section, the leave-one-out approach is used to assess the capacity of the models of predicting new data. In addition, the linear and power models are compared based on the results.

Table 5.12: Errors from the leave-one-out cross-validation approach.

	Blower door	**Pulse method**
Linear model	7.1%	12.7%
Power model	3.5%	4.9%

Table 5.12 shows the average error for the linear and power models obtained using the leave-one-out approach. The independent variable in the models was the air leakage rate measured with the steady pressurisation and Pulse methods. The power model, showed in the previous section, to be a better fit than the linear model, with a higher r-squared value. Moreover, in this analysis, the power model showed better results, only 3.5% and 4.9% of average error for the steady pressurisation and pulse methods respectively.

The errors were higher in both cases for the linear model. In conclusion, this cross-validation showed that the power models (Equations 5.8 and 5.10) describe better the data obtained and are better to predict new data.

Although the power model showed an accuracy of more than 70% (R-squared), the data used to validate it was the same one as the one used to create it. That is why two dwellings were re-tested in the summer of 2019. The objectives of these tests were first, to see if the airtightness of the dwellings changed, and second, to assess the model predictions using new data.

The selected properties for a re-test were property 4 and 5; these re-tests are going to be referred to as tests 4b and 5b. Table 5.13 includes the measurements from the re-tested properties. The methodology to carry out the re-tests was the same one used in the field data collection phase.

Table 5.13: Results from re-test of properties 4 and 5.

Property	**Blower door** n_{50} (h^{-1})	**Pulse method** $n_4(h^{-1})$	**Air infiltration rate, tracer gas** n_1 (h^{-1})
4b	6.2123	1.1176	0.0971
5b	4.1225	0.7389	0.0583

In both cases, the airtightness of the dwellings changed from the initial tests to the later tests. That is to say that the air leakage rate at both 4 and 50 Pa increased, meaning that there was some deterioration of the envelope. The infiltration rate was expected to be different due to different conditions; however,

despite the increase in air leakage rate, the infiltration rate decreased; probably due to the low wind and low temperature difference expected in the summertime. This illustrates why having a model that only takes airtightness into account to predict infiltration will not deliver accurate results.

To test the models, the newly measured airtightness values were input in the empirical models; the results can be found in Table 5.14.

Table 5.14: Air infiltration rate (h^{-1}) predictions based on steady pressurisation and pulse airtightness measurements, and, error using the empirical models in the re-tested properties.

Property 4b

	Blower door		**Pulse**	
	Prediction (h^{-1})	Error (%)	Prediction (h^{-1})	Error (%)
Linear model	0.1668	72	0.1569	62
Power model	0.1586	63	0.1394	44

Property 5b

	Blower door		**Pulse**	
	Prediction (h^{-1})	Error (%)	Prediction (h^{-1})	Error (%)
Linear model	0.1044	79	0.1137	95
Power model	0.0993	70	0.0913	57

It was known that the empirical power model was more accurate than the linear one; this was demonstrated in this analysis as well, with a lower error. However, the errors created were large; for instance, when using the steady pressurisation method measurements, the errors were 63% and 70% for tests 4b and 5b respectively. On the other hand, when the Pulse's measurements were used, the errors returned to be lower (44% and 57%); despite being lower, they remain high.

High errors mean that the model created was only valid for data set used to create it, and a model not accounting for external factors such as wind and temperature, will not be able to predict the infiltration rate accurately. An empirical model such as the one developed would only be accurate when all environmental, shielding and terrain parameters are similar for all tests. Predicting using these models will be useful only in a specific scenario, namely when the parameters are as the ones assumed in the model. Therefore it is not recommended to use this kind of models.

A different example of models only correlating airtightness and air infiltration are the airtightness-infiltration ratios and the *"divide-by-20"* rule of thumb. These

ratios sometimes are modified by weather and shielding conditions; however, they have been questioned due to their crude nature. The following Chapter will analyse the use of these ratios.

5.5 Chapter conclusions

After several months of tests, the field trials phase of this project was completed; 20 different properties were tested using the steady pressurisation and Pulse methods for airtightness measuring and; the tracer gas decay method for air infiltration measurements. Additionally, the indoor and outdoor weather conditions were measured while the tracer gas tests were being carried out.

The lack of tank temperature measurement delivered a big question on whether the results were accurate or not. It was seen that the method produced more accurate results once the empirical temperature correction was developed. The step-test feature in the Pulse method is relatively new and represents an opportunity to cover a broader pressure range. The inclusion of the temperature correction for step tests improves the test accuracy and aids to the development of the testing method. Hence why all the airtightness measurements in the field data collection stage had this temperature correction.

There were several lessons learnt on performing airtightness and air infiltration tests such as duration, and advantages or disadvantages of the methods. In the end, the results were used to start creating a correlation between air infiltration and all the influencing parameters, i.e. environmental, shielding and terrain conditions.

All the airtightness tests were carried out according to standard. Regarding the measurements, most of the houses comply with an air permeability value below 10 $m^3h^{-1}m^{-2}$ at 50 Pa.

From all tracer gas tests, only three did not comply with the minimum test duration required by the standard. The calculated uncertainties of the tests were low in most of the cases, meaning that the results could be used for the completion of this project.

In conclusion, the data obtained and the measurements carried out provided good-quality information that can be used to create and test infiltration models.

Empirical models, which only took into account airtightness to predict air infiltration were created and; it was seen that a power model is the one better-describing the measured data, the model was cross-validated. Despite being the best model for the data, it was not accurate enough, when tested with new data; errors larger than 57% were encountered.

The primary conclusion from these models was that they do not predict correctly when environmental, shielding and terrain conditions are not taken into account. A model only correlating airtightness and air infiltration will not have any practical use because of the changing nature of air infiltration. This was proved when the air leakage rate of the dwellings increased, but the air infiltration decreased, in the re-test of two dwellings.

Taking into account that computing technology is available, and also external affecting parameters can be measured, more robust and sophisticated models should be used to calculate infiltration rates. The following chapter carries out an analysis of the model used by the UK government (airtightness-infiltration ratios) to predict infiltration rates.

Chapter 6

Leakage-infiltration ratios, testing the simplest way of predicting air infiltration

Part of the work covered in this chapter was previously presented as a short presentation at the Air Infiltration and Ventilation Centre conference 2019 in:

A. Vega Pasos, X. Zheng, M. Gillott, and C. Wood. Comparison between infiltration rate predictions using the divide-by-20 rule of thumb and real measurements. In *40th AIVC Conference Proceedings*, Ghent, Belgium, 2019b

6.1 Introduction

The previous chapters of this thesis described airtightness and air infiltration measurement methods. The importance of correlating infiltration and airtightness lies in the fact that the former is used to predict heat losses associated with it, and also to size ventilation systems, thus enhancing energy efficiency.

Chapter 5 provided insights into an empirical model. Linear and power models were developed using data measured from twenty different dwellings. However, these type of models only represents the data measured and do not have any theoretical background.

Various infiltration predicting models exist already, such as those summarised in Liddament [1986], Orme and Leksmono [2005]. However, they rely on measurements from the steady pressurisation method. Such models have not been tested and validated from airtightness measurements taken at low pressure difference; for example with measurements taken by the Pulse technique. With the advent of Pulse for measuring airtightness at low pressure, an opportunity exists

to re-purpose these already developed models by re-calibration and validation.

Despite the existence of robust infiltration models, the (probably) best-known relation for predicting infiltration is that of a simple ratio, whose creation and development are still not clear[Jones et al., 2013a]. This ratio, the simplest, and arguably the less accurate of the studied models (in this project), is used in UK legislation and is colloquially referred as the "divide by 20 rule". In this chapter, testing and validating of the mentioned ratio is carried out based on the measurements described in the previous chapter.

6.1.1 UK context

Measurement of airtightness is the starting point to obtain the air infiltration rate. Air permeability ($m^3h^{-1}m^{-2}$) is the airtightness metric used in the United Kingdom and is referred to as "q". Another metric adopted to define the airtightness level of the house is air change rate or air leakage rate (h^{-1}), referred to as "n". Both these measurements are usually referenced to a pressure difference, for instance, in the United Kingdom, air permeability is quoted at a pressure difference of 50 Pa, because of the method used to take the airtightness value, the steady pressurisation method (q_{50}). The steady (fan) pressurisation method, typically referred to as "blower door", has been described in earlier chapters.

The pressure difference experienced by the building under natural conditions is in the range of 1-4 Pa [Cooper and Etheridge, 2007a, Vega Pasos et al., 2018a, 2019a], which is lower than the pressure range in that the steady pressurisation test is performed. Therefore, a leakage-infiltration correlation is required to evaluate the corresponding infiltration rate when a steady pressurisation test is available. As discussed earlier there are a number of different ways of predicting the air infiltration rate occurred in the building under natural conditions. The leakage - infiltration ratio (Equation 6.1) which represents the simplest way to predict air infiltration is given as follows:

$$\frac{n_{50}}{n_1} = N \tag{6.1}$$

A study carried out in the United States [Sherman, 1987] determined that a representative value of N is 20. n_{50} describes the air leakage rate occurring at 50 Pa, measured by the steady pressurisation method; and n_1 refers to the air infiltration rate. Both in air changes units (h^{-1}). This study created the "divide-by-20" rule of thumb (Equation 6.2), also known as "Sherman's ratio" [Jones et al., 2016].

$$\frac{n_{50}}{20} = n_1 \tag{6.2}$$

In the United Kingdom, Equation 6.2 was adopted by the government as the way to predict the air change rate in natural conditions (air infiltration). This is stated in the Standard Assessment Procedure (SAP) [Building Research Establishment, 2013], which is the UK's standard used to obtain the energy rating and consumption of a dwelling. The usage of this ratio has already been questioned due to its crudeness [Keig et al., 2016, Johnston and Stafford, 2016, Jones et al., 2013a].

Despite the American study, which delivered the "divide-by-20 rule" using values of n_{50} and n_1, in Equation 6.2 the UK would then go on to use q_{50} ($m^3h^{-1}m^{-2}$) directly in place of n_{50} as seen in Equation 6.3. This change suggests an assumption that the ratio of volume to envelope area is close to 1. As a result, a lower infiltration rate is calculated for narrow or tall dwellings compared to those who have a near cubic form.

$$\frac{q_{50}}{20} = n_1 \tag{6.3}$$

The objective of this chapter is to assess the accuracy of infiltration predictions when using Equation 6.3 in the building regulation in the United Kingdom. This study is based on the field tests performed in a range of dwellings (introduced in Chapter 5). The approach taken herein is similar to that in other studies [Johnston and Stafford, 2016, Keig et al., 2016]. By implication of this assessment to therefore identify a more accurate value to N from Equation 6.1, for the steady pressurisation tests performed on dwellings within this study. Furthermore, this study also aims to determine a single ratio for measurements taken by utilising the Pulse technique.

6.2 Chapter methodology

The results obtained by the tracer gas decay method, namely air infiltration rates, are only representative of the conditions present during the tests. The air infiltration rate is given in the unit of air changes per hour (n_1, h^{-1}).

The steady pressurisation tests results are presented in the form of air permeability (q_{50}) quoted at 50 Pa ($m^3h^{-1}m^{-2}$). For further analysis, an air leakage rate at 50 Pa is also given (n_{50}, h^{-1}).

Air permeability (q_{50}) test results are divided-by-20 as per the SAP requirements and these values are then compared with measurements of air infiltration

rate given by the tracer gas. Since the "divide-by-20" rule of thumb in the USA originally uses n_{50} (rather than q_{50}), a comparison against n_1 is also analysed. Ultimately, final thoughts are given regarding the use of the "divide-by-20" rule of thumb employed in the SAP

The calculations will also be made as per SAP requires, including the modifying factors of shelter, wind and ventilation factors. An analysis of the usage of the "divide-by-20" rule in SAP will be made.

There is no "simple" ratio for low-pressure airtightness measurements such as the Pulse method. For this reason, based on the results, a ratio is proposed for airtightness measurements quoted at 4 Pa. The ratios obtained from measurements from both, the steady pressurisation and Pulse methods, are tested aiming to assess how they then predict infiltration rates in re-tested properties (4b and 5b).

6.3 Results and discussion

From Chapter 5, Tables 5.7, 5.8 show the airtightness measurements, and Table 5.9 presents the air infiltration results from the concentration decay method. These measurements are compared with predictions using different airtightness - infiltration ratios, such as the divide-by-20 rule of thumb.

6.3.1 Air Permeability q_{50} (air leakage rate n_{50}) – infiltration n_1 ratios.

In Table 6.1 the "divide-by-20" rule is used to predict the infiltration rate from steady state pressurisation/depressurisation tests and compares it with the actual infiltration rate determined by the tracer gas tests. The q_{50} value used is the average of the pressurisation and depressurisation test. Finally, the last column presents an actual $q_{50} - infiltration$ ratio. This initial analysis does not include any modification factors when determining the infiltration rate from the q_{50} result and using the "divide-by-20" rule.

Table 6.1: Air permeability (@50 Pa) - infiltration ratios.

Dwelling	**Air permeability @50 Pa (q_{50})** $m^3h^{-1}m^{-2}$	$q_{50}/20$	**Infiltration** $(n_1)h^{-1}$	**Error**	q_{50}/n_1
1	7.88	0.3938	0.1484	165%	53.07
2	6.03	0.3015	0.2093	44%	28.81
3	7.90	0.3948	0.2080	90%	37.96
4	4.40	0.2200	0.1241	77%	35.46
5	3.86	0.1930	0.0787	145%	49.05
6	7.60	0.3800	0.3171	20%	23.97
7	7.22	0.3608	0.3512	3%	20.54
8	6.04	0.3020	0.1645	84%	36.72
9	6.81	0.3405	0.1514	125%	44.98
10	10.04	0.5020	0.2344	114%	42.83
11	8.77	0.4383	0.2284	92%	38.38
12	5.85	0.2923	0.2533	15%	23.08
13	13.61	0.6805	0.4192	62%	32.47
14	4.68	0.2338	0.0849	175%	55.06
15	5.33	0.2665	0.1504	77%	35.44
16	11.16	0.5580	0.5189	8%	21.51
17	4.29	0.2145	0.0998	115%	42.99
18	9.92	0.4960	0.3594	38%	27.60
19	13.43	0.6713	0.2928	129%	45.85
20	13.87	0.6933	0.2753	152%	50.36

Assuming that the measured infiltration rate is a representative parameter, it is clear that by only dividing the air permeability by 20, delivers an infiltration rate with a significant error. The usage of this ratio overestimates the infiltration rate, i.e. ratings would assume higher heat losses than the ones experienced by a dwelling. Moreover, results suggest that a much larger value of N (Equation 6.1) is more representative of this sample. On the other hand, dwellings 6, 7, 12 and 16 demonstrated that the ratio can be close to 20; though these properties represent less than a quarter of the sample.

Table 6.2: q_{50}/n_1 statistical figures.

	q_{50}/n_1 **(N)**
average	37.31
min	20.54
max	55.06
std dev (σ)	10.70
std error	2.39

Table 6.2 presents the statistical figures for the values taken by N if a ratio using q_{50} is to be used to predict the air infiltration rate. Results suggest that a value of N closer to 37.31 represents better the leakage - infiltration relationship. This number is almost twice the figure that is utilised initially. It is interesting to observe that the minimum value taken by N in the sample is larger than 20 (20.54) with no values for N lower than 20.

In the USA, where it was created, the divide-by-20 rule of thumb uses the value of n_{50} (air change or air leakage rate) instead of q_{50}. A similar analysis is made in Tables 6.3 and 6.4 for the measured values of n_{50}. Since most of the houses were close to a cubical shape (1:1 volume-envelope ratio), there is no significant change compared with what was previously presented.

Table 6.3: Air change rate(@50 Pa) - infiltration ratios.

Dwelling	**ACH @50 Pa** (n_{50}) h^{-1}	$n_{50}/20$	**Infiltration** $(n_1)h^{-1}$	**Error**	n_{50}/n_1
1	7.62	0.3810	0.1484	157%	51.35
2	5.76	0.2878	0.2093	38%	27.50
3	8.59	0.4296	0.2080	107%	41.31
4	5.31	0.2656	0.1241	114%	42.81
5	3.51	0.1756	0.0787	123%	44.63
6	7.86	0.3931	0.3171	24%	24.79
7	8.61	0.4306	0.3512	23%	24.52
8	5.77	0.2883	0.1645	75%	35.05
9	7.10	0.3548	0.1514	134%	46.86
10	10.45	0.5224	0.2344	123%	44.57
11	9.73	0.4864	0.2284	113%	42.59
12	8.33	0.4164	0.2533	64%	32.88
13	14.97	0.7486	0.4192	79%	35.71
14	5.07	0.2535	0.0849	199%	59.73
15	5.58	0.2788	0.1504	85%	37.08
16	13.27	0.6634	0.5189	28%	25.57
17	4.13	0.2064	0.0998	107%	41.35
18	11.34	0.5671	0.3594	58%	31.56
19	13.29	0.6644	0.2928	22%	45.38
20	12.24	0.6121	0.2753	122%	44.46

Table 6.4: n_{50}/n_1 statistical figures.

	n_{50}/n_1 **(N)**
average	38.99
min	24.52
max	59.73
std dev (σ)	9.35
std error	2.09

These results imply that the ratios must be used with care. The dwellings used in this study do not follow the same rules as the North-American stock and it is therefore possible that the same would be experienced in the wider UK building stock. The prediction of infiltration rate should be made using different ratios or a more accurate infiltration model [Orme and Leksmono, 2005]. This is also

suggested by Keig et al. [2016] which suggests that a divide-by-30 rule would be more accurate for the four houses the study tested in the Belfast region.

6.3.1.1 Error analysis

The derivation of leakage-infiltration ratio is based on the measurements of the air leakage results at 50 Pa using the blower door unit and the infiltration rate using the tracer gas decay method. Although the leakage-infiltration ratio used in the UK context is based on the air permeability at 50 Pa (q_{50}), the ratio of the air change rate at 50 Pa (n_{50}) to the infiltration rate is also appraised in order to provide the international context. The leakage-infiltration ratios based on the q_{50} and n_{50} are given by Eq.6.4 and

$$\frac{q_{50}}{n_1} = N_{UK} \tag{6.4}$$

$$\frac{n_{50}}{n_1} = N_{IT} \tag{6.5}$$

Where the subscripts UK and IT refer to the United Kingdom and international context. Therefore, the errors in deriving N_{UK} and N_{IT} are based on the measurement errors of the combination of q_{50} and n_1, and the combination of n_{50} and n_1, respectively. Both q_{50} and n_{50} are calculated by respectively normalising the air leakage rate at 50 Pa, Q_{50} (m^3h^{-1}) with the envelope area and volume of the building.

According to the BS EN ISO 9972 [International Organization for Standardization, 2015], the error in obtaining the building parameters is between 3% and 10% and does not specify the difference between the envelope area and volume. It is assumed that the measurement errors of both building parameters are the same and therefore the error analysis herein will be only performed to the derivation of N_{UK}. The associated error sources of N_{UK} are summarised and listed in Table 6.5.

Table 6.5: Sources or error in obtaining N_{UK}.

Source	**Error denotation**	**Error value**
Air flow rate at 50 Pa, Q_{50} (m^3h^{-1})	δQ_{50}	1.24% - 3.77%
Envelope area of the dwelling, E_a (m^2)	δE_a	3% - 10%
Air infiltration rate, n_1 (h^{-1})	δn_1	0.17% - 12.53%

Based on Eq.6.4, the calculation of N_{UK} can be described by Eq.6.6 using the error sources listed in Table 6.5.

$$\frac{Q_{50}}{(E_a n_1)} = N_{UK} \tag{6.6}$$

Therefore, the error in obtaining the leakage-infiltration ratio based on the air permeability at 50 Pa (q_{50}) can be quantified by Eq.6.7:

$$\delta N_{UK} = \sqrt{\delta Q_{50}^2 + \delta E_a^2 + \delta n_1^2} \tag{6.7}$$

Where, δQ_{50} is determined by the instrumentation error of the blower door unit used in the test, the precision error caused by environmental conditions and manual readings and the model specification error that is used to quantify Q_{50} [Sherman and Palmiter, 1995].

The instrumentation error or bias error, is given by the manufacturers of the DG-1000 gauge (pressure) used with the blower door. The precision error is calculated by the procedure described in Annex of the ISO 9972 standard [International Organization for Standardization, 2015] which is based on the error by each of the pressure and flow readings in each pressurisation test. Finally, the model error was calculated through the propagation of the error in the procedure given in section 6.2 from the ISO 9972 standard; this approach is based on the uncertainty given by the measuring device, and, how it propagates through the algorithm.

Figure 6.1 shows the leakage-infiltration ratio of all the test dwellings with the error bands. The boxes in Figure 6.1 represent the lowest uncertainty range, when $\delta E_a = 3\%$; and the lines represent the highest uncertainty when $\delta E_a = 10\%$. For example, in dwelling one the calculated N is 53.07, the range of values that N can take when $\delta E_a = 3\%$ is between 51.3 and 54.8; on the other hand when $\delta E_a = 10\%$ N can be between 47.7 and 58.4.

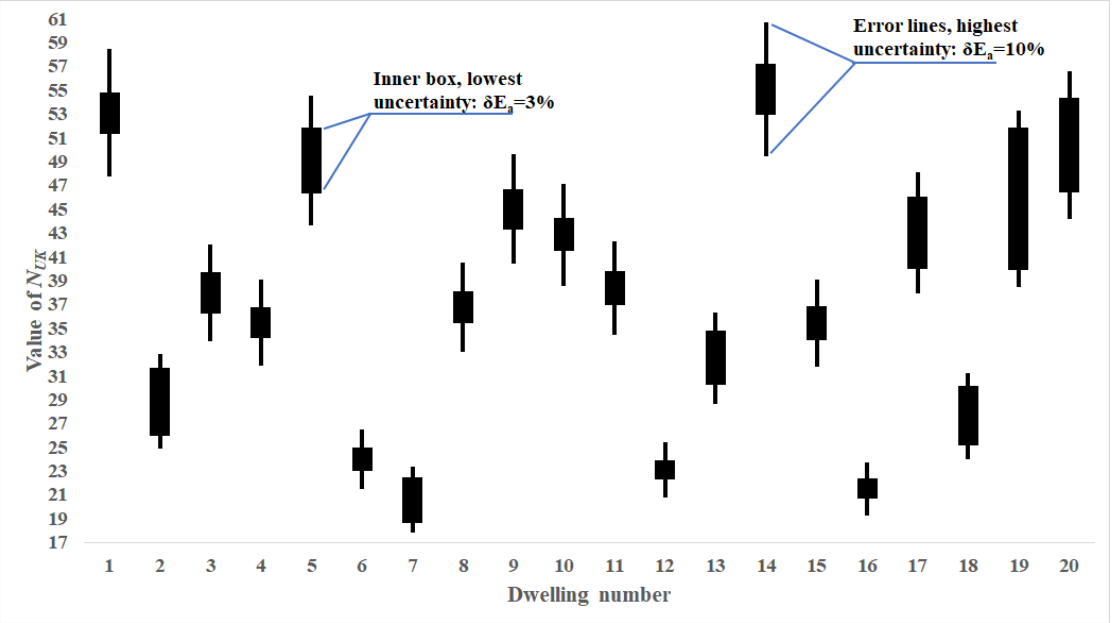


Figure 6.1: N_{UK} of all testing dwellings with their uncertainties, boxes representing the best case scenario for $\delta E_a = 3\%$ and, lines representing the worst case scenario $\delta E_a = 10\%$.

It is important to remark that each uncertainty is particular for each dwelling and depend on the uncertainty of each measurement. On average, the calculation of the uncertainty in q_{50} was 1.81% as mentioned in Table 6.5 the range of the uncertainty in this parameter is from 1.24% to 3.77% which is small, compared to the one given in the calculation of the uncertainty in n_1; 13 dwellings had their Q_{50} uncertainty under 2%. Dwelling 19 has a large uncertainty mainly due to a large uncertainty in the calculation of air infiltration (n_1); on the other hand, dwelling 10 presents a small uncertainty due to a low uncertainty in n_1. Finally, the uncertainty in the measurement of the envelope area is fixed, in this case set as 3 to 10%. This particularly remarks the importance of having a good measurement of the envelope area (or volume if n_{50} is used) of the dwelling; an inaccurate value of envelope area leads to the calculation of an inaccurate N.

The previous analysis implies that despite the uncertainties in each factor (Q_{50}, n_1 and E_a) most of the values of N are above 20 used in the divide-by-20 rule. Only 2 dwellings include 20 in the range within the uncertainty. In conclusion, a higher value for N represents better the sample taken in this study.

According to the ISO 9972 [International Organization for Standardization, 2015], the measurement uncertainty of blower door test is ±10% under calm conditions and ±20% under windy conditions. Considering the calculation of N_{UK} is arrived from the aforementioned multiple measurements, the probability of N_{UK} of

each dwelling lying within ±20% of the average ($\overline{N_{UK}}$) is evaluated. Such assumption might be crude and have the tendency of being conservative considering N_{UK} is affected by a range of factors, but it gives us a benchmark estimate so a better understanding can be obtained.

The value of N of twelve dwellings would fall in a range of $\overline{N_{UK}}$ ±20% (37.31±20%) when considering the ranges of uncertainty calculated for each N, which represents 57% of the test dwellings. However, the overall probability in this sample of an infiltration being correctly predicted using $\overline{N_{UK}}$ ±20% is only 44% (When using the worst case scenario of $\delta E_a = 10\%$). When using the original divide-by-20±20% rule the probability of correctly predicting infiltration is 16%. If $\delta E_a = 3\%$ is considered, the probability of predicting correctly are 47% for the new $\overline{N_{UK}}$ ±20% and 18% for the original divide-by-20±20%, respectively. In both cases the ratio proposed in this study is more accurate than the divide-by-20 rule; nevertheless, in both cases the accuracy is low.

These results indicate that it is possible that a divide-by-20 rule be accurate as Johnston and Stafford [2016] mentioned; however, it is more probable that a higher value of N be more accurate, such as the one proposed by Keig et al. [2016], or the one recommended in this study (37.31). This study followed a similar approach as the on taken by Keig et al. [2016], however the starting concentration in the tracer gas tests was lower (between 1700 and 3300 ppm) than the ones used in this study (above 4000 ppm). The Johnston and Stafford [2016] study considered multiple test in each of the 4 dwellings tested, however, in a graph presented the initial concentration of CO_2 was under 700 ppm, this only allowed a decay of less than 300 ppm (over a long time), this small decay can lead to an inaccurate calculation of infiltration; for this reason Johnston and Stafford [2016] obtained higher infiltration rates even when the air permeability (q_{50}) is in all cases under 8.48 $m^3h{-}1m{-}2$. Johnston and Stafford [2016] does not present the uncertainties for the steady pressurisation (three types) tests or the tracer gas tests, only mentioned that these are under 10%, and therefore it is difficult to assess the accuracy of the data taken.

The sample used in this study is larger than the ones presented by the previous studies, however, different results have been obtained. These results suggest that the spread of the value of N is high and dwelling (or sample) dependent; a single fixed ratio will not deliver accurate infiltration predictions for most dwellings.

6.3.1.2 SAP calculated infiltration rates

The procedure to calculate the effective air change rate in dwellings by the Standard Assessment Procedure (SAP) is to divide the air permeability value ($m^3h^{-1}m^{-2}$) by 20 and then modify it by shelter, wind and ventilation factors.

The wind factors used in SAP are obtained depending on the location of the dwelling. In this study, all dwellings were situated in two UK regions: East Pennines and Midlands. The wind measured at all test sites was smaller in magnitude than the one given in SAP. Furthermore, it is required to say that SAP does not include factors to modify the infiltration rate by the temperature difference, even when the theory recognizes its importance when wind speed is low [Liddament, 1986, Vega Pasos et al., 2018a].

Table 6.6 shows the air infiltration rates calculated as per SAP after including the modifying factors; two cases are considered: first,using the SAP monthly wind speed figure for the month when the tracer gas test was carried out and; second, an annual average of the wind speed. Furthermore, Table 6.6 also includes the values that N would take if a direct ratio is to be used. Finally, the table mentions the relative percentage difference when using the air change rates calculated by SAP compared with measurements.

Table 6.6: Air change rates(h^{-1}) calculated using SAP, values of N from values calculated, and their error compared to measured values.

Dwelling	SAP n_1 during month	SAP n_1 annual average	N SAP month	N SAP annual	Infiltration (tracer gas, h^{-1})	Error SAP month	Error SAP annual average
1	0.5938	0.5938	13.2625	13.2625	0.1484	300%	300%
2	0.5449	0.5470	11.0654	11.0228	0.2093	160%	161%
3	0.5703	0.5943	13.8432	13.2855	0.2080	174%	186%
4	0.5207	0.5293	8.4501	8.3132	0.1241	320%	326%
5	0.5159	0.5225	7.4816	7.3871	0.0787	556%	564%
6	0.5529	0.5747	13.7468	13.2235	0.3171	74%	81%
7	0.5470	0.5569	13.1898	12.9563	0.3512	56%	59%
8	0.5352	0.5472	11.2852	11.0380	0.1645	225%	233%
9	0.5448	0.5600	12.5008	12.1606	0.1514	260%	270%
10	0.5922	0.6304	16.9524	15.9258	0.2344	153%	169%
11	0.5531	0.5656	15.8464	15.4965	0.2284	142%	148%
12	0.5327	0.5404	10.9725	10.8164	0.2533	110%	113%
13	0.7289	0.7397	18.6709	19.4003	0.4192	74%	76%
14	0.7289	0.7330	6.4135	6.3780	0.0849	759%	763%
15	0.5320	0.5336	10.0179	9.9891	0.1504	254%	255%
16	0.6202	0.6260	17.9937	17.8285	0.5189	20%	21%
17	0.6850	0.6883	6.2628	6.2328	0.0998	586%	590%
18	0.6027	0.6075	16.4592	16.3289	0.3594	68%	69%
19	0.7033	0.7130	19.0880	18.8279	0.2928	140%	144%
20	0.6856	0.6944	20.2244	19.9662	0.2753	149%	152%

Once again, SAP overestimates the infiltration rate of all test houses; this can be translated as a step backwards in energy efficiency due to the over-sizing of heating and ventilation equipment. An approximate average value that N would take after SAP is used is 12.94, meaning that is – close to - one-third of the 37 that was presented as a more accurate value. It is observed that in the case of airtight dwellings, i.e. $q_{50} < 5m^3h^{-1}m^{-2}$ (dwellings 4, 5, 14 and 17) that the difference is higher than 320% or as high as 763% for dwelling 14.

SAP extremely overestimates the air change rate and for some cases, the error compared to the measured values is greater than 500% (it can be as high as 763%). The average percentage difference is 229% and 234% for month and annual predictions, respectively. The author suggests revising the correction factors and

the usage of the divide-by-20 rule to provide a more adequate way to predict the air infiltration rate of a dwelling.

It is essential to mention that the majority of dwellings in the sample of this study were fairly new build (after 1990) and presented modifications that improved the airtightness of the houses. This represents a bias towards the "tightness" of the stock. Nevertheless, new build houses are expected to have good airtightness, and refurbishment will also aim to improve this feature. Consequently, the estimation of infiltration will overpredict the air change rate value and end in a low efficiency of the dwellings.

As mentioned, SAP uses measured wind speeds depending on the region where the dwelling is located. Table 6.7 shows the predictions by SAP when the on-site measured wind speeds are used instead of the one provided by the standard. In this case, only one case is taken, the day when the tracer gas tests were performed. This analysis makes a fairer comparison using a measured wind speed.

Table 6.7: Air change rates(h^{-1}) calculated using SAP and measured wind speeds, values of N from values calculated, and their error compared to measured values.

Dwelling	SAP n_1 during test day	N SAP test day	Infiltration (tracer gas, h^{-1})	Error SAP test day
1	0.5363	14.6848	0.1484	261%
2	0.5033	11.9798	0.2093	140%
3	0.5016	15.7409	0.2080	141%
4	0.5018	8.7691	0.1241	304%
5	0.5006	7.7109	0.0787	536%
6	0.5033	15.0989	0.3171	59%
7	0.5022	14.3681	0.3512	43%
8	0.5070	11.9121	0.1645	208%
9	0.5008	13.5980	0.1514	231%
10	0.5017	20.0112	0.2344	114%
11	0.5025	17.4424	0.2284	120%
12	0.5022	11.6386	0.2533	98%
13	0.5056	26.9207	0.4192	21%
14	0.5425	8.6175	0.0849	539%
15	0.5019	10.6191	0.1504	234%
16	0.5047	22.1107	0.5189	-3%
17	0.5141	8.3445	0.0998	415%
18	0.5059	19.6089	0.3594	41%
19	0.5049	26.5893	0.2928	72%
20	0.5371	25.8128	0.2753	95%

As can be seen, the errors reduced significantly, this means that a revision of wind speeds in addition to a revision of the divide-by-20 rule can make the standard accurate. The properties with errors above 500% were the ones where the reduction in error was more significant. It is also important to mention that in property 16 SAP underestimated the infiltration rate by 3%, it was the only dwelling where a underestimation occurred; furthermore, this dwelling had the most accurate prediction. By using the measured wind speed, the average value that N would take after introduced the correction factors in SAP is 15.58.

Despite the improvement in the results, errors are still as large as 539% and 184% on average; hence, the usage of the methodology employed in SAP is still not accurate enough to produce reliable infiltration predictions.

6.3.2 Air Permeability q_4 (air change rate n_4) – infiltration n_1 ratios.

So far, the "divide-by-20" rule has been examined, and a more accurate value for the ratio was proposed for the sample of dwellings in this study for airtightness measurements taken at 50 Pa. However, a value for N has not been provided if the ratio uses low-pressure airtightness measurements. If a similar approach is taken; but utilising low pressure airtightness measurements, a (low pressure) leakage-infiltration ratio can be obtained.

Table 6.8 shows the calculated ratios for twenty properties using both, air permeability and air leakage rate measurements from the Pulse method.

Table 6.8: Airtightness measurements (@4Pa) and estimated infiltration ratios using air permeability and air change rate as metrics.

Dwelling	**Air permeability @4 Pa** (q_{50}) $m^3h^{-1}m^{-2}$	**ACH @4Pa** (n_4) h^{-1}	**Infiltration** (n_1)h^{-1}	q_4/n_1	n_4/n_1
1	1.576	1.525	0.1484	10.619	10.275
2	1.279	1.221	0.2093	6.110	5.833
3	1.906	2.074	0.2080	9.162	9.970
4	0.836	1.010	0.1241	6.739	8.137
5	0.788	0.717	0.0787	10.006	9.106
6	1.361	1.408	0.3171	4.293	4.441
7	1.495	1.785	0.3512	4.258	5.083
8	1.285	1.227	0.1645	7.812	7.457
9	1.577	1.643	0.1514	10.416	10.852
10	2.292	2.385	0.2344	9.778	10.175
11	1.699	1.886	0.2284	7.439	8.256
12	1.190	1.696	0.2533	4.698	6.694
13	3.362	3.698	0.4192	8.020	8.822
14	0.836	0.907	0.0849	9.845	10.678
15	1.134	1.186	0.1504	7.540	7.889
16	2.220	2.640	0.5189	4.279	5.087
17	1.067	1.027	0.0998	10.693	10.287
18	1.844	2.109	0.3594	5.131	5.867
19	3.190	3.158	0.2928	10.896	10.784
20	2.819	2.489	0.2753	10.240	9.041

Since a low-pressure measurement was used, the airtightness measurements (quoted at 4 Pa) are smaller in magnitude than those measured at high-pressure difference (and quoted at 50 Pa). Therefore the ratio is expected to be smaller than the proposed 37 for high-pressure measurements. The statistical figures for the ratios are given in Table 6.9.

Table 6.9: q_4/n_1 and n_4/n_1 statistical figures.

	q_4/n_1 **(N)**	n_4/n_1 **(N)**
average	7.899	8.237
min	4.258	4.441
max	10.896	10.852
std dev (σ)	2.423	2.114
std error	0.542	0.473

The value proposed for N when using air permeability(q_4) 7.9. The corresponding for air leakage rate (n_4) is 8.2. The standard error for both results is approximately ± 0.5. Meaning that if a ratio between this range is used, most of the predictions will be relatively accurate. This uncertainty (standard error) represents the 6.86% and 5.74% (converting the standard error as a percentage of N) respectively for permeability and air leakage rate. The ratios obtained from the steady pressurisation method have an uncertainty of 6.40% and 5.34% for permeability and air leakage rate respectively. Hence, the uncertainty is comparable in both techniques. Equally, it is much smaller than if a crude divide-by-20 rule is used.

It can be concluded that if new ratios are applied (the ones proposed in this chapter), both measurements are equally accurate to predict air infiltration. However, these ratios do not take into account parameters such as wind speed or temperature difference that, are known to affect the total infiltration rate of a building.

Properties 4 and 5 were re-tested (as mentioned in Chapter 5, and the results are given in Figure 6.2. For both dwellings, the newly proposed ratio overpredicted infiltration rates. The errors in re-tested property 4 (named 4b) are 64% and 40% when using n_{50} and n_4 measurements respectively. For property 5b the errors are 81% and 54%. Consequently, low-pressure measurements and the newly developed ratios better predicted the infiltration rate for these dwellings.

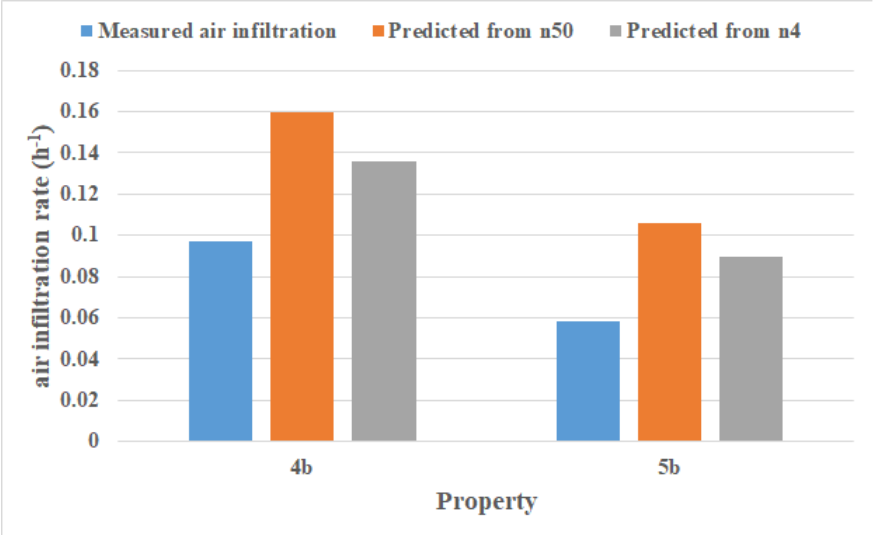


Figure 6.2: Comparison of measured and predicted air infiltration in re-tested dwellings

It is relevant to mention that the tested properties are generally more airtight than seen in the average UK building stock, this suggests that for relatively airtight buildings, low-pressure airtightness measurements produce more accurate air infiltration predictions. Nonetheless, these predictions are very different from the actual measurements. Therefore, the newly proposed ratios would work better for "average" properties (if it is considered that the average airtightness measured in this study is representative of the housing stock). With the improvement of building materials and construction techniques, more airtight buildings will be constructed, that is why a simple ratio is somewhat problematic when used by building regulation to predict infiltration heat losses.

6.4 Chapter conclusion

Twenty houses in the East Midlands region of the UK were tested by means of steady pressurisation, Pulse and tracer gas methods. All tests were carried out according to standards. Results of both, air permeability ($m^3h^{-1}m^{-2}$) and air change rate (h^{-1}) measured at both high and low pressure difference were presented to show the airtightness of the test dwellings. Likewise, tracer gas tests were carried out in the dwellings to calculate the actual unintended air change rate during the tests.

In the United Kingdom, the Standard Assessment Procedure (SAP) evaluates the energy efficiency of dwellings. An essential factor in SAP is the air change

rate (n_1) and it is obtained through dividing the air permeability (q_{50}) value of the house (obtained by a steady pressurisation test) by 20; the value is then modified using shelter, wind and ventilation factors.

The "divide-by-20" rule of thumb was evaluated, and results from this study suggest that, a number for a simple ratio is closer to 37 (divide-by-37). This was (approximately) correct when using either q_{50} or n_{50}. The error of using the rule of thumb ranged from 3% to 175%. After an error analysis it was seen that based on the dwellings from this sample there is a 44% probability that the value for N $37.31 \pm 20\%$ represents the infiltration rate of a dwelling.

After adding the modifying factors, SAP overestimated the air change rate creating errors larger than 700% in airtight houses. A bias found was that the majority of the houses were built in the last 30 years, or at least had a refurbishment which improved the airtightness of the houses. Even so, new built houses are expected to have low air permeability values; thus, the error in the air change rate calculations will be large, leading to a low energy efficiency.

When using the Pulse method, a ratio proposed to predict infiltration rate is a divide-by 8.2 rule, using air leakage rate (n_4) as airtightness metric. This ratio has a similar uncertainty compared to the one proposed for the steady pressurisation method. In both cases the uncertainty is lower than when using the "divide-by-20" rule of thumb.

When predicting infiltration in tight houses, the ratio developed using Pulse's measurements became more accurate; yet the error was still substantial. The crudeness of these ratios realises these large errors. The inclusion of environmental and building factors is mandatory if better accuracy is to be achieved.

Suggestions about the revision of the modifying factors and the utilisation of the "divide-by-20" rule of thumb were given. The subsequent part of this study is to evaluate the usage of more complex air infiltration models or new technologies to have a more accurate prediction of the unintended air change rate.

The following chapters will analyse the usage of different infiltration models. Predictions will be made from high and low-pressure airtightness measurements. Their integration to airtightness measuring technologies will be assessed.

Chapter 7

Prediction of infiltration from low-pressure leakage measurements using the LBL model

7.1 Introduction

So far, in the analysis of infiltration prediction, only models which are either empirical (Chapter 5) or developed from statistics (Chapter 6) have been analysed. Other than airtightness, these models do not consider other variables that act on air infiltration. On the other hand, more robust infiltration models such as the ones described in Chapter 2 take into account these other acting variables e.g. environmental conditions, shielding factors or leakage distribution. An infiltration model which considers all these variables should be more accurate than one who does not.

This chapter analyses one of the most used, validated and tested models for predicting infiltration rate: the Lawrence Berkeley Laboratory infiltration model, or LBL model. The model has been used since the 1980s and is still used due to a proven accuracy and simplicity [Hayati et al., 2014]. The Lawrence Berkeley Laboratory infiltration model (LBL) is a simplified single zone-model, which means that the computational capacity required is nor significant. The model was created by Sherman in the 1980's [Sherman, 1980], which was updated to include the stack effect [Sherman and Grimsrud, 1982].

LBL uses the power law as a governing equation, $Q = C\Delta P^b$ as defined in Equation 2.8. Where Q is the flow through the envelope (m^3/s), ΔP the pressure

difference (Pa), b the flow exponent which varies from 0.5 to 1 from turbulent to laminar; and, C is the flow coefficient ($m^3h^{-1}Pa^{-b}$). C and b, are obtained from pressurization tests, or in the case od his sudy; the Pulse method. LBL was created to produce infiltration predictions based on airtightness measurements taken at a high-pressure differential (50 Pa). These then are extrapolated to low pressure using the power law. More information about the algorithm of the model was given in Chapter 2.

Both airtightness measurements from the Pulse and the steady pressurisation method are used as inputs for the model. For the first time in this project, the measured environmental conditions are accounted for while predicting infiltration rates.

This is the first step on understanding how predictions from low-pressure airtightness measurements compare with standard predictions. The Pulse is tested on its capacity to predict and reproduce infiltration in already validated models.

The objective of this chapter is to assess the accuracy of the model using both airtightness measurement methods; and provide guidance on the prediction of infiltration when a Pulse test is used as basis of the model.

7.2 Chapter methodology

The airtightness and environmental conditions measurements taken from the field data collection stage (Chapter 5) were used as inputs for the LBL model. LBL typically takes airtightness measurements from the steady pressurisation method (blower door). Additionally, airtightness measurements taken using the Pulse method will be used. Typically the model uses the airtightness measurements referenced at 50 Pa of pressure difference and extrapolates them to low pressure (4 Pa) when calculating the Effective Leakage Area (ELA). The high-pressure model (LBL50)is taken as the original model, and the low pressure (LBL4) avoids this extrapolation and uses Pulse measurements directly as inputs. The collected data from the survey carried out provided the inputs for volume, envelope area, shielding and terrain factors (Table 5.1).

In the original model created by Sherman and Grimsrud [1980], wind speed is taken from a nearby weather station and then modified to be accounted as site wind speed. For this study, the wind speed was directly measured on-site; therefore, there was no need to correct the measured wind speed. All the measured environmental conditions used for the LBL model are included in Table 7.1. It is important to remark that the environmental condition inputs are averaged from

all the measurements taken during the air infiltration tests.

Table 7.1: Average environmental conditions measured for every dwelling to be used as inputs for the LBL model.

Number	**Wind speed (m/s)**	**Wind direction (°)**	**Indoor temperature (°C)**	**Outdoor temperature (°C)**	**Temperature difference (K)**
1	2.74	224	13.20	8.47	4.73
2	1.16	185	22.25	20.2	2.05
3	0.57	192	19.43	18.3	1.13
4	1.08	250	29.16	25.47	3.69
5	0.71	216	21.27	17.87	3.4
6	0.93	87	25.05	24.86	0.19
7	0.86	170	20.50	17.63	2.87
8	1.70	195	21.09	19.38	1.71
9	0.51	177	25.40	23.74	1.66
10	0.51	193	20.64	18.99	1.65
11	0.76	205	19.91	16.19	3.72
12	0.91	249	21.38	21.37	0.01
13	0.67	121	20.12	13.99	6.13
14	0.85	197	20.88	19.57	1.31
15	0.93	227	18.87	16.91	1.96
16	0.75	199	20.70	15.87	4.83
17	0.36	178	17.55	6.47	11.08
18	1.03	163	22.36	23.06	0.70
19	0.59	229	17.79	13.88	3.91
20	1.70	83	14.93	11.38	3.55

The model was programmed using MATLAB and run for all the twenty properties. LBL uses airtightness measurements from steady pressurisation tests, but it requires an input of the leakage at 4 Pa, which is derived from extrapolation using the power law equation. (Equation 2.8). When Pulse was utilised to measure airtightness, there was no need to extrapolate; the air leakage rate was directly measured at 4 Pa.

To assess the model accuracy, predictions given by the LBL model are compared with air infiltration rates measured using the tracer gas decay method. The airtightness inputs and the measured infiltration rates are given in Tables 5.7, 5.8

and 5.9. The required airtightness data is given in air leakage rate units (n_{50} and n_4). The comparisons are made in terms of their accuracy and uncertainty. The accuracy is assessed through the capabilities of the model to reproduce the measured data, the metric is the relative percentage difference (RPD) shown in Equation 7.1. The RPD is obtained by comparing the measured infiltration with the prediction. The standard error (Equation 7.2)is calculated from the measured and predicted data and evaluates the uncertainty in the predictions. Overall statistical figures were also calculated for the group sample of dwellings, such as the mean, minimum and maximum RPD and standard error. Finally and importantly, the overall uncertainty (standard error) of the RPD and standard errors of the sample. The models were renamed depending on the airtightness method used: LBL50 when the steady pressurisation method was used to measure airtightness, and LBL4 when Pulse was utilised.

$$RPD = \frac{Predictedinfiltration - Measuredinfiltration}{Measuredinfiltration} \tag{7.1}$$

$$SE = \frac{\sigma}{\sqrt{k}} \tag{7.2}$$

Where SE stands for the standard error, σ is the standard deviation and k is the number of measurements.

Despite having compared real air infiltration measurements and predicted values, it is relevant to have a more extensive data set to provide a complete analysis on how variables interact within the model. A Monte Carlo random sampling method is used to produce large samples from simulations based on the measured variables' distributions. These samples were used to validate and test the model. Finally, a sensitivity analysis was made to find which variables affect the most the model when based on high and low-pressure airtightness measurements.

A summary of the contents of this chapter is given in Figure 7.1. Additionaly Figure 7.1 depicts a diagram of the methodology used in the present chapter and can be used as a guideline to follow its contents.

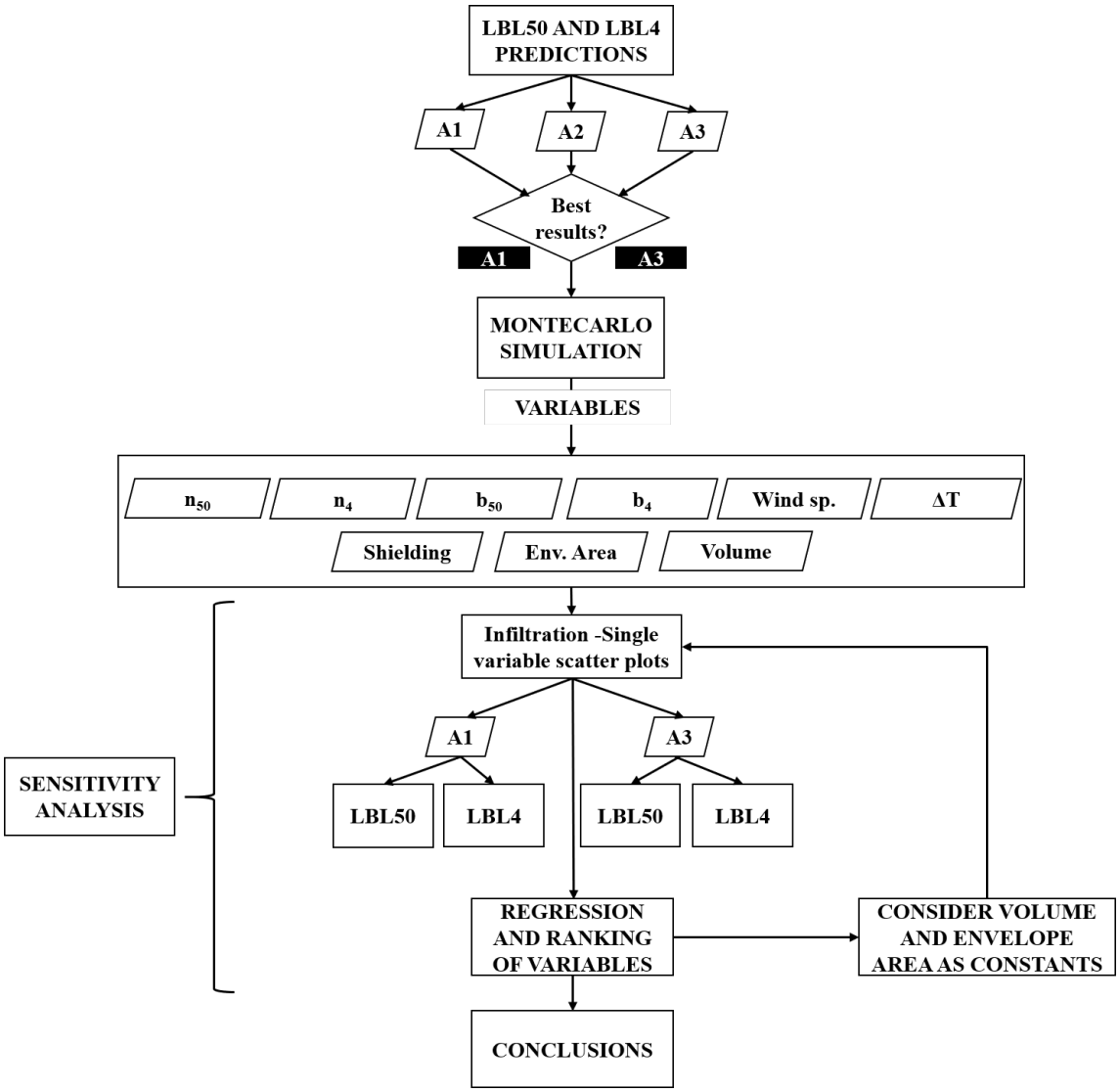


Figure 7.1: Diagram of the evaluation of the LBL model during the present Chapter.

This Chapter evaluates the predictions given by the LBL models using different assumptions and compare them with real air infiltration measurements. A simulation of the variables used as inputs in the model is given, 100,000 samples are obtained for each variable, this leads to 100,000 simulations of the models. Due to the results obtained only 2 assumptions are evaluated for each model. As part of the sensitivity analysis scatter plots using the infiltration rate and the different variables is given and the ranking of importance of variables is assessed. The previous steps are repeated taking the envelope Area and the volume as constants. Finally, conclusions are given.

7.3 Predicting infiltration rates with the LBL model

When solving Equations 2.15 and 2.16 the leakage areas of the ceiling and floor (A_c and A_f) had to be assumed or calculated. Three different assumptions were considered for this study:

1. the ceiling (A_c) and floor (A_f) leakages are so small that can be neglected, therefore are equal to zero.

2. all the leakage area is equally distributed across every façade; therefore A_c and A_f are equal to all the effective leakage area (ELA, Equation 2.13) divided by 6: $A_c = ELA/6$ and $A_f = ELA/6$; and

3. Sherman and Grimsrud [1980], in their study, found that the wind and stack factors (Equations 2.18 and 2.20), can be assumed as 0.12 and 0.123, respectively; these factors already account for the leakage distribution in the building. Therefore $f_w = 0.12$ and $f_s = 0.123$.

For brevity, LBL4 and LBL50 are used to represent the models that are utilised to predict infiltration rate from the Pulse measurement and blower door measurement, respectively. The assumptions are used to predict infiltration rate results; therefore, infiltration results are given and presented for all the assumptions. The full MATLAB code from both models can be found in Appendix F.

7.3.1 From high- pressure airtightness measurements: Steady pressurisation method

The model was run using the steady pressurisation method for all three assumptions, the air leakage value used is the average between depressurisation and pressurisation tests. The predicted air infiltration rates (h^{-1}) are given in Table 7.2. Furthermore, the measured values are given in the second column of the table. It can be seen that the predictions vary between assumptions. When using assumption 1 or 2, the results do not differ much, but the results obtained using assumption 3 differ from the other two. The is a range of predictions between 0.077 and 0.486 h^{-1} when using assumption 1, between 0.0816 and 0.553 h^{-1} when using assumption 2, and between 0.04 and 0.235 h^{-1} when using assumption 3; from these is clear that assumption 3 predicts lower infiltration rates than the other two assumptions.

Table 7.2: Air infiltration rate predictions using the LBL50 model. The letter A stands for the assumption used.

Number	LBL50 (n_1, h^{-1})			
	Measured	**A.1**	**A.2**	**A.3**
1	0.1484	0.4859	0.4594	0.2348
2	0.2093	0.1839	0.1788	0.0756
3	0.2080	0.1797	0.1868	0.0710
4	0.1241	0.1619	0.1652	0.0648
5	0.0787	0.1118	0.1241	0.0444
6	0.3171	0.1212	0.1108	0.0770
7	0.3512	0.1793	0.1968	0.0824
8	0.1645	0.2416	0.2230	0.1018
9	0.1514	0.1185	0.1322	0.0517
10	0.2344	0.1816	0.1978	0.0745
11	0.2284	0.2801	0.2982	0.1089
12	0.2533	0.1444	0.1264	0.0739
13	0.4192	0.4857	0.5527	0.1968
14	0.0849	0.0777	0.0816	0.0400
15	0.1504	0.1525	0.1536	0.0615
16	0.5189	0.4455	0.4810	0.1714
17	0.0998	0.1961	0.2266	0.0707
18	0.3594	0.1798	0.1762	0.1047
19	0.2928	0.4447	0.4962	0.1667
20	0.2753	0.3131	0.3216	0.1686

Table 7.3 lists the uncertainty and errors calculated from the standard error (SE) and RPD, respectively. Table 7.3 is divided into three sections, one for each assumption, and each section is divided into three columns. The first column represents the standard error of comparing the measured and predicted value. The second column gives the standard error in percentage. The third column provides an estimate of the relative percentage difference (RPD) between the measured and predicted infiltration rates.

In addition, the statistical figures for every assumption are presented. These were calculated by taking into account all twenty dwellings.

Table 7.3: Standard error and percentage difference between measurements for all the assumptions in the LBL50 model

	Assumption 1			Assumption 2			Assumption 3		
	SE	**SE%**	**R.P.D.**	**SE**	**SE%**	**R.P.D.**	**SE**	**SE%**	**R.P.D.**
1	0.1193	25%	227%	0.1099	24%	210%	0.0306	13%	58%
2	0.0090	5%	-12%	0.0108	6%	-15%	0.0473	63%	-64%
3	0.0100	6%	-14%	0.0075	4%	-10%	0.0484	68%	-66%
4	0.0134	8%	30%	0.0145	9%	33%	0.0210	32%	-48%
5	0.0117	10%	42%	0.0161	13%	58%	0.0121	27%	-44%
6	0.0693	57%	-62%	0.0729	66%	-65%	0.0849	110%	-76%
7	0.0608	34%	-49%	0.0546	28%	-44%	0.0950	115%	-77%
8	0.0273	11%	47%	0.0207	9%	36%	0.0221	22%	-38%
9	0.0116	10%	-22%	0.0068	5%	-13%	0.0352	68%	-66%
10	0.0187	10%	-23%	0.0129	7%	-16%	0.0565	76%	-68%
11	0.0183	7%	23%	0.0247	8%	31%	0.0422	39%	-52%
12	0.0385	27%	-43%	0.0449	35%	-50%	0.0634	86%	-71%
13	0.0235	5%	16%	0.0472	9%	32%	0.0786	40%	-53%
14	0.0025	3%	-8%	0.0012	1%	-4%	0.0159	40%	-53%
15	0.0007	0%	1%	0.0011	1%	2%	0.0314	51%	-59%
16	0.0260	6%	-14%	0.0134	3%	-7%	0.1229	72%	-67%
17	0.0340	17%	96%	0.0448	20%	127%	0.0103	15%	-29%
18	0.0635	35%	-50%	0.0648	37%	-51%	0.0901	86%	-71%
19	0.0537	12%	52%	0.0719	14%	69%	0.0446	27%	-43%
20	0.0134	4%	14%	0.0164	5%	17%	0.0377	22%	-39%
AVERAGE	0.0313	15%	13%	0.0328	15%	17%	0.0495	54%	-51%
STD DEV	0.0285	14%	63%	0.0289	16%	63%	0.0301	30%	28%
STD ERROR	0.0064	3%	14%	0.0065	4%	14%	0.0067	7%	6%
MIN	0.0007	0%	-62%	0.0011	1%	-65%	0.0103	13%	-77%
MAX	0.1193	57%	227%	0.1099	66%	210%	0.1229	115%	58%

By looking at the minimum standard error (uncertainty), it can be seen that it comes from assumption one (ceiling and floor leakage equals to zero) with 0% of uncertainty, on the contrary, the highest minimum error comes from assumption three (13%).

Assumption one has a range of standard error from 0 to 57% and, a relative percentage difference range between -62 to 227%. Assumption 2 has standard errors between 1 to 66% and RPD's between -65 to 210%. Finally, assumption three's standard errors vary from 13 to 115% and RPD from -77% to 58%.

Figure 7.2 shows the RPD of all dwellings sorted by dwelling number. It can be seen from the images and inferred from the numbers that, assumption 3 has a lower variance between the predicted infiltration rates. On the other hand, assumptions

1 and 2 have similar RPD for all properties, and a significant variance (large range in the RPD)

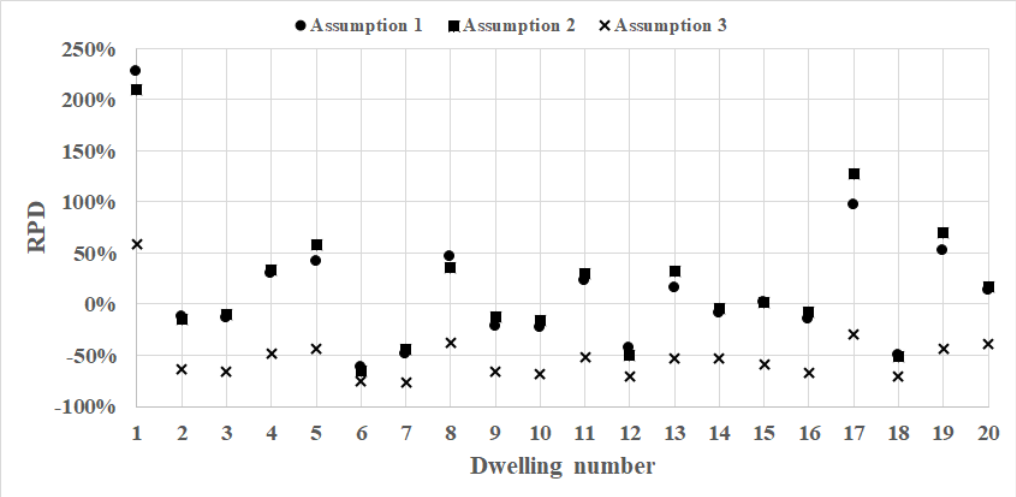


Figure 7.2: Relative percentage differences (RPD) in the LBL50 model.

These results have to be analysed carefully, because, even when the average error is less for assumptions one and two, assumption three has the lowest standard deviation for the relative percentage difference; therefore, the variance is less. If the standard errors are compared for all assumptions, it can clearly be seen that the error is almost the same for all of them (0.0064, 0.0065 and 0.0067 h^{-1} for assumptions one, two and three, respectively). This also indicates that the uncertainty is similar for all assumptions.

There is no clear definition from these measurements about which assumption delivers more accurate results. However, a smaller range of predictions and a lower variance in RPD is a good indicator of less variability and uncertainty (when compared with measured data). For assumptions 1 and 2 there are ten properties with positive RPD, this means that the model overpredicted the infiltration rate. Alternatively, for the remaining ten properties, the RPD is negative and therefore, LBL50 underpredicted the infiltration rate. In regard to the overall RPD from the LBL50 model it can be seen that the underestimation and overestimation tend to compensate each other; for this reason the overall error is small, mainly for assumptions 1 and 2.

The reported RPD with their standard error (or error and uncertainty, respectively) are 13% ±14%, 17% ±14% and -51% ±6% respectively for assumptions 1, 2 and 3 . For example, there are two-thirds of probability that a prediction of infiltration using assumption one lies between -1% to 27%. In this case, it is clear that the error is less for assumption one, and it would be better when predicting

new data. On the other hand, the assumption with less uncertainty is assumption 3.

A different approach of analysing the error is to add the absolute value of the RPD. By doing this change all the differences would turn positive, and therefore, the overall error would be different. Table 7.4 presents the calculated statistical figures for this approach. Furthermore, Figure 7.3 graphically presents these results when a) the RPD is sorted by dwelling number and, b) when arranging the RPD from the lowest to the highest.

Table 7.4: Statistical figures for the overall relative percentage difference between measurements for all the assumptions in the LBL50 model when taking the absolute value of each RPD

	Assumption 1 R.P.D.	**Assumption 2 R.P.D.**	**Assumption 3 R.P.D.**
AVERAGE	42%	44%	57%
STD DEV	48%	48%	13%
STD ERROR	11%	11%	3%
MIN	1%	2%	29%
MAX	227%	210%	77%

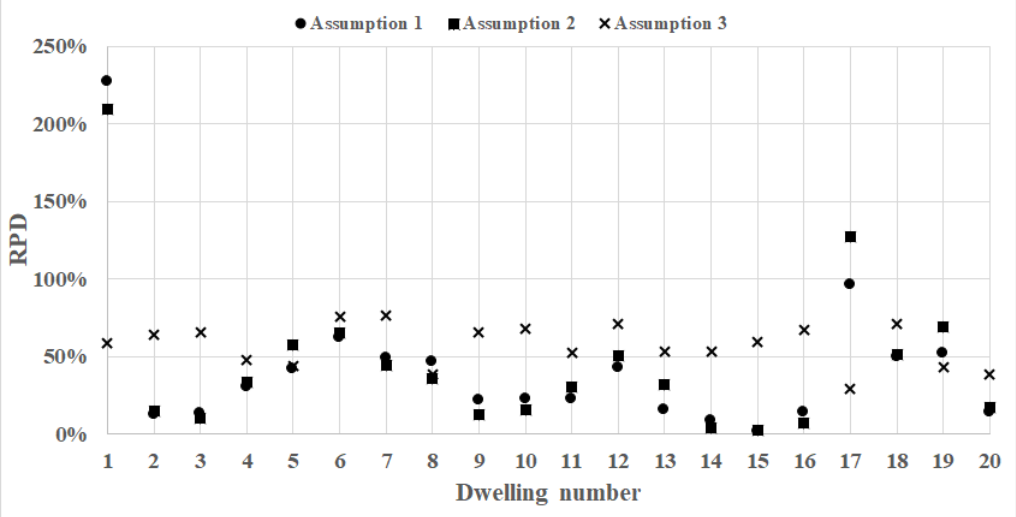


Figure 7.3: Absolute value of the relative percentage differences (RPD) in the LBL50 model.

The standard error does not vary with this change, but the reported error value does. The new overall errors and their uncertainty are 42% ±11%, 44% ±11%

and 57% ±3% for assumptions 1, 2 and 3, respectively. There is no compensation between under and overpredictions, that is why the errors (RPD) increase notably. Despite this, the uncertainties decreased, for assumption three, only 3% of uncertainty was found.

It is noteworthy to mention that the assumptions given by Sherman and Grimsrud [1980] (assumption three in this study) were taken from single-story houses. Even when a single space is considered, the dwellings tested for this sample were not single-storied; consequently the height is higher than the ones assumed by LBL authors. This inconsistency might create an error since a higher dwelling would be influenced differently by the environmental conditions.

7.3.2 From low-pressure airtightness measurements: Pulse method

In the LBL4 model, the Pulse measurements are used as direct inputs. The resulting predictions of the infiltration rate using the LBL model under the assumptions presented before are listed in Table 7.5. As for the previous results, assumption 3 predicts lower infiltration rates than the other two assumptions. Dwelling number 14 is the one with the lowest infiltration rate for all assumptions; dwelling number 13 is the one with the highest infiltration when using assumptions 1 and 2, and the dwelling number 20 when using assumption 3.

Table 7.5: Air infiltration rate predictions using the LBL4 model.

Number	LBL4 (h^{-1})			
	Measured	**A.1**	**A.2**	**A.3**
1	0.1484	0.4465	0.4221	0.2158
2	0.2093	0.1896	0.1843	0.0779
3	0.2080	0.1901	0.1976	0.0751
4	0.1241	0.1626	0.1658	0.0650
5	0.0787	0.1028	0.1141	0.0409
6	0.3171	0.0996	0.0910	0.0633
7	0.3512	0.2148	0.2357	0.0987
8	0.1645	0.2498	0.2306	0.1053
9	0.1514	0.1356	0.1513	0.0592
10	0.2344	0.2079	0.2266	0.0853
11	0.2284	0.2577	0.2743	0.1002
12	0.2533	0.1437	0.1257	0.0735
13	0.4192	0.5372	0.6113	0.2177
14	0.0849	0.0842	0.0884	0.0433
15	0.1504	0.1611	0.1623	0.0649
16	0.5189	0.3864	0.4173	0.1487
17	0.0998	0.2245	0.2594	0.0810
18	0.3594	0.1895	0.1857	0.1104
19	0.2928	0.4713	0.5260	0.1767
20	0.2753	0.4292	0.4407	0.2310

Table 7.6 shows the standard error and relative percentage differences between measured and predicted infiltration rates using the LBL4 model. Finally, the statistical figures for all twenty dwellings are presented.

Table 7.6: Standard error and percentage difference between measurements for all the assumptions in the LBL4 model

	Assumption 1			Assumption 2			Assumption 3		
	SE	**SE%**	**R.P.D.**	**SE**	**SE%**	**R.P.D.**	**SE**	**SE%**	**R.P.D.**
1	0.1054	24%	201%	0.0968	23%	184%	0.0238	11%	45%
2	0.0070	4%	-9%	0.0088	5%	-12%	0.0464	60%	-63%
3	0.0063	3%	-9%	0.0037	2%	-5%	0.0470	63%	-64%
4	0.0136	8%	31%	0.0148	9%	34%	0.0209	32%	-48%
5	0.0085	8%	31%	0.0125	11%	45%	0.0134	33%	-48%
6	0.0769	77%	-69%	0.0799	88%	-71%	0.0897	142%	-80%
7	0.0482	22%	-39%	0.0408	17%	-33%	0.0893	90%	-72%
8	0.0302	12%	52%	0.0234	10%	40%	0.0209	20%	-36%
9	0.0056	4%	-10%	0..0000	0%	0%	0.0326	55%	-61%
10	0.0094	4%	-11%	0.0028	1%	-3%	0.0527	62%	-64%
11	0.0103	4%	13%	0.0162	6%	20%	0.0453	45%	-56%
12	0.0388	27%	-43%	0.0451	36%	-50%	0.0636	86%	-71%
13	0.0417	8%	28%	0.0679	11%	46%	0.0713	33%	-48%
14	0.0003	0%	-1%	0.0012	1%	4%	0.0147	34%	-49%
15	0.0038	2%	7%	0.0042	3%	8%	0.0302	47%	-57%
16	0.0468	12%	-26%	0.0359	9%	-20%	0.1309	88%	-71%
17	0.0441	20%	125%	0.0564	22%	160%	0.0066	8%	-19%
18	0.0601	32%	-47%	0.0614	33%	-48%	0.0881	80%	-69%
19	0.0631	13%	61%	0.0824	16%	80%	0.0410	23%	-40%
20	0.0544	13%	56%	0.0585	13%	60%	0.0157	7%	-16%
AVERAGE	0.0337	15%	17%	0.0356	16%	22%	0.0472	51%	-49%
STD DEV	0.0283	17%	61%	0.0304	19%	63%	0.0320	33%	27%
STD ERROR	0.0063	4%	14%	0.0068	4%	14%	0.0071	7%	6%
MIN	0.0003	0%	-69%	0.0000	0%	-71%	0.0066	7%	-80%
MAX	0.1054	77%	201%	0.0968	88%	184%	0.1309	142%	45%

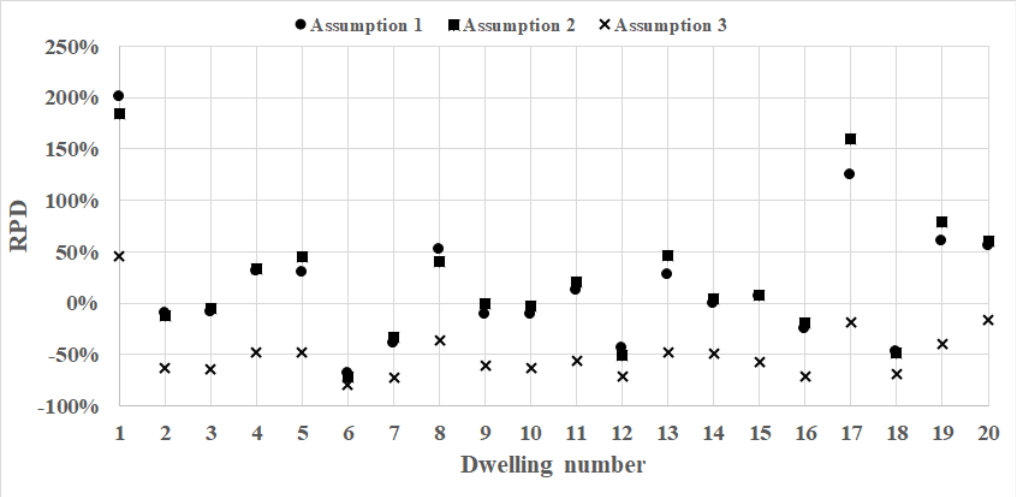


Figure 7.4: Relative percentage differences (RPD) in the LBL4 model.

The results from the LBL4 model are consistent with results from the LBL50, strictly speaking about the assessment of all the assumptions. The average error is less (in both standard error and RPD) for assumptions one and two and assumption three has the lowest standard deviation for the RPD.

While the standard error is a useful metric to quantify the uncertainty in a data set, it might not be suitable when only two values are being compared. For this case, only the predicted and measured values are compared. Conversely, when analysing all twenty dwellings, the standard error is indeed a reliable parameter to assess the uncertainty created for the model. When comparing two values only, the RPD might be a more telling figure, because it directly compares the predicted with the measured data. Therefore the RPD is a quantification of the error between the measured and predicted values.

The calculated differences with their uncertainty for the LBL4 model are: 17% ± 14%, 22% ±14% and -49% ±6% for assumption 1, 2 and 3, respectively. The conclusions made from LBL50 are maintained for LBL4: the error is less for assumption one, and the uncertainty (standard error) is lower for assumption 3. Additionaly, it can be seen how errors are larger and have more variance when using assumptions 1 and 2.

If as before, the absolute value of the RPD is computed, new statistical figures are calculated. Table 7.7 show these new figures and, Figure 7.5 depicts how the RPD changes depending on the assumption used in the LBL4 model.

Table 7.7: Standard error and percentage difference between measurements for all the assumptions in the LBL4 model

	Assumption 1 R.P.D.	**Assumption 2 R.P.D.**	**Assumption 3 R.P.D.**
AVERAGE	43%	46%	54%
STD DEV	46%	48%	17%
STD ERROR	10%	11%	4%
MIN	1%	0%	16%
MAX	201%	184%	80%

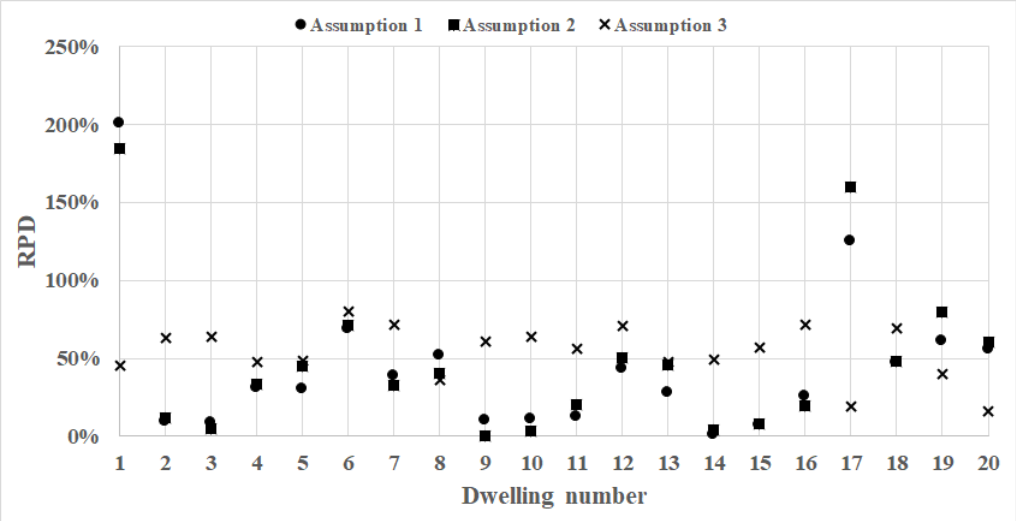


Figure 7.5: Absolute value of the relative percentage differences (RPD) in the LBL4 model.

The reported errors and their uncertainty when taking the absolute value are 43% ± 10%, 46% ±11% and 54% ±4% for assumptions 1, 2 and 3, respectively. As with the LBL50 model, the error increased substantially and the uncertainty decreased.

Given the results mentioned above, assumption 3 delivered the lowest standard error in the relative percentage difference (RPD) in both models. Hence there is less uncertainty in the calculation of the sample's average RPD. However, assumption 1 resulted as the one with the lowest error. Therefore, assumptions one and three will be used to test the variables used as input of the LBL50 and LBL4 models (namely, sensitivity analysis).

If both, Tables 7.3 and 7.6 are compared (for assumption one only), it can be seen that the standard error of RPD is 14% for both LBL50 and LBL4. More-

over,the RPD average is 13% and 17% for the LBL50 and LBL4 models, then:

- LBL50 RPD = $13\% \pm 14\%$. This means that two-thirds of the results will have an error between -1 and 27%,
- LBL4 RPD = $17\% \pm 14\%$. This means that two-thirds of the results will have an error between 3 and 31%.

And for assumption 3:

- LBL50 RPD = $-51\% \pm 6\%$. This means that two-thirds of the results will have an error between -57 and -45%,
- LBL4 RPD = $-49\% \pm 6\%$. This means that two-thirds of the results will have an error between -55 and -43%.

If the absolute value is included in the RPD, the new RPD for assumption one is:

- LBL50 RPD = $42 \pm 11\%$. This means that two-thirds of the results will have an error between 31 and 53%,
- LBL4 RPD = $43 \pm 10\%$. This means that two-thirds of the results will have an error between 33 and 53%.

And for assumption 3:

- LBL50 RPD = $57\% \pm 3\%$. This means that two-thirds of the results will have an error between 54 and 60%,
- LBL4 RPD = $54\% \pm 4\%$. This means that two-thirds of the results will have an error between 50 and 58%.

It can be concluded that both models predict the infiltration rates with similar accuracy and uncertainty. These conclusions are given based on using assumptions one (ignoring ceiling and floor leakage) and three (fixed wind and stack factors). It is critical to define which assumption to use or to quantify the ceiling and floor leakage areas.

Using the real errors, accounting for under and overpredictions, both models yield the same uncertainty. However, when using assumption 3, the model is likely to underestimate the infiltration rate. Assumption 1, is more likely to deliver accurate results. When adding the absolute value to the RPD, the uncertainties are similar, slightly lower for LBL4 when using assumption one, but slightly larger when using assumption 3.

Finally, the LBL models are simplified models. Their advantage is to have quick (and easy) results, at the cost of (theoretically) reduced accuracy compared to other (more computationally expensive) models. Therefore, by using assumption 3 the simplification is even more significant.

7.4 Monte Carlo analysis

Monte Carlo methods are a method to determine numerical results using repeated random sampling. They are based on performing several evaluations of a model with randomly selected inputs. A Monte Carlo calculation is useful to determine the model uncertainty and understand the significance of a result from a model or experiment [Hughes and Hase, 2010, Saltelli et al., 2003, Bevington and Robinson, 2003, Morgan, 2009].

Before utilizing random sampling, the statistical distribution of each simulated variable has to be defined. Different variables might have different distributions [Saltelli et al., 2003].

For this study, the distributions were calculated according to the field measured data for wind speed and direction, temperature, air leakage rate, flow exponent, house volume and envelope area and shielding and dwelling factor. 1x10^5 random samples were simulated for each variable. The Monte Carlo analysis is used to carry out a sensitivity analysis of the LBL models.

7.4.1 Defining distributions

In order to obtain a representative simulated sample, the distributions of all independent variables have to be defined. Different infiltration models require different inputs. For the LBL models (both 50 Pa and 4 Pa, assumptions one and three), six variables are defined:

- air leakage rate (n_{50} or n_4, h^{-1}),
- flow exponent (b_{50} or b_4),
- wind speed (m/s),
- temperature difference (ΔT, K),
- shielding factor,
- house volume (m^3), and,

- envelope area (m^2).

Other models are also analysed in the following chapters; two other variables are therefore defined as below:

- wind direction (°), and,
- dwelling factor.

In addition, the data used to define the distributions simulates as accurately as possible the conditions presented during the testing campaigns. The only variable whose distribution was not defined from the field measurements is the temperature difference, ΔT where the data was acquired from historical regional data. The need to use historical data as opposed to field measurements is discussed later in section 7.4.1.3. The data was organized to obtain statistical figures such as mean, standard deviation and type of distribution followed. The data presented in Chapter 5 in Tables 5.9 and 5.10 is used to define distributions from airtightness parameters.

7.4.1.1 Air leakage rate

The measurements of air leakage rate taken in the test dwellings using both testing methods help define the distribution range of air leakage rate. The mean air leakage rate measured with the blower door and Pulse is respectively 8.53 h^{-1} and 1.78 h^{-1}.

In both cases the distribution assumed was a log-normal distribution in order to obtain non-negative samples; the standard deviation (σ) of the sample for n_{50} was 3.21 h^{-1}, and for n_4 0.76 h^{-1}. Figures 7.6 and 7.7 show the final distribution after producing 100 000 of random samples.

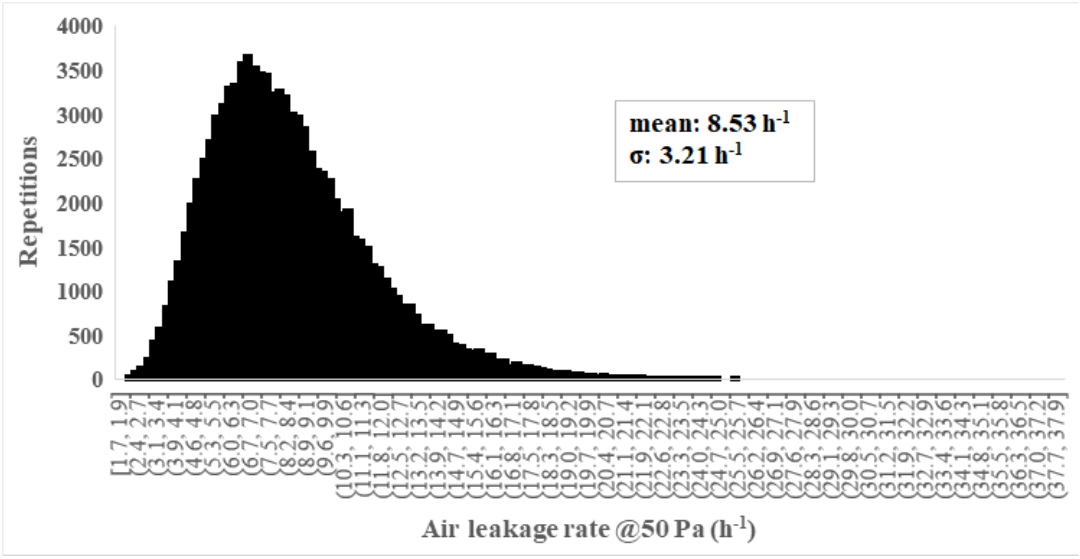


Figure 7.6: Air leakage rate @50 Pa(n_{50}) distribution from $1x10^5$ samples.

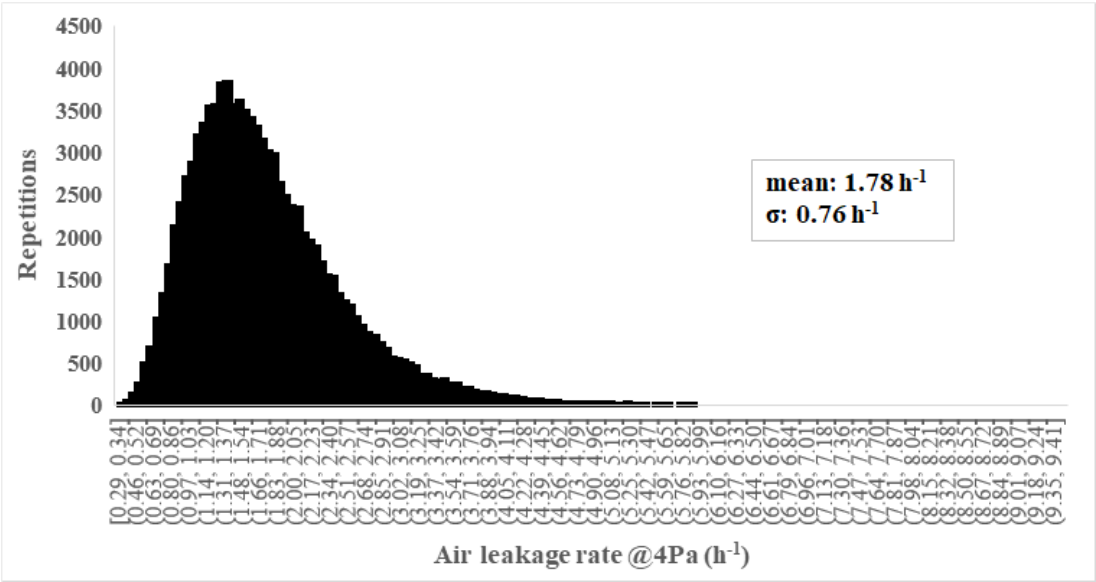


Figure 7.7: Air leakage rate @4 Pa(n_4) distribution from $1x10^5$ samples.

7.4.1.2 Flow exponent

For the flow exponent (b), the distributions are samples based on the measurements taken in the field data collection stage as shown in Chaper 5. The value for flow exponent has to lie between 0.5 and 1, depending on the type of flow (turbulent to laminar). The distribution followed a normal distribution, with means of 0.63 and 0.69 for b_{50} and b_4 respectively. When there is no information, a typically assumed value for the flow exponent is 0.66, which is close to the mean of the samples.

The variation is small, the standard deviation (σ) for b_{50} was 0.045 and for b_4, 0.059. It was reviewed that the simulations were in the correct range. The information to describe the distributions from the airtightness measurements is summarised in Table 7.8.

Table 7.8: Mean and standard deviation from all the measurements (Chapter 5) of airtightness using the blower door and Pulse methods.

	Blower door		Pulse	
	n_{50} (h^{-1})	b_{50}	n_4 (h^{-1})	b_4
Mean	8.53	0.63	1.78	0.69
Standard deviation	3.21	0.045	0.76	0.059

7.4.1.3 Environmental conditions

Variables such as wind speed and wind direction, present large variability due to the different measurements taken in the field. Table 7.9 shows a summary of the measured environmental conditions, a total of 359,623 measurements across all 20 tests for each variable were taken to produce the wind speed and direction figures presented. In the case of temperature, the approach to define the distribution was different. When the indoor and outdoor temperature measurements taken were computed to randomly simulate temperature difference scenarios, it was seen that for several simulations the temperature differential was negative, i.e. the outdoor temperature was higher than the indoor temperature. Therefore when calculating the stack infiltration in Equation 2.17 the model produces unrealistic values.

The LBL model was put to the test using these in-situ temperature measurements and the results obtained are shown in Figure 7.8. It is clear from the graph, that for an n_{50} value lower than $13h^{-1}$ infiltration is inversely proportional to the airtightness of the building, which contradicts the theory.

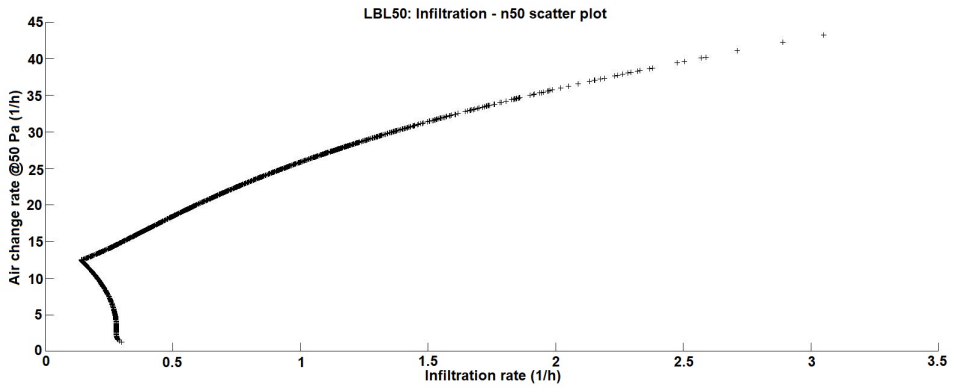


Figure 7.8: Predicted air infiltration rates (using LBL50 model) against air leakage rate.

These results are explained from the simplified nature of the model. It is known that leakage distribution across the building's façades affects the infiltration rate of a building. The LBL model does not account for these distributions and does not differentiate from infiltration and exfiltration. This means that the part of Figure 7.8 where airtightness and infiltration are inversely proportional, is where infiltration and exfiltration flows are acting together.

Most of the measurements were taken during summer time; therefore, a bias towards a small (or negative) temperature difference was found and small stack induced infiltration is calculated. When this happens, Lyberg [1997] states that the model violates the mass conservation; therefore leading to unrealistic results. Additionally, infiltration is more relevant (in the UK) during winter than it is for summer, i.e. during the heating season. Infiltration heat losses mainly occur when heating is in use.

Given the above, it was decided to obtain historical temperature data from the East-Midlands region of the United Kingdom. Outdoor temperature data was obtained using the met office data from a weather station located in Sutton Bonnington, U.K. Average temperatures from the months of October, November, December, January, February and March of 1959 to 2019 were used to calculate a mean outdoor temperature and a standard deviation of the data; these figures are included in Table 7.9. The indoor temperature was fixed to 20.0 °C. This was set as a winter design temperature according to CIBSE Guide A [CIBSE, 2015].

Table 7.9: Mean and standard deviation from all the measurements of environmental conditions.

	Wind speed (m/s)	**Wind direction (°)**	**Outdoor temperature (°C)**	**Indoor temperature (°C)**
Mean	0.758	190.18	6.12	20.0
Standard deviation	0.542	101.42	2.83	N/A

As presented in Table 7.9, the mean wind speed from the measurements was 0.758 m/s, with a σ of 0.542. The large variation (large σ when compared to the mean) accounts for very different readings. The figure was obtained from all measurements recorded in all test days; therefore, many different wind speeds could be captured. The distribution utilised was a log-normal distribution to account only for positive values of wind speed, the final distribution of $1x10^5$ samples can be found in Figure 7.9. The majority of velocities lie under 3 m/s.

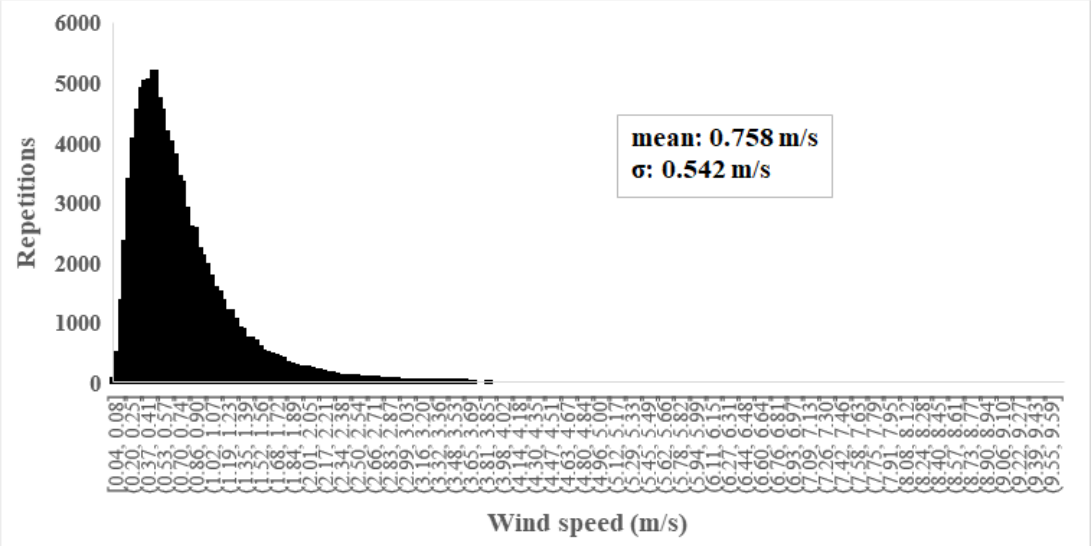


Figure 7.9: Wind speed distribution from $1x10^5$ samples.

The wind direction simulation was a different case compared to other variables because only values from 0 to 360 degrees were simulated. That is why a beta distribution was selected. A beta distribution is defined through an interval, 0 to 360 in this case, and shape parameters, alpha and beta parametrise it. The alpha and beta parameters were calculated as 0.4454 and 0.5965, respectively, taken from the measured data. The distribution for 100,000 random samples is shown in the

histogram presented in Figure 7.10.

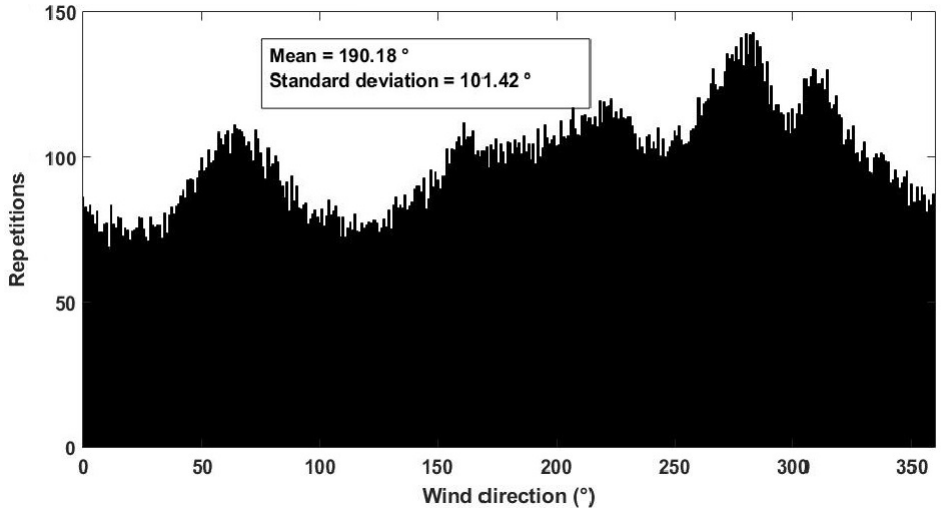


Figure 7.10: Wind direction distribution from $1x10^5$ samples.

The temperature difference (ΔT) was calculated by subtracting the outdoor temperature to the indoor temperature. The distribution of temperature difference is what drives the stack induced infiltration of the LBL model. A final graph of the distribution is given in Figure 7.11.

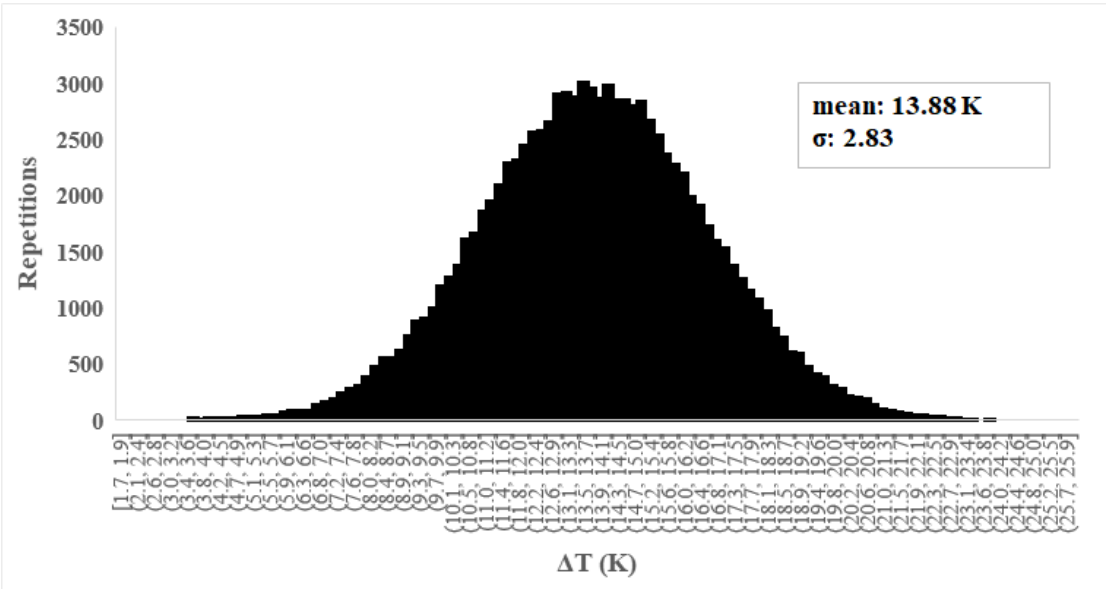


Figure 7.11: Temperature difference distribution from $1x10^5$ samples.

It can be seen that the temperature difference follows a normal distribution with a mean of 13.88 K and a standard deviation of 2.83 K.

7.4.1.4 Volume and envelope area

For the same reasoning as before, where only positive values were required, a log-normal distribution was considered for the volume and envelope area. Table 7.10 summarises the statistical information from the measurements of twenty dwellings. Volume and envelope area are inputs of the models. However, these parameters are constant whereas the weather conditions are non-steady, and the air leakage rate might vary from test to test. Therefore, analysing the models assuming that the volume and envelope area do not add to the uncertainty of the output, would be a way of analysing the interaction of the remaining non-steady variables. For this study, both scenarios (uncertainty introduced from measuring volume and envelope area, and taking them as constants) are considered.

Table 7.10: Mean and standard deviation from all the measurements of Volume and Envelope Area.

	Volume (m^3)	**Envelope Area** (m^2)
Mean	251.05	260.80
Standard deviation	81.53	64.90

Figures 7.12 and 7.13 show the final sample of volume and envelope area, respectively.

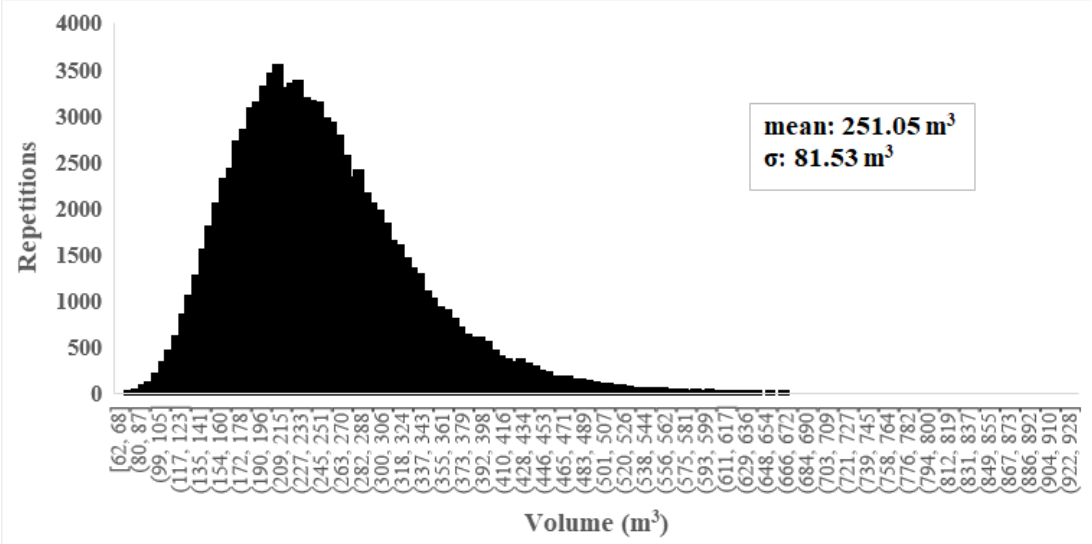


Figure 7.12: Dwelling volume distribution from $1x10^5$ samples.

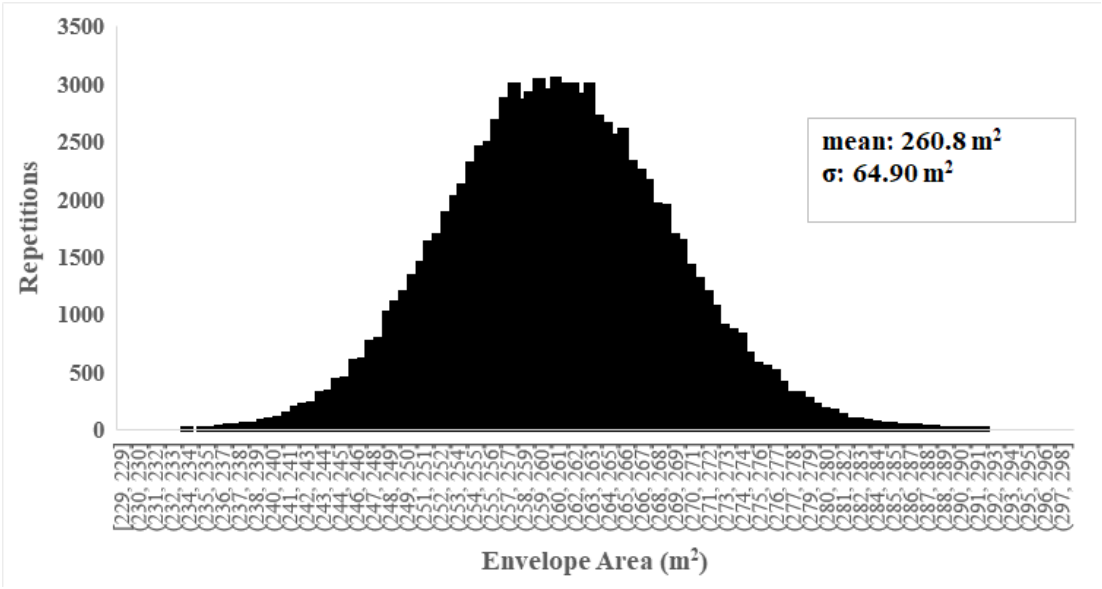


Figure 7.13: Dwelling envelope area distribution from $1x10^5$ samples.

7.4.1.5 Shielding and dwelling factors

The shielding and dwelling factors are simulated according to their probability. Depending on the data obtained from the dwellings survey, a probability is assigned to each parameter. Numbers from 0 to 1 are simulated and, depending on the probability, the shielding and dwelling factors are assigned. Table 7.11 presents the probabilities of the shielding and dwelling factors.

Table 7.11: Probability of shielding and dwelling factor.

Shielding		**Dwelling**	
Factor	**Probability**	**Factor**	**Probability**
Heavy shielding	0.35	End of terrace	0.15
Moderate shielding	0.20	Mid terrace	0.15
Light shielding	0.40	Semi-detached	0.35
No shielding	0.05	Detached	0.35

The majority of the dwellings tested have light or heavy shielding and are detached or semi-detached. This is because the majority of houses are located in urban or suburban areas in the East-Midlands of the United Kingdom, i.e. none were located in the city centre of a big city such as London.

7.5 Sensitivity analysis

7.5.1 Introduction to sensitivity analysis

With the samples generated through the Monte Carlo random sampling method, 100 000 different predictions were made using the LBL model, from measurements using both airtightness measuring techniques. It is important to mention that, as seen in previous sections, assumption 3 provided less variance, and assumption one less mean RPD; therefore a sensitivity analysis is made for both assumptions.

The predicted infiltration rates are used to carry out a sensitivity analysis of the LBL50 and LBL4 models. Saltelli et al. [2003] defines a sensitivity analysis as *"the study of how the variation in the output of a model can be apportioned, qualitatively or quantitatively, to different sources of variation, and how the given model depends upon the information fed to it"*. In other words, a sensitivity analysis evaluates the impact of each variable that is fed into the model on the uncertainty of its output.

Sensitivity analyses are model dependent, the analyses made were carried out according to Chapter 6 in Saltelli et al. [2003]. The procedure is described as follows:

1. Definition of distributions: these were defined in the Section 7.4.1.

2. Sampling: Monte Carlo random sampling selected and explained in Section 7.4.1. Additionally, the model is run for the same number of times the variables were sampled; in these models, one hundred thousand.

3. Evaluation of model: A model fitting the data is compared to the original model. Samples are used to determine predictions from the model and all this predicted data is fitted into a regression.

4. Uncertainty analysis. The variables are analysed comparing the predicted results with the ones obtained with the regression model.

5. Sensitivity analysis. Analysis of the effect of each variable into the final output.

The sensitivity analysis was made through a regression analysis; assuming that the model created (in step 3) is from the form:

$$\hat{y} = b_0 + \sum_{j=1}^{n_x} b_j x_j \tag{7.3}$$

Where x_j are the input variables and b_j are the coefficients that are determined from the created model ($\hat{y}$); n_x represent the number of independent variables. For each variable k Equation 7.3 becomes:

$$y_k = b_0 + \sum_{j=1}^{n} b_j x_{kj} + \varepsilon_k, k = 1, ..., m \tag{7.4}$$

m is the number of inputs or independent variables, and the error terms $\varepsilon_k = y_k - \hat{y_k}$, with y_k as the original model results. To determine the values of b_j, the matrix for $\mathbf{b}$ in Equation 7.5 has to be solved (section 6.2.2 from Saltelli et al. [2003]).

$$\boldsymbol{y} = \boldsymbol{x}\boldsymbol{b} + \boldsymbol{\varepsilon} \tag{7.5}$$

Finally, the least-squares regression model is defined by:

$$\sum_{k=1}^{m} (y_k - \bar{x})^2 = \sum_{k=1}^{m} (\hat{y_k} - \bar{x})^2 + \sum_{k=1}^{m} (\hat{y_k} - y_k)^2 \tag{7.6}$$

where: $\sum_{k=1}^{m} (y_k - \bar{x})^2 = SS_{tot}$, $\sum_{k=1}^{m} (\hat{y_k} - \bar{x})^2 = SS_{reg}$ and, $\sum_{k=1}^{m} (\hat{y_k} - y_k)^2 = SS_{res}$. Then the previous equation can be written as $SS_{tot} = SS_{reg} + SS_{res}$. The R^2 of the regression model is given by:

$$R^2 = \frac{SS_{reg}}{SS_{tot}} \tag{7.7}$$

A value close to 1 means that the model accounts for most of the uncertainty. An element of b_j is given for each variable used as input of the model, these are called "*Regression coefficients*". The regression model can be re-defined as:

$$\frac{\hat{y} - \bar{y}}{\hat{s}} = \sum_{j=1}^{n} \frac{b_j \hat{s}_j}{\hat{s}} \frac{x_j - \bar{x}_j}{\hat{s}_j} \tag{7.8}$$

where

$$\hat{s} = \Big[\sum_{j=1}^{n} \frac{(y_k - \bar{y})^2}{m-1} \Big]^2 \tag{7.9}$$

and

$$\hat{s}_j = \Big[\sum_{j=1}^{n} \frac{(x_{kj} - \bar{x}_j)^2}{m-1} \Big]^2 \tag{7.10}$$

Standardised regression coefficients (SRC) are metrics to determine the importance of a variable in a model, and are given by the coefficients $\frac{b_j \hat{s}_j}{\hat{s}}$ from Equation 7.8.

In addition, the level of dependency of the model to a variable is defined by the correlation. For instance, the correlation coefficients (CC) r_{xy} represent the relationship between x and y, for the model described before. Nevertheless, these coefficients are known to describe the relationship when only one independent variable (x_j) is used [Saltelli et al., 2003].

$$r_{xy} = \frac{\sum_{k=1}^{m}(x_k - \bar{x})(y_k - \bar{y})}{\left[\sum_{k=1}^{m} x_k - \bar{x}^2\right]^{1/2}\left[\sum_{k=1}^{m} y_k - \bar{y}^2\right]^{1/2}} \tag{7.11}$$

For this study, the variables are ranked according to the SRC's and CC's, which then determine the corresponding impact of each variable on the uncertainty of the output.

The regression model is evaluated for $1x10^5$ samples for each variable, giving 100,000 infiltration rates. Figure 7.14 shows the cumulative distribution function (CDF) for the LBL models using assumptions 1 and 3. It can be seen that the mean infiltration value for the LBL50 model is 1.42 h^{-1} with a standard deviation (σ) of 0.23 h^{-1} (16%)for assumption 1 and, a mean of 0.52 h^{-1} and standard deviation of 0.09 h^{-1} (17%) for assumption 3.

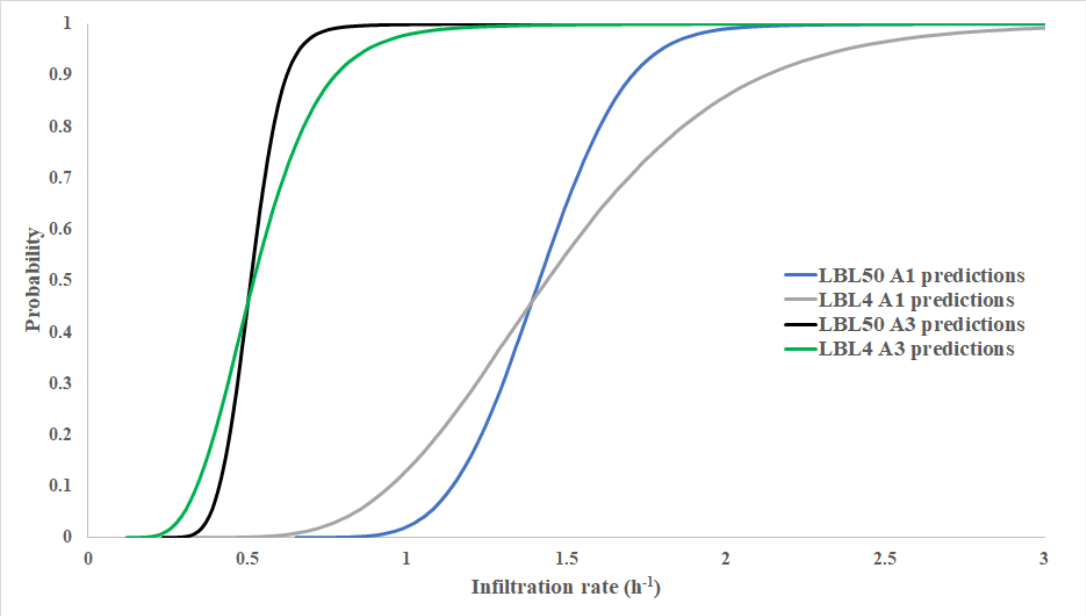


Figure 7.14: Cumulative distribution function (CDF) for predicted infiltration rates using the LBL models for assumptions 1 and 3.

For the LBL4 model the obtained mean was 1.50 h^{-1} with a standard deviation (σ) of 0.49 h^{-1} (33%) for assumption 1 and mean of $0.55h^{-1}$ and standard deviation $0.19h^{-1}$ (34%) of for assumption 3. The LBL4 model has a higher variance,

therefore the overall uncertainty is larger. It can also be seen that assumption one yields larger infiltration rates. By looking only at the mean values of each model, if assumption 1 is used, the result is 2.7 times higher than when using assumption 3. This remarks the importance of choosing the right assumption for the floor and ceiling distribution. Additionally it also tells how a result can differ from reality if the inputs are selected incorrectly.

7.5.2 Scatter plots LBL50 and LBL4 assumptions 1 and 3

For a correct sensitivity analysis, Saltelli et al. [2003] recommends to start by analysing the variables in scatter plots, this step was also followed by Das et al. [2014] in its indoor air quality sensitivity analysis. Different scatter plots using the different variables in the LBL50 and LBL4 models were produced. Scatter plots are good to provide observational evidence of correlation.

The variables analysed in the LBL50 and LBL4 models (assumptions 1 and 3) include:

- wind speed,
- temperature difference,
- air leakage rate (at 50 and 4 Pa of pressure difference),
- flow exponent, and
- shielding.

7.5.2.1 Infiltration-Environmental conditions (wind and temperature)

Figure 7.15 shows in the X axis the predicted infiltration rates (h^{-1}) and on the Y axis, the wind speed. Furthermore, Figure 7.16 has a similar configuration. Each figure represents the LBL50 and LBL4 models, respectively, in both cases, using assumption one.

For the LBL50 model (Figure 7.15), it can be seen that both variables are positively correlated (directly proportional), the higher the wind speed, the higher the infiltration rate. However, for wind speed higher than 2 m/s the rate at which infiltration increases is higher. For low wind (less than 2 m/s), the correlation is not linear. On the other hand, for the LBL4 model (Figure 7.16) the graph is closer to a line, infiltration increases steadily with higher wind velocities.

It is noticeable that the minimum infiltration rate predicted with the LBL50 model is 0.7 h^{-1} whereas for the LBL4 model is 0.4 h^{-1}. This means that the

LBL50 model predicts higher infiltration rates overall. These two figures are obtained when the wind speed is 0.

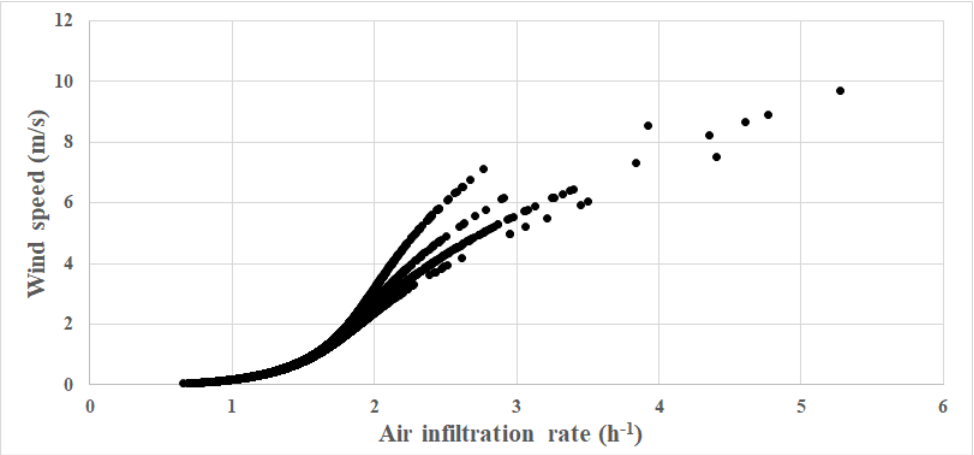


Figure 7.15: Predicted air infiltration rates (using LBL50 model Assumption 1) against wind speed.

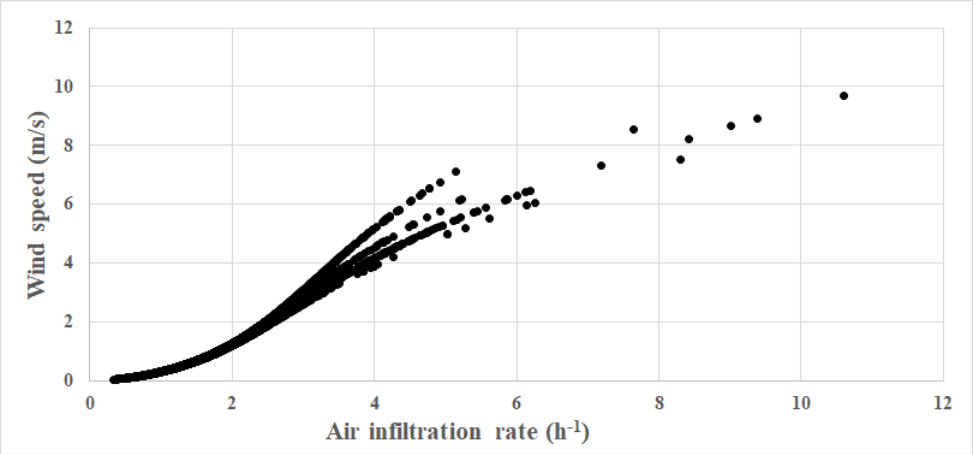


Figure 7.16: Predicted air infiltration rates (using LBL4 model Assumption 1) against wind speed.

Figure 7.17 shows the predicted infiltration rate obtained using the LBL50 model assumption 3 against wind speed; and, Figure 7.18 shows a similar graph for the LBL4 model assumption 3. Both models show a similar trend as the ones produced for assumption 1. The difference is, being assumption 3 a simplification of the model, the graphs follow only one path whereas in assumption 1 the graphs include four "tails"; these tails are produced by the shielding factors, in assumption 3 the shielding factor is already included in the simplification. LBL50 also predicts higher infiltration rates, when the wind speed is 0 the infiltration rate is 0.25 h^{-1}

whereas for the LBL4 is 0.16 h^{-1}. However, the opposite occurs at high wind speeds, LBL4 predicts higher infiltration. By using assumption 3, the overall predictions are smaller than when using assumption 1.

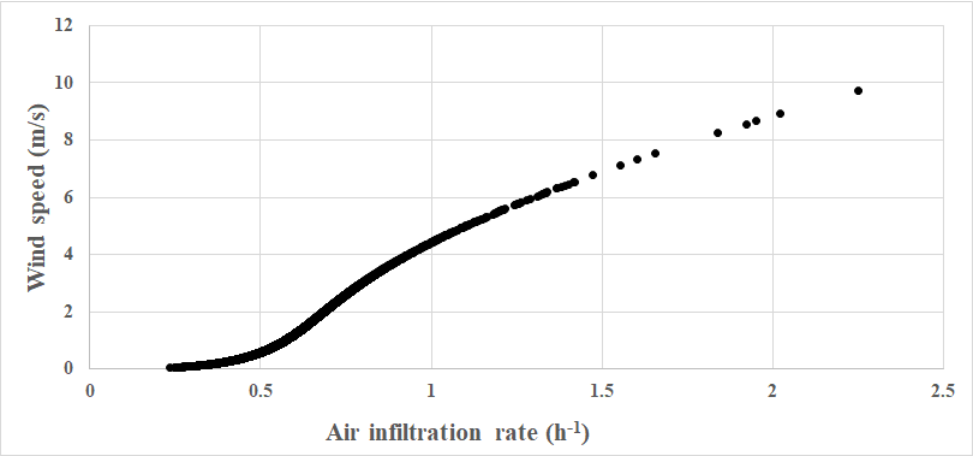


Figure 7.17: Predicted air infiltration rates (using LBL50 model Assumption 3) against wind speed.

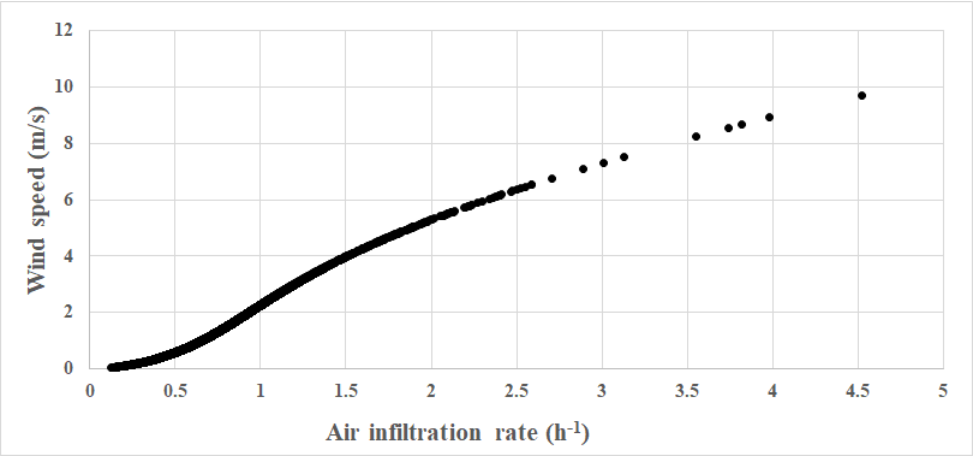


Figure 7.18: Predicted air infiltration rates (using LBL4 model Assumption 3) against wind speed.

Figures 7.19 and 7.20 show how the infiltration rate (X) and temperature difference (Y) interact in the LBL50 and LBL4 models assumption 1, respectively. Additionally, Figures 7.21 and 7.22 show the same interaction for assumption 3. For all cases, the figures show an inversely proportional trend between infiltration rate and temperature difference, which, contradicts the theory. To explain this, first, it has to be pointed out that the graphs only show two variables; however, they were obtained from running the models using all variables. Second, as

mentioned before, the model uses a superposition technique and does not include exfiltration flows, i.e. does not recognize an interaction between infiltration and exfiltration flows, hence it is a simplified model; infiltration and exfiltration act together responding to the outdoor-indoor pressure differential, both exist and interact and must be taken into account when analysing air movement and ventilation. That being said, the graphs show that at low infiltration rate, temperature difference is more relevant. For high infiltration rate, variables such as wind are more important. This was also mentioned in Chapter 4 and presented in Vega Pasos et al. [2018a] and Liddament [1996]. Aditionally, the simulations were used using winter temperatures, or high temperature differences. This represents a bias since most of the cases will have a similar temperature difference, in other words, the sample is not as spread. With a larger spread of temperature differences, different conditions would be simulated; however, as mentioned earlier, the model does not produce realistic results for negative temperature differences.

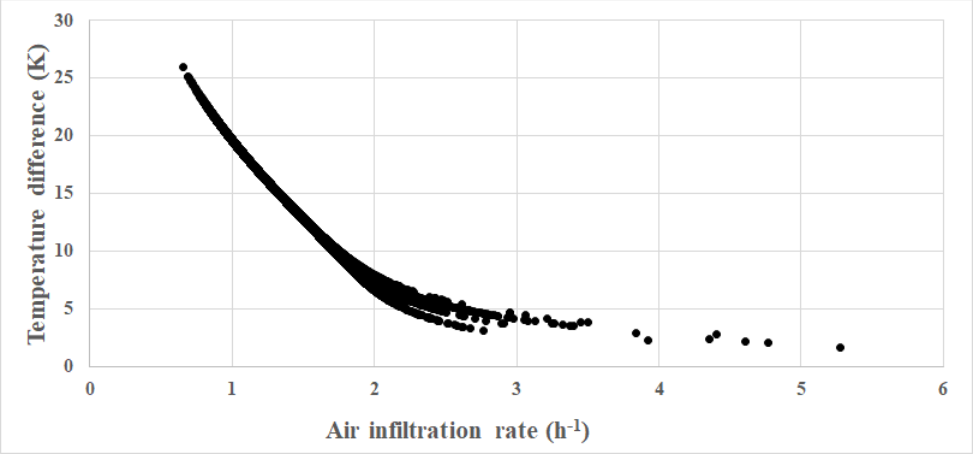


Figure 7.19: Predicted air infiltration rates (using LBL50 model Assumption 1) against temperature difference.

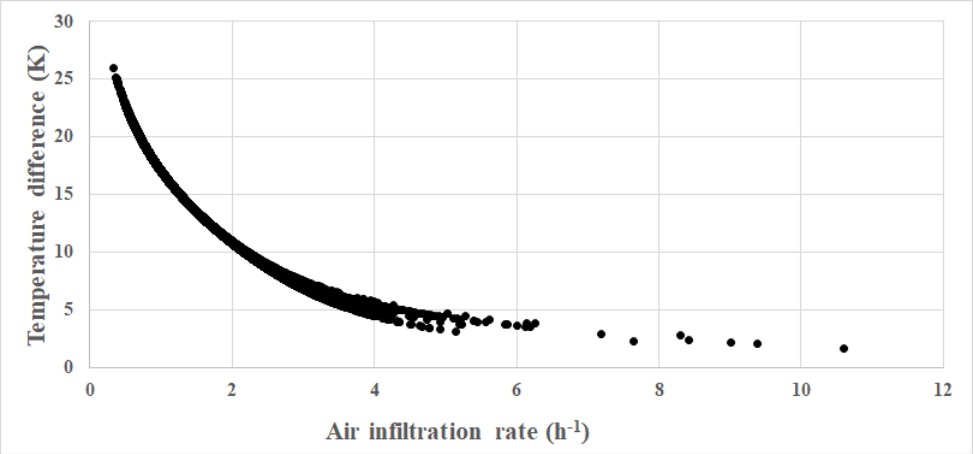


Figure 7.20: Predicted air infiltration rates (using LBL4 model Assumption 1) against temperature difference.

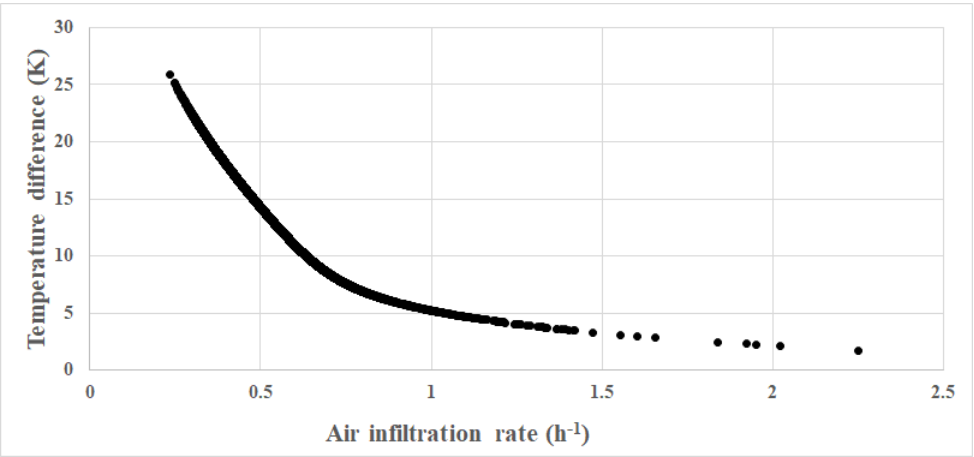


Figure 7.21: Predicted air infiltration rates (using LBL50 model Assumption 3) against temperature difference.

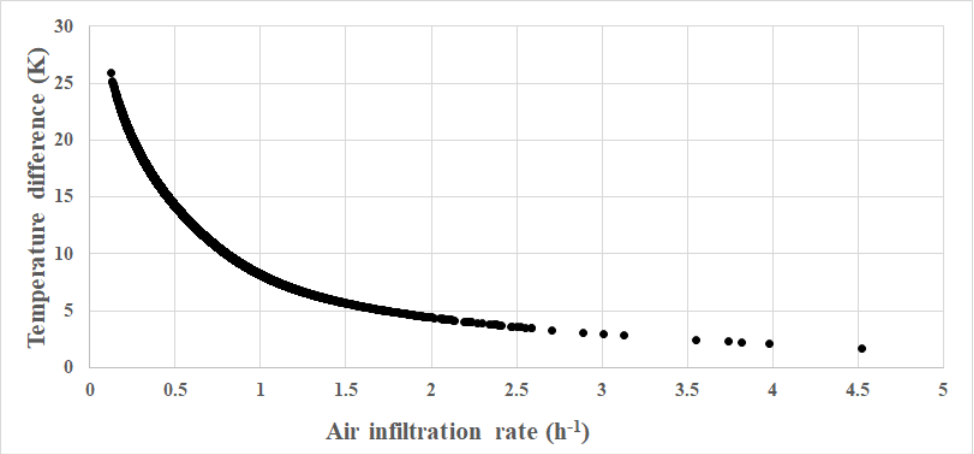


Figure 7.22: Predicted air infiltration rates (using LBL4 model Assumption 3) against temperature difference.

Despite the model or assumption it can be inferred from the previous graphs that at low infiltration (low wind), temperature difference is the main driving force for air infiltration. And that for most of the curve other variables have a more significant effect on the output of the model. The algorithm of the LBL models show that the stack effect, apart from the temperature difference is only dependant on the leakage distribution. The wind effect is dependant also on the shielding of the building. Hence, different variable interaction makes the model more sensitive to wind particularly, which explains why temperature difference follows that trend.

The differences when using assumption 1 compared to the results when using assumption 3, are more model-related than variable-related, i.e. what was mentioned for the infiltration - wind scatter plot is still valid. In assumption 3, infiltration only follows one trend, whereas for assumption 1, at high infiltration there are different options (multiple variable interaction). Infiltration is higher when using assumption one, and the LBL50 model.

For a deeper analysis, Figure 7.23 overlaps the effect of wind (left Y-axis) and temperature difference (right Y-axis) against the predicted infiltration rate (X-axis) for the LBL50 model assumption 1. When wind speed is 0 and the temperature difference is high (above 20K), infiltration is low. This supports the discussion given in the previous paragraphs, temperature difference is the main driving force at low wind speed but inducing low infiltration. Furthermore, Infiltration increases with an increase in wind speed.

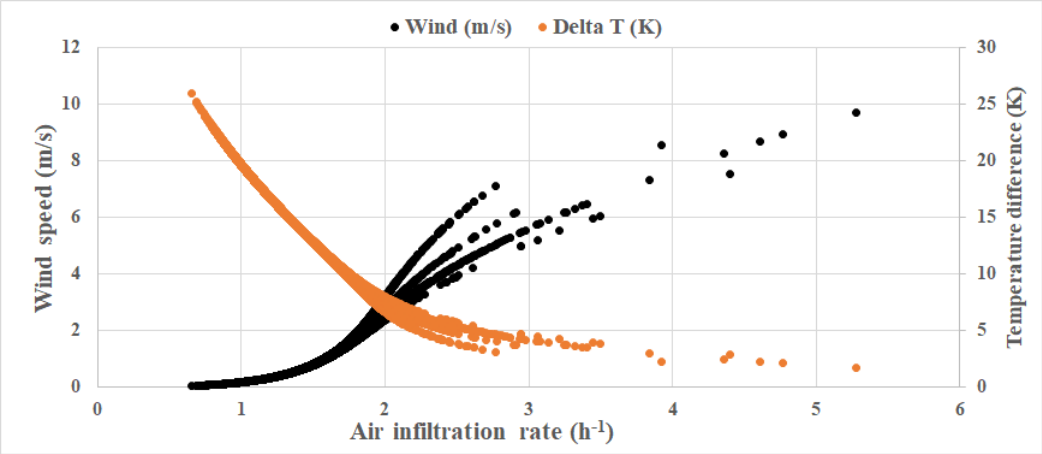


Figure 7.23: Predicted air infiltration rates (using LBL50 model Assumption 1) against wind speed and temperature difference

A temperature difference between 5 and 10 K means that there is an outdoor temperature between 11 and 16 °C. Between those differences, is when the model start becoming highly sensitive to an increase in wind speed. The majority of predictions occur in this range of temperature differences; it can be said that when the temperature difference is in this range (wind speed lies between 1.8 and 2.1 m/s), the wind has a more dominant effect, but temperature difference also induces some infiltration.

A similar analysis is given for the LBL4 model assumption 1, which is graphically given in Figure 7.24. In this case, it can be seen that wind effect (on infiltration) is bigger for lower velocities; however, the conclusions are the same as for the LBL50 model when referring to temperature difference.

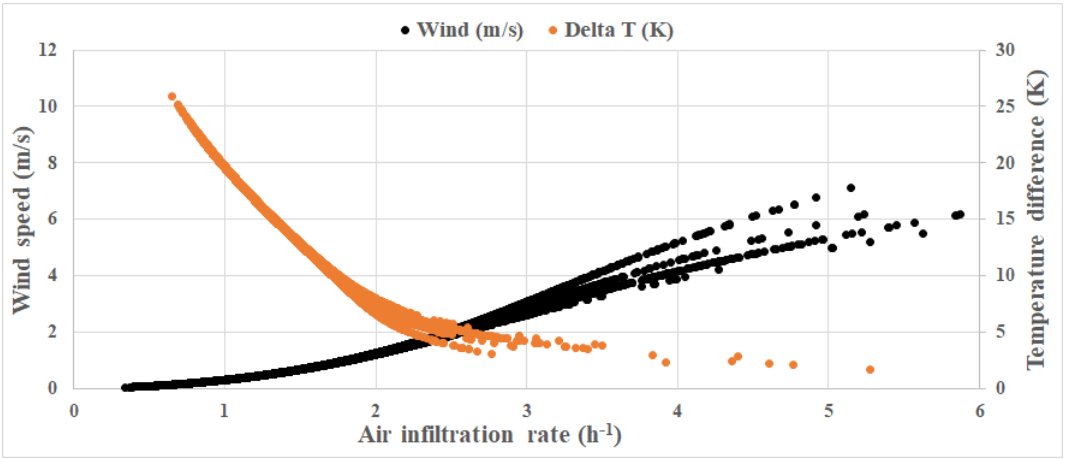


Figure 7.24: Predicted air infiltration rates (using LBL4 model Assumption 1) against wind speed and temperature difference form low infiltration

This is telling that for this case, wind seems to have a dominating effect at most points, probably given by the fact that at high pressure noise from wind is shadowed. It can be seen for both cases, that the majority of infiltration rates lie between a wind speed of 1.8 and 2.1 m/s. For temperature difference between and 5 to 10 K for LBL 50 and, between 4 to 8 K for the LBL4, these ranges are the parts of the graphs with most infiltration predictions. In conclusion, infiltration depends on both environmental conditions; however, the one which is the main driving force for infiltration according to these models, will be dependent upon their individual magnitudes.

7.5.2.2 Infiltration-air leakage rate (n_{50} and n_4) and flow exponent (b)

Air leakage rate is known as the base line for infiltration rate to be predicted, it can be said that infiltration is mainly affected by the air leakage rate. For the LBL50 model, measurements from air leakage rate at 50 Pa were used (n_{50}), using the blower door method; for the LBL4 model, n_4 was obtained from the Pulse method. Another important parameter obtained when measuring the air leakage rate, is the flow exponent, b_{50} and b_4 were obtained from the blower door and Pulse methods respectively, and, used in the LBL50 and LBL4 models.

Figures 7.25 and 7.26 depict the infiltration rate against the air leakage rate, n_{50} for the LBL50 model for assumptions 1 and 3 respectively.

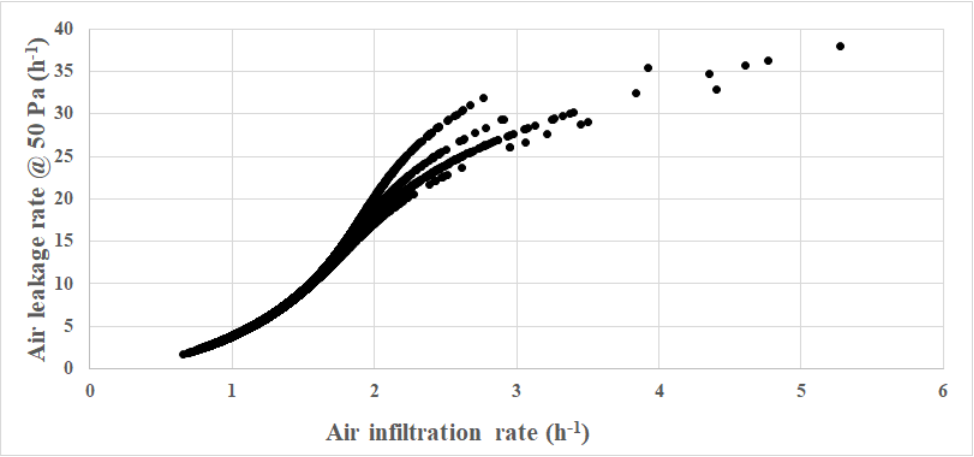


Figure 7.25: Predicted air infiltration rates (using LBL50 model Assumption 1) against air leakage rate (n_{50}).

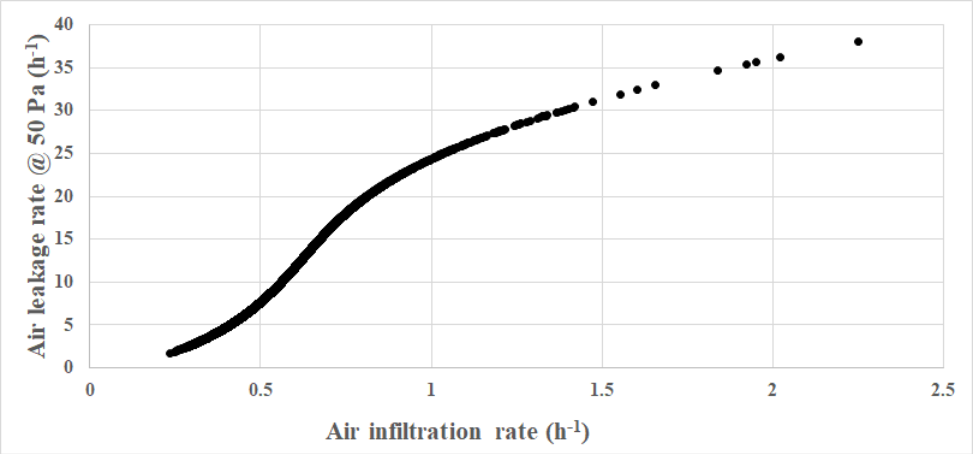


Figure 7.26: Predicted air infiltration rates (using LBL50 model Assumption 3) against air leakage rate (n_{50}.

For Figure 7.25, the majority of infiltration predictions occur for air leakage rates lower than 20 h^{-1}; however, there are predictions for air leakage rates up to 38 h^{-1}. Precisely, 99% of the air leakage rate samples are lower than 20 h^{-1}, 96% of samples are lower than 15 h^{-1}, 73% of the samples are lower than $10h^{-1}$, and only 10% of the samples are tighter than $5h^{-1}$ It can be seen that the air leakage rate is proportional to the infiltration rate.

For assumption 3, the results are similar as for assumption 1; however, the simplification used in assumption 3 is reflected in a lower spread of the infiltration predictions (following one single line).

On the other hand, Figures 7.27 and 7.28 show the interaction between air infiltration and n_4 for the LBL4 model assumptions 1 and 3, respectively.

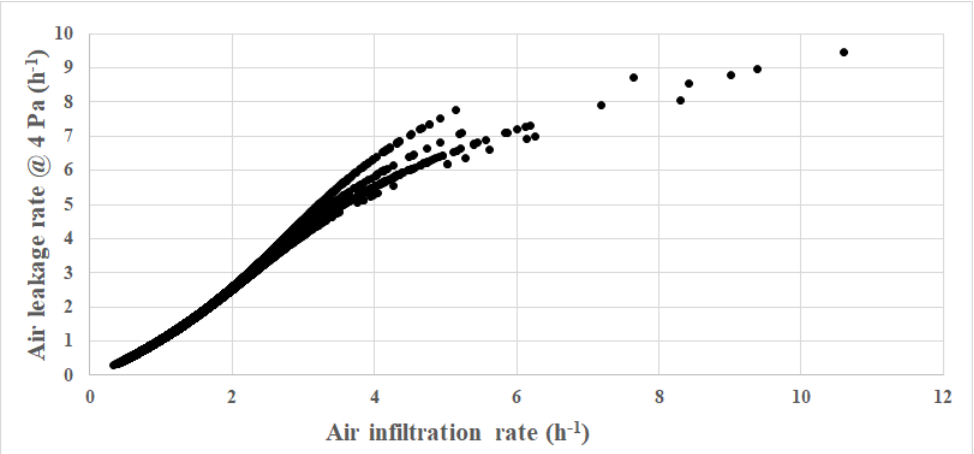


Figure 7.27: Predicted air infiltration rates (using LBL4 model Assumption 1) against air leakage rate (n_4).

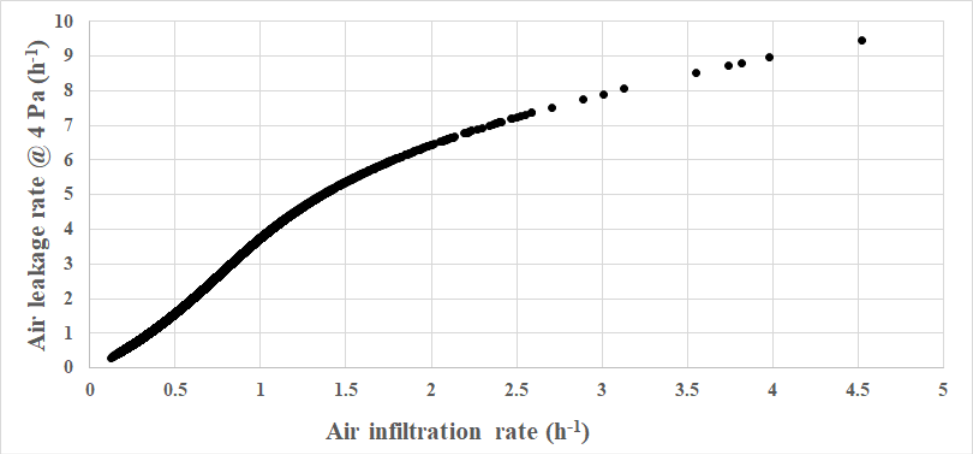


Figure 7.28: Predicted air infiltration rates (using LBL4 model Assumption 3) against air leakage rate (n_4).

For LBL4 model assumptions 1 and 3, the model is closer to a straight line characteristic for air leakage rates lower than 5 h^{-1} @4 Pa. For the samples of n_4, almost 100% of the sample have an air leakage rate lower than 5 h^{-1}, 93% lower than 3 h^{-1}, 69% lower than 2 h^{-1}, and only 11% lower than 1 h^{-1}.

As before, air infiltration is directly proportional to the air leakage rate. Both models have shown sensitivity to the air leakage rate measurement.

The flow exponent, which was measured alongside the air leakage rate varies between 0.5 and 1 from turbulent to laminar flow in leakage paths. Figures 7.29 and 7.30 show the interaction between air infiltration and flow exponent b_{50} and b_4 respectively for the LBL and LBL4 assumption 1 models.

For both figures, the results are similar, there are infiltration predictions for all simulated flow exponents. It appears as the infiltration rate grows with an increase in flow exponent i.e. higher infiltration for a closer-to laminar flow. For the LBL50 model the prediction is closer to a line, whereas for the LBL4 model it resembles a parabola. These graphs might be misleading because 99% of the simulated flow exponents are lower than 0.75, and 96% of the simulation lie between 0.5 and 0.75 for both cases. This means that the majority of predictions of infiltration have an average exponent. It is expected for airtight dwellings to have a greater flow exponent than leaky ones. This interaction might not be reflected in the graphs presented, however it leads to point that the air leakage rate impacts more (than flow exponent) when predicting infiltration rates.

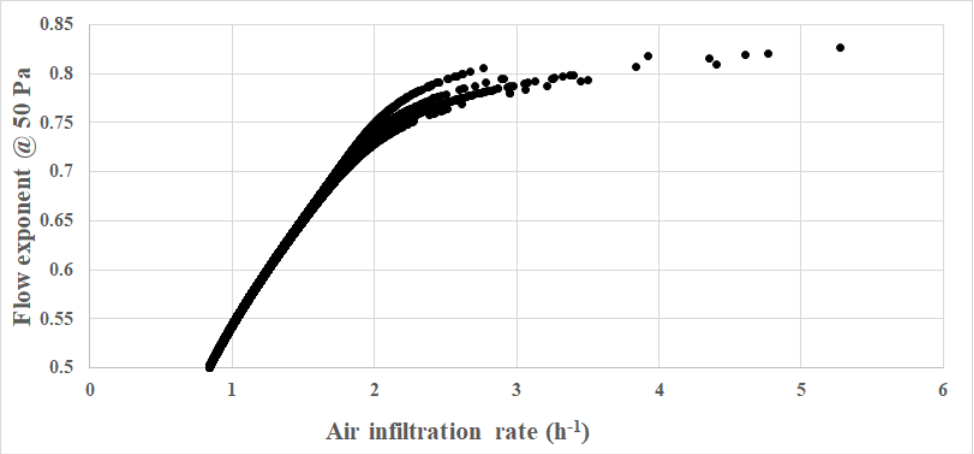


Figure 7.29: Predicted air infiltration rates (using LBL50 model Assumption 1) against flow exponent.

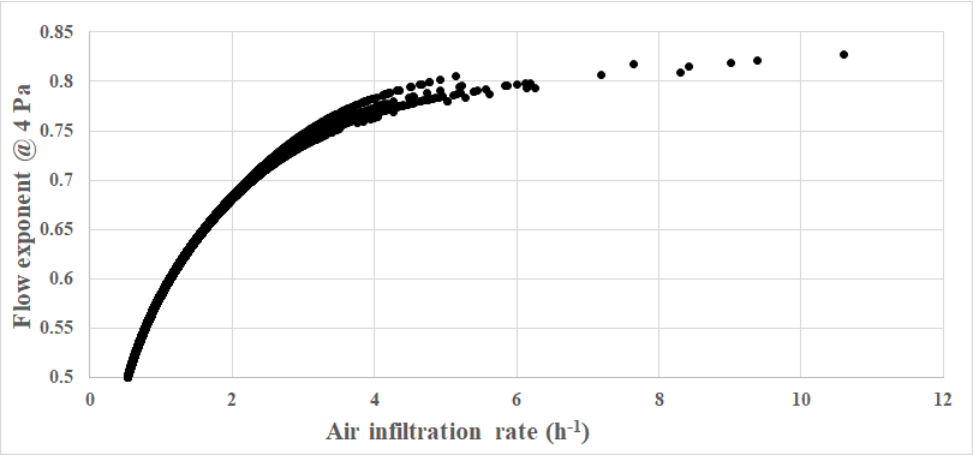


Figure 7.30: Predicted air infiltration rates (using LBL4 model Assumption 1) against flow exponent.

Figures 7.31 and 7.32 show the interaction between air infiltration and flow exponent b_{50} and b_4 respectively for the LBL assumption 3 models. The results are similar as the ones presented for assumption 1. For the majority of flow exponent simulations (0.55 to 0.75), both variables show proportionality.

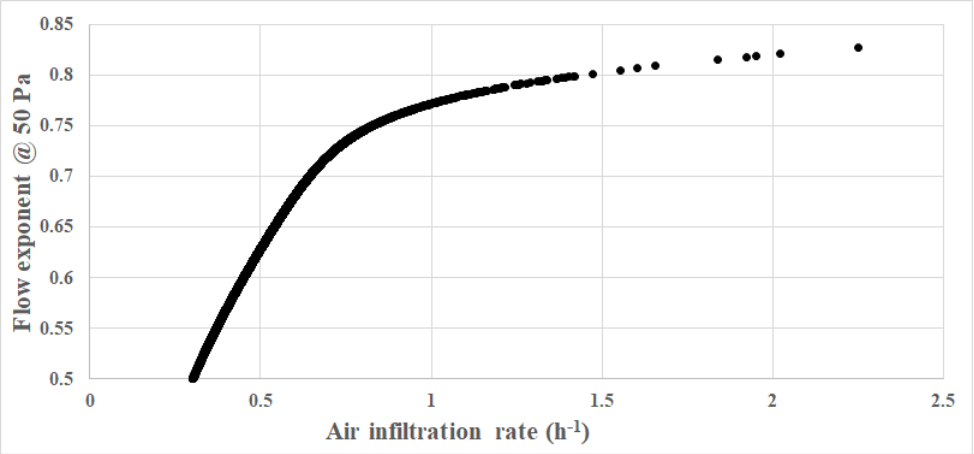


Figure 7.31: Predicted air infiltration rates (using LBL50 model Assumption 3) against flow exponent.

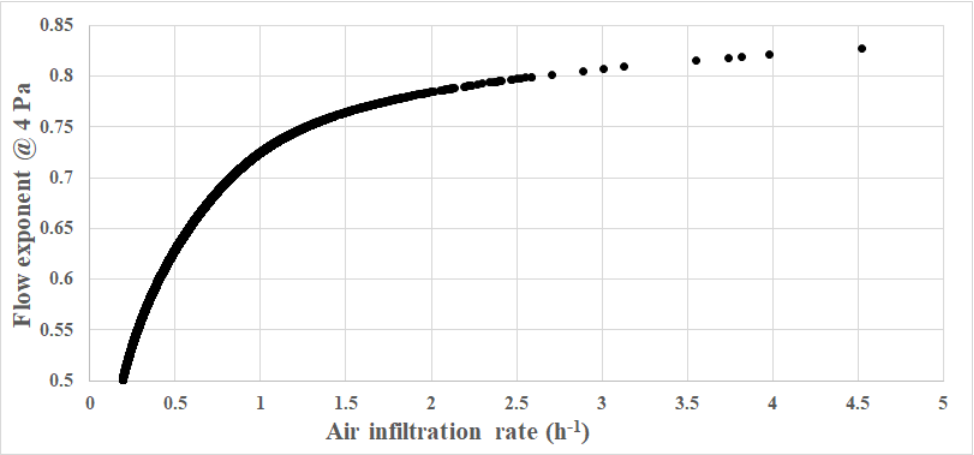


Figure 7.32: Predicted air infiltration rates (using LBL4 model Assumption 3) against flow exponent.

Despite the results shown in the airtightness (air leakage rate and flow exponent) scatter plots, it is difficult to assign total output dependence to a particular variable. It is known that all variables interact together. It is also known that the flow exponent is obtained through airtightness testing, therefore the air leakage rate and flow exponent are related to the capacity of the testing method of providing accurate results; in other words, their uncertainties and their effect on the output (infiltration rate) are closely related.

7.5.2.3 Infiltration - dwelling parameters (volume, envelope area and shielding)

Figures 7.33, 7.34 and 7.35 show the interaction between infiltration rate and house volume, envelope area and shielding condition, respectively for assumption 1 of the LBL50 model. On the other hand Figures 7.36 and 7.37 represent the interaction between air infiltration and house volume and envelope area for assumption 3 of the LBL model; in assumption 3, the shielding condition is simplified, therefore, it is not used directly in the model.

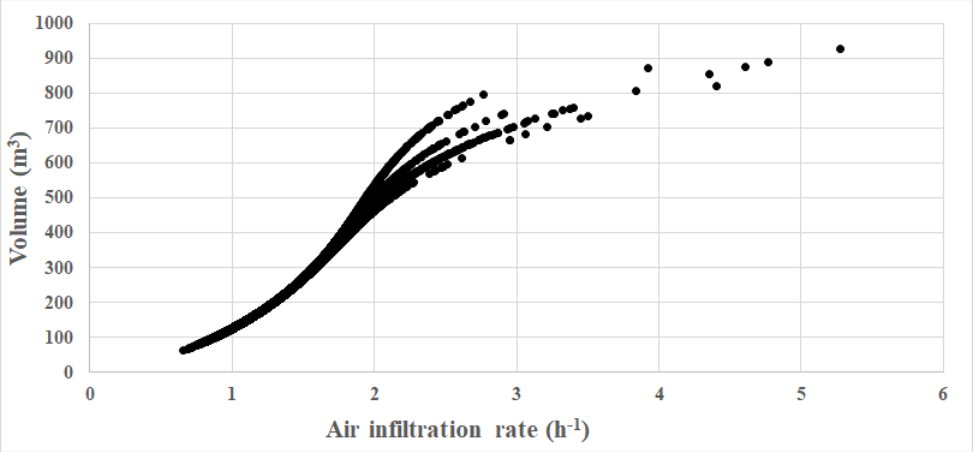


Figure 7.33: Predicted air infiltration rates (using LBL50 model Assumption 1) against house volume.

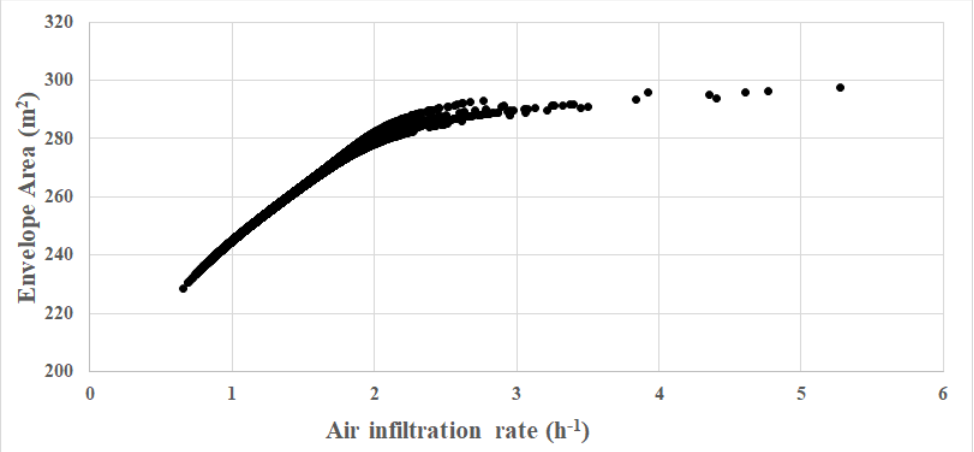


Figure 7.34: Predicted air infiltration rates (using LBL50 model Assumption 1) against house envelope area.

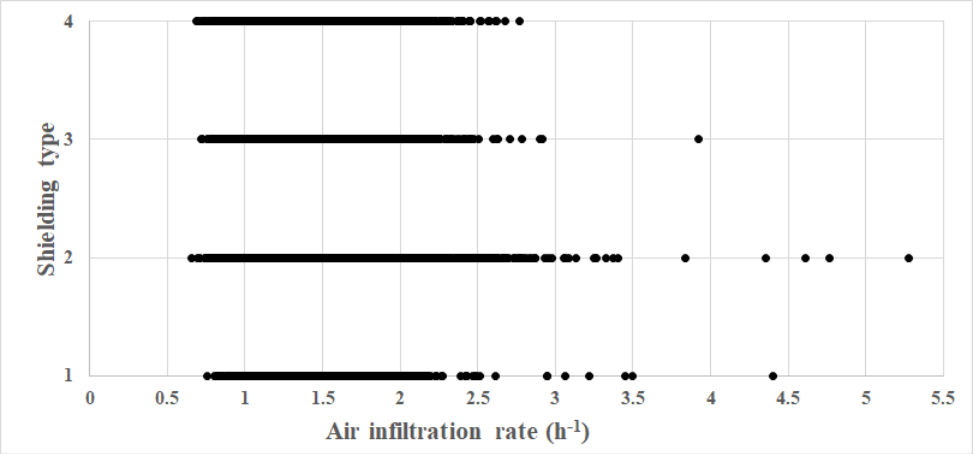


Figure 7.35: Predicted air infiltration rates (using LBL50 model Assumption 1) against shielding condition.

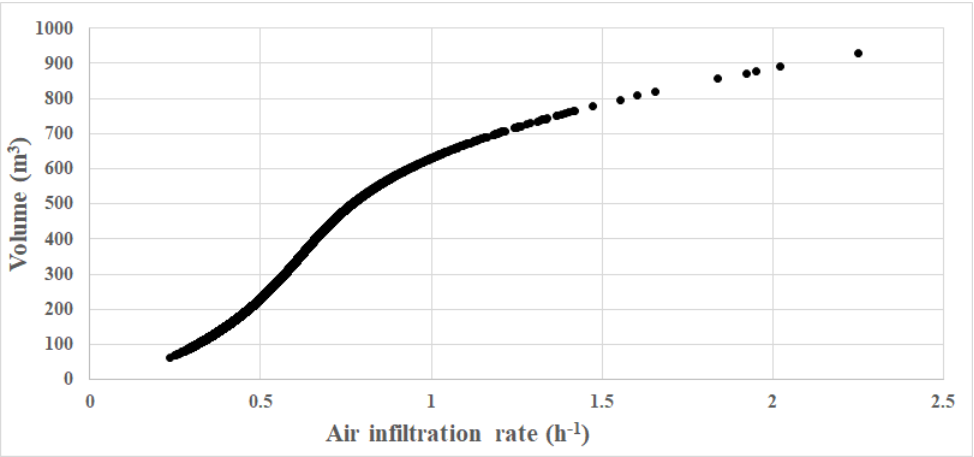


Figure 7.36: Predicted air infiltration rates (using LBL50 model Assumption 3) against house volume.

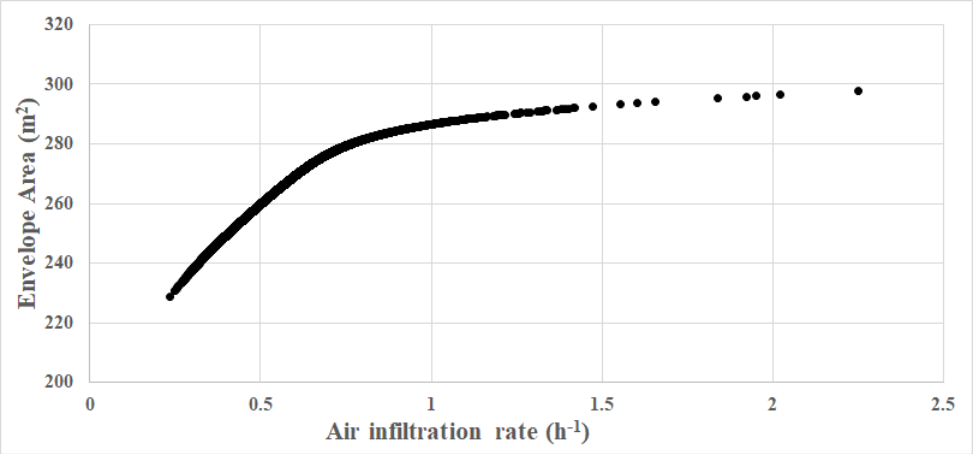


Figure 7.37: Predicted air infiltration rates (using LBL50 model Assumption 3) against house envelope area.

For volume and envelope area, as expected, it is seen that infiltration increases with larger dwellings, this is valid for both assumptions. The main difference is that the infiltration-volume graphs follow a curve with two points of inflection. The envelope area graphs follow a closer-to linear shape.

There is little which is remarkable concerning the infiltration-shielding graph. What is apparent however, is that for all graphs plotted using assumption 1 regardless of the independent variable, the curves have four "tails", this does not happen for assumption 3 (assumption three does not use a shielding factor since it is already accounted in the simplifying factors). These tails are given by the shielding factor, a different shielding scenario leads to a different end of the curve. This means that for high infiltration shielding plays a major role, and it is clearly seen in all graphs. Shielding modifies the infiltration and is a main variable when large infiltration is present (approximately above $2h^{-1}$).

Figures 7.38, 7.39 and 7.40 show the interaction between infiltration rate and house volume, envelope area and shielding condition, respectively for assumption 1 of the LBL4 model.On the other hand Figures 7.41 and 7.42 represent the interaction between air infiltration and house volume and envelope area for assumption 3 of the LBL4 model.

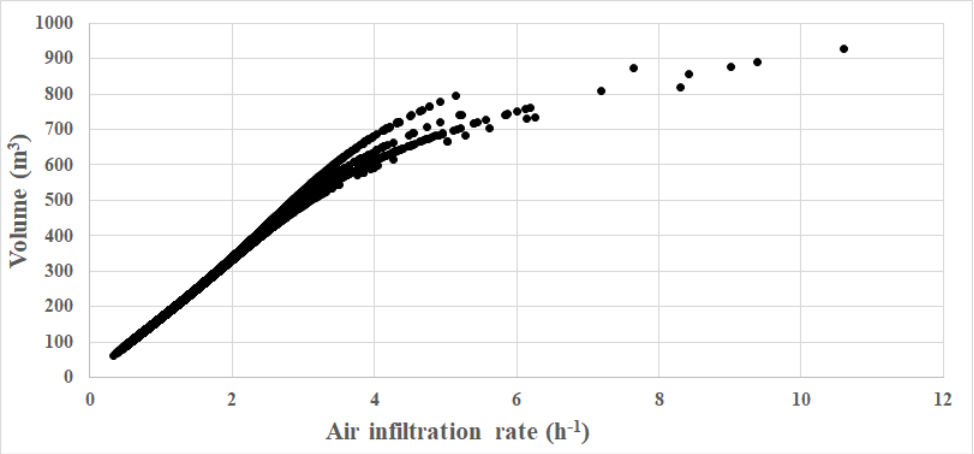


Figure 7.38: Predicted air infiltration rates (using LBL4 model Assumption 1) against house volume.

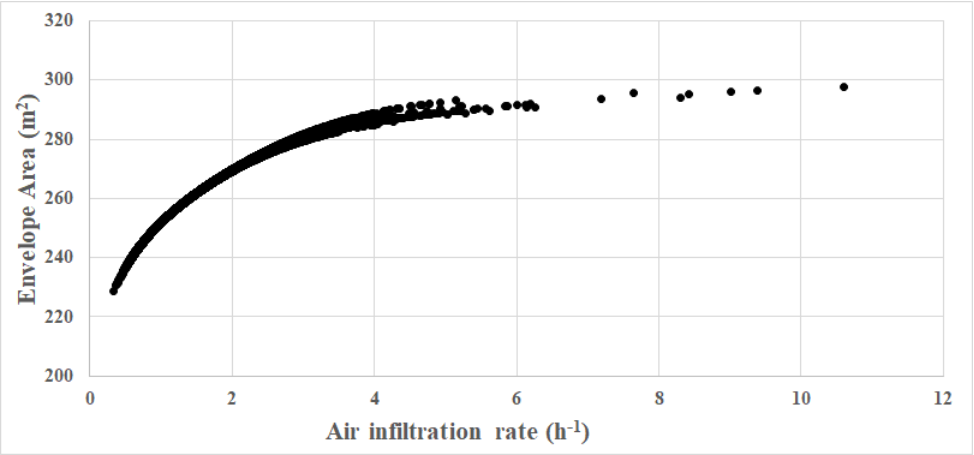


Figure 7.39: Predicted air infiltration rates (using LBL4 model Assumption 1) against house envelope area.

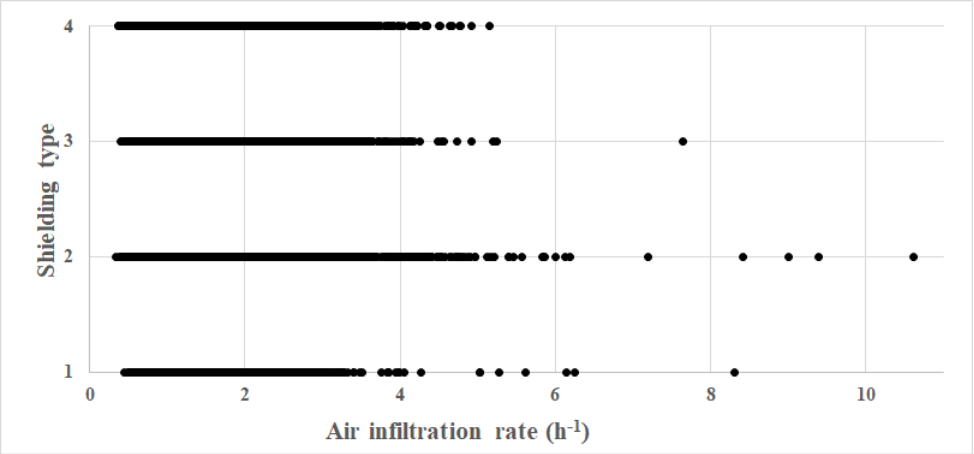


Figure 7.40: Predicted air infiltration rates (using LBL4 model Assumption 1) against shielding condition.

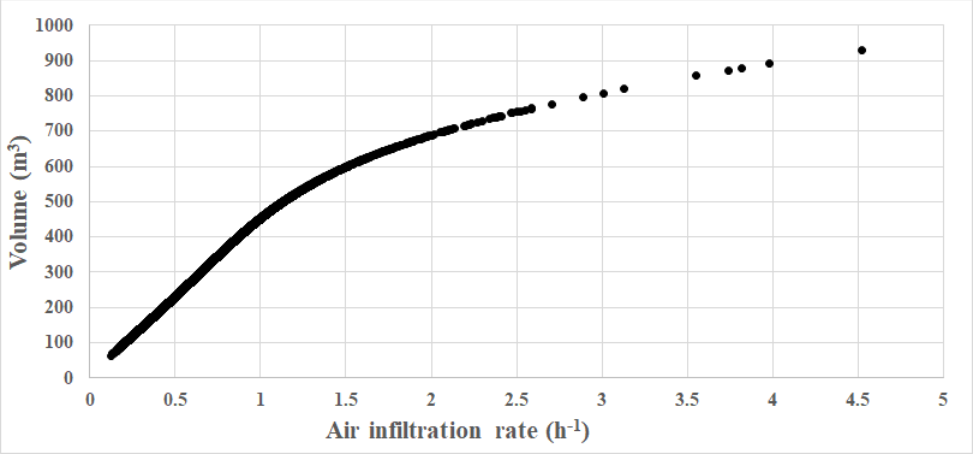


Figure 7.41: Predicted air infiltration rates (using LBL4 model Assumption 3) against house volume.

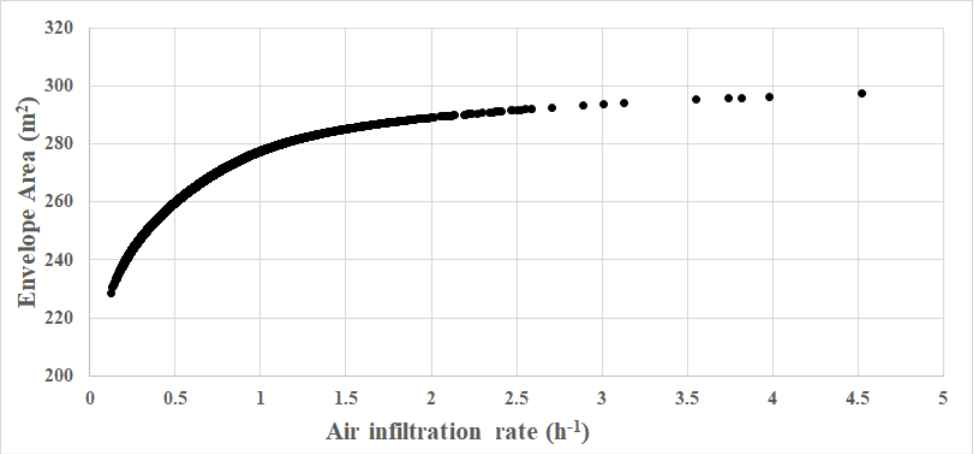


Figure 7.42: Predicted air infiltration rates (using LBL4 model Assumption 3) against house envelope area.

The graphs are similar as the ones presented for the LBL50 model, and the analysis is valid also for the LBL4 graphs.

7.5.2.4 Summary of scatter plots

In summary, from the scatter plots, it was found that all the variables interact with each other, therefore it is difficult to find a correlation or a complete output dependence on only one single variable. Infiltration is proportional to air leakage rate and wind speed. The scatter plots from temperature difference showed that it is particularly relevant when all the other variables are small, for example, when the wind speed is low or the house is tight. The shielding condition proved to be important at high infiltration, this was seen only for assumption 1 graphs (assumption 3 simplifies the model assuming a fixed shielding). LBL models need to be treated as a combination of independent variables acting to predict infiltration rates; it is difficult to assign importance to only one variable without considering the rests.

7.5.3 Regression and ranking of variables

7.5.3.1 LBL50 and LBL4 assumption 1

After running all the samples, a fitting model was created, whereby the predicted data was fitted and the sum of squares (Equation 7.6) and coefficients of multiple determination (R^2, Equation 7.7), were calculated. The results from the LBL models assumption 1 are given in Table 7.12; the coefficients are obtained when

comparing the predictions from the original model (given in the previous sections) and the predictions of the regression model (sensitivity analysis).

Table 7.12: Sum of squares (SS) and coefficient of multiple determination (R^2) for sensitivity analysis of LBL50 and LBL4 infiltration models (assumption 1) for $1x10^5$ samples.

SS	**LBL50**	**LBL4**
Regression	5127.300	23888
Residual	23.066	82.187
Total	5150.366	23970.187
R^2	0.996	0.997

It is clearly seen that, the model fits the data almost perfectly, the R^2 coefficients are close to one for both models. This is probably due to the simplified nature of the LBL model. Figures 7.43 and 7.44 show the predicted data using respectively the LBL50 and LBL4 models, and the newly created regression models fitting that data. The red dashed lines represents a perfect correlation (where all points overlap each other resembling a straight line).

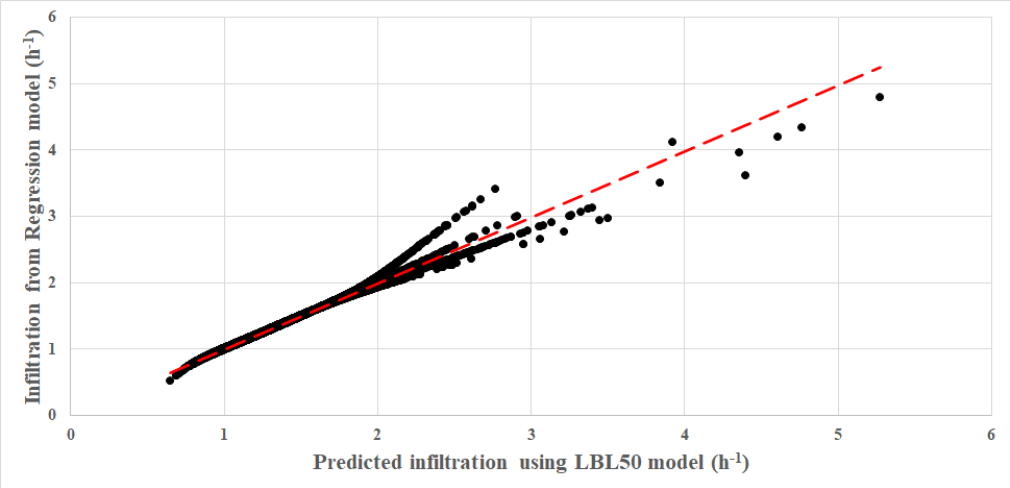


Figure 7.43: Predicted and regression values of infiltration rate for LBL50 Assumption 1 sensitivity analysis, $R^2 = 0.996$.

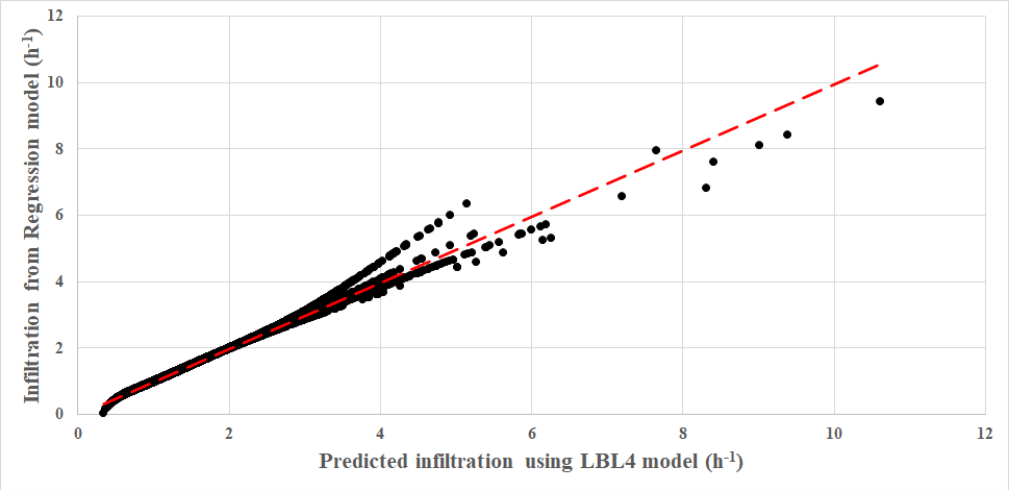


Figure 7.44: Predicted and regression values of infiltration rate for LBL4 Assumption 1 sensitivity analysis, $R^2 = 0.997$.

As can be seen, the correlation lines overlap for most of the graph, except for the last part (or the four "tails" in the model). It can be said that the data is well represented by the regression model, which is to be used in the calculation of the Standard Regression Coefficients (SRC). This is valid for both LBL50 and LBL4 models.

When the coefficients from the best fit regression model (b_n) are determined, the SRC's can be calculated, as mentioned, SRC's are relevant when finding the importance of variables upon the output. For this case, the dependent variable (output) is the infiltration rate and the independent variables are the inputs of the models.

Table 7.13 shows the coefficients of the regression models (Equation 7.8) for the LBL50 and LBL4 models sensitivity analysis, in both cases only for assumption 1. The Standardised Regression Coefficients (SRC) are also presented; and, in addition, the Correlation Coefficients (CC) are included. The CC's are good when using models with only one variable. Here are shown to prove that there is no single correlation because they all are very small.

Table 7.13: Model coefficients (b_n), Standardised Regression Coefficients (SRC) and, Correlation Coefficients (CC) for the model created in the Sensitivity analysis for LBL50 and LBL 4 assumption 1.

Variable	**Regression coefficient**(b_n)	**SRC**		**CC**	
		Value	**Rank**	**Value**	**Rank**
LBL50 Assumption 1					
Volume	0.647	218.625	1	$-1.123x10^{-05}$	5
Air leakage rate (n_{50})	-14.894	-194.848	2	$1.104x10^{-05}$	6
Envelope Area	-4.145	-143.944	3	$1.168x10^{-05}$	2
Flow exponent (b_{50})	415.614	80.510	4	$1.166x10^{-05}$	3
Temperature difference	-2.544	-31.030	5	$-1.170x10^{-5}$	4
Wind speed	5.091	9.576	6	$9.400x10^{-06}$	7
Shielding	-0.005	-0.035	7	$-2.093x10^{-05}$	1
LBL4 Assumption 1					
Envelope Area	-8.364	-140.977	1	$-1.117x10^{-05}$	2
Volume	0.726	119.018	2	$1.074x10^{-05}$	5
Air leakage rate (n_4)	-67.140	-99.059	3	$1.036x10^{-05}$	6
Flow exponent (b_4)	1031.266	96.946	4	$1.115x10^{-05}$	3
Temperature difference	-2.277	-13.483	5	$-1.115x10^{-5}$	3
Wind speed	12.664	11.561	6	$8.990x10^{-06}$	7
Shielding	-0.006	-0.022	7	$-2.002x10^{-05}$	1

7.5.3.2 LBL50 and LBL4 assumption 3

A similar analysis as the one performed for assumption 1 was carried for assumption 3. The coefficients of multiple determination obtained from the regresison models for the LBL models assumption 3 are given in Table 7.14.

Table 7.14: Sum of squares (SS) and coefficient of multiple determination (R^2) for sensitivity analysis of LBL50 and LBL4 infiltration models (assumption 3) for $1x10^5$ samples.

SS	**LBL50**	**LBL4**
Regression	864.852	3591.9
Residual	72.183	8.030
Total	937.035	3599.930
R^2	0.923	0.998

For assumption 3, the LBL4 represents better the data than the LBL50 model. Nevertheless, both are well represented, 92% and 99% of accuracy. Figures 7.45

and 7.46 shown the predicted infiltration results using the original LBL models (X axis) against the predicted infiltration using the regression model (Y axis), with the perfect correlation (red dashed) line.

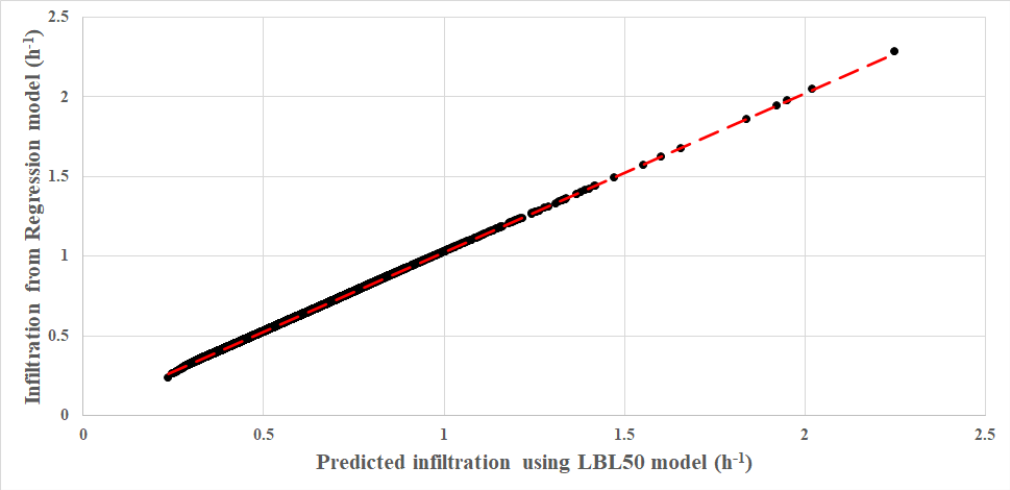


Figure 7.45: Predicted and regression values of infiltration rate for LBL50 Assumption 3 sensitivity analysis, $R^2 = 0.923$.

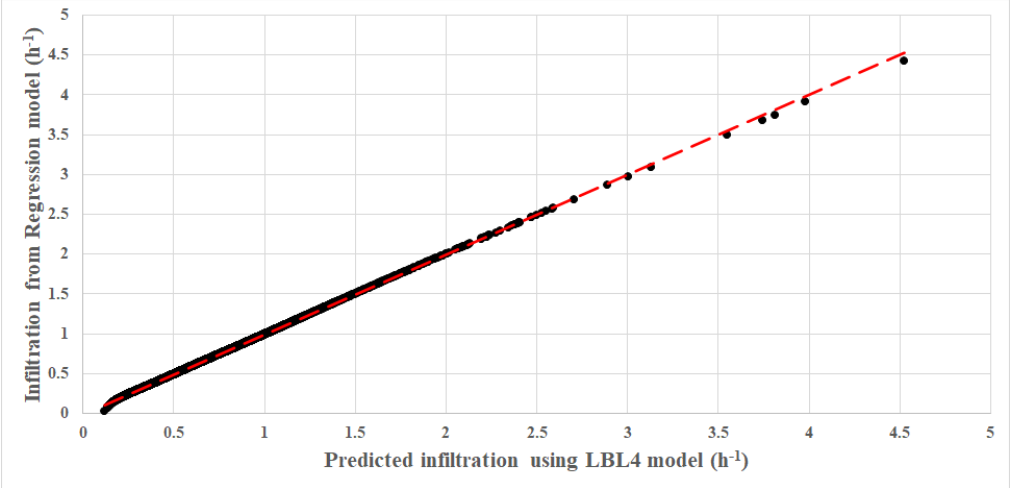


Figure 7.46: Predicted and regression values of infiltration rate for LBL4 Assumption 3 sensitivity analysis, $R^2 = 0.998$.

Different from assumption 1 and as mentioned before, by using assumption 3 the data is more close together (less variance in the infiltration rate) due to the simplifications made. Nevertheless, both models are well represented by the regression model. The model coefficients (b_n) for the regression created for the LBL50 and LBL4 models assumption 3 are given in Table 7.15. Additionally, the

SRC and CC are given. The table ranks the variables according to both SRC and CC, however, it can be seen that the CC are small in magnitude, hence, there is no direct correlation to one particular variable.

Table 7.15: Model coefficients (b_n), Standardised Regression Coefficients (SRC) and, Correlation Coefficients (CC) for the model created in the Sensitivity analysis for LBL50 and LBL 4 assumption 3.

Variable	**Regression coefficient**(b_n)	**SRC**		**CC**	
		Value	**Rank**	**Value**	**Rank**
LBL50 Assumption 3					
Volume	0.216	209.114	1	$9.981x10^{-06}$	4
Air leakage rate (n_{50})	-5.071	-189.833	2	$9.818x10^{-06}$	5
Envelope Area	-1.244	-123.609	3	$1.039x10^{-05}$	1
Temperature difference	-1.421	-49.603	4	$-1.037x10^{-5}$	2
Flow exponent (b_{50})	81.529	45.196	5	$1.037x10^{-05}$	2
Wind speed	1.955	10.525	6	$9.360x10^{-06}$	6
LBL4 Assumption 3					
Envelope Area	-2.943	-140.570	1	$-1.023x10^{-05}$	1
Volume	0.273	126.860	2	$9.836x10^{-06}$	4
Air leakage rate (n_4)	-25.890	-108.272	3	$9.497x10^{-06}$	5
Temperature difference	-4.484	-75.218	4	$-1.022x10^{-05}$	2
Flow exponent (b_4)	128.310	34.177	5	$1.022x10^{-05}$	2
Wind speed	5.255	13.592	6	$8.235x10^{-06}$	6

First, for assumption 1, the LBL50 model ranks the volume as the parameter which induces most uncertainty to the predicted infiltration rate. Air leakage rate, n_{50}, is the second place in terms of importance, meaning that, as expected, the uncertainty created when carrying out a steady pressurisation test, and its extrapolation, is more relevant than the environmental conditions. This was expected due to the nature of the high pressure airtightness testing method. What is important to remark is that volume and envelope area rank 1st and 3rd; this means that if there are errors while measuring the volume and envelope area, they are carried to the prediction of the infiltration rate.

In the LBL4 model, envelope area and volume rank 1st and 2nd place, followed by the airtightness parameters. In this case, the dwelling parameters induce more uncertainty than n_4, probably because it is directly measured at low pressure, and the extrapolation is avoided.

Shielding ranks last place for both models, this was expected. The "tails" seen in the scatter plots are only present for high infiltration, which represents less

than 2% of the simulations. The environmental conditions in both cases (LBL50 and LBL4) are ranked after the house parameters and airtightness measurements. As mentioned before, very small CC's show no individual correlation from one variable to the output.

Second, for assumption 3, once again volume and envelope area are in the first places (1st and 3rd for LBL50, 1st and 2nd for LBL4), n_{50} ranks in second place (LBL50) whereas n_4 ranks third (LBL4). The flow exponent is the fifth place for both models and wind speed ranked last.

It is important to remark that for both cases, LBL50 and LBL4, volume and envelope area were in the top 3 of relevance, this is because these are used to calculate leakage areas, and façade dimensions. However, the objective from this section is to see the interaction between the airtightness parameters, namely air leakage rate and flow exponent, and the environmental conditions. That is why, a similar analysis was made taking the volume and envelope area as true constants of the building. This introduces the assumption that these do not introduce uncertainty to the calculation of air infiltration. For these new regression models, the volume and envelope area were taken as the mean of the measured from the dwellings: 251.05 m^3 and 260.8 m^2 respectively.

7.5.4 Scatter plots LBL50 and LBL4 assuming volume and envelope area as constants

7.5.4.1 Infiltration - environmental conditions

The scatter plots from these new models with volume and envelope area as constants are given below. Figures 7.47 and 7.48 show the interaction between air infiltration (X) and wind speed (Y) for the LBL50 and LBL4 models assumption 1, respectively. On the other hand, Figures 7.49 and 7.50 show the interaction between air infiltration (X) and wind speed (Y) for the LBL50 and LBL4 models assumption 3, respectively.

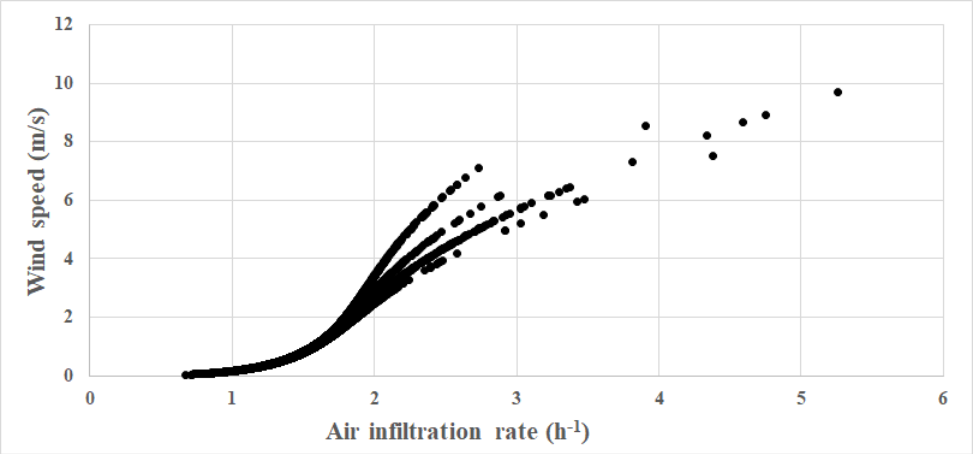


Figure 7.47: Predicted air infiltration rates (using LBL50 model Assumption 1) against wind speed with Volume and Envelope Area as true constants.

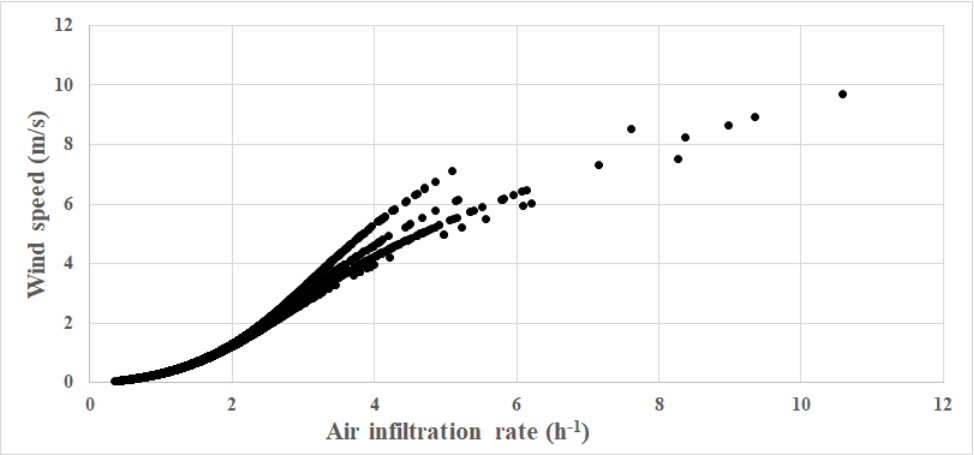


Figure 7.48: Predicted air infiltration rates (using LBL4 model Assumption 1) against wind speed with Volume and Envelope Area as true constants.

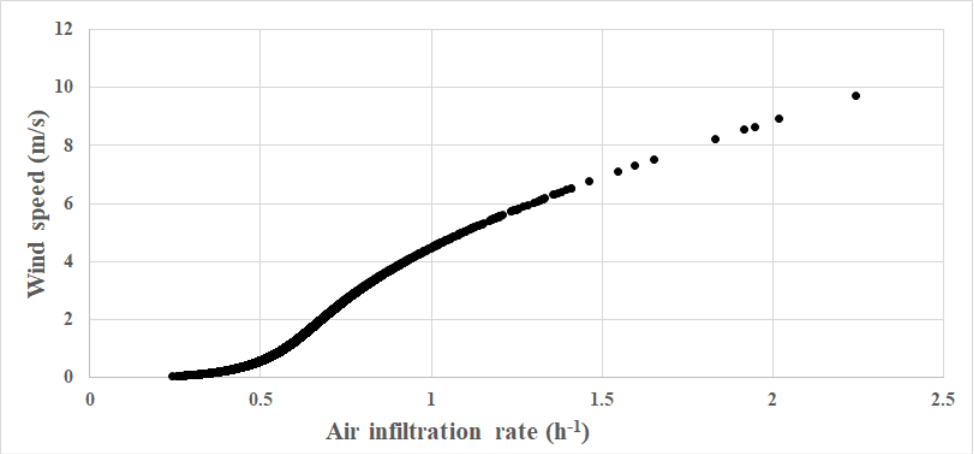


Figure 7.49: Predicted air infiltration rates (using LBL50 model Assumption 3) against wind speed with Volume and Envelope Area as true constants.

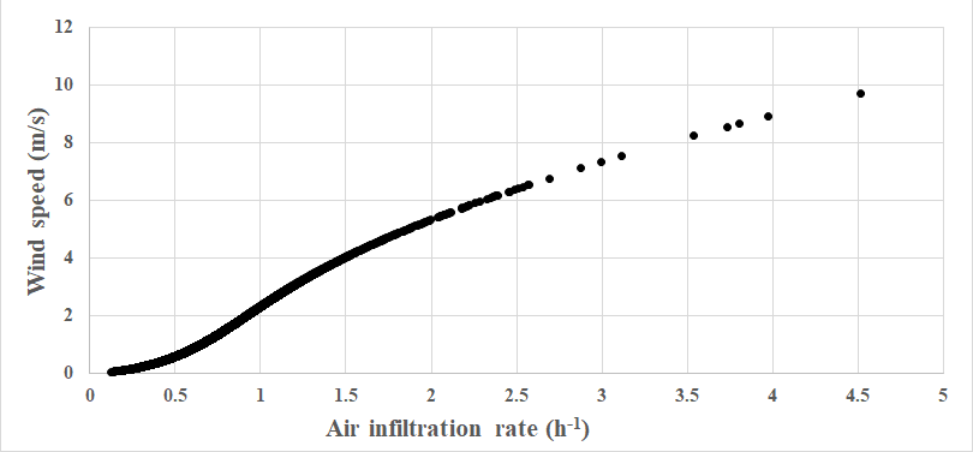


Figure 7.50: Predicted air infiltration rates (using LBL4 model Assumption 3) against wind speed with Volume and Envelope Area as true constants.

Figures 7.51 and 7.52 show the scatter plots of air infiltration against temperature difference for assumption 1 of the LBL50 and LBL4 models respectively. For assumption 3 of the LBL50 model Figure 7.53 shows the same interaction. Additionaly, for the LBL4 assumption 3 model the interaction between n_1 and ΔT is given in Figure 7.52.

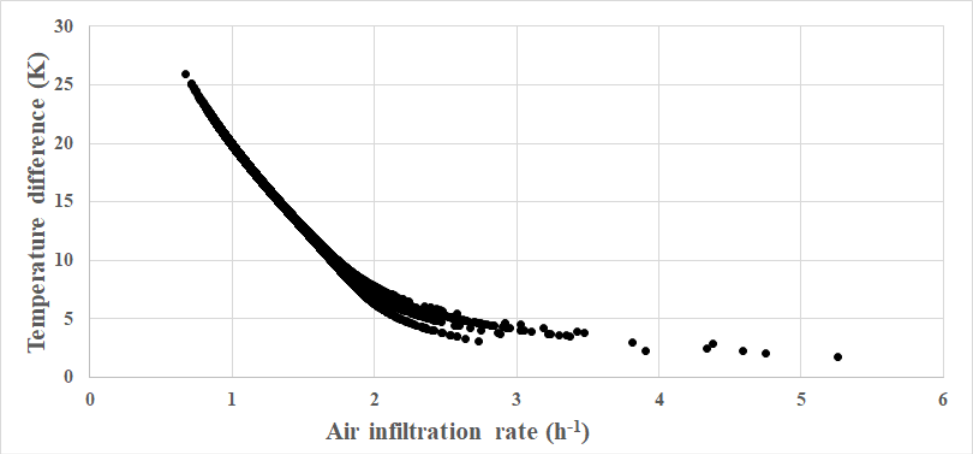


Figure 7.51: Predicted air infiltration rates (using LBL50 model Assumption 1) against temperature difference with Volume and Envelope Area as true constants.

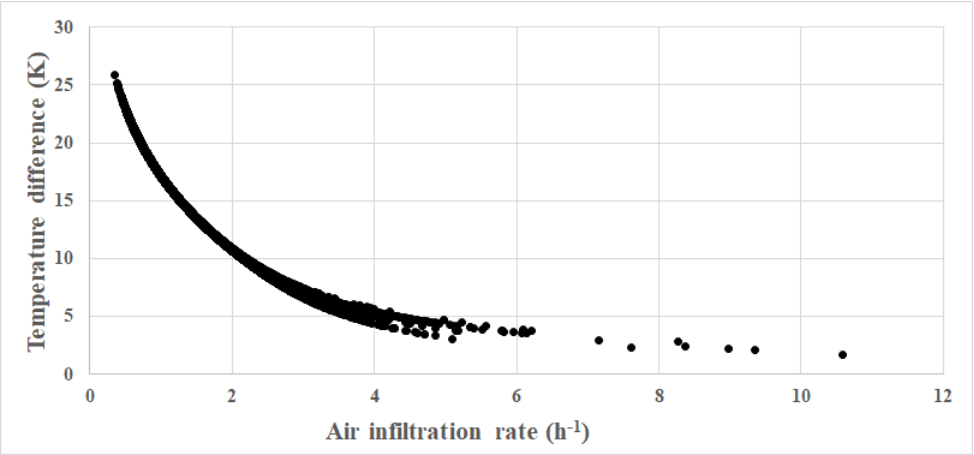


Figure 7.52: Predicted air infiltration rates (using LBL4 model Assumption 1) against temperature difference with Volume and Envelope Area as true constants.

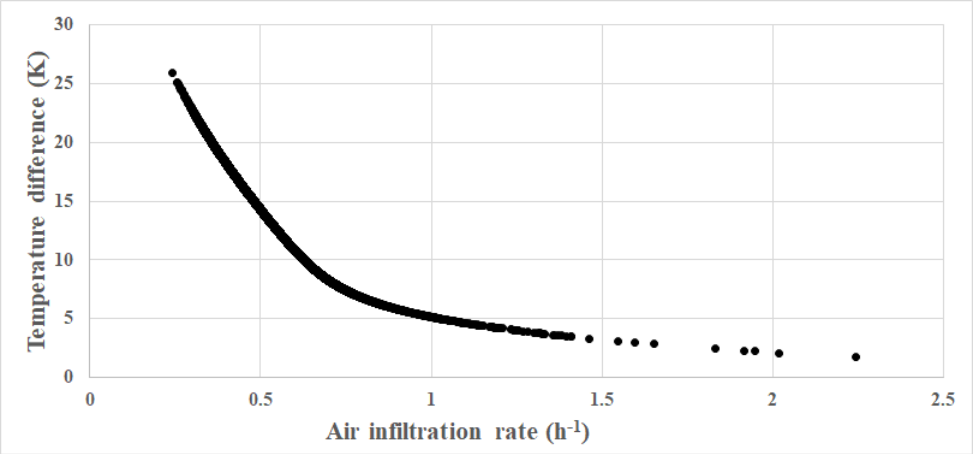


Figure 7.53: Predicted air infiltration rates (using LBL50 model Assumption 3) against temperature difference with Volume and Envelope Area as true constants.

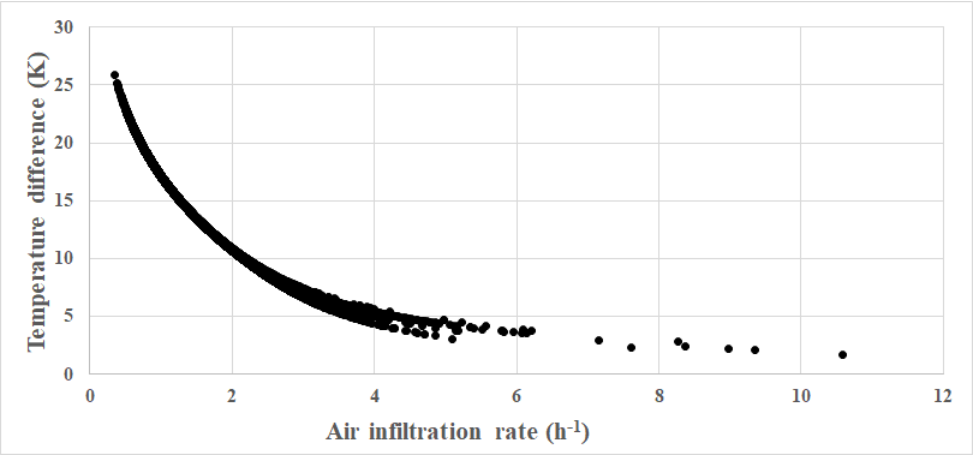


Figure 7.54: Predicted air infiltration rates (using LBL4 model Assumption 3) against temperature difference with Volume and Envelope Area as true constants.

7.5.4.2 Infiltration-air leakage rate (n_{50} and n_4) and flow exponent (b)

The scatter plots between air infiltration (X) and air leakage rate when volume and envelope are taken as constants are given in: Figure 7.55 for LBL50 assumption 1, Figure 7.56 for LBL50 assumption 3, Figure 7.57 for LBL4 assumption 1, and, Figure 7.58 for LBL4 assumption 3.

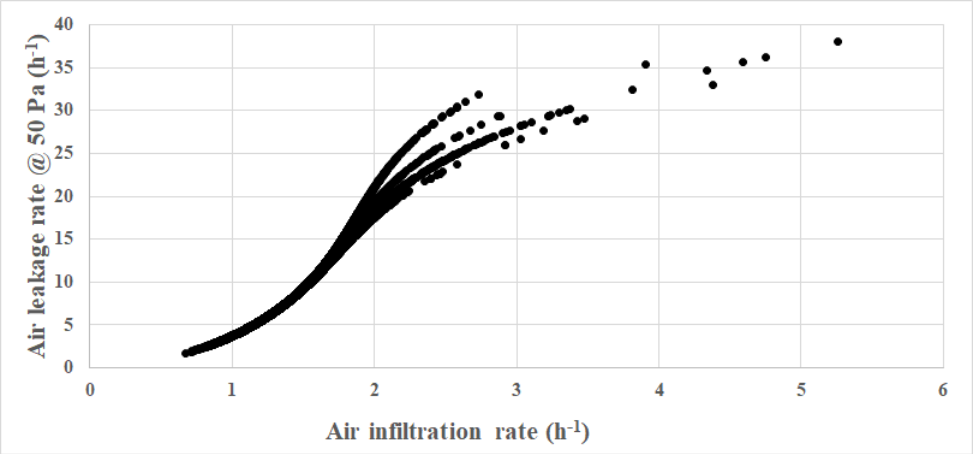


Figure 7.55: Predicted air infiltration rates (using LBL50 model Assumption 1) against air leakage rate with Volume and Envelope Area as true constants.

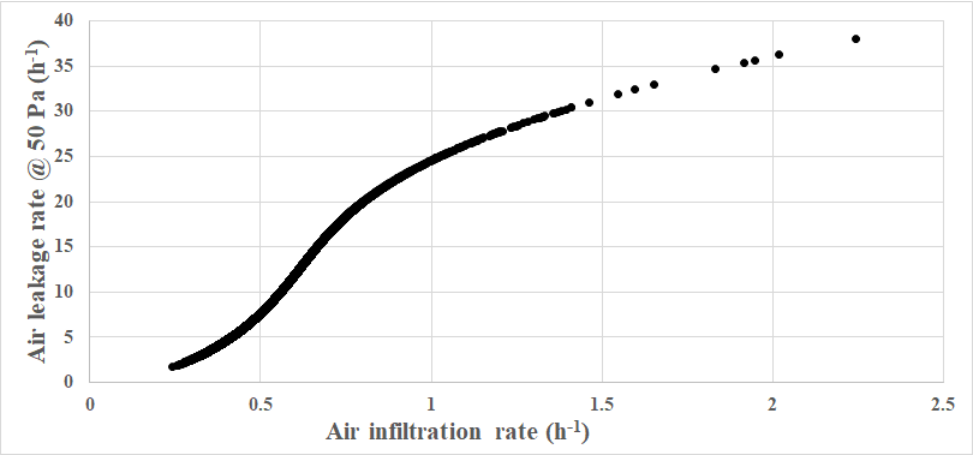


Figure 7.56: Predicted air infiltration rates (using LBL50 model Assumption 3) against air leakage rate with Volume and Envelope Area as true constants.

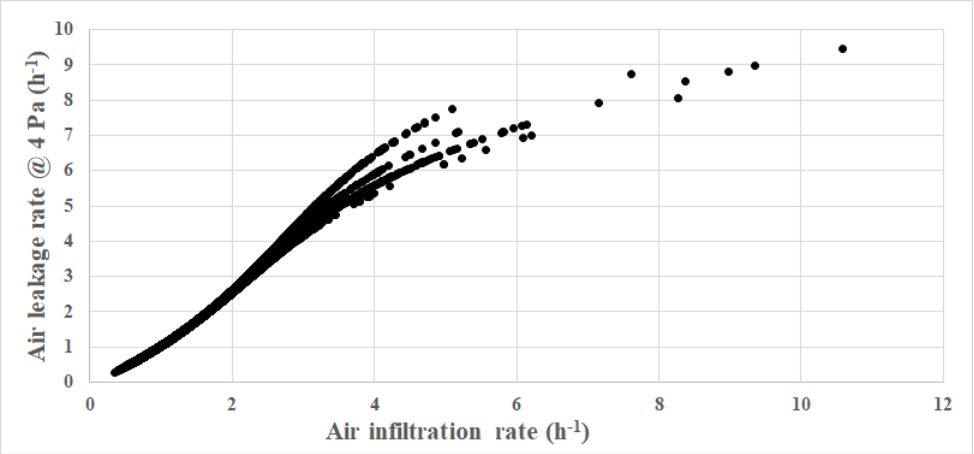


Figure 7.57: Predicted air infiltration rates (using LBL4 model Assumption 1) against air leakage rate with Volume and Envelope Area as true constants.

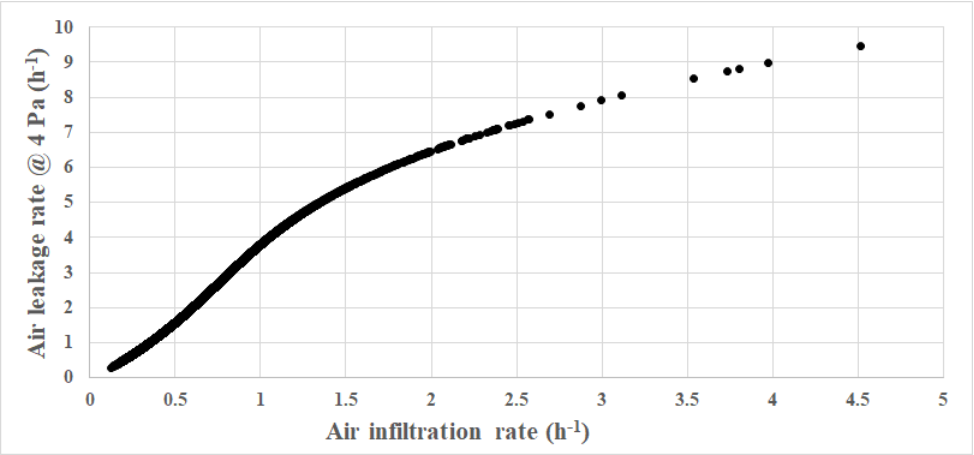


Figure 7.58: Predicted air infiltration rates (using LBL4 model Assumption 3) against air leakage rate with Volume and Envelope Area as true constants.

The scatter plots for air infiltration and flow exponent when volume and envelope area are considered constants are given in Figures 7.59 and 7.60 for assumption 1 of the LBL50 and LBL4 models, respectively. Additionally, Figures 7.61 and 7.62 show the relationship between the mentioned variables for the assumption 3 of the LBL50 and LBL4 models, respectively.

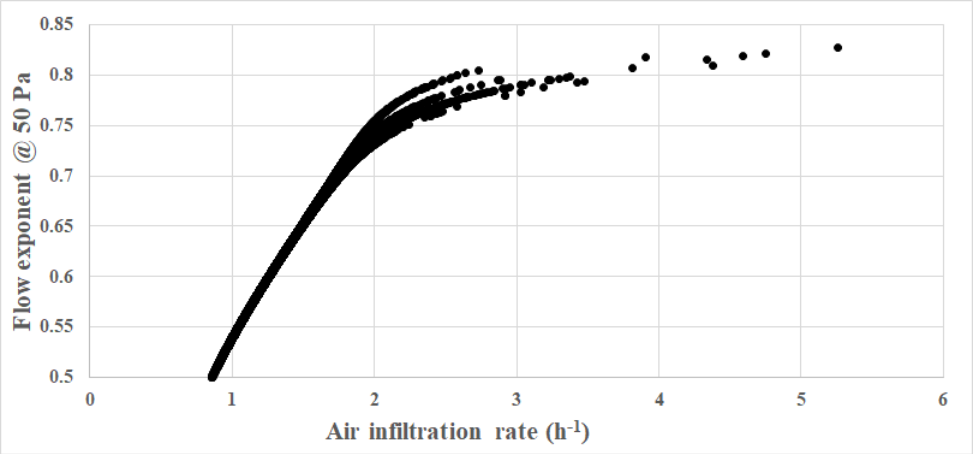


Figure 7.59: Predicted air infiltration rates (using LBL50 model Assumption 1) against flow exponent with Volume and Envelope Area as true constants.

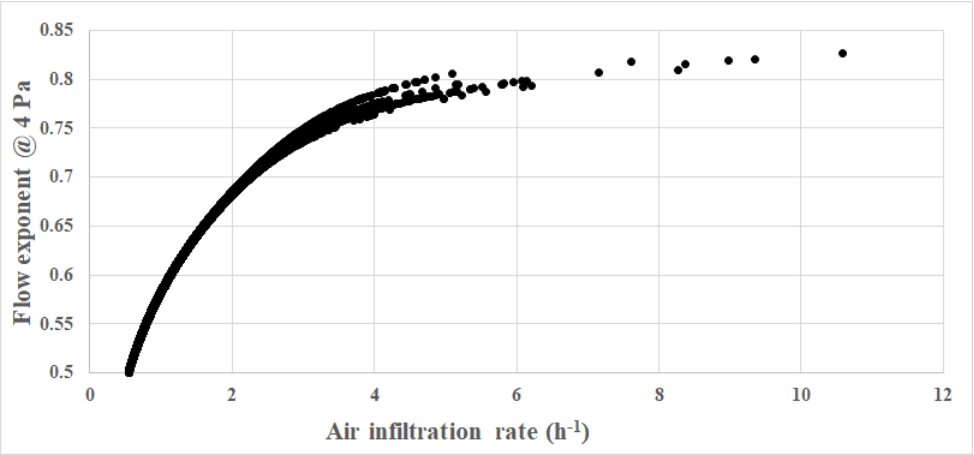


Figure 7.60: Predicted air infiltration rates (using LBL4 model Assumption 1) against flow exponent with Volume and Envelope Area as true constants.

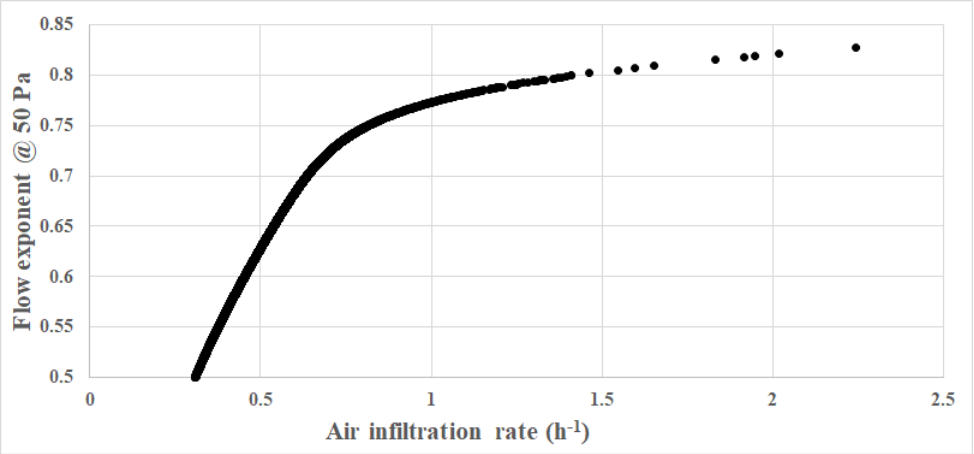


Figure 7.61: Predicted air infiltration rates (using LBL50 model Assumption 3) against flow exponent with Volume and Envelope Area as true constants.

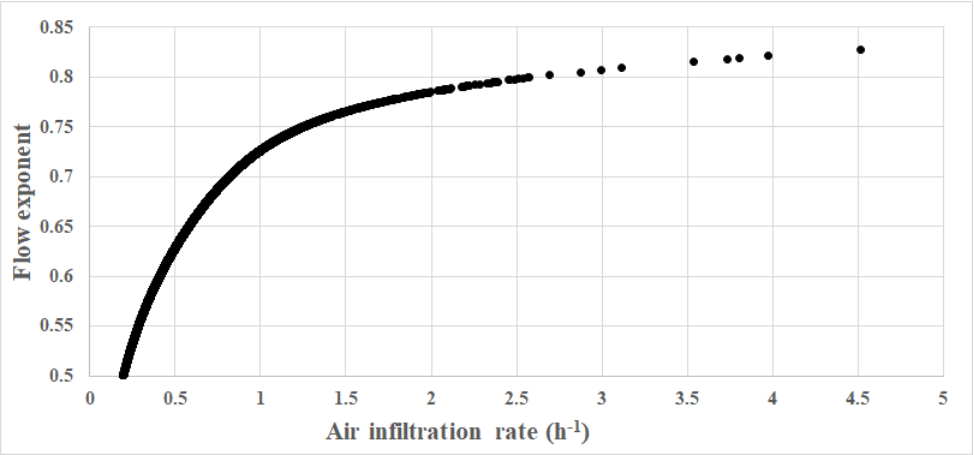


Figure 7.62: Predicted air infiltration rates (using LBL4 model Assumption 3) against flow exponent with Volume and Envelope Area as true constants.

7.5.4.3 Summary of scatter plots

The graphs presented above are almost identical to those ones presented for the models where volume and envelope area were considered as variables. The conclusions drawn before also apply for these models. Infiltration is directly proportional to wind and air leakage rate. The conclusion is that infiltration depends on wind and air leakage rate (quoted aT high or low-pressure difference) regardless of the dwelling parameters. At low infiltration, temperature difference is the main driving force, but at high infiltration other variables induce more uncertainty to the output. Both models showed being sensitive to the air leakage rate measurement.

Finally, in the way the predictions (data points) are spread in the graphs, considering the dwelling parameters as constants does not change the interaction of each of the other variables with infiltration. However, there might be a higher importance given to one variable compared to others. As mentioned, when eliminating the contribution of the uncertainty of the dwelling parameters to the output, other variables are adding to the overall uncertainty. It is pertinent to carry out a new sensitivity analysis for each of the models with volume and envelope area taken as constants.

7.5.5 Regression and ranking of variables taking volume and envelope area as constants

As a start, the new sum of squares (SS) and coefficient of multiple determination for the LBL50 and LBL4 models assumption 1 (with volume and envelope area taken as constants) are given in Table 7.16.

Table 7.16: Sum of squares (SS) and coefficient of multiple determination (R^2) for sensitivity analysis of LBL50 and LBL4 infiltration models (assumption 1) for $1x10^5$ samples when the Volume and Envelope area are considered as constants.

SS	**LBL50**	**LBL4**
Regression	4538.2	22761
Residual	70.635	381.393
Total	4608.835	23142.393
R^2	0.985	0.984

Both R^2 values are close to one, therefore once again, represent the predicted data. The regression models against the predicted infiltration values for the LBL50 and LBL4 models (when volume and envelope area do not introduce uncertainty) are given in Figures 7.63 and 7.64, respectively.

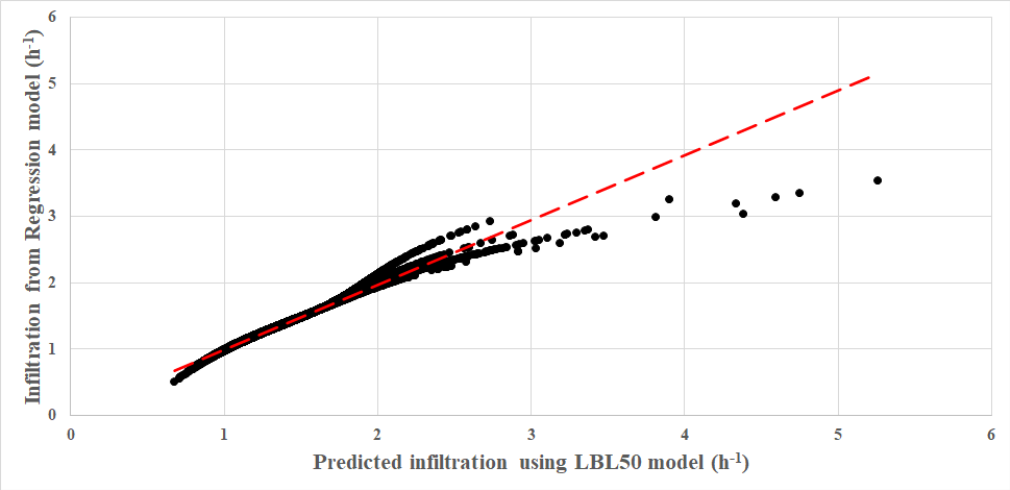


Figure 7.63: Predicted and regression values of infiltration rate for LBL50 Assumption 1 sensitivity analysis with Volume and Envelope Area as true constants, $R^2 = 0985$.

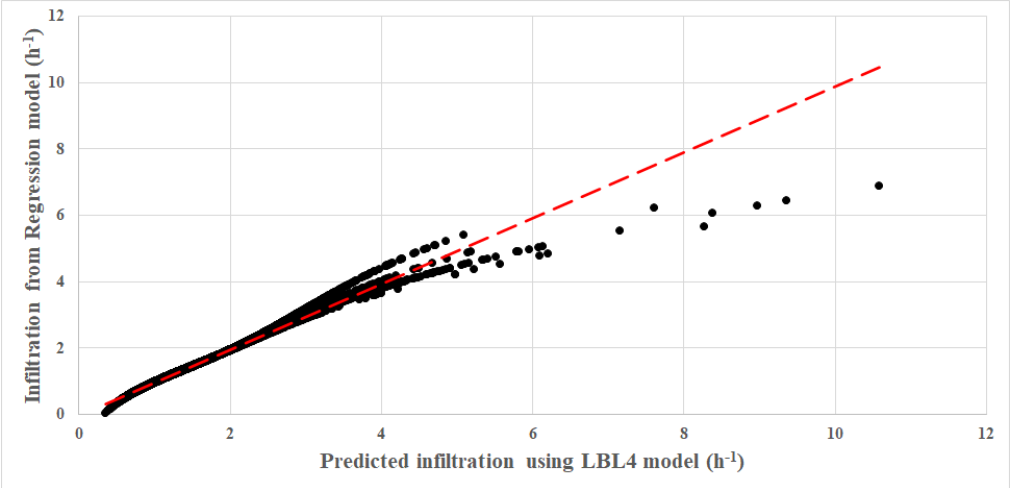


Figure 7.64: Predicted and regression values of infiltration rate for LBL4 Assumption 1 sensitivity analysis with Volume and Envelope Area as true constants, $R^2 = 0984$.

The best fit regression models have a large R^2 value, over 98% for both cases, therefore it can be said once again, that the regression models represent the predicted data. It has been seen from all the regression models analysed that the simplified nature of the LBL models, makes them easy to reproduce using empirical or simulation data; that is why the regression models have large coefficients of multiple determination.

As before, the new b_n coefficients, SRC's and CC's with their ranks, in the

new regression models predictions, are given in Tables 7.17 for LBL50 and LBL4's predictions.

Table 7.17: Model coefficients (b_n), Standardised Regression Coefficients (SRC) and, Correlation Coefficients (CC) for the model created in the Sensitivity analysis for LBL50 and LBL4 models assumption 1 when Volume and Envelope are taken as constants.

Variable	**Regression coefficient**(b_n)	**SRC**		**CC**	
		Value	**Rank**	**Value**	**Rank**
LBL50 Assumption 1					
Air leakage rate (n_{50})	-0.078	-1.076	1	$1.102x10^{-05}$	4
Temperature difference	-0.0702	-0.900	2	$-1.164x10^{-5}$	2
Wind speed	0.362	0.714	3	$9.383x10^{-06}$	5
Flow exponent (b_{50})	1.764	0.359	4	$1.164x10^{-05}$	2
Shielding	-0.005	-0.038	5	$-2.089x10^{-05}$	1
LBL4 Assumption 1					
Wind speed	0.627	0.587	1	$8.989x10^{-06}$	5
Flow exponent (b_4)	4.615	0.445	2	$1.116x10^{-05}$	2
Air leakage rate (n_4)	-0.190	-0.288	3	$1.037x10^{-05}$	4
Temperature difference	-0.031	-0.190	4	$-1.116x10^{-05}$	2
Shielding	-0.006	-0.024	5	$-2.002x10^{-05}$	1

A similar analysis was done when using assumption 3 of the LBL models. The sum of squares and coefficient of multiple determination are given in Table 7.18. It can be seen that the R^2 values are above 98% in both cases; this means that the regression models used for the sensitivity analysis represents the predicted data.

Table 7.18: Sum of squares (SS) and coefficient of multiple determination (R^2) for sensitivity analysis of LBL50 and LBL4 infiltration models (assumption 3) for $1x10^5$ samples when the Volume and Envelope area are considered as constants.

SS	**LBL50**	**LBL4**
Regression	741.210	3474.600
Residual	13.738	40.288
Total	754.947	3514.888
R^2	0.982	0.989

Figure 7.65 and 7.66 show the original predicted infiltration rates using the LBL50 and LBL4 models assumption 3 (X axis) against the infiltration rates predicted using the newly developed regression models (Y axis).

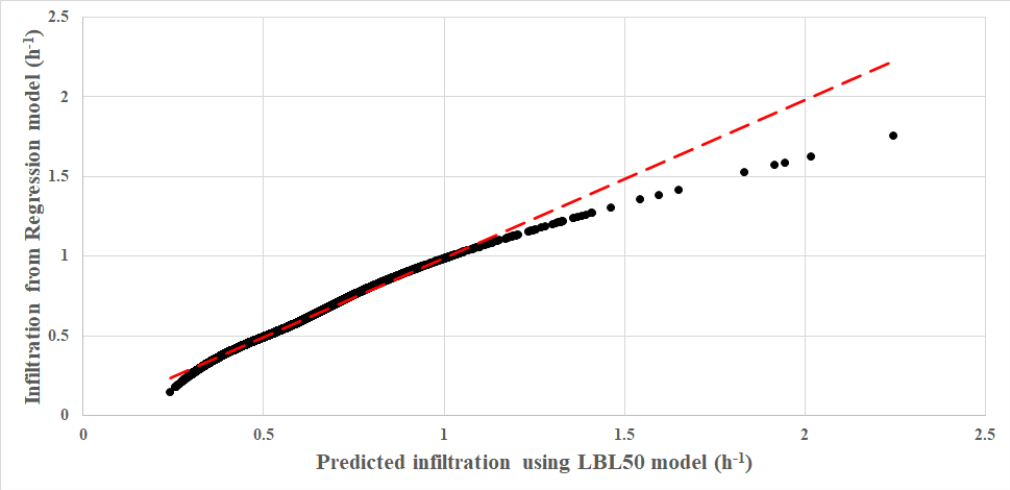


Figure 7.65: Predicted and regression values of infiltration rate for LBL50 Assumption 3 sensitivity analysis with Volume and Envelope Area as true constants, $R^2 = 0982$.

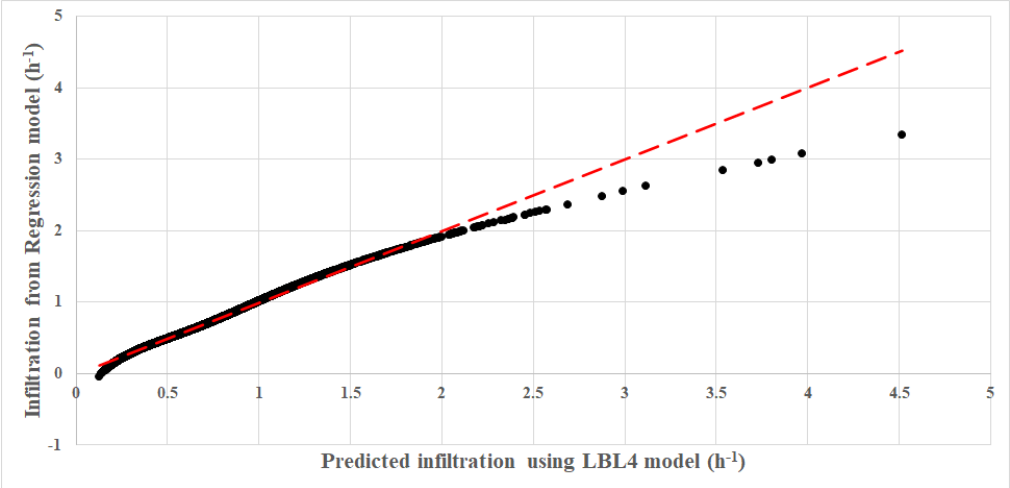


Figure 7.66: Predicted and regression values of infiltration rate for LBL4 Assumption 3 sensitivity analysis with Volume and Envelope Area as true constants, $R^2 = 0989$.

Despite the large coefficient of multiple determination, it can be seen that the regression models underpredict on the lower and top parts of the infiltration scale; however, most of the predictions do not lie within these sections of the graphs, hence a good correlation.

The coefficients b_n of the regression models for each variable, the standardised regression coefficients SRC and, the correlation coefficients of the sensitivity analyses for the LBL50 and LBL4 assumption 3 models are given in 7.19.

Table 7.19: Model coefficients (b_n), Standardised Regression Coefficients (SRC) and, Correlation Coefficients (CC) for the model created in the Sensitivity analysis for LBL50 and LBL4 models assumption 3 when Volume and Envelope are taken as constants.

Variable	Regression coefficient(b_n)	SRC		CC	
		Value	Rank	Value	Rank
LBL50 Assumption 3					
Air leakage rate (n_{50})	-0.057	-2.228	1	$9.730x10^{-06}$	2
Temperature difference	-0.047	-1.706	2	$-1.028x10^{-5}$	1
Wind speed	0.263	1.488	3	$8.281x10^{-06}$	3
Flow exponent (b_{50})	-0.008	-0.004	4	$1.028x10^{-05}$	1
LBL4 Assumption 3					
Air leakage rate (n_4)	-0.316	-1.355	1	$9.465x10^{-06}$	2
Wind speed	0.509	1.350	2	$8.207x10^{-06}$	3
Flow exponent (b_4)	2.813	0.769	3	$1.019x10^{-05}$	1
Temperature difference	-0.0120	-0.206	4	$-1.019x10^{-05}$	1

The results from assumption 1 (Table 7.17) showed that the LBL50 model is more sensitive to the air leakage rate (n_{50}) and then to the environmental conditions. The model showed to be more sensitive to temperature difference than wind. On the other hand, the LBL4 model is more sensitive to wind speed, this because this force acts mainly at a pressure closer to 4 Pa (than 50 Pa), and it is difficult to shadow. What was not expected is to have the flow exponent ranked second in the analysis, the air leakage rate ranked third.

Different from the analysis when the volume and envelope area were considered, for both models using assumption 3, the air leakage rate (quoted @50 and @4 Pa depending on the model) ranks first place. For the LBL50 model, the temperature difference supplies more uncertainty than the wind speed, which rank in 2nd and 3rd place, respectively; finally the flow exponent is the less influential variables of the LBL50 model. On the other hand, the LBL4 model is more sensitive to wind speed (2nd place) than to the flow exponent (3rd place) and temperature difference (4th place).

The fact that wind and temperature difference's effects are added in quadrature in the LBL models, makes the environmental conditions model dependent (depend on the data fed to the model). However, it has been seen from the scatter plots, that the model is more sensitive to temperature difference when there is no wind, low infiltration and the ΔT is high.

If the SRC's are analysed, it can be seen that the absolute value of the SRC for n_4 and wind speed in the LBL4 model sensitivity analysis are close to each other

(1.355 and 1.350) meaning that the LBL4 model is similarly sensitive to both. It can be therefore said for the LBL4 model that it is important to have accurate wind speed as well as air leakage measurements.

7.5.6 Sensitivity analysis: major findings

The sensitivity analysis of the LBL models, delivered two main results, first, both models had similar results, and they can be compared against one another, there is not a substantial difference between the LBL50 and LBL4 model regardless of the assumption used; taking the LBL50 model as benchmark, the results from the LBL4 model are comparable. Second, it was seen that the dwelling parameters (volume and envelope area) introduce most of the uncertainty in the LBL models; this is mainly because initial values such as dwelling dimensions and effective leakage area are calculated using the dwelling parameters, and their uncertainty is carried through the algorithm.

Regarding the effect of each variable, the importance of having accurate air-tightness measurements was demonstrated: air leakage rate appeared in both scenarios in the first places of the ranking of variables, mainly when removing the dwelling parameters of the analysis. The shielding condition (assumption 1) showed that it is relevant when there is high infiltration. Each shielding condition drives a different path of infiltration; however, for low or normal infiltration the difference between conditions is not substantial or is shadowed by the effect of other variables, but is relevant at high infiltration. Shielding ranked last in the sensitivity analyses, this is because high infiltration represents less than 2% of the samples.

For all models analysed the correlation coefficients (CC) were low and therefore all variables should be analysed together.

The main drawback of this analysis is that it was based on the assumptions made to describe the distributions of the variables. If the analysis is carried out for different assumptions, and with different distributions, a different result might be obtained. The objective of this study was not to test the uncertainty of the LBL model, but to compare the LBL4 and LBL50 models' capacity of predicting infiltration rates. The sensitivity analysis confirmed that both models have similar advantages and shortcomings.

7.6 Conclusions

This chapter used information from twenty dwellings as inputs to run the LBL model. The standard LBL model was used with high pressure airtightness measurements taken as inputs (LBL50) and additionally, the model was modified to use the data coming from low pressure airtightness measurements (LBL4).

Three different assumptions were defined to run the LBL models, each one depending on the leakage distribution from ceiling and floor. It was seen that assumptions 1 and 2 (no leakage form floor and ceiling and, equally distributed leakage), had the lowest errors, however, they also had the largest deviations; this means that the variance of the results was large. On the other hand, assumption 3 (fixed wind and stack factors) had a larger mean error, but lower variance.

It is key to know which assumption is going to be used when running the LBL models, each one will give a different result. Comparing both LBL50 and LBL4, it can be concluded that both have similar uncertainty using assumption 1($13\pm14\%$ and $17\pm14\%$, respectively), and assumption 3 ($-51\pm6\%$ and $-49\pm6\%$, respectively). The error is considerable, mainly for assumption 3, nevertheless, the mean error calculated using the infiltration ratios as seen in Chapter 6 was 95%; therefore, using a simplified model has been shown to be more accurate than using a leakage - infiltration ratio. In addition, the accuracy can be improved by selecting the right assumption or accounting for the leakage distribution.

The error is increased if the absolute value of the RPD is added to the calculations; this means that the overall error of the sample does not account for the compensation created by under and overpredictions. In this case, assumption one is the most accurate with $42 \pm 11\%$ and $43 \pm 10\%$ from the LBL50 and LBL4 models respectively.

When analysing the effect of variables upon the predicted infiltration, 100,000 samples were created of assumptions one and three, and tested to predict 100,000 infiltration rates. It was found that for both the LBL50 and LBL4 models, the variables have similar performance. By analysing scatter plots it was found that regardless of which model or assumptions were used, variables interact similarly. The infiltration rate is proportional to wind and air leakage rate. It was found that the temperature differences are the main driving force of infiltration at low-infiltration with low wind and low air leakage rate. Furthermore, shielding is relevant at high infiltration scenarios. Having a greater diversity of properties in terms of their variables would help define more representative distributions, and therefore, more representative samples of the housing stock, hence an analysis of

greater accuracy could be performed.

A sensitivity analysis was made, and a regression model was used to fit the predicted data for each model in assumptions 1 and 3. In both models, results showed that the variables interact similarly. The volume and envelope area were found to create most of the uncertainty in the infiltration rate. When these variables were taken out of the calculation, and taken as constants, for assumption 1 the rank of variables of the LBL4 model showed that the model is more sensitive to wind than air leakage rate. In other words, measuring the airtightness parameters induces less uncertainty to the prediction than the occurring wind speed. The LBL50 model was shown to be more sensitive to the air leakage rate than any other variable. For the simplified assumption 3, the results were as expected; the air leakage rate (both n_{50} and n_4) showed to be the most important variables affecting the uncertainty of the model. However, for both models, the results were similar; therefore, the LBL model can be implemented using airtightness measurements at 50 or 4 Pa pressure difference.

There are several ways at which this analysis can be improved, one suggestion is to measure multiple times the infiltration rate and environmental conditions in the same building, and to use the models to predict infiltration rates, and finally, to compare both measurements. Therefore airtightness parameters, volume and envelope area, would have been constants of the models. Unfortunately the resources and time allowed in the properties did not allow for that to happen in this study.

A larger number of data points would also have helped to simulate a more accurate sample, and define better the distributions used in the Monte Carlo analysis. These recommendations are valid when using any infiltration model, which uses more than one variable as input.

Finally, the main conclusion from this chapter is that the LBL model, can be used within the Pulse technique to predict infiltration rates, without compromising the accuracy. In fact it can be more accurate, it showed a lower average error when assumption 3 was used, and the airtightness parameters contribute less to the uncertainty (depending on the assumption used). Given the above, the infiltration rates predicted using the LBL4 model, can be as statistically accurate or more accurate than the predictions obtained using the LBL50 model.

It is important to highlight that the LBL model is a simplified model and the assumptions enable a simple calculation at the cost of reduced accuracy. More complex models should be more accurate when predicting infiltration. In the following chapter a similar investigation is performed using a different infiltration

model, DOMVENT3D.

Chapter 8

Modifying an infiltration model to predict based on low pressure airtightness measurements

Part of the work covered in this chapter was previously presented as a short presentation at the Air Infiltration and Ventilation Centre conference 2019 in:

A. Vega Pasos, X. Zheng, B. Jones, M. Gillott, and C. Wood. On the experimental validation of the infiltration model domvent3d. In *40th AIVC Conference Proceedings*, Ghent, Belgium, 2019c

8.1 Introduction

In earlier chapters, ratios and simplified models have been tested. It was shown that the absolute error when predicting infiltration is large, but the accuracy is better when using simplified models. Regarding the airtightness measurement techniques, low pressure measurements have been proved comparable with high pressure ones. Similar accuracy and uncertainty has been found.

However, in addition to ratios and simplified models, there are also other infiltration models. DOMVENT3D has been introduced as a single zone infiltration predicting model. This chapter will evaluate the performance of DOMVENT3D when predicting infiltration rates from high and low pressure airtightness measurements. In addition, DOMVENT3D has not yet been field-validated, however, it has been proven to predict infiltration for a whole-stock scenario [Jones et al., 2015], with good results.

The work within this study using DOMVENT3D is bases upon an algorithm in the form of MATLAB code. The algorithm and the code is based on: Lyberg

[1997], Lowe [2000], Jones et al. [2013b, 2014, 2015], Das et al. [2014]. Dr. Benjamin Jones is acknowledged for providing the code for use in this work.

The advantage of using DOMVENT3D is that it was modelled for the English housing stock, compared to the previous LBL model, which was developed in the USA. In addition, DOMVENT3D considers more variables such, as orientation of the building, exposed façades, shielding coefficients, amongst others.

DOMVENT3D started when Lyberg [1997] showed that superposition techniques (LBL or AIM-2 models) do not represent real flows. Based on Lyberg's study, Lowe [2000] created a two-dimensional model. Lowe [2000] identified four zones in a building: windward and leeward exfiltration, and windward and leeward infiltration. Jones et al. [2013b] created a modified version of the Lowe's model: DOMVENT3D [Jones et al., 2013a]. This new version (three-dimensional) addressed the problems created by the two-dimensional nature of DOMVENT2D. In DOMVENT3D, every façade's airflow is taken into account. DOMVENT3D's algorithm was given in Chapter 2.

8.2 Chapter method

The method followed in this chapter is similar to that used in Chapter 7. DOMVENT3D was re-coded using MATLAB, and calibrated to run with low pressure airtightness measurements. The relative leakage area is the parameter to modify when calibrating the model.

$$E = \frac{q_P E_a \rho}{3600 E_a a_P P^{b_P}} \tag{8.1}$$

Where E is the relative leakage area (m^2),q is the measured air permeability ($m^3 h^{-1} m^{-2}$), ρ is the mean (exterior-interior) air density ($\frac{kg}{m^3}$), E_a is the envelope area (m^2), b is the flow exponent and a_P is given by:

$$a_P = \rho(\frac{2}{\rho})^{b_P} \tag{8.2}$$

For the previous equations P refers to the reference pressure: 50 for the steady pressurisation method and 4 for the Pulse method.

The model that uses high pressure (or blower door) airtightness measurements, will be named DOMVENT3D-50, which is the current version of the model. Additionally, the model will be named DOMVENT3D-4 when using the Pulse method airtightness measurements (low pressure) as input. Equations 8.1 and 8.2 are the basis for the DOMVENT3D models. Using P as 50 Pa and the measurements taken

by the pressurisation method will lead to the DOMVENT3D-50 model and taking P as 4 Pa will lead to DOMVENT3D-4. In both cases the equations are part of the algorithm introduced in Chapter 2 The predictions given by both models will be compared with real measurements. The dwellings survey, and, measurements taken in chapter 5 were used as DOMVENT3D's inputs.

The standard error and relative percentage difference (RPD) are calculated and comparisons from measurements and predictions are used as DOMVENT3D field validation. Furthermore, DOMVENTD3D-50 and DOMVENT3D-4 are compared and their accuracy will be assessed.

Finally, as in the previous chapter, a sensitivity analysis is carried out. DOMVENT3D models have more variables than the LBL model presented in chapter 7; therefore, the analysis includes a greater number of variables. Different from the previous chapter, DOMVENT3D does not need to make extra assumptions, therefore only two scenarios will be tested: DOMVENT3D-50 and DOMVENT3D-4. Figure 8.1 presents the contents of the present chapter and can be used as a guideline to follow the analysis made.

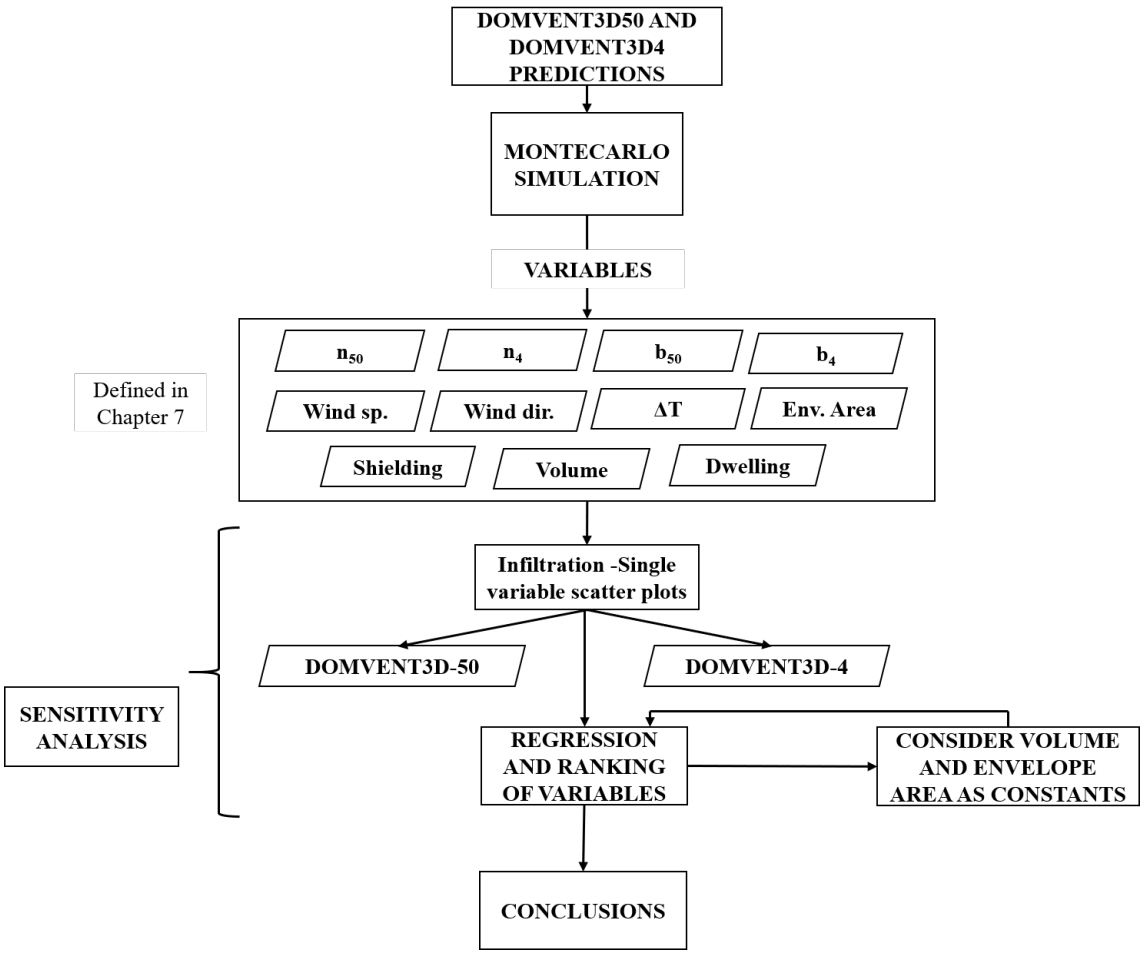


Figure 8.1: Diagram of the evaluation of the DOMVENT3D model during the present Chapter.

This Chapter will evaluate the predictions given by the DOMVENT3D models followed by a simulation of 100,000 cases using the distributions of variables given in Chapter 7. Furthermore, an analysis of scatter plots using the infiltration rate and the different variables is given and the ranking of importance of variables is assessed. The previous analysis is also given when the envelope Area and the volume are taken as constants. Finally, conclusions are given.

8.3 Predicting infiltration rates with DOMVENT3D

The DOMVENT3D models (DOMVENT3D-50 and DOMVENT3D-4) were re-coded in MATLAB. In order to obtain the DOMVENT3D-4 model, the original model was calibrated for use with low-pressure airtightness measurements. The code was designed to open a spreadsheet with the data obtained in the field data collection period, which has been described in Chapters 5 and 7. The code for

both models can be found in Appendix G.

The code was run to predict the infiltration rates for all twenty properties; DOMVENT3D-50 and DOMVENT3D-4's infiltration (h^{-1}) predictions are given in Table 8.1.

Table 8.1: Air infiltration rate (h^{-1}) predictions from the DOMVENT3D model, from high and low pressure difference airtightness measurements.

	Air infiltration rate (h^{-1})	
Number	**DOMVENT3D-50**	**DOMVENT3D-4**
1	0.3069	0.2611
2	0.1779	0.1670
3	0.2526	0.2233
4	0.2091	0.1941
5	0.1620	0.1289
6	0.0966	0.0452
7	0.0878	0.1048
8	0.2203	0.2346
9	0.1036	0.1219
10	0.1522	0.1302
11	0.1563	0.1180
12	0.1768	0.1536
13	0.5150	0.4341
14	0.0617	0.0623
15	0.1757	0.1805
16	0.4405	0.3100
17	0.2297	0.2789
18	0.0755	0.0851
19	0.6444	0.4551
20	0.2133	0.3704

As can be seen, for DOMVENT3D-50, the predictions range from 0.0617 to 0.644 h^{-1}, and for DOMVENT3D-4 from 0.0452 to 0.4551 h^{-1}. In most cases, the results are similar between models. However, in some cases the results differ, e.g. dwelling number 6 has a predicted infiltration of 0.0966 h^{-1} in the DOMVENT3D-50 model, and, 0.0452 in the DOMVENT3D-4 model, which is half of the first value. Predictions from dwellings 6, 11, 16, 19 and 20 vary more than 30% between models. This means, that there are differences between models caused by using n_4

and b_4 as input rather than n_{50} and b_{50}. Nevertheless, 15 properties have similar predictions from model to model, this is an indicator that both models are comparable. Therefore, despite the airtightness measurement technique, it is possible to obtain a reliable prediction, assuming an accuracy of the DOMVENT3D model. It is important to remark that the remaining (besides airtightness values) inputs are the same for both models.

Standard errors between measured and predicted vales for both DOMVENT3D models are given in Table 8.2. Furthermore, the relative percentage difference (RPD) between infiltration measured by tracer gas means and predictions are also included. The first RPD represents the absolute value of the RPD, and the second removing the absolute value to account for the overestimation or underestimation between predictions. Finally, at the bottom of the table, the statistical figures obtained from all the properties are also presented.

Table 8.2: Standard error and relative percentage difference between assumptions for the DOMVENT3D models

	DOMVENT3D-50				DOMVENT3D-4			
	SE	**SE%**	**|R.P.D.|**	**R.P.D.**	**SE**	**SE%**	**|R.P.D.|**	**R.P.D.**
1	0.0560	18%	107%	107%	0.0398	15%	76%	76%
2	0.0111	6%	15%	-15%	0.0150	9%	20%	-20%
3	0.0158	6%	21%	21%	0.0054	2%	7%	7%
4	0.0301	14%	68%	68%	0.0248	13%	56%	56%
5	0.0294	18%	106%	106%	0.0177	14%	64%	64%
6	0.0780	81%	70%	-70%	0.0961	213%	86%	-86%
7	0.0931	106%	75%	-75%	0.0871	83%	70%	-70%
8	0.0197	9%	34%	34%	0.0248	11%	43%	43%
9	0.0169	16%	32%	-32%	0.0104	9%	19%	-19%
10	0.0290	19%	35%	-35%	0.0368	28%	44%	-44%
11	0.0255	16%	32%	-32%	0.0390	33%	48%	-48%
12	0.0271	15%	30%	-30%	0.0353	23%	39%	-39%
13	0.0339	7%	23%	23%	0.0053	1%	4%	4%
14	0.0082	13%	27%	-27%	0.0080	13%	27%	-27%
15	0.0089	5%	17%	17%	0.0106	6%	20%	20%
16	0.0277	6%	15%	-15%	0.0739	24%	40%	-40%
17	0.0459	20%	130%	130%	0.0633	23%	179%	179%
18	0.1004	33%	79%	-79%	0.0970	114%	76%	-76%
19	0.1243	19%	120%	120%	0.0574	13%	55%	55%
20	0.0219	10%	23%	-23%	0.0336	9%	35%	35%
AVERAGE	0.0401	27%	53%	10%	0.0391	33%	51%	3%
STD DEV	0.0323	35%	37%	64%	0.0295	49%	37%	63%
STD ERROR	0.0072	8%	8%	14%	0.0066	11%	8%	14%
MIN	0.0082	5%	15%	N/A	0.0053	1%	4%	N/A
MAX	0.1243	133%	130%	N/A	0.0970	213%	179%	N/A

For the DOMVENT3D-50 model, the average standard error was 27% ±8%, and the minimum standard error was 5% of the measurement. However, as with the LBL model, the standard error might not be the best metric for only two data points. The RPD might be better for a direct comparison. The average RPD was 53% ±8%; with difference ranging from 15% to 30%. DOMVENT3D-50 underestimated the infiltration for 11 dwellings and overestimated it for 9. If the absolute value is deleted, the average RPD is reduced to 10% ±14% due to the compensations.

For the DOMVENT3D-4 model the average standard error was 33% ±11%, with values ranging from 1% to 213%. The average RPD was 51% ±8%, varying

from 4% to 179%. If the absolute value of the error is used, the average RPD is reduced to 3% ±14%.

These results suggest when large number of data points are used, the underestimation will compensate the overestimation to finally, deliver an accurate average result, with high uncertainty. However, for the DOMVENT-4 model, these are still under 20% maximum error (17%). Nevertheless, when using the absolute value of RPD, the overall error for both models is large.

Comparing both models, they both seem to have similar behaviours, overall they deliver similar results and similar uncertainty. Despite DOMVENT3D-50 having smaller variation of results, the variance is the same for both; furthermore, DOMVENT3D-4 presented the smallest SE and RPD for a single data point from the analysis. Using these results the clear conclusion is that both models are comparable. DOMVENT3D models can be used despite the airtightness measurement technique. Moreover, when analysing large numbers of properties, the models become more accurate due to the underestimation-overestimation compensation, and in this case the DOMVENT3D-4 became more accurate. Both models showed the same uncertainty.

8.4 Montecarlo simulations

Using the same method as in the previous chapter, 100000 samples for each variable were simulated. The technique was, a random sampling approach and the distributions were the ones described in Chapter 7. These samples aided to create a regression model, and finally, carry out a sensitivity analysis with the following variables:

- Wind speed (m/s),
- Wind direction ($^\circ$),
- Temperature difference (ΔT, K),
- Air leakage rate (n_{50} or n_4, h^{-1}),
- Flow exponent (b_{50} or b_4),
- House volume (m^3),
- Envelope area (m^2),
- Shielding factor, and,

- Dwelling factor.

All the mean values, standard deviations and, distributions are defined and described in section 7.4.1 from Chapter 7.

8.5 Sensitivity analysis

Following the methodology given by Saltelli et al. [2003] and explained in Chapter 7 a sensitivity analysis was performed. The model was programmed in MATLAB to run for 100000 samples of each variable. The code was run twice: considering all variables, and assuming volume and envelope area as constants.

The variables were ranked based on the standard regression coefficients (SRC) obtained from the regression model fitting the data. Nevertheless, the first step was to analyse the scatter graphs comparing one of the independent variables with the dependent variable, or output: air infiltration rate (h^{-1}).

Figure 8.3 shows the cumulative distribution function of the predictions from both DOMVENT3D models. It can be seen that DOMVENT3D-4 follows a curve closer to a normal distribution. The CDF for DOMVENT3D-50 resembles the normal distribution, however it can be seen that there are more predictions between 0.5 h^{-1} and 0.6 h^{-1} than the ones expected if the results followed a perfect normal distribution. These results can be seen in Figure 8.2 where a second peak of results is seen in the mentioned range. The consideration of exfiltration flows in the models cause also this second peak of infiltration. This anomaly was only seen for the DOMVENT3D-50 model and it is also attributed to the simulated results; despite having changed the values of other variables, the simulation for air change rate @50 Pa delivered this second peak in predictions. It can be concluded that the distribution of infiltration results does not follows a perfect normal distribution due to the factors mentioned above.

For DOMVENT3D-50, it can be seen that 85% of the predictions are under 0.6 h^{-1}, whereas for DOMVENT3D-4 85% of the predictions are under 0.7 h^{-1}. This means that DOMVENT3D-4 tends to predict higher infiltration rates than DOMVENT3D-50.

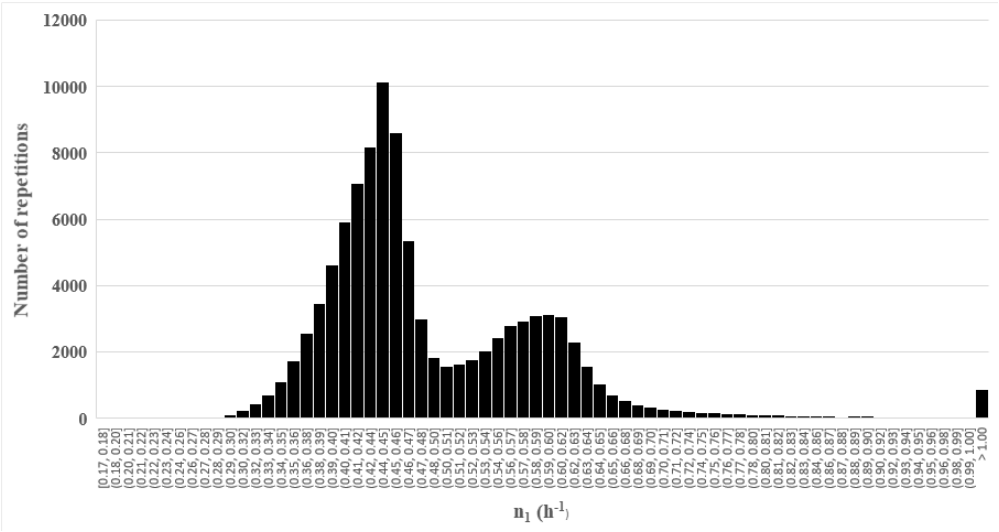


Figure 8.2: Distribution of infiltration predictions (n_1, h^{-1}) in the DOMVENT3D-50 model.

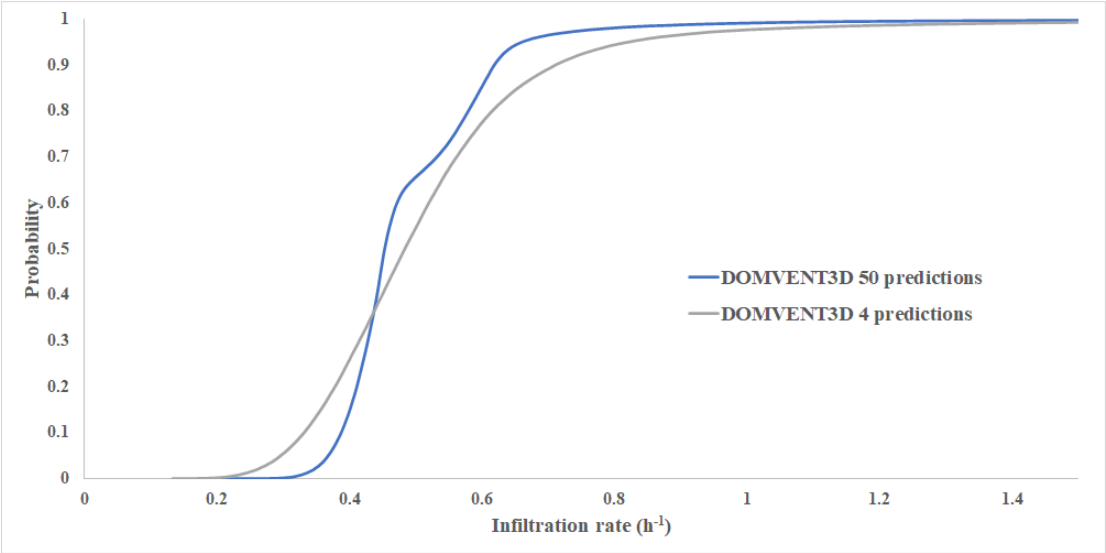


Figure 8.3: Cumulative Distribution Function (CDF) for the predictions of the DOMVENT3D models .

8.5.1 Scatter plots DOMVENT3D-50 and DOMVENT3D-4

8.5.1.1 Infiltration-Environmental conditions (wind and temperature)

Different from the results given in the LBL models, the scatter plots from the DOMVENT3D were more widely spread, and therefore more difficult to approxi-

mate to a line or curve. The relation between infiltration and wind speed in the DOMVENT3D-50 model is shown in Figure 8.4. And, for the DOMVENT3D-4 model is given in Figure 8.5.

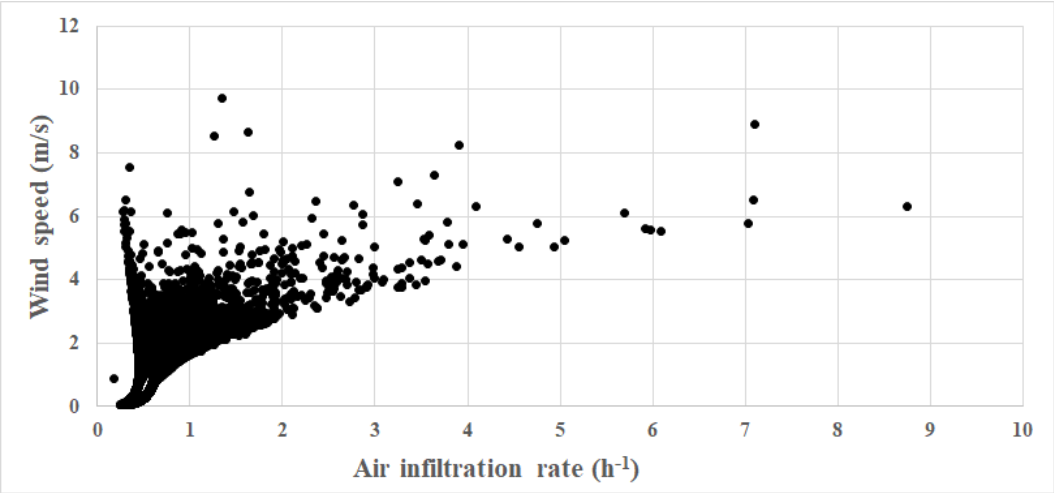


Figure 8.4: Predicted air infiltration rates (using DOMVENT3D-50 model) against wind speed.

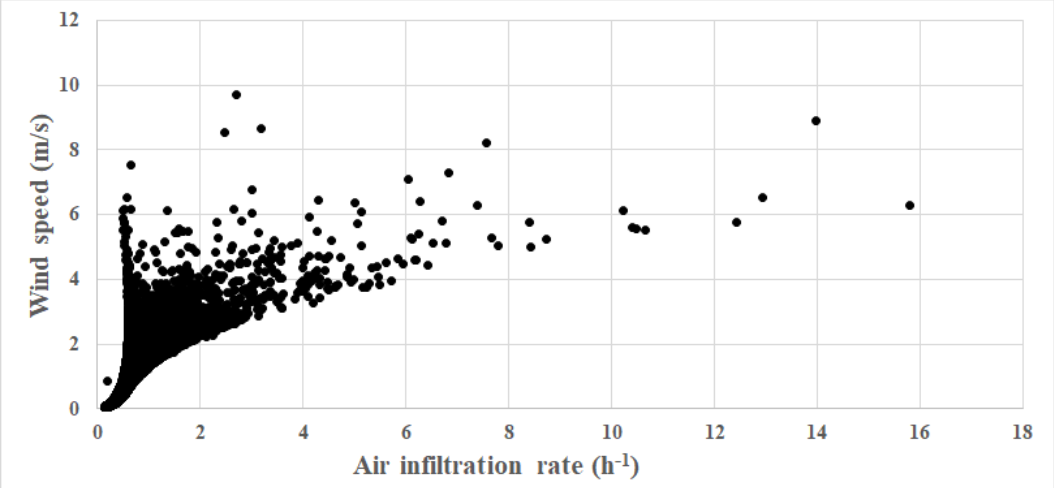


Figure 8.5: Predicted air infiltration rates (using DOMVENT3D-4 model) against wind speed.

Due to the spread of the values it is difficult to give an accurate analysis. It was discussed before that for both models the majority of infiltration predictions are lower than 0.7 h^{-1}; for this range only, there seems to be an overall proportionality between infiltration and wind. Nevertheless, when infiltration is lower than 0.45 h^{-1}, a part of the graph follows a different trend. A similar trend is found in most

scatter plots. This trend can be explained as when exfiltration flows are large. DOMVENT3D takes exfiltration into account and therefore, when exfiltration is large, it creates the effect that at high wind there is less infiltration. However, when wind speed is larger, the infiltration is directly proportional to the wind speed. Similar results are found for both DOMVENT3D models. It is noteworthy that for DOMVENT3D-4, these sections of the graphs where exfiltration is considerable are much more smaller (in number of points) than for DOMVENT3D-50. Only a few points were found to follow a different trend; the majority depicts proportionality between infiltration and wind velocity. The interaction of many variables also creates the effect of the "tails" at when high-pressure measurements are used.

The temperature difference is analysed in Figures 8.6 and 8.7 for DOMVENT3D-50 and DOMVENT3D-4, respectively.

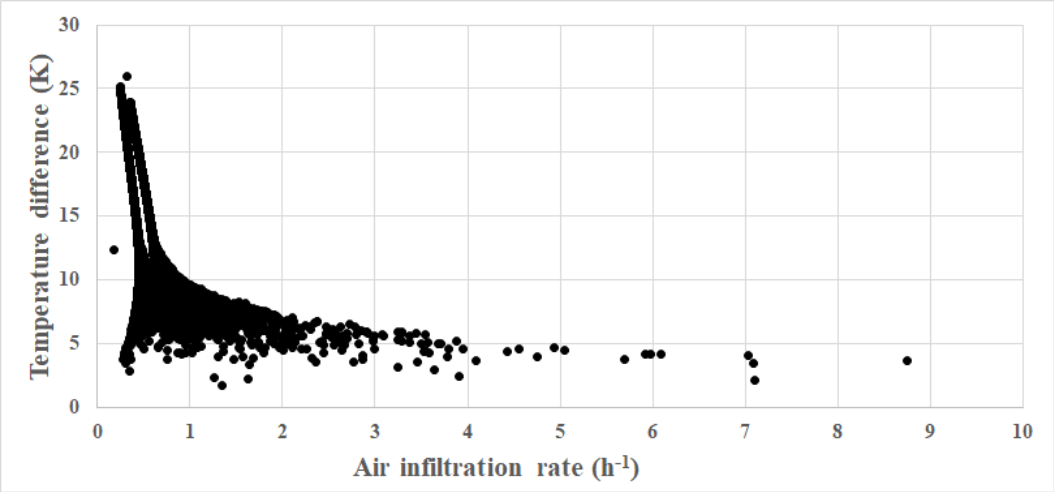


Figure 8.6: Predicted air infiltration rates (using DOMVENT3D-50 model) against temperature difference.

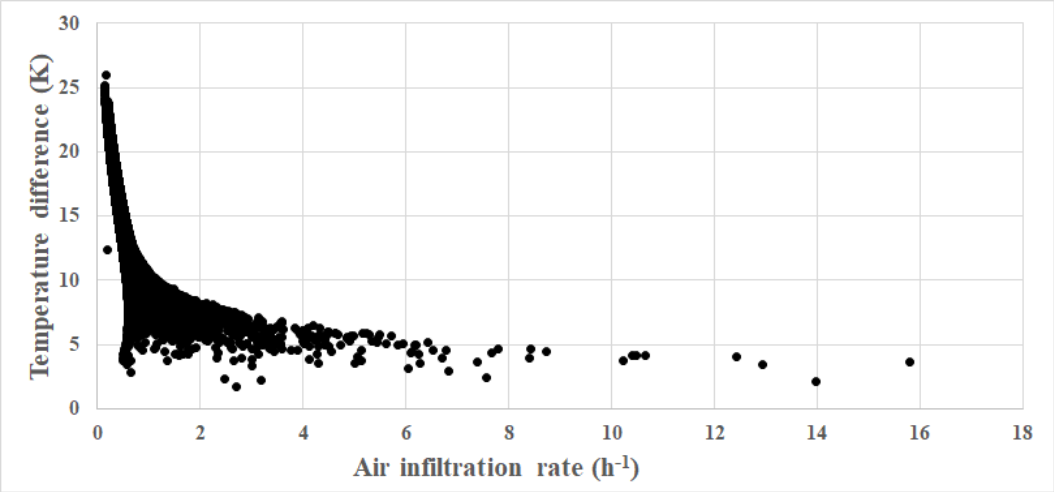


Figure 8.7: Predicted air infiltration rates (using DOMVENT3D-4 model) against temperature difference.

The graphs for temperature difference show a similar effect as the ones for the wind. For the majority of points in the scatter plots, infiltration is proportional to the temperature difference. The only place where it is not is when exfiltration flows are substantial. The majority of infiltration occurs for temperature differences between 5 and 10 K.

When comparing the graphs of infiltration-temperature and infiltration-wind, it is seen that the "tails" of the graph are facing forwards (downwards for wind); therefore, the majority of points are in the opposite direction. This leads to the same conclusion as with the LBL model that the temperature difference is the main driving force at low infiltration and low wind. It is important to mention that it is clear from the scatter plot that there is considerable interaction from the variables; this is seen in the spread of the points. As seen before, the "tails" in the DOMVENT3D-4 plot are smaller, and the graphs resemble those ones presented in the previous chapter for the LBL models.

8.5.1.2 Infiltration-air leakage rate (n_{50} and n_4) and flow exponent (b)

Stepping apart from the environmental conditions and their effect on infiltration, Figures 8.8 and 8.9 show the relationship of air infiltration with the air leakage rate, measured using the high pressure steady pressurisation method (DOMVENT3D-50), and the low-pressure Pulse method (DOMVENT3D-4) respectively.

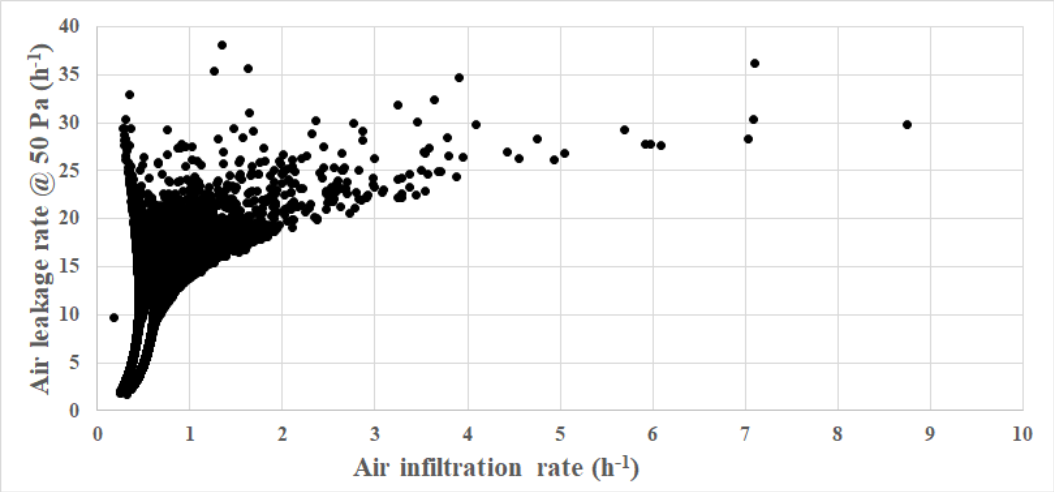


Figure 8.8: Predicted air infiltration rates (using DOMVENT3D-50 model) against air leakage rate.

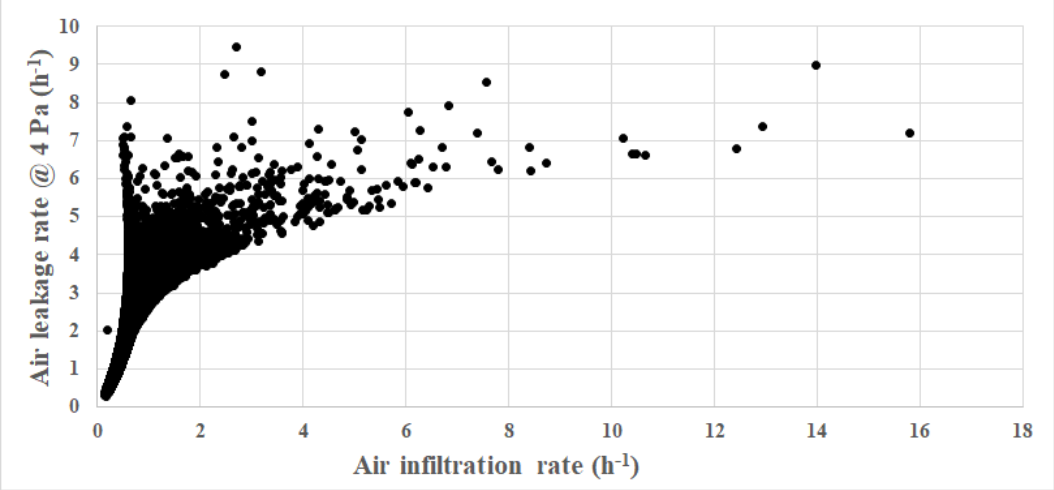


Figure 8.9: Predicted air infiltration rates (using DOMVENT3D- model) against air leakage rate.

The graphs look very similar to those given for the infiltration-wind scatter plots. The majority of infiltration occurs between 10 h^{-1} and 20 h^{-1} for DOMVENT3D-50 and between 2 h^{-1} and 4 h^{-1} in DOMVENT3D-4 model. For most of the plots, the infiltration is proportional to the air leakage rate (regardless of the reference pressure). However, as seen for the other variables, the plot for DOMVENT3D-4 has smaller "tail", and seems to follow the theory.

Infiltration was also compared against the flow exponents taken in the airtightness tests from both methods. Figures 8.10 and 8.11 show the scatter plots from these two variables.

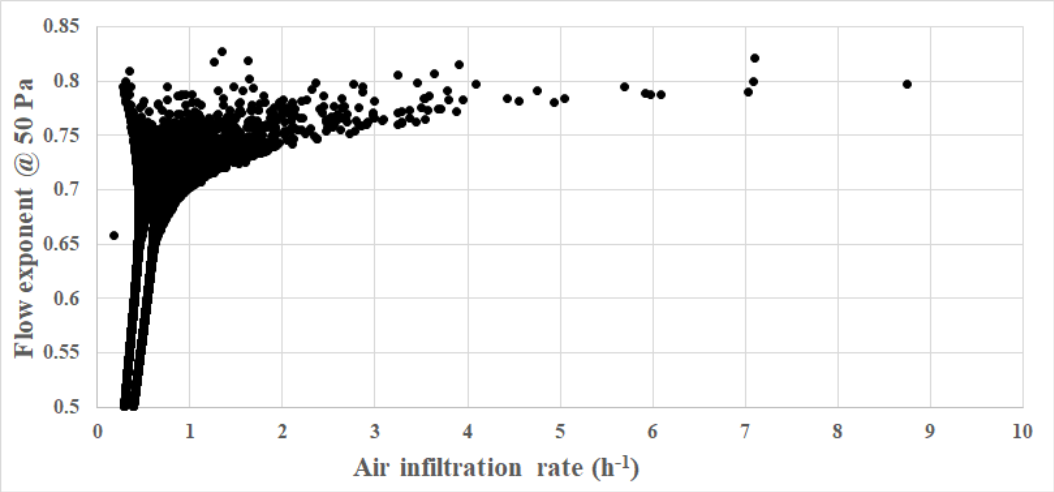


Figure 8.10: Predicted air infiltration rates (using DOMVENT3D-50 model) against flow exponent.

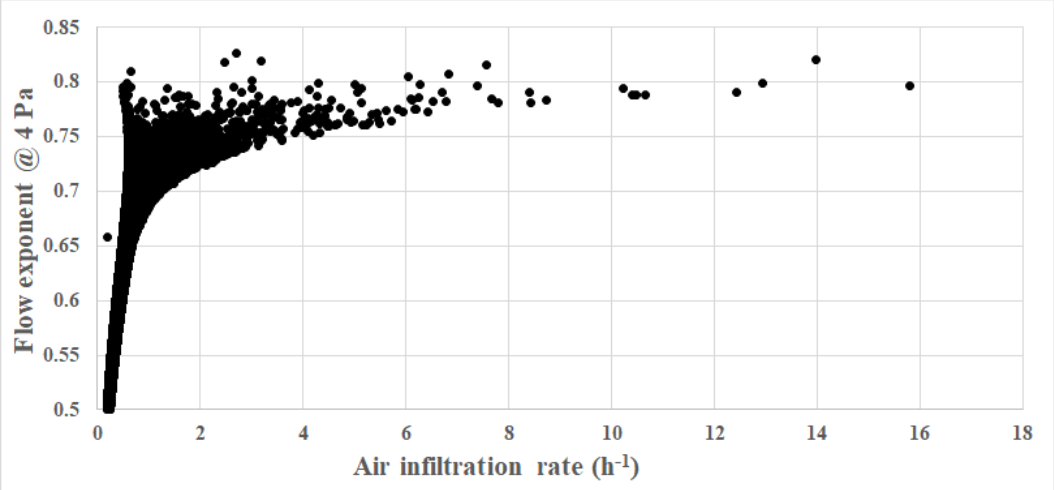


Figure 8.11: Predicted air infiltration rates (using DOMVENT3D-4 model) against flow exponent.

There are infiltration predictions for most simulated flow exponents; however, in both cases most of the flow exponents are between 0.65 and 0.75. It appears as the infiltration rate grows with an increase in flow exponent.

8.5.1.3 Infiltration - dwelling parameters (volume, envelope area, shielding and dwelling factors)

Figures 8.12 and 8.13 show the interaction between predicted infiltration and dwelling volume using DOMVENT3D-50 and DOMVENT3D-4, respectively. On

the other hand, Figures 8.14 and 8.15 show the interaction between infiltration and envelope area for both models.

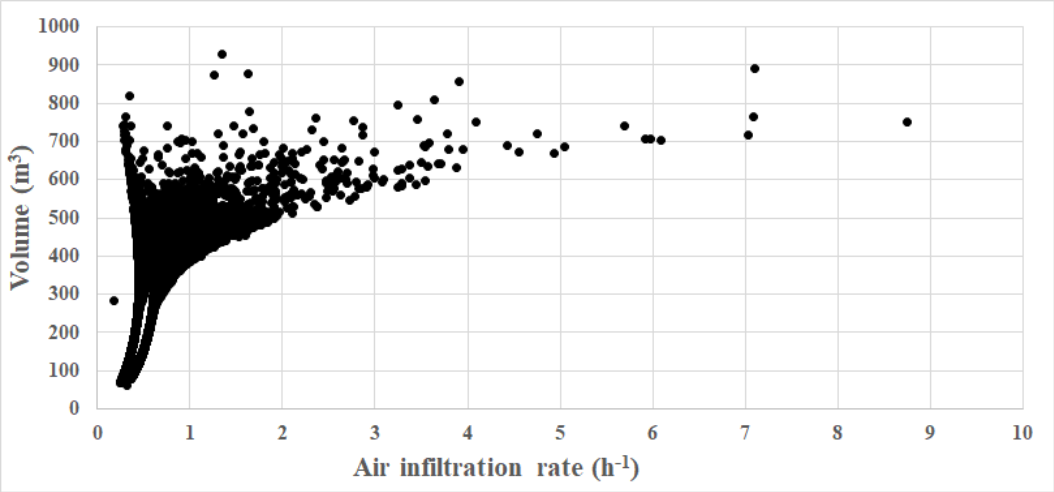


Figure 8.12: Predicted air infiltration rates (using DOMVENT3D-50 model) against dwelling volume.

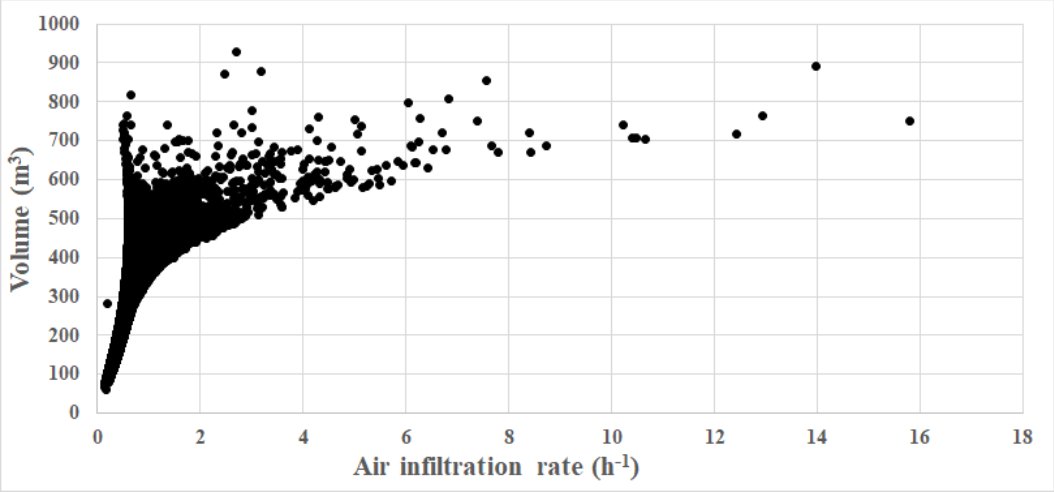


Figure 8.13: Predicted air infiltration rates (using DOMVENT3D-4 model) against dwelling volume.

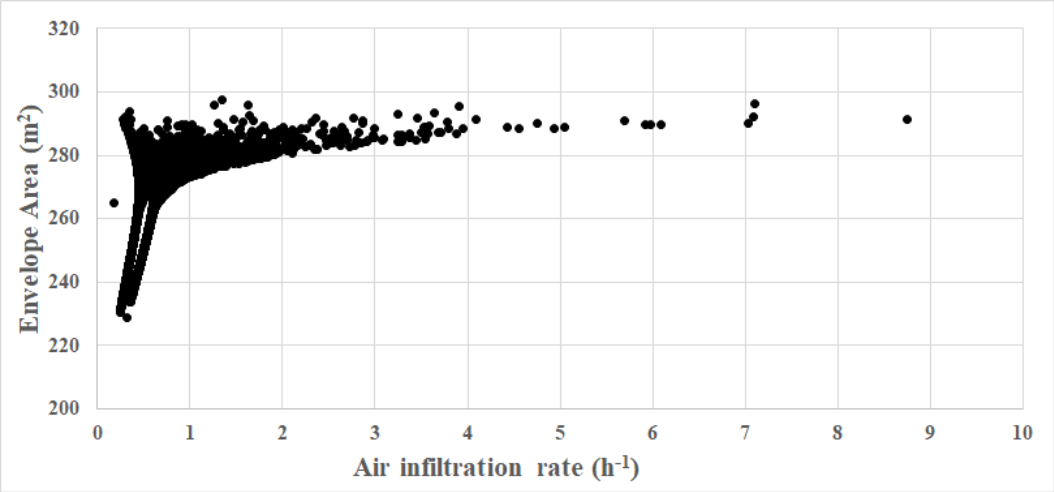


Figure 8.14: Predicted air infiltration rates (using DOMVENT3D-50 model) against dwelling envelope area.

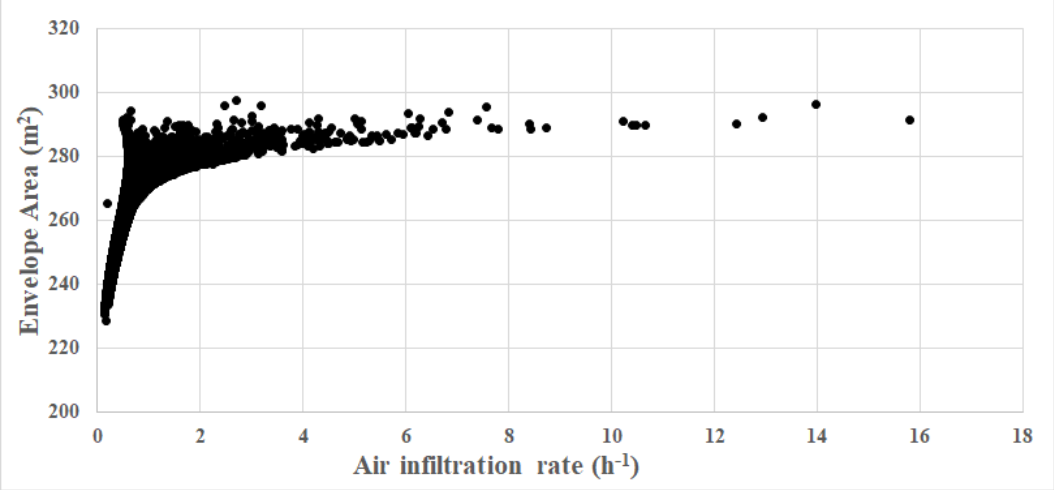


Figure 8.15: Predicted air infiltration rates (using DOMVENT3D-4 model) against dwelling envelope area.

For both, volume and envelope area, it seems that there is a positive correlation between these variables and infiltration rate. However, their effect seem not to change infiltration as other variables. Or if seen differently, they set a basis for the infiltration; in other words, the size of the dwelling gives a minimum infiltration.

Finally, the last variables to analyse are the shielding and dwelling types. Figures 8.16 and 8.17 depict the relationship between predicted infiltration and shielding type. Additionally, Figures 8.18 and 8.19 show the interaction between infiltration and dwelling type. In both cases using the DOMVENT3D-50 and DOMVENT3D-4 models.

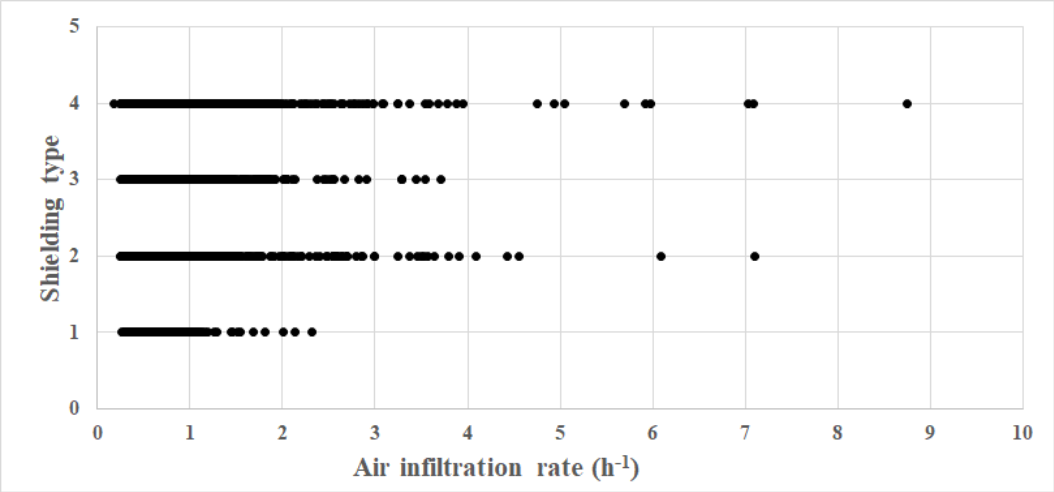


Figure 8.16: Predicted air infiltration rates (using DOMVENT3D-50 model) against shielding type.

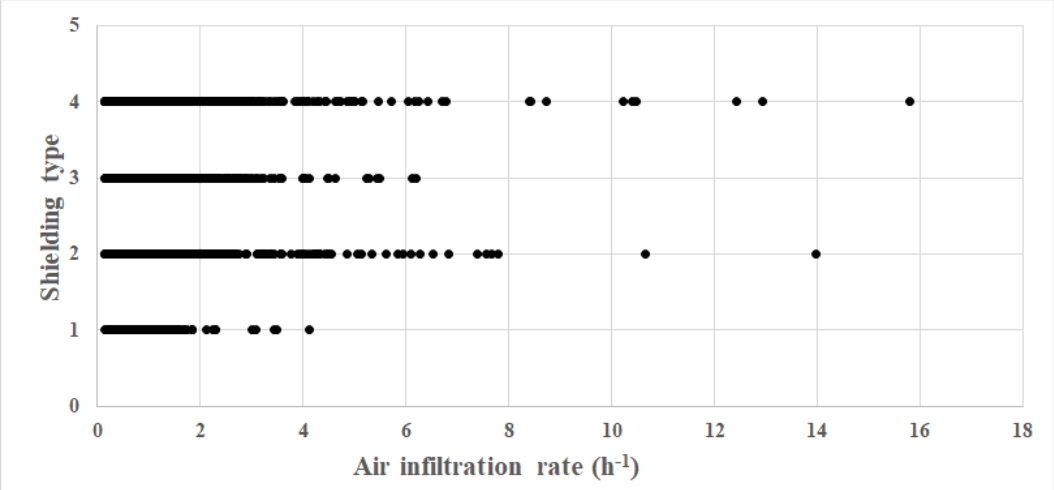


Figure 8.17: Predicted air infiltration rates (using DOMVENT3D-4 model) against shielding type.

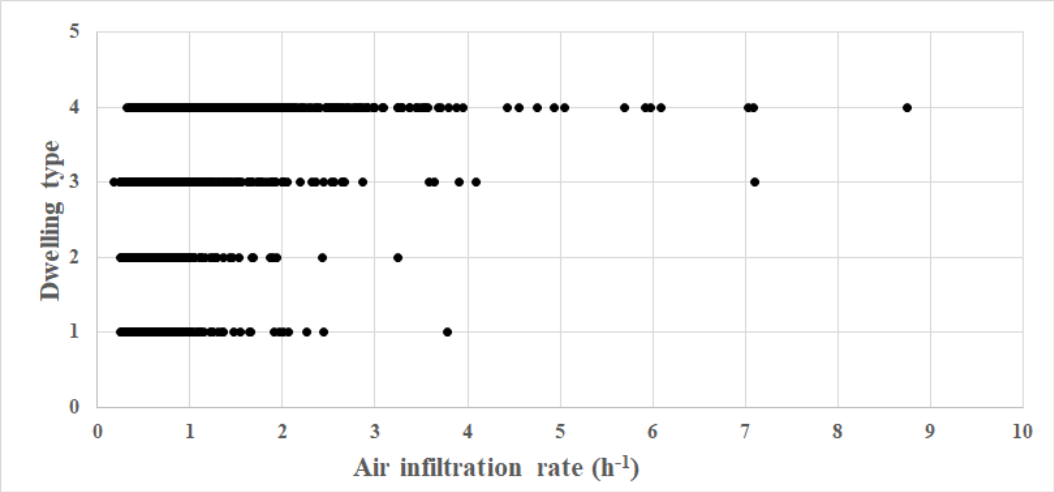


Figure 8.18: Predicted air infiltration rates (using DOMVENT3D-50 model) against dwelling type.

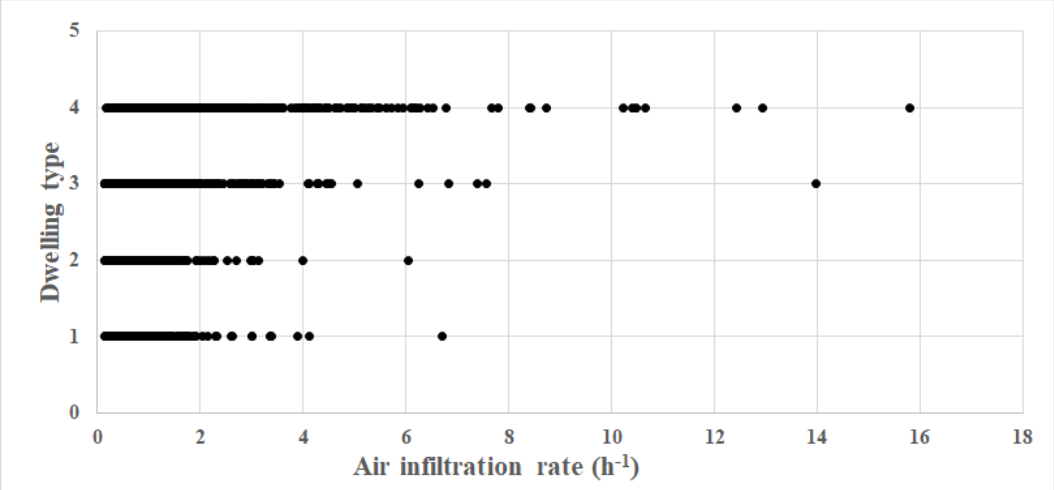


Figure 8.19: Predicted air infiltration rates (using DOMVENT3D-4 model) against dwelling type.

These last graphs showed how infiltration predictions considered all scenarios. For shielding conditions, no shielding (type 4) delivered higher infiltration rates, but moderate shielding (type 2) showed a wider variety of predictions. For the dwelling conditions, as expected, a detached house (type 4) showed a higher infiltration rate; dwellings in an end or a mid terrace (types 1 and 2) showed similar results between each other.

8.5.1.4 Summary of scatter plots

At typical infiltration rates the variables interact and there appears to be little or no correlation or dependence to one particular variable. However, the complexity of the DOMVENT3D models made the results more spread and an approximation to a single line or curve, becomes elusive. The temperature difference drives infiltration when there is no wind, but only at low infiltration. The DOMVENT3D-4 models seems to follow theory better, because the "tails" are more an anomaly in this model rather than a trend for some points.

The analysis of the scatter plots in the previous and the current Chapters leads to the conclusions that both models (LBL and DOMVENT) represent similarly the effect of variables. Nevertheless, in the DOMVENT3D models more variables are involved. A sensitivity analysis using a regression method is a better method to understand the effect of each variable in the output's uncertainty.

8.5.2 Regression and ranking of variables

The predicted data was fitted to regression models (one for each DOMVENT3D model), the sum of squares and coefficient of multiple determination (R^2) were calculated. The results are given in Table 8.3.

Table 8.3: Sum of squares and (SS) and coefficient of multiple determination (R^2) for sensitivity analysis of DOMVENT3D-50 and DOMVENT3D-4 infiltration models for $1x10^5$ samples.

SS	**DOMVENT3D-50**	**DOMVENT3D-4**
Regression	1384	4887
Residual	1067.3	2540.1
Total	2451.3	7427.1
R^2	0.5646	0.6580

Compared to the LBL models where the R^2 value was close to one (almost perfect correlation between the original model and the regression), the DOMVENT3D models show lower correlation, the coefficients of multiple determination are closer to 0.6, which means that the data is not well represented by the model. This is clearly observed in Figure 8.20 for the DOMVENT3D-50 model and in Figure 8.21 form the DOMVENT3D-4 model.

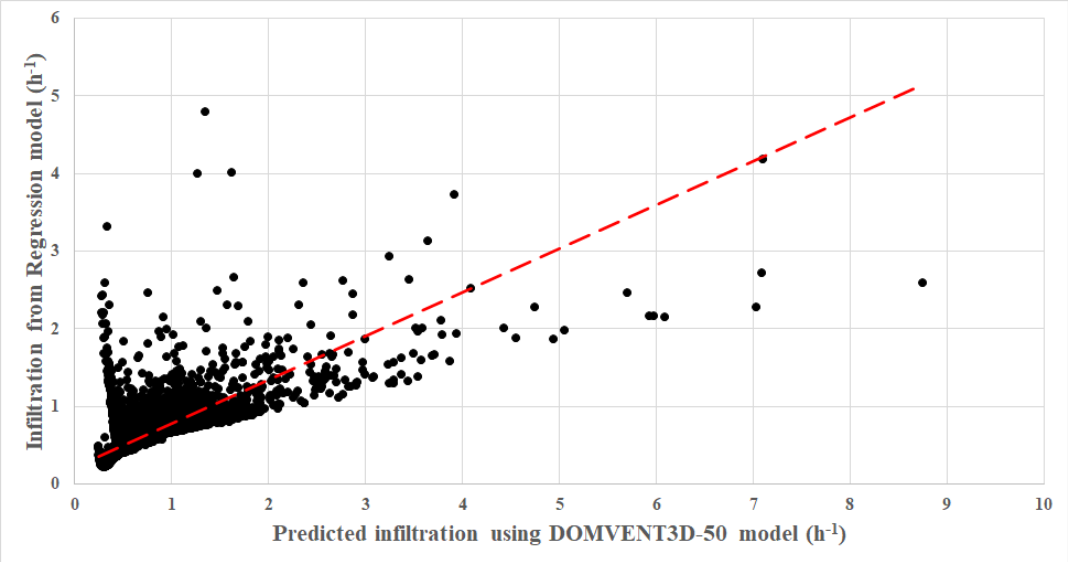


Figure 8.20: Predicted and regression values of infiltration rate for DOMVENT3D-50 sensitivity analysis, $R^2 = 0.5646$.

In the figures both axes represent infiltration rates (h^{-1}), the predicted values given by the DOMVENT3D models are given in the X axis, and the regression model predictions (created for the sensitivity analysis) are given in the Y axis. The dashed line represents a perfect fit of the model.

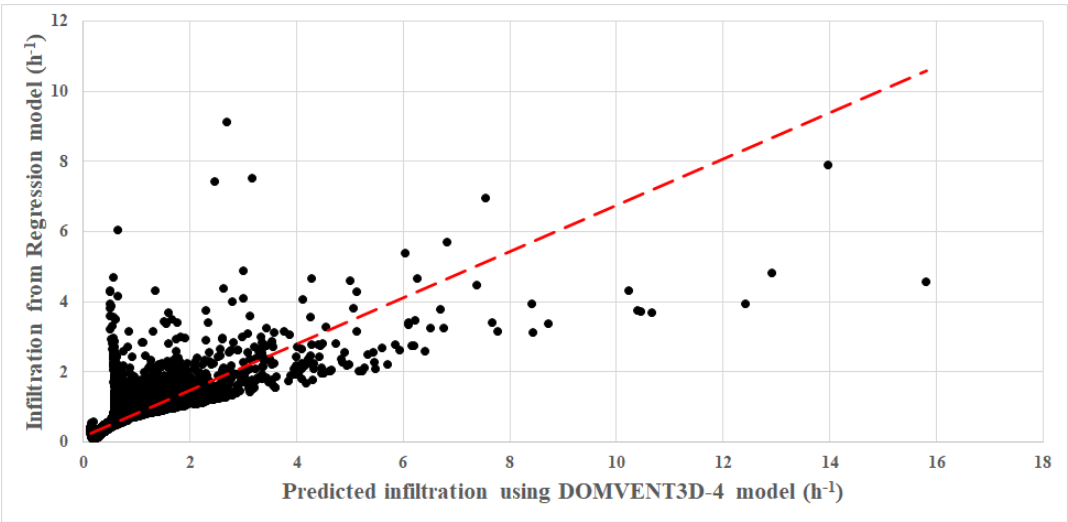


Figure 8.21: Predicted and regression values of infiltration rate for DOMVENT3D-4 sensitivity analysis, $R^2 = 0.6580$.

The least squares regression model (OLS) does not account for variations in the lower zone, this is also due to the complexity of the model, and its algorithm, three equations have to be solved for every data point; that is why the coefficient

of determination is reduced to a 56 and 65%. It is difficult to approximate a line with a large spread of predictions.

If both models are compared, the regression model for the DOMVENT3D-4 is more accurate (9.3%). Therefore the uncertainty from these predictions is lower.

The comparisons between predictions and the regression models were made using the same assumptions, only changing the airtightness inputs. That is why they were used to determine the relevance of each variable. Table 8.4 shows the order of importance of each variable in terms of Standardised Regression Coefficients (SRC); additionally, the regression model coefficients (b_n), and the individual correlation coefficients (CC) are given.

Table 8.4: Model coefficients (b_n), Standardised Regression Coefficients (SRC) and, Correlation Coefficients (CC) for the models created in the Sensitivity Analysis for DOMVENT3D.

Variable	**Regression coefficient**(b_n)	**SRC**		**CC**	
		Value	**Rank**	**Value**	**Rank**
DOMVENT3D-50					
Envelope Area	3.592	207.005	1	$1.021x10^{-05}$	3
Volume	-0.285	-159.585	2	$9.811x10^{-06}$	7
Flow exponent (b_{50})	-401.024	-128.905	3	$1.019x10^{-05}$	4
Air leakage rate (n_{50})	5.470	118.735	4	$9.651x10^{-06}$	8
Temperature difference	1.899	38.433	5	$-1.019x10^{-05}$	4
Wind speed	0.461	1.438	6	$8.214x10^{-06}$	9
Dwelling factor	0.062	0.459	7	$1.004x10^{-05}$	6
Shielding factor	0.004	0.258	8	$-1.139x10^{-05}$	1
Wind direction	$3.849x10^{-05}$	0.036	9	$-1.066x10^{-05}$	2
DOMVENT3D-4					
Envelope Area	2.519	85.454	1	$9.980x10^{-06}$	3
Flow exponent (b_4)	-301.672	-57.076	2	$9.965x10^{-06}$	4
Air leakage rate (n_4)	-5.527	-16.412	3	$9.261x10^{-06}$	8
Temperature difference	1.338	15.949	4	$-9.965x10^{-06}$	4
Wind speed	4.587	8.428	5	$8.030x10^{-06}$	9
Volume	-0.012	-3.991	6	$9.591x10^{-06}$	7
Dwelling factor	0.068	0.270	7	$9.817x10^{-06}$	6
Shielding factor	0.006	0.152	8	$-1.114x10^{-05}$	1
Wind direction	$5.255x10^{-05}$	0.029	9	$-1.042x10^{-05}$	2

As mentioned in the previous chapter, the model coefficients, are calculated to represent the regression model and the correlation coefficients are given to determine each variable's correlation. The CC are small which means that there is no individual correlation and that is because the model has 9 different variables.

That being stated, the SRC's, are a metric to determine the relevance when more than one variable interacts. For the DOMVENT3D-50 model, the dwelling parameters (envelope are and volume) are the most important variables affecting the model. The flow exponent (b_{50}) and air leakage rate (n_{50}) measured in the blower door test ranked third and fourth. In fifth and sixth place of relevance were the environmental conditions, temperature difference and wind speed. Shielding and dwelling factors were ranked seventh and eighth place. Finally, the wind direction showed to provide the less uncertainty to the output.

For the DOMVENT3D-4 model, envelope area ranked first place. Different from the DOMVENT3D-50 model, the flow exponent (b_4) and air leakage rate (n_4) ranked second and third place respectively. The fourth and fifth place were temperature difference and wind speed. In the DOMVENT3D-4 model, the house volume ranked sixth in the sensitivity analysis from all the variables. Finally shielding factor, dwelling factor and wind direction ranked last.

The house geometry is defined by dwelling envelope area and volume, and these parameters have the effect of increasing the uncertainty as they directly affect the façade areas and therefore the impact of environmental conditions upon the building. Nevertheless, it is clear that when low-pressure airtightness parameters are used, the importance of the dwelling volume reduces.

When considering only the environmental conditions, the temperature differences ranked above wind in both cases. The wind impact on a building is directly related to the exposed façades and geometry which are obtained using the envelope area, hence the effect of the wind in the uncertainty is reduced and the envelope area's impact is increased. A similar reason is given for the airtightness parameters results. In both cases the flow exponent ranked above the air leakage rate; this is because the air leakage rate depends on the dwelling parameters, and the flow exponent in the airflow through leakage paths.

It is also important to mention that the wind direction in both cases is the least important variable, this is because the models address the building type (dwelling factor) and location of the shielded façades with higher importance. Therefore, the permeability (or impermeability) of certain sides of the dwelling is assessed before entering the effect of the direction of wind.

8.5.3 Regression and ranking of variables taking volume and envelope area as constants

It can clearly be seen that the dwelling parameters are important when calculating the effect of other variables such as wind or air leakage rate. By using them as a subject of uncertainty, a bias towards their relevance is obtained; however, this study focuses on assessing the impact of using air leakage rates taken at different pressure difference. Hence, as done for the LBL model, if the volume and envelope area are considered as constants, the number of variables is reduced, and a new sensitivity analyses can be done. Table 8.5 shows the SS and R^2 values for these new sensitivity analyses.

Table 8.5: Sum of squares and (SS) and coefficient of multiple determination (R^2) for sensitivity analysis of DOMVENT3D-50 and DOMVENT3D-4 infiltration models for $1x10^6$ samples when the Volume and Envelope area are considered as constants.

SS	**DOMVENT3D-50**	**DOMVENT3D-4**
Regression	1310.6	4643.1
Residual	1087	2597.5
Total	2397.6	7240.6
R^2	0.5466	0.6413

The correlation is similar as the one given when envelope area and volume were considered as variables. The correlation is, again higher for the DOMVENT3D-4 model. Figures 8.22 and 8.23 provide the comparisons between the predicted values against the regression model used for the DOMVENT3D-50 and the DOMVENT3D-4 models respectively. The values of volume and envelope area were assumed as the average measured values.

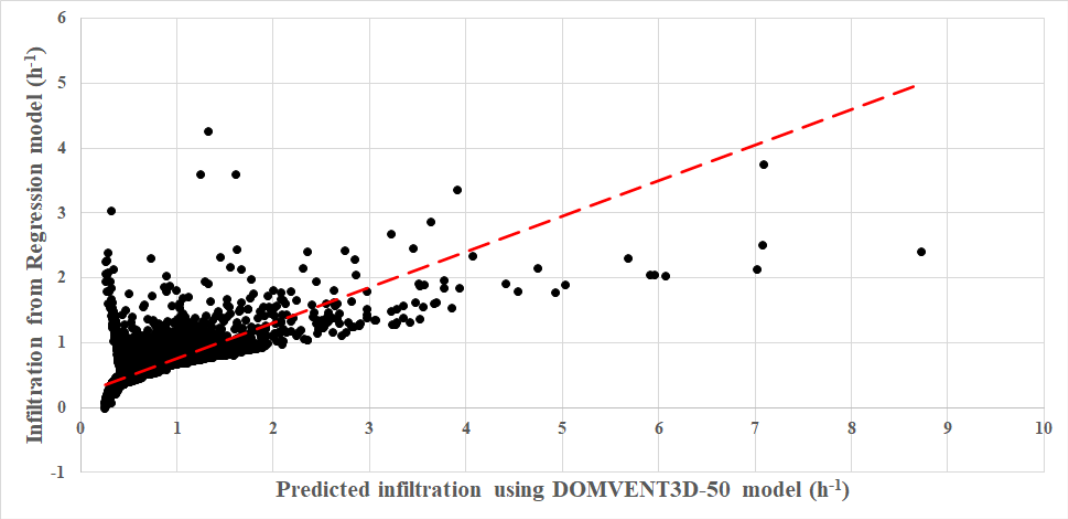


Figure 8.22: Predicted and regression values of infiltration rate for DOMVENT3D-50 sensitivity analysis with Volume and Envelope Area as true constants, $R^2 = 0.5466$.

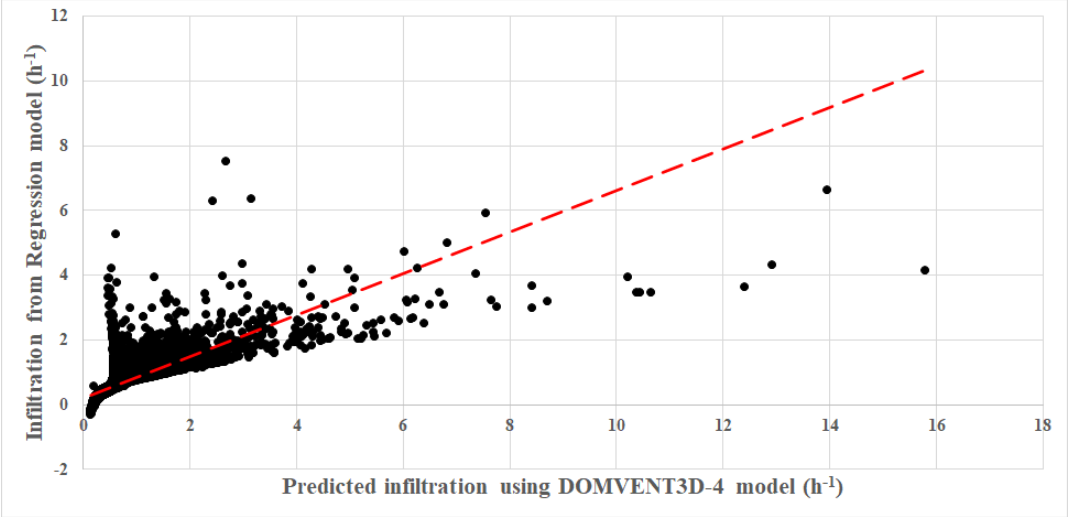


Figure 8.23: Predicted and regression values of infiltration rate for DOMVENT3D-4 sensitivity analysis with Volume and Envelope Area as true constants, $R^2 = 0.6413$.

It can be seen from the comparisons of these models, that the spread of points makes it difficult to provide a perfect correlation between regression and original models. Scatter plots showed similar results as the ones presented in the previous analysis when envelope area and volume were included as variables.

The scatter plots between the output (infiltration) and the variables is omitted from these sections. The scatter plots were similar to those ones presented when

the dwelling parameters were considered in the analysis. The conclusions made before, remain for these new created models with volume and envelope area taken as constants.

Table 8.6 gives the new values of b_n, SRC and CC when volume and envelope area are taken as constants for both DOMVENT3D models.

Table 8.6: Model coefficients (b_n), Standardised Regression Coefficients (SRC) and, Correlation Coefficients (CC) for the models created in the Sensitivity Analysis for DOMVENT3D with Volume and Envelope Area as true constants.

Variable	**Regression coefficient**(b_n)	**SRC**		**CC**	
		Value	**Rank**	**Value**	**Rank**
DOMVENT3D-50					
Air leakage rate (n_{50})	-0.275	-6.255	1	$9.336x10^{-06}$	6
Wind speed	1.147	3.745	2	$7.946x10^{-06}$	7
Temperature difference	-0.100	-2.113	3	$-9.861x10^{-06}$	3
Flow exponent (b_{50})	1.832	0.616	4	$9.861x10^{-06}$	3
Dwelling factor	0.062	0.480	5	$9.714x10^{-06}$	5
Wind direction	$3.872x10^{-05}$	0.038	6	$-1.031x10^{-05}$	2
Shielding factor	0.004	0.036	7	$-1.102x10^{-05}$	1
DOMVENT3D-4					
Air leakage rate (n_4)	-1.991	-6.089	1	$9.098x10^{-06}$	6
Wind speed	2.233	4.225	2	$7.888x10^{-06}$	7
Flow exponent (b_4)	5.898	1.149	3	$9.790x10^{-06}$	3
Temperature difference	-0.092	-1.130	4	$-9.790x10^{-06}$	3
Dwelling factor	0.068	0.305	5	$9.644x10^{-06}$	5
Wind direction	$5.2537x10^{-05}$	0.030	6	$-1.023x10^{-05}$	2
Shielding factor	0.006	0.028	7	$-1.094x10^{-05}$	1

It can be seen that for these new models the air leakage rate (n_{50} and n_4) and wind speed provide most of the uncertainty to the output (infiltration rate). When removing the dwelling parameters, these variables show their objective interaction with the infiltration rate, this is what is expected. These results confirm that when accounting correctly for the dwelling parameters, the accuracy of the predictions improve.

The third and fourth place are the temperature difference and the flow exponent for the DOMVENT3D-50 model, and flow exponent and temperature difference, respectively for the DOMVENT3D-4 model. This was also expected considering that the effect of wind is greater for most of the scenarios and; that the flow exponent is also related to the air leakage rate. The wind direction is not ranked last for this analysis.

It is also important to point out that defining the dwelling condition in the model is more relevant than both, the shielding condition and the wind direction. If a different analysis is made assuming that the shielding and the dwelling condition are constants (which are in the short term) and do not add uncertainty, the results would not differ since these variables are ranked last; however, the effect of wind direction might be greater.

When comparing these two new models, the most important result found is that the air leakage rate is as important for the DOMVENT3D-4 model as it is for DOMVENT3D-50. This means that the uncertainty in the prediction of infiltration due to the air leakage rate is similar for low and high-pressure airtightness measurements when predicting infiltration rates. If it is considered that environmental conditions are usually obtained from data bases or meteorological stations where the measurement accuracy is greater than for those measured in this work (due to the limited availability to place the anemometer and temperature sensors, as explained in Chapter 5), then the prediction of infiltration will have similar uncertainty when coming from low pressure airtightness measurements than when coming from high-pressure differences.

The DOMVENT3D models showed how different variables interact when predicting air infiltration. Even when a regression model was fitted to the data, it is difficult to determine if the results found are accurate to validate the model. The results in Jones et al. [2015] only agree with the ones presented here when the dwelling parameters were removed. That may be due to the data collection phase, mainly related to environmental conditions. Jones et al. [2015] performed a stochastic model, which fitted data from data bases, and the environmental conditions did not contain the uncertainty defined in this project. In addition, the distributions simulated here, came from measured data and might not represent a whole-stock scenario.

Despite what was mentioned, the results showed that both models (DOMVENT3D-50 and DOMVENT3D-4) are comparable,in terms of model fitting and the determined ranking of variables. Both have similar coefficients of determination, and predict data in a similar manner, this suggests that the DOMVENT3D model can be used to predict infiltration rate regardless of the airtightness measurement method. The model needs only to be calibrated, and a similar code as the one presented in Appendix G (for low pressure), must be used. It is important to remark that the results of the sensitivity analyses when removing the dwelling parameters, seem to follow previous findings [Liddament, 1996] and demonstrated a good description of the infiltration phenomena; therefore, it can be said that

DOMVENT3D have been seen to be in good agreement with actual infiltration rates as determined by tracer gas in the range of 3 - 10% ±14%.

8.6 Conclusions

The infiltration model DOMVENT3D was modified to accept low pressure airtightness measurements as its input as opossed to high pressure measurements. Model predictions of air infiltration rates were assessed against known rates from tracer gas studies. The model was re-coded in MATLAB to read the measured data and predict accordingly. In addition, the model was recalibrated to produce results from low-pressure airtightness measurements. The models were named DOMVENT3D-50 when reading high-pressure airtightness data, and, DOMVENT3D-4 when reading low-pressure airtightness data.

The DOMVENT3D model is more complex than the previous models analysed, and the code (appendix G) and results showed it. When predictions from both models were compared against real measurements, DOMVENT3D-4 was shown to have a slightly lower RPD error, though both models had similar uncertainty. However, if the absolute value of the RPD error is removed, the overestimations and the underestimations compensate each other, and the average RPD is reduced but with larger uncertainty. The DOMVENT3D-4 model also provided predictions with an RPD accuracy of 3% ± 14%, which translates to less than 17% of error for two thirds of the predictions .Hence, this demonstrates that it was reasonable by Jones et al. [2015] to use this model to assess cumulative impacts of infiltration at the level of the housing stock. The main conclusion from this analysis is that both models are comparable and can be used regardless the airtightness inputs, with slightly better overall performance when using low-pressure airtightness inputs: 10% ±14% for high pressure airtightness inputs and 3% ±14% for low pressure airtightness inputs.

Comparisons between the output and each independent variable was made in scatter plots, it was difficult to determine correlation to a particular variable. However, it was clear that wind and air leakage rate have positive correlation with infiltration. On the other hand, temperature difference is the main driving force when infiltration and wind are low. Furthermore, the DOMVENT3D-4 showed to have results which were closer together than those seen with the DOMVENT3D-50 model. The DOMVENT3D-50 model appeared to have two “tails” in the scatter plots due to the consideration of the exfiltration flows.

When performing a sensitivity analysis, a regression model was developed for

each model, the coefficient of determination (R^2) was low for both models, but slightly higher for DOMVENT3D-4. The model represented the data with around 60% of accuracy. Standardised regression coefficients were used to rank the variables and for both models the dwelling parameters were seen as the most important. However, when the volume and envelope area were set as constants, the air leakage rate and wind speed ranked as the dominant factors. This is more in line with what was expected from the theory. It is understood that the dwelling parameters play a role also in the effect of other variables such as wind and air leakage rate.

The results of the sensitivity analyses, when the dwelling parameters were set constant, matched the ones provided by the author of the DOMVENT3D model [Jones et al., 2015], which also ranked air leakage rate and wind as the most relevant variables when accounting for uncertainty.

The main objective of this chapter was to field validate the original model, and, to compare the performance of both DOMVENT3D models. The DOMVENT3D-4 model showed a better accuracy (3% ±14%) than the DOMVENT3D-50 (10% ±14%) model. Hence it has been shown that the DOMVENT3D model can be modified to utilise low pressure airtightness measurements as an input and deliver infiltration rate predictions with comparable accuracy and uncertainty of those seen with high pressure inputs.

Chapter 9

Discussion, conclusion and recommendation for future research

9.1 Discussion

9.1.1 Airtightness testing

The steady pressurisation method (or blower door) has been through a long development process over the last four decades. There are standards and legislation relating to airtightness testing, which already include it as the test methodology. A number of different countries require the blower door test to be performed so to comply with energy efficiency policies. Nevertheless, research concerning the method still continues. Uncertainty due to the background pressure reading has been a topic of discussion in recent times. Additionally, uncertainties caused by steady and unsteady wind have been studied. The blower door test has been shown in this study to provide good repeatability, and consistency between results, even during adverse climate conditions.

Despite the widespread use and maturity of the incumbent steady pressurisation (blower door) method, this project has highlighted some shortcomings. The disadvantages of not maintaining the building's integrity and, the extrapolation from high to low pressure are the most significant sources of concern. It was seen in Chapter 3 when testing in small and airtight enclosures that the blower door measurements in airtight environments are affected by the modification of the building integrity due to the blower door being cited within the building envelope. And it was also seen from the analysis of the infiltration models in Chapter 7 and 8 that

the extrapolation caused more uncertainty than low- pressure measurements, this was shown when the air leakage rate ranked higher as a source of uncertainty in the high-pressure models.

There will be a continuation of airtightness testing research investigating the uncertainties associated with blower door measurements by the scientific community. However, more research is required in the field of evaluating how airtightness measurements actually relate to building energy use.

A new research field has been opened in relation to low-pressure airtightness measurements, due to the advent of the Pulse technology. This project saw part of Pulse's development. The Pulse device changed its appearance in a short time. A more robust and sophisticated piece of equipment was developed from having a composite tank in a trolley to an aluminium tank in a resistant box. Additionally, the analogue control box was switched into a LED tablet with digital graphic display. These changes aided in both the robustness in the equipment and the accuracy of the results. However, one of the most significant changes seen was the modification of the reference pressure tank. The reference pressure tank is now enclosed within the box. This improvement erased the variations in the results created because of loose connections, or wear due to transportation. Finally, the inclusion of tank temperature corrections aided the accuracy of results.

When this project started in 2016, the reproducibility of the Pulse test was lower (10% RPD) than the current one (5% RPD). It was seen that there were anomalies in certain tests, whereas now, the repeatability is lower than 5% RPD. However, the technology is not yet perfect; therefore, more research has to be carried out. It was also seen that this repeatability level is similar as the one obtained with the steady pressurisation method (5% RPD).

The main disadvantage of Pulse is that multiple testing is required. The tank has to be charged multiple times if the results need to be validated; this eliminates the time advantage of the method. Nevertheless, in a commercial practice one valid test is sufficient to determine the airtightness of a building. Moreover, determining the validity of tests requires a knowledgeable professional analysing the results: even when results are printed on the screen, a person has to determine their validity. This human involvement might eliminate the advantage of easy-to-perform tests. These two shortcomings are solvable with more development of the method. The research reported in this thesis was also part of the product development and provided feedback for the Pulse to overcome these technical and practical issues.

The Pulse method has the potential to be included in the airtightness testing

market. The inclusion of Pulse does not mean that the steady pressurisation method will cease to be valid; on the contrary, both methods will be able to coexist with their advantages and disadvantages. Pulse can be a reliable tool when quick measurements in multiple dwellings are required; while the blower door keeps the advantage of leakage detection (in combination with a thermal camera or smoke pen).

The Pulse technique has been developed to a commercial point and can be able to predict in large scale testing campaigns as the one performed in this project. However, it will still be compared with the blower door, at least in the near future. In an economic point of view, one method could serve different purposes to different testers.

From the analyses made to infiltration models and their capabilities to predict infiltration, it was seen that despite which airtightness measuring technique is used the models deliver similar results. This was clearer for the DOMVENT3D model. Infiltration prediction and consequently heat losses calculation can be done despite the way airtightness is measured. Therefore, both techniques are comparable when predicting infiltration. In other words, despite their differences, airtightness measuring techniques work similarly when serving their ultimate purpose, estimating infiltration heat and energy losses.

9.1.2 Air infiltration rate measurements: tracer gas

Air infiltration is the value needed to calculate the unintended ventilation heat losses. It has been discussed in this study as to why it is impractical to measure infiltration directly in buildings in most cases. Tracer gas tests are accurate; however, they are invasive and require long periods, at least 2 hours in an unoccupied space.

A large number of tracer gas tests were performed during this study and described in Chapters 4 and 5. The first contact with air infiltration testing was with the constant concentration tracer gas test. It was seen that the constant concentration test provided good results of high accuracy; however, expensive high-specification equipment is required, plus the need for long test duration. However, it has the advantage of real-time results despite the changing weather conditions. With this method, it was discerned that temperature difference plays a dominant role in air infiltration when the wind speed is lower than 2.5 m/s. This conclusion could only be possible when analysing scatter plots, and could not be seen from the analysis of infiltration models.

The constant concentration tracer gas method was also used to compare with

pressure differentials in a building. It was challenging to correlate one infiltration measurement (every 3.5 minutes), with more than 200 pressure measurements. Despite this, it was found that the pressures measured in a building at around 2 meters high, mainly occur between a pressure difference of 1 and 5 Pa.

The second tracer gas test used was the concentration decay test. The tests explained in Chapter 4 set the basis for developing the methodology to carry out a tracer gas testing campaign for the wider field data collection stage of the project. The time taken to perform a decay test is much less than the constant concentration test, but has the disadvantage of reporting a one point infiltration rate; the mean rate across the duration of the test. The cost of the concentration decay method is also much lower than the constant concentration method. It was seen that a decay could be fast or very slow, and an initial low concentration would increase the uncertainty of the result and in consequence, make the test inaccurate. If using carbon dioxide as tracer gas, an initial average concentration of 4500 ppm provided reliable results, if the decay was long enough. A minimum of 3500 ppm of initial average concentration was seen to be required. Also, a way to improve accuracy is to increase the number of thermal zones, but consequently, the number of sensors (and cost) will increase. Time was a significant constraint in the concentration decay tests. It is challenging to obtain dwellings to test for long times, and for tight dwellings, a decay of more than 2000 ppm could take more than 8 hours. Despite this, the concentration decay method, due to its simplicity, is the most realistic proposition when obtaining large data sets of air infiltration. For example, when infiltration models are to be field-validated, this method would be the most efficient to employ.

Air infiltration measurement will still continue to be performed despite advances in airtightness testing and infiltration models. Novel methods such as the technique created by Liu et al. [2018] have also been developed; however, due to standardisation, documentation and over-50-years usage, tracer gas methods will still be used.

It was learnt during this study that air infiltration predictions can be included as a result of Pulse's measurements. However, it will require constant validation and, good understanding from the phenomena from the tester: air infiltration has to be understood as a result of different variables interacting.

9.1.3 The correlation between airtightness and air infiltration: predictions using models

It is known that airtightness and air infiltration are closely related, or in statistical words, correlated. The level of that correlation depends on how different variables interact. Wind, temperature, shielding, orientation, among others, cannot be ignored when predicting infiltration rates.

It was seen during this study, that airtightness represents a baseline for infiltration, which is then increased by weather conditions. Therefore, there will not be a -close to- perfect correlation between airtightness and air infiltration. To clarify, it has to be understood that air infiltration changes all the time, whereas airtightness can be considered constant in the short term.

Empirical models were tested in Chapter 5, and a relatively good correlation was found with a 0.7 r-squared value, meaning that by only relating airtightness and air infiltration there was only a 30% of uncertainty in the regression. A 0.7 value may not represent high accuracy; however, taking into account infiltration depends on many changing factors, this number was higher than expected. The most accurate empirical model was a power model, with an exponent close to one. Based on low-pressure airtightness measurements; the model was proved good with only 5% error when predicting new data. This model, despite being the most accurate, did not have a basis in theory and was one hundred percent empirical, and therefore solely based on the measured data. This lack of theoretical background meant that the 70% accuracy would only be valid for the data used and therefore using this model in different dwellings, would not predict accurately.

Using these kind of empirical models is not recommended, except when it is specifically required. Nevertheless, the exercise of developing these empirical relations was the first way of proving that both airtightness measuring technologies (blower door and Pulse) can be used to predict air infiltration with similar outcomes. For this reason, empirical correlations cannot be compared with the models, as a comparison would present a bias towards the data utilised to create them. The model will most of the time be inaccurate when tested in different scenarios. Nevertheless, the objective was fulfilled and it was demonstrated that despite the origin of the airtightness data, the empirical models were similarly accurate. However, it was seen that the errors created were in both cases large when tested in new conditions, with errors as large as 70%.

There are several infiltration models with different levels of complexity, but based on solid theoretical background; and therefore it is considered that the

uncertainty of using them will be lower than using a random empirical model when predicting AIR from airtightness measurements.

Chapter 2 described how infiltration predicting models have changed. From the use of simple single-zone models to complex multi-zone ones. Despite this, it is worth mentioning that, the most used model is the divide-by-20 rule of thumb presented in Chapter 6.

This project evaluated three different models: the divide-by-20 rule of thumb, the simplified model LBL, and DOMVENT3D. The last two were programmed in this study to predict infiltration from low-pressure airtightness measurements. It was seen that for the LBL model, the use of low pressure measurements meant that the only difference it was that the extrapolation was removed; DOMVENT3D, on the other hand required a certain level of calibration by means of changing the calculation of the relative leakage area to accept low pressure airtightness measurements .

The first model (divide-by-20) proved to be obsolete, with tighter houses, the model will extremely over-predict infiltration and differences as large as 175% were obtained. The trend is to build tighter. However, if the conditions measured are taken as representatives of the season, the errors when predicting infiltration by British legislation (SAP) [Building Research Establishment, 2013], are extremely high, over 500% in some cases. A new value for N in the ratio was proposed, which was almost twice as the current one, this new N is 37.31 when using q_{50} as airtightness metric (UK) and 38.99 when using n_{50} (USA). This new N is only representative of the sample used. Despite being more accurate, it is not recommended to be used, because, in some cases, the error when using it will be significant since these ratios do not take into account weather and shielding conditions.

A ratio was also defined based on low-pressure airtightness measurements given by the Pulse method, a close to divide-by-8 rule. Despite being -slightly- more accurate when predicting new data (than the proposed divide-by-37 when based on the pressurisation method measurements), the differences are still considerable. A different approach to predict infiltration from Pulse measurements using leakage-infiltration ratios, is to extrapolate the low-pressure values to high-pressure using the power law and then using the divide-by-20 rule as described in Zheng et al. [2019b] and Zheng et al. [2019a]. By using this approach, the uncertainty created is higher than using directly high-pressure measurements due to the double extrapolation. All these factors lead to the conclusion that leakage-infiltration ratios must not be included within the Pulse algorithm to predict infiltration rates; therefore, they should not be considered in legislation either.

Using the new proposed and more accurate ratios, it was once again demonstrated that both airtightness measuring techniques are comparable when used to predict infiltration. The uncertainties calculated for both new ratios were 6.86% and 6.40% for the steady pressurisation and the Pulse method, respectively when using q_{50} as metric. It can be concluded that both techniques have the same potential to predict infiltration through leakage-infiltration ratios. Nevertheless, large error was found when testing the ratios in new properties with differences between 64-81% when using the pressurisation measurements and 40-54% when using the Pulse technique measurements.

The LBL model provided better results than the rule of thumb; however, its simplicity was witnessed in the sensitivity analysis, the scatter plot showed single lines as a result of infiltration predictions; in other words, there is not much variation in results despite the inputs. The superposition assumption proved not to be realistic and led to not-expected results when the temperature difference was negative (higher outdoor temperature), which agrees with previous findings [Lyberg, 1997].

Despite the simplified nature of the LBL model, dwelling-particular errors reduced to half of those obtained from using ratios; and the overall errors of the whole sample up to almost one-seventh (87% when using the ratio to 13% using the LBL model). The most important factor affecting the accuracy was seen to be the way the leakage distribution was assumed. Three different assumptions of the leakage distributions were tested. In this case, the LBL models were more accurate for assumption 1 (floor and ceiling leakages are equal to zero), and had less uncertainty for assumption 3 (factors given by the authors of the models). Nevertheless, despite the airtightness inputs the results were similar.

On the other hand, DOMVENT3D was seen to work with a similar accuracy as the LBL models when the absolute error is accounted; and better when the overall error was taken into account. If it is assumed that the dwelling parameters do not add uncertainty, the results show that the most influencing variables when using DOMVENT3D are the air leakage rate and the wind speed. DOMVENT3D-4 (low pressure airtightness measurement inputs, 4 Pa) proved to be more accurate than DOMVENT3D-50 (50 Pa inputs) mainly when the overall error is accounted, and proved to be the most accurate model tested in this project. Both DOMVENT3D-50 and DOMVENT3D-4 lead to the same uncertainty: ±14%.

Table 9.1 presents a comparison of all models tested, the mean RPD and the uncertainty.

Table 9.1: Comparisons of average and standard error reported values between three different infiltration models, using high and low-pressure airtightness inputs

Model	**High pressure (50Pa)**	**Low pressure (4Pa)**
divide-by-20	95% ±10%	N/A
|LBL assumption 1|	42% ±11%	43% ±10%
LBL assumption 1	13% ±14%	17% ±14%
|LBL assumption 3|	57% ±3%	54% ±4%
LBL assumption 3	-51% ±6%	-49% ±6%
|DOMVENT3D|	53% ±8%	51% ±8%
DOMVENT3D	10% ±14%	3% ±14%

As mentioned, DOMVENT3D-4 was the most accurate model (mean RPD), whereas the LBL50 assumption three was the most repeatable (low SE) one. As expected, the least accurate is the divide-by-20 rule of thumb. The rule of thumb always overpredicts the infiltration rate. The other two models sometimes overpredict and sometimes underpredict, thus creating a low mean RPD. When having large data sets, these two models will be more accurate, even when for some properties, the prediction could be inaccurate.

It was found that in both LBL and DOMVENT3D models, all the variables interact simultaneously. However, it could be seen that the temperature difference can be the main driving force when wind speed is under 1.8 m/s and the building is tight (less than $1h^{-1}$@4 Pa). Shielding and dwelling factors proved to be more relevant when infiltration is high. In fact, for the DOMVENT3D models, it was proven that the dwelling factor is more important than the shielding factor and wind direction. However, the dwelling factor is a value that is defined only by inspection and should not lead to much uncertainty in reality.

An important conclusion of the sensitivity analyses is that the dwelling parameters (house volume and envelope area) introduce most of the uncertainty. This is because these parameters are then used to calculate different values, such as, the area of each façade and therefore the effect of wind in the exposed façades. It is essential to calculate the dwelling parameters accurately. In practice it is almost impossible to measure the dwelling parameters perfectly, with errors between 3-10% [International Organization for Standardization, 2015], but it is concluded that an accurate measurement will lead to an accurate prediction.

Moreover, from the sensitivity analyses it was seen that the DOMVENT3D models follow the theory more accurately. The results obtained were expected, with air leakage rate and wind as dominating variables. The LBL4 model in com-

parison, ranked the flow exponent higher than the air leakage rate for assumption 1. However, for assumption 3, both LBL50 and LBL4 ranked the air leakage rate first, but the environmental conditions in different places. This leads to three conclusions:

- The DOMVENT3D models represent better the infiltration flows and how the variables interact, mainly airtightness values and environmental conditions.
- It is essential to determine the ceiling and floor leakage distribution, in this case there is no need to assume them. In reality this is difficult, therefore it is very important to decide this value for each case, which depends on the dwelling type, shielding and configuration.
- The LBL models and the superposition do not represent the interaction of the environmental conditions and airtightness values realistically. This is because first, the superposition assigns equal importance to stack and wind induced infiltration and; second, the model does not account for exfiltration.

In conclusion, DOMVENT3D-4 represented a reliable correlation between air infiltration and low-pressure airtightness measurements; mainly when working with large data sets. Additionally, the model showed to be less affected by the airtightness measuring method. Finally, it is important to remark, that the findings in this study have shown that despite the model utilised and, when using low-pressure airtightness measurements (Pulse method) as input, the models are as or more accurate than when using high-pressure measurements (blower-door) as input (Table 9.1).

9.1.4 Implication of the impact of the findings on the practice.

First of all, supporting evidence on Pulse proficiency to measure airtightness has been given. The results from Pulse are comparable to those one given by the steady pressurisation method. Therefore, it is concluded that Pulse can be used in practice to measure the airtightness of buildings.

In a scenario where Pulse is accepted for use regulation and one of the infiltration models is used, a large number of measurements (and predictions) would be taken and reported across the housing stock. The efficiency of the overall stock would therefore be improved since the calculations will be more accurate, in a range of 3% $\pm$14%.

Since the error in DOMVENT3D-4 is low (maximum of 17%), it is recommended to include it within the Pulse technology; hence, in Pulse's interface, the tester should be able to input the average weather conditions to plot an immediate infiltration value, which should appear together with the airtightness value. If this is included in Pulse's algorithm and, the technology is accepted in UK regulation, the current version of SAP [Building Research Establishment, 2013] must be revised to allow the option for this.

9.2 Conclusion

A number of particular conclusions are given:

- Over two hundred Pulse tests were carried out from 2016 to 2020; there were changes in the technology during this period. However, the fundamentals were the same. The Pulse technique showed to be easy-to-use in terms of practicality and was useful when carrying out the experimental part of this investigation.
- A lengthy discussion was made on the benefits and shortcomings of the Pulse method. A quick measurement can be achieved without compromising the building's integrity; however, the lack of development makes it difficult to determine the validity of tests, and, the time required to charge the tank can be seen as a shortcoming. Further discussion has been done on the possibility of measuring airtightness at low-pressure.
- Blower door's main advantage is its development and maturity. There has been much research surrounding it; on the other hand, the facts that it has to increase the pressure and that it does not maintain the building's integrity are its main shortcomings.
- Both, the blower door and Pulse methods are accurate with reproducible results, with an RPD of 0-10%..
- Natural infiltration was seen to occur for the vast majority of time between 1.5 and 5.5 Pa of pressure difference.
- An empirical power model was created, the r^2 value was -close to- 0.7; despite this, the model could not predict new data with precision. It is concluded that an empirical model does not predict infiltration accurately. The main reason is that these models will not take into account the weather conditions, which were different for every data point.

- The simplified LBL model and DOMVENT3D were shown to be useful in predicting air infiltration rates regardless of the airtightness measuring method. Using the blower door and Pulse delivered similar results in terms of accuracy and uncertainty (Table 9.1).
- The best performing model was DOMVENT3D-4, accuracy of 3% ±14% .
- Pulse has the potential to be included in legislation; the reproducibility and accuracy have been proven. By including Pulse as an option in legislation, it will mean that different needs in the industry can be fulfilled, such as multiple testing where quick results are needed.
- This study concludes that a feature that would fit the development of Pulse, is the direct prediction of air infiltration, with immediate results; it was suggested to include the DOMVENT3D-4 model as part of the predicting algorithm.

The final answer to the research question is: there is no direct correlation between airtightness and air infiltration. Different variables interact, it was seen during the length of this thesis, that airtightness sets a base for air infiltration, and it is then modified by weather and shielding conditions. However, it was found that low pressure airtightness measurements can predict infiltration with similar accuracy as high pressure measurements. In the sensitivity analyses made, a complete interaction of variables was seen mainly for average infiltration rates, however airtightness showed to interact similarly with all the variables despite the measurement method and the pressure difference used. The main conclusion obtained is that under normal climate conditions all variables interact to develop infiltration flows, and that low pressure airtightness measurements can predict air infiltration with similar or better accuracy than high-pressure measurements.

On the other hand, infiltration models are the most reliable available option to predict infiltration. For the analyses made in this thesis, DOMVENT3D showed the choicest results and can be said that by using it, the best possible correlation can be obtained, mainly for large data sets. The results are improved if DOMVENT3D is used with low-pressure airtightness measurements given by methods such as the Pulse technique.

9.3 Future research

There are various channels for continuing this study. The Pulse method is still under development, and there is not as many research as with the blower door.

Infiltration prediction with Pulse is only a way of comparing its accuracy with traditional airtightness testing methods. The effect of wind on Pulse's measurements, the reading of background pressures, the definition of a quasi-steady period, are a few options where a research guideline can be directed.

The effect of steady and changing wind during a Pulse tests can be studied; different tests in different wind conditions with changing leakages can give insights on how Pulse performs compared to the steady pressurisation method. Wind also affects the background pressure readings, and therefore a study on the uncertainty of the background pressure readings will lead to a more accurate result within the technique; Pulse uses a pressure reference tank when analysing the pressure difference, then the uncertainty when using this tank can be revised by changing methods or materials. Finally, during the quasi-steady period in a Pulse graph is when the airtightness is calculated; studying if the quasi-steady period can be obtained in a different time frame or without the need of fully charging a tank can be useful when describing more accurate airtightness characteristics.

There is a future ahead on airtightness testing, mainly in those places where there is no legislation or characterisation of buildings. The current methods are only two ways of determining the airtightness properties of a building; however, it is unknown if more accurate techniques will be developed. The only fact is that more testing will be required in the future as the basis of predicting infiltration heat and energy losses in buildings. Many countries mainly in Asia and Latin America have no protocol for airtightness testing, and therefore, there is no airtightness regulation. Testing campaigns in different countries will eventually take place with the goal of increasing building energy efficiency. Studies such as the present can aid the policy makers in different countries to develop standards and best-practice policies to improve their building stock. For these, methodologies for large testing campaigns are to be designed; such methodologies will depend on building type, construction, year, terrain and environmental conditions. A well planned testing methodology leads to a correct characterisation and therefore more efficient regulation.

On the other hand, infiltration prediction is essential when calculating heat loss and dwelling energy efficiency. The most worrying fact demonstrated here, is how legislation, at least in the United Kingdom, has to be modified. Times have changed and with that tighter dwellings are being built. It was shown that the infiltration overprediction for airtight dwellings is considerable, and therefore, the energy efficiency is compromised. A revision of wind and shelter factors must be performed; additionally a research direction when modifying legislation is to

evaluate a simple but accurate model that can substitute the current divide-by-20 rule of thumb. A continuation of this study with a larger data set considering different locations can be useful when serving this purpose.

More interdisciplinary research about air infiltration can be performed in the air quality field. Different urban environments have different contaminants, sometimes infiltration (or exfiltration) might aid to remove them, but sometimes might take them to the indoor environment; case studies are needed. However, these are not accurate if the infiltration prediction is not accurate.

In hot climates where air conditioning is needed, understanding of infiltration can lead to more comfortable dwellings. A research on leakage paths and how infiltration varies with weather can lead to more efficient houses.

Revision of dwelling energy efficiency must include the effect of air infiltration when being reconsidered. The effect of heat transfer, energy generation, ventilation strategies, air infiltration, etc, must be considered as an interaction of all of them, and not as a result of adding them. Research of how changes in, for example, the fabric of a building affect each parameter is to be done. More accurate and complex energy models must be designed, and for that several studies must be performed.

There are still a number of paths to follow to accomplish the building's energy efficiency; nevertheless, airtightness and air infiltration research must continue to contribute to the achievement of de-carbonising the building sector in this century.

References

F. Allard, editor. *Natural ventilation in buildings: a design handbook*. James & James (Science Publishers) Ltd., London, U.K., 1998.

American Society for Testing and Materials. Standard test method for determining air change in a single zone by means of tracer gas dilution. Technical Report ASTM designation E741-11, U.S.A., 2011.

American Society for Testing and Materials. Standard test method for determining air leakage rate by fan pressurization. Technical Report ASTM designation E779-19, U.S.A., 2019.

American Society of Heating, Refrigerating and Air Conditioning Engineers. *ASHRAE Fundamentals Handbook*. ASHRAE, U.S.A., 2017.

American Society of Testing and Materials. *ASTM Book of Standards Vol. 04.07*. American Society of Testing and Materials, 1991.

ASHRAE. Technical report.

P. Baker and Ward I. Sharples, S. Air flow through cracks. *Building and Environment*, 22(4):293–304, 1987.

G. Benedetto and E. Brosio. A relation between transmission loss and air infiltration characteristics in windows. Technical report, Turin, Italy, 1981.

P. R. Bevington and D. K. Robinson. *Data reduction and error analyisis for the physical sciences*. McGraw-Hill higher education, New York, NY, U.S.A., third edition edition, 2003.

A. Blomsterberg, M. Sherman, and D. Grimsrud. A model correlating air tightness and air infiltration in houses. In *Conference on Thermal Performance of the Exterior Envelopes of Buildings*, Orlando, FL, U.S.A., 1979.

D. Bohac, M. Hewett, J. Fitzgerald, and D. Grimsrud. Measured change in multi-family unit air leakage and airflow due to air sealing and ventilation treatments. In *Proceedings of building X: Thermal Performance of the Exterior Envelopes of Whole Buildings*, Clearwater, Florida, U.S.A., 2007.

Building Research Establishment. *The Government's Standard Assessment Procedure for Energy Rating of Dwellings*. Building Research Establishment on behalf of the Deparment of Energy and Climate Change, Watford, United Kingdom., 2013.

Canadian commission on Building and Fire Codes. National energy code of canada. Technical Report NRC-CONST-56215, Ottawa, Canada, 2017.

W. Card, A. Sallman, R. Graham, and E. Drucker. Air leakage measurement of buildings by an infrasonic method. Technical Report TR-78-1, 1978.

P. Carey and D. Etheridge. Leakage measurements using unsteady techniques with particular reference to large buildings. *Building Serv. Eng. Res. Technol.*, 22: 69–82, 2001.

W. Chan, P. Prinche, M. Sohn, and A. Gadgil. Analysis of u.s. residential houses air leakage database. Technical Report Report 53367, California, U.S.A., 2003.

W. Chen, D. Claridge, C. Rohrs, and J. Liao. Modeling to predict positive pressurization required to control mold growth from infiltration in buildings in a hot and humid climate. *Building and Environment*, 104:102–113, 2016.

Y. Chiu and D. Etheridge. Calculations and notes on the quadratic and power law equations for modelling infiltration. *International Journal of Ventilation*, 1(1): 65–77, 2002.

CIBSE. Cibse guide a: Environmental design. Technical report, United Kingdom, 2015.

D. Clark. *What colour is your building? Measuring and reducing the energy carbon footprint of buildings*. RIBA Publishing, London, United Kingdom., 2013.

P. Condon, D. Grimsrud, M. Sherman, and R. Kammerud. An automated controlled-flow air infiltration measurement system. In *Proceedings of the Symposium on Air Infiltration and Air Exchange Rate Measurements*, Washington D.C., U.S.A., 1978.

E. Cooper and D. Etheridge. Masurement of building leakage by unsteady pressurisation. In *Air Infiltration and Ventilation Centre*, Prague, Czech Republic, 2004.

E. Cooper and D. Etheridge. Determining the adventitious leakage of buildings at low pressure, part 1: Uncertainties. *Building Services Engineers Research Technology*, 28:71–80, 2007a.

E. Cooper and D. Etheridge. Determining the adventitious leakage of buildings at low pressure, part 2: Pulse technique. *Building Services Engineers Research Technology*, 28:81–96, 2007b.

E. Cooper and Y. Zu. A nozzle pulse pressurisation technique for measurement of building leakage at low pressure. In *10th International Conference on Sustainable Energy Technologies*, Istanbul, Turkey, 2011.

E. Cooper, Z. Zheng, M. Gillott, and Y. Zu. A nozzle pressurization technique for measurements of building leakage at low pressures. In *35th AIVC Conference: Ventilation and Airtightness in Transforming the Building Stock to high Performance*, Poznan, Poland, 2014.

E. Cooper, X. Zheng, C. Wood, M. Gillott, D. Tetlow, S. Riffat, and L. De Simon. Field trialling of a new airtightness tester in a range of uk homes. *International Journal of Ventilation*, 18(1):1–18, 2016.

P. Das, S. Shrubsole, B. Jones, I. Hamilton, Z. Chalabi, M. Davies, A. Mavrogianni, and J. Taylor. Using probabilistic sampling-based sensitivity analyses for indoor air quality modelling. *Building and Environment*, 78:171–182, 2014.

C. Delmotte. Airtightness of buildings – considerations regarding the zero-flow pressure and the weighted line of organic correlation. In *38th AIVC conference*, Nottingham, U.K., 2017.

W. Dols, G. Walton, and Denton K. Contamw 1.0 user manual. Technical Report NISTIR 6476, Gaithersburg, MD, USA, 2000.

S. Emmerich and A. Persily. Energy impacts of infiltration & ventilation in u.s.office buildings using multizone airflow simulation. In *Proceedings IAQ and energy 98 Conference*, New Orleans, LA, U.S.A., 1998.

Energy Conservatory. Minneapolis blower door operation manual for model 3 and model 4 systems. Technical report, Minneapolis, U.S.A., 2017.

Energy Saving Trust. *Good Practice Guide 268- Energy efficient ventilation in dwellings - a guide for specifiers*. Energy Saving Trust, London, UK., 2006.

D. Etheridge. *Natural ventilation of buildings: theory, measurement and design*. Wiley and Sons, U.K., 2012.

D. Etheridge. A perspective of fifty years of natural ventilation research. *Building and environment*, 97:51–60, 2015.

J. Feijo-Muñoz, R. A. Gonzalez-Lezcano, I. Poza-Casado, M. A. Padilla-Marcos, and A. Meiss. Airtightness of residential buildings in the continental area of spain. *Building and Environment*, 148:299–308, 2019.

J. Fernandez-Aguera, S. Dominguez-Amarillo, J.J. Sendra, and R. Suarez. An approach to modelling envelope airtightness in multi-family social housing in mediterranean europe based on the situation in spain. *Energy and Buildings*, 128:236–253, 2016.

J. Fernandez-Aguera, S. Dominguez-Amarillo, J. J. Sendra, R. Suarez, and I. Oteiza. A method to quantify uncertainties in airtightness measurements: Zero-flow and envelope pressure. *Energy and Buildings*, 183:377–391, 2019.

P. Francisco and L. Palmiter. Infiltration and ventilation measurements on three electrically-heated multifamily buildings. *Proceedings ACEEE Summer Study on Energy Efficiency in Buildings*, 5:97–104, 1994.

H. Gough, Z. Luo, C. Halios, M. King, C. Noakes, C. Grimmond, J. Barlow, R. Hoxey, and A. Quinn. Field measurements of natural ventilation rate in an idealised full-scale building located in a staggered urban array: Comparison between tracer gas and pressure-based methods. *Building and Environment*, 137:246–256, 2018.

Government of Abu Dhabi. 2013 abu dhabi international energy conservation code. Technical Report ADIECC, ISBN 978-1-60983-577-4, Abu Dhabi, UAE, 2014.

F. Granne. Air and water tightness in building envelopes – evaluation of methods for quality assurance. Technical Report Report R-01/187-SE, Stockholm, KTH., 2001.

R. Grot and A. Persily. *Measured Air Infiltration and Ventilation Rates in Eight Large Office Buildings*, pages 151–183. American Society for Testing Materials, Philadelphia, U.S.A., 1986.

O. Hassan. An alternative method for evaluating the air tightness of building components. *Building and Environment*, 67:82–86, 2013.

A. Hayati, M. Mattsson, and M. Sandberg. Evaluation of the lbl and aim-2 air infiltration models on large single zones: Three historical churches. *Building and Environment*, 81:365–379, 2014.

HM government. The building regulations 2010: Conservation of fuel and power. approved document l1a. Technical Report L1A, United Kingdom, 2013.

I. Hughes and T. Hase. *Measurements and their uncertainties: a practical guide to modern error analysis*. Oxford University Press, Oxford, U.K., 2010.

International Energy Agency. Tracking buildings. Technical report, Paris, 2019a.

International Energy Agency. The critical role of buildings. Technical report, Paris, 2019b.

International Organization for Standardization. Iso 9972:2015 thermal performance of buildings - determination of air permeability of buildings- fan pressurisation method. Technical Report ISO 9972:2015, United Kingdom, 2015.

International Organization for Standardization. Iso 12569:2017 thermal performance of buildings ans materials - determination of specific aiflow rate in buildings - tracer gas dilution method. Technical Report ISO 12569:2017, United Kingdom, 2017.

V. Iordache and T. Catalina. Acoustic approach for building air permeability estimation. *Building and Environment*, 57:18–27, 2012.

ISO. Energy performance of buildings - energy needs for heating and cooling, internal temperatures and sensible and latent heat loads. Technical Report BS EN ISO 52016-1:2017, United Kingdom, 2017.

Y. Ji, L. Duanmu, and X. Li. Building air leakage analysis for individual apartments in north china. *Building and Environment*, 122:105–115, 2017.

D. Johnston and D. Miles-Shenton. The airtightness and air leakage characteristics of new uk holiday homes. *Buildin Serv. Eng. Res. Technol.*, 39(3):343–361, 2018.

D. Johnston and A. Stafford. Estimating the background ventilation rates in new-build uk dwellings - is n50/20 appropriate? *Indoor and Built Environment*, 26 (4):502–513, 2016.

J. Jokisalo, J. Kurnitski, T. Kalamees, and J. Vinha. Building leakage, infiltration and energy performance analyses for finnish detached houses. *Building and Environment*, 44(2):377–387, 2009.

B. Jones, Z. Chalabi, M. Davies, I. Hamilton, R. Lowe, A. Mavrogianni, D. Robinson, C. Shrubsole, and J. Taylor. A stochastic approach to predict the relationship between dwelling permeability and infiltration in english apartments. In *34th AIVC - 3rd TightVent - 2nd Cool Roofs - 1st Venticool Conference*, Athens, Greece, 2013a.

B. Jones, P. Das, Z. Chalabi, M. Davies, I. Hamilton, R. Lowe, J. Milner, I. Ridley, C. Shrubsole, and P. Wilkinson. The effect of party wall permeability on estimations of infiltration from air leakage. *International Journal of Ventilation*, 12(1):17–29, 2013b.

B. Jones, R. Lowe, M. Davies, Z. Chalabi, P. Das, and I. Ridley. Modelling uniformly porous facades to predict dwelling infiltration rates. *Building Services Engineering Research and Technlogy*, 35(4):408–416, 2014.

B. Jones, P. Das, Z. Chalabi, M. Davies, I Hamilton, R. Lowe, A. Mavrogianni, D. Robinson, and J. Taylor. Assessing uncertainty in housing stock infiltration rates and associated heat loss: English and uk case studies. *Building and Environment*, 92:644–656, 2015.

B. Jones, A. Persily, and M. Sherman. The origin and application of leakage-infiltration ratios. In *ASHRAE AIVC IAQ 2016, Defining Indoor Air Quality: Policy, standards and Best Practices*, Alexandria, Virginia, U.S.A., 2016.

T. Kalamees, U. Alev, and M. Parnalaa. Air leakage levels in timber frame building envelope joints. *Building and Environment*, 116:121–129, 2017.

D. Keast and H. Pei. The use of sound to locate infiltration openings in buildings. In *ASHRAE/DOE Conference: Thermal Performance of the Exterior Envelopes of Buildings*, Florida, U.S.A., 1979.

P. Keig, T. Hyde, and G. McGill. A comparison of the estimated natural ventilation rates of four solid wall houses with the measured ventilation rates and the implications flor low-energy retrofits. *Indoor and Built Environment*, 25(1): 169–179, 2016.

D. Kraniotis. *Dynamic characteristics of wind-driven air infiltration in buildings - The impact of wind gusts under unsteady wind conditions.* PhD thesis, Norwegian University of Life Sciences, Oslo, Norway, 2014.

D. Kraniotis, T. Thiis, and T. Aurlien. Wind direction and leakage distribution. a cfd transient analysis of their impact on air exchange rates under unsteady wind conditions. In *6th European - African Conference in Wind Engineering (EACWE)*, Cambridge, UK, 2013.

D. Kraniotis, T. Aurlien, and T. Thiis. Investigating instantaneous wind-driven infiltration rates using the co2 concentration decay method. *International Journal of Ventilation*, 13(2):111–124, 2014a.

D. Kraniotis, T. Thiis, and T. Aurlien. A numerical study on the impact of wind gust frequency on air exchanges in buildings with variabhle external and internal leakages. *Buildings*, 4(1):27–42, 2014b.

B. Lapillonne, K. Pollier, and N. Samci. Monitoring of energy efficiency trends for households in the eu: an analysis based on the odyssee and mure databases. Technical report, 2015.

D. Laussmann and D. Helm. *Air Change Measurements Using Tracer Gases: Methods and Results. Significance of air change for indoor air quality*, pages 365–406. InTech, 2011.

C. Lerma, E. Barreira, and R.M.S.F. Almeida. A discussion concerning active infrared thermography in the evaluation of buildings air infiltration. *Energy and Buildings*, 168:56–66, 2018.

M. Liddament. Air infiltration calculation techniques an applications guide. Technical report, Coventry, United Kingdom, 1986.

M. Liddament. Aida. *Air Infiltration Review*, 11(1), 1989.

M. Liddament. A guide to energy efficient ventilation. Technical report, 1996.

M. Liddament and C. Allen. Technical note aic 11: The validation and comparison of mathematical models of air infiltration. Technical report, Great Britain, 1983.

W. Liu, X. Zhao, and Q. Chen. A novel method for measuring air infiltration rate in buildings. *Energy and Buildings*, 168:309–318, 2018.

J. Logue, M. Sherman, I. Walker, and B. Singer. Energy impacts of envelope tightening and mechanical ventilation for the u.s. residential sector. *Energy and Buildings*, 65:281–291, 2013.

J. Love, J. Wingfield, A.Z.P. Smith, P. Biddulph, T. Oreszczyn, R. Lowe, and C.A. Elwell. 'hitting the target and missing the point': Analysis of air permeability data for new uk dwellings and what it reveals about the testing procedure. *Energy and Buildings*, 155:88–97, 2017.

R. Lowe. Ventilation strategy, energy use and co2 emissions in dwellings - a theoretical approach. *Building services engineering research and technology*, 21 (3):179–185, 2000.

M. Lyberg. Basic air infiltration. *Building and Environment*, 32(2):95–100, 1997.

B. Mattsson. A transient pressurisation method for measurements of airtightness. *Journal of Building Physics*, 31(1):35–53, 2007.

J. McWilliams. Review of airflow measurement techniques. Technical Report LBNL-49747, California, U.S.A., 2003.

Ministerio de vivienda y urbanismo. Estándares de construcción sustentable para viviendas de chile. tomo ii energía. Technical Report ISBN: 978-956-9432-46-0, Santiago, Chile, 2018.

E. Moller, T. Rasmussen, and A. Nicolajsen. A simplified method using compressed air to determine air leakage. In *Buildings XI Proceedings*, 2010.

Byron J. T. Morgan. *Applied stochastic modelling*. CRC Press, Boca Raton, FL, U.S.A., second edition edition, 2009.

K. J. Moss. *Heat and Mass Transfer in Buildings*. ITaylor and Francis Ltd, London, United Kingdom, 2007.

T. Nishioka, Q. Chen, N. Arai, K. Fujiwara, N. Unemiya, and R. Okura. Unsteady pressuriation method to measure the airtightness of the building envelope. *Research in Building Physics*, 2003.

H. Okuyama and Y. Onishi. Uncertainty analysis and optimum concentration decay term for air exchange rate measurements: Estimation methods for effective volume and infiltration rate. *Building and Environment*, 49:182–192, 2012.

M. Orme and N. Leksmono. *AIVC guide 5: Ventilation modelling data guide*. International Energy Agency, AIVC, Brussels, Belgium, 2005.

M. Orme, M. Liddament, and A. Wilson. An analysis and data summary of the aivc's numerical database. Technical Report Technical Note 44, Coventry, U.K., 1994.

L. Palmiter. Mass flow for aida. *Air Infiltration Review*, 11(2), 1990.

W. Pan. Relatioship between air-tightness and its influencing factors of post-2006 new-build dwellings in the uk. *Building and Environment*, 45:2387–2399, 2010.

A. Persily, A. Musser, and D. Leber. A collection of homes to represent the u.s. housing stock. Technical Report NISTIR 7330, Washington, U.S.A., 2006.

M. Prignon, A. Dawans, S. Altomonte, and G. Van Moeseke. A method to quantify uncertainties in airtightness measurements: Zero-flow and envelope pressure. *Energy and Buildings*, 188-189:12–24, 2019.

G. Raman, K. Chelliah, M. Prakash, and R. Muehleisen. Detection and quantification of building air infiltration using remote acoustic methods. In *Inter Noise 2014*, Melbourne, Australia, 2014.

N.M.M. Ramos, R.M.S.F. Almeida, A. Curado, P.F. Pereira, S. Manuel, and J. Maia. Airtightness and ventilation in a mild climate country rehabilitated social housing buildings e what users want and what they get. *Building and Environment*, 92:97–110, 2015.

RDH Building Engineering Ltd. Air leakage control in multi-unit residential buildings. Technical report, Vancouver, Canada, 2013.

F. Remi Carrie and V. Leprince. Uncertainties in building pressurization tests due to steady wind. *Energy and Buildings*, 116:656–665, 2016.

M. Ringger and P. Hartmann. Evaluation of an acoustical method for detecting air leaks. *Air Infiltration Review*, 11(1), 1989.

A. Salehi, I. Torres, and A. Ramos. Experimental analysis of building airtightness in traditional residential portuguese buildings. *Energy and Buildings*, 151:198–205, 2017.

A. Saltelli, K. Chan, and Scott E.M., editors. *Sensitivity analysis*. Willey series in probability and statistics. Wiley & Sons Ltd., West Sussex, England., 2003.

M. Sandberg and C. Blomqvist. A quantitative estimate of the accuracy of tracer gas methods for the determination of the ventilation flow rate in buildings. *Building and Environment*, 20(3):139–150, 1985.

M. Sandberg and J. Sundberg. The use of detector tubes with carbon dioxide as a tracer gas. *Air Infiltration Review*, 8(3), 1987.

M. Santamouris and D. Asimakopoulos. *Passive Cooling of Buildings*. James & James (Science Publishers) Ltd., 1996.

S. Sharples and Thompson D. Experimental study of crack flow with varying pressure differentials. In *Proceedings: Optimum Ventilation and Air Flow Control in Buildings, 17th Air Infiltration and Ventilation Centre Conference*, Gothenburg, Sweden, 1996.

C. Shaw. A correlation between air infiltration and air-tightness for houses in a developed residential area. Technical report, Ottawa, Canada, 1981.

M. Sherman. *Air infiltration in buildings*. PhD thesis, Lawrence Berkeley Laboratory, University of California, Berkeley, California, U.S.A., oct 1980.

M. Sherman. Air infiltration research at the lawrence berkeley laboratory. Technical Report EEB-epb 83-6, California, U.S.A., 1983.

M. Sherman. Estimation of infiltration from leakage and climate indicators. *Energy and Buildings*, 10:81–86, 1987.

M. Sherman. Uncertainty in air flow calculations using tracer gas measurements. *Building and Environment*, 24(4):347–354, 1989.

M. Sherman. Single-zone stack-dominated infiltration modelling. In *Proceedings 12th Air Infiltration and Ventilation Conference*, Ottawa, Canada, 1991.

M. Sherman. Air infiltration measurement techniques. Technical Report LBL-10705, California, U.S.A., 1998.

M. Sherman. On the valuation of infiltration towards meeting residential ventilation needs. Technical report, California, U.S.A., 2008.

M. Sherman and B. Dickinson. The prediction of air infiltration. In *Proceedings of the CLIMA 2000 Conference*, Copenhagen, Denmark, 1985.

M. Sherman and D. Grimsrud. Infiltration-pressurization correlation: simplified physical modelling. In *Conference of the American Society of Heating, Refrigeration and Air Conditioning Engineers*, Denver, Colorado, U.S.A., 1980.

M. Sherman and D. Grimsrud. Wind and infiltration interaction for small buildings. In *Annual Meeting of the American Society of Civil Engineers*, New Orleans, U.S.A., 1982.

M. Sherman and M. Modera. Low frequency measurement of the leakage in enclosures. *Review of Scientific Instruments.*, 57(7):557–561, 1986.

M. Sherman and M. Modera. Signal attenuation due to cavity leakage. *The Journal of the Acoustical Society of America*, 84(6):2163–2169, 1988.

M. Sherman and L. Palmiter. Uncertainties in fan pressurization measurements. *Airflow Performance of Building Envelopes, Components and Systems*, ASTM STP 1255:266–283, 1995.

D. Sinott and M. Dyer. Air-tightness field data for dwellings in ireland. *Building and Environment*, 51:269–275, 2012.

K. Siren. A modification of the power law equation to account for large-scale wind turbulence. In *Ventilation and Cooling, 18th Air Infiltration and Ventilation Centre Conference*, Athens, Greece, 1997.

T. Sonoda and F. Peterson. A sonic method for building air-leakage measurements. *Appl Energy*, 22(3):205–224, 1986.

Standards Council of Canada. Standard test method for determining air leakage rate by fan pressurization. Technical Report AN/CGSB-149.15-96, Canada, 1996.

Standards New Zealand. Thermal insultation - housing and small buildings. Technical Report NZS 4218:2009, New Zealand, 2009.

Ali Murat Tanyer, A. Tavukcuoglu, and M. Bekboliev. Assessing the airtightness performance of container houses in relation to its effect on energy efficiency. *Building and Environment*, 134:59–73, 2018.

The Air Tightness Testing and Measurements Association. Technical standar l1: Measuring air permeability of buildings - fan pressurization method. Technical Report BS EN ISO 9972:2015, Buckinghamshire, United Kingdom, 2016.

W. Turner, M. Sherman, and I. Walker. Infiltration as ventilation: Weather-induced dilution. *HVAC&R Research*, 18(6):1122–1135, 2012.

United Nations. Paris agreement. Technical report, 2015.

United Nations' World Commission on Environment and Development. Technical report.

R. Urquhart, R. Richman, and G. Finch. The effect of an enclosure retrofit on air leakage rates for a multi-unit residential case-study building. *Energy and Buildings*, 86:35–44, 2015.

K. Varshney, J. Rosa, I. Shapiro, and D. Scott. Air-infiltration measurements in buildings using sound transmission loss through small apertures. *International Journal of Green Energy*, 10(5):482–493, 2013.

A. Vega Pasos, X. Zheng, V. Sougkakis, M. Gillott, J. Meulemans, O. Samin, F. Alzetto, L. Smith, S. Jackson, and C. Wood. Experimental investigation of the impact of environmental conditions on the measurement of building infiltration, and its correlation with airtightness. In *39th AIVC Conference Proceedings*, Juan-les-Pins/Antibes, France, 2018a.

A. Vega Pasos, X. Zheng, V. Sougkakis, M. Gillott, J. Meulemans, O. Samin, F. Alzetto, L. Smith, S. Jackson, and C. Wood. Experimental study on the measurement of building infiltration and air leakage rates (at 4 and 50 pa) by means of tracer gas, blower door and the novel pulse technique in a detached uk home. In *39th AIVC Conference Proceedings*, Juan-les-Pins/Antibes, France, 2018b.

A. Vega Pasos, X. Zheng, M. Gillott, and C. Wood. Experimental study on the pressure differential at which building air leakage should be measured. In *SET (Sustainable Energy Technlogies) 2019 Conference Proceedings*, Kuala Lumpur, Malaysia, 2019a.

A. Vega Pasos, X. Zheng, M. Gillott, and C. Wood. Comparison between infiltration rate predictions using the divide-by-20 rule of thumb and real measurements. In *40th AIVC Conference Proceedings*, Ghent, Belgium, 2019b.

A. Vega Pasos, X. Zheng, B. Jones, M. Gillott, and C. Wood. On the experimental validation of the infiltration model domvent3d. In *40th AIVC Conference Proceedings*, Ghent, Belgium, 2019c.

J. Vinha, E. Manelius, M. Korpi, K. Salminen, M. Kurnitski, J. Kiviste, and A. Laukkarinen. Airtigthness of residential buildings in finland. *Building and Environment*, 93:128–140, 2015.

I. Walker and D. Wilson. Aim-2 the alberta air infiltration model. Technical Report Report 71, 1990.

I. Walker and D. Wilson. Evaluating models for superposition of wind and stack effects in air infiltration. *Building and Environment*, 28(2):201–210, 1993.

I. Walker and D. Wilson. Field validation of algebraic equations for stack and wind driven air infiltration calculations. *ASHRAE HVAC&R Research Journal*, 4(2):119–140, 1998.

I. Walker, D. Wilson, and M. Sherman. A comparison of the power law to quadratic formulations for air infiltration calculations. *Energy and Buildings*, 27(3):293–299, 1997.

W. Wang, I. Beausoleil-Morrison, and J. Reardon. Evaluation of the alberta air infiltration model using measurements and inter-model comparisons. *Building and Environment*, 44:309–318, 2009.

Y Watanabe, H. Kobayashi, and Y. Utsumi. Development of validation of acpressurization measuring of leakage area of houses. In *Proceedings: BuildingSimulation '99, Sixth International IBPSA Conference*, Kyoto, Japan, 1999.

C. Wood, X. Zheng, A. Vega Pasos, Y. Hsu, and L. Smith. An extended pressure range comparison of the blower door and novel pulse method for measuring the airtightness of two outdoor chambers with different levels of airtightness. In *39th AIVC Conference Proceedings*, Juan-les-Pins/Antibes, France, 2018.

X. Zheng, I. Wallis, and C. Wood. Experimental study of enclosure airtightness of an outdoor chamber using the pulse technique and blower door method under various leakage and wind conditions. In *39th AIVC Conference Proceedings*, Juan-les-Pins/Antibes, France, 2018.

X. Zheng, E. Cooper, J. Mazzon, I. Wallis, and C. J Wood. Experimental insights into the airtightness measurement of a house-sized chamber in a sheltered environment using blower door and pulse methods. *Building and Environment*, 162, 2019a.

X. Zheng, E. Cooper, Y. Zu, M. Gillott, D. Tetlow, S. Riffat, and C. J Wood. Experimental studies of a pulse pressurisation technique for measurig building airtightness. *Future Cities and Environment*, 5:1–17, 2019b.

Appendices

Appendix A

Temperature correction code

The following code is the ones used to obtain all the raw data from different files stored in a folder in the personal computer of the author. This code also overwrites the files to include the corrected temperatures. This code is only valid for those files containing Pulse raw data in the right spreadsheet format used once the Pulse data is exported.

```
% Getting the results when the temperature is corrected
% Specify the folder where the files live.
myFolder = 'C:\Users\ezxaev\OneDrive - The University of Nottingham\Alan
Vega\PhD Building Technology\Field tests\Tracer gas\BTS Field trials\MATLAB\Tests';
% Check to make sure that folder actually exists. Warn user if it doesn't. if
isdir(myFolder)
 errorMessage = sprintf('Error: The following folder does not exist:\n %s',
myFolder);
 uiwait(warndlg(errorMessage));
 return;
end
% Get a list of all files in the folder with the desired file name pattern.
filePattern = fullfile(myFolder, '*.xlsx'); % Change to needed pattern
theFiles = dir(filePattern);
for k = 1 : length(theFiles)
 baseFileName = theFiles(k).name;
 fullFileName = fullfile(myFolder, baseFileName);
 fprintf(1, 'Now reading % s \n', fullFileName);
Tam = xlsread(fullFileName,'Data Dump & Results','F8'); T0A=Tam+3;
P1=xlsread(fullFileName,'PULSE 1 PROCESSED','I19');
P2=xlsread(fullFileName,'PULSE 2 PROCESSED','I19');
```

```
P3=xlsread(fullFileName,'PULSE 3 PROCESSED','I19');
DeltaP1=P1-P2;
TempFall1=(15.077.*log(DeltaP1))+27.552;
Warmingeffect1=0.2807.*(Tam-(T0A-TempFall1))-8.1002;
T0B=T0A-TempFall1+Warmingeffect1; DeltaP2=P2-P3;
TempFall2=(15.077.*log(DeltaP2))+27.552;
Warmingeffect2=0.2807.*(Tam-(T0B-TempFall2))-8.1002;
T0C=T0B-TempFall2+Warmingeffect2;
xlswrite(fullFileName,T0A,'Data Dump & Results','F9');
xlswrite(fullFileName,T0B,'Data Dump & Results','F11');
xlswrite(fullFileName,T0C,'Data Dump & Results','F13');
 end
```

Writing results in the Pulse test files

```
% Specify the folder where the files live.
myFolder = 'C:\Users\ezxaev\OneDrive - The University of Nottingham\Alan
Vega\PhD Building Technology\Field tests\Tracer gas\BTS Field trials\MATLAB\Tests';
% Check to make sure that folder actually exists. Warn user if it doesn't.
if  isdir(myFolder)
 errorMessage = sprintf('Error: The following folder does not exist:\n % s',
myFolder);
 uiwait(warndlg(errorMessage));
 return;
end
% Get a list of all files in the folder with the desired file name pattern.
filePattern = fullfile(myFolder, '*.xlsx'); % Change to whatever pattern you
need.
theFiles = dir(filePattern);
for k = 1 : length(theFiles)
 baseFileName = theFiles(k).name;
 fullFileName = fullfile(myFolder, baseFileName);
 fprintf(1, 'Now reading %s\n', fullFileName);
ID = string(baseFileName);
C3 = xlsread(fullFileName,'Data Dump & Results','F8');
C4 = xlsread(fullFileName,'Data Dump & Results','F9');
C5 = xlsread(fullFileName,'Data Dump & Results','F11');
C6 = xlsread(fullFileName,'Data Dump & Results','F13');
A = [ID C3 C4 C5 C6];
```

```
all(k,:) = A;
filename = 'Summary of results 2.xlsx';
end
colheader = 'ID', 'Room temp', 'P1 tank temp', 'P2 tank temp', 'P3 tank temp';
xlswrite(filename, colheader, 'Sheet1', 'A1');
 xlswrite(filename, all, 'Sheet1', 'A2');
```

Appendix B

Tracer gas tests in the case study house

The tracer gas constant concentration tests were carried out according to International Organization for Standardization [2017], the calculations were done accordingly. Results were compared first against the temperature difference occurring during the tests.

In addition, the measured infiltration rates were calculated agains the changing wind.

Figures B.15 and B.30 only show the infiltration rate when the requirements were accomplished.

For the concentration decay tests, the calculations were made using the regression method given in both standards [American Society for Testing and Materials, 2011, International Organization for Standardization, 2017], the following images include the calculation of the uncertainty of the regression and the confidence limits with a 99% level of confidence. The infiltration rate is given by the slope in the best fit linear equation of the regression; such equation is given in the figures.

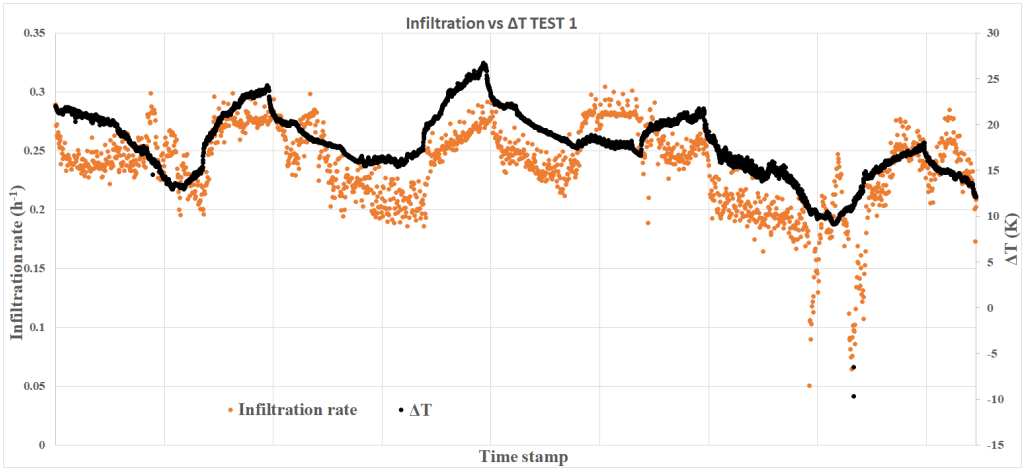


Figure B.1: Comparison between occurring temperature difference and measured infiltration rate in test 1

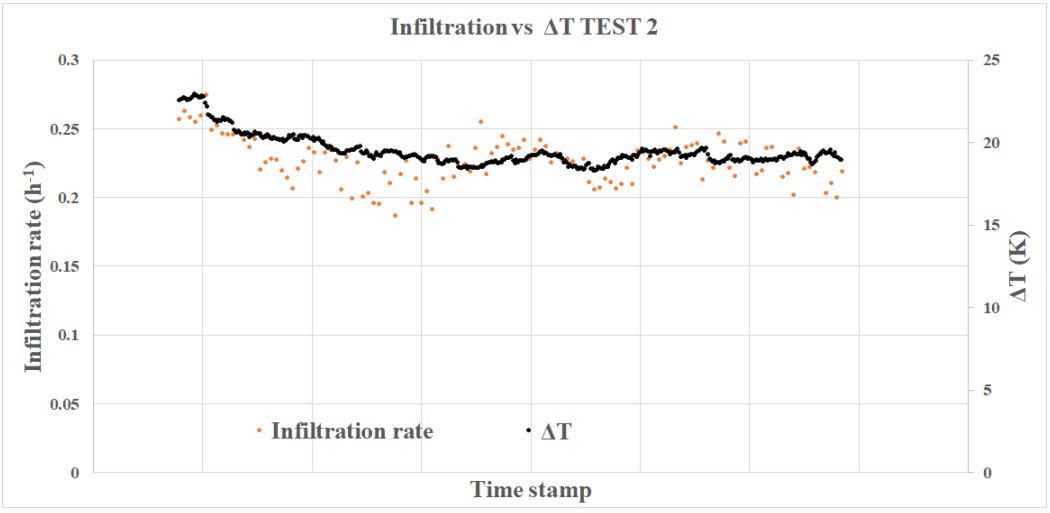


Figure B.2: Comparison between occurring temperature difference and measured infiltration rate in test 2

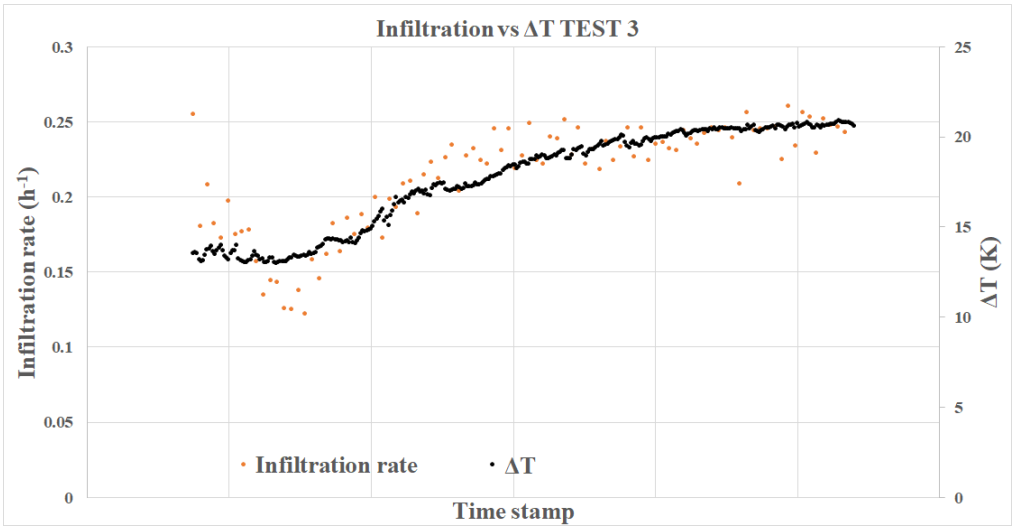


Figure B.3: Comparison between occurring temperature difference and measured infiltration rate in test 3

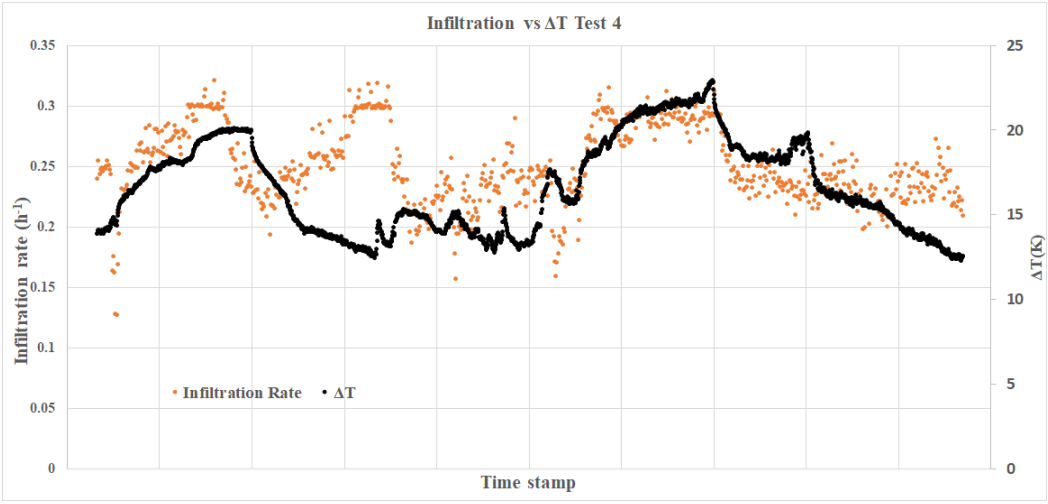


Figure B.4: Comparison between occurring temperature difference and measured infiltration rate in test 4

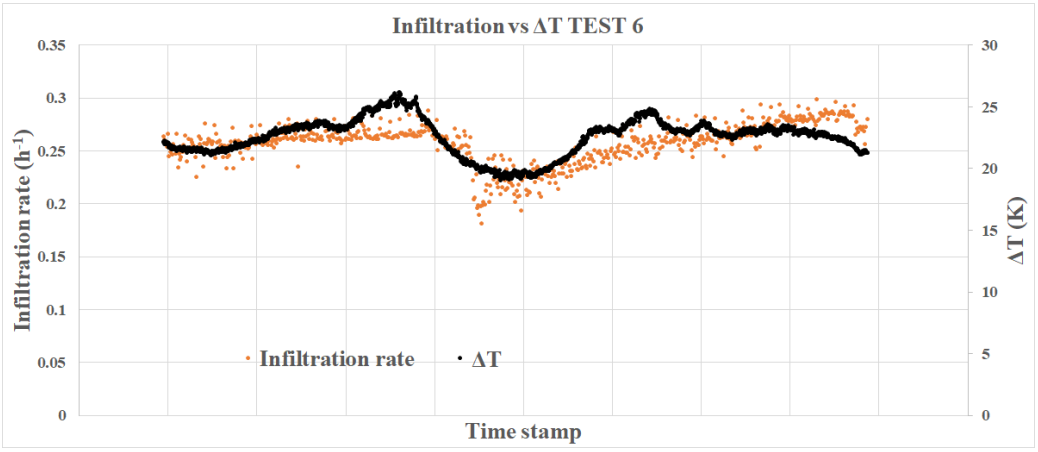


Figure B.5: Comparison between occurring temperature difference and measured infiltration rate in test 6

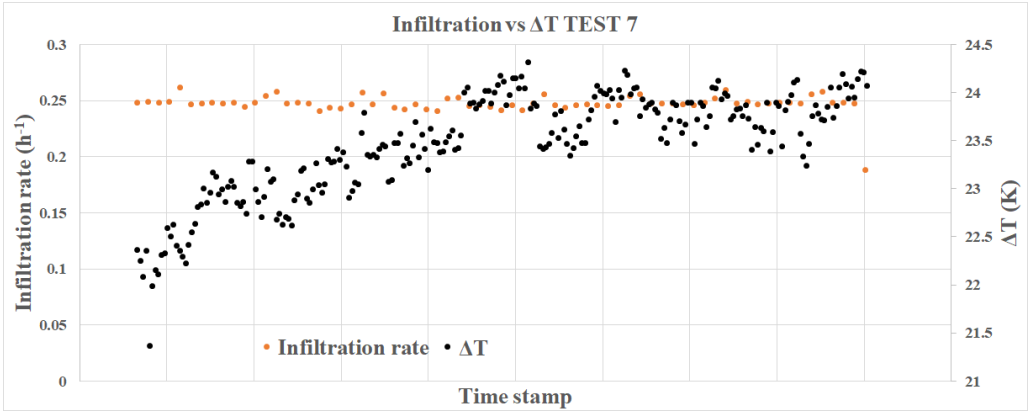


Figure B.6: Comparison between occurring temperature difference and measured infiltration rate in test 7

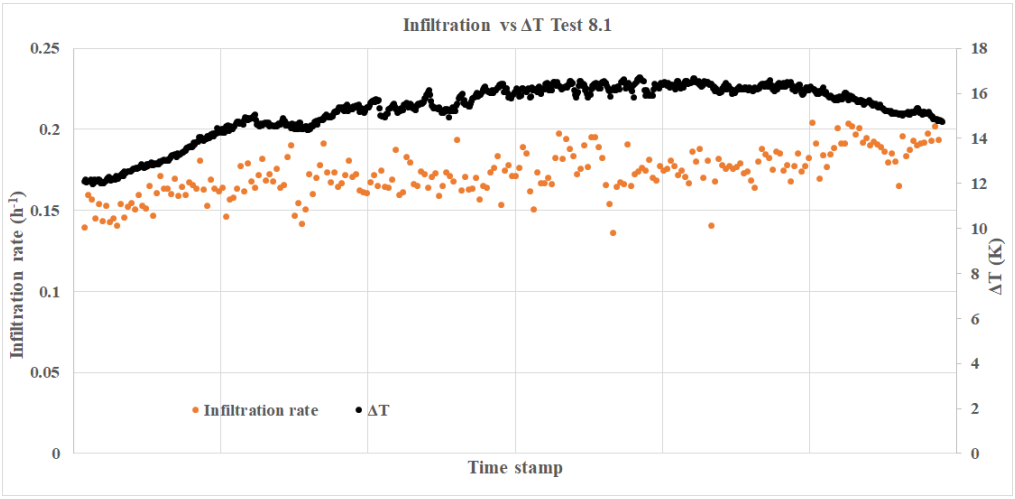


Figure B.7: Comparison between occurring temperature difference and measured infiltration rate in test 8.1

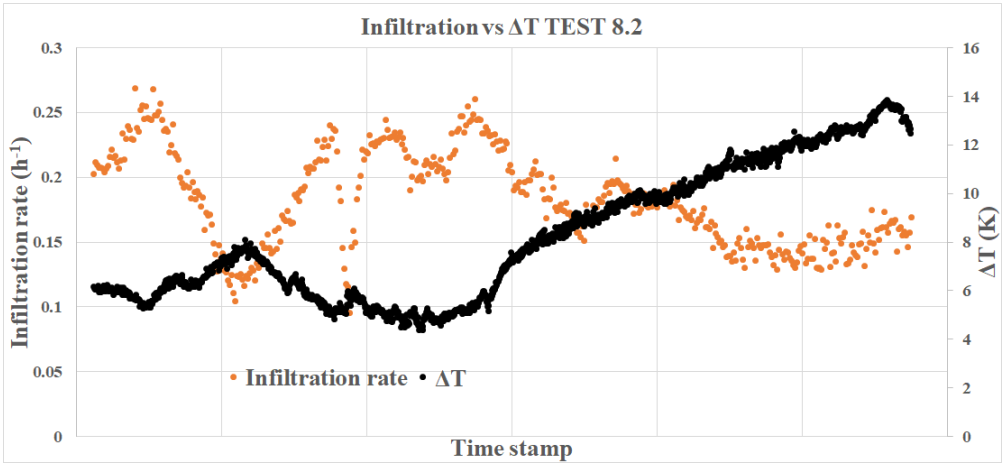


Figure B.8: Comparison between occurring temperature difference and measured infiltration rate in test 8.2

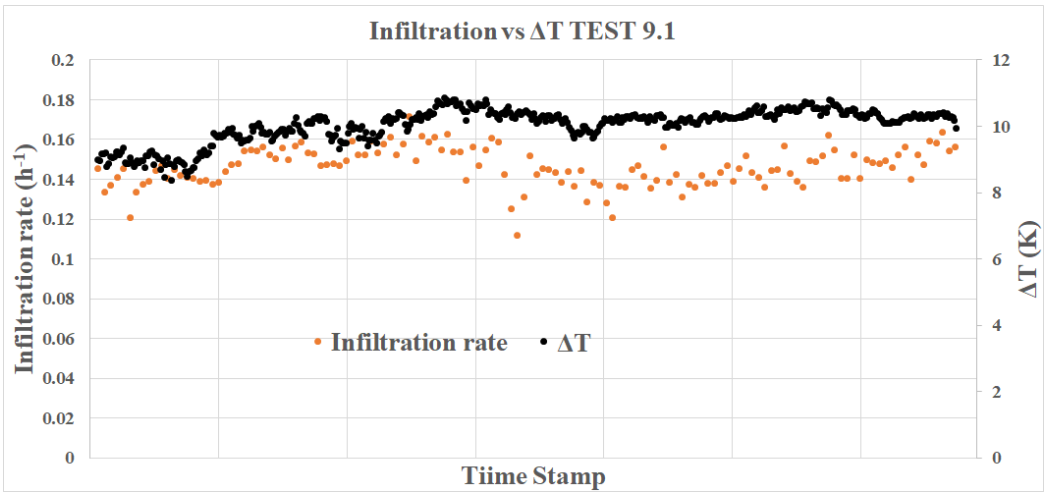


Figure B.9: Comparison between occurring temperature difference and measured infiltration rate in test 9.1

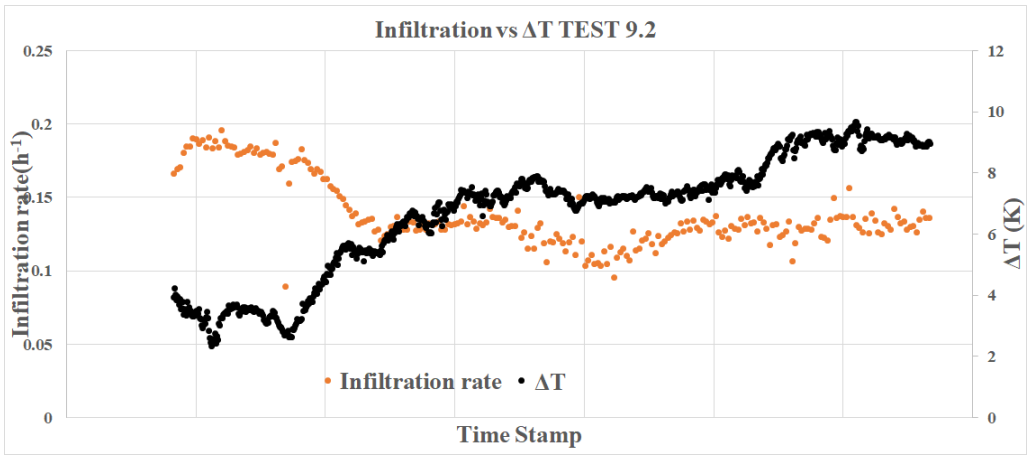


Figure B.10: Comparison between occurring temperature difference and measured infiltration rate in test 9.2

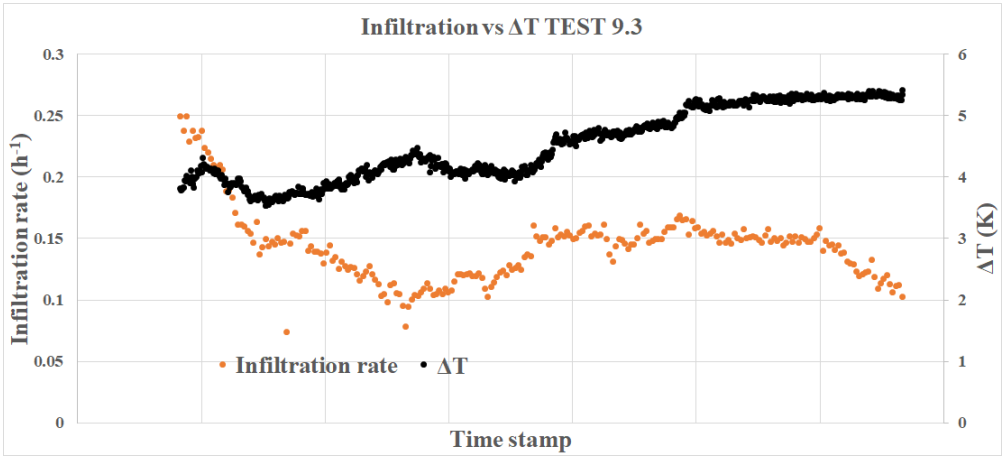


Figure B.11: Comparison between occurring temperature difference and measured infiltration rate in test 9.3

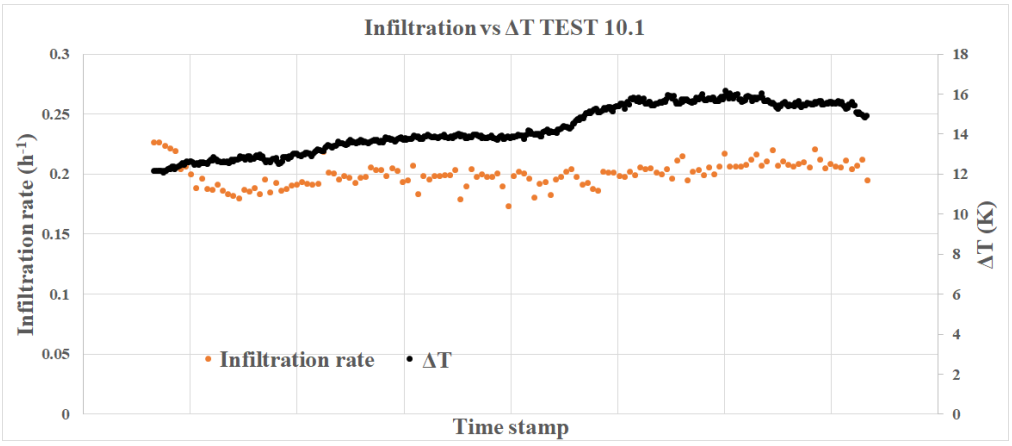


Figure B.12: Comparison between occurring temperature difference and measured infiltration rate in test 10.1

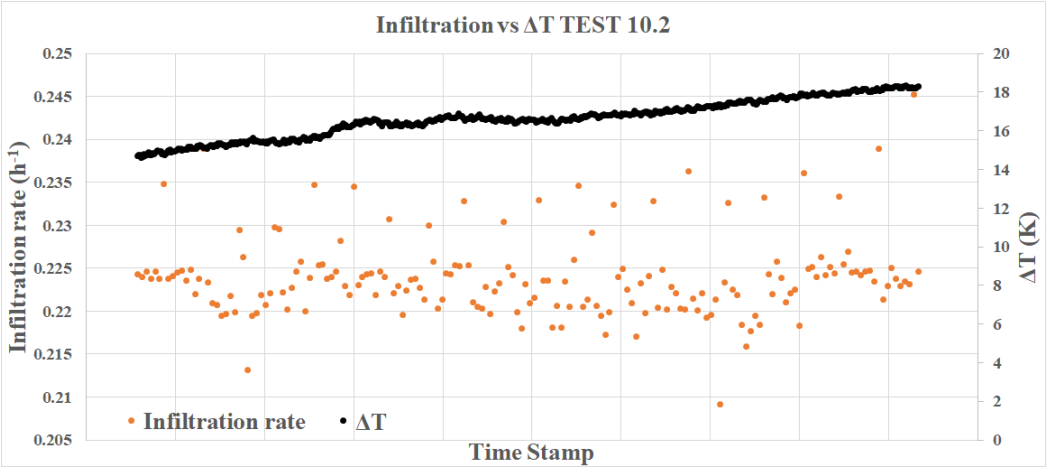


Figure B.13: Comparison between occurring temperature difference and measured infiltration rate in test 10.2

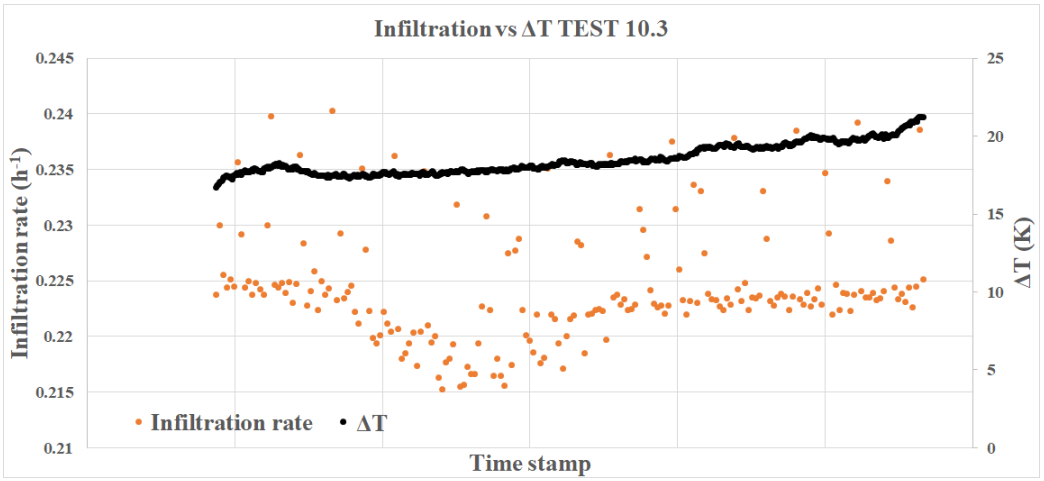


Figure B.14: Comparison between occurring temperature difference and measured infiltration rate in test 10.3

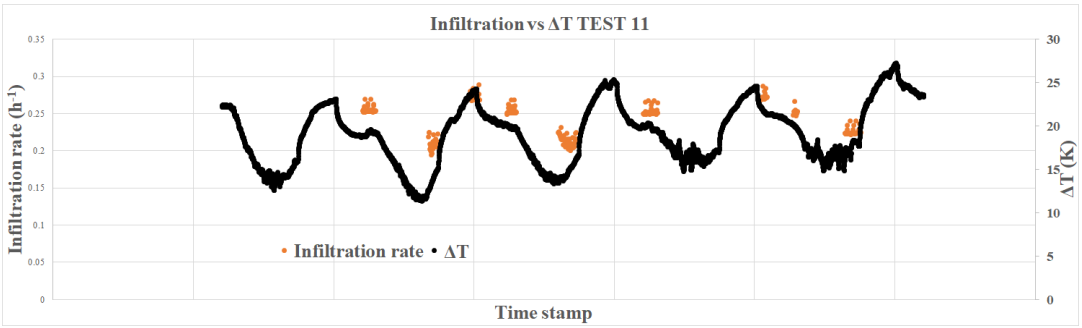


Figure B.15: Comparison between occurring temperature difference and measured infiltration rate in test 11

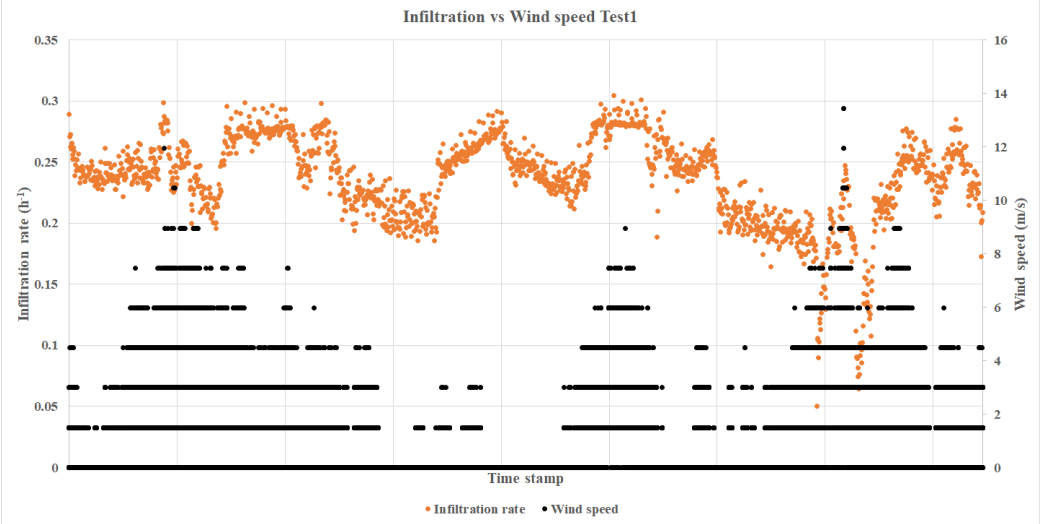


Figure B.16: Comparison between occurring wind velocities and measured infiltration rate in test 1

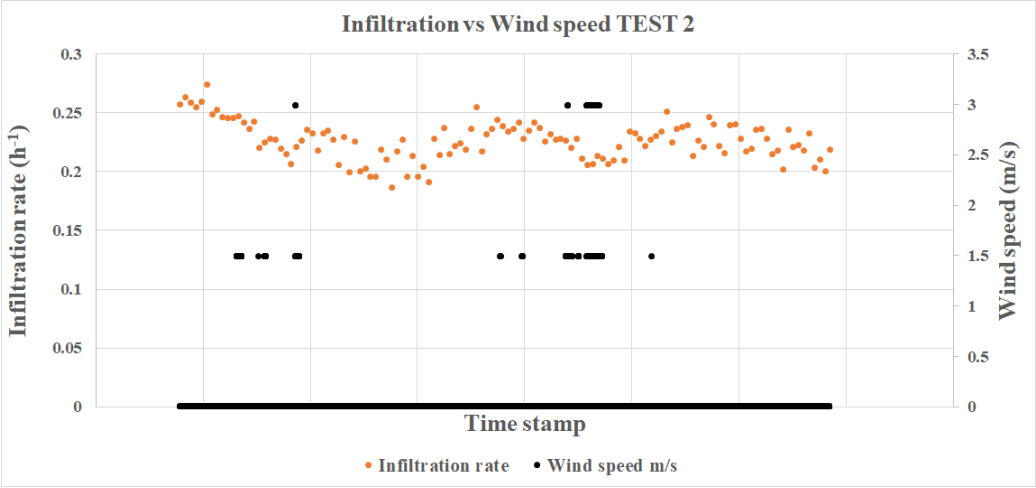


Figure B.17: Comparison between occurring wind velocities and measured infiltration rate in test 2

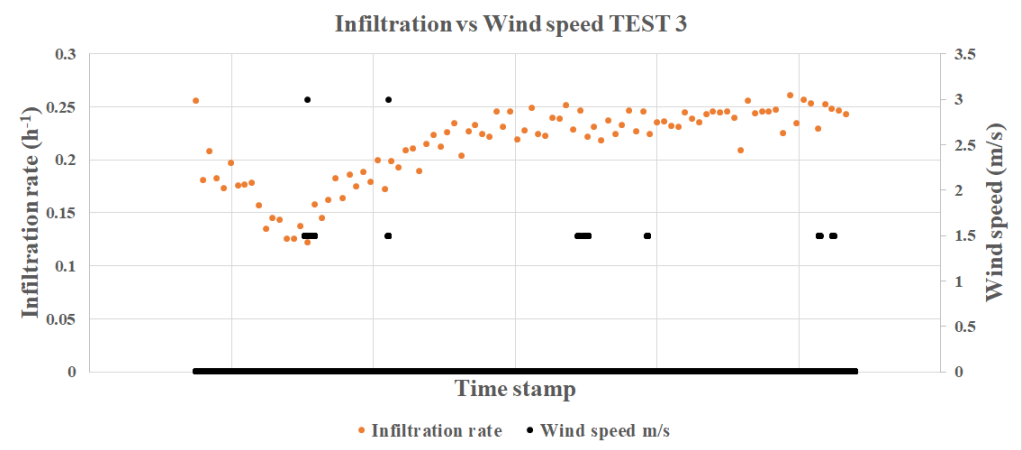


Figure B.18: Comparison between occurring wind velocities and measured infiltration rate in test 3

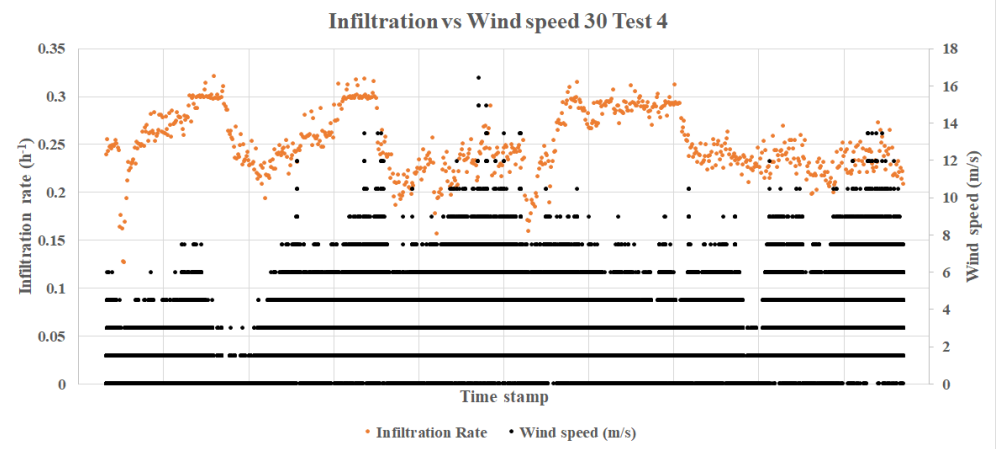


Figure B.19: Comparison between occurring wind velocities and measured infiltration rate in test 4

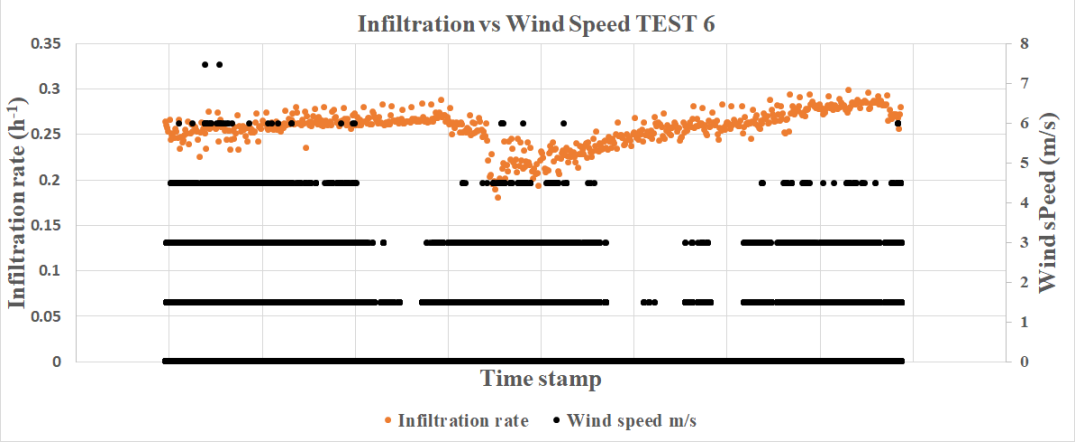


Figure B.20: Comparison between occurring wind velocities and measured infiltration rate in test 6

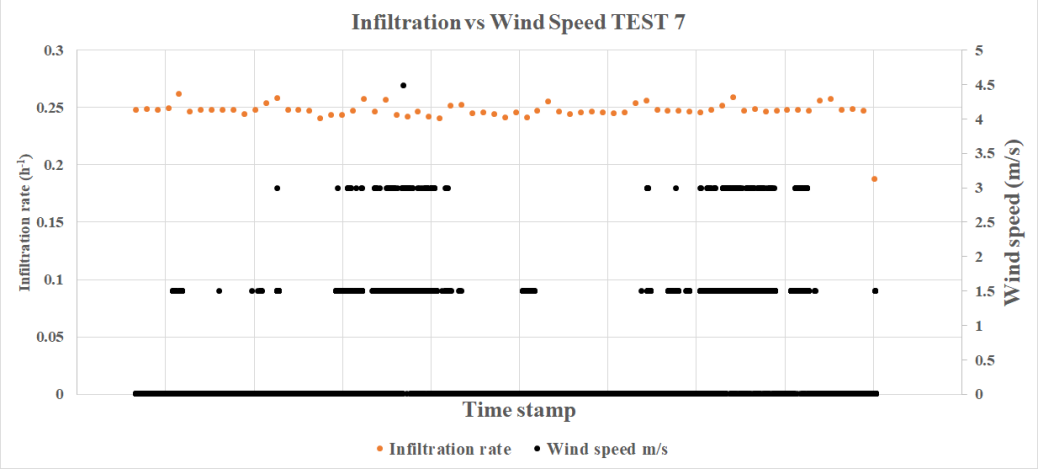


Figure B.21: Comparison between occurring wind velocities and measured infiltration rate in test 7

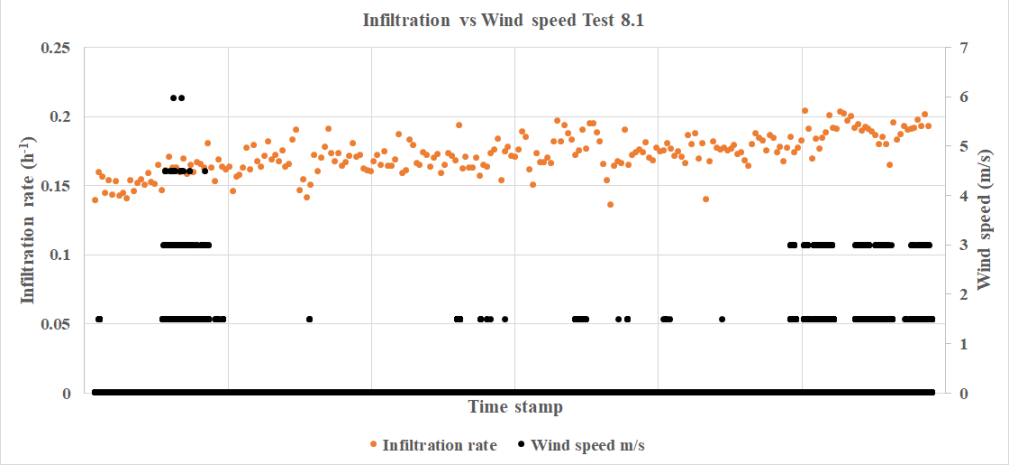


Figure B.22: Comparison between occurring wind velocities and measured infiltration rate in test 8.1

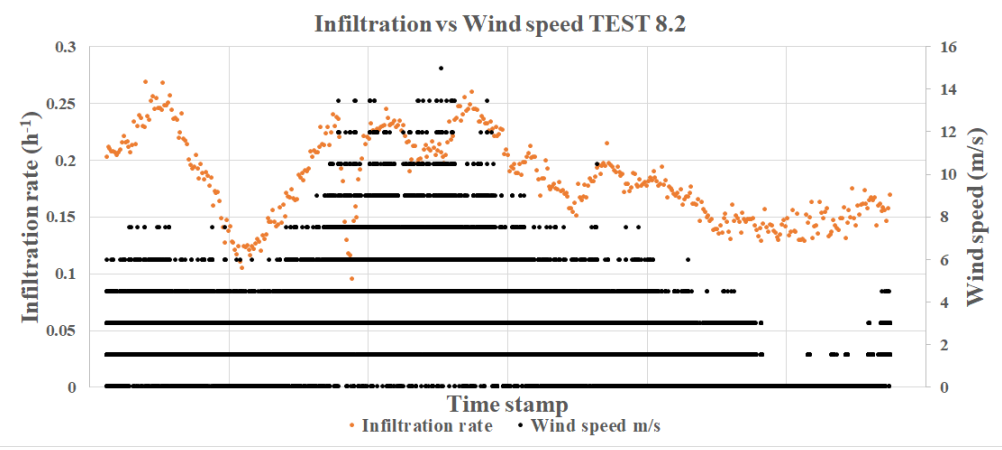


Figure B.23: Comparison between occurring wind velocities and measured infiltration rate in test 8.2

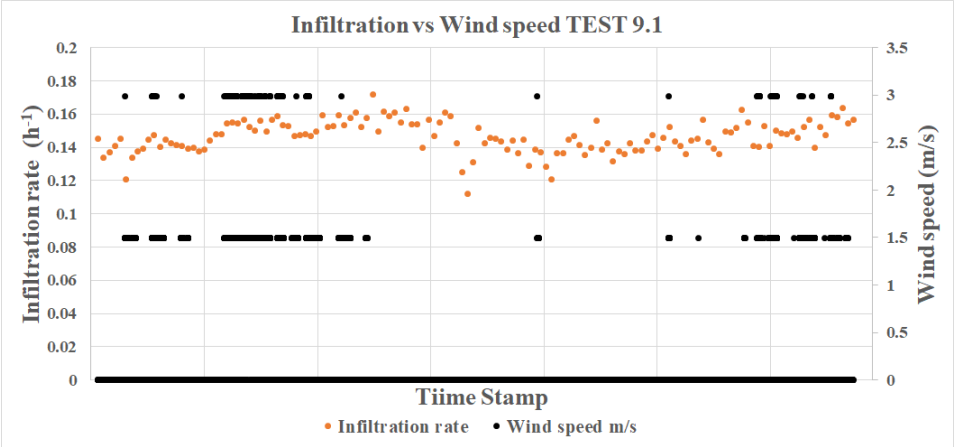


Figure B.24: Comparison between occurring wind velocities and measured infiltration rate in test 9.1

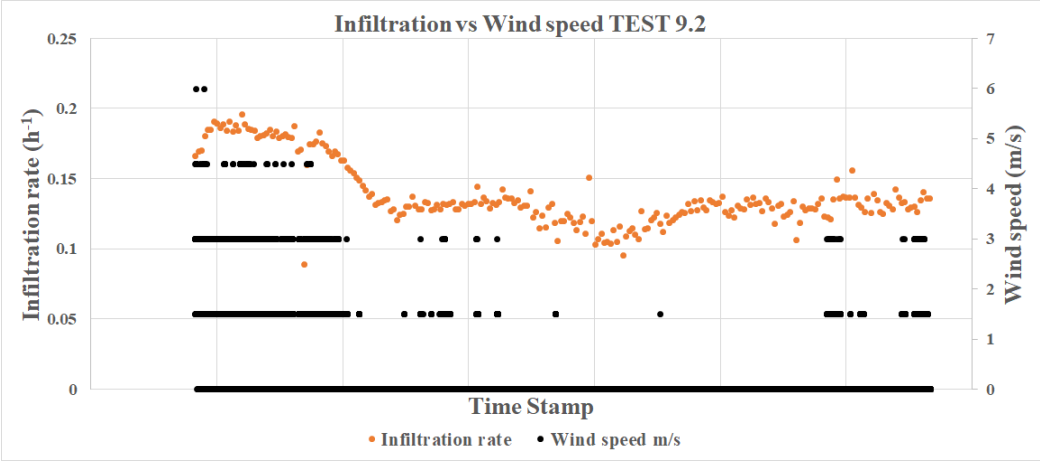


Figure B.25: Comparison between occurring wind velocities and measured infiltration rate in test 9.2

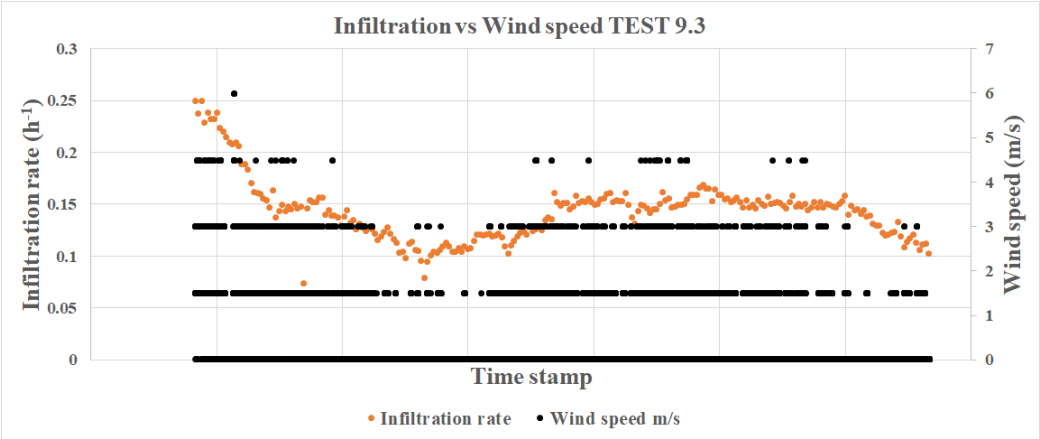


Figure B.26: Comparison between occurring wind velocities and measured infiltration rate in test 9.3

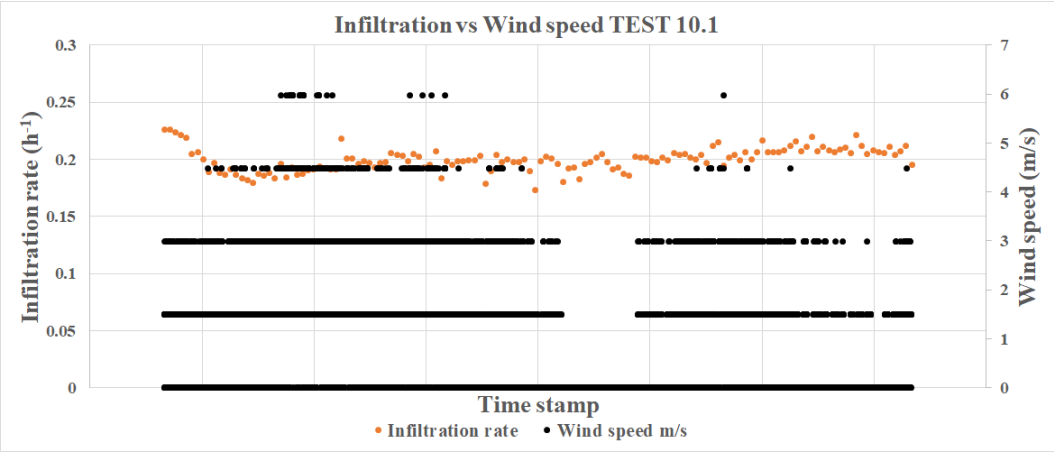


Figure B.27: Comparison between occurring wind velocities and measured infiltration rate in test 10.1

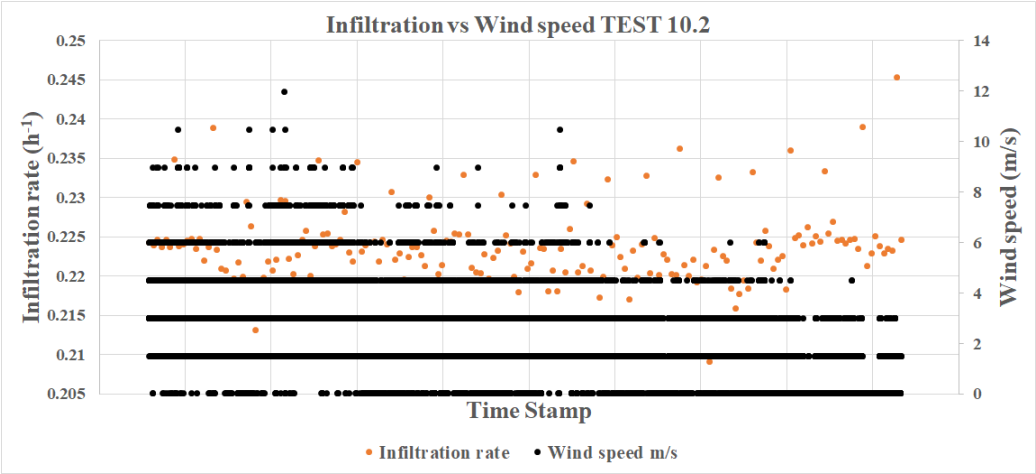


Figure B.28: Comparison between occurring wind velocities and measured infiltration rate in test 10.2

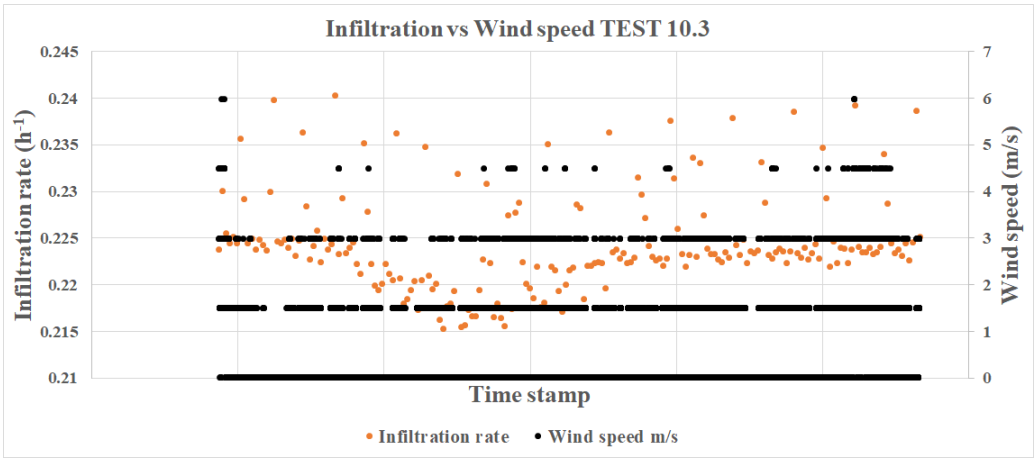


Figure B.29: Comparison between occurring wind velocities and measured infiltration rate in test 10.3

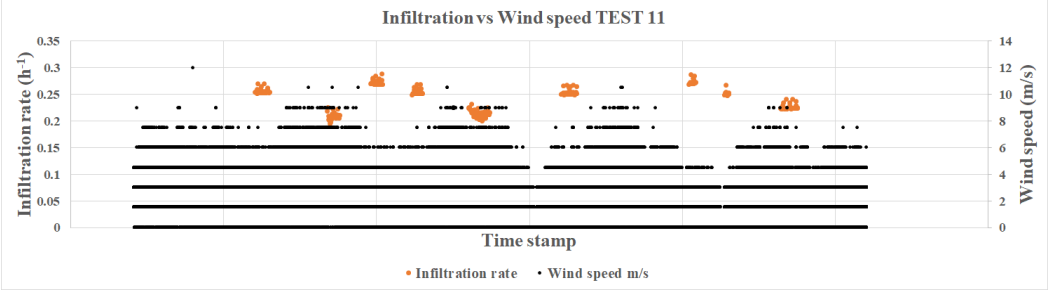


Figure B.30: Comparison between occurring wind velocities and measured infiltration rate in test 11

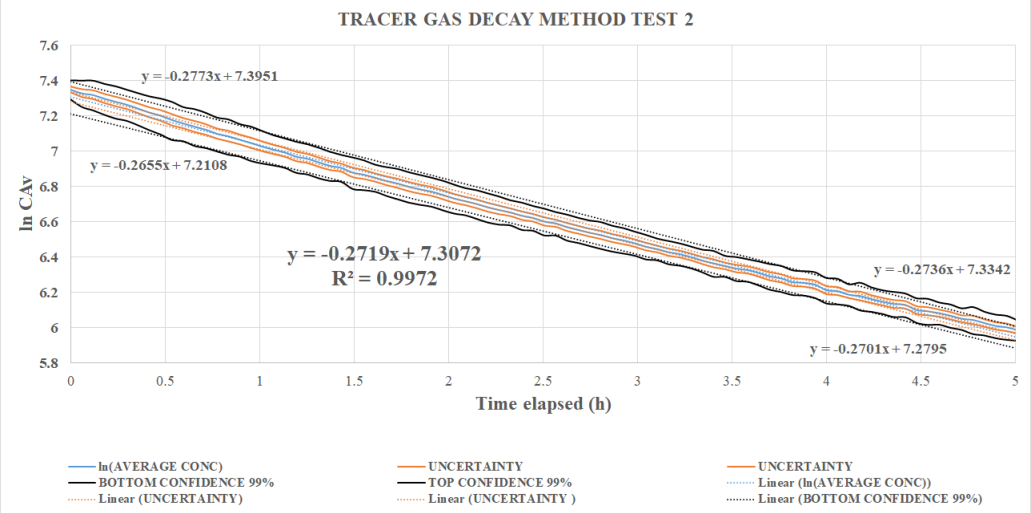


Figure B.31: Tracer gas concentration decay calculation for test 2

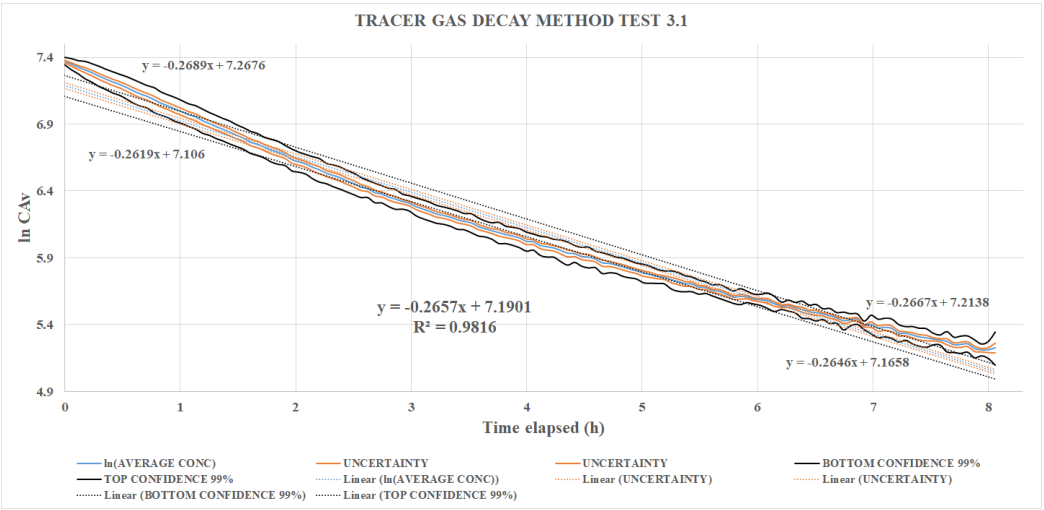


Figure B.32: Tracer gas concentration decay calculation for test 3.1

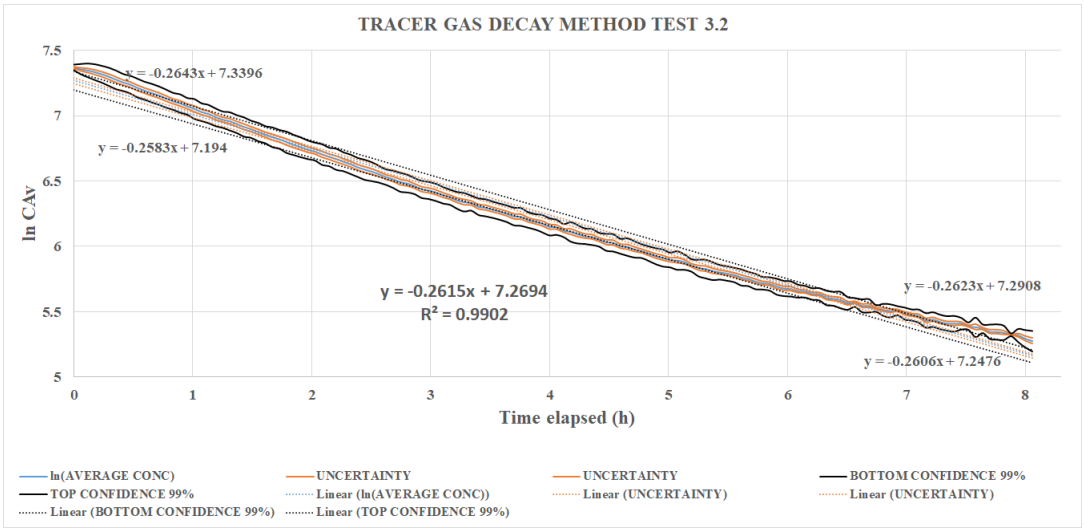


Figure B.33: Tracer gas concentration decay calculation for test 3.2

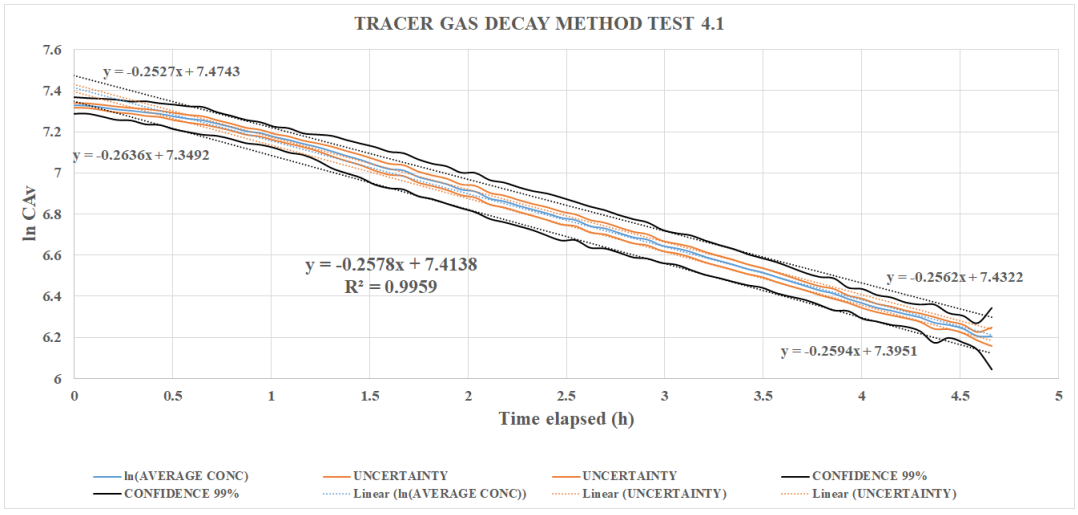


Figure B.34: Tracer gas concentration decay calculation for test 4.1

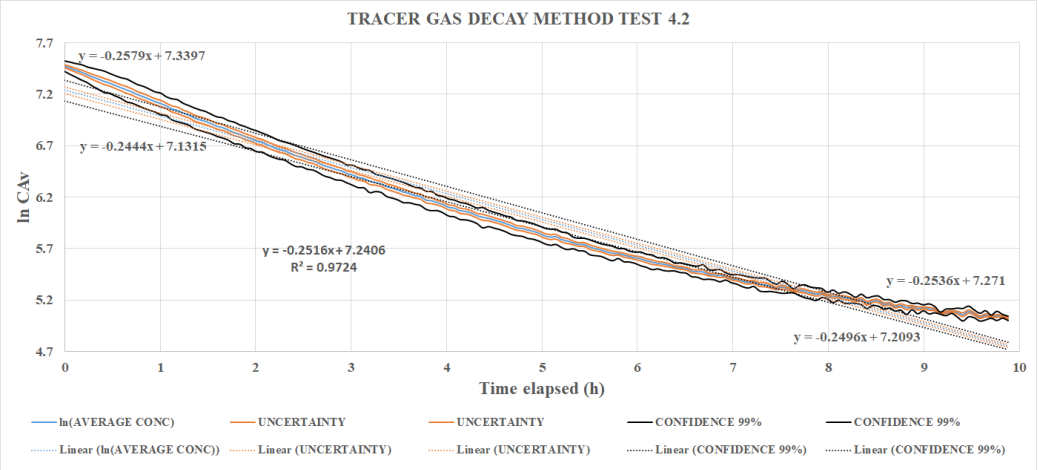


Figure B.35: Tracer gas concentration decay calculation for test 4.2

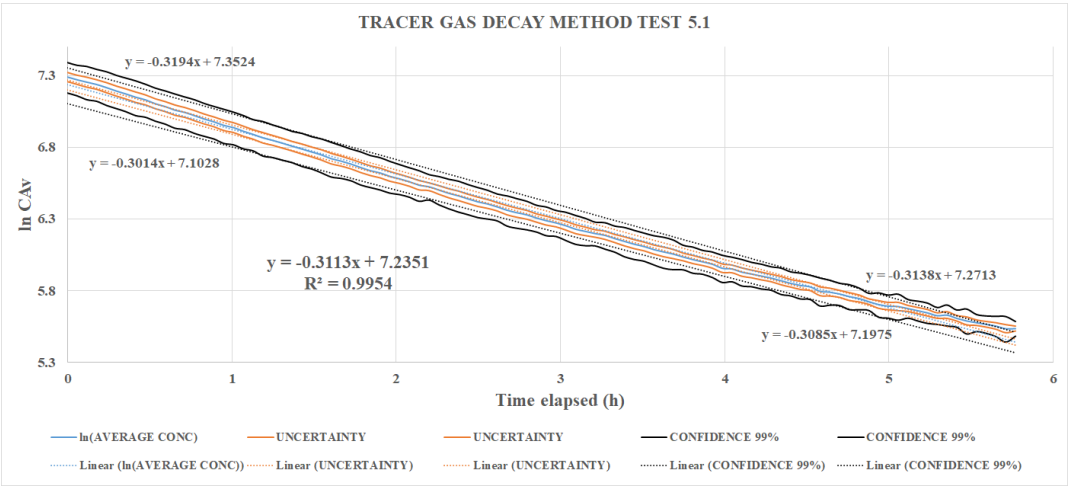


Figure B.36: Tracer gas concentration decay calculation for test 5.1

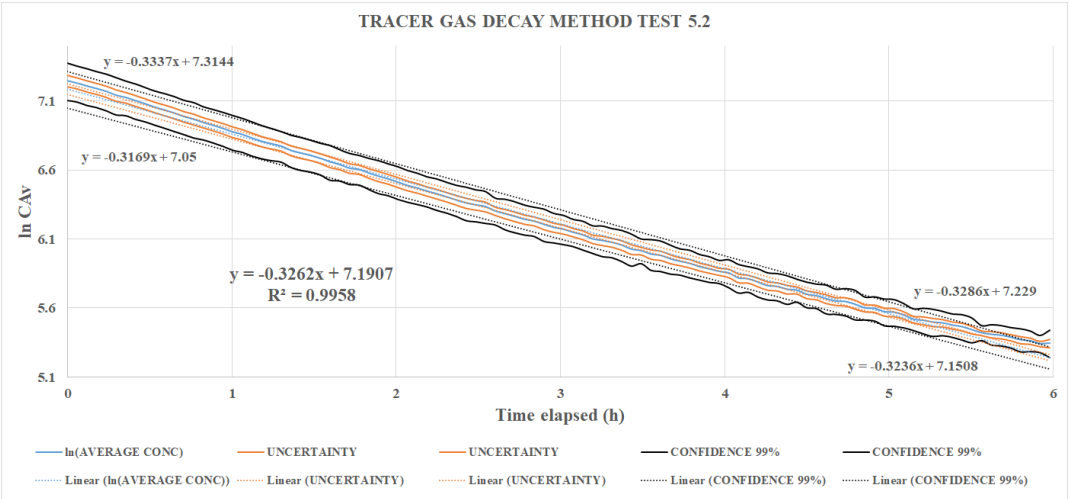


Figure B.37: Tracer gas concentration decay calculation for test 5.2

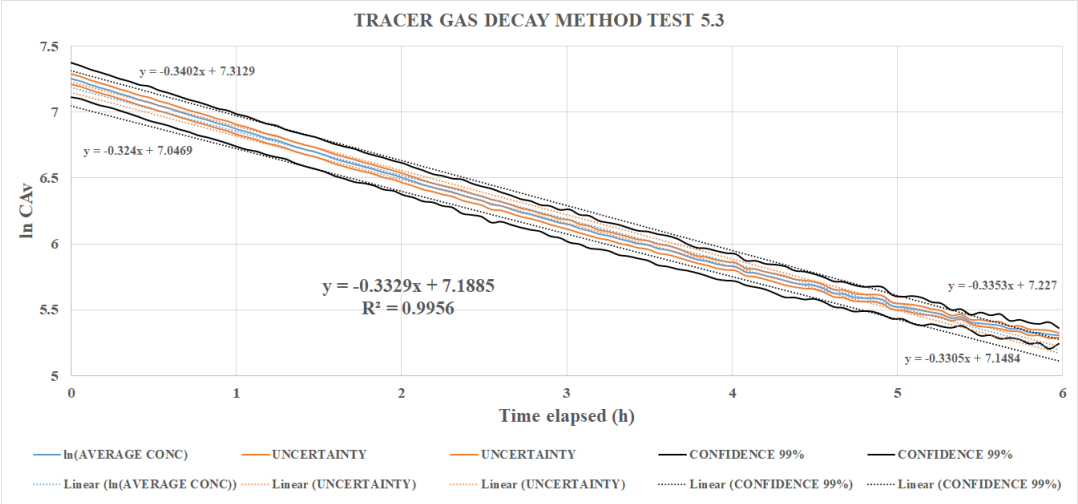


Figure B.38: Tracer gas concentration decay calculation for test 5.3

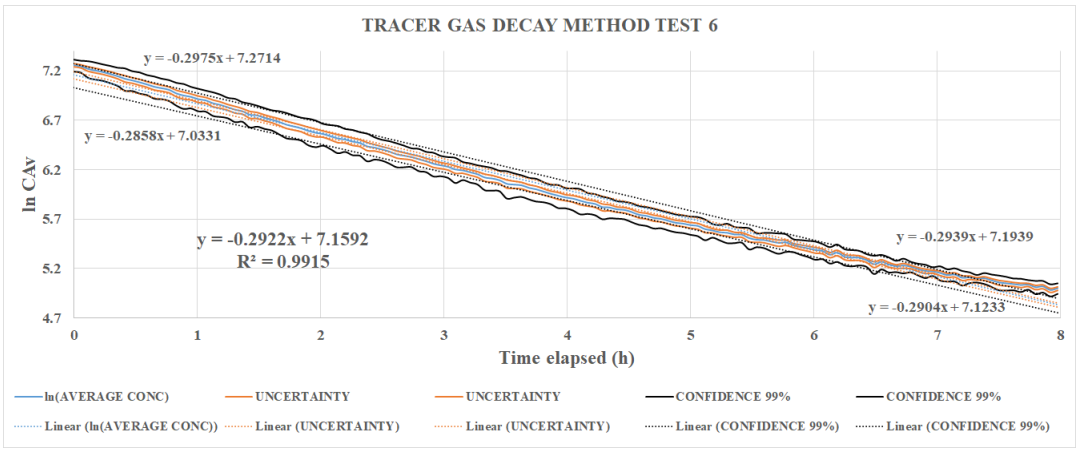


Figure B.39: Tracer gas concentration decay calculation for test 6

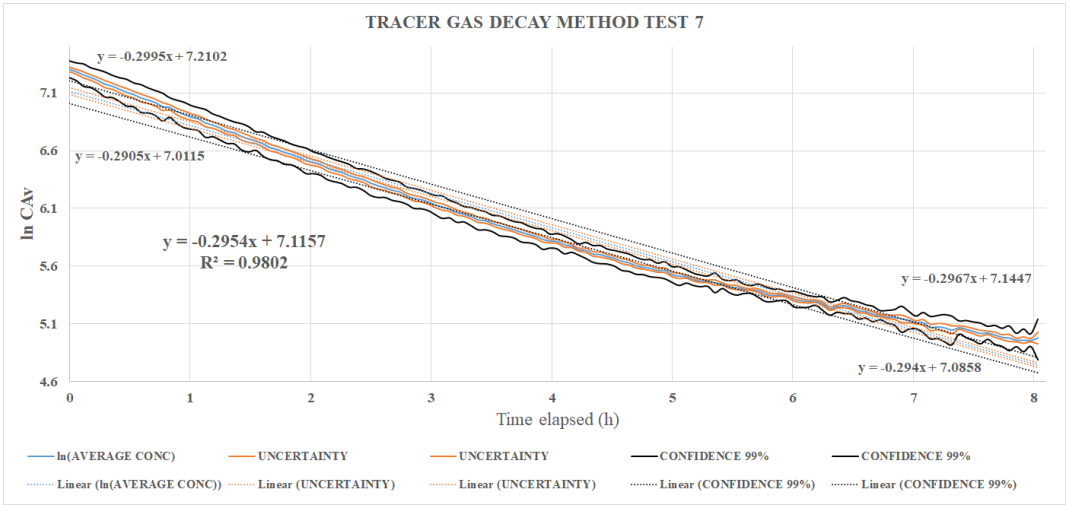


Figure B.40: Tracer gas concentration decay calculation for test 7

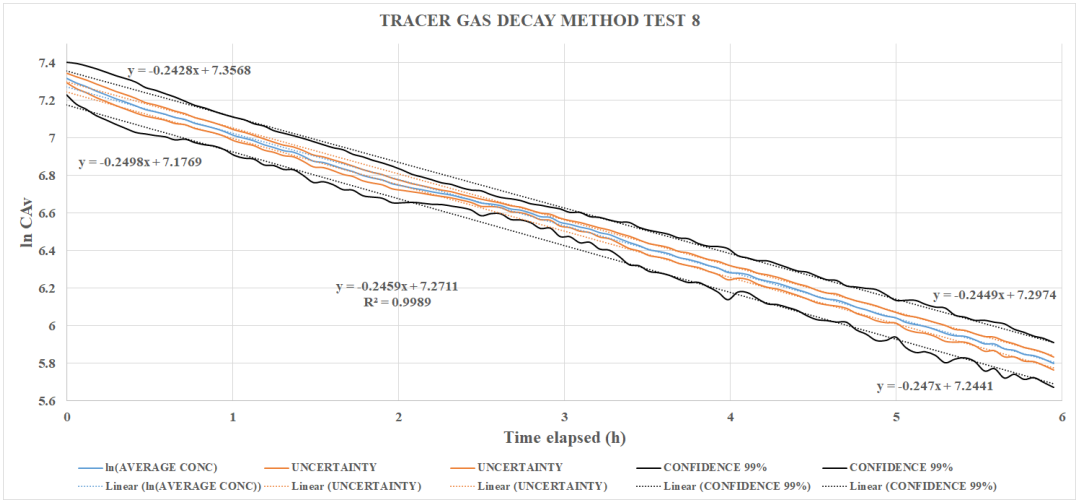


Figure B.41: Tracer gas concentration decay calculation for test 8

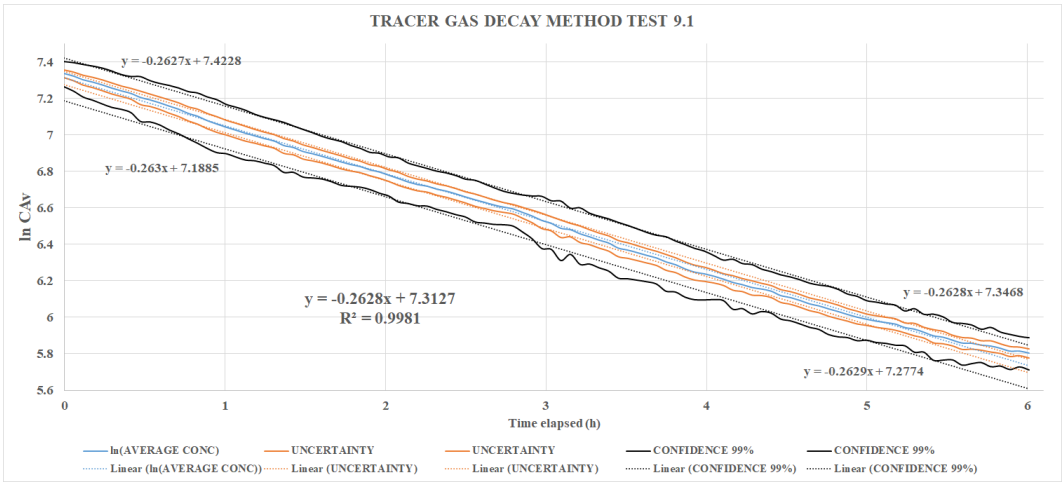


Figure B.42: Tracer gas concentration decay calculation for test 9.1

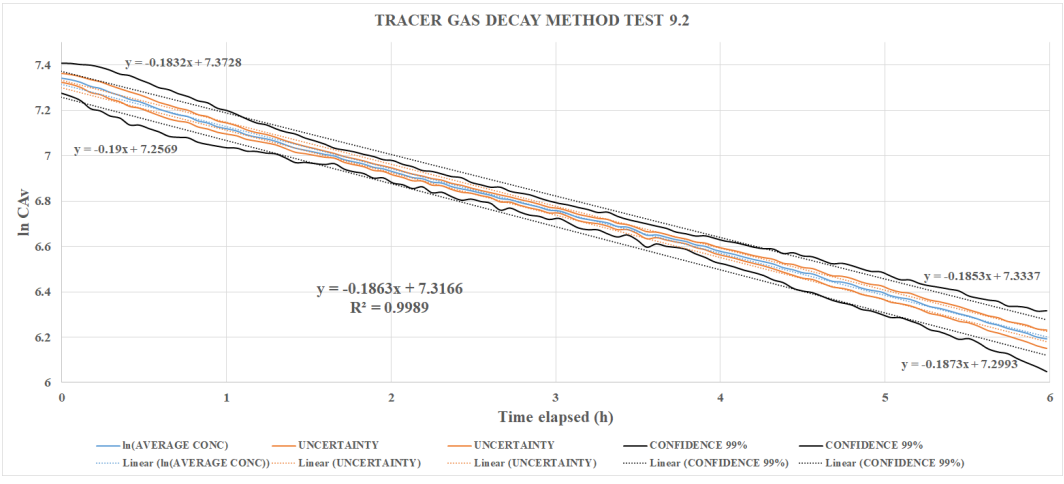


Figure B.43: Tracer gas concentration decay calculation for test 9.2

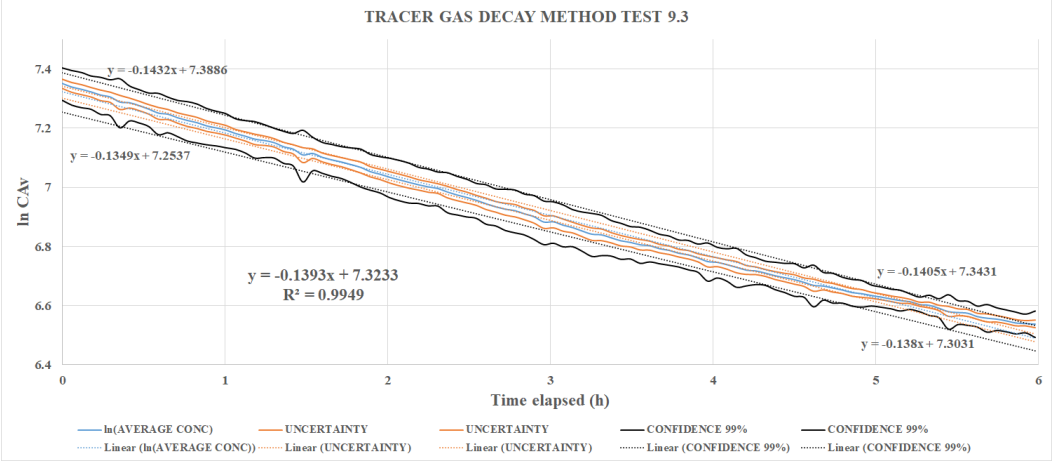


Figure B.44: Tracer gas concentration decay calculation for test 9.3

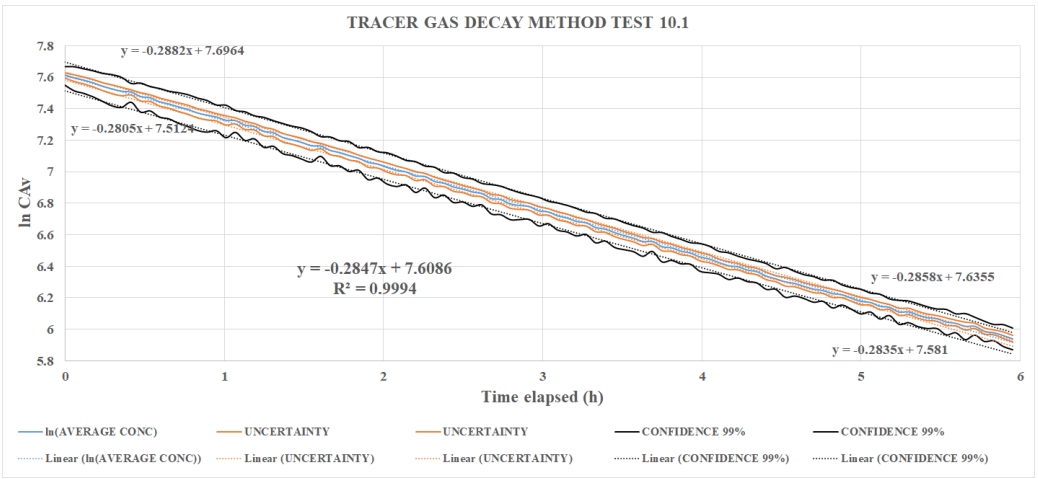


Figure B.45: Tracer gas concentration decay calculation for test 10.1

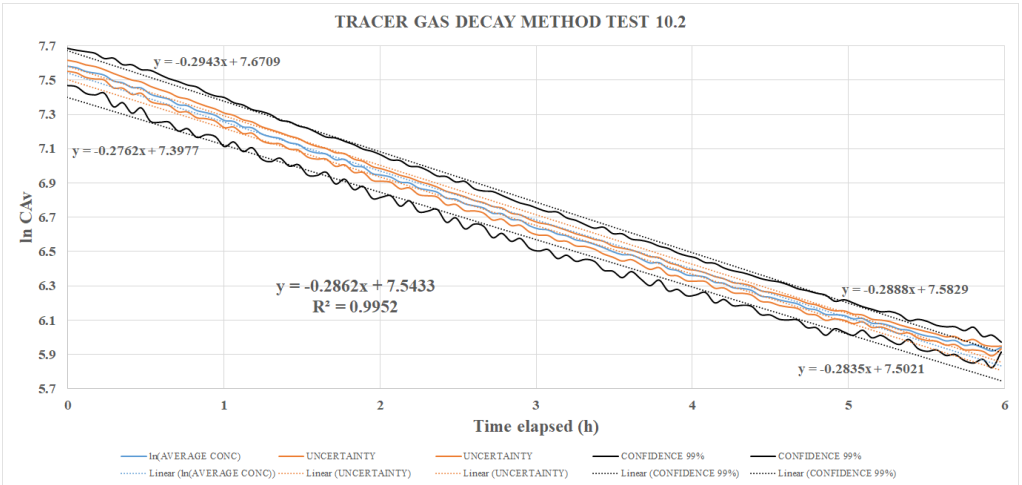


Figure B.46: Tracer gas concentration decay calculation for test 10.2

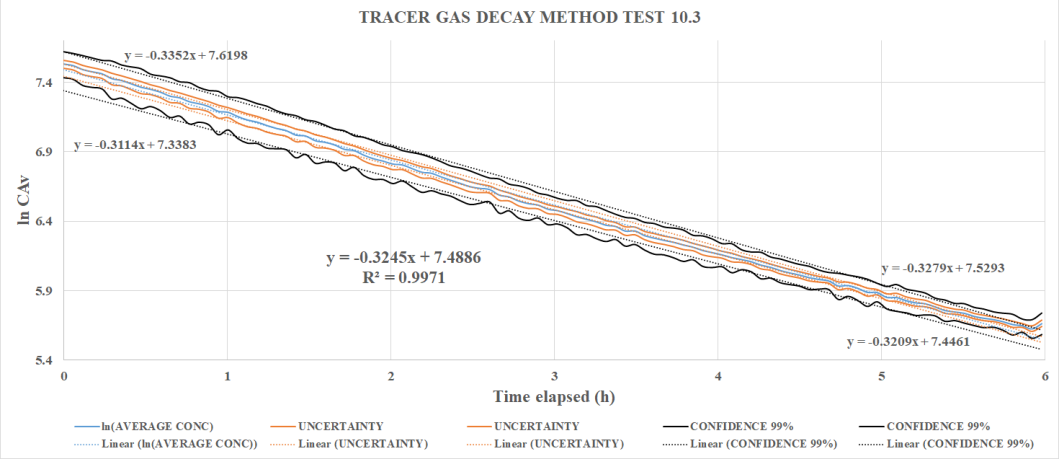


Figure B.47: Tracer gas concentration decay calculation for test 10.3

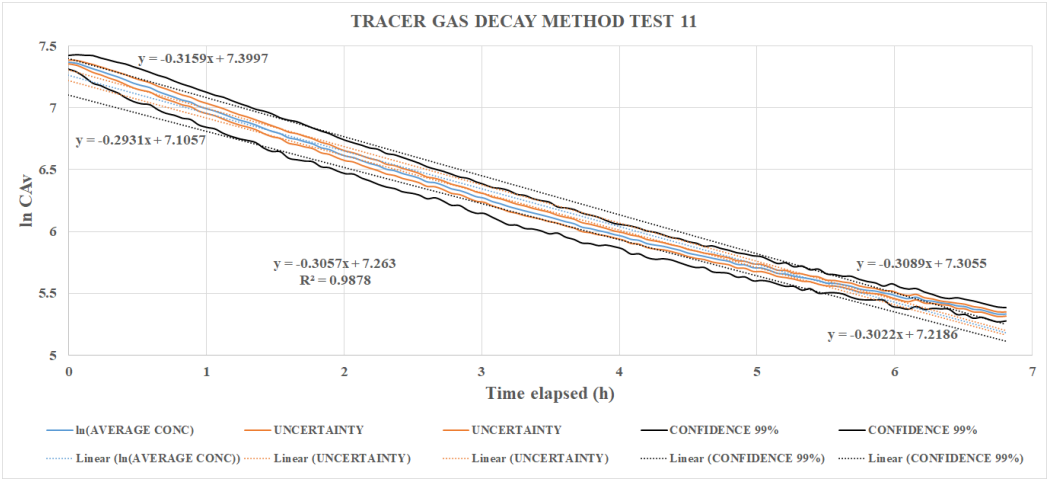


Figure B.48: Tracer gas concentration decay calculation for test 11

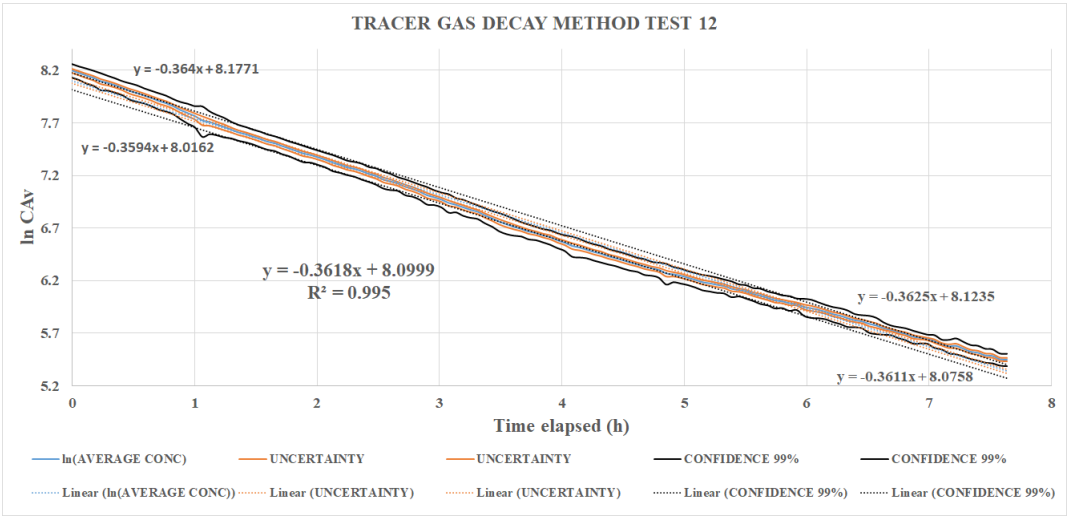


Figure B.49: Tracer gas concentration decay calculation for test 12

Appendix C

Wind and pressure graphs from the case study house tests

The wind has a great effect on the pressure profile on the facades of a building. Even when it is difficult to analyse, figure C.4 clearly shows that at high wind, the pressure profiles are higher as well. this led the decision to analyse shorter time gaps.

The following images are the ones used to perform the analysis in chapter 4. The time frame is represented in the images.

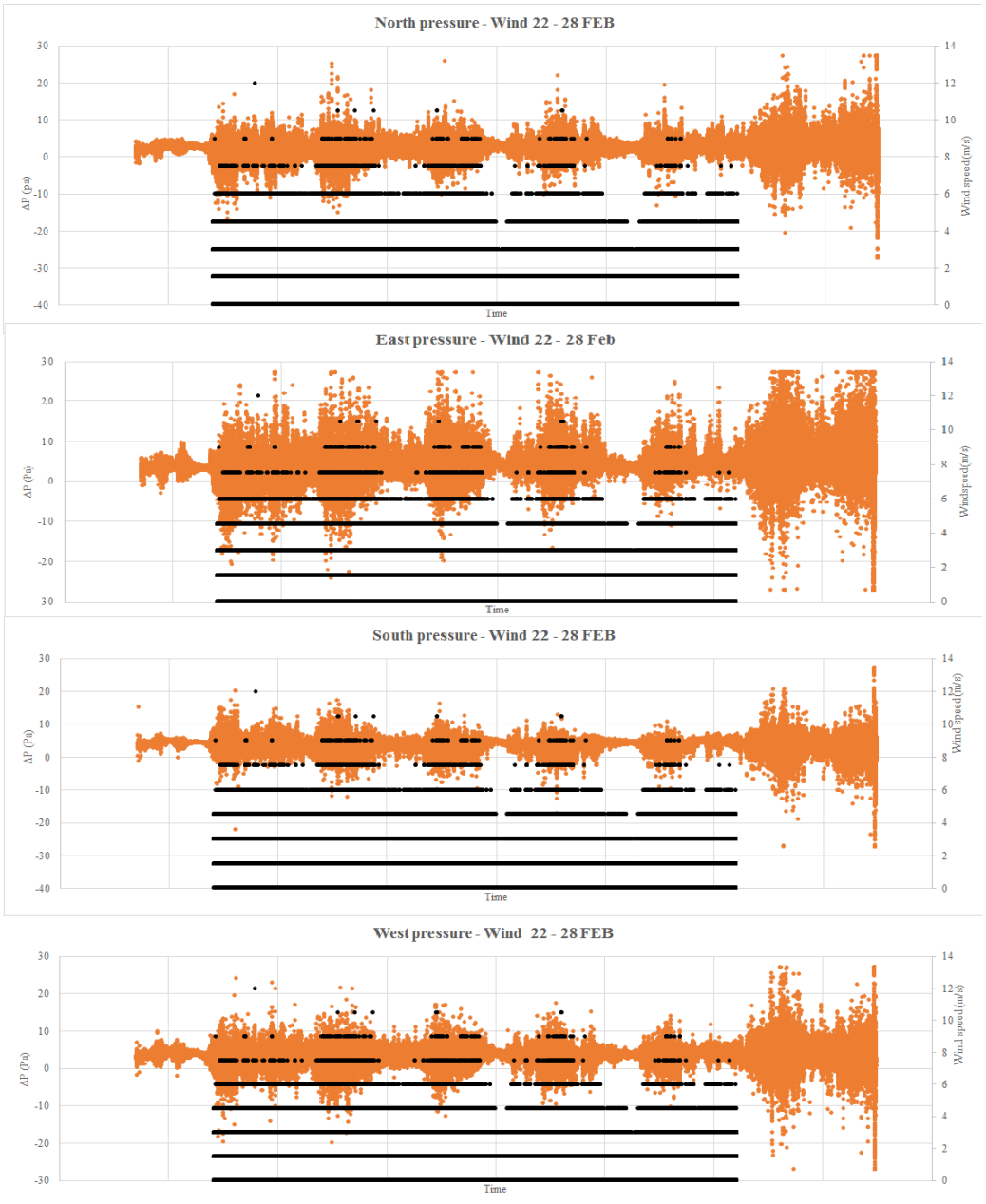


Figure C.1: Wind speed against measured pressure in all the façades of the case study house

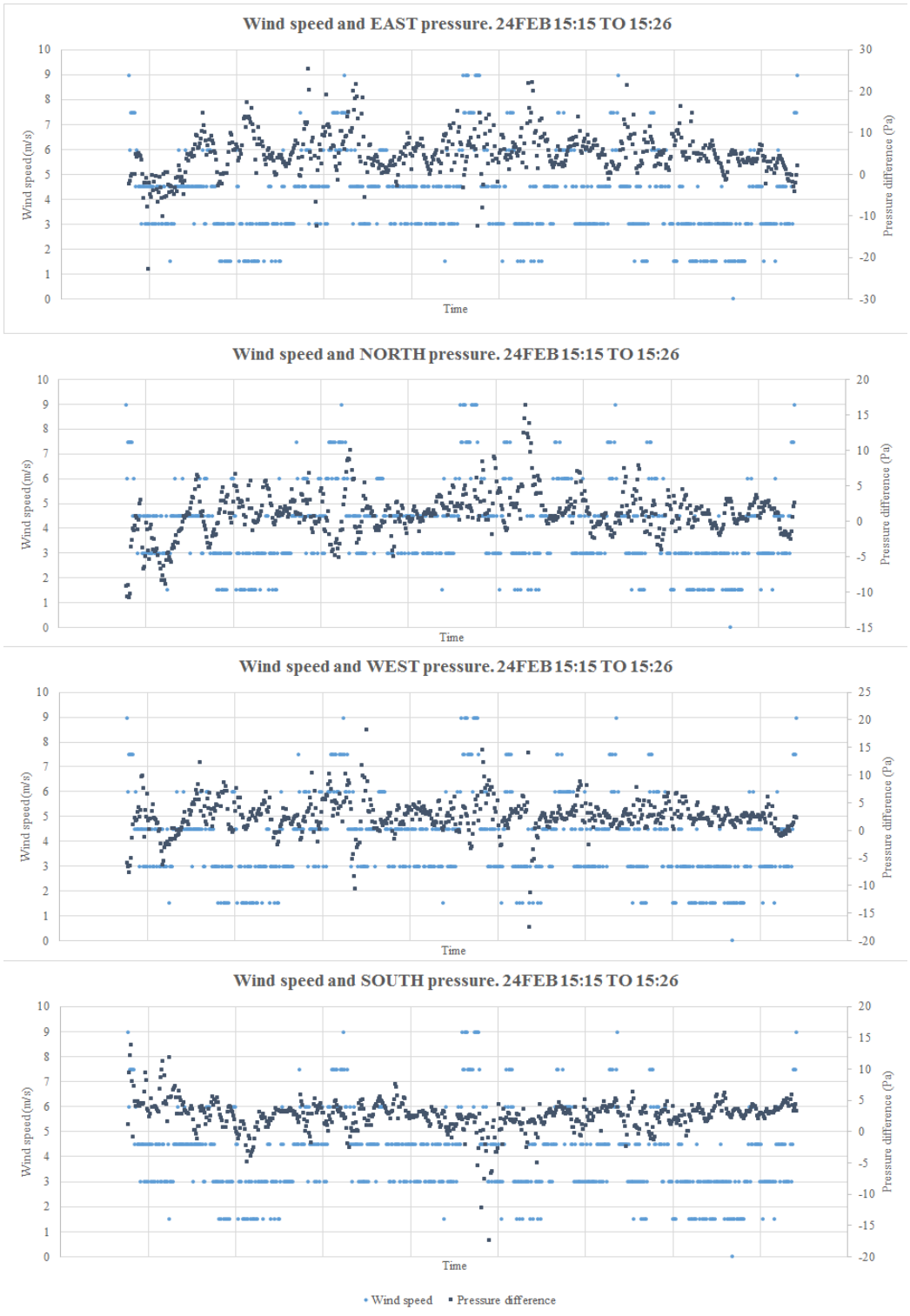


Figure C.2: Wind speed against measured pressure in all the façades of the case study house in the 24th of February 2018

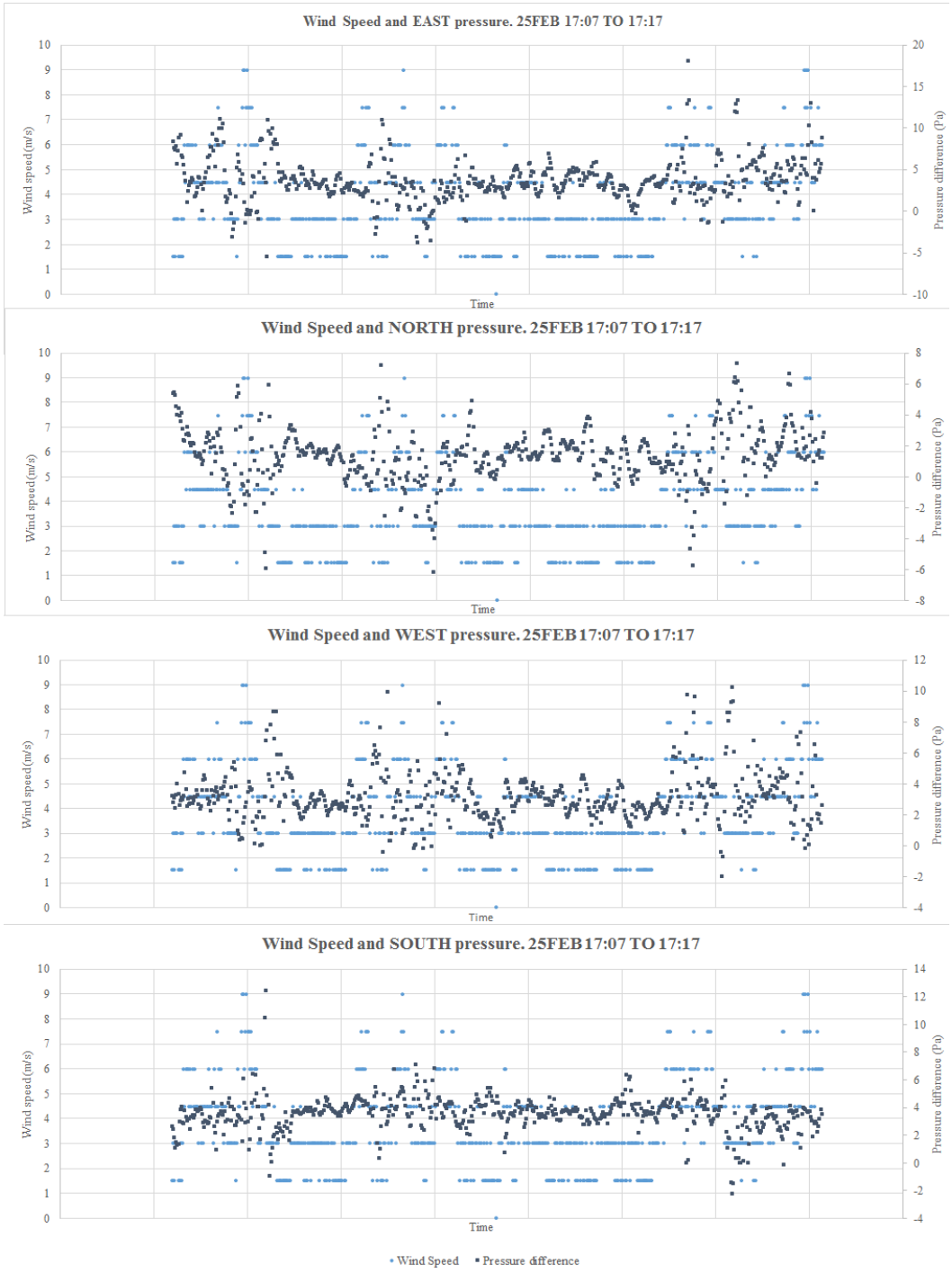


Figure C.3: Wind speed against measured pressure in all the façades of the case study house in the 25th of February 2018

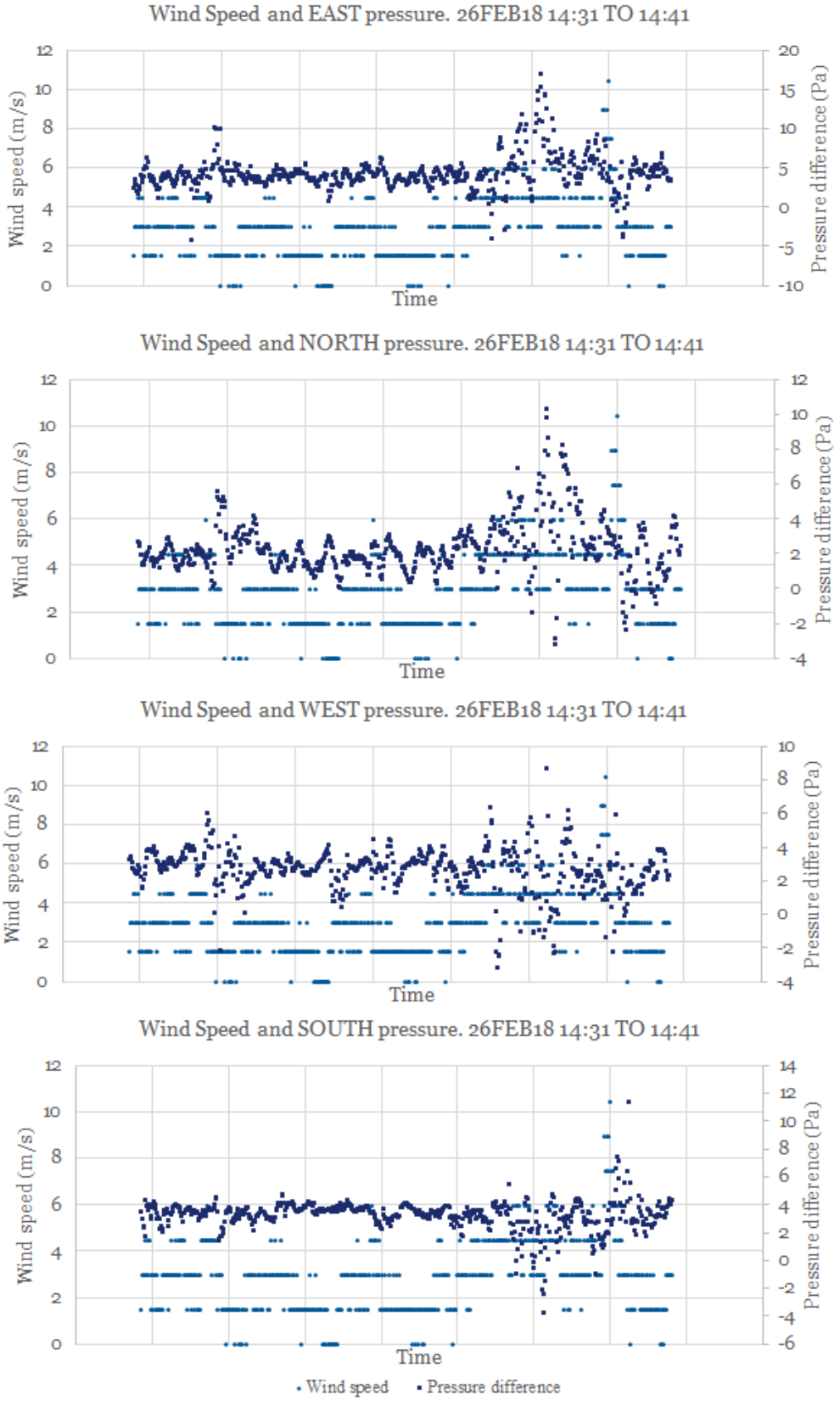
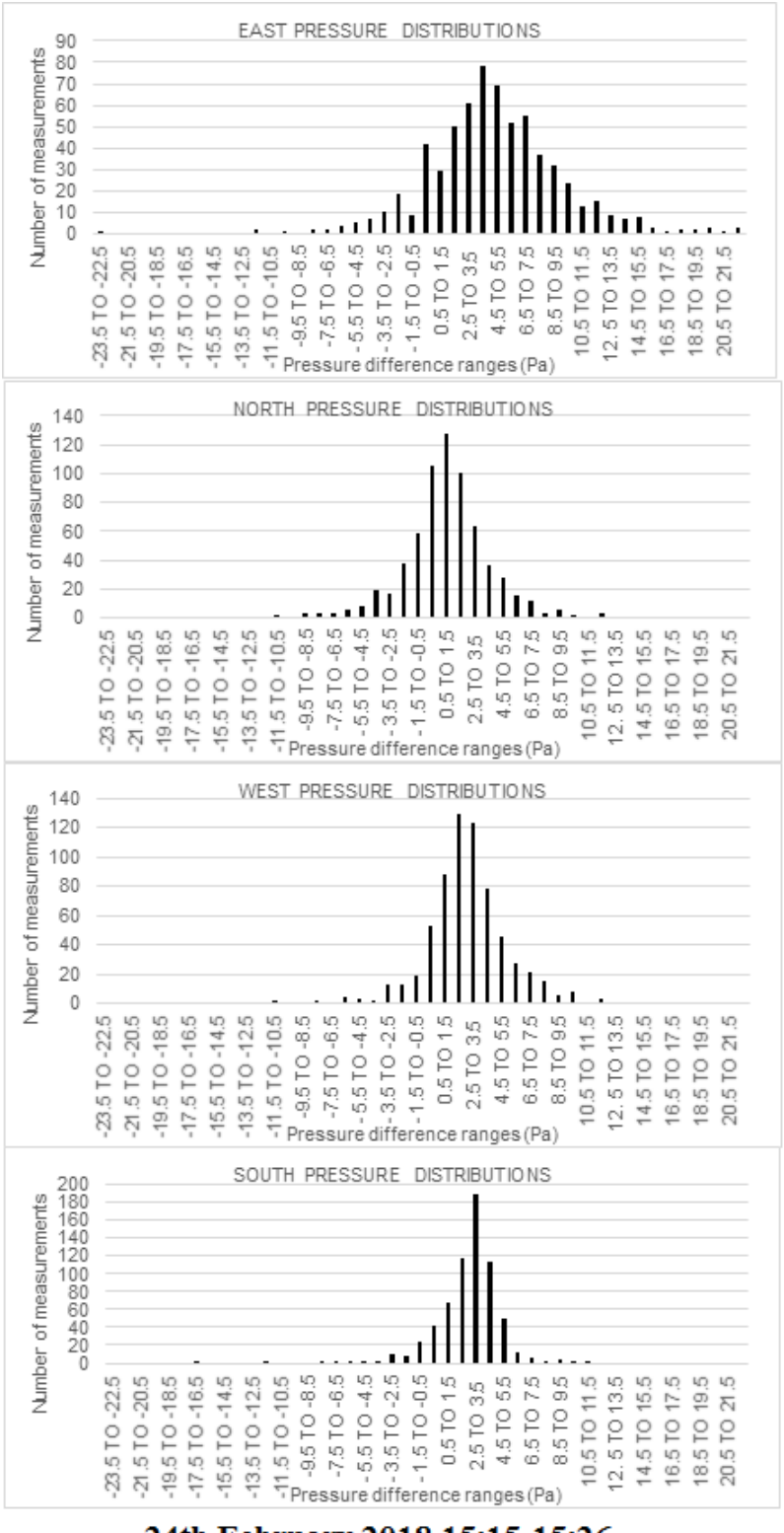


Figure C.4: Wind speed against measured pressure in all the façades of the case study house in the 26th of February 2018

Appendix D

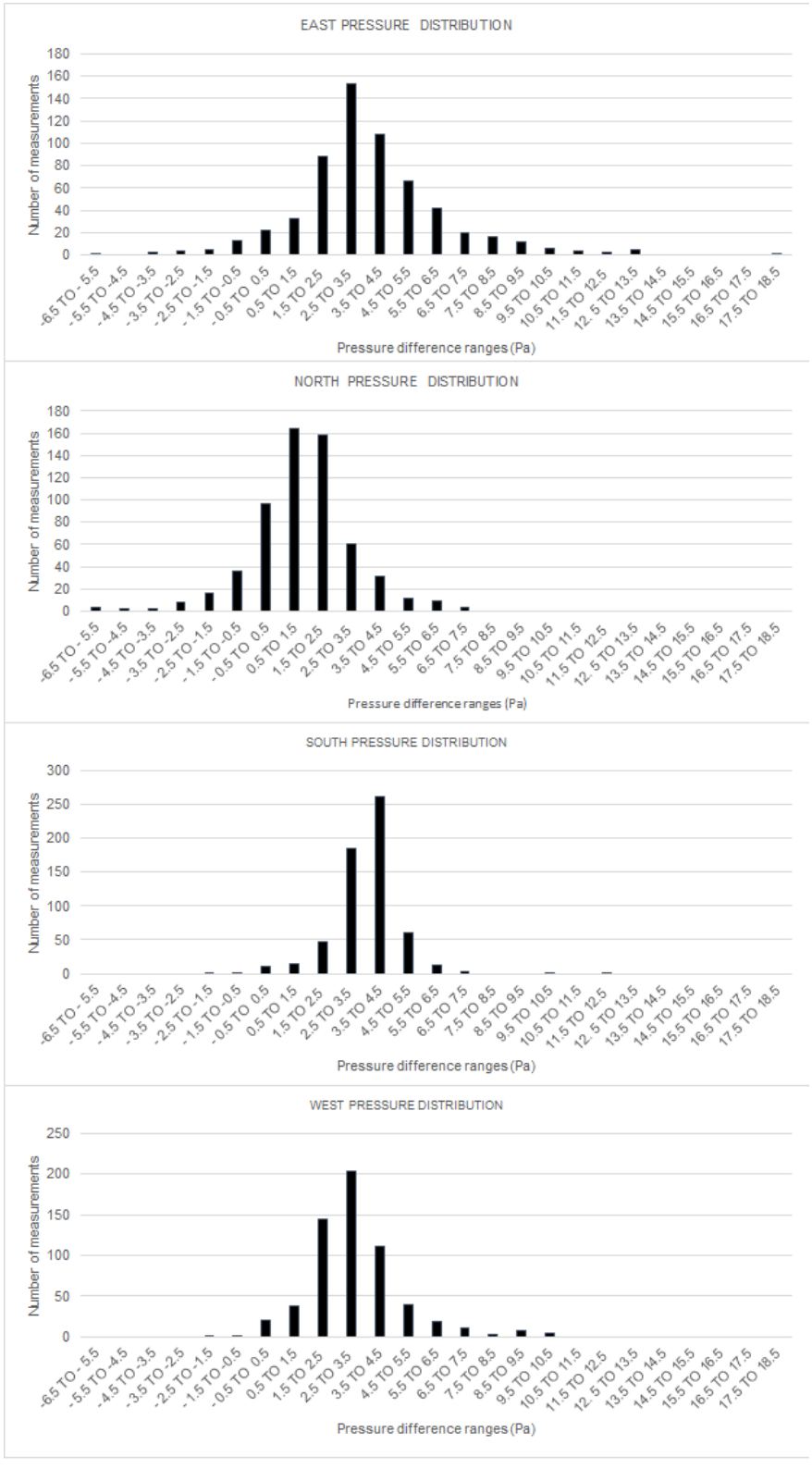
Statistical distributions of pressure tests in the case study house

The statistical analysis of on which pressure differences occur at "natural conditions" was made based on the following images.



24th February 2018 15:15-15:26

Figure D.1: Distribution of measured pressures in different facades of the case study house in the 24th of February 2018



25th February 2018 17:07-17:17

Figure D.2: Distribution of measured pressures in different facades of the case study house in the 25th of February 2018

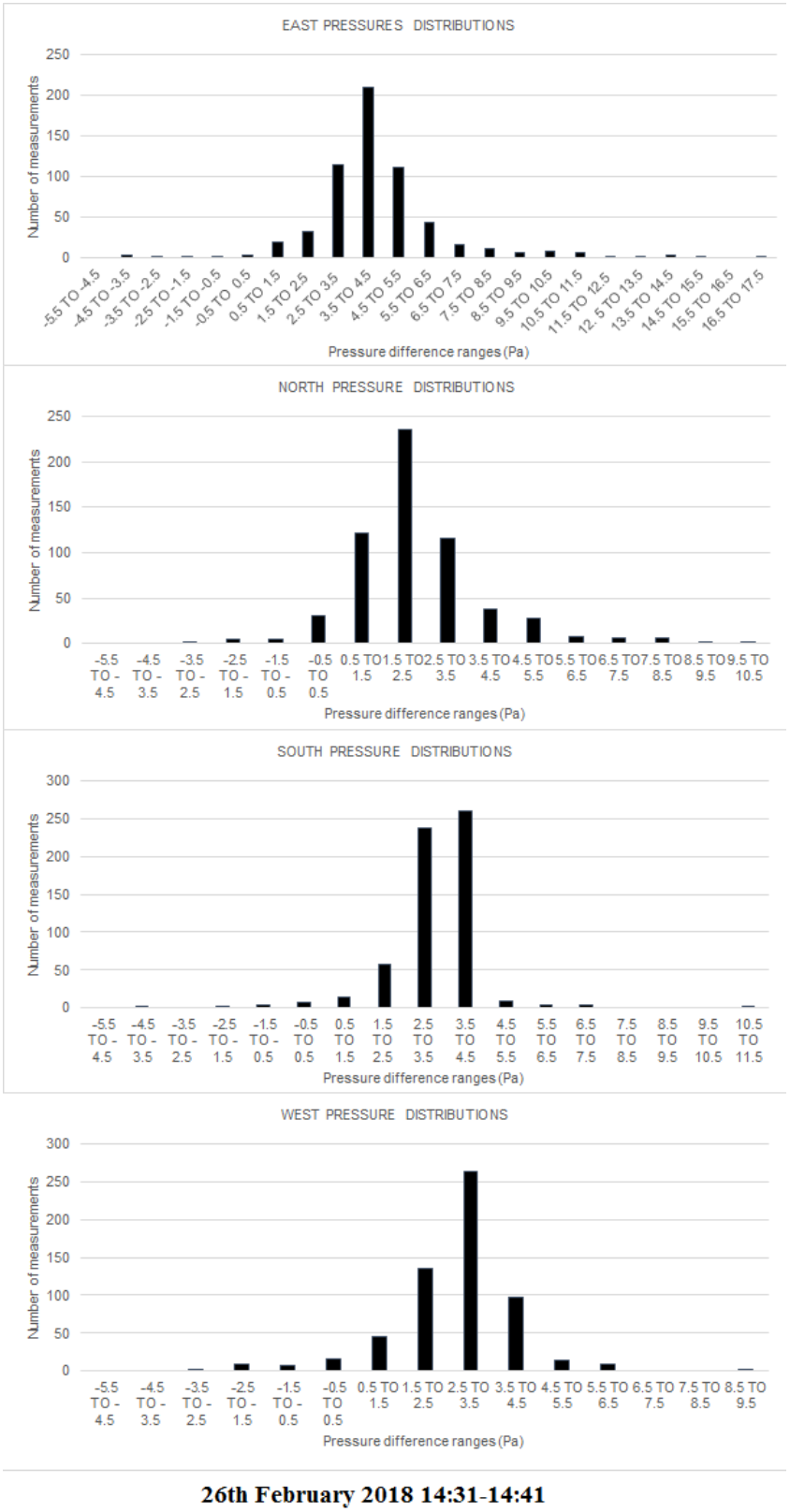


Figure D.3: Distribution of measured pressures in different facades of the case study house in the 26th of February 2018

Appendix E

Tracer gas tests and environmental conditions measurements in Field Trials stage.

E.1 Tracer gas concentration decay tests and uncertainty calculation

The following figures represent the calculations of infiltration rates in the test dwellings. The measurements were taken using the concentration decay method. The gas used as tracer gas was carbon dioxide. The calculations account for CO_2 levels in the environment.

The figures include the calculation of the infiltration rate (middle blue line) with its best fit. The slope in the equation of the line represents the infiltration rate (h^{-1}). The orange lines represent the uncertainty calculations and; the black lines account for a 99% confidence level of the measurements. Both the uncertainty and the confidence intervals were fitted with a line. The slope of the ebst fit line represents the infiltration rate (h^{-1}) equivalent to the uncertainty and 99% confidence intervals respectively.

For more information on the theory of the tracer gas concentration decay method, refer to Chapter 2. For more information on the test dwellings refer to Chapter 5.

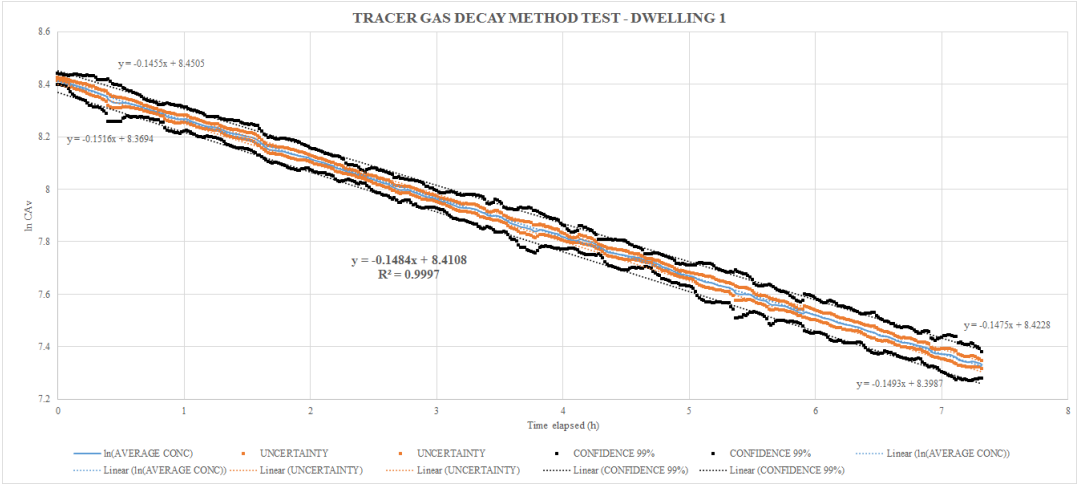


Figure E.1: Tracer gas decay test graph for dwelling 1 with best fit for uncertainty and confidence at 99%.

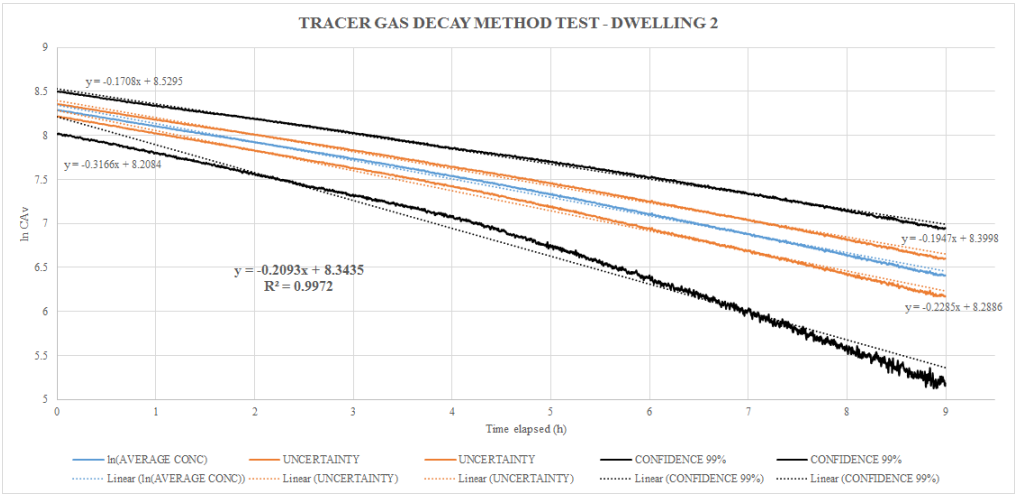


Figure E.2: Tracer gas decay test graph for dwelling 2 with best fit for uncertainty and confidence at 99%.

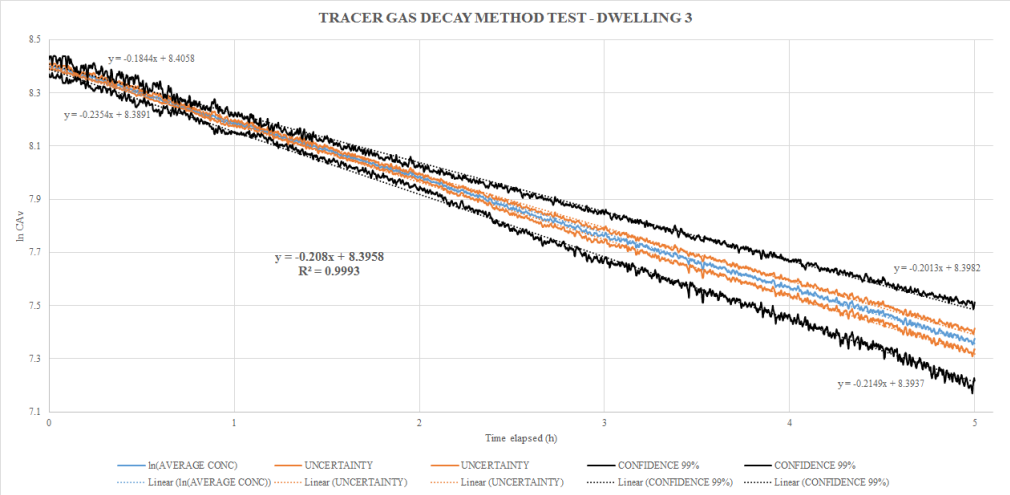


Figure E.3: Tracer gas decay test graph for dwelling 3 with best fit for uncertainty and confidence at 99%.

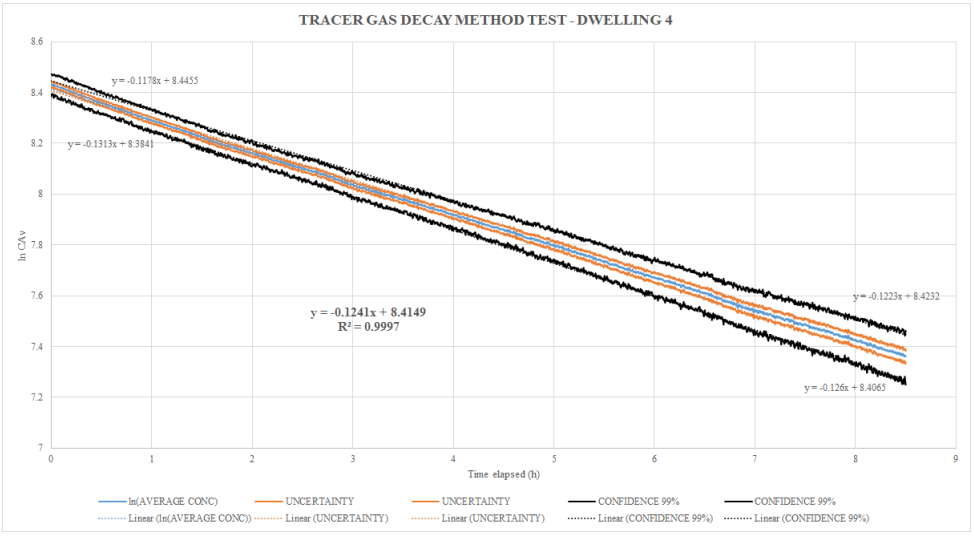


Figure E.4: Tracer gas decay test graph for dwelling 4 with best fit for uncertainty and confidence at 99%.

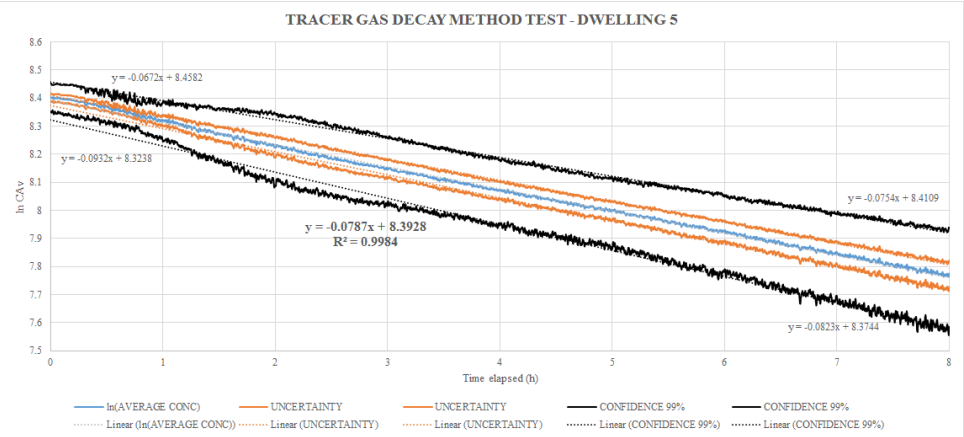


Figure E.5: Tracer gas decay test graph for dwelling 5 with best fit for uncertainty and confidence at 99%.

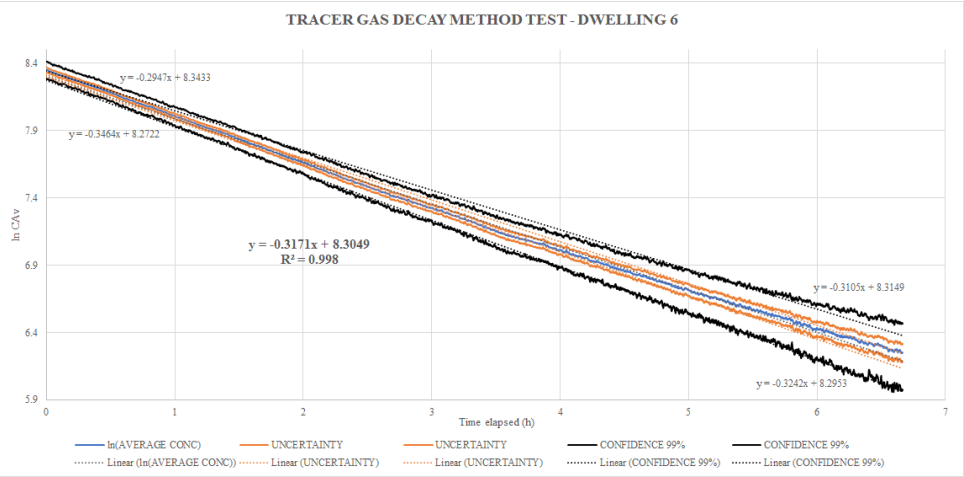


Figure E.6: Tracer gas decay test graph for dwelling 6 with best fit for uncertainty and confidence at 99%.

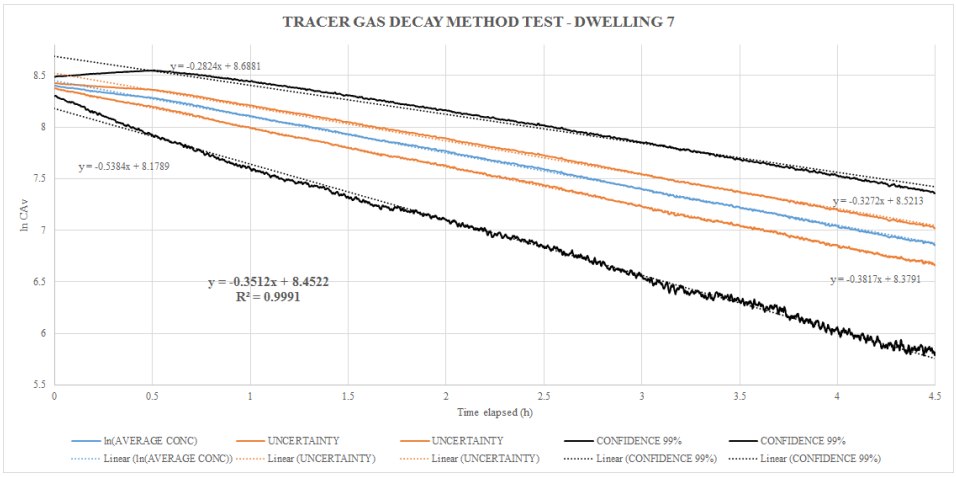


Figure E.7: Tracer gas decay test graph for dwelling 7 with best fit for uncertainty and confidence at 99%.

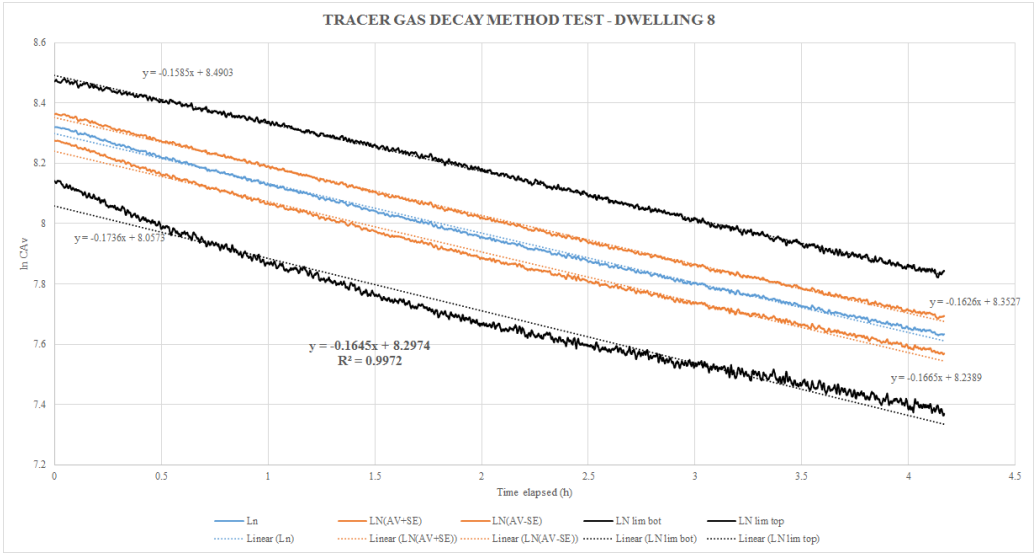


Figure E.8: Tracer gas decay test graph for dwelling 8 with best fit for uncertainty and confidence at 99%.

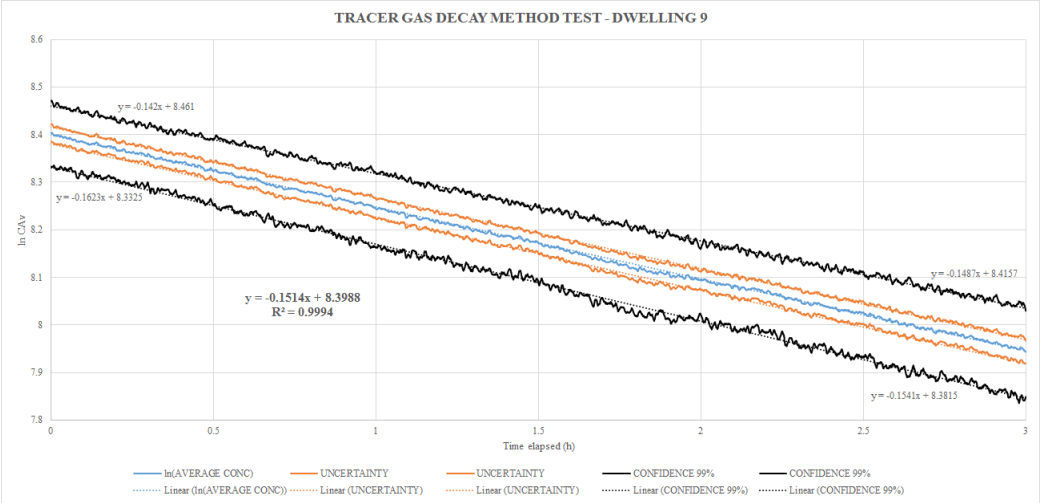


Figure E.9: Tracer gas decay test graph for dwelling 9 with best fit for uncertainty and confidence at 99%.

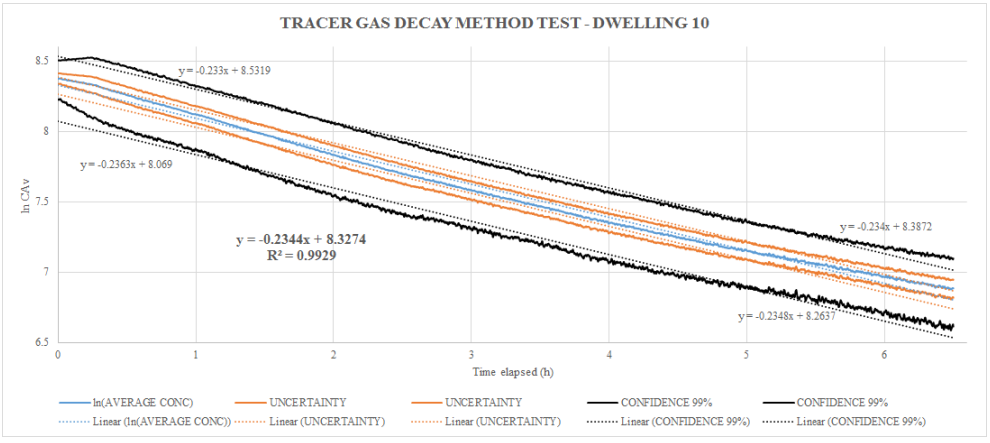


Figure E.10: Tracer gas decay test graph for dwelling 10 with best fit for uncertainty and confidence at 99%.

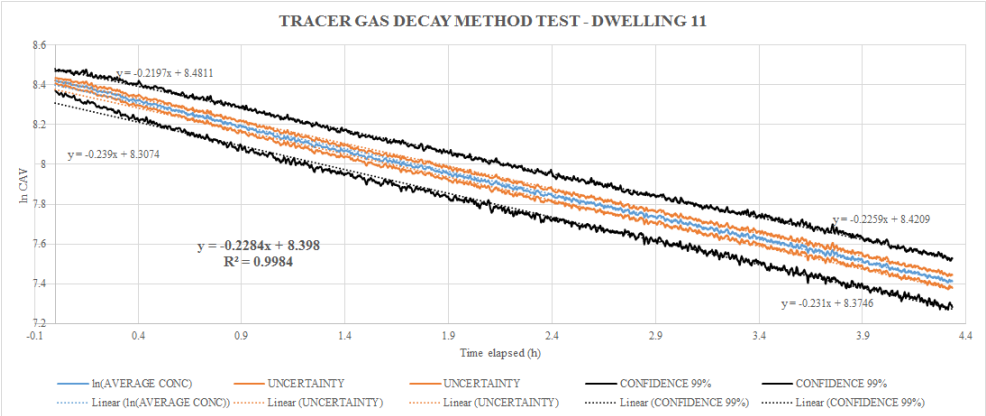


Figure E.11: Tracer gas decay test graph for dwelling 11 with best fit for uncertainty and confidence at 99%.

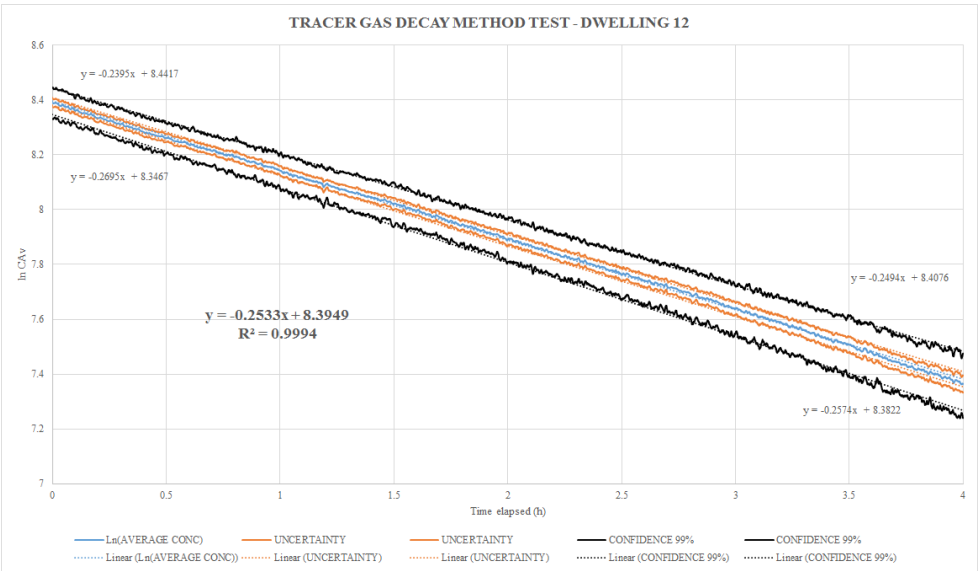


Figure E.12: Tracer gas decay test graph for dwelling 12 with best fit for uncertainty and confidence at 99%.

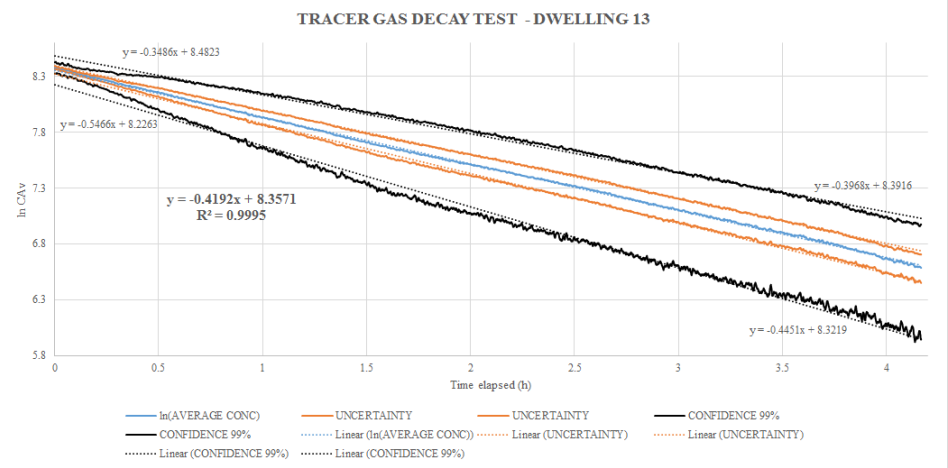


Figure E.13: Tracer gas decay test graph for dwelling 13 with best fit for uncertainty and confidence at 99%.

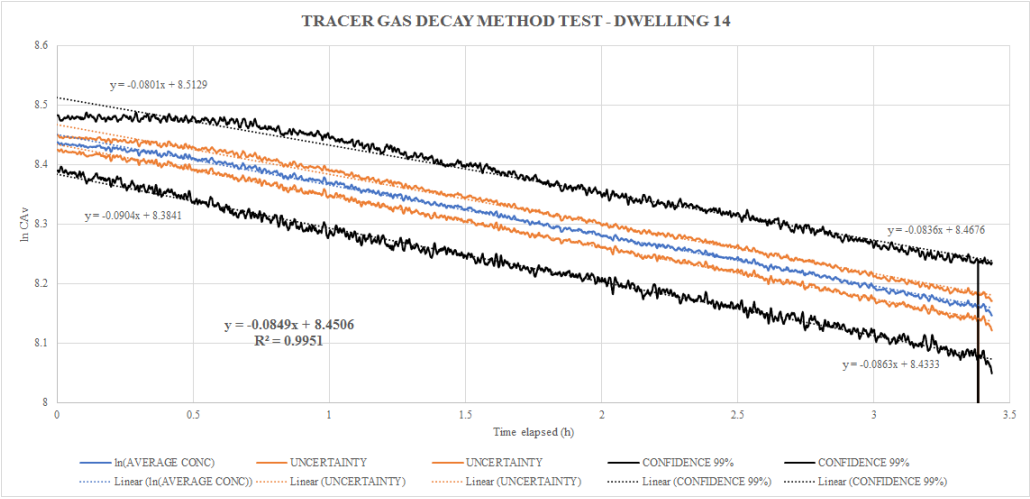


Figure E.14: Tracer gas decay test graph for dwelling 14 with best fit for uncertainty and confidence at 99%.

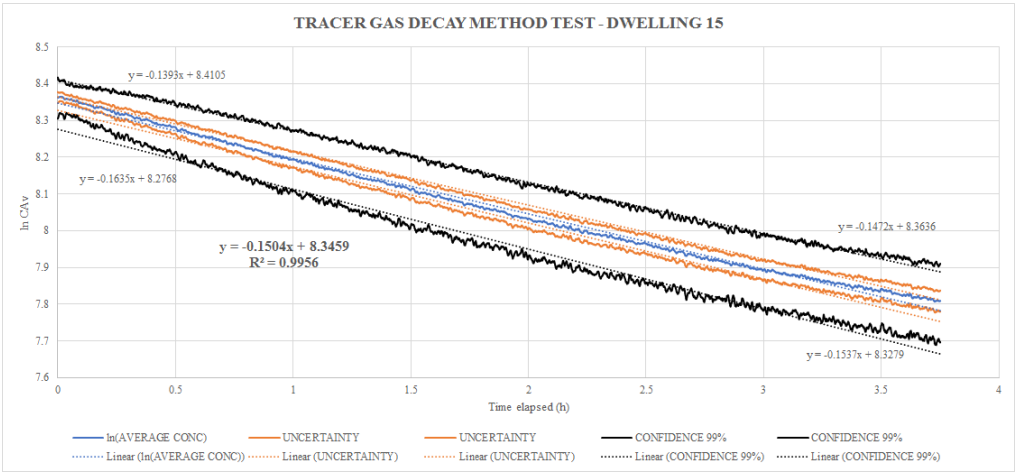


Figure E.15: Tracer gas decay test graph for dwelling 15 with best fit for uncertainty and confidence at 99%.

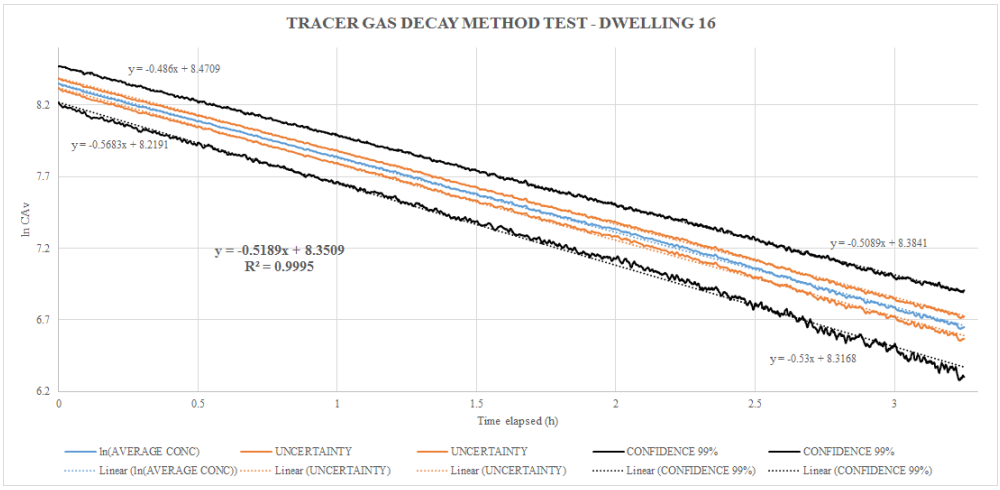


Figure E.16: Tracer gas decay test graph for dwelling 16 with best fit for uncertainty and confidence at 99%.

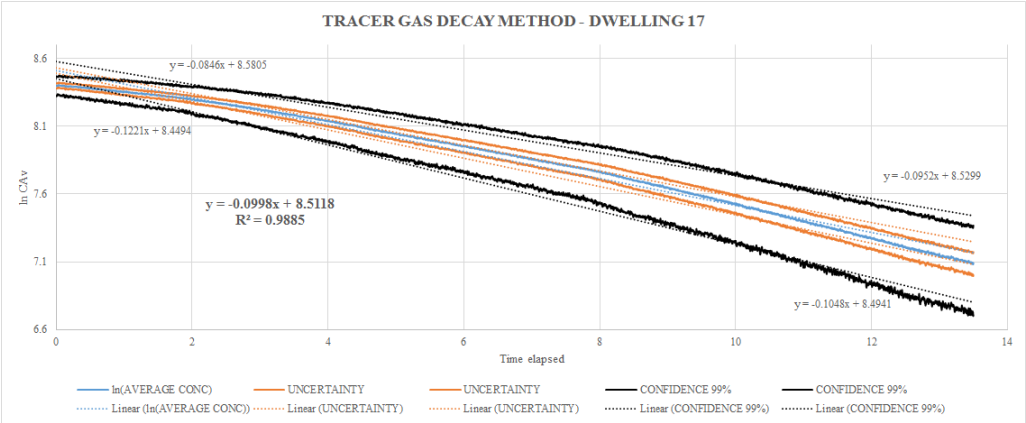


Figure E.17: Tracer gas decay test graph for dwelling 17 with best fit for uncertainty and confidence at 99%.

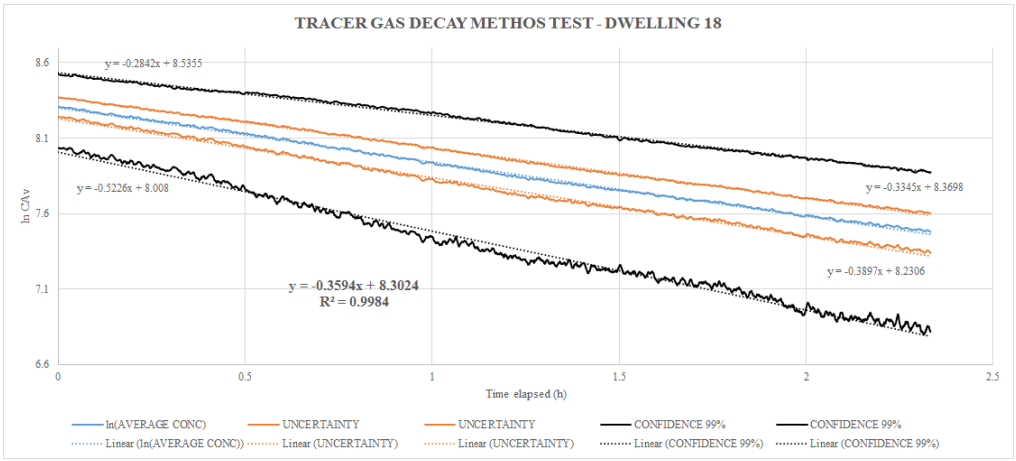


Figure E.18: Tracer gas decay test graph for dwelling 18 with best fit for uncertainty and confidence at 99%.

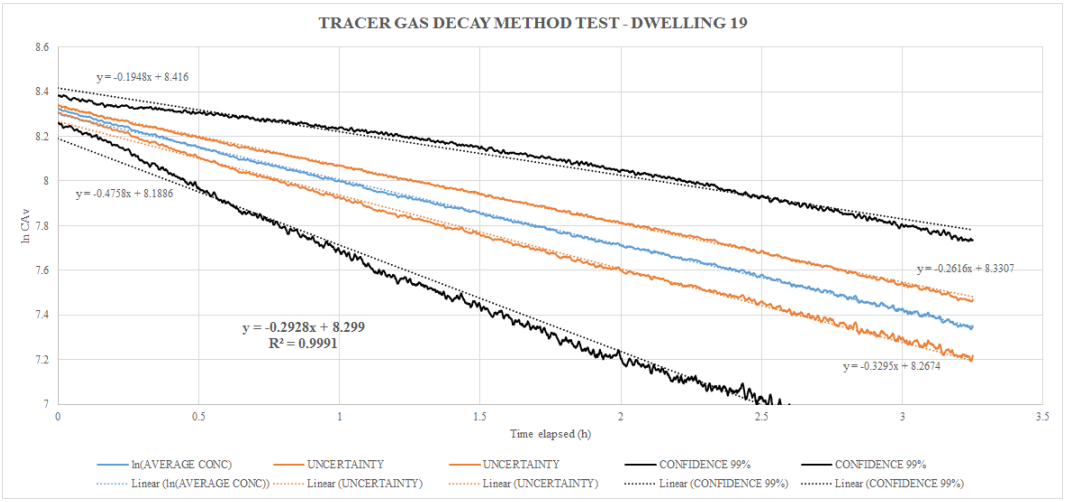


Figure E.19: Tracer gas decay test graph for dwelling 19 with best fit for uncertainty and confidence at 99%.

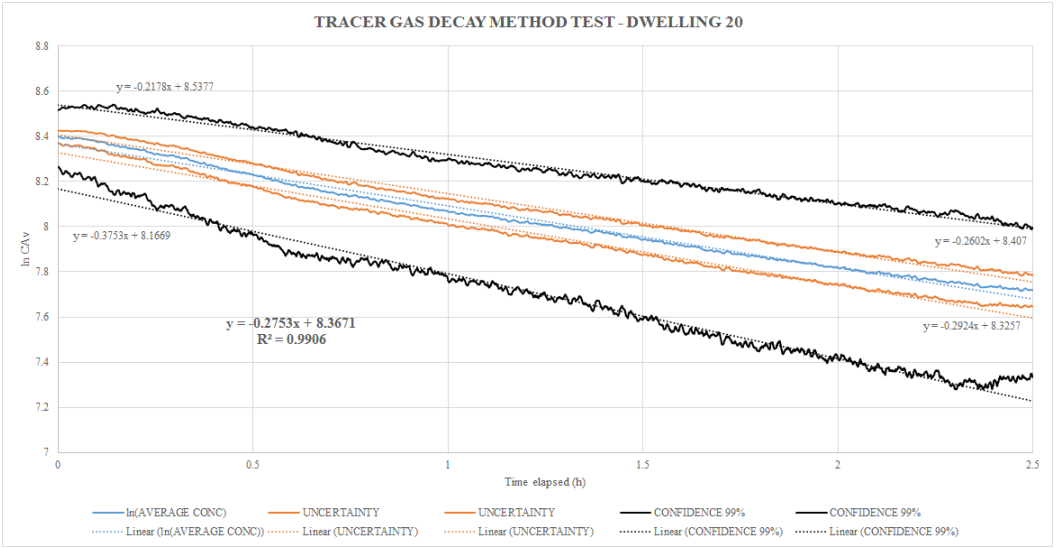


Figure E.20: Tracer gas decay test graph for dwelling 20 with best fit for uncertainty and confidence at 99%.

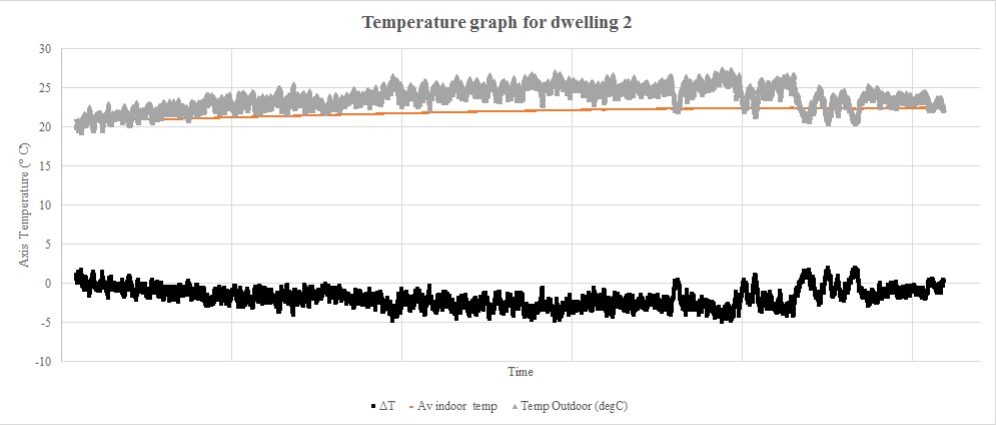


Figure E.21: Temperature difference, indoor and outdoor temperatures in dwelling 2.

E.2 Environmental conditions measurements in test dwellings

The following figures depict the indoor and outdoor temperatures occurring during the tracer gas decay. this means that these temperatures were measured for the time used to calculate the infiltration rate. In addition the temperature difference variation with time is presented. Moreover, wind graphs represent the measured wind speed for the same period.

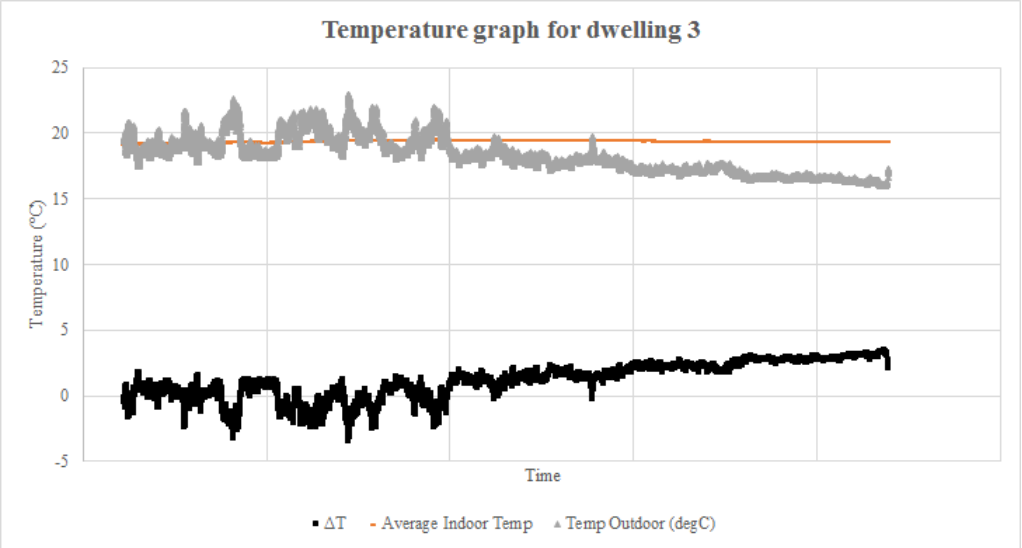


Figure E.22: Temperature difference, indoor and outdoor temperatures in dwelling 3.

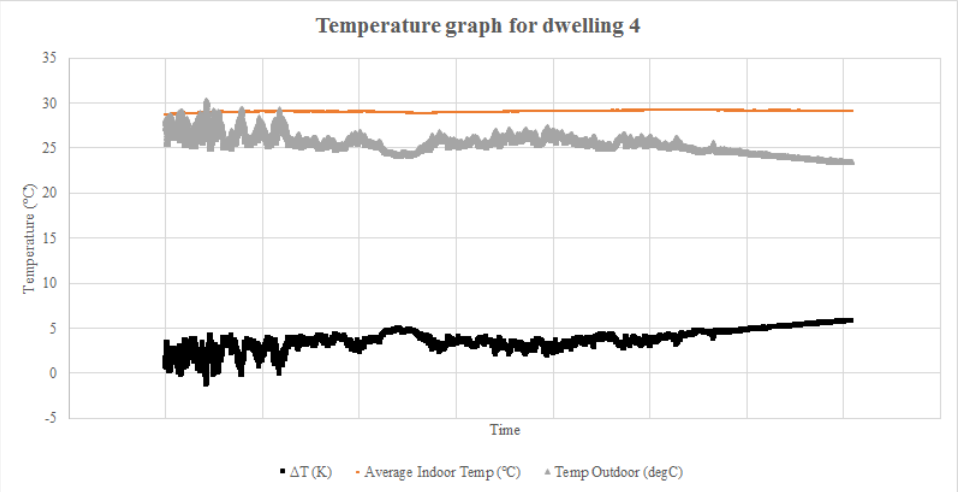


Figure E.23: Temperature difference, indoor and outdoor temperatures in dwelling 4.

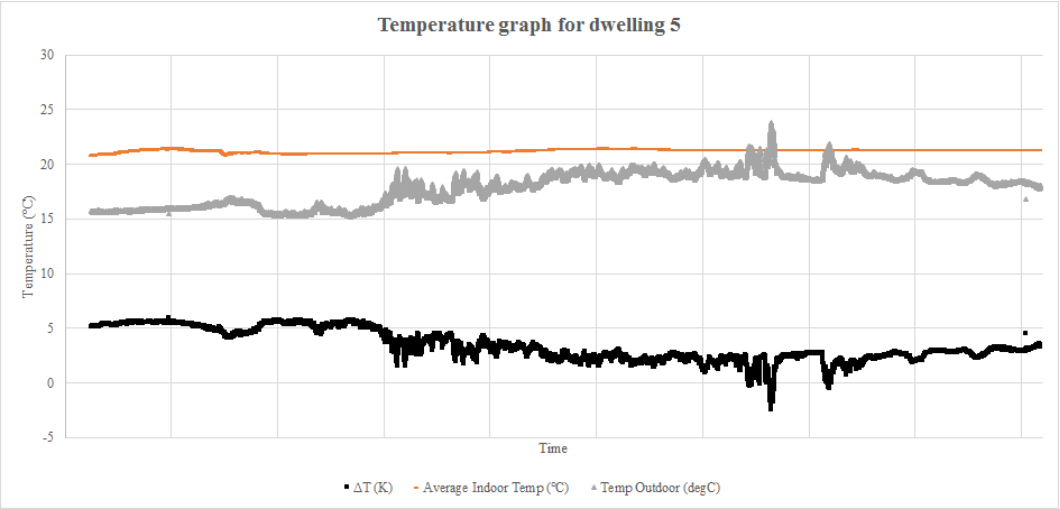


Figure E.24: Temperature difference, indoor and outdoor temperatures in dwelling 5.

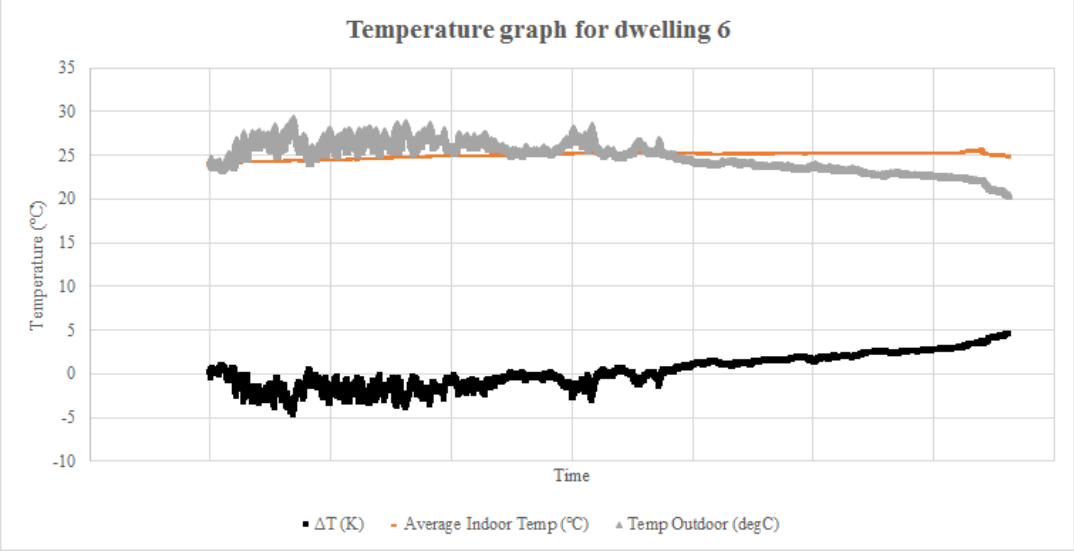


Figure E.25: Temperature difference, indoor and outdoor temperatures in dwelling 6.

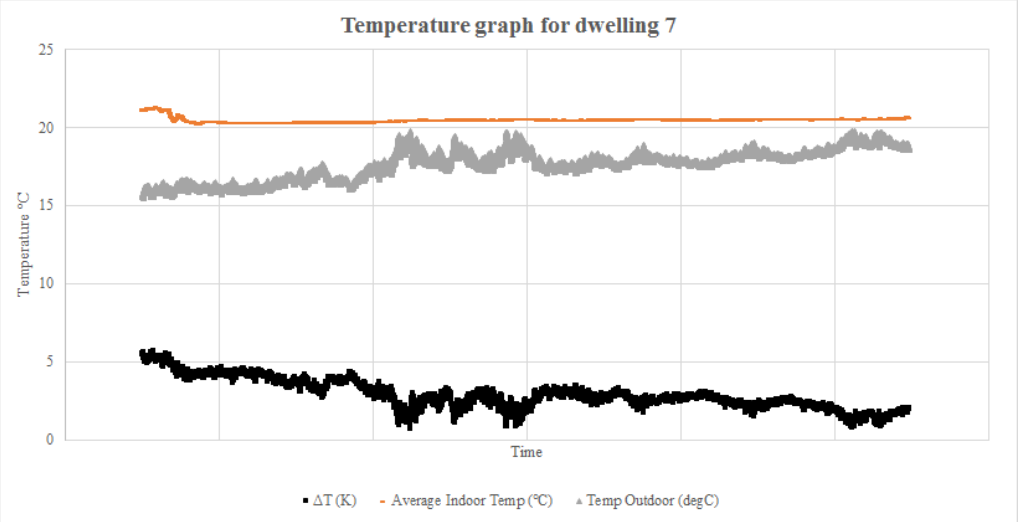


Figure E.26: Temperature difference, indoor and outdoor temperatures in dwelling 7.

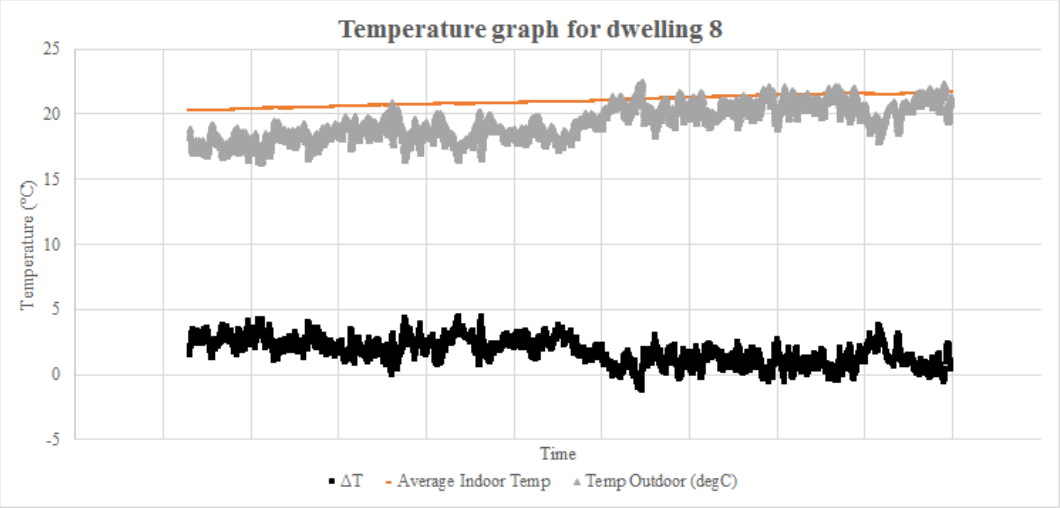


Figure E.27: Temperature difference, indoor and outdoor temperatures in dwelling 8.

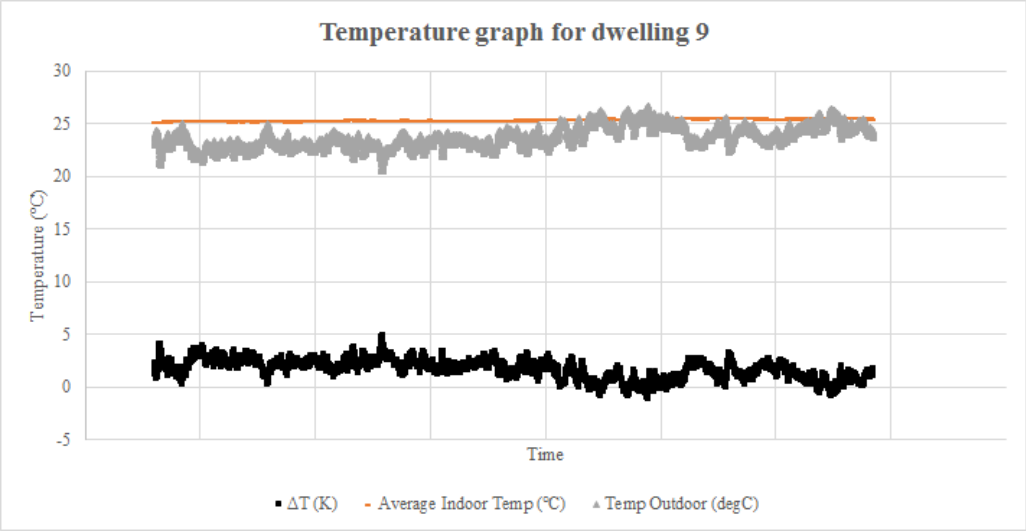


Figure E.28: Temperature difference, indoor and outdoor temperatures in dwelling 9.

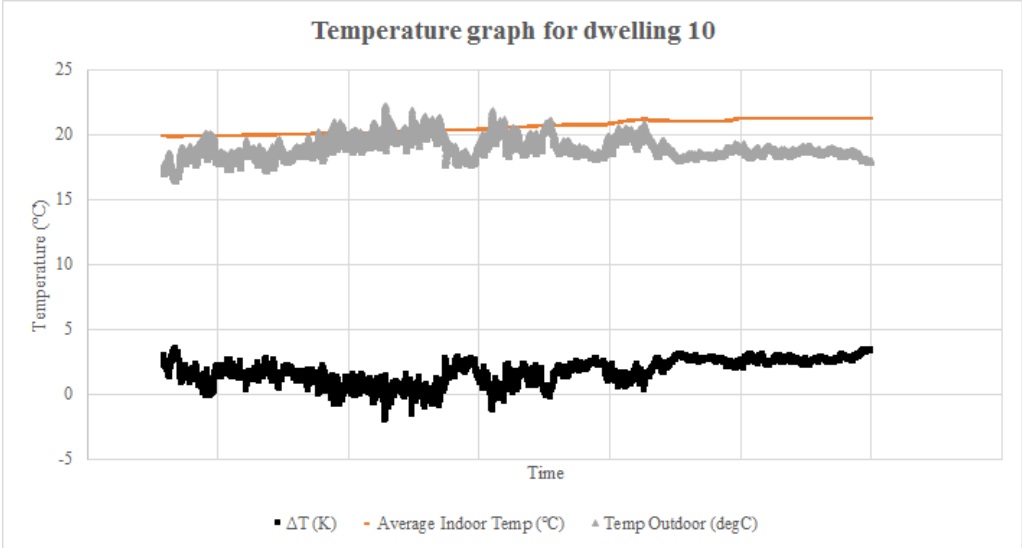


Figure E.29: Temperature difference, indoor and outdoor temperatures in dwelling 10.

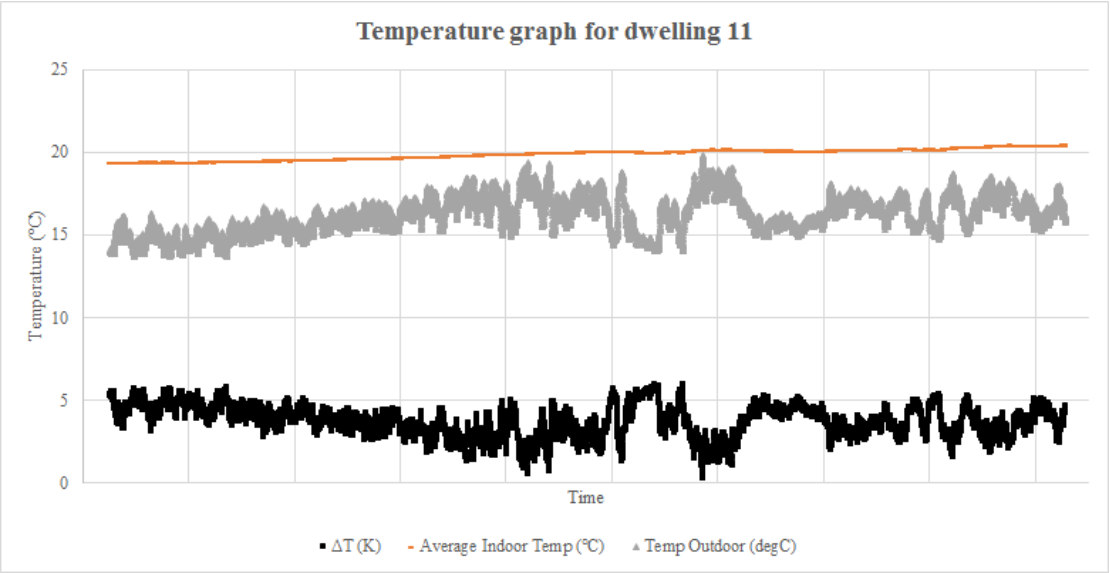


Figure E.30: Temperature difference, indoor and outdoor temperatures in dwelling 11.

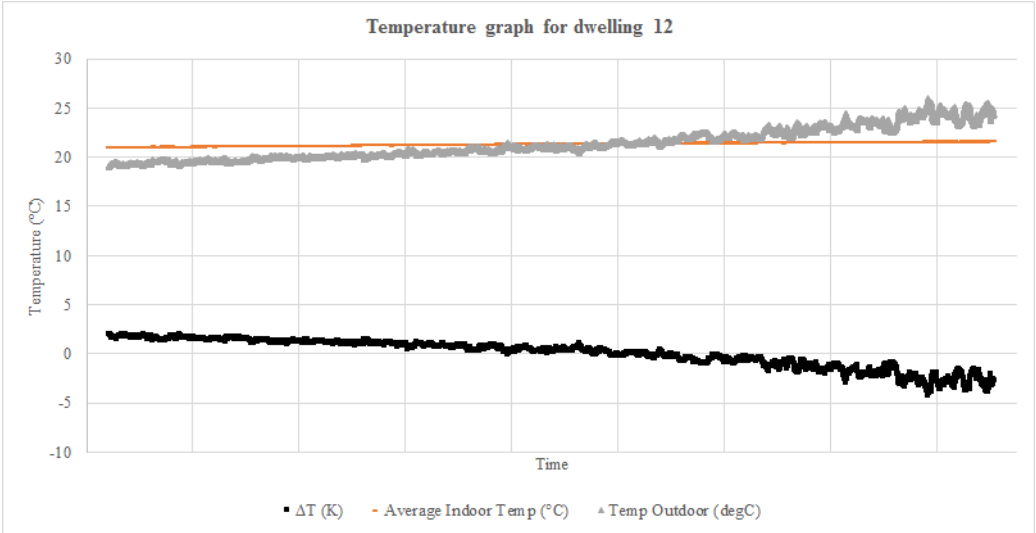


Figure E.31: Temperature difference, indoor and outdoor temperatures in dwelling 12.

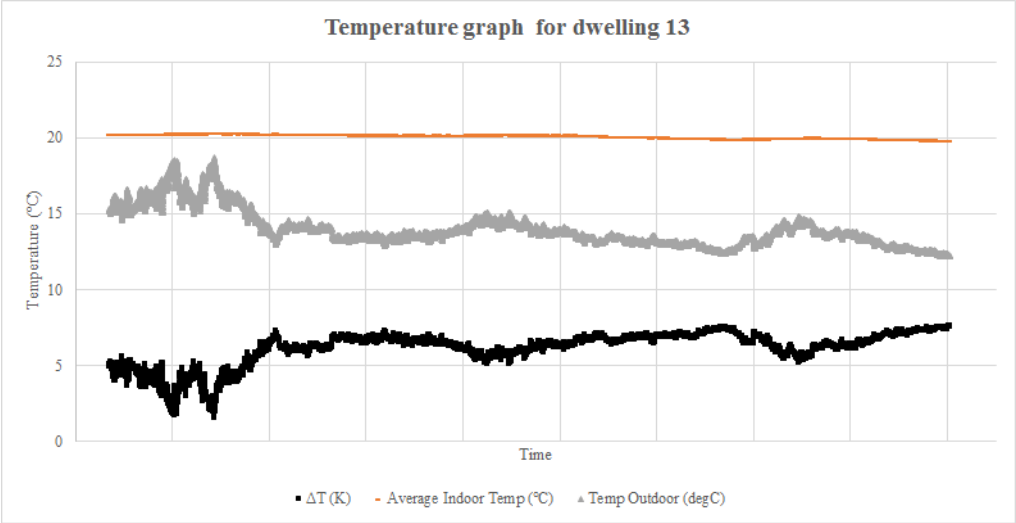


Figure E.32: Temperature difference, indoor and outdoor temperatures in dwelling 13.

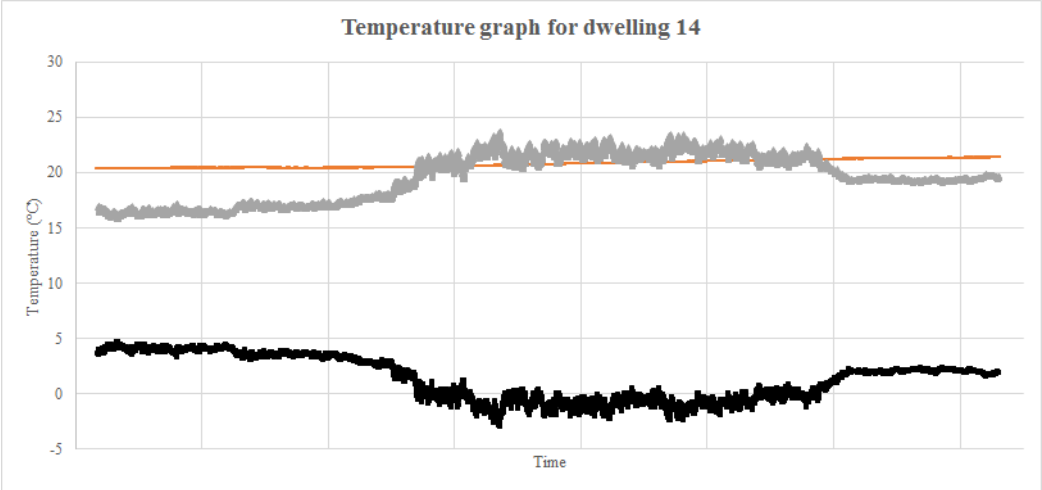


Figure E.33: Temperature difference, indoor and outdoor temperatures in dwelling 14.

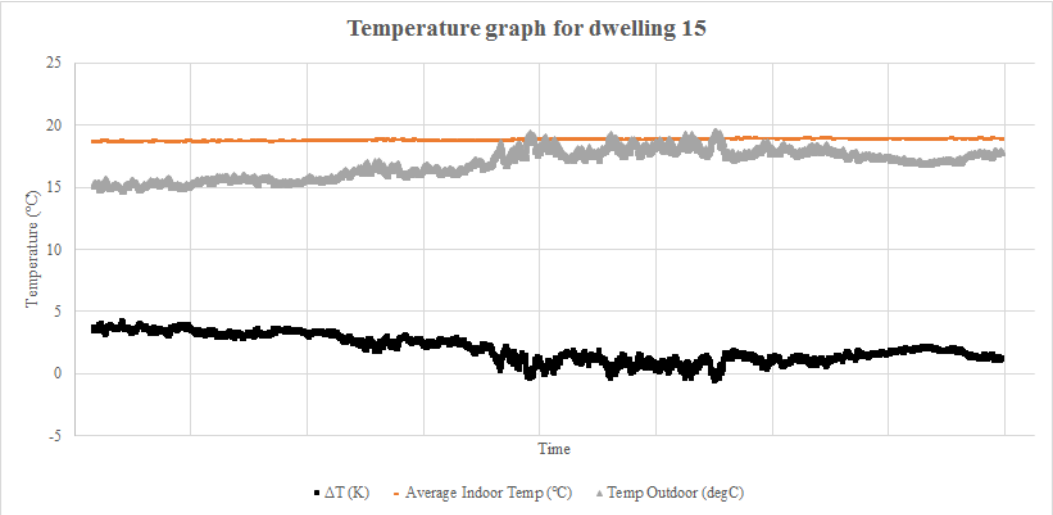


Figure E.34: Temperature difference, indoor and outdoor temperatures in dwelling 15.

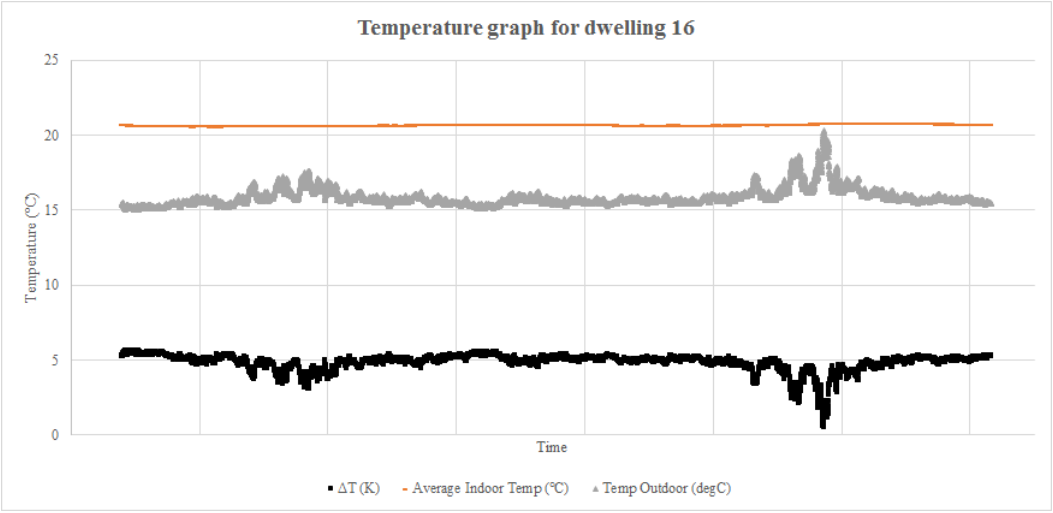


Figure E.35: Temperature difference, indoor and outdoor temperatures in dwelling 16.

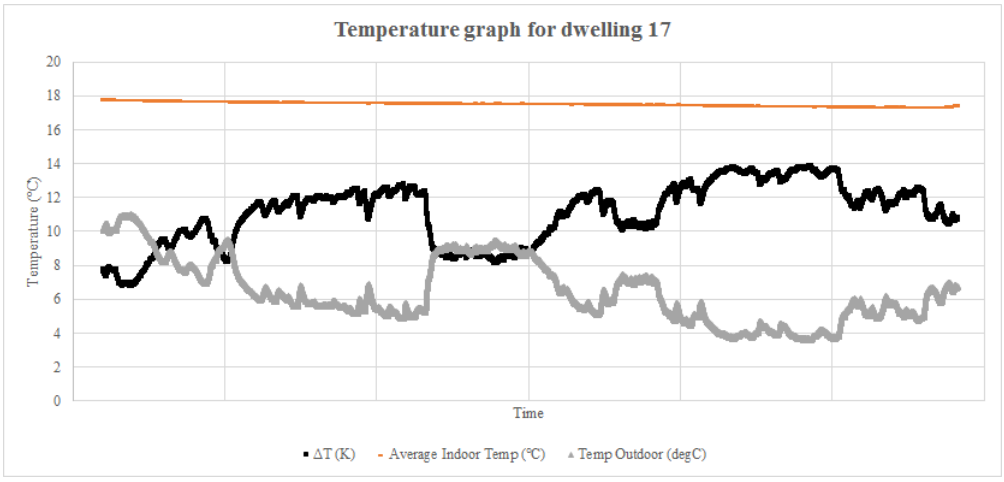


Figure E.36: Temperature difference, indoor and outdoor temperatures in dwelling 17.

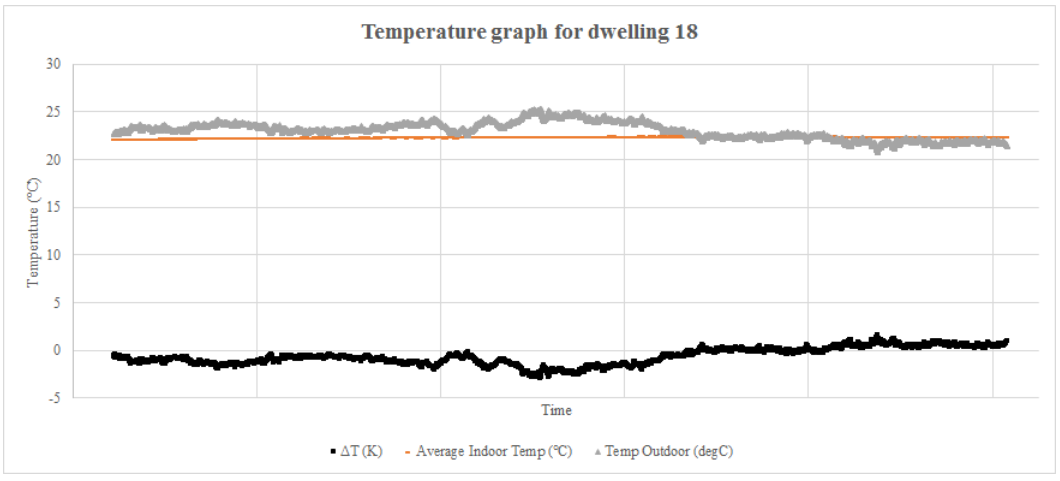


Figure E.37: Temperature difference, indoor and outdoor temperatures in dwelling 18.

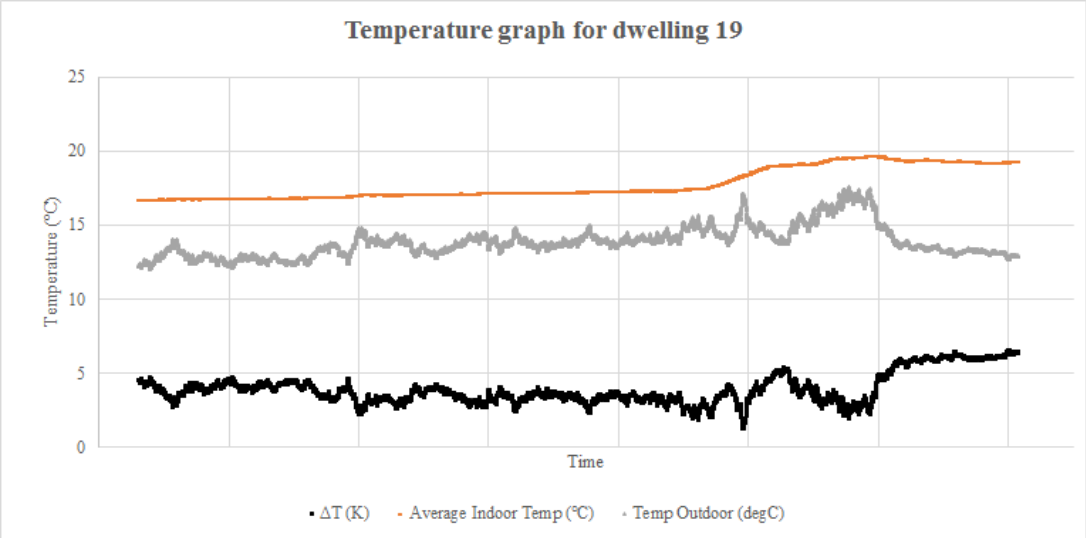


Figure E.38: Temperature difference, indoor and outdoor temperatures in dwelling 19.

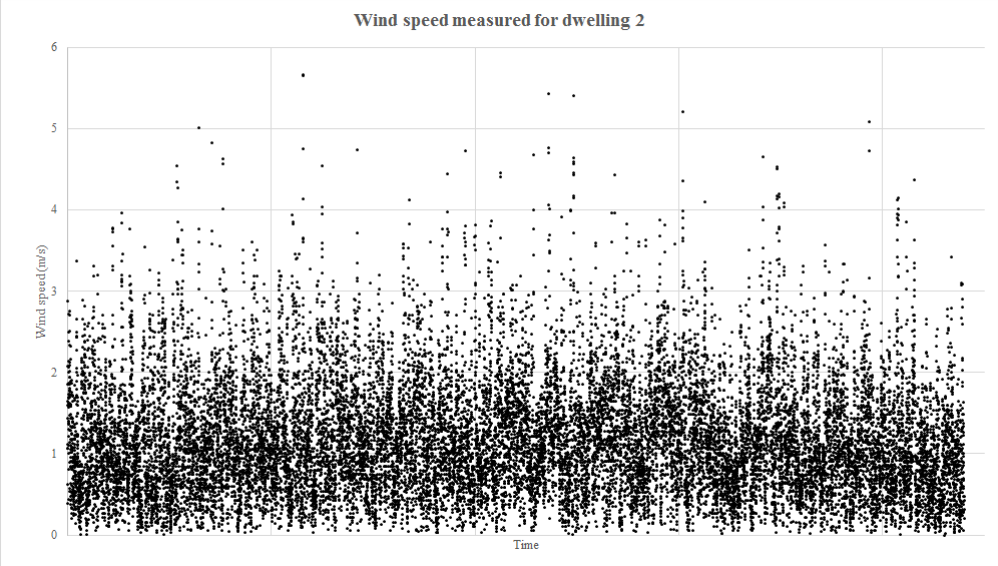


Figure E.39: Measurements of wind speed in dwelling 2.

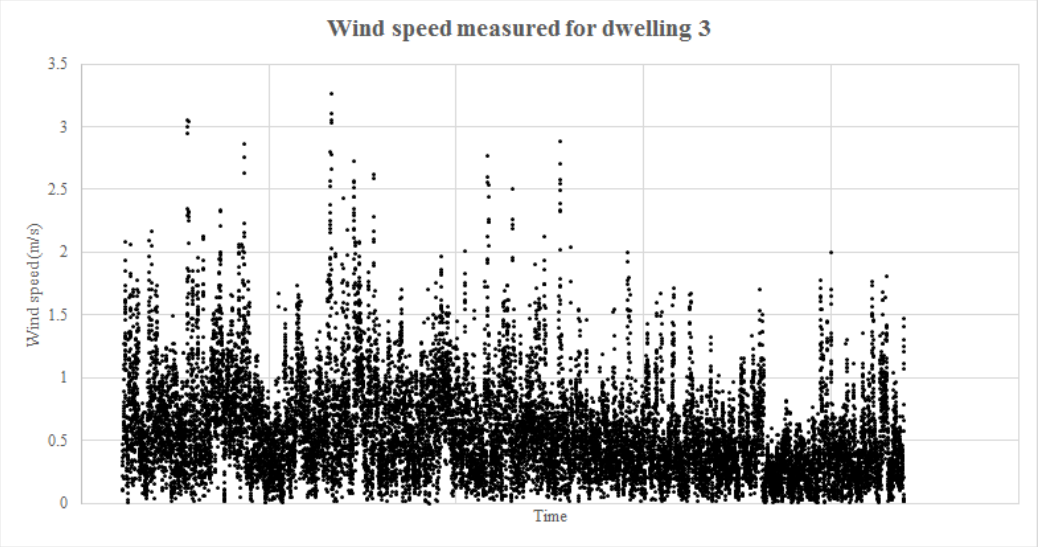


Figure E.40: Measurements of wind speed in dwelling 3.

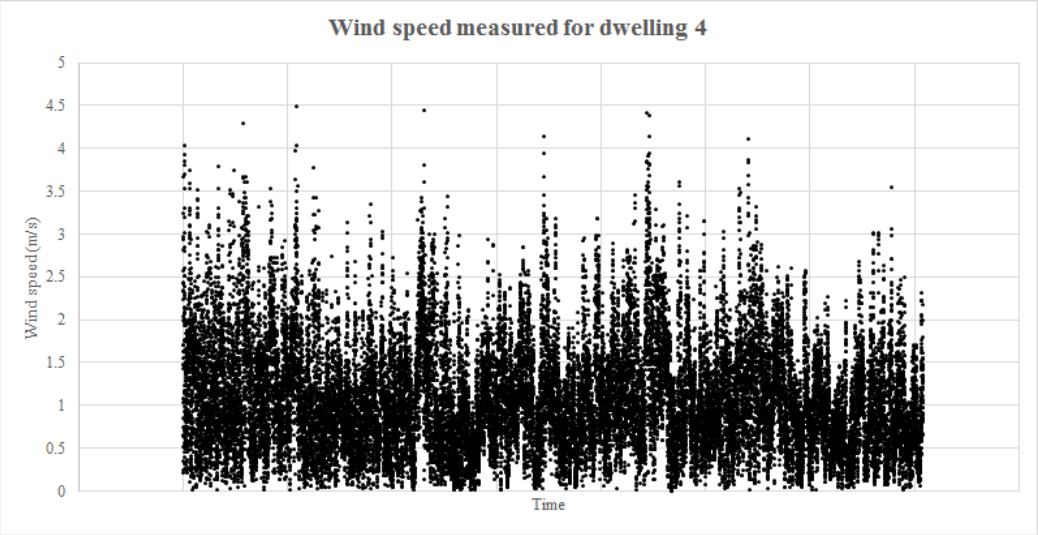


Figure E.41: Measurements of wind speed in dwelling 4.

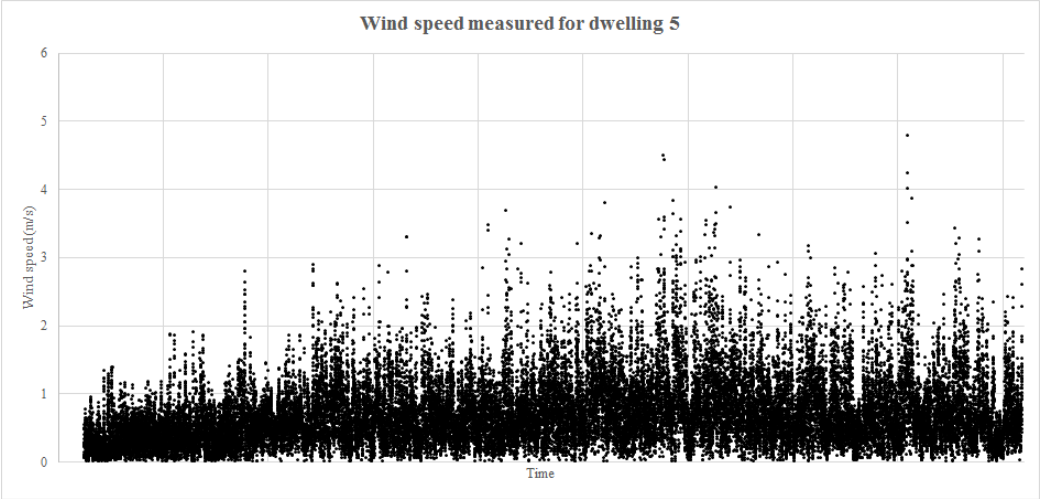


Figure E.42: Measurements of wind speed in dwelling 5.

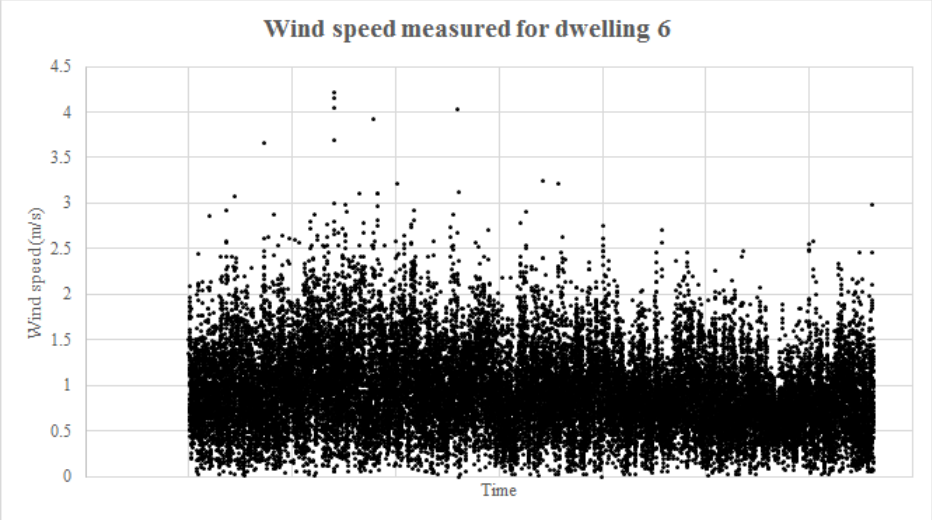


Figure E.43: Measurements of wind speed in dwelling 6.

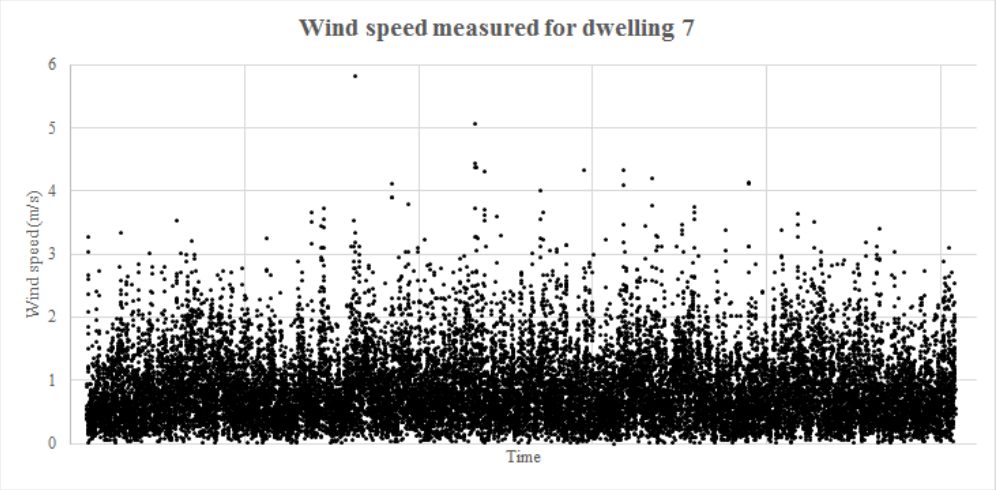


Figure E.44: Measurements of wind speed in dwelling 7.

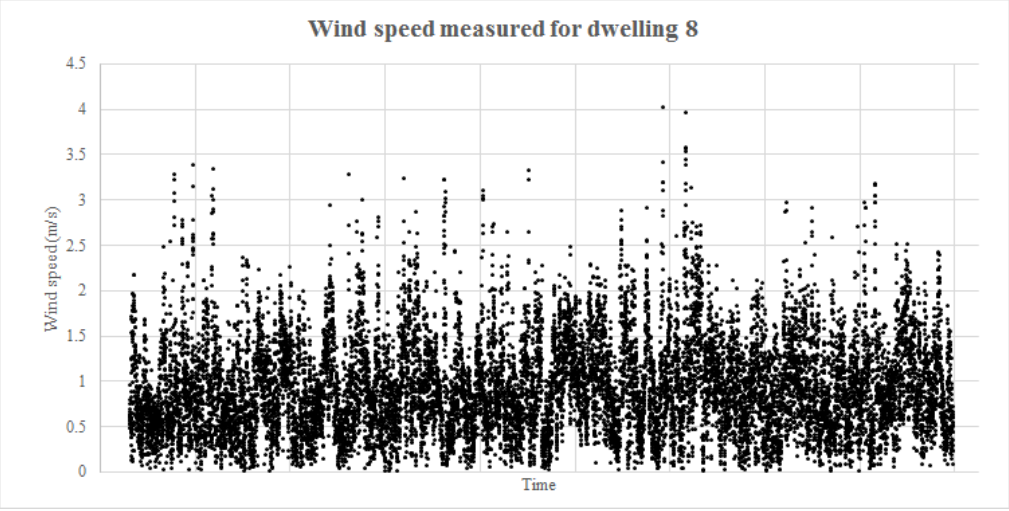


Figure E.45: Measurements of wind speed in dwelling 8.

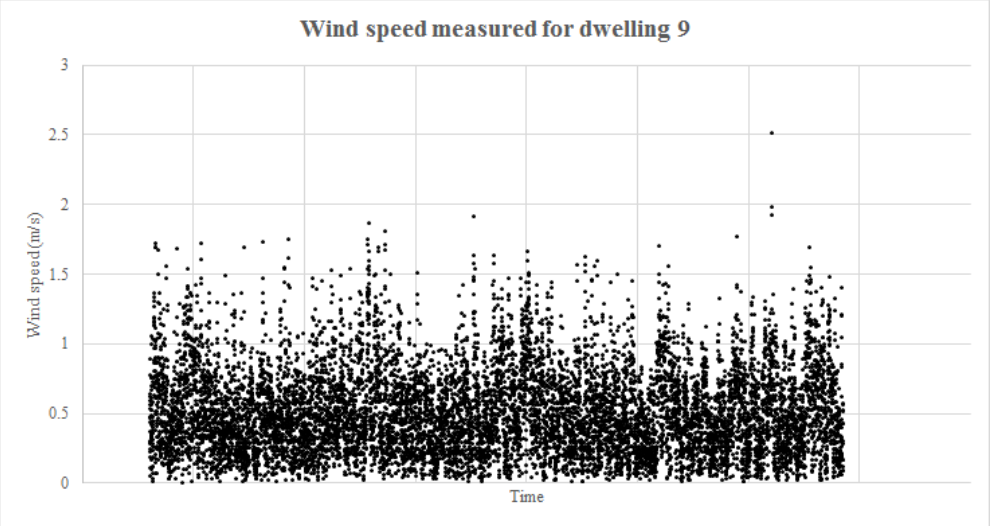


Figure E.46: Measurements of wind speed in dwelling 9.

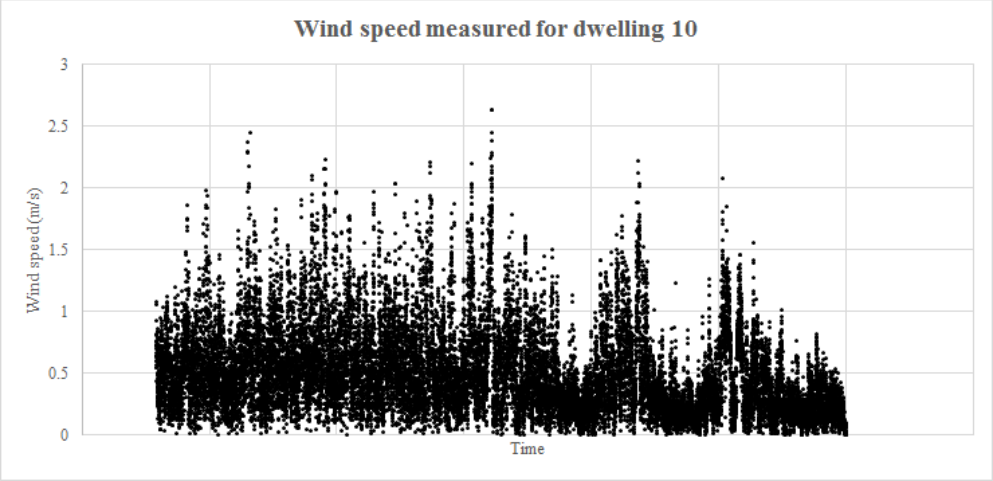


Figure E.47: Measurements of wind speed in dwelling 10.

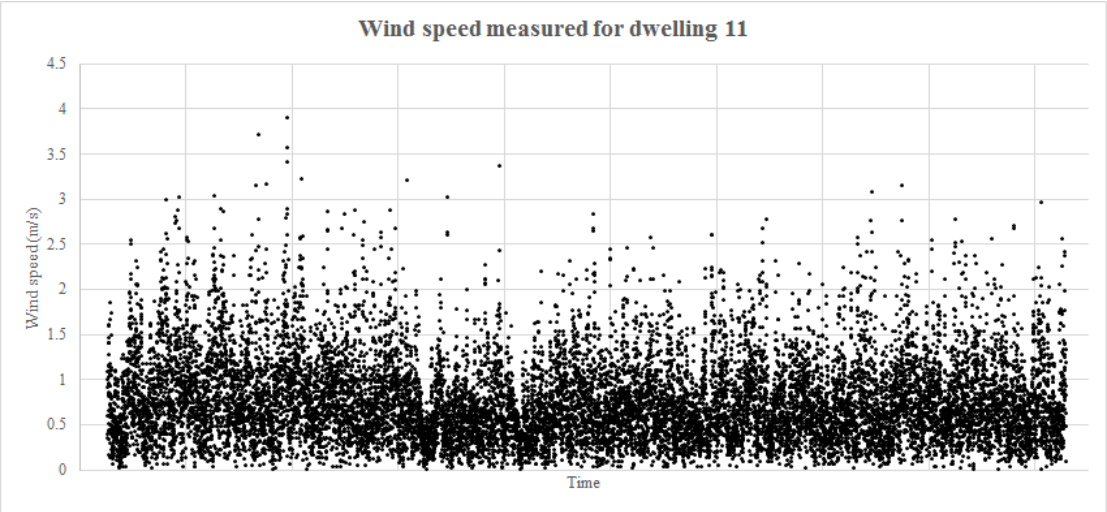


Figure E.48: Measurements of wind speed in dwelling 11.

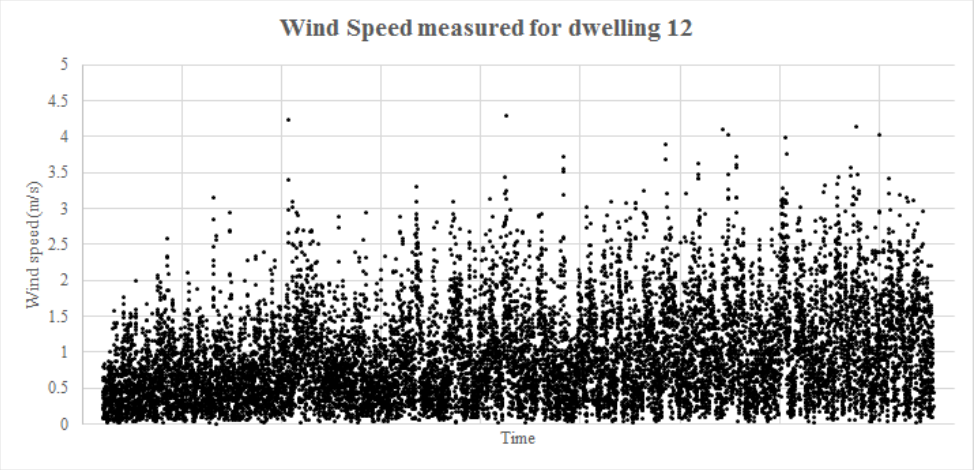


Figure E.49: Measurements of wind speed in dwelling 12.

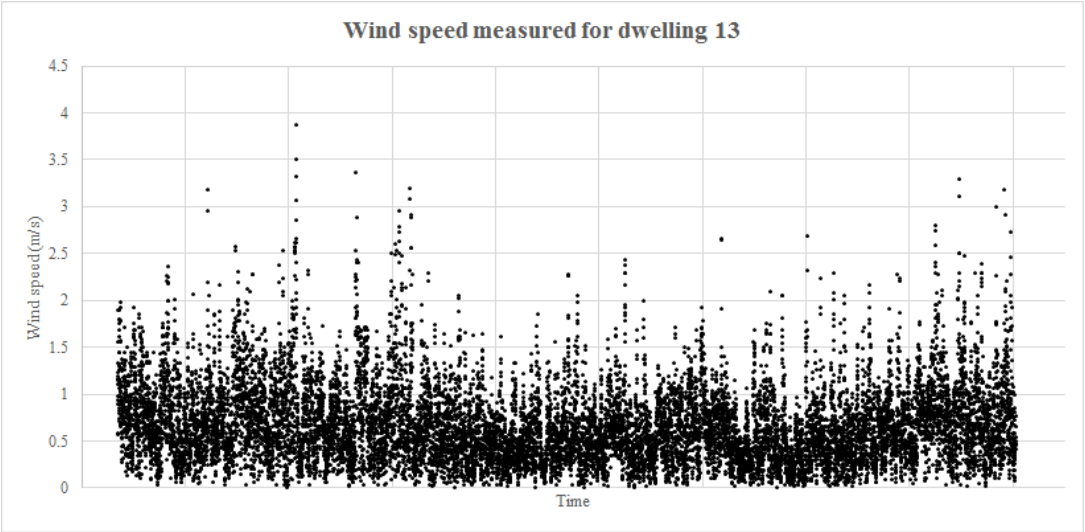


Figure E.50: Measurements of wind speed in dwelling 13.

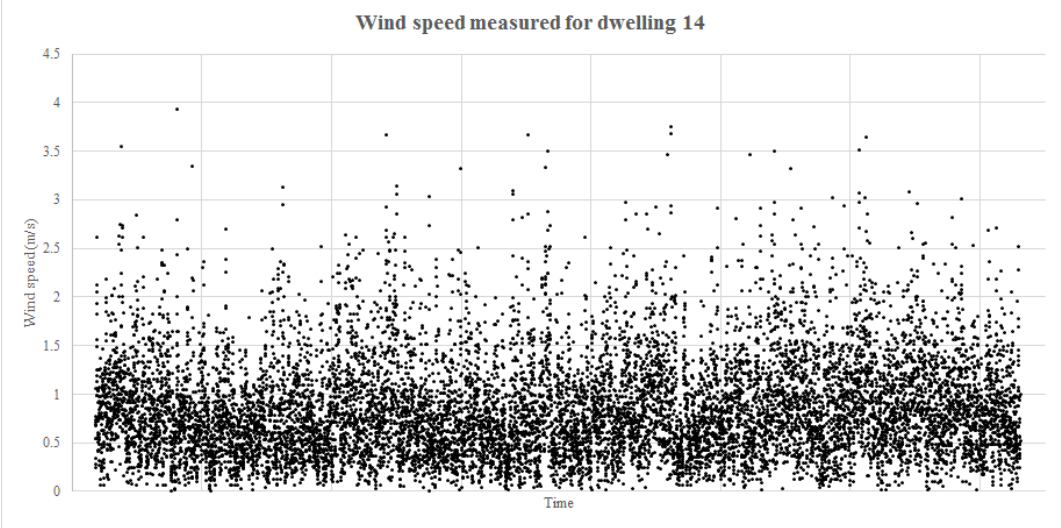


Figure E.51: Measurements of wind speed in dwelling 14.

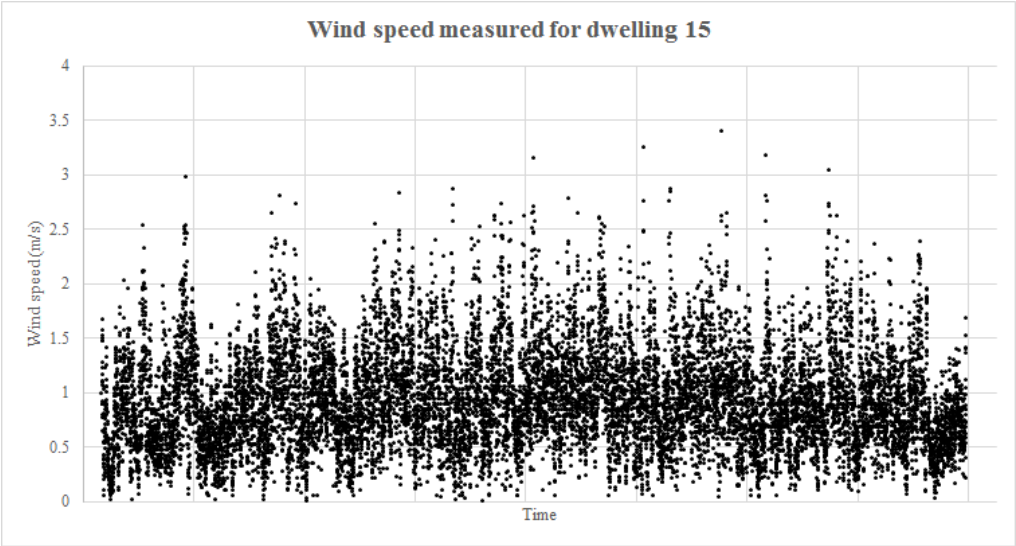


Figure E.52: Measurements of wind speed in dwelling 15.

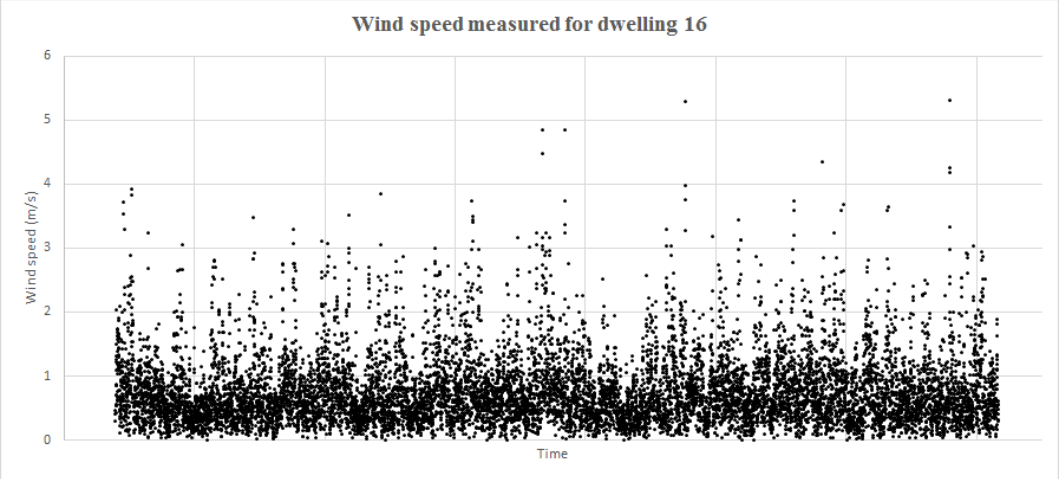


Figure E.53: Measurements of wind speed in dwelling 16.

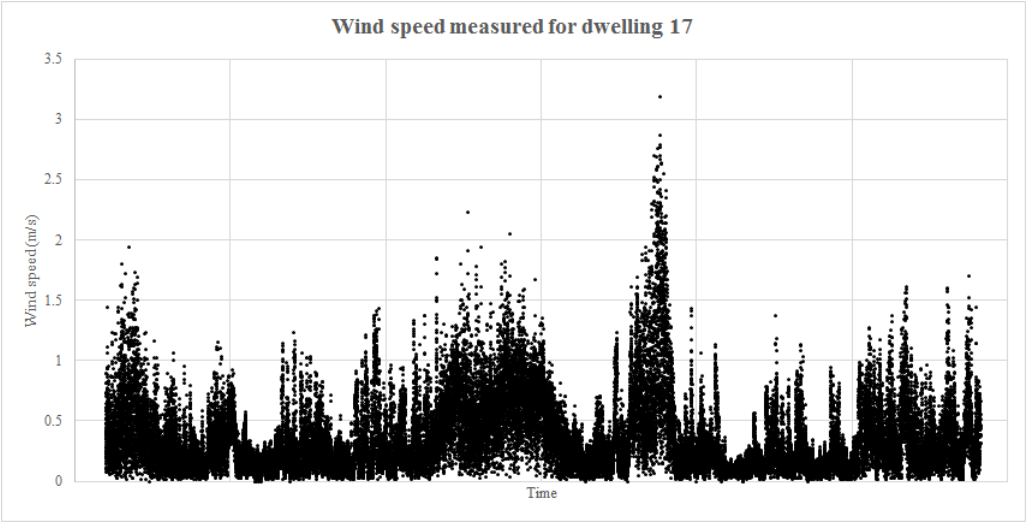


Figure E.54: Measurements of wind speed in dwelling 17.

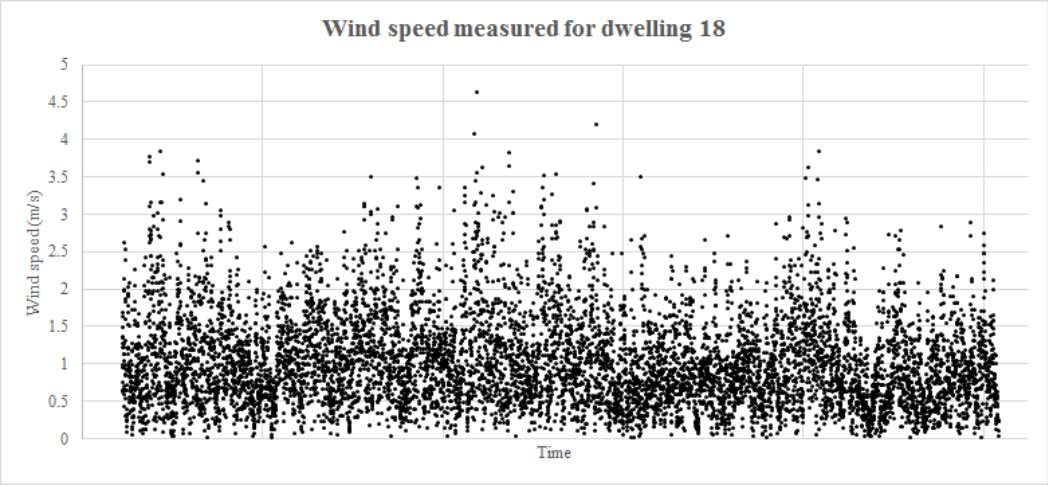


Figure E.55: Measurements of wind speed in dwelling 18.

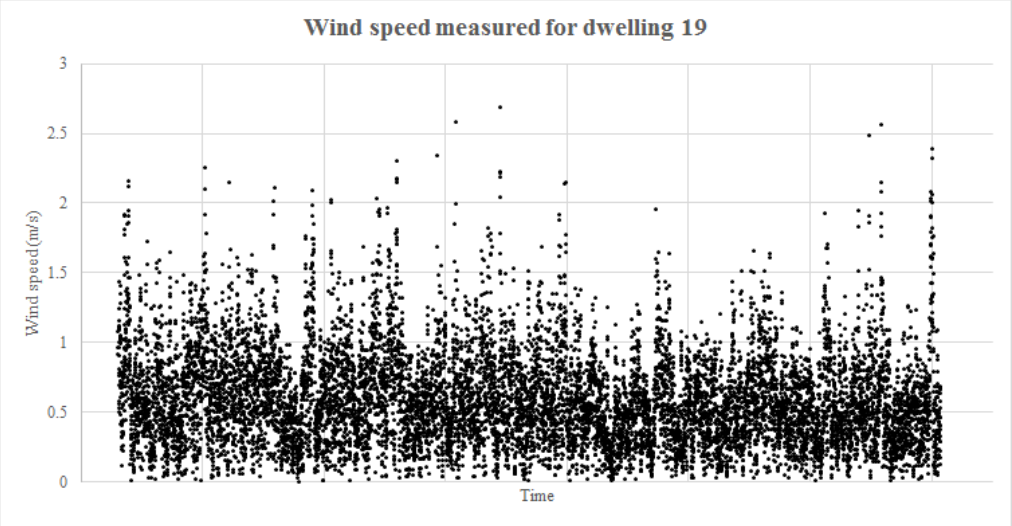


Figure E.56: Measurements of wind speed in dwelling 19.

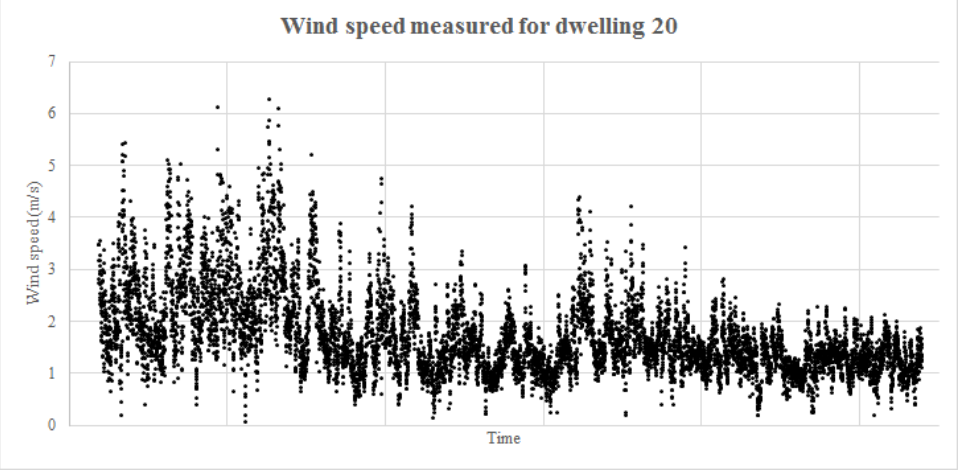


Figure E.57: Measurements of wind speed in dwelling 20.

Appendix F

LBL50 and LBL4 MATLAB code

The following code runs the LBL model for airtightness measurements at high (50 Pa) and low (4 Pa) pressure measurements, along with different inputs.

```
%% SECTION 1, initial calculations and definitions
%This section gets the information from field tests,
%enters the needed constants, and does the calculations to
%get the needed information tu run the model.
filename = 'LBL_data.xlsx';
%Reading the excel file including the data
sheet = 1; %sheet 1 from the document
A=xlsread(filename,sheet);

%Reading all the information from field data
Test_code = A(:,2); %Property test code
Vol = A(:,5); %Volume (m^3)
EnvArea = A(:,6); %Envelope area (m^2)
N50 = A(:,10);
%Airtightnes measured with the blower door (h-1) @50 Pa
b50 = A(:,21); %Blower door flow exponent
N4 = A(:,9); %Airtightnes measured with the Pulse (h-1) @4 Pa
b4 = A(:,22); %Pulse flow exponent

%Shielding condition according to LBL:
%1 = N0 = No shielding
%2 = LS = Light shielding
%3 = MS = Moderate shielding
%4 = HS = Heavy shielding
```

```
Shielding = A(:,13);

%Inputing measured weather conditions.
U = A(:,15); %Wind speed, m/s
Tint = (A(:,18))+ 273.15; %Average indoor temperature, K
Text = (A(:,19))+ 273.15; %Average outdoor temperature, K


%Entering the neccesary constants.
R = 287.055; %Gas constant, J/Kg.K
P0 = 101325; %Atmospheric pressure, Pa
Chc = 1004; %Specific heat capacity of air, J/Kg/K
g = 9.81; %Gravitational accelaration on earth m/s^2

%Initial calculations, density means, and differences
if  Tint-Text==0
%Temperature difference, a DeltaT = 0 will create an error
    %Revising that DeltaT is not 0
    fprintf('Error in AlanLBL, the temperature difference is 0');
else
    DeltaT = abs(Tint-Text);
    %if DeltaT is not 0, asign the variable, K
end
rext = (P0./R./Text); %External air density, kg/m^3
rint = (P0./R./Tint); %Internal air density, kg/m^3
rmean = ((rext+rint)./2); %Average air density
%calculate density multiplier that makes the rla dimensionless

%Calculating dwelling dimmensions, due to the lack of data,
%this model assumes the house as a cube and calculates the
%dimmension of each  dwelling accordingly, nevertheless,
%the envelope area and volume are accounted as measured .
H = (EnvArea./6).^(0.5); %Height
%Blower door
Q50 = N50.*(Vol./3600); %Air flow @50 Pa, m^3/s
C50 = Q50./(50.^b50); %constant from power law
Q50to4= C50.*(4.^b50);
```

```
%Air flow extrapolated from 50 to 4 Pa   m^3/s
ELA50 = Q50to4./(((4.*2)./rmean).^0.5);%Effective leakage area
%Pulse
Q4 = N4.*(Vol./3600); %Air flow @4 Pa, m^3/s
ELA4 = Q4./(((4.*2)./rmean).^0.5);%Effective leakage area



%% SECTION 2, Main, Calculation of the infiltration rate using
%Blower door measurements
%% Section 2.1, Calculations from measurements of the blower door
% Assumption 1: the ceiling and floor leakages are so small that
%can be neglected, therefore are 0
Ac1=0; %leakage area from the ceiling
Af1=0; % leakage area from the floor
for i=1:20
R1(i,1)= (Ac1+Af1)./ELA50(i,1);
X1(i,1)=(Ac1-Af1)./ELA50(i,1);
end

for i=1:20
fs1(i,1) =
((1+(R1(i,1)./2))./3).*((1-((X1(i,1).^2)./
((2-R1(i,1)).^2))).^(3./2));
%Stack factor
end

ShFac=[0.324;0.285;0.240;0.185;0.102]; %shielding factors from
%Sherman  and Dickinson (1985)
for i=1:20
    if Shielding(i,1)==1
        fw1(i,1) = ShFac(1).*((1-R1(i,1)).^(1./3)).*1 ;
    elseif Shielding(i,1)==2
        fw1(i,1) = ShFac(2).*((1-R1(i,1)).^(1./3)).*1 ;
    elseif Shielding(i,1)==3
        fw1(i,1) = ShFac(3).*((1-R1(i,1)).^(1./3)).*1 ;
```

```
    elseif Shielding(i,1)==4
        fw1(i,1) = ShFac(4).*((1-R1(i,1)).^(1./3)).*1 ;
    else
        disp('error in the shielding condition');
    end
end %wind factor, wind velocity is taken on site,
%therefore does not have to be corrected.

Qs1= ELA50.*fs1.*((g.*H.*(DeltaT./Tint)).^0.5);
%stack infiltration
Qw1= ELA50.*U.*fw1; %wind infiltration

Q1final = ((Qs1.^2)+(Qw1.^2)).^0.5 ;
%infiltration rate in m^3/s
N1final =  Q1final.*(3600./Vol) ;%infiltration in h^-1

%% Section 2.2, Calculations from measurements of the blower door
% Assumption 2: all the leakage area is equally distributed
% across every facade, therefore Ac and Af = ELA/6
for i=1:20
Ac2(i,1)= ELA50(i,1)./6; %leakage area from the ceiling
Af2(i,1)= ELA50(i,1)./6; % leakage area from the floor
end
for i=1:20
R2(i,1)= (Ac2(i,1)+Af2(i,1))./ELA50(i,1);
X2(i,1)=(Ac2(i,1)-Af2(i,1))./ELA50(i,1);
end

for i=1:20
fs2(i,1) = ((1+(R2(i,1)./2))./3).*((1-((X2(i,1).^2)./
((2-R2(i,1)).^2))).^(3./2));
%Stack factor
end

ShFac=[0.324;0.285;0.240;0.185;0.102]; %shielding factors
%from Sherman  and Dickinson (1985)
for i=1:20
```

```
    if Shielding(i,1)==1
        fw2(i,1) = ShFac(1).*((1-R2(i,1)).^(1./3)).*1 ;
    elseif Shielding(i,1)==2
        fw2(i,1) = ShFac(2).*((1-R2(i,1)).^(1./3)).*1 ;
    elseif Shielding(i,1)==3
        fw2(i,1)= ShFac(3).*((1-R2(i,1)).^(1./3)).*1 ;
    elseif Shielding(i,1)==4
        fw2(i,1)= ShFac(4).*((1-R2(i,1)).^(1./3)).*1 ;
    else
        disp('error in the shielding condition');
    end
end %wind factor, wind velocity is taken on site,
%therefore does not have to be corrected.

Qs2= ELA50.*fs2.*((g.*H.*(DeltaT./Tint)).^0.5); %stack infiltration
Qw2= ELA50.*U.*fw2; %wind infiltration

Q2final =((Qs2.^2)+(Qw2.^2)).^0.5 ;  %infiltration rate in m^3/s
N2final =  Q2final.*(3600./Vol) ; %infiltration in h^-1
%% Section 2.3, Calculations from measurements of the blower door
% Assumption 3: Using the values given by Sherman and
% Grimsrud (1980) for the stack and wind factor for a single
% story dwelling.
fs3= 0.12 ;
%stack factor using value given by Sherman and Grimsrud (1980)
fw3= 0.123;
%wind factor using value given by Sherman and Grimsrud (1980)

Qs3= ELA50.*fs3.*((g.*H.*(DeltaT./Tint)).^0.5);
%stack infiltration
Qw3= ELA50.*U.*fw3; %wind infiltration

Q3final = ((Qs3.^2)+(Qw3.^2)).^0.5 ;
%infiltration rate in m^3/s
N3final =  Q3final.*(3600./Vol) ; %infiltration in h^-1
```

```
%% SECTION 3, Main, Calculation of the infiltration rate using
%Pulse measurements
%% Section 3.1, Calculations from measurements of the Pulse
% Assumption 1: the ceiling and floor leakages are so small
%that can be  neglected, therefore are 0
AcP1=0; %leakage area from the ceiling
AfP1=0; % leakage area from the floor
for i=1:20
RP1(i,1)= (AcP1+AfP1)./ELA4(i,1);
XP1(i,1)=(AcP1-AfP1)./ELA4(i,1);
end

for i=1:20
fsP1(i,1) = ((1+(RP1(i,1)./2))./3).*((1-((XP1(i,1).^2)./
((2-RP1(i,1)).^2))).^(3./2));
%Stack factor
end

ShFac=[0.324;0.285;0.240;0.185;0.102]; %shielding factors
%from Sherman  and Dickinson (1985)
for i=1:20
    if Shielding(i,1)==1
        fwP1(i,1) = ShFac(1).*((1-RP1(i,1)).^(1./3)).*1 ;
    elseif Shielding(i,1)==2
        fwP1(i,1) = ShFac(2).*((1-RP1(i,1)).^(1./3)).*1 ;
    elseif Shielding(i,1)==3
        fwP1(i,1) = ShFac(3).*((1-RP1(i,1)).^(1./3)).*1 ;
    elseif Shielding(i,1)==4
        fwP1(i,1) = ShFac(4).*((1-RP1(i,1)).^(1./3)).*1 ;
    else
        disp('error in the shielding condition');
    end
end %wind factor, wind velocity is taken on site,
%therefore does not have to be corrected.

QsP1= ELA4.*fsP1.*((g.*H.*(DeltaT./Tint)).^0.5);
```

```
%stack infiltration
QwP1= ELA4.*U.*fwP1; %wind infiltration

QP1final = ((QsP1.^2)+(QwP1.^2)).^0.5 ;
%infiltration rate in m^3/s
NP1final =  QP1final.*(3600./Vol) ;%infiltration in h^-1

%% Section 3.2, Calculations from measurements of the Pulse
% Assumption 2: all the leakage area is equally distributed
% across every facade, therefore Ac and Af = ELA/6
for i=1:20
AcP2(i,1)= ELA4(i,1)./6; %leakage area from the ceiling
AfP2(i,1)= ELA4(i,1)./6; % leakage area from the floor
end

for i=1:20
RP2(i,1)= (AcP2(i,1)+AfP2(i,1))./ELA4(i,1);
XP2(i,1)=(AcP2(i,1)-AfP2(i,1))./ELA4(i,1);
end

for i=1:20
fsP2(i,1) = ((1+(RP2(i,1)./2))./3).*((1-((XP2(i,1).^2)./
((2-RP2(i,1)).^2))).^(3./2));
%Stack factor
end

ShFac=[0.324;0.285;0.240;0.185;0.102]; %shielding factors
%from Sherman  and Dickinson (1985)
for i=1:20
    if Shielding(i,1)==1
        fwP2(i,1) = ShFac(1).*((1-RP2(i,1)).^(1./3)).*1 ;
    elseif Shielding(i,1)==2
        fwP2(i,1) = ShFac(2).*((1-RP2(i,1)).^(1./3)).*1 ;
    elseif Shielding(i,1)==3
        fwP2(i,1) = ShFac(3).*((1-RP2(i,1)).^(1./3)).*1 ;
    elseif Shielding(i,1)==4
        fwP2(i,1) = ShFac(4).*((1-RP2(i,1)).^(1./3)).*1 ;
```

```
    else
        disp('error in the shielding condition');
    end
end %wind factor, wind velocity is taken on site,
%therefore does not have to be corrected.

QsP2= ELA4.*fsP2.*((g.*H.*(DeltaT./Tint)).^0.5);
%stack infiltration
QwP2= ELA4.*U.*fwP2; %wind infiltration

QP2final = ((QsP2.^2)+(QwP2.^2)).^0.5 ;
%infiltration rate in m^3/s
NP2final =  QP2final.*(3600./Vol) ;%infiltration in h^-1

%% Section 3.3, Calculations from measurements of the
% Assumption 3: Using the values given by Sherman and
% Grimsrud (1980) for the stack and wind factor for a
%single story dwelling.
fsP3= 0.12 ;
%stack factor using value given by Sherman and Grimsrud (1980)
fwP3= 0.123;
%wind factor using value given by Sherman and Grimsrud (1980)

QsP3= ELA4.*fsP3.*((g.*H.*(DeltaT./Tint)).^0.5);
%stack infiltration
QwP3= ELA4.*U.*fwP3; %wind infiltration

QP3final = ((QsP3.^2)+(QwP3.^2)).^0.5 ;
%infiltration rate in m^3/s
NP3final =  QP3final.*(3600./Vol) ;%infiltration in h^-1

%% SECTION 4, outputs
filename = 'LBL_data.xlsx';
sheet = 1;
xlRange='AA1:AA20';
xlswrite(filename,N1final,sheet,xlRange);
```

```
filename = 'LBL_data.xlsx';
sheet = 1;
xlRange='AB1:AB20';
xlswrite(filename,N2final,sheet,xlRange);

filename = 'LBL_data.xlsx';
sheet = 1;
xlRange='AC1:AC20';
xlswrite(filename,N3final,sheet,xlRange);

filename = 'LBL_data.xlsx';
sheet = 1;
xlRange='AD1:AD20';
xlswrite(filename,NP1final,sheet,xlRange);

filename = 'LBL_data.xlsx';
sheet = 1;
xlRange='AE1:AE20';
xlswrite(filename,NP2final,sheet,xlRange);

filename = 'LBL_data.xlsx';
sheet = 1;
xlRange='AF1:AF20';
xlswrite(filename,NP3final,sheet,xlRange);

display('finished, go to your file with the results')
```

Appendix G

DOMVENT3D-50 and DOMVENT3D-4 MATLAB code

The following MATLAB code runs the infiltration predicting model DOMVENT3D for airtightness measurements at high (50 Pa) and low (4 Pa) pressure measurements, along with different inputs.

```
%Alan_domvent runs the DOMVENT 3D model using the field data
%and predicts the infiltration rate. The programme reads
%an excel file including all the variales and writes in the
%same file the predicted infiltration rate and heat losses.

%% SECTION 1, initial calculations and definitions
%This section gets the information from field tests,
%enters the needed constants, and does the calculations to get
%the needed information tu run the model.
filename = 'DOMVENT3D_data.xlsx';
%Reading the excel file including the data
sheet = 1; %sheet 1 from the document
A=xlsread(filename,sheet);

%Reading all the information from field data
Test_code = A(:,2); %Property test code
Vol = A(:,5); %Volume (m^3)
EnvArea = A(:,6); %Envelope area (m^2)
N50 = A(:,10);
%Airtightnes measured with the blower door (h-1) @50 Pa
b50 = A(:,21); %Blower door flow exponent
```

```
N4 = A(:,9); %Airtightnes measured with the Pulse (h-1) @4 Pa
b4 = A(:,22); %Pulse flow exponent

%Shielding condition according to LBL:
%1 = HS = Heavy shielding
%2 = MS = Moderate shielding
%3 = LS = Light shielding
%4 = N0 = No shielding
Shielding = A(:,13);


%Terrain conditions:
%city=1
%urban=2
%suburban town=3
%rural residential=4
%village centre=5
%rural=6
Terrain = A(:,14);

%Dwelling type, this model does not account for flats:
%end of terrace = 1
%mid terrace = 2
%semi detached = 3
%detached = 4
dwelling_type = A(:,17);

%Inputing measured weather conditions.
U = A(:,15); %Wind speed, m/s
Ud = A(:,20); %Wind direction, degrees
Tint = (A(:,18))+ 273.15; %Average indoor temperature, K
Text = (A(:,19))+ 273.15; %Average outdoor temperature, K

%Calculating dwelling dimensions, due to the lack of data,
%this model assumes the house as a cube and calculates the
%dimension of each dwelling accordingly, nevertheless, the
%envelope area and volume are accounted as measured .
```

```
W = (EnvArea./6).^(0.5); %Width
H = (EnvArea./6).^(0.5); %Height
D = (EnvArea./6).^(0.5); %Depth
P50 = N50.*(Vol./EnvArea);%Air permeability @50 Pa, m^3/h/m^2
P4 = N4.*(Vol./EnvArea);%Air permeability @4 Pa, m^3/h/m^2

%Entering the neccesary constants.
R = 287.055; %Gas constant, J/Kg.K
P0 = 101325; %Atmospheric pressure, Pa
Chc = 1004; %Specific heat capacity of air, J/Kg/K
g = 9.81; %Gravitational accelaration on earth m/s^2

%Initial calculations, density means, and differences
Tmean = (Tint+Text)./2; %Average temperature
if  Tint-Text==0 %Temperature difference,
% a DeltaT = 0 will create an error
    %Revising that DeltaT is not 0
    fprintf('Error in Alan_domvent, the temperature difference is 0');
else
    DeltaT = Tint-Text;
    %if DeltaT is not 0, asign the variable, K
end
rext = (P0./R./Text); %External air density, kg/m^3
rint = (P0./R./Tint); %Internal air density, kg/m^3
rmean = ((rext+rint)./2); %Average air density
Deltar = rint-rext; %Air density difference
% calculate the density multiplier that makes the rla
%dimensionless
a50  = rmean.*(2./rmean).^b50;
% this statement assumes airtighness measurements with the
%blower door
a4 = rmean.*(2./rmean).^b4;
% this statement assumed airtighness measurements with the
%Pulse
E50 = (P50.*EnvArea.*rmean)./(3600.*EnvArea.*a50.*50.^b50);
%relative leakage area @50 Pa
E4 = (P4.*EnvArea.*rmean)./(3600.*EnvArea.*a4.*4.^b4);
```

```
%relative leakage area @4 Pa

%% SECTION 2, Main, calculation of Pi using blower door.
%This section runs the model according to Jones et. al. 2013
%and Jones et. al. 2015 and the original DOMVENT3D model
%by Jones.

%Getting the exposed facades.is a boolean parameter, 1 means
%exposed facade, and 0 represent an unexposed facade, the
%number after the EF represents the orientation of the
%mentioned facade.
EF0 = A(:,23);
EF90 = A(:,24);
EF180 = A(:,25);
EF270 = A(:,26);
%Calculating the areas of every facade
A0 = W.*H;
A90 = D.*H;
A180 = W.*H;
A270 = D.*H;
Afloor = W.*D;
Aroof = W.*D;
%Defining orientation vectors, the transposed is used
%considering each one represents one element (file).
O0 = [0,0,0,0,0,0,0,0,0,0,0,0,0,0,0,0,0,0,0,0,0]';
O90 = [90,90,90,90,90,90,90,90,90,90,90,90,90,90,90,
90,90,90,90,90]';
O180 = [180,180,180,180,180,180,180,180,180,180,180,
180,180,180,180,180,180,180,180,180]';
O270 = [270,270,270,270,270,270,270,270,270,270,270,270,270,270,
270,270,270,270,270,270]';
%Calculating the wind incidence in radians in every facade
Ui0=zeros(size(Ud));
Ui90=zeros(size(Ud));
Ui180=zeros(size(Ud));
Ui270=zeros(size(Ud));
%first facade 0 degrees
```

```
for j=1:20
if Ud(j,1)<=180
    Ui0(j,1) = Ud(j,1).*pi()./180;
else
    Ui0(j,1) = (360-Ud(j,1)).*pi()./180;
end
end
%second facade 90 degress
for j=1:20
if abs(O90(j,1)-Ud(j,1))<=180
    Ui90(j,1) = (abs(O90(j,1)-Ud(j,1))).*pi()./180;
else
    Ui90(j,1) = (360-abs(O90(j,1)-Ud(j,1))).*pi()./180;
end
end
%third facade 180 degrees
for j=1:20
if abs(O180(j,1)-Ud(j,1))<=180
    Ui180(j,1) = (abs(O180(j,1)-Ud(j,1))).*pi()./180;
else
    Ui180(j,1) = (360-abs(O180(j,1)-Ud(j,1))).*pi()./180;
end
end
%fourth facade 270 degrees
for j=1:20
if abs(O270(j,1)-Ud(j,1))<=180
    Ui270(j,1) = (abs(O270(j,1)-Ud(j,1))).*pi()./180;
else
    Ui270(j,1) = (360-abs(O270(j,1)-Ud(j,1))).*pi()./180;
end
end
%Calculation of Cp
%C is the constant vector of wind pressure coefficients
C = [1.248;-0.703;-1.175;0.131;0.769;0.071;0.717];
 % set the aspect of low-rise flats or terraced houses
 aspect=zeros(size(dwelling_type));
 for i=1:20
```

```
if dwelling_type(i,1) == 1
%aspect_terr_max = 20
%aspect_terr_min = 3
     aspect(i,1)= rand(1).*(20-3)+3;
     aspect(i,1)= round(aspect(i,1),0)*W(i,1)./D(i,1);
elseif dwelling_type(i,1) == 2
%aspect_terr_max = 20
%aspect_terr_min = 3
%these parameters were obtained from the original domvent
     aspect(i,1) = rand(1).*(20-3)+3;
     aspect(i,1) = round(aspect(i,1),0)*W(i,1)./D(i,1);
 % detached
 elseif dwelling_type(i,1) == 4
       aspect(i,1) = W(i,1)./D(i,1);
 % sem-detached
elseif dwelling_type(i,1) == 3
        aspect(i,1) = 2.*W(i,1)./D(i,1);
 else
     disp('error');
end
 end
%G is the aspect coeficcient
G = log(aspect);
%Cp are the coefficient of pressure for the calculation of
%wind pressuresacting in every facade.
Cp0 = log(C(1)+C(2).*sin(Ui0./2)+C(3).*sin(Ui0).^2
+C(4).*sin(2.*Ui0.*G).^3
+C(5).*cos(Ui0./2)+C(6).*G.^2.*sin(Ui0./2).^2+
C(7).*cos(Ui0./2).^2);
Cp90 = log(C(1)+C(2).*sin(Ui90./2)+C(3).*sin(Ui90).^2
+C(4).*sin(2.*Ui90.*G).^3+C(5).*cos(Ui90./2)+
C(6).*G.^2.*sin(Ui90./2).^2+C(7).*cos(Ui90./2).^2);
Cp180 = log(C(1)+C(2).*sin(Ui180./2)+C(3).*sin(Ui180).^2
+C(4).*sin(2.*Ui180.*G).^3+C(5).*cos(Ui180./2)+
C(6).*G.^2.*sin(Ui180./2).^2+C(7).*cos(Ui180./2).^2);
Cp270 = log(C(1)+C(2).*sin(Ui270./2)+C(3).*sin(Ui270).^2
+C(4).*sin(2.*Ui270.*G).^3+C(5).*cos(Ui270./2)
```

```
+C(6).*G.^2.*sin(Ui270./2).^2+C(7).*cos(Ui270./2).^2);

ShFac=[0.6;0.528;0.446;0.3426;0.189];
for i=1:20
 if Shielding(i,1)==4
Cp0(i,1)=Cp0(i,1).*ShFac(1);
Cp90(i,1)=Cp90(i,1).*ShFac(1);
Cp180(i,1)=Cp180(i,1).*ShFac(1);
Cp270(i,1)=Cp270(i,1).*ShFac(1);
    elseif Shielding(i,1)==3
Cp0(i,1) =Cp0(i,1).*ShFac(2);
Cp90(i,1) =Cp90(i,1).*ShFac(2);
Cp180(i,1) =Cp180(i,1).*ShFac(2);
Cp270(i,1) =Cp270(i,1).*ShFac(2);
    elseif Shielding(i,1)==2
Cp0(i,1) =Cp0(i,1).*ShFac(3);
Cp90(i,1) =Cp90(i,1).*ShFac(3);
Cp180(i,1) =Cp180(i,1).*ShFac(3);
Cp270(i,1) =Cp270(i,1).*ShFac(3);
    elseif Shielding(i,1)==1
Cp0(i,1) =Cp0(i,1).*ShFac(4);
Cp90(i,1) =Cp90(i,1).*ShFac(4);
Cp180(i,1) =Cp180(i,1).*ShFac(4);
Cp270(i,1) =Cp270(i,1).*ShFac(4);
    else
disp('error in the shielding condition');
    end
end
%Calculating the wind pressure for every facade
Pwind0=0.5.*rext.*U.*U.*Cp0;
Pwind90=0.5.*rext.*U.*U.*Cp90;
Pwind180=0.5.*rext.*U.*U.*Cp180;
Pwind270=0.5.*rext.*U.*U.*Cp270;

%Determinating the internal pressure using the
    % NEWTON RAPHSON SOVLER
 %definig the initial parameter for the solver
```

```
    % initial caclulation,
    %i have to include the new code here.
%here last_qnet is calculated using an assumed Pi
    % Loop until the net flow rate is zero
this_Pi = [1,0,0,0,0,0,0,0,0,0,0,0,0,0,0,0,0,0,0,0,0]';
Qnet       = [1,1,1,1,1,1,1,1,1,1,1,1,1,1,1,1,1,1,1,1,1]';
last_Qnet=zeros(size(Qnet));
    for i=1:20
iteration_max_raphson(i,1) = 50;
dPi                   = 0.0001;
last_Pi   = this_Pi(i,1) - 2.*dPi;
criterion(i,1)  = 1e-3;
iterations(i,1) = 0;
overshoots(i,1) = 0;
%facade neutral height relative to ground level
z0(i,1) = (Pwind0(i,1)-last_Pi)./((rext(i,1)-rint(i,1)).*g);
z90(i,1) = (Pwind90(i,1)-last_Pi)./((rext(i,1)-rint(i,1)).*g);
z180(i,1) = (Pwind180(i,1)-last_Pi)./((rext(i,1)-rint(i,1)).*g);
z270(i,1) = (Pwind270(i,1)-last_Pi)./((rext(i,1)-rint(i,1)).*g);
%Vertical facades
% facade mass flow rate in and out
% infiltration when tint>text and visa versa
negz0(i,1)= z0(i,1)>0; % negative neutral height ***
negz90(i,1)= z90(i,1)>0; % negative neutral height ***
negz180(i,1)= z180(i,1)>0; % negative neutral height ***
negz270(i,1)      = z270(i,1)>0; % negative neutral height ***
highz0(i,1)     = z0(i,1)>H(i,1);
% neutral height above the facade height
highz90(i,1)     = z90(i,1)>H(i,1);
% neutral height above the facade height
highz180(i,1)     = z180(i,1)>H(i,1);
% neutral height above the facade height
highz270(i,1)     = z270(i,1)>H(i,1);
% neutral height above the facade height
integral_A0(i,1) =
```

```
sign(z0(i,1)).*abs(z0(i,1).^(b50(i,1)+1));
% between floor level and neutral height ***
integral_A90(i,1) =
 sign(z90(i,1)).*abs(z90(i,1).^(b50(i,1)+1));
% between floor level and neutral height ***
integral_A180(i,1) =
sign(z180(i,1)).*abs(z180(i,1).^(b50(i,1)+1));
% between floor level and neutral height ***
integral_A270(i,1)  =
sign(z270(i,1)).*abs(z270(i,1).^(b50(i,1)+1));
% between floor level and neutral height ***
integral_A0(~negz0(i,1)) = 0; % no infiltration
integral_A90(~negz90(i,1))  = 0; % no infiltration
integral_A180(~negz180(i,1))  = 0; % no infiltration
integral_A270(~negz270(i,1))  = 0;  % no infiltration
integral_B0(i,1) = -(sign(z0(i,1)-H(i,1)))
.*abs((z0(i,1)-H(i,1)).^(b50(i,1)+1));
% remove flow between facade height and neutral height
integral_B90(i,1) = -(sign(z90(i,1)-H(i,1)))
.*abs((z90(i,1)-H(i,1)).^(b50(i,1)+1));
% remove flow between facade height and neutral height
integral_B180(i,1) = -(sign(z180(i,1)-H(i,1)))
.*abs((z180(i,1)-H(i,1)).^(b50(i,1)+1));
% remove flow between facade height and neutral height
integral_B270(i,1) = -(sign(z270(i,1)-H(i,1)))
.*abs((z270(i,1)-H(i,1)).^(b50(i,1)+1));
% remove flow between facade height and neutral height
integral_B0(~highz0(i,1)) = 0;
integral_B90(~highz90(i,1)) = 0;
integral_B180(~highz180(i,1)) = 0;
integral_B270(~highz270(i,1)) = 0;
% exfiltration when tint>text and visa versa
integral_C0(i,1) = sign((H(i,1)-z0(i,1)))
.*abs(((H(i,1)-z0(i,1))).^(b50(i,1)+1));
% between neutral height and facade height ***
integral_C90(i,1) = sign((H(i,1)-z90(i,1)))
.*abs(((H(i,1)-z90(i,1))).^(b50(i,1)+1));
```

```
% between neutral height and facade height ***
integral_C180(i,1) = sign((H(i,1)-z180(i,1)))
.*abs(((H(i,1)-z180(i,1))).^(b50(i,1)+1));
% between neutral height and facade height ***
integral_C270(i,1) = sign((H(i,1)-z270(i,1)))
.*abs(((H(i,1)-z270(i,1))).^(b50(i,1)+1));
% between neutral height and facade height ***
integral_C0(highz0(i,1))  = 0;% no exfiltration
integral_C90(highz90(i,1))  = 0; % no exfiltration
integral_C180(highz180(i,1))  = 0; % no exfiltration
integral_C270(highz270(i,1))  = 0; % no exfiltration
integral_D0(i,1)  = -(sign(abs(z0(i,1))))
.*abs((abs(z0(i,1))).^(b50(i,1)+1));
% remove flow between floor level and negative neutral height
integral_D90(i,1)  = -(sign(abs(z90(i,1))))
.*abs((abs(z90(i,1))).^(b50(i,1)+1));
% remove flow between floor level and negative neutral height
integral_D180(i,1)  = -(sign(abs(z180(i,1))))
.*abs((abs(z180(i,1))).^(b50(i,1)+1));
% remove flow between floor level and negative neutral height
integral_D270(i,1)  = -(sign(abs(z270(i,1))))
.*abs((abs(z270(i,1))).^(b50(i,1)+1));
% remove flow between floor level and negative neutral height
integral_D0(negz0(i,1))   = 0;
integral_D90(negz90(i,1))   = 0;
integral_D180(negz180(i,1))   = 0;
integral_D270(negz270(i,1))   = 0;

% coefficient
Coeff(i,1) = W(i,1).*((1./(b50(i,1)+1)).*E50(i,1).*a50(i,1)
.*((abs(rint(i,1)-rext(i,1)).*g).^b50(i,1)));
% Mass flow rates (kg/s)
if Tint(i,1)>Text(i,1)
minf0(i,1) = Coeff(i,1).*(integral_A0(i,1)
+integral_B0(i,1));
minf90(i,1) = Coeff(i,1).*(integral_A90(i,1)
+integral_B90(i,1));
```

```
minf180(i,1) = Coeff(i,1).*(integral_A180(i,1)
+integral_B180(i,1));
minf270(i,1) = Coeff(i,1).*(integral_A270(i,1)
+integral_B270(i,1));
mexf0(i,1) = Coeff(i,1).*(integral_C0(i,1)
+integral_D0(i,1));
mexf90(i,1) = Coeff(i,1).*(integral_C90(i,1)
+integral_D90(i,1));
mexf180(i,1) = Coeff(i,1).*(integral_C180(i,1)
+integral_D180(i,1));
mexf270(i,1) = Coeff(i,1).*(integral_C270(i,1)
+integral_D270(i,1));
        else
mexf0(i,1) = Coeff(i,1).*(integral_A0(i,1)+integral_B0(i,1));
mexf90(i,1) = Coeff(i,1).*(integral_A90(i,1)+integral_B90(i,1));
mexf180(i,1) = Coeff(i,1).*(integral_A180(i,1)
+integral_B180(i,1));
mexf270(i,1) = Coeff(i,1).*(integral_A270(i,1)
+integral_B270(i,1));
minf0(i,1) = Coeff(i,1).*(integral_C0(i,1)+integral_D0(i,1));
minf90(i,1) = Coeff(i,1).*(integral_C90(i,1)+integral_D90(i,1));
minf180(i,1) = Coeff(i,1).*(integral_C180(i,1)
+integral_D180(i,1));
minf270(i,1) = Coeff(i,1).*(integral_C270(i,1)
+integral_D270(i,1));
        end

    % HORIZONTAL FACADE FUNCTIONS
% function to calculate flow rate through horizontal given the
% internal air pressure Pi
pc(i,1) = (rint(i,1)-rext(i,1)).*g.*H(i,1) - last_Pi;
% pressure difference across facade (Pa)
% Buoyancy flow calculation only ceiling
pf(i,1) = - last_Pi; % pressure difference across facade (Pa)
% Buoyancy flow calculation only floor
mc(i,1) = sign(pc(i,1)).*rmean(i,1).*Coeff(i,1)
.*abs(pc(i,1)).^b50(i,1);
```

```
% volume flow rate through facade (kg/s)
mf(i,1) = sign(pf(i,1)).*rmean(i,1).*Coeff(i,1)
.*abs(pf(i,1)).^b50(i,1);
% volume flow rate through facade (kg/s)
%multiplied by mean density rmean
        if mc(i,1)>=0
minfhc(i,1) = mc(i,1);     % infiltration (kg/s)
        else
minfhc(i,1)=0;
        end
        if mf(i,1)>=0
minfhf(i,1) = mf(i,1);     % infiltration (kg/s)
        else
minfhf(i,1)=0;
        end
        if mc(i,1)<0
mexfhc(i,1) = abs(mc(i,1)); % exfiltration (kg/s)
        else
mexfhc(i,1)=0;
        end
        if mf(i,1)<0
mexfhf(i,1) = abs(mf(i,1)); % exfiltration (kg/s)
        else
mexfhf(i,1)=0;
        end

for j=1:20
     if EF0(i,1)==0
minf0(i,1)=0;
mexf0(i,1)=0;
     end
      if EF90(i,1)==0
minf90(i,1)=0;
mexf90(i,1)=0;
      end
       if EF180(i,1)==0
minf180(i,1)=0;
```

```
mexf180(i,1)=0;
       end
        if EF270(i,1)==0
minf270(i,1)=0;
mexf270(i,1)=0;
        end
 end
% total airflow rate
minft(i,1)  = minf0(i,1)+minf90(i,1)+minf180(i,1)
+minf270(i,1)+minfhc(i,1)+minfhf(i,1);
% infiltration (kg/s)
mexft(i,1)  = mexf0(i,1)+mexf90(i,1)+mexf180(i,1)
+mexf270(i,1)+mexfhc(i,1)+mexfhf(i,1);
% exfiltration (kg/s)
mtotal(i,1) = minft(i,1) - mexft(i,1);
% net mass flow rate (kg/s)
qtotal(i,1) = 1000.*(minft(i,1) - mexft(i,1))./rmean(i,1);
% net volume flow rate (l/s)
last_Qnet(i,1)=qtotal(i,1);

    while((abs(Qnet(i,1)) > criterion(i,1))
& (iterations(i,1) < iteration_max_raphson(i,1)))
iterations(i,1) = iterations(i,1) + 1;
% if the difference between current pi and last calculated pi is
% too small then re-scale the last calculated value
if (abs(this_Pi(i,1)-last_Pi) < abs(dPi))
last_Pi = this_Pi(i,1) - (this_Pi(i,1)-last_Pi)./10.0;
        end

% estimate mass flow rates through all facade
%here starts the calculation for Qnet using this_pi
z0(i,1) =
(Pwind0(i,1)-this_Pi(i,1))./((rext(i,1)-rint(i,1)).*g);
z90(i,1) =
(Pwind90(i,1)-this_Pi(i,1))./((rext(i,1)-rint(i,1)).*g);
z180(i,1) =
(Pwind180(i,1)-this_Pi(i,1))./((rext(i,1)-rint(i,1)).*g);
```

```
z270(i,1) =
(Pwind270(i,1)-this_Pi(i,1))./((rext(i,1)-rint(i,1)).*g);
%Vertical facades
% facade mass flow rate in and out
% infiltration when tint>text and visa versa
negz0(i,1)      = z0(i,1)>0; % negative neutral height
negz90(i,1)      = z90(i,1)>0; % negative neutral height
negz180(i,1)      = z180(i,1)>0; % negative neutral height
negz270(i,1)      = z270(i,1)>0; % negative neutral height
highz0(i,1)     = z0(i,1)>H(i,1);
% neutral height above the facade height
highz90(i,1)     = z90(i,1)>H(i,1);
% neutral height above the facade height
% neutral height above the facade height
highz270(i,1)     = z270(i,1)>H(i,1);
% neutral height above the facade height
integral_A0(i,1) =
sign(z0(i,1)).*abs(z0(i,1).^(b50(i,1)+1));
% between floor level and neutral height ***
integral_A90(i,1) =
sign(z90(i,1)).*abs(z90(i,1).^(b50(i,1)+1));
% between floor level and neutral height ***
integral_A180(i,1) =
sign(z180(i,1)).*abs(z180(i,1).^(b50(i,1)+1));
% between floor level and neutral height ***
integral_A270(i,1)  =
sign(z270(i,1)).*abs(z270(i,1).^(b50(i,1)+1));
% between floor level and neutral height ***
integral_A0(~negz0(i,1)) = 0; % no infiltration
integral_A90(~negz90(i,1))  = 0;% no infiltration
integral_A180(~negz180(i,1))  = 0;% no infiltration
integral_A270(~negz270(i,1))  = 0;% no infiltration
integral_B0(i,1) = -(sign(z0(i,1)-H(i,1))).*abs((z0(i,1)
        -H(i,1)).^(b50(i,1)+1));
% remove flow between facade height and neutral height
integral_B90(i,1) = -(sign(z90(i,1)-H(i,1))).*abs((z90(i,1)
        -H(i,1)).^(b50(i,1)+1));
```

```
% remove flow between facade height and neutral height
integral_B180(i,1) = -(sign(z180(i,1)-H(i,1))).*abs((z180(i,1)
        -H(i,1)).^(b50(i,1)+1));
% remove flow between facade height and neutral height
integral_B270(i,1) = -(sign(z270(i,1)-H(i,1))).*abs((z270(i,1)
        -H(i,1)).^(b50(i,1)+1));
% remove flow between facade height and neutral height
integral_B0(~highz0(i,1)) = 0;
integral_B90(~highz90(i,1)) = 0;
integral_B180(~highz180(i,1)) = 0;
integral_B270(~highz270(i,1)) = 0;
% exfiltration when tint>text and visa versa
integral_C0(i,1) = sign((H(i,1)-z0(i,1)))
        .*abs(((H(i,1)-z0(i,1))).^(b50(i,1)+1));
% between neutral height and facade height
integral_C90(i,1) = sign((H(i,1)-z90(i,1)))
        .*abs(((H(i,1)-z90(i,1))).^(b50(i,1)+1));
% between neutral height and facade height ***
integral_C180(i,1) = sign((H(i,1)-z180(i,1)))
        .*abs(((H(i,1)-z180(i,1))).^(b50(i,1)+1));
% between neutral height and facade height ***
integral_C270(i,1) = sign((H(i,1)-z270(i,1)))
        .*abs(((H(i,1)-z270(i,1))).^(b50(i,1)+1));
% between neutral height and facade height ***
integral_C0(highz0(i,1))  = 0;  % no exfiltration
integral_C90(highz90(i,1))  = 0; % no exfiltration
integral_C180(highz180(i,1))  = 0;% no exfiltration
integral_C270(highz270(i,1))  = 0;% no exfiltration
integral_D0(i,1)  = -(sign(abs(z0(i,1))))
        .*abs((abs(z0(i,1))).^(b50(i,1)+1));
% remove flow between floor level and negative neutral height
integral_D90(i,1)  = -(sign(abs(z90(i,1))))
        .*abs((abs(z90(i,1))).^(b50(i,1)+1));
% remove flow between floor level and negative neutral height
integral_D180(i,1)  = -(sign(abs(z180(i,1))))
        .*abs((abs(z180(i,1))).^(b50(i,1)+1));
% remove flow between floor level and negative neutral height
```

```
integral_D270(i,1)  = -(sign(abs(z270(i,1))))
        .*abs((abs(z270(i,1))).^(b50(i,1)+1));
% remove flow between floor level and negative neutral height
integral_D0(negz0(i,1)) = 0;
integral_D90(negz90(i,1)) = 0;
integral_D180(negz180(i,1))= 0;
integral_D270(negz270(i,1)) = 0;
        % coefficient
Coeff(i,1) = W(i,1).*((1./(b50(i,1)+1)).*E50(i,1).*a50(i,1)
        .*((abs(rint(i,1)-rext(i,1)).*g).^b50(i,1)));
% Mass flow rates (kg/s)
        if Tint(i,1)>Text(i,1)
minf0(i,1) = Coeff(i,1).*(integral_A0(i,1)+integral_B0(i,1));
minf90(i,1) = Coeff(i,1).*(integral_A90(i,1)+integral_B90(i,1));
minf180(i,1) = Coeff(i,1).*(integral_A180(i,1)
+integral_B180(i,1));
minf270(i,1) = Coeff(i,1).*(integral_A270(i,1)
+integral_B270(i,1));
mexf0(i,1) = Coeff(i,1).*(integral_C0(i,1)+integral_D0(i,1));
mexf90(i,1) = Coeff(i,1).*(integral_C90(i,1)+integral_D90(i,1));
mexf180(i,1) = Coeff(i,1).*(integral_C180(i,1)
+integral_D180(i,1));
mexf270(i,1) = Coeff(i,1).*(integral_C270(i,1)
+integral_D270(i,1));
        else
mexf0(i,1) = Coeff(i,1).*(integral_A0(i,1)+integral_B0(i,1));
mexf90(i,1) = Coeff(i,1).*(integral_A90(i,1)+integral_B90(i,1));
mexf180(i,1) = Coeff(i,1).*(integral_A180(i,1)
+integral_B180(i,1));
mexf270(i,1) = Coeff(i,1).*(integral_A270(i,1)
+integral_B270(i,1));
minf0(i,1) = Coeff(i,1).*(integral_C0(i,1)+integral_D0(i,1));
minf90(i,1) = Coeff(i,1).*(integral_C90(i,1)+integral_D90(i,1));
minf180(i,1) = Coeff(i,1).*(integral_C180(i,1)
+integral_D180(i,1));
minf270(i,1) = Coeff(i,1).*(integral_C270(i,1)
+integral_D270(i,1));
```

```
        end

    % HORIZONTAL FACADE FUNCTIONS
% function to calculate flow rate through horizontal given the
% internal air pressure Pi
pc(i,1) = (rint(i,1)-rext(i,1)).*g.*H(i,1) - this_Pi(i,1);
% pressure difference across facade (Pa)
% Buoyancy flow calculation only ceiling
pf(i,1) = - this_Pi(i,1);
% pressure difference across facade (Pa)
% Buoyancy flow calculation only floor
mc(i,1) = sign(pc(i,1)).*rmean(i,1).*Coeff(i,1)
       .*abs(pc(i,1)).^b50(i,1);
% volume flow rate through facade (kg/s)
mf(i,1) = sign(pf(i,1)).*rmean(i,1).*Coeff(i,1)
       .*abs(pf(i,1)).^b50(i,1);
% volume flow rate through facade (kg/s)
%multiplied by mean density rmean
        if mc(i,1)>=0
minfhc(i,1) = mc(i,1);     % infiltration (kg/s)
        else
minfhc(i,1)=0;
        end
        if mf(i,1)>=0
minfhf(i,1) = mf(i,1);     % infiltration (kg/s)
        else
minfhf(i,1)=0;
        end
        if mc(i,1)<0
mexfhc(i,1) = abs(mc(i,1)); % exfiltration (kg/s)
        else
mexfhc(i,1)=0;
        end
        if mf(i,1)<0
mexfhf(i,1) = abs(mf(i,1)); % exfiltration (kg/s)
        else
mexfhf(i,1)=0;
```

```
        end

for j=1:20
     if EF0(i,1)==0
minf0(i,1)=0;
mexf0(i,1)=0;
     end
      if EF90(i,1)==0
minf90(i,1)=0;
mexf90(i,1)=0;
      end
       if EF180(i,1)==0
minf180(i,1)=0;
mexf180(i,1)=0;
       end
        if EF270(i,1)==0
minf270(i,1)=0;
mexf270(i,1)=0;
        end
 end
% total airflow rate
minft(i,1)  = minf0(i,1)+minf90(i,1)+minf180(i,1)
    +minf270(i,1)+minfhc(i,1)+minfhf(i,1);
% infiltration (kg/s)
mexft(i,1)  = mexf0(i,1)+mexf90(i,1)+mexf180(i,1)
    +mexf270(i,1)+mexfhc(i,1)+mexfhf(i,1);
% exfiltration (kg/s)
mtotal(i,1) = minft(i,1) - mexft(i,1);
% net mass flow rate (kg/s)
qtotal(i,1) = 1000.*(minft(i,1) - mexft(i,1))./rmean(i,1);
% net volume flow rate (l/s)
Qnet(i,1)=qtotal(i,1);
%Here the model ends
% compare this prediction against the last

slope(i,1)=
(Qnet(i,1) - last_Qnet(i,1))./(this_Pi(i,1)-last_Pi);
```

```
% update variables for next iteration
last_Pi = this_Pi(i,1);
% calculate the next guess
this_Pi(i,1) = this_Pi(i,1) - Qnet(i,1)./slope(i,1);


% check if we've overshot the zero value
        if ((Qnet(i,1).*last_Qnet(i,1)) < 0.0)
overshoots(i,1) = overshoots(i,1) + 1;
        end

% update variables for next iteration
last_Qnet(i,1) = Qnet(i,1);
    end


%From now on, the last calculations will be done, basically it
%will repeat the last iteration of the solver.

Pi(i,1) = this_Pi(i,1);
    end
    %% SECTION 2.1, Main, Calculation of the infiltration rate
%here starts the calculation for Qnet using this_pi
z0(i,1) = (Pwind0(i,1)-Pi(i,1))./((rext(i,1)-rint(i,1)).*g);
z90(i,1) = (Pwind90(i,1)-Pi(i,1))./((rext(i,1)-rint(i,1)).*g);
z180(i,1) = (Pwind180(i,1)-Pi(i,1))./((rext(i,1)-rint(i,1)).*g);
z270(i,1) = (Pwind270(i,1)-Pi(i,1))./((rext(i,1)-rint(i,1)).*g);
%Vertical facades
% facade mass flow rate in and out
% infiltration when tint>text and visa versa
negz0(i,1)      = z0(i,1)>0; % negative neutral height
negz90(i,1)      = z90(i,1)>0; % negative neutral height ***
negz180(i,1)      = z180(i,1)>0; % negative neutral height ***
negz270(i,1)      = z270(i,1)>0; % negative neutral height ***
highz0(i,1)     = z0(i,1)>H(i,1);
% neutral height above the facade height
highz90(i,1)     = z90(i,1)>H(i,1);
```

```
% neutral height above the facade height
highz180(i,1)     = z180(i,1)>H(i,1);
% neutral height above the facade height
highz270(i,1)     = z270(i,1)>H(i,1);
% neutral height above the facade height
integral_A0(i,1) = sign(z0(i,1)).*abs(z0(i,1).^(b50(i,1)+1));
% between floor level and neutral height ***
integral_A90(i,1) =
sign(z90(i,1)).*abs(z90(i,1).^(b50(i,1)+1));
% between floor level and neutral height ***
integral_A180(i,1) =
sign(z180(i,1)).*abs(z180(i,1).^(b50(i,1)+1));
% between floor level and neutral height ***
integral_A270(i,1)  =
 sign(z270(i,1)).*abs(z270(i,1).^(b50(i,1)+1));
% between floor level and neutral height ***
integral_A0(~negz0(i,1)) = 0; % no infiltration
integral_A90(~negz90(i,1))  = 0;    % no infiltration
integral_A180(~negz180(i,1))  = 0;    % no infiltration
integral_A270(~negz270(i,1))  = 0;  % no infiltration
integral_B0(i,1) = -(sign(z0(i,1)-H(i,1)))
        .*abs((z0(i,1)-H(i,1)).^(b50(i,1)+1));
% remove flow between facade height and neutral height
integral_B90(i,1) = -(sign(z90(i,1)-H(i,1)))
        .*abs((z90(i,1)-H(i,1)).^(b50(i,1)+1));
% remove flow between facade height and neutral height
integral_B180(i,1) = -(sign(z180(i,1)-H(i,1)))
        .*abs((z180(i,1)-H(i,1)).^(b50(i,1)+1));
% remove flow between facade height and neutral height
integral_B270(i,1) = -(sign(z270(i,1)-H(i,1)))
        .*abs((z270(i,1)-H(i,1)).^(b50(i,1)+1));
% remove flow between facade height and neutral height
integral_B0(~highz0(i,1)) = 0;
integral_B90(~highz90(i,1)) = 0;
integral_B180(~highz180(i,1)) = 0;
integral_B270(~highz270(i,1)) = 0;
% exfiltration when tint>text and visa versa
```

```
integral_C0(i,1) = sign((H(i,1)-z0(i,1)))
        .*abs(((H(i,1)-z0(i,1))).^(b50(i,1)+1));
% between neutral height and facade height ***
integral_C90(i,1) = sign((H(i,1)-z90(i,1)))
        .*abs(((H(i,1)-z90(i,1))).^(b50(i,1)+1));
% between neutral height and facade height ***
integral_C180(i,1) = sign((H(i,1)-z180(i,1)))
        .*abs(((H(i,1)-z180(i,1))).^(b50(i,1)+1));
% between neutral height and facade height ***
integral_C270(i,1) = sign((H(i,1)-z270(i,1)))
        .*abs(((H(i,1)-z270(i,1))).^(b50(i,1)+1));
% between neutral height and facade height ***
integral_C0(highz0(i,1))  = 0;% no exfiltration
integral_C90(highz90(i,1))  = 0; % no exfiltration
integral_C180(highz180(i,1))  = 0; % no exfiltration
integral_C270(highz270(i,1))  = 0; % no exfiltration
integral_D0(i,1)  = -(sign(abs(z0(i,1))))
        .*abs((abs(z0(i,1))).^(b50(i,1)+1));
% remove flow between floor level and negative neutral height
integral_D90(i,1)  = -(sign(abs(z90(i,1))))
        .*abs((abs(z90(i,1))).^(b50(i,1)+1));
% remove flow between floor level and negative neutral height
integral_D180(i,1)  = -(sign(abs(z180(i,1))))
        .*abs((abs(z180(i,1))).^(b50(i,1)+1));
% remove flow between floor level and negative neutral height
integral_D270(i,1)  = -(sign(abs(z270(i,1))))
        .*abs((abs(z270(i,1))).^(b50(i,1)+1));
% remove flow between floor level and negative neutral height
integral_D0(negz0(i,1))   = 0;
integral_D90(negz90(i,1))   = 0;
integral_D180(negz180(i,1))   = 0;
integral_D270(negz270(i,1))   = 0;

        % coefficient
Coeff(i,1) = W(i,1).*((1./(b50(i,1)+1)).*E50(i,1).*a50(i,1)
        .*((abs(rint(i,1)-rext(i,1)).*g).^b50(i,1)));
        % Mass flow rates (kg/s)
```

```
        if Tint(i,1)>Text(i,1)
minf0(i,1) = Coeff(i,1).*(integral_A0(i,1)+integral_B0(i,1));
minf90(i,1) = Coeff(i,1).*(integral_A90(i,1)
+integral_B90(i,1));
minf180(i,1) = Coeff(i,1).*(integral_A180(i,1)
+integral_B180(i,1));
minf270(i,1) = Coeff(i,1).*(integral_A270(i,1)
+integral_B270(i,1));
mexf0(i,1) = Coeff(i,1).*(integral_C0(i,1)
+integral_D0(i,1));
mexf90(i,1) = Coeff(i,1).*(integral_C90(i,1)
+integral_D90(i,1));
mexf180(i,1) = Coeff(i,1).*(integral_C180(i,1)
+integral_D180(i,1));
mexf270(i,1) = Coeff(i,1).*(integral_C270(i,1)
+integral_D270(i,1));
        else
mexf0(i,1) = Coeff(i,1).*(integral_A0(i,1)+integral_B0(i,1));
mexf90(i,1) = Coeff(i,1).*(integral_A90(i,1)+integral_B90(i,1));
mexf180(i,1) = Coeff(i,1).*(integral_A180(i,1)
+integral_B180(i,1));
mexf270(i,1) = Coeff(i,1).*(integral_A270(i,1)
+integral_B270(i,1));
minf0(i,1) = Coeff(i,1).*(integral_C0(i,1)+integral_D0(i,1));
minf90(i,1) = Coeff(i,1).*(integral_C90(i,1)+integral_D90(i,1));
minf180(i,1) = Coeff(i,1).*(integral_C180(i,1)
+integral_D180(i,1));
minf270(i,1) = Coeff(i,1).*(integral_C270(i,1)
+integral_D270(i,1));
        end

    % HORIZONTAL FACADE FUNCTIONS
% function to calculate flow rate through horizontal given the
% internal air pressure Pi
pc(i,1) = (rint(i,1)-rext(i,1)).*g.*H(i,1) - Pi(i,1);
% pressure difference across facade (Pa)
% Buoyancy flow calculation only ceiling
```

```
pf(i,1) = - Pi(i,1); % pressure difference across facade (Pa)
% Buoyancy flow calculation only floor
mc(i,1) =
sign(pc(i,1)).*rmean(i,1).*Coeff(i,1).*abs(pc(i,1)).^b50(i,1);
% volume flow rate through facade (kg/s)
mf(i,1) =
sign(pf(i,1)).*rmean(i,1).*Coeff(i,1).*abs(pf(i,1)).^b50(i,1);
% volume flow rate through facade (kg/s)
%multiplied by mean density rmean
    if mc(i,1)>=0
minfhc(i,1) = mc(i,1);     % infiltration (kg/s)
        else
minfhc(i,1)=0;
        end
        if mf(i,1)>=0
minfhf(i,1) = mf(i,1);     % infiltration (kg/s)
        else
minfhf(i,1)=0;
        end
        if mc(i,1)<0
mexfhc(i,1) = abs(mc(i,1)); % exfiltration (kg/s)
        else
mexfhc(i,1)=0;
        end
        if mf(i,1)<0
mexfhf(i,1) = abs(mf(i,1)); % exfiltration (kg/s)
        else
mexfhf(i,1)=0;
        end

for j=1:20
     if EF0(i,1)==0
minf0(i,1)=0;
mexf0(i,1)=0;
     end
      if EF90(i,1)==0
minf90(i,1)=0;
```

```
mexf90(i,1)=0;
      end
       if EF180(i,1)==0
minf180(i,1)=0;
mexf180(i,1)=0;
       end
        if EF270(i,1)==0
minf270(i,1)=0;
mexf270(i,1)=0;
        end
 end
% total airflow rate
minft(i,1)  = minf0(i,1)+minf90(i,1)+minf180(i,1)
+minf270(i,1)+minfhc(i,1)+minfhf(i,1);
% infiltration (kg/s)
mexft(i,1)  = mexf0(i,1)+mexf90(i,1)+mexf180(i,1)
+mexf270(i,1)+mexfhc(i,1)+mexfhf(i,1);
% exfiltration (kg/s)
mtotal(i,1) = minft(i,1) - mexft(i,1);
% net mass flow rate (kg/s)
qtotal(i,1) = 1000.*(minft(i,1) - mexft(i,1))./rmean(i,1);
% net volume flow rate (l/s)
Qinft50  = 1000*minft./rmean;  % infiltration (l/s)
 Ninft50  = 3600*minft./rmean./Vol;
 % total air changes per hour (h^-1)

    %% SECTION 2, Main, calculation of Pi using Pulse.
%This section runs the model according to Jones et. al. 2013
%and Jones et. al. 2015 and the original DOMVENT3D model by
%Jones.

%Determinating the internal pressure using the
    % NEWTON RAPHSON SOVLER
 %definig the initial parameter for the solver

% initial caclulation,
%here last_qnet is calculated using an assumed Pi
```

```
% Loop until the net flow rate is zero
fthis_Pi = [1,0,0,0,0,0,0,0,0,0,0,0,0,0,0,0,0,0,0,0]';
fQnet       = [1,1,1,1,1,1,1,1,1,1,1,1,1,1,1,1,1,1,1,1]';
flast_Qnet=zeros(size(fQnet));
for i=1:20
fiteration_max_raphson(i,1) = 50;
fdPi                  = 0.0001;

flast_Pi   = this_Pi(i,1) - 2.*dPi;
fcriterion(i,1)  = 1e-3;
fiterations(i,1) = 0;
fovershoots(i,1) = 0;
%facade neutral height relative to ground level
fz0(i,1) =
(Pwind0(i,1)-flast_Pi)./((rext(i,1)-rint(i,1)).*g);
fz90(i,1) =
(Pwind90(i,1)-flast_Pi)./((rext(i,1)-rint(i,1)).*g);
fz180(i,1) =
(Pwind180(i,1)-flast_Pi)./((rext(i,1)-rint(i,1)).*g);
fz270(i,1) =
(Pwind270(i,1)-flast_Pi)./((rext(i,1)-rint(i,1)).*g);
%Vertical facades
% facade mass flow rate in and out
% infiltration when tint>text and visa versa
fnegz0(i,1)      = fz0(i,1)>0; % negative neutral height ***
fnegz90(i,1)      = fz90(i,1)>0; % negative neutral height ***
fnegz180(i,1)      = fz180(i,1)>0; % negative neutral height ***
fnegz270(i,1)      = fz270(i,1)>0; % negative neutral height ***
fhighz0(i,1)     = fz0(i,1)>H(i,1);
% neutral height above the facade height
fhighz90(i,1)     = fz90(i,1)>H(i,1);
% neutral height above the facade height
fhighz180(i,1)     = fz180(i,1)>H(i,1);
% neutral height above the facade height
fhighz270(i,1)     = fz270(i,1)>H(i,1);
% neutral height above the facade height
fintegral_A0(i,1) = sign(fz0(i,1)).*abs(fz0(i,1).^(b4(i,1)+1));
```

```
% between floor level and neutral height ***
fintegral_A90(i,1) =
sign(fz90(i,1)).*abs(fz90(i,1).^(b4(i,1)+1));
% between floor level and neutral height ***
fintegral_A180(i,1) =
sign(fz180(i,1)).*abs(fz180(i,1).^(b4(i,1)+1));
% between floor level and neutral height ***
fintegral_A270(i,1)  =
sign(fz270(i,1)).*abs(fz270(i,1).^(b4(i,1)+1));
% between floor level and neutral height ***
fintegral_A0(~fnegz0(i,1)) = 0; % no infiltration
fintegral_A90(~fnegz90(i,1))  = 0;   % no infiltration
fintegral_A180(~fnegz180(i,1))  = 0;  % no infiltration
fintegral_A270(~fnegz270(i,1))  = 0;  % no infiltration
fintegral_B0(i,1) = -(sign(fz0(i,1)-H(i,1)))
        .*abs((fz0(i,1)-H(i,1)).^(b4(i,1)+1));
% remove flow between facade height and neutral height
fintegral_B90(i,1) = -(sign(fz90(i,1)-H(i,1)))
        .*abs((fz90(i,1)-H(i,1)).^(b4(i,1)+1));
% remove flow between facade height and neutral height
fintegral_B180(i,1) = -(sign(fz180(i,1)-H(i,1)))
        .*abs((fz180(i,1)-H(i,1)).^(b4(i,1)+1));
% remove flow between facade height and neutral height
fintegral_B270(i,1) = -(sign(fz270(i,1)-H(i,1)))
        .*abs((fz270(i,1)-H(i,1)).^(b4(i,1)+1));
% remove flow between facade height and neutral height
fintegral_B0(~fhighz0(i,1)) = 0;
fintegral_B90(~fhighz90(i,1)) = 0;
fintegral_B180(~fhighz180(i,1)) = 0;
fintegral_B270(~fhighz270(i,1)) = 0;
% exfiltration when tint>text and visa versa
fintegral_C0(i,1) = sign((H(i,1)-fz0(i,1)))
        .*abs(((H(i,1)-fz0(i,1))).^(b4(i,1)+1));
% between neutral height and facade height ***
fintegral_C90(i,1) = sign((H(i,1)-fz90(i,1)))
        .*abs(((H(i,1)-fz90(i,1))).^(b4(i,1)+1));
% between neutral height and facade height ***
```

```
fintegral_C180(i,1) = sign((H(i,1)-fz180(i,1)))
        .*abs(((H(i,1)-fz180(i,1))).^(b4(i,1)+1));
% between neutral height and facade height ***
fintegral_C270(i,1) = sign((H(i,1)-fz270(i,1)))
        .*abs(((H(i,1)-fz270(i,1))).^(b4(i,1)+1));
% between neutral height and facade height ***
fintegral_C0(fhighz0(i,1))  = 0;  % no exfiltration
fintegral_C90(fhighz90(i,1))  = 0;    % no exfiltration
fintegral_C180(fhighz180(i,1))  = 0;% no exfiltration
fintegral_C270(fhighz270(i,1))  = 0;  % no exfiltration
fintegral_D0(i,1)  = -(sign(abs(fz0(i,1))))
        .*abs((abs(fz0(i,1))).^(b4(i,1)+1));
% remove flow between floor level and negative neutral height
fintegral_D90(i,1)  = -(sign(abs(fz90(i,1))))
        .*abs((abs(fz90(i,1))).^(b4(i,1)+1));
% remove flow between floor level and negative neutral height
fintegral_D180(i,1)  = -(sign(abs(fz180(i,1))))
        .*abs((abs(fz180(i,1))).^(b4(i,1)+1));
% remove flow between floor level and negative neutral height
fintegral_D270(i,1)  = -(sign(abs(fz270(i,1))))
        .*abs((abs(fz270(i,1))).^(b4(i,1)+1));
% remove flow between floor level and negative neutral height
fintegral_D0(fnegz0(i,1)) = 0;
fintegral_D90(fnegz90(i,1))= 0;
fintegral_D180(fnegz180(i,1))= 0;
fintegral_D270(fnegz270(i,1))= 0;

        % coefficient
fCoeff(i,1) = W(i,1).*((1./(b4(i,1)+1)).*E4(i,1).*a4(i,1)
.*((abs(rint(i,1)-rext(i,1)).*g).^b4(i,1)));
% Mass flow rates (kg/s)
        if Tint(i,1)>Text(i,1)
fminf0(i,1) = fCoeff(i,1).*(fintegral_A0(i,1)
+fintegral_B0(i,1));
fminf90(i,1) = fCoeff(i,1).*(fintegral_A90(i,1)
+fintegral_B90(i,1));
fminf180(i,1) = fCoeff(i,1).*(fintegral_A180(i,1)
```

```
+fintegral_B180(i,1));
fminf270(i,1) = fCoeff(i,1).*(fintegral_A270(i,1)
+fintegral_B270(i,1));
fmexf0(i,1) = fCoeff(i,1).*(fintegral_C0(i,1)
+fintegral_D0(i,1));
fmexf90(i,1) = fCoeff(i,1).*(fintegral_C90(i,1)
+fintegral_D90(i,1));
fmexf180(i,1) = fCoeff(i,1).*(fintegral_C180(i,1)
+fintegral_D180(i,1));
fmexf270(i,1) = fCoeff(i,1).*(fintegral_C270(i,1)
+fintegral_D270(i,1));
        else
fmexf0(i,1) = fCoeff(i,1).*(fintegral_A0(i,1)
+fintegral_B0(i,1));
fmexf90(i,1) = fCoeff(i,1).*(fintegral_A90(i,1)
+fintegral_B90(i,1));
fmexf180(i,1) = fCoeff(i,1).*(fintegral_A180(i,1)
+fintegral_B180(i,1));
fmexf270(i,1) = fCoeff(i,1).*(fintegral_A270(i,1)
+fintegral_B270(i,1));
fminf0(i,1) = fCoeff(i,1).*(fintegral_C0(i,1)
+fintegral_D0(i,1));
fminf90(i,1) = fCoeff(i,1).*(fintegral_C90(i,1)
+fintegral_D90(i,1));
fminf180(i,1) = fCoeff(i,1).*(fintegral_C180(i,1)
+fintegral_D180(i,1));
fminf270(i,1) = fCoeff(i,1).*(fintegral_C270(i,1)
+fintegral_D270(i,1));
        end

    % HORIZONTAL FACADE FUNCTIONS
% function to calculate flow rate through horizontal given the
% internal air pressure Pi
fpc(i,1) = (rint(i,1)-rext(i,1)).*g.*H(i,1) - flast_Pi;
% pressure difference across facade (Pa)
% Buoyancy flow calculation only ceiling
fpf(i,1) = - flast_Pi; % pressure difference across facade (Pa)
```

```
% Buoyancy flow calculation only floor
fmc(i,1) =
sign(fpc(i,1)).*rmean(i,1).*fCoeff(i,1).*abs(fpc(i,1)).^b4(i,1);
% volume flow rate through facade (kg/s)
fmf(i,1) =
sign(fpf(i,1)).*rmean(i,1).*fCoeff(i,1).*abs(fpf(i,1)).^b4(i,1);
% volume flow rate through facade (kg/s)
%multiplied by mean density rmean
        if fmc(i,1)>=0
fminfhc(i,1) = fmc(i,1);     % infiltration (kg/s)
        else
fminfhc(i,1)=0;
        end
        if fmf(i,1)>=0
fminfhf(i,1) = fmf(i,1);     % infiltration (kg/s)
        else
fminfhf(i,1)=0;
        end
        if fmc(i,1)<0
fmexfhc(i,1) = abs(fmc(i,1)); % exfiltration (kg/s)
        else
fmexfhc(i,1)=0;
        end
        if fmf(i,1)<0
fmexfhf(i,1) = abs(fmf(i,1)); % exfiltration (kg/s)
        else
fmexfhf(i,1)=0;
        end

 for j=1:20
     if EF0(i,1)==0
fminf0(i,1)=0;
fmexf0(i,1)=0;
     end
      if EF90(i,1)==0
fminf90(i,1)=0;
fmexf90(i,1)=0;
```

```
      end
       if EF180(i,1)==0
fminf180(i,1)=0;
fmexf180(i,1)=0;
       end
        if EF270(i,1)==0
fminf270(i,1)=0;
fmexf270(i,1)=0;
        end
 end
% total airflow rate
fminft(i,1)  = fminf0(i,1)+fminf90(i,1)+fminf180(i,1)
    +fminf270(i,1)+fminfhc(i,1)+fminfhf(i,1);
% infiltration (kg/s)
fmexft(i,1)  = fmexf0(i,1)+fmexf90(i,1)+fmexf180(i,1)
    +fmexf270(i,1)+fmexfhc(i,1)+fmexfhf(i,1);
% exfiltration (kg/s)
fmtotal(i,1) = fminft(i,1) - fmexft(i,1);
    % net mass flow rate (kg/s)
fqtotal(i,1) = 1000.*(fminft(i,1) - fmexft(i,1))./rmean(i,1);
% net volume flow rate (l/s)
flast_Qnet(i,1)=fqtotal(i,1);

while((abs(fQnet(i,1)) > fcriterion(i,1))
& (fiterations(i,1) < fiteration_max_raphson(i,1)))
fiterations(i,1) = fiterations(i,1) + 1;
% if the difference between current pi and last calculated pi
%is too small then re-scale the last calculated value
        if (abs(fthis_Pi(i,1)-flast_Pi) < abs(fdPi))
flast_Pi = fthis_Pi(i,1) - (fthis_Pi(i,1)-flast_Pi)./10.0;
        end

% estimate mass flow rates through all facade
%here starts the calculation for Qnet using this_pi
fz0(i,1) =
(Pwind0(i,1)-fthis_Pi(i,1))./((rext(i,1)-rint(i,1)).*g);
fz90(i,1) =
```

```
(Pwind90(i,1)-fthis_Pi(i,1))./((rext(i,1)-rint(i,1)).*g);
fz180(i,1) =
(Pwind180(i,1)-fthis_Pi(i,1))./((rext(i,1)-rint(i,1)).*g);
fz270(i,1) =
(Pwind270(i,1)-fthis_Pi(i,1))./((rext(i,1)-rint(i,1)).*g);
%Vertical facades
% facade mass flow rate in and out
% infiltration when tint>text and visa versa
fnegz0(i,1)      = fz0(i,1)>0; % negative neutral height
fnegz90(i,1)      = fz90(i,1)>0; % negative neutral height
fnegz180(i,1)      = fz180(i,1)>0; % negative neutral height ***
fnegz270(i,1)      = fz270(i,1)>0; % negative neutral height ***
fhighz0(i,1)     = fz0(i,1)>H(i,1);
% neutral height above the facade height
fhighz90(i,1)     = fz90(i,1)>H(i,1);
% neutral height above the facade height
fhighz180(i,1)     = fz180(i,1)>H(i,1);
% neutral height above the facade height
fhighz270(i,1)     = fz270(i,1)>H(i,1);
% neutral height above the facade height
fintegral_A0(i,1) = sign(fz0(i,1))
        .*abs(fz0(i,1).^(b4(i,1)+1));
% between floor level and neutral height ***
fintegral_A90(i,1) = sign(fz90(i,1))
        .*abs(fz90(i,1).^(b4(i,1)+1));
% between floor level and neutral height ***
fintegral_A180(i,1) = sign(fz180(i,1))
        .*abs(fz180(i,1).^(b4(i,1)+1));
% between floor level and neutral height ***
fintegral_A270(i,1)  = sign(fz270(i,1))
        .*abs(fz270(i,1).^(b4(i,1)+1));
% between floor level and neutral height
fintegral_A0(~fnegz0(i,1)) = 0;  % no infiltration
fintegral_A90(~fnegz90(i,1))  = 0; % no infiltration
fintegral_A180(~fnegz180(i,1))  = 0; % no infiltration
fintegral_A270(~fnegz270(i,1))  = 0; % no infiltration
fintegral_B0(i,1) = -(sign(fz0(i,1)-H(i,1)))
```

```
        .*abs((fz0(i,1)-H(i,1)).^(b4(i,1)+1));
% remove flow between facade height and neutral height
fintegral_B90(i,1) = -(sign(fz90(i,1)-H(i,1)))
        .*abs((fz90(i,1)-H(i,1)).^(b4(i,1)+1));
% remove flow between facade height and neutral height
fintegral_B180(i,1) = -(sign(fz180(i,1)-H(i,1)))
        .*abs((fz180(i,1)-H(i,1)).^(b4(i,1)+1));
% remove flow between facade height and neutral height
fintegral_B270(i,1) = -(sign(fz270(i,1)-H(i,1)))
        .*abs((fz270(i,1)-H(i,1)).^(b4(i,1)+1));
% remove flow between facade height and neutral height
fintegral_B0(~fhighz0(i,1)) = 0;
fintegral_B90(~fhighz90(i,1)) = 0;
fintegral_B180(~fhighz180(i,1)) = 0;
fintegral_B270(~fhighz270(i,1)) = 0;
% exfiltration when tint>text and visa versa
fintegral_C0(i,1) = sign((H(i,1)-fz0(i,1)))
        .*abs(((H(i,1)-fz0(i,1))).^(b4(i,1)+1));
% between neutral height and facade height ***
fintegral_C90(i,1) = sign((H(i,1)-fz90(i,1)))
        .*abs(((H(i,1)-fz90(i,1))).^(b4(i,1)+1));
% between neutral height and facade height ***
fintegral_C180(i,1) = sign((H(i,1)-fz180(i,1)))
        .*abs(((H(i,1)-fz180(i,1))).^(b4(i,1)+1));
% between neutral height and facade height ***
fintegral_C270(i,1) = sign((H(i,1)-fz270(i,1)))
        .*abs(((H(i,1)-fz270(i,1))).^(b4(i,1)+1));
% between neutral height and facade height ***
fintegral_C0(fhighz0(i,1))  = 0; % no exfiltration
fintegral_C90(fhighz90(i,1))  = 0;  % no exfiltration
fintegral_C180(fhighz180(i,1))  = 0; % no exfiltration
fintegral_C270(fhighz270(i,1))  = 0; % no exfiltration
fintegral_D0(i,1)  = -(sign(abs(fz0(i,1))))
        .*abs((abs(fz0(i,1))).^(b4(i,1)+1));
% remove flow between floor level and negative neutral height
fintegral_D90(i,1)  = -(sign(abs(fz90(i,1))))
        .*abs((abs(fz90(i,1))).^(b4(i,1)+1));
```

```
% remove flow between floor level and negative neutral height
fintegral_D180(i,1)  = -(sign(abs(fz180(i,1))))
        .*abs((abs(fz180(i,1))).^(b4(i,1)+1));
% remove flow between floor level and negative neutral height
fintegral_D270(i,1)  = -(sign(abs(fz270(i,1))))
        .*abs((abs(fz270(i,1))).^(b4(i,1)+1));
% remove flow between floor level and negative neutral height
fintegral_D0(fnegz0(i,1))   = 0;
fintegral_D90(fnegz90(i,1))   = 0;
fintegral_D180(fnegz180(i,1))   = 0;
fintegral_D270(fnegz270(i,1))   = 0;

% coefficient
fCoeff(i,1) = W(i,1).*((1./(b4(i,1)+1)).*E4(i,1).*a4(i,1)
.*((abs(rint(i,1)-rext(i,1)).*g).^b4(i,1)));
% Mass flow rates (kg/s)
        if Tint(i,1)>Text(i,1)
fminf0(i,1) = fCoeff(i,1).*(fintegral_A0(i,1)
+fintegral_B0(i,1));
fminf90(i,1) = fCoeff(i,1).*(fintegral_A90(i,1)
+fintegral_B90(i,1));
fminf180(i,1) = fCoeff(i,1).*(fintegral_A180(i,1)
+fintegral_B180(i,1));
fminf270(i,1) = fCoeff(i,1).*(fintegral_A270(i,1)
+fintegral_B270(i,1));
fmexf0(i,1) = fCoeff(i,1).*(fintegral_C0(i,1)
+fintegral_D0(i,1));
fmexf90(i,1) = fCoeff(i,1).*(fintegral_C90(i,1)
+fintegral_D90(i,1));
fmexf180(i,1) = fCoeff(i,1).*(fintegral_C180(i,1)
+fintegral_D180(i,1));
fmexf270(i,1) = fCoeff(i,1).*(fintegral_C270(i,1)
+fintegral_D270(i,1));
        else
fmexf0(i,1) = fCoeff(i,1).*(fintegral_A0(i,1)
+fintegral_B0(i,1));
fmexf90(i,1) = fCoeff(i,1).*(fintegral_A90(i,1)
```

```
+fintegral_B90(i,1));
fmexf180(i,1) = fCoeff(i,1).*(fintegral_A180(i,1)
+fintegral_B180(i,1));
fmexf270(i,1) = fCoeff(i,1).*(fintegral_A270(i,1)
+fintegral_B270(i,1));
fminf0(i,1) = fCoeff(i,1).*(fintegral_C0(i,1)
+fintegral_D0(i,1));
fminf90(i,1) = fCoeff(i,1).*(fintegral_C90(i,1)
+fintegral_D90(i,1));
fminf180(i,1) = fCoeff(i,1).*(fintegral_C180(i,1)
+fintegral_D180(i,1));
fminf270(i,1) = fCoeff(i,1).*(fintegral_C270(i,1)
+fintegral_D270(i,1));
        end

    % HORIZONTAL FACADE FUNCTIONS
% function to calculate flow rate through horizontal given the
% internal air pressure Pi
fpc(i,1) = (rint(i,1)-rext(i,1)).*g.*H(i,1) - fthis_Pi(i,1);
% pressure difference across facade (Pa)
% Buoyancy flow calculation only ceiling
fpf(i,1) = - fthis_Pi(i,1); % pressure difference across
%facade (Pa) Buoyancy flow calculation only floor
fmc(i,1) =
sign(fpc(i,1)).*rmean(i,1).*fCoeff(i,1).*abs(fpc(i,1)).^b4(i,1);
% volume flow rate through facade (kg/s)
fmf(i,1) =
sign(fpf(i,1)).*rmean(i,1).*fCoeff(i,1).*abs(fpf(i,1)).^b4(i,1);
% volume flow rate through facade (kg/s)
%multiplied by mean density rmean
        if fmc(i,1)>=0
fminfhc(i,1) = fmc(i,1);     % infiltration (kg/s)
        else
fminfhc(i,1)=0;
        end
        if fmf(i,1)>=0
fminfhf(i,1) = fmf(i,1);     % infiltration (kg/s)
```

```
        else
fminfhf(i,1)=0;
        end
        if fmc(i,1)<0
fmexfhc(i,1) = abs(fmc(i,1)); % exfiltration (kg/s)
        else
fmexfhc(i,1)=0;
        end
        if fmf(i,1)<0
fmexfhf(i,1) = abs(fmf(i,1)); % exfiltration (kg/s)
        else
fmexfhf(i,1)=0;
        end

for j=1:20
     if EF0(i,1)==0
fminf0(i,1)=0;
fmexf0(i,1)=0;
     end
      if EF90(i,1)==0
fminf90(i,1)=0;
fmexf90(i,1)=0;
      end
       if EF180(i,1)==0
fminf180(i,1)=0;
fmexf180(i,1)=0;
       end
        if EF270(i,1)==0
fminf270(i,1)=0;
fmexf270(i,1)=0;
        end
 end
% total airflow rate
fminft(i,1)  = fminf0(i,1)+fminf90(i,1)+fminf180(i,1)
    +fminf270(i,1)+fminfhc(i,1)+fminfhf(i,1);
% infiltration (kg/s)
fmexft(i,1)  = fmexf0(i,1)+fmexf90(i,1)+fmexf180(i,1)
```

```
    +fmexf270(i,1)+fmexfhc(i,1)+fmexfhf(i,1);
% exfiltration (kg/s)
fmtotal(i,1) = fminft(i,1) - fmexft(i,1);
    % net mass flow rate (kg/s)
fqtotal(i,1) = 1000.*(fminft(i,1) - fmexft(i,1))./rmean(i,1);
    % net volume flow rate (l/s)
fQnet(i,1)=fqtotal(i,1);
%Here the model ends

% compare this prediction against the last
 fslope(i,1) =
 (fQnet(i,1) - flast_Qnet(i,1))./(fthis_Pi(i,1)-flast_Pi);
% update variables for next iteration
flast_Pi = fthis_Pi(i,1);
% calculate the next guess
fthis_Pi(i,1) = fthis_Pi(i,1) - fQnet(i,1)./fslope(i,1);

 % check if we've overshot the zero value
        if ((fQnet(i,1).*flast_Qnet(i,1)) < 0.0)
foversshoots(i,1) = fovershoots(i,1) + 1;
        end
 % update variables for next iteration
flast_Qnet(i,1) = fQnet(i,1);
    end

%From now on, the last calculations will be done, basically
% it will repeat the last iteration of the solver.
fPi(i,1) = fthis_Pi(i,1);
    end

    %% SECTION 2.1, Main, Calculation of the infiltration rate
%here starts the calculation for Qnet using this_pi
fz0(i,1) =
(Pwind0(i,1)-fPi(i,1))./((rext(i,1)-rint(i,1)).*g);
fz90(i,1) =
 (Pwind90(i,1)-fPi(i,1))./((rext(i,1)-rint(i,1)).*g);
fz180(i,1) =
```

```
 (Pwind180(i,1)-fPi(i,1))./((rext(i,1)-rint(i,1)).*g);
fz270(i,1) =
(Pwind270(i,1)-fPi(i,1))./((rext(i,1)-rint(i,1)).*g);
%Vertical facades
% facade mass flow rate in and out
% infiltration when tint>text and visa versa
fnegz0(i,1)      = fz0(i,1)>0; % negative neutral height ***
fnegz90(i,1)      = fz90(i,1)>0; % negative neutral height ***
fnegz180(i,1)      = fz180(i,1)>0; % negative neutral height
fnegz270(i,1)      = fz270(i,1)>0; % negative neutral height ***
fhighz0(i,1)     = fz0(i,1)>H(i,1);
% neutral height above the facade height
fhighz90(i,1)     = fz90(i,1)>H(i,1);
% neutral height above the facade height
fhighz180(i,1)     = fz180(i,1)>H(i,1);
% neutral height above the facade height
fhighz270(i,1)     = fz270(i,1)>H(i,1);
% neutral height above the facade height
fintegral_A0(i,1) =
 sign(fz0(i,1)).*abs(fz0(i,1).^(b4(i,1)+1));
% between floor level and neutral height ***
fintegral_A90(i,1) =
sign(fz90(i,1)).*abs(fz90(i,1).^(b4(i,1)+1));
% between floor level and neutral height ***
fintegral_A180(i,1) =
 sign(fz180(i,1)).*abs(fz180(i,1).^(b4(i,1)+1));
% between floor level and neutral height ***
fintegral_A270(i,1)  =
 sign(fz270(i,1)).*abs(fz270(i,1).^(b4(i,1)+1));
% between floor level and neutral height ***
fintegral_A0(~fnegz0(i,1)) = 0; % no infiltration
fintegral_A90(~fnegz90(i,1))  = 0;  % no infiltration
fintegral_A180(~fnegz180(i,1))  = 0;% no infiltration
fintegral_A270(~fnegz270(i,1))  = 0;% no infiltration
fintegral_B0(i,1) = -(sign(fz0(i,1)-H(i,1)))
        .*abs((fz0(i,1)-H(i,1)).^(b4(i,1)+1));
% remove flow between facade height and neutral height
```

```
fintegral_B90(i,1) = -(sign(fz90(i,1)-H(i,1)))
        .*abs((fz90(i,1)-H(i,1)).^(b4(i,1)+1));
% remove flow between facade height and neutral height
fintegral_B180(i,1) = -(sign(fz180(i,1)-H(i,1)))
        .*abs((fz180(i,1)-H(i,1)).^(b4(i,1)+1));
% remove flow between facade height and neutral height
fintegral_B270(i,1) = -(sign(fz270(i,1)-H(i,1)))
        .*abs((fz270(i,1)-H(i,1)).^(b4(i,1)+1));
% remove flow between facade height and neutral height
fintegral_B0(~fhighz0(i,1)) = 0;
fintegral_B90(~fhighz90(i,1)) = 0;
fintegral_B180(~fhighz180(i,1)) = 0;
fintegral_B270(~fhighz270(i,1)) = 0;
% exfiltration when tint>text and visa versa
fintegral_C0(i,1) = sign((H(i,1)-fz0(i,1)))
        .*abs(((H(i,1)-fz0(i,1))).^(b4(i,1)+1));
% between neutral height and facade height
fintegral_C90(i,1) = sign((H(i,1)-fz90(i,1)))
        .*abs(((H(i,1)-fz90(i,1))).^(b4(i,1)+1));
% between neutral height and facade height ***
fintegral_C180(i,1) = sign((H(i,1)-fz180(i,1)))
        .*abs(((H(i,1)-fz180(i,1))).^(b4(i,1)+1));
% between neutral height and facade height ***
fintegral_C270(i,1) = sign((H(i,1)-fz270(i,1)))
        .*abs(((H(i,1)-fz270(i,1))).^(b4(i,1)+1));
% between neutral height and facade height ***
fintegral_C0(fhighz0(i,1))  = 0; % no exfiltration
fintegral_C90(fhighz90(i,1))  = 0; % no exfiltration
fintegral_C180(fhighz180(i,1))  = 0; % no exfiltration
fintegral_C270(fhighz270(i,1))  = 0; % no exfiltration
fintegral_D0(i,1)  = -(sign(abs(fz0(i,1))))
        .*abs((abs(fz0(i,1))).^(b4(i,1)+1));
% remove flow between floor level and negative neutral height
fintegral_D90(i,1)  = -(sign(abs(fz90(i,1))))
        .*abs((abs(fz90(i,1))).^(b4(i,1)+1));
% remove flow between floor level and negative neutral height
fintegral_D180(i,1)  = -(sign(abs(fz180(i,1))))
```

```
        .*abs((abs(fz180(i,1))).^(b4(i,1)+1));
% remove flow between floor level and negative neutral height
fintegral_D270(i,1)  = -(sign(abs(fz270(i,1))))
        .*abs((abs(fz270(i,1))).^(b4(i,1)+1));
% remove flow between floor level and negative neutral height
fintegral_D0(fnegz0(i,1))= 0;
fintegral_D90(fnegz90(i,1))= 0;
fintegral_D180(fnegz180(i,1))= 0;
fintegral_D270(fnegz270(i,1)) = 0;

% coefficient
fCoeff(i,1) = W(i,1).*((1./(b4(i,1)+1)).*E4(i,1).*a4(i,1)
.*((abs(rint(i,1)-rext(i,1)).*g).^b4(i,1)));
% Mass flow rates (kg/s)
        if Tint(i,1)>Text(i,1)
fminf0(i,1) = fCoeff(i,1).*(fintegral_A0(i,1)
+fintegral_B0(i,1));
fminf90(i,1) = fCoeff(i,1).*(fintegral_A90(i,1)
+fintegral_B90(i,1));
fminf180(i,1) = fCoeff(i,1).*(fintegral_A180(i,1)
+fintegral_B180(i,1));
fminf270(i,1) = fCoeff(i,1).*(fintegral_A270(i,1)
+fintegral_B270(i,1));
fmexf0(i,1) = fCoeff(i,1).*(fintegral_C0(i,1)
+fintegral_D0(i,1));
fmexf90(i,1) = fCoeff(i,1).*(fintegral_C90(i,1)
+fintegral_D90(i,1));
fmexf180(i,1) = fCoeff(i,1).*(fintegral_C180(i,1)
+fintegral_D180(i,1));
fmexf270(i,1) = fCoeff(i,1).*(fintegral_C270(i,1)
+fintegral_D270(i,1));
        else
fmexf0(i,1) = fCoeff(i,1).*(fintegral_A0(i,1)
+fintegral_B0(i,1));
fmexf90(i,1) = fCoeff(i,1).*(fintegral_A90(i,1)
+fintegral_B90(i,1));
fmexf180(i,1) = fCoeff(i,1).*(fintegral_A180(i,1)
```

```
+fintegral_B180(i,1));
fmexf270(i,1) = fCoeff(i,1).*(fintegral_A270(i,1)
+fintegral_B270(i,1));
fminf0(i,1) = fCoeff(i,1).*(fintegral_C0(i,1)
+fintegral_D0(i,1));
fminf90(i,1) = fCoeff(i,1).*(fintegral_C90(i,1)
+fintegral_D90(i,1));
fminf180(i,1) = fCoeff(i,1).*(fintegral_C180(i,1)
+fintegral_D180(i,1));
fminf270(i,1) = fCoeff(i,1).*(fintegral_C270(i,1)
+fintegral_D270(i,1));
        end

    % HORIZONTAL FACADE FUNCTIONS
% function to calculate flow rate through horizontal given the
% internal air pressure Pi
fpc(i,1) = (rint(i,1)-rext(i,1)).*g.*H(i,1) - fPi(i,1);
% pressure difference across facade (Pa)
% Buoyancy flow calculation only ceiling
fpf(i,1) = - fPi(i,1); % pressure difference across facade (Pa)
% Buoyancy flow calculation only floor
fmc(i,1) =
sign(fpc(i,1)).*rmean(i,1).*fCoeff(i,1).*abs(fpc(i,1)).^b4(i,1);
% volume flow rate through facade (kg/s)
fmf(i,1) =
sign(fpf(i,1)).*rmean(i,1).*fCoeff(i,1).*abs(fpf(i,1)).^b4(i,1);
% volume flow rate through facade (kg/s)
%multiplied by mean density rmean
        if fmc(i,1)>=0
fminfhc(i,1) = fmc(i,1); % infiltration (kg/s)
        else
fminfhc(i,1)=0;
        end
        if fmf(i,1)>=0
fminfhf(i,1) = fmf(i,1);     % infiltration (kg/s)
        else
fminfhf(i,1)=0;
```

```
        end
        if fmc(i,1)<0
fmexfhc(i,1) = abs(fmc(i,1)); % exfiltration (kg/s)
        else
fmexfhc(i,1)=0;
        end
        if fmf(i,1)<0
fmexfhf(i,1) = abs(fmf(i,1)); % exfiltration (kg/s)
        else
fmexfhf(i,1)=0;
        end

for j=1:20
     if EF0(i,1)==0
fminf0(i,1)=0;
fmexf0(i,1)=0;
     end
      if EF90(i,1)==0
fminf90(i,1)=0;
fmexf90(i,1)=0;
      end
       if EF180(i,1)==0
fminf180(i,1)=0;
fmexf180(i,1)=0;
       end
        if EF270(i,1)==0
fminf270(i,1)=0;
fmexf270(i,1)=0;
        end
 end

% total airflow rate
fminft(i,1)  = fminf0(i,1)+fminf90(i,1)+fminf180(i,1)
    +fminf270(i,1)+fminfhc(i,1)+fminfhf(i,1);
% infiltration (kg/s)
fmexft(i,1)  = fmexf0(i,1)+fmexf90(i,1)+fmexf180(i,1)
    +fmexf270(i,1)+fmexfhc(i,1)+fmexfhf(i,1);
```

```
% exfiltration (kg/s)
fmtotal(i,1) = fminft(i,1) - fmexft(i,1);
% net mass flow rate (kg/s)
fqtotal(i,1) = 1000.*(fminft(i,1) - fmexft(i,1))./rmean(i,1);
% net volume flow rate (l/s)
Qinft4  = 1000*fminft./rmean;  % infiltration (l/s)
Ninft4  = 3600*fminft./rmean./Vol;
% total air changes per hour (h^-1)

    %% SECTION 4, outputs
filename = 'DOMVENT3D_data.xlsx';
sheet = 1;
xlRange='AA1:AA20';
xlswrite(filename,Ninft50,sheet,xlRange);

filename = 'DOMVENT3D_data.xlsx';
sheet = 1;
xlRange='AB1:AB20';
xlswrite(filename,Ninft4,sheet,xlRange);

display('finished, go to your file with the results')
```